Petal cell shape and flower-pollinator interaction in *Nicotiana*

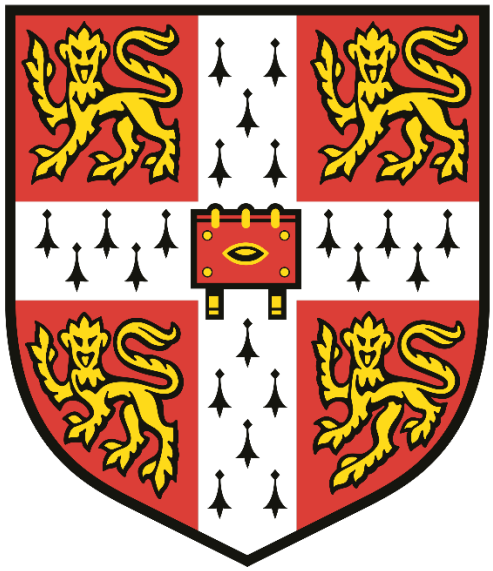

Maria Gabriela Doria Ramirez

Department of Plant Sciences

University of Cambridge

Cambridge, United Kingdom

This dissertation is submitted for the degree of

Doctor of Philosophy

Wolfson College

April 2019

Declaration

This thesis is the result of my own work and includes nothing which is the outcome of work done in collaboration except as declared in the Preface and specified in the text. It is not substantially the same as any that I have submitted, or, is being concurrently submitted for a degree or diploma or other qualification at the University of Cambridge or any other University or similar institution except as declared in the Preface and specified in the text. I further state that no substantial part of my thesis has already been submitted, or, is being concurrently submitted for any such degree, diploma or other qualification at the University of Cambridge or any other University or similar institution except as declared in the Preface and specified in the text. It does not exceed the 60.000 prescribed word limit for the Degree Committee of the Faculty of Biology.

Petal cell shape and flower-pollinator interaction in *Nicotiana*

Maria Gabriela Doria Ramirez

Petal epidermal cell shape has been shown to affect pollination success in flowering plants. Conical epidermal cells may increase grip for insect pollinators and enhance flower colouration compared to non-conical cells. *Nicotiana* (Solanaceae) presents a diverse range of petal cell shapes. Interestingly, sister species in at least two phylogenetically distinct clades of the genus have contrasting petal epidermal cell shapes (conical vs. non-conical). This project aims to further understand character evolution of petal cell shape in *Nicotiana* and its implications in pollination systems, combining tools of molecular biology, morphology and pollinator behaviour experiments. First, using a candidate gene approach, I explore in parallel the molecular mechanisms involved in petal cell shape differentiation of sister species with contrasting cell shape *N. cordifolia* and *N. solanifolia* (Section *Paniculatae*) and *N. bonariensis* and *N. forgetiana* (Section *Alatae*). Subgroup 9 R2R3 MYB transcription factors are potentially responsible for the molecular control of petal cell shape. Differential expression of subgroup 9 R2R3 MYBs in petals of the sister species, rather than sequence differences in these genes, might be explaining the contrasting cell morphologies. Next, I develop an *Agrobacterium tumefaciens* mediated transformation protocol for the non-model species *N. forgetiana*, a methodological advance crucial for further exploration of the molecular mechanisms and functional implications of petal cell shape. Lastly, I explore how petal colour and petal cell shape interact in the perception of flowers by model pollinator *Bombus terrestris* using biomimetic artificial flowers. Pollinator behaviour experiments indicate that the bumblebees can discriminate flowers with conical from flowers with non-conical surfaces, on a red and on a white background, using visual cues alone as well as tactile cues alone. This investigation improves our understanding of the molecular mechanisms involved in petal epidermal cell morphogenesis and of the functional implications of petal cell shape in the interaction flower-pollinator in *Nicotiana*.

Acknowledgements

I would like to thank my supervisor, Professor Beverley Glover, for her guidance and encouragement during my PhD. It has been invaluable to be part of her research group, learn from her expertise and passion for flowers and pollination, and receiving her support in all aspects of academic life in and out the laboratory. I specially thank her for proofreading this manuscript and for providing important insights during the writing process.

My research would have been impossible without the contributions of Dr. Lin Taylor to the understanding of the evolution of petal cell shape in *Nicotiana* during her PhD at the Department of Plant Sciences, University of Cambridge.

I would like to thank my examiners Professor John P. Carr and Professor Andrew Leitch for insightful discussion and constructive comments to improve this manuscript.

I am profoundly grateful to Matthew Dorling for his support in all aspects of laboratory and office organisation, and for lovingly taking care of the *Nicotiana* plants and the bees.

Access to specialized equipment was crucial for this investigation. I extend my acknowledgments to Raymond Wightman and Gareth Evans from the Cryogenic Scanning Microscope Facility at the Sainsbury Laboratory, and to Jeremy Skepper at the Cambridge Advanced Imaging Centre, for their support obtaining hundreds of scanning electron microscopy images for my work. I would like to thank the Department of Plant Sciences staff, specially to Pawel Baster for coordinating the use of the tissue lyser and the qPCR machines, and to Susana Sauret-Gueto for training and coordinating the use of the Keyence microscope.

Many people have contributed with their expertise in several aspects of this research. I have received invaluable training on molecular biology from Dr. Chiara Arioldi, Dr. Edwige Moyroud, Dr. Greg Mellers, Dr. Emily Bailes, and other members of the Glover Lab, since the early stages of my PhD. Dr. Chiara Arioldi, Dr. Saumya Awathi and Roísín Fattorini contributed with insightful discussion and trobleshutting about quantitative analyses of gene expression. Dr. Jonathan Pattrick and Dr. Roman Kellenberger provided advise on the design and selection of materials for the fabrication of artificial flowers used in the bee experiments. Johnathan Patrick, Hamish Symington, Jake Moscrop, Netsai Mhlanga and Anna Platoni shared the space, the knowledge and the love for bees in the Bee Lab. Dr. Carlos Lugo, Dr. Boris Delahaie and Dr. Nik

Cuniffe gave me invaluable help with the statistics analyses of bumblebee behaviour. I am deeply thankful to all of them.

None of this work would have been possible without having access to plants from different corners of the world. I would like to thank Jessica Nifong, from the US *Nicotiana* Germplasm Collection, for providing seeds of several *Nicotiana* species. My sincere thanks go to Dr. Angela Cano-Schütz, Alex Summers, Paul Aston, and other staff members of the Cambridge University Botanic Gardens, for their help on using the garden's collection and for taking good care of the nicotianas with 'special needs'. Sincere acknowledgements go to Felipe Andrés Saéz Quintana, from Corporación Nacional Forestal de Chile-CONAF, in the Juan Fernández Archipelago, for significant information from the field about *Nicotiana cordifolia.* Also, to Constanza Valdivieso, from the Department of Animal Sciences, University of Cambridge, for keeping and eye on this mysterious plant species while doing her investigations on fur seals in the islands. Moreover, I would like to thank Carolina Carrasco for kindly providing important literature about field observations and archeological research on *Nicotiana solanifolia* from the Atacama Desert in Chile.

My investigations and stay at Cambridge were possible thanks to my academic sponsors, the Colombian Administrative Department of Science, Technology and Innovation-COLCIENCIAS, the British Council, the Newton-Caldas Fund and the Commonwealth, European and International Cambridge Trust. I am also thankful for the generous financial support I have received over the course of this PhD from Wolfson College, the Philosophical Society of Cambridge, the New Phytologist Trust, and the Swiss National Science Foundation and University of Zürich, to participate in scientific conferences abroad.

Writing this dissertation required a boost of inspiration and encouragement. I would like to thank the "Cavendish Hall Writing Group" for generating a space for mutual motivation and for their company during the writing process.

On a personal note, I am deeply thankful to all, past and present, permanent and transient, members of the Glover Lab from whom I have learnt and with whom I have shared the past four years. Thank you to Chiara Airoldi, Saumya Awathi, Erin Cullen, Gwen Davis, Chris Davis, Boris Delahaie, Matthew Dorling, Alice Fairnie, Róisín Fattorini, Mario Fernández-Mazuecos, Jordan Ferria, Mike Imburgia, Benjamin Fisk, Roman Kellenberger, Thea Kongsted, Lize Joubert, Victoria Hernández-Ruiz, Carlos Lugo-Vélez, Cecilia Martínez-Pérez, Greg Mellers, Jake Moscrop, Edwige Moyroud, Alex Summers, Miranda Sinnott-Armstrong, Hamish Symington,

Lin Taylor and Qi Wang. It has been fantastic to share with such a group of brilliant minds with similar interests and fascination for science, the natural world, flowers, pollination and baking goods.

Special thanks to my friends and colleagues from the Department of Plant Sciences Alfonso Timoneda-Monfort and Ana Bravo for sharing my PhD adventure from the beginning to the end. Thanks to all members of the Department for their smiles in the corridors, shared moments in the tearoom and for making of Plant Sciences a loving space to work and learn, specially to Aleix Gorsch Rovira, Hester Sheehan and all members of the Brockington Lab. Thanks to my friends from Wolfson College and the University of Cambridge Colombian Society for the fun times and their affection. Thanks to my friends and colleagues from Universidad Nacional de Colombia for their lifelong friendship, support and company along the uncertain path of being a biologist and pursuing a career inspired by love and curiosity for biodiversity and the natural world.

Finally, thank you to my family for their constant love and support from all corners of the world. To my mother, Gladys Ramírez, for being and infinite source of positive energy, beauty and inspiration. To my father, Eliécer Doria, for always being proud and encouraging. To my siblings, Iván Rey, Marcela Rey, Javier Rey, Alejandro Rey and Olga Lucía Doria, my nephew Pablo Nicolás Fuentes, my nieces María Camila Rey, Laura Rozo and Gianna Lynn Rey, my closer relatives from multiple lines Sonia, Alberto, Anita, Jeannine, Gustavo, Juan Carlos, Valentino, Emilio, Doreen, Claudia, Nicolas, Diana, Rob, Greyson, the Ramirez family, the Doria family, and my quadrupedal relatives Alaska, Deseo, Elliot, Emily, Duque, Napoleón and Morris, for their encouragement on pursuing my goals and for keeping an eye on me, my flowers and my bees from the distance.

TABLE OF CONTENTS

LIST OF ABBREVIATIONS

BAP	6-Benzylaminopurine
bp	Base pairs (s)
CaMV	cauliflower mosaic virus
Cβ	carbon beta terminus
cDNA	complementary deoxyribonucleic acid
Ct	cycle threshold
dH_20	deionised water
DNA	deoxyribonucleic acid
dNTP	deoxyribonucleotide triphosphate
evo-devo	evolutionary developmental biology
GARLI	genetic algorithm for rapid likelihood inference
IAA	indole-3-acetic acid
IPTG	isopropyl thiogalactoside
kb	kilobase pairs
kDa	kilodalton
L	liter
m	meter
µ	micro
M	molar
LiCl	lithium chloride
MLBS	Maximum Likelihood bootstrap
MYB	family of transcription factors named for myeloblastosis
m.y.a.	million years ago
O.D.	optical density
PCR	polymerase chain reaction
RNA	Ribonucleic acid
qPCR	quantitative reverse transcriptase PCR
rpm	revolutions per minute
RT-PCR	reverse transcriptase PCR
SEM	scanning electron microscopy
WT	wild type
X-gal	5-bromo-4-chloro-3-indolyl-β-D-galactopyranoside

LIST OF FIGURES

LIST OF TABLES

LIST OF APPENDICES

Chapter 1.

INTRODUCTION

1 INTRODUCTION

1.1 Flowering plant diversity and mechanisms of diversification

An estimated 369,000 species of flowering plants (angiosperms) are known to science, making them the most diverse group of plants on Earth (RBG-Kew, 2016). In the last few decades there has been an increase in studies of genetics, morphology, development, reproductive biology, fossil record and phylogenetic relationships of the angiosperms. These studies have allowed the re-analysis of one of the most interesting problems of contemporary botany, which Charles Darwin referred to as "an abominable mystery": the origin and rapid diversification of flowering plants (Stebbins, 2006; Friedman & Ryerson, 2009; Crepet & Niklas, 2009; Buggs, 2017). Today there is consensus on the phylogenetic pattern among living angiosperms based on molecular and/or morphological data enhanced by sophisticated laboratory and computational techniques (Savolainen et al., 2000; Wikström et al., 2001; Doyle & Endress, 2002; Qiu et al., 2002; Soltis & Soltis, 2004; APG, 2009; Bell et al., 2010; Soltis et al., 2011; Doyle, 2012; Magallón et al., 2015; Sauquet et al., 2017). Moreover, paleobotanical findings have provided direct evidence of the structure and biology of plant groups crucial to elucidate the relationships among living angiosperms (Friis *et al.*, 2007, 2009; Stockey & Rothwell, 2009; Taylor & Taylor, 2009), and have documented major diversification patterns through the evolution of the clade (Crepet *et al.*, 2004; Friis *et al.*, 2006, 2011; Wing *et al.*, 2012; Gomez *et al.*, 2015; Herendeen *et al.*, 2017). However, the mechanisms that have resulted in such diversity of forms and natural histories is an active matter of debate.

Reproduction by means of flowers and fruits is often invoked as one of the main causes of the evolutionary success of angiosperms (Pellmyr, 1992; Stebbins, 2006; Mitchell *et al.*, 2009; Armbruster, 2014). Adaptive radiation driven by the interaction between plants and their beneficial animal pollinators and/or dispersers is thought to be one of the main drivers resulting in the huge number of flowering plant species (Lunau, 2004; Labandeira & Currano, 2013; Yuan *et al.*, 2013). Special attention has been paid to the patterns and mechanisms of structural diversification of the flower itself (Crepet, 1984; Grant, 1994; Soltis & Soltis, 2004, 2014; Friis *et al.*, 2006; Damerval & Nadot, 2007; Ronse De Craene, 2007; Kramer, 2007; Armbruster, 2014; Bruce, 2015; Glover *et al.*, 2015; Chanderbali *et al.*, 2016; Sauquet *et al.*, 2017). Most of the diversity in angiosperms is diagnosed by variation in floral features, and, in fact, speciation often involves shifts in floral characters, such as size, shape, colour, phenology, scent and reward, among others (Kay & Sargent, 2009; Chase *et al.*, 2010; Givnish, 2010). Often associated with

variation in floral features is a shift in pollinators, such that animal pollinators are thought to drive patterns of floral diversity (Lunau, 2004; Mitchell *et al.*, 2009; Armbruster, 2014; Bruce, 2015). Understanding the structural diversity of floral features, the evolutionary mechanisms involved in defining such features, and how the interaction between flowers and their pollinators is driving patterns of flower diversity, is then crucial to understand the enormous diversity of flowering plants.

1.1.1 Flower-pollinator interaction as a mechanism of flowering plant diversification

Pollination is the successful transfer of pollen from the pollen sacs (microsporangia) into proximity to the ovule. It is the essential precursor to fertilisation in gymnosperms (Owens *et al.*, 1998; Bolinder *et al.*, 2015) and angiosperms (Stebbins, 1970; Endress & Steiner-Gafner, 1996; Endress, 2010). Some flowering plants and gymnosperms can self-pollinate (Wang *et al.*, 2004; Wright *et al.*, 2013; Abdelaziz *et al.*, 2019), but most use external vectors to maximize the probability of outcrossing. The great variety of modes of pollination using external vectors can broadly be divided into pollination involving animals (biotic) (Mitchell *et al.*, 2009) or wind/water (abiotic) (Culley *et al.*, 2002; Friedman & Barrett, 2009). Biotic pollination is especially important in flowering plants and is thought to have an important role in underpinning the structural diversity and high speciation rate of the group (Bawa, 1990; Pellmyr, 1992; Kay & Sargent, 2009). Pollinators may exert selective pressure over floral traits, eventually directing the evolution of both flowers and pollinators. Speciation in flowering plants is commonly assumed to be derived in part from reproductive isolation associated with morphological divergence and specificity in interactions with pollinators (Ippolito *et al.*, 2004; Kay & Sargent, 2009).

A great variety of animals, including insects, birds and mammals, participate in pollination of angiosperms. Flowers of different taxa that are pollinated by similar animal pollinators often show similar specialisation in structure and other features (*e.g.* morphology, colour, odour, size, rewards, phenology). These similarities have been used to recognise "syndromes" among the diversity of angiosperm floral form that distinguish flowers visited by certain kinds of pollinators (Faegri & Van Der Pijl, 1979; Proctor *et al.*, 1996; Fenster *et al.*, 2004). For instance, flowers pollinated by bees are often blue, yellow or ultraviolet with nectar guides, and are open in the early morning (*e.g.* Peterson *et al.*, 2015), whereas flowers pollinated by noctuid moths tend to be light in colour, presumably aiding recognition in the dark (*e.g.* Martins & Johnson, 2007;

Riffell *et al.*, 2008). In both cases the floral reward for the pollinator is usually nectar. Pollination syndromes could have predictive value in inferring potential pollinators for plants with specific floral traits. However, this assumption could be misleading in some cases, such as for generalist flowers and/or generalist pollinators (Johnson & Steiner, 2000). Although multiple works report pollination syndromes for certain plant lineages (*e.g.* Fenster *et al.*, 2004; Armbruster, 2014), and a recent quantitative evaluation of the concept found strong support even across angiosperms (Rosas-Guerrero *et al.*, 2014), other studies have criticised the utility of the concept (Chittka & Waser, 1997; Ollerton *et al.*, 2009; Dellinger *et al.*, 2019).

1.2 Floral features influencing flower-pollinator interactions

The interaction of flowers with pollinators (and herbivores or pollen robbers) is influenced by different communication channels, with visual clues as some of the most important floral features that structure the flower-visitor composition (Chittka & Thomson, 2002). Flowers of angiosperms pollinated by animals are usually large, showy and coloured. In most cases the organs generating visual attractiveness to animal pollinators are the petals, although in several taxa bracts, sepals and/or stamens (staminodia) are also involved in the attraction of pollinators (Endress & Steiner-Gafner, 1996; Ronse De Craene, 2007; Endress, 2010; Ronse De Craene & Brockington, 2013).

1.2.1 Flower epidermal features and pollination

The flower epidermis is crucial to understanding petal function, as it is both the primary point of contact with the abiotic environment (influencing light capture and reflectance, evaporation, temperature and wettability) and the primary point of contact with the biotic environment, providing visual, tactile and olfactory cues to pollinating animals (Whitney *et al.*, 2011a). The diversity of flower colour in angiosperms is mainly attributed to pigments derived from different biochemical pathways, their combinations, variable concentrations as well as additional co-pigments, the prevalent pH in the vacuole, metal ions, pigment packaging and location within the tissue layers (Grotewold, 2006). Along with these factors epidermal cell structure of petals also affects the visual appearance of flowers (Noda *et al.*, 1994; Gorton & Vogelmann, 1996; Baumann *et al.*, 2007; Whitney *et al.*, 2011a,b, Vignolini *et al.*, 2012b,a; Moyroud *et al.*, 2017).

Two petal epidermal morphologies are known to influence light and pollinator behaviour: epidermal cell shape on the micro-scale (*e.g.* conical cells), and the presence of cuticular nano-

scale structures such as folds or striations. Cuticular nanostructures are sculptures, such as ordered ridges, on top of the outermost layer of the petal. These sculptures can result in diffraction gratings known to produce 'structural colours' (Antoniou Kourounioti *et al.*, 2013). Recent studies demonstrate the role of cuticular nanostructures in generating optical effects that are visible to insect pollinators, such as floral iridescence and blue light scattering (Whitney *et al.*, 2009d; Glover & Whitney, 2010; Vignolini *et al.*, 2015; Moyroud *et al.*, 2017). In angiosperms floral gratings have been identified and characterised in plants belonging to nine orders including members of the monocots, basal eudicots, asterids and rosids (Whitney *et al.*, 2009c,d; Glover & Whitney, 2010; Vignolini *et al.*, 2015; Moyroud *et al.*, 2017).

Conical cells are cone-shaped epidermal cells (also referred to in some studies as papillate). A first survey of epidermal cell structure revealed that 79% of the investigated plant species show some form of conical epidermal cells (Kay *et al.*, 1981). They have been best studied in flowering plants where they are most commonly found on the stigma, where they function to trap pollen grains, and on the petals of flowers where may play a role in pollinator attraction (Glover *et al.*, 1998; Whitney *et al.*, 2009b). Conical epidermal cells can act as lenses and light traps, changing optical properties by refracting and focusing light into the pigment-containing tissue layer of petals (Gorton & Vogelmann, 1996; Zhang *et al.*, 2015). Besides visual appearance, it has been shown that conical epidermal cells increase grip by providing contact between small pollinators and the flower (Whitney *et al.*, 2009b,a; Alcorn *et al.*, 2012; Alcorn, 2013). Moreover, the epidermal cell structure also determines floral temperature (Comba *et al.*, 2000), floral shape (Baumann *et al.*, 2007), wettability (Whitney *et al.*, 2011c) and microsculptural pattern forming nectar guides (Kevan & Lane, 1985).

1.2.2 Functional aspects of petal cell shape related to pollination

Plants with conical cells on the petals have been shown to provide a distinct advantage for animal pollination, specifically by insects, when compared to those with non-conical cells (Glover & Martin, 1998; Alcorn *et al.*, 2012; Alcorn, 2013). The effect of conical cells on colour saturation, on pollinator grip and on floral temperature and wettability, are the main processes through which conical cells influence pollinator interactions, with pollinator grip the most important of these.

1.2.2.1 Effect of petal cell shape on colour saturation

Figure 1.1 illustrates the effect of petal cell shape on the appearance of petal colouration in *Anthirrinum majus*. Wild type flowers in *A. majus* (left) are deep magenta in colour with a velvety texture to the petal lobes. The flower to the right is a *mixta* mutant of *A. majus*, in which the activity of the transcription factor MIXTA, responsible for the formation of conical cells in this species (Noda *et al.*, 1994)(Section 1.3.2), has been blocked, resulting in non-conical cells on the surface of the petals (Glover & Martin, 1998). Mutant flowers appear paler in colour, in spite of an equal amount of pigment, and have a dull texture.

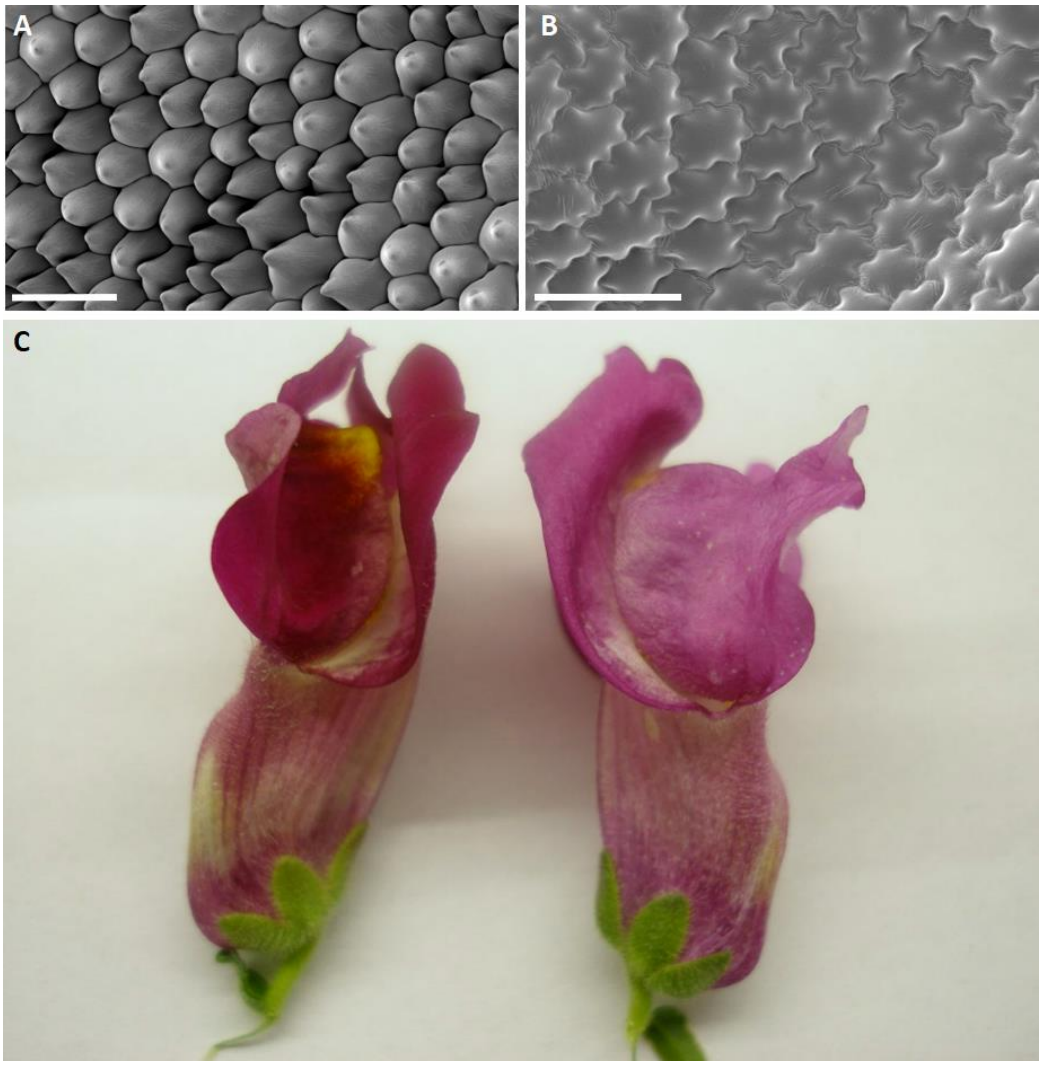

Figure 1.1. Petal cell shape in *Antirrhinum majus* and its effect on colouration.
Petal texture influences flower colour. (A) Scanning electron micrograph of wild-type *Antirrhinum* petal epidermis, showing conical cells. (B) Scanning electron micrograph of a *mixta* mutant with flat (non-conical) petal epidermal cells. (C) Photograph illustrating the colour difference between these flowers. Figure from Whitney & Glover (2007).

Conical cells focus light onto internal floral pigments, thus enhancing a petal's colour intensity (Kay *et al.*, 1981). Two types of light are reflected from a petal when irradiated with light at a 90° angle to its surface (vertical irradiation)(Zhang *et al.*, 2015). One is exterior reflected light (Rs),

which is reflected from the surface and seen as sparkling spots at the centres of the epidermal cells. The characteristics of the Rs are influenced by epidermal cell shape and the colour is similar to that of the light source (Gorton & Vogelmann, 1996; Zhang *et al.*, 2015). The other type of reflected light is interior reflected light (Ri), which is reflected from inside the petal and influenced by the pigment contents and internal structures of the petal, especially the parenchyma determining the petal's base colour (Kay *et al.*, 1981; Zhang *et al.*, 2015). Figure 1.2 shows the role of epidermal cell differentiation in light absorption and reflection. In a conical epidermis (1) incident light is reflected by the angled cell walls into the cells, including light arriving at a low angle of incidence. On flat cells (2) such light is reflected off the cell walls. Therefore, conical cells enhance the relative amount of light absorbed by the epidermal cells and reduce the amount of reflected white light to enhance the intensity of pigmentation (Noda *et al.*, 1994). Light reflected out from the mesophyll below the epidermis (Figure 1.2B) will be reflected in many directions by the angled walls of conical-papillate cells, giving the epidermis a bright appearance when viewed from a variety of angles (Kay *et al.*, 1981; Noda *et al.*, 1994).

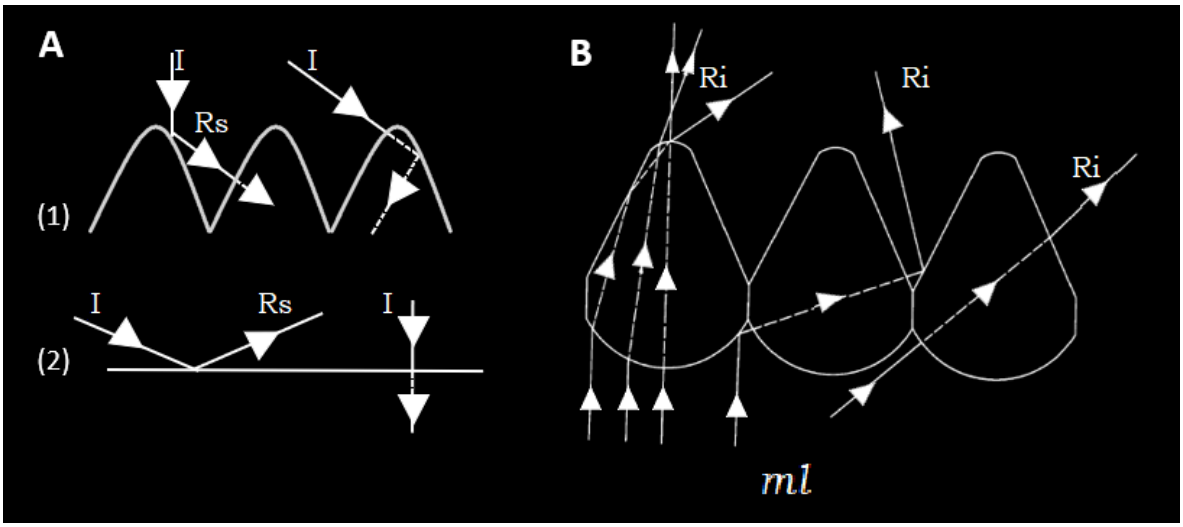

Figure 1.2. Conical cells increase the saturation of petal colouration compared to flat cells.
A. Light absorption and reflection by a conical-papillate petal surface (1) and a flat-non-conical petal surface (2). Incident light (I) is reflected by the angled cell walls of conical cells into the cells, including light arriving at a low angle of incidence whereas incident light is reflected off the cell walls of flat cells. Therefore, conical cells enhance the relative amount of light absorbed by the epidermal cells (dashed lines) and reduce the amount of reflected white light reflected by the surface (Rs) to enhance the intensity of pigmentation. B. Paths of light rays emerging from the reflective mesophyll layer (ml) of a petal with conical-papillate epidermal cells. Light reflected out from the interior (Ri) is reflected in many directions by the angled walls of conical-papillate cells, giving the epidermis a bright appearance when viewed from a variety of angles. Adapted from Kay *et al.*, 1981 and Noda *et al.*, 1994.

Experimental evidence on the effect of colour saturation associated with petal cell shape in pollination is discussed in Chapter 5 (section 5.1.4).

1.2.2.2 Effect of petal cell shape on pollinator grip

Along with the different visual appearance of the petals of the *mixta* mutant compared to the wild type *A. majus (*Figure 1.1) these lines also present different petal textures defined by their epidermal cell shape (Glover & Martin, 1998). Although petal texture, at the microscopic scale, might be indiscernible for humans, pollinators such as bees are able to discriminate between conical and non-conical-celled surfaces by tactile cues alone (Kevan & Lane, 1985; Erber *et al.*, 1997, 1998; Whitney *et al.*, 2009a). The effect of petal cell shape as an enhancer of grip by insect pollinators has been tested extensively (Whitney *et al.*, 2009a; Rands *et al.*, 2011; Alcorn *et al.*, 2012; Alcorn, 2013; Pattrick, 2017). While grip is not irrelevant for larger pollinators such as birds and mammals, the structures important for grip for these pollinators are likely to be of a different order and magnitude to those for insects (Pattrick, 2017).

In a series of experiments using flowers from isogenic lines of *A. majus* (Figure 1.1), Whitney *et al.* (2009a) showed that the bumblebee *Bombus terrestris* preferred the conical-celled wild type over the non-conical celled *mixta* mutant, when the flowers were presented in a vertical orientation and required opening. Similarly, when presented with biomimetic epoxy casts of the petals of *A. majus* of the same pigment background but contrasting cell shape, bumblebees preferred the conical-celled surfaces when foraging from casts in a vertical position (Whitney *et al.*, 2009a). These experiments confirmed that the bumblebees were able to discriminate between the surfaces by touch alone. Moreover, they indicated that in situations where the flowers are harder to handle, as is the case for the complex morphology of the flowers of *A. majus* or the epoxy cast in a vertical position, an advantage of conical cells may be that they offer enhanced grip for small pollinators. The interaction between floral texture, orientation, and reward was investigated by Pattrick (2017). Lab-based foraging trials on *B. terrestris* visiting artificial flowers varying in slope, surface texture and sugar reward revealed a trade-off between the biomechanical difficulty of visiting and handling the 'flowers' and the quality of the reward offered. Flowers that were difficult to grip (*e.g.* "smooth surface" in a vertical position) were often avoided even if they offered a higher reward (Pattrick, 2017).

Most flowering plants have conical cells on their petals (Kay *et al.*, 1981), but considering flower morphology or presentation angle, not all species with conical celled species are necessarily difficult to handle by pollinators. A study of 183 angiosperm species found no association between presence of conical cells on the adaxial surface of the petal and the orientation of flowers (vertical or horizontal) (Rands *et al.*, 2011). Why are then conical cells equally prevalent amongst complex and simpler flowers? In a laboratory setup, using isogenic lines of *Petunia*

hybrida, Alcorn *et al.*, (2012) tested *B. terrestris* preference for conical- or non-conical-celled flowers under different conditions of motion. For the relatively easy to handle flowers of *Petunia,* they found that when the flowers were moving, bees always learned to favour conical-celled flowers (Alcorn *et al.*, 2012; Alcorn, 2013). Simpler flowers then may still benefit from producing petal surfaces that enhance pollinator grip under certain conditions.

Considering the advantage of having conical cells, the remaining question is then, why some flowers have non-conical/slippery cells on their petal surfaces? In wind pollinated species such as *Thalictrum dioicum*, which has flat-celled petals (Di Stilio *et al.*, 2009), having flowers that are easy to grip is irrelevant to pollination success. Another possibility is that a smooth petal surface, coupled with other areas of the flower that are easier to grip, helps to direct pollinator movement whilst on the flowers. In a field based exploration, Pattrick, (2017) showed that bumblebees avoided the slippery (non-conical) surface of the petals of hollyhocks (*Alcea rosea*, Malvaceae), instead these pollinators would grasp on the long staminal column of the flowers, which would result in greater contact with the anthers or stigma than simply gripping onto the base of the column while foraging for nectar, and much greater contact than only walking on the petals. This combination of structures seems to direct pollinator visiting behaviour, and is likely to be beneficial for the plant by enhancing pollen transfer. The slippery petals of hollyhocks may improve pollination efficiency for the plant when it is being visited by bumblebees, by encouraging the bees to hold onto the staminal column (Pattrick, 2017). Slippery petals are also found as an adaptation in some specialised pollination systems, such as the slippery trap flowers of *Arisaema* (Araceae) and *Aristolochia* (Aristolochiaceae) (Vogel & Martens, 2000; Oelschlägel *et al.*, 2009) and some orchids (Bäzinger *et al.*, 2005).

Non-conical petal surfaces have also been proposed to result from secondary loss of conical cells in some species that have transitioned from bee to bird pollination, as microscale grip is not important for birds (Ojeda *et al.*, 2012, 2016). Ojeda et al., (2009) found that four species of *Lotus* (Fabaceae) that have shifted to bird pollination from bee-pollinated ancestors completely lack conical cells on their dorsal petals. Similarly, Papiorek et al., (2014) found from a survey of epidermal cell shape in 58 species from 26 families that conical cells are more common in bee pollinated flowers, whereas bird pollinated flowers are more likely to have flat epidermal cells. These authors suggest that changes in cell shape could be associated with other adaptations that specialise a flower to attracting hovering pollinators, such as birds, rather than bees.

1.2.2.3 Effect of petal cell shape on floral temperature and wettability

Another hypothesis for the advantage of conical cells is that they absorb more sunlight than flat cells, and so are warmer than their surroundings; this increase in temperature could speed up the development of floral organs, and act as a metabolic reward for pollinators (Comba *et al.*, 2000; Whitney *et al.*, 2008). However, experiments comparing the temperatures of conical celled to flat celled flowers found that cell shape has limited effects on floral warming, and that pigmentation is much more of a factor in this process (Whitney *et al.*, 2011a). The hydrophobicity or wettability of a petal surface (the ability of water to bead up and roll off it, as on a lotus leaf) also influences its function. Petals with conical cells are generally less wettable (more hydrophobic) than those with flat cells (Whitney *et al.*, 2011c). This has the potential to increase reproductive success in a number of ways: for example, hydrophobicity may generate a self-cleaning effect, allowing dust, dirt, virus particles and fungal spores to be carried away. Similarly, self-cleaning may remove insect scent marks, masking when a flower has been recently visited and emptied of nectar. Hydrophobic petals may also prevent the flower from becoming waterlogged and losing its shape (Whitney *et al.*, 2011c). However, the effect of petal wettability on pollinator behaviour has not been tested.

1.3 Molecular mechanisms underlying the evolution of plant form

Morphological differences between species, from simple single-character differences to large-scale variation in body plans, can be traced to changes in the timing and location of developmental events (Purugganan, 1998). Evolutionary developmental biology (evo-devo) aims to define how developmental programs are modified to generate novel or labile morphologies (Glover *et al.*, 2015). Understanding gene structure, function, and interactions is crucial to disentangle the molecular mechanisms underlying the evolution of plant form (Doebley & Lukens, 1998).

Developmental pathways consist of signal(s), transducers, transcriptional regulator(s) and targets (Doebley & Lukens, 1998). The signals may be environmental (*e.g.*, photoperiod) or internal (*e.g.*, auxin). The transducers compose the signal transduction pathway and include those gene products that participate in signal production, perception, transmission, and modification (*e.g.*, ligands, receptor kinases, phytochromes, and proteins/enzymes involved in hormone synthesis/deactivation). Transcriptional regulators are the proteins involved specifically in the regulation of gene expression through direct binding to regions of non-coding DNA. Finally, target genes can be any type of gene (Doebley, 1993; Doebley & Lukens, 1998).

A hypothesis with historical and continuing importance in evo-devo is that the majority of phenotypic change between species is brought about by changes in the regulation of genes, rather than changes in structural proteins themselves (Doebley, 1993; Doebley & Lukens, 1998; Carroll, 2000, 2008; Swinnen *et al.*, 2016). Transcription factors are proteins that either activate or repress transcription of other genes by binding to short *cis*-regulatory elements that lie in the vicinity of the target genes (Pabo & Sauer, 2003; Chen & Rajewsky, 2007). Transcription factors recruit and instruct RNA polymerase (RNA pol II) to initiate RNA synthesis at specific genes by recognizing and biding to DNA elements called promoters (Mitchell & TjiAN, 1989). In complex multicellular organisms, transcription factors generally do not work in isolation, but instead, together with co-regulators, they form large networks of cooperating and interacting transcription factors (Chen & Rajewsky, 2007; Carroll, 2008).

Some transcription factors have key positions, so that alterations in their expression levels or patterns of expression, or in those of their downstream genes, cause the multi-gene configurations or phenotypic state that emerges as a result of such complex regulatory networks to switch into another state (Rodríguez-Mega *et al.*, 2015). The cases in which alteration of transcriptional regulatory mechanisms have been associated with important phenotypic changes in plants are numerous (Rodríguez-Mega *et al.*, 2015; Moyroud & Glover, 2017). For instance, the position of organs within a flower can be radically altered by the mutation of a single MADS box gene (Coen & Meyerowitz, 1991), and there are numerous examples of *cis*-regulatory element modifications underlying crop initial domestication or improvement phenotypes (Swinnen *et al.*, 2016), for instance several alleles of a barley *APETALA2* ortholog, named *HvAP2*, are associated with increased spike density (Houston *et al.*, 2013).

1.3.1 Molecular control of petal epidermal cell morphology

MYB proteins are a diverse class of transcription factors of particular importance in transcriptional regulation in plants (Jin & Martin, 1999). The extensive expansion of this family in plants suggests that its members perform diverse functions in plant-specific processes (Du *et al.*, 2012). The characteristic common to all MYB proteins is the structurally conserved MYB DNA-binding domain. This domain consists of about 52 amino acids (the R motif) that bind DNA in a sequence-specific manner. The most common type of plant MYB transcription factor is the subfamily R2R3 MYB (containing two repeats of the R motif) (Du *et al.*, 2012). The R2R3 MYB proteins are plant specific (Martin & Paz-Ares, 1997; Dubos *et al.*, 2010; Brockington *et al.*,

2013). The R2R3 MYB subfamily is incredibly diverse and the proteins have been found to be involved in the regulation of secondary metabolism, cell fate and identity, developmental processes, and response to biotic and abiotic stress (Jin & Martin, 1999; Stracke *et al.*, 2001; Dubos *et al.*, 2010).

Phylogenetic analyses of R2R3 MYB genes from *Arabidopsis thaliana*, *Zea mays* and other plants support 37 subgroups (Figure 1.3) (Du *et al.*, 2012; Stracke *et al.*, 2001). These subgroups are defined based on conserved sequence motifs, and in some cases MYB proteins within a subgroup appear to have similar functions (Stracke *et al.*, 2001; Jaffé *et al.*, 2007; Brockington *et al.*, 2013)

Figure 1.3 Phylogeny and classification of R2R3 MYB proteins of *Arabidopsis thaliana.*
(Next page) Phylogenetic tree showing the classification of 125 *A. thaliana* R2R3 MYB proteins into subgroups according to shared amino acid motifs. Some landmark R2R3 MYB transcription factors from other species (ZmMYBC1, X06333; AmMYBMIXTA, X79108; AmMYBPHAN, AJ005586; HvMYBGA, X87690; NtMYB1, U72762; PhMYBAN2, AF146702; and Mmc-Myb, X02774) were included for comparison. The consensus motif for each subgroup and the location of this in relation to the R2R3 repeats is shown on the right. Subgroup 9 is indicated by an arrow. The prototypic MIXTA protein, AmMYBMIXTA (referred to in this thesis as AmMIXTA), is shown in subgroup 9 along with the three known *Arabidopsis* subgroup 9 proteins, AtMYB16, AtMYB17 and AtMYB107. Figure adapted from (Stracke *et al.*, 2001).

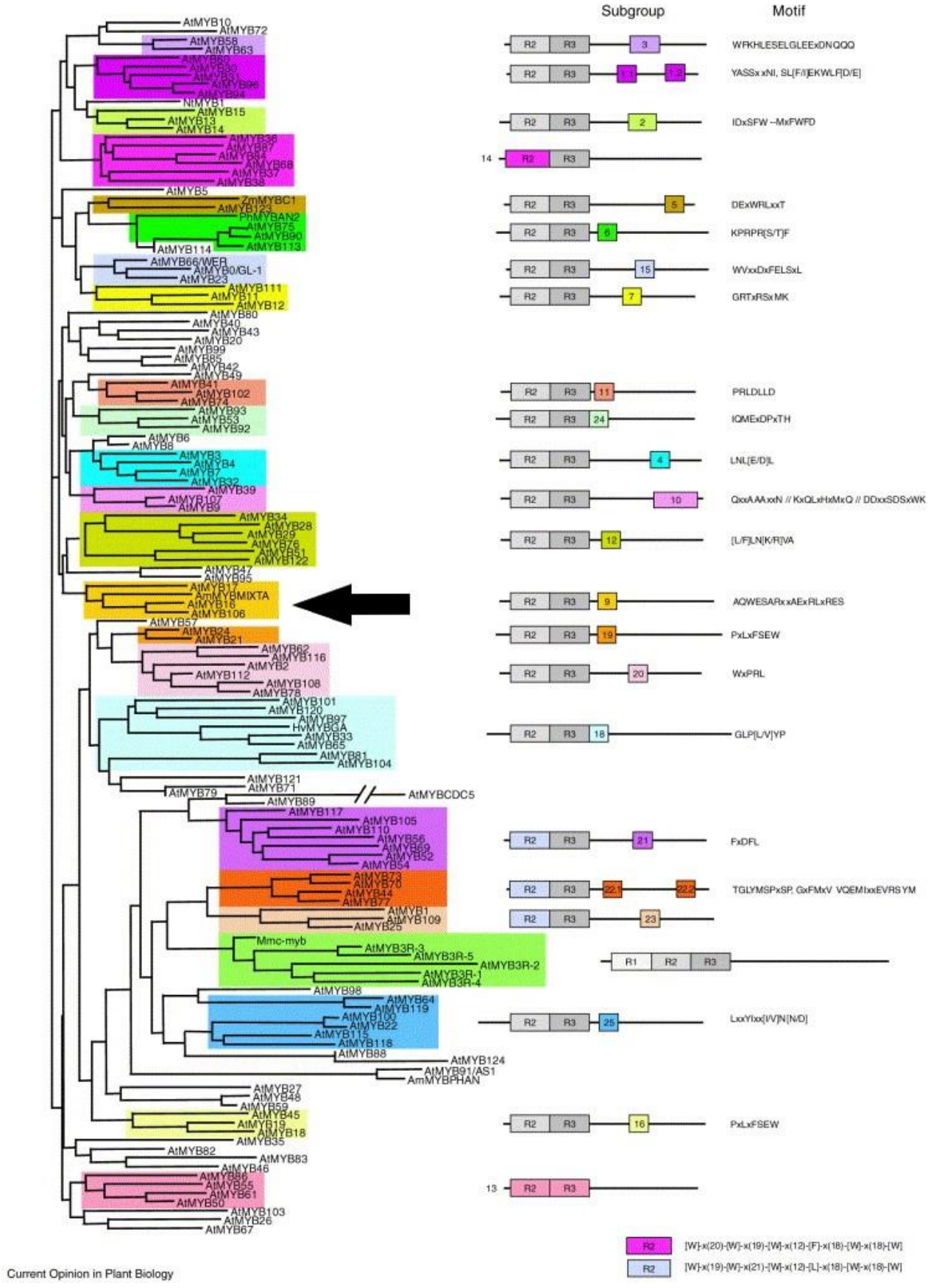
Subgroup
Motif
AtMYB10
AtMYB72
AtMYB58
AtMYB63
AtMYB90
AtMYB30
AtMYB31
AtMYB96
AtMYB94
NtMYB1
AtMYB15
AtMYB13
AtMYB14
AtMYB36
AtMYB87
AtMYB84
AtMYB68
AtMYB37
AtMYB38
AtMYB5
ZmMYBC1
AtMYB123
PhMYBAN2
AtMYB75
AtMYB90
AtMYB113
AtMYB114
AtMYB66/WER
AtMYB0/GL-1
AtMYB23
AtMYB111
AtMYB11
AtMYB12
AtMYB60
AtMYB40
AtMYB43
AtMYB20
AtMYB99
AtMYB85
AtMYB42
AtMYB49
AtMYB41
AtMYB102
AtMYB24
AtMYB93
AtMYB53
AtMYB92
AtMYB6
AtMYB8
AtMYB3
AtMYB4
AtMYB7
AtMYB32
AtMYB39
AtMYB107
AtMYB9
AtMYB34
AtMYB28
AtMYB29
AtMYB76
AtMYB51
AtMYB122
AtMYB47
AtMYB95
AtMYB17
AmMYBMIXTA
AtMYB16
AtMYB106
AtMYB57
AtMYB24
AtMYB21
AtMYB62
AtMYB116
AtMYB2
AtMYB112
AtMYB108
AtMYB78
AtMYB101
AtMYB120
AtMYB97
HvMYBGA
AtMYB33
AtMYB65
AtMYB81
AtMYB104
AtMYB121
AtMYB71
AtMYB79
AtMYBCDC5
AtMYB89
AtMYB117
AtMYB105
AtMYB110
AtMYB56
AtMYB69
AtMYB52
AtMYB54
AtMYB73
AtMYB70
AtMYB44
AtMYB77
AtMYB1
AtMYB109
AtMYB25
Mmc-myb
AtMYB3R-3
AtMYB3R-5
AtMYB3R-2
AtMYB3R-1
AtMYB3R-4
AtMYB98
AtMYB64
AtMYB119
AtMYB103
AtMYB22
AtMYB115
AtMYB118
AtMYB88
AtMYB124
AtMYB91/AS1
AmMYBPHAN
AtMYB27
AtMYB48
AtMYB59
AtMYB45
AtMYB19
AtMYB18
AtMYB35
AtMYB82
AtMYB83
AtMYB46
AtMYB86
AtMYB55
AtMYB61
AtMYB50
AtMYB103
AtMYB26
AtMYB67
R2 R3 3 WFKHLESELGLEExDNQQQ
R2 R3 11 12 YASSxxNI, SL[F/I]EKWLF[D/E]
R2 R3 2 IDxSFW --MxFWFD
14 R2 R3
R2 R3 5 DExWRLxxT
R2 R3 6 KPRPR[S/T]F
R2 R3 15 WVxxDxFELSxL
R2 R3 7 GRTxRSxMK
R2 R3 11 PRLDLLD
R2 R3 24 IQMExDPxTH
R2 R3 4 LNL[E/D]L
R2 R3 10 QxxAAAxxN // KxQLxHxMxQ // DDxxSDSxWK
R2 R3 12 [L/F]LN[K/R]VA
R2 R3 9 AQWESARxxAExRLxRES
R2 R3 19 PxLxFSEW
R2 R3 20 WxPRL
R2 R3 18 GLP[L/V]YP
R2 R3 21 FxDFL
R2 R3 22.1 22.2 TGLYMSPxSP. GxFMxV VQEMIxxEVRSYM
R2 R3 23
R1 R2 R3
R2 R3 25 LxxYIxx[I/V]N[N/D]
R2 R3 16 PxLxFSEW
13 R2 R3
R2 [W]-x(20)-[W]-x(19)-[W]-x(12)-[F]-x(18)-[W]-x(18)-[W]
R2 [W]-x(19)-[W]-x(21)-[W]-x(12)-[L]-x(18)-[W]-x(18)-[W]
Current Opinion in Plant Biology

Genes in subgroup 9 of the R2R3 MYB family (black arrow in Figure 1.3), are known to be involved in the regulation of epidermal cell differentiation and the formation of epidermal projections including conical cell Together these studies suggest that the SBG9 lineage of R2R3 MYB proteins as a whole perform roles in the regulation of cellular differentiation and particularly in the formation of epidermal projections such as trichomes, conical cells, and root hairs development in a range of angiosperm species (Noda et al., 1994; Glover et al., 1998; Baumann et al., 2007; Mintz-Oron et al., 2008; Machado et al., 2009).

The first R2R3 subgroup 9 gene (SBG9 R2R3 MYB) to be characterized was the *MIXTA* gene from the snapdragon *Antirrhinum majus* (Plantaginaceae), which controls the development of conical cell shape in the petal epidermis (Noda *et al.*, 1994) and appears to be both necessary and sufficient to drive the formation of conical epidermal cells from flat epidermal cells, as further introduced in section 1.3.2 (Noda *et al.*, 1994; Glover & Martin, 1998; Martin *et al.*, 2002). Additional SBG9 R2R3 MYB genes (*MIXTA-like 1*, *MIXTA-like 2*, and *MIXTA-like 3*) are also expressed in petals of *A. majus* and perform similar but non-redundant roles with respect to *MIXTA* (Perez-Rodriguez *et al.*, 2005; Jaffé *et al.*, 2007; Baumann *et al.*, 2007).

SBG9 R2R3 MYB genes have been functionally analysed in a number of other plant species (Appendix 1). In cotton plants (*Gossypium hirsuta*, Malvaceae), for example, *MIXTA-like* MYBs play a role in regulating specialized outgrowths of epidermal cells, including cotton fibres (Machado *et al.*, 2009; Bedon *et al.*, 2014; Wu *et al.*, 2018). Regulation of epidermal cell outgrowths by SBG9 MYB genes has also been demonstrated in *Arabidopsis thaliana* (Brassicaceae, Folkers *et al.*, 1997; Jakoby *et al.*, 2008; Gilding & Marks, 2010), *Populus trichopoda* (Salicaceae, Wilkins *et al.*, 2009; Plett *et al.*, 2010), *Dendrobium crumenatum* (Orchidaceae; Scoville *et al.*, 2011), *Mimulus guttatus* (Phyrmaceae; Scoville *et al.*, 2011), *Medicago truncatula* (Fabaceae; Gilding & Marks, 2010), *Solanum* spp. (Solanaceae; Alcorn, 2013; Lashbrooke *et al.*, 2015), *Aristolochia ringens* (Suárez-Baron *et al.*, 2019), among others. Besides *Antirrhinum majus*, the role of SBG9 R2R3 MYBs in regulating conical cell growth specifically has been demonstrated in petals of *Arabidopsis thaliana* (Baumann *et al.*, 2007), *Petunia hybrida* (Solanaceae; Baumann *et al.*, 2007), petaloid organs of *Thalictrum spp.* (Ranunculaceae; Di Stilio *et al.*, 2009) and in petaloid tepals of the basal angiosperm *Cabomba caroliniana* (ANA grade; Reed, 2014).

Subgroup 9 of the R2R3 MYB protein family has a deep evolutionary history within the land plants. Phylogenetic analyses of the gene family (Brockington *et al.*, 2013) (Figure 1.4) show a

deep duplication event that occurred before the evolution of seed plants, splitting the MYB subgroup 9 family into two distinct subclades (subgroup 9A and 9B). Two further major duplications occurred independently within these subclades giving rise to the MIXTA and MIXTA-like clades (within subgroup 9A clade) and the MYB17 and MYB17-like clades (within subgroup 9B). Both of these duplications occurred at the base of the eudicots.

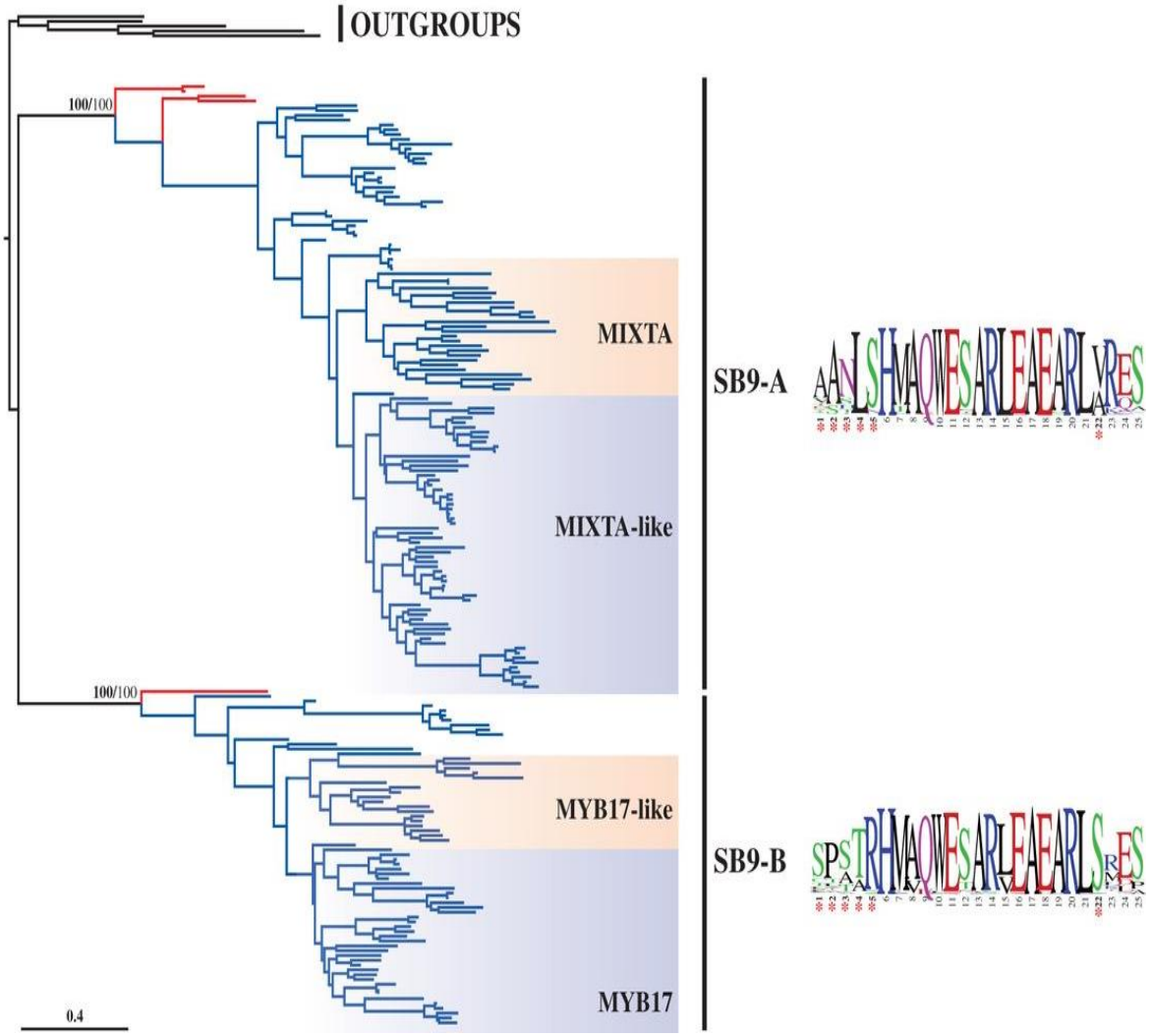

Figure 1.4. GARLI phylogram of the subgroup 9 R2R3 MYB genes in angiosperms
GARLI (Genetic Algorithm for Rapid Likelihood Inference) maximum likelihood phylogram of 220 members of the subgroup 9 R2R3 MYB genes revealing the two major subclades, SBG9-A and SBG9-B, and the major clades resulting from core eudicot duplication, MIXTA, MIXTA-like, MYB17, and MYB17-like. Blue lines indicate angiosperm taxa, and red lines indicate gymnosperm taxa. Outgroups: *Selaginella mollendorfii*, *Physcomitrella patens*, and *Marchantia polymorpha*. Numbers next to nodes are Bayesian Posterior probabilities (in bold) and MLBS support values greater than 50% from 100 replicates. Logo types depict the conserved SBG9 motif for SBG9-A and SB9-B clades—red stars beneath these logos indicate residues that are most diagnostic between the two clades. Figure from Brockington *et al.*, (2013).

1.3.2 Molecular control of epidermal cell differentiation in *Antirrhinum majus*

Antirrhinum majus is one of the more widely used plant models in studies related to gene regulation and development of the flower (Schwarz-Sommer *et al.*, 2003). Several key floral genes were first identified in *Antirrhinum* including MYB genes controlling petal epidermal cell shape (*MIXTA*, section 1.3.1). In *A. majus MIXTA* encodes a transcription factor that is necessary for the development of conical cells on the inner epidermis of the petals (Noda *et al.*, 1994). Ectopic expression of the *MIXTA* gene in tobacco (Glover *et al.*, 1998) and overexpression of *MIXTA* in *A. majus* (Martin *et al.*, 2002) results in the formation of two distinct cell types on leaves. All plants ectopically expressing *MIXTA* produce outgrowths on their leaf epidermal cells which resemble conical cells. Some lines also produce ectopic trichomes on their leaves and petals. These experiments show *MIXTA* to be sufficient for conical cell formation, but also indicate that two specialised cell forms, trichomes and conical cells, can be induced by *MIXTA* expression in both tobacco and *Antirrhinum,* and therefore these species probably share at least part of a common developmental programme (Perez-Rodriguez *et al.*, 2005). *MIXTA* expression in *Antirrhinum* is limited to a narrow window of time relatively late in development of the petal epidermis, only after cell division has ceased, and is confined to the adaxial epidermal cells (Glover *et al.*, 1998).

In addition to *MIXTA*, in *A. majus* there are three other Subgroup 9 R2R3 MYB genes described: *AmMYBML1* in the subgroup 9A *MIXTA* clade, and *AmMYBML2* and *AmMYBML3* in the subgroup 9A *MIXTA-like* clade. These genes have similar but non-redundant functions to *MIXTA*. *AmMYBML1* controls trichome formation in the corolla tube, conical epidermal cell and mesophyll cell morphogenesis in ventral petals, and hinge formation (Perez-Rodriguez *et al.*, 2005). *AmMYBML2* is responsible for cone elongation in conical cells (Baumann *et al.*, 2007) and *AmMYBML3* can induce conical cell outgrowth and is expressed in trichomes (Jaffé *et al.*, 2007). No genes in the R2R3 Subgroup 9B MYB have been identified in *A. majus* so far, however, a near-complete genome assembly of *A. majus* cultivar JI7 is currently available (Li *et al.*, 2019), which will allow the exploration of this subclade in *Antirrhinum*.

The detailed understanding of the role of subgroup 9 R2R3 MYB genes in epidermal cell differentiation in *A. majus* has provided a platform from which to expand the analysis of petal cell shape differentiation to other plants, including non-model species, through a "candidate gene approach". In this approach, the findings in a model species suggest promising genes that seem likely to be involved in the development of the trait in question (Haag & True, 2001). The

characteristics of a good candidate gene include a well-known developmental function that is clearly associated with the trait in question, a tissue specific expression pattern, and a high degree of sequence conservation (Kramer, 2007).

This investigation uses a candidate gene approach to explore the role of subgroup 9 R2R3 MYB genes in the identity of petal cell shape in non-model species of the genus of flowering plants *Nicotiana*.

1.4 The genus *Nicotiana*

The genus of flowering plants *Nicotiana* belongs to the hyperdiverse and economically important family Solanaceae (order Solanales, Asteridae I; (APG, 2009, 2016). *Nicotiana* contains about 75 species of herbs, shrubs to small trees, widely distributed in warm temperate regions of both hemispheres, mostly centred in America (mainly in Andean South America and Mexico) with several species in Australia and South Pacific Islands, and one in West Africa (Goodspeed, 1954; Vignoli-Silva & Auler Mentz, 2005; RBG-Kew, 2016b). Members of the genus are important in traditional medicine in both South America and Australia (Carrasco *et al.*, 2015; Ballester *et al.*, 2016; Moghbel *et al.*, 2017), and *N. tabacum* is one of the most widely used drug plants, reaching world production of about 6.5 million tonnes of leaves from 4.2 million hectares (FAO, 2017). Moreover, various *Nicotiana* species are cultivated as ornamental garden plants (RHS, 2019). *N. tabacum* and *N. benthamiana* have served as model species for the plant sciences for since the 1950's (Goodspeed, 1954; Clemente, 2006), and non-model *Nicotiana* species are recurrent objects of study in multiple fields of plant biology (*e.g.* Baldwin, 1998; Kaczorowski *et al.*, 2005; Ollerton *et al.*, 2012; Haverkamp *et al.*, 2019).

Nicotiana is one of the most comprehensively studied flowering plant genera with numerous studies having accumulated a large body of information concerning evolution, cytology, taxonomy and biogeography (Goodspeed, 1954; Aoki & Ito, 2000; Chase *et al.*, 2003; Clarkson *et al.*, 2004; Leitch *et al.*, 2008; Knapp, 2010; Ladiges *et al.*, 2011).Within the Solanaceae, *Nicotiana* is sister to the Australian endemic tribe Anthocercidae (including *Cyphanthera*, *Duboisia*, *Anthocercis* and *Symonanthus*), together forming the subfamily Nicotianoideae, which is sister to the large subfamily Solanoideae including *Solanum*, *Capsicum*, *Datura*, *Lycium*, *Nolana* and many other genera (Olmstead *et al.*, 1999, 2008; Garcia & Olmstead, 2003; Martins & Barkman, 2005; Särkinen *et al.*, 2013). Polyploidy is common in the genus, with approximately 40% of species being allotetraploid (Goodspeed, 1954; Leitch *et al.*, 2008; Clarkson *et al.*, 2017).

Based on cytological studies and floral morphology, combined with sequence data from plastid and nuclear genes (Goodspeed, 1954; Aoki & Ito, 2000; Chase *et al.*, 2003; Leitch *et al.*, 2008; Clarkson *et al.*, 2010), there is currently a robust phylogenetic hypothesis of relationship among the members of *Nicotiana* and the likely parentage of nearly all allotetraploid species has now been determined (Figure 1.5).

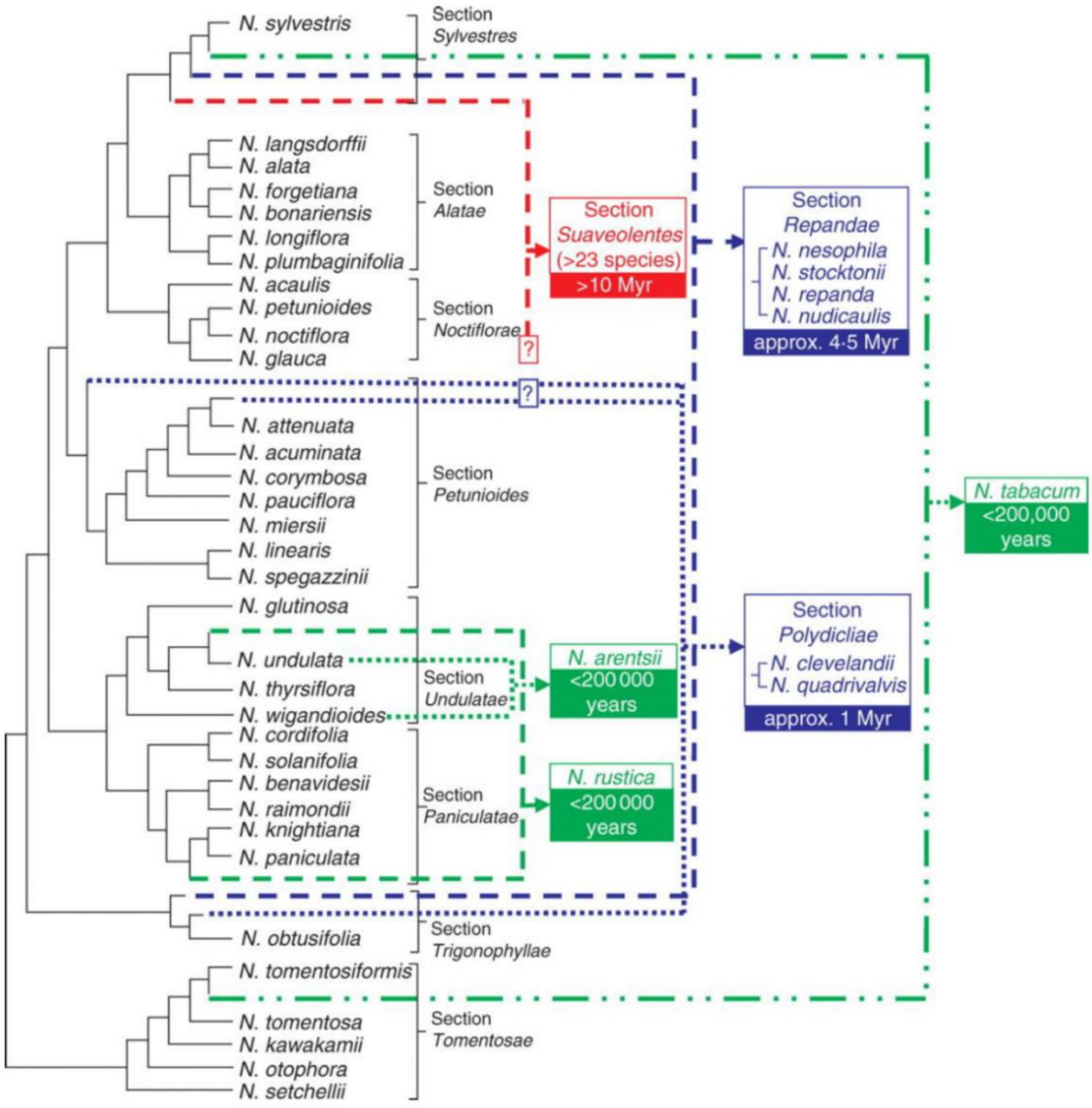

Figure 1.5. Summary of phylogenetic relationships of *Nicotiana* species with proposed origins of polyploids.
Data used in analyses include plastid and internal transcribed spacer loci. Figure modified and adapted from Knapp *et al.* (2004) using more recent phylogenetic information taken from the glutamine synthase marker (Clarkson *et al.*, 2010). Uncertainty concerning one of the parental genome donors for sections *Polydicliae* and *Suaveolentes* is indicated by question marks. Figure from Leitch *et al.*, (2008).

A general structural plan can be recognised in *Nicotiana* flowers. Flowers in the genus have four distinguishable whorls. The calyx is formed by five fused sepals and is usually shorter than the

corolla. The corolla is also pentamerous of fused petals having a tubular appearance. Three zones are distinguishable in the corolla of *Nicotiana* flowers from base to apex: tube, throat and limb (Figure 1.6). The tube is the narrow elongated basal part, the throat is the more or less swollen area distal to the tube, and the limb is the open, distal most zone, formed by the corolla lobes. The corolla lobes are usually colourful and constitute the attractive parts for pollinators. The androecium in *Nicotiana* is of five anthers fused at least partially to the inner corolla, each stamen is differentiated into filament and anther, and their length relative to the corolla varies. The ovary is bottle shaped, of two fused carpels, with long style terminating in a donut-shaped stigma.

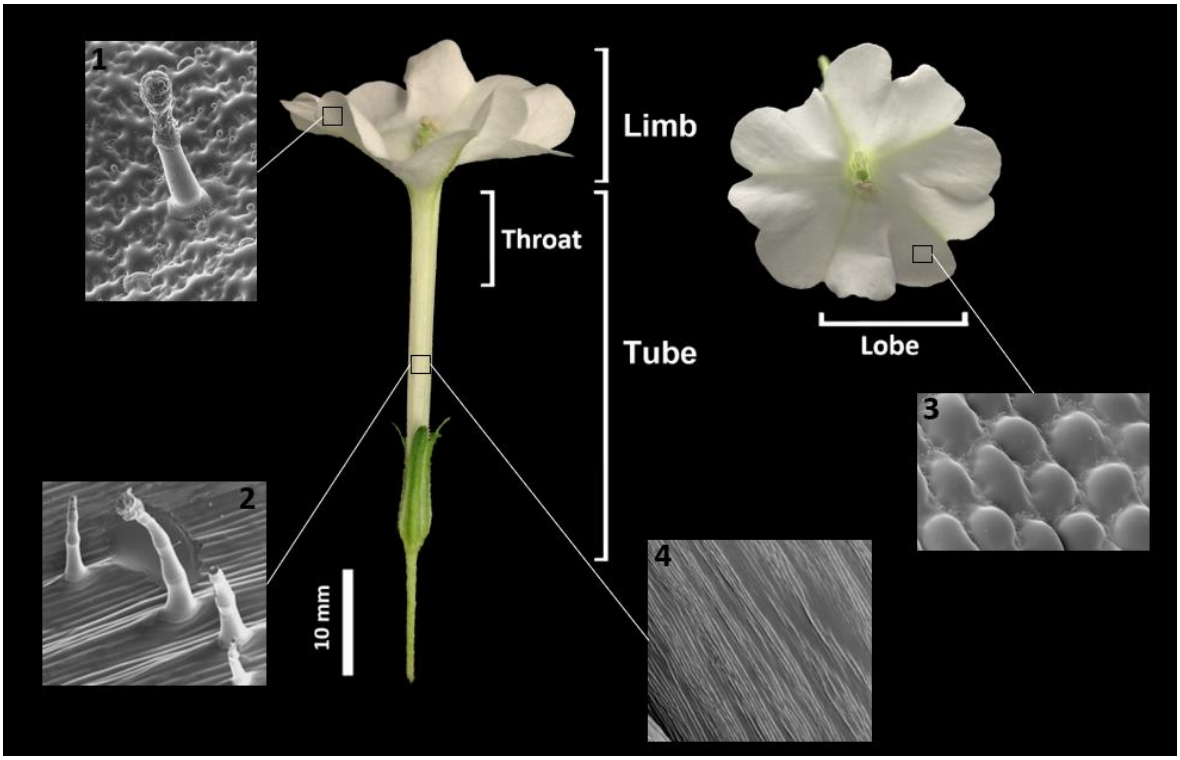

Figure 1.6. Corolla zones and petal epidermal cell morphology in different zones of *Nicotiana* petals.

A typical trumpet shape *Nicotiana* flower can be divided in limb and tube. The limb is constituted by the petal lobes and the limb by the fused bases of adjacent petals. A swollen region at the top pf the tube is referred as the troath. The epidermal cells on each area have diverse characteristics in terms of shape and epidermal features. This figure shows macro- and micromorphology of the corolla in *N. occidentalis* H.-M.Wheeler (Section *Suaveolentes*). 1: Abaxial lobe with jigsaw epidermal cells and simple trichomes; 2: Abaxial tube with parallel striations and simple trichomes; 3: Adaxial lobe with non-conical (dome shaped) cells; 4: Adaxial tube with fine irregular striations.

Despite a relatively fixed floral structure, *Nicotiana* species are very diverse in floral attributes that are potentially associated with a wide diversity of pollination systems present in the genus. *Nicotiana* flower symmetry, for instance, varies from almost actinomorphic to strongly zygomorphic, and corolla lobes range from narrow and well differentiated from each other, to

broad in which only the tip of each petal can be distinguishable individually (Marks *et al.*, 2011). *Nicotiana* flowers differ visually in size (ranging from 1-9 cm in length) and colour (including yellow to green, white, pink, purple or red)(Goodspeed, 1954; Knapp *et al.*, 2004). Species also differ in insect perceived colour (McCarthy *et al.*, 2015), scent and nectar characteristics (Kaczorowski *et al.*, 2005; Kessler & Baldwin, 2007; Kessler *et al.*, 2008).

The diversity of floral traits potentially important in the interaction between flowers and pollinators, and the well established phylogenetic hypotheses of relationships among *Nicotiana* species, makes this genus of flowering plants an exceptional model to explore how individual floral traits have evolved in the group and how these patterns may be directing diversification.

1.4.1 Petal epidermal cell morphology of *Nicotiana*

In angiosperms, epidermal cells are not homogeneous along all the surfaces of the petal (Figure 1.6). The adaxial epidermis of the petal lobe is the part of the flower that is exposed to pollinators, and so is most likely to be under the influence of pollinator-mediated selection. The morphology of the mature adaxial petal surface has been studied for a majority of the species of *Nicotiana* (Taylor, 2015; this work, Appendix 2). Character mapping of conical and non-conical petal epidermal cells on the phylogeny of the diploid species of *Nicotiana* demonstrates shifts in petal epidermal cell form observed between sister species and provides bases for the interpretation of character evolution of epidermal cells in the genus (Figure 1.7). The main shifts in petal cell shape observed in the *Nicotiana* phylogeny of diploid clades are the independent losses of conical cells in Section *Alatae* and in Section *Paniculatae*.

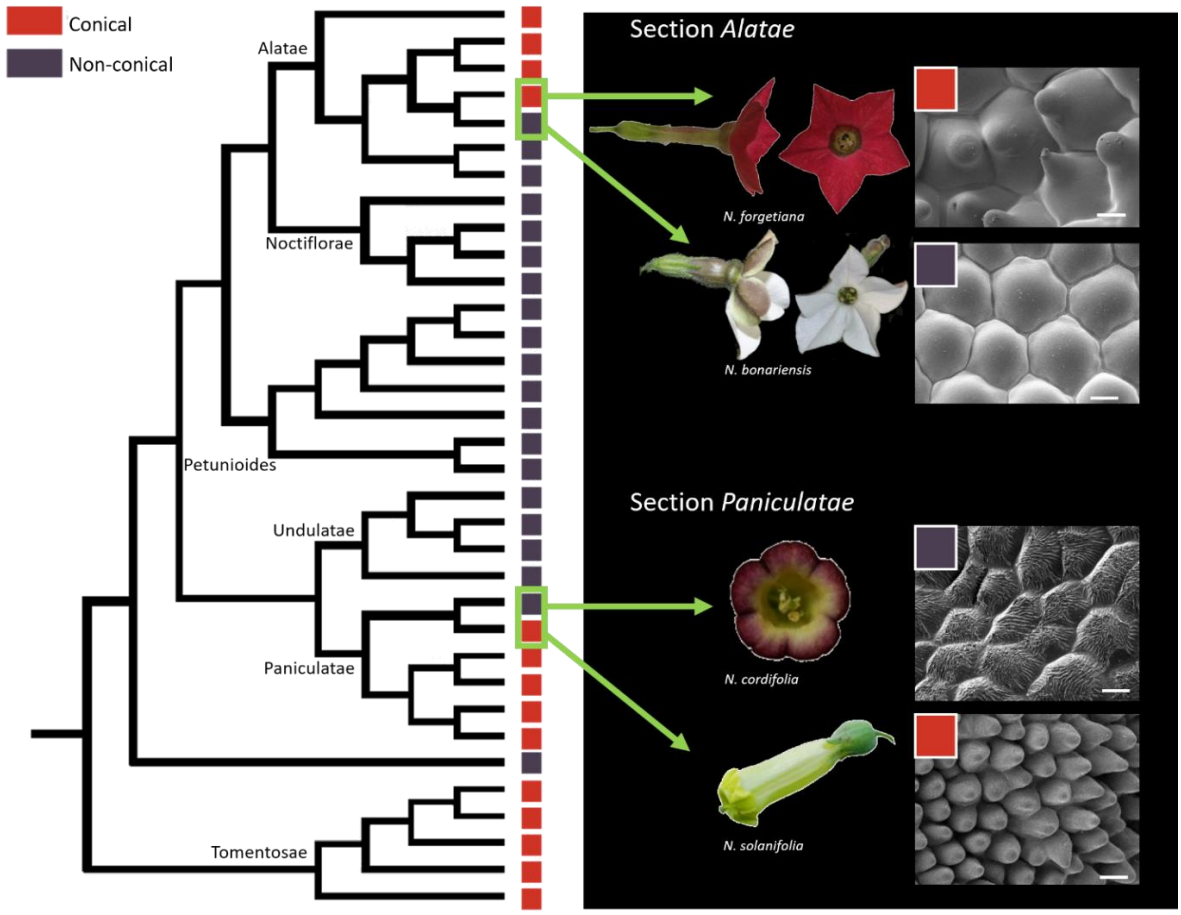

Figure 1.7. Character mapping of conical and non-conical petal epidermal cells on the phylogeny of the diploid species of the genus *Nicotiana*.
Sister species *N. forgetiana* and *N. bonariensis* (Section *Alatae*) and *N. cordifolia* and *N. solanifolia* (Section *Paniculatae*) present contrasting cell shape (scanning electron microscopy-SEM images). This scenario of sister species with contrasting characteristics provides a unique opportunity to explore the evolution of petal cell shape in *Nicotiana.* Species represented in the tree from top to bottom: *N. sylvestris, N. langsdorfii, N. alata, N. forgetiana, N. bonariensis, N. longiflora, N. plumbaginifolia* (Section Alatae), *N. acaulis, N. petunioides, N. noctiflora, N. glauca* (Section *Noctiflorae*), *N. attenuata, N. acuminata, N. corymbosa, N. pauciflora, N. miersi, N. linearis, N. spegazzinii* (Section *Petunioides*), *N. glutinosa, N. undulata, N. thyrsiflora, N. wigandioides* (Section *Undulatae*), *N. cordifolia, N. solanifolia, N. benavidesii, N. raimondii, N. knightiana, N. paniculate* (Section *Paniculatae*), *N. obtusifolia* (Section *Trygonophyllae*), *N. tomentosiformis, N. tomentosa, N. kawakamii, N. otophora, N. setchelii* (Section *Tomentosae*). Modified from Taylor (2015). Scale bars for SEM images = 10 µm.

Sister species *N. forgetiana* Hemsl. and *N. bonariensis* Lehm. in Section *Alatae* (Figure 1.7) are native to South East Brazil, northern Argentina, and Uruguay. *N. forgetiana* has purple-red to white flowers that seem to be mostly pollinated by hummingbirds (Ippolito *et al.*, 2004). *N. bonariensis* has white petals and is thought to be pollinated by perching moths (Ippolito, 2000; Kaczorowski *et al.*, 2005). In Section *Paniculatae* (Figure 1.7) *N. cordifolia* Phil. is endemic to the Juan Fernandez Islands off the Pacific coast of Chile, it has dark red to yellow flowers and it is known to be visited by hummingbirds and other birds for pollination (Anderson *et al.*, 2001). *N. solanifolia* Walp. occurs in the northern part of continental Chile, has a green corolla and is

thought to be pollinated by birds (Goodspeed, 1954; Ballester *et al.*, 2016). Petal epidermal cells in *N. forgetiana* (Section *Alatae*) and *N. solanifolia* (Section *Paniculate*) have been characterized as typical conical cells, whereas those of *N. bonariensis* (Section *Alatae*) and *N. cordifolia* (Section *Paniculatae*) have been classed as non-conical (Taylor, 2015)(Figure 1.7). This scenario of sister pairs of species with contrasting character states provides an exceptional opportunity to investigate the molecular changes that have given rise to differences in petal epidermal cell morphology, and how these mechanisms differ or converge between distantly related clades of *Nicotiana*.

1.4.2 R2R3 MYB Subgroup 9 transcription factors in *Nicotiana*

In addition to the phylogenetic hypothesis proposed by Brockington *et al.*, (2013), Taylor (2015) performed phylogenetic analysis based on publicly available sequences of the R2R3 MYB subgroup 9 clade within the Solanales. This was done both to predict how many subgroup 9 genes to expect in *Nicotiana* (by estimating the number of gene duplications for each subclade) and also to inform primer design by using consensus sequences from other closely-related genes (Taylor, 2015). The results indicated that genes belonging to three of the four main subclades of the gene family are present in *Nicotiana*: Subgroup 9A *MIXTA* (two genes) and *MIXTA-like* (one gene), and subgroup 9B *MYBI7* (two genes). None of the Solanales sequences segregated alongside previously-described *MYBI7-like* genes in the preliminary tree, suggesting that this subfamily is absent from this order of plants (Taylor, 2015).

The phylogenetic analysis was able to partially resolve the pattern of subgroup 9 gene evolution within the Solanales. It showed clear evidence of a duplication within the *MYBI7* clade that occurred within the Solanaceae family, as there were *MYBI7* homologues from *N. tabacum, Lycium barabum, Atropa belladonna* and *Solanum lycopersicum* segregated into two separate clades (*MYBI7-1* and *MYBI7-2*) (Taylor, 2015).

Conversely, there did not appear to have been a gene duplication within the *MIXTA-like* subclade: the genes from the represented species fell out into a topology that tracked the species phylogeny very well, as was expected if there was only one *MIXTA-like* gene copy in the order (Taylor, 2015).

In contrast to the *MYBI7* and *MIXTA-like* trees, Taylor's *MIXTA* gene tree was too poorly-populated to resolve the relationships between the two *N. tabacum MIXTA* genes detected. One

of the genes (*MIXTA-1*) appeared to be a clear orthologue of genes in other Solanales species, as it fell out into a clade with other genes from *Solanum* species. However, the other gene (*MIXTA-2)* was on a branch on its own that appeared to be basal to the *MIXTA-2* genes. Taylor proposed three possible explanations to this topology, it could be because the duplication event would have occurred within or prior the evolution of the Solanales, but its not represented in other Solanales because of poor sequencing coverage in these species, or because it was subsequently lost from other lineages. Alternatively, the genes may had been the result of a duplication event within *Nicotiana*, hence why there were no other Solanales copies of *MIXTA-2*. Lastly, *NtMIXTA-1* and *NtMIXTA-2* could be homeologues of the same gene inherited from the parents of *N. tabacum*. *N. tabacum* is a tetraploid derived from hybridization between the diploid species *N. sylvestris* (Section *Sylvestres*) and *N. tomentosiformis* (Section *Tomentosae*) (Figure 1.5). However, given the tree topology, the last two scenarios seem unlikely, as if the two *MIXTA* copies were paralogues or homeologues they would be expected to fall out as sister to each other.

Draft genomes and transcriptomes for both the polyploid and the parental species became available later during Taylor's investigation. Via nucleotide BLAST of the genomes, Taylor found copies of both *MIXTA* genes (*MIXTA-1* and *MIXTA*-2) in *N. tomentosiformis,* but only one, *MIXTA-2,* in *N. sylvestris*. This pattern was confirmed in the current investigation (Appendices). BLAST search of the *N. tabacum MIXTA-1* and *MIXTA-2* genes in the sequenced genomes of several *Solanum* species showed that individual *MIXTA* genes from these species contain motifs that are specific to both *Nicotiana* genes (Taylor, 2015). This suggested that *MIXTA*-1 and *MIXTA*-2 genes might be the result of a lineage specific duplication before the split between the Solanoideae (containing *Solanum*) and the *Nicotinoideae* (including *Nicotiana*) clades (Solanales phylogeny from Stevens, 2001), and that the *MIXTA-1* gene had been lost in *N. sylvestris.* After Taylor's investigation, the genome of the diploid species *N. attenuata* (Section *Petunioides*) became available. BLAST search of the *NaMIXTA*-1 and *NaMIXTA*-2 nucleotide sequences showed that this species has a single gene nested with the *N. tabacum* and *N. tomentosiformis MIXTA*-1 genes and another one nested with the *MIXTA*-2 genes.

Additional putative sequences of R2R3 Subgroup 9 MYBs retrieved from the *Solanum lycopersicum* genome and from other *Nicotiana* species for which whole genome sequences became available after the start of this project were included in an updated phylogenetic analysis (Appendix 3). The updated results confirm the general phylogenetic pattern indicated by Taylor (2015) for *MYBl7* (two genes), *MYBl7-like* (no genes) and *MIXTA-like* (one gene), and provide evidence suggesting that the duplication of the MIXTA clade (two genes) occurred before the split of the Solanoideae and the Nicotinoideae. This allows to predict the number of R2R3 MYB

Subgroup 9 in the diploid species of *Nicotiana* to be two in the MIXTA clade, one in the MIXTA-like clade, two in the MYB17 clade and no representatives of the MYB17-like clade. This work focused on four candidate genes in the species of interest: one in the MIXTA clade (*MIXTA-2*), one in the MIXTA-like clade (*MIXTA-like*) and two in the MYB17 clade (*MYB17-1* and *MYB17-2*).

1.5 Aims of this project

This project aims to further understand character evolution of petal cell shape in species of the genus *Nicotiana* (Solanaceae) and its implications in pollination systems, combining tools of molecular biology, morphology and pollinator behaviour experiments.

- In chapters two and three, I explore in parallel the molecular mechanisms involved in petal cell shape in two distantly related clades of *Nicotiana*. Sister species *N. cordifolia* and *N. solanifolia* (Section *Paniculatae*, Chapter 2) and *N. bonariensis* and *N. forgetiana* (Section Alatae, Chapter 3) have contrasting petal cell shape (conical vs. non-conical). This system provides an exceptional opportunity to explore independent evolutionary pathways leading to the same phenotype. First, I fully characterize the coding sequences of four subgroup 9 R2R3 MYB candidate genes potentially responsible for the molecular control of petal cell shape from each species. Second, I test whether any sequence differences detected between the orthologues of sister species have implications in the protein function by using heterologous expression of the genes in model species *N. tabacum*. Third, I asses any differences in gene expression of the candidate genes in the petals of sister species *N. forgetiana* and *N. bonariensis*. The combined result provides an understanding of the prevailing molecular mechanism involved in petal cell identity in these species, and gives clues to differentiate between convergent and parallel evolution in the transition from conical to non-conical petal cell shape.

- In Chapter 4, I present an *Agrobacterium tumefaciens* mediated transformation protocol for the non-model species *Nicotiana forgetiana,* a methodological advance crucial for further exploration of the molecular mechanisms and functional implications of petal cell shape in *Nicotiana.*

- In Chapter 5, I explore how petal colour and petal cell shape interact in the perception of flowers by model pollinator *Bombus terrestris*. Using biomimetic artificial flowers reproducing the colouration and texture of *N. bonariensis* (white, non-conical) and *N. forgetiana*

(red, conical), I test whether bumblebees can discriminate between floral textures on pigment backgrounds usually described as “invisible” for bees.

The integrated approach used in this thesis allows an investigation of the evolution and development of a floral trait, petal cell shape, and its potential implications in the interaction between flowers and their animal pollinators. Because flowers are linked to reproductive isolation and thus to speciation, by inspecting the mechanisms behind the variation of a single floral trait in a specific group of plants, the genus *Nicotiana,* this investigation contributes to the overarching question of the mechanisms of diversification and radiation of flowering plants.

Chapter 2

Evolution and molecular control of petal cell shape in Nicotiana *Section* Paniculatae

2 Evolution and molecular control of petal cell shape in *Nicotiana* Section *Paniculatae*

2.1 SUMMARY

Sister species *Nicotiana cordifolia* and *N. solanifolia*, Section *Paniculatae*, present contrasting petal epidermal cell shape: *N. cordifolia* has non-conical cells whereas *N. solanifolia* has conical cells. This chapter focuses on assessing the role of candidate genes from the R2R3 MYB Subgroup 9 transcription factors in petal cell shape identity of these sister species. Entire coding sequences of the four candidate genes: *MIXTA-2* and *MIXTA-like* (Subgroup 9A) and *MYBl7-1* and *MYBl7-2* (Subgroup 9B) were obtained for both species. *MIXTA-2*, *MYBl7-1* and MYBl7-2 sequences were found to be conserved when comparing the two species. However, six amino acid differences were detected between the predicted sequences of MIXTA-like when comparing *N. cordifolia* to *N. solanifolia. In silico* comparisons of these sequences allowed an approximation of the potential effect of the differences detected on the function of the putative coded protein. To confirm the functional effect of these differences, the two orthologues of *MIXTA-like*, one from *N. cordifolia* (*NcMIXTA-like*) and one from *N. solanifolia* (*NsMIXTA-like*), were ectopically expressed in *Nicotiana tabacum* using *Agrobacterium tumefaciens* mediated stable transformation. Both sets of *N. tabacum* transgenic lines, expressing *NcMIXTA-like* or *NsMIXTA-like*, presented incipient conical cells on the surface of the carpel, a phenotype not present in the wild type of *N. tabacum*. This confirmed that the two orthologues of *MIXTA-like* are positive regulators of epidermal outgrowths. These results thus suggest that the sequence differences detected in *MIXTA-like* between the species are not responsible for the different petal epidermal cell shape phenotypes. Gene expression analyses would be necessary to assess the role of *MIXTA-like* and the other R2R3 Subgroup 9 MYB candidate genes in petal cell identity of *N. cordifolia* and *N. solanifolia*. The role of petal cell shape in *Nicotiana* Section *Paniculatae*, specifically in *N. cordifolia* and *N. solanifolia,* is discussed.

2.2 INTRODUCTION

Petal cell shape has been characterized extensively across species of the genus *Nicotiana* (Taylor, 2015; this work). Character mapping of petal cell shape on the well-established phylogenetic tree of *Nicotiana* (Clarkson *et al.*, 2004) has provided a working hypothesis of the evolution of the petal cell shape character in the genus (Taylor, 2015; Figure 1.5). This chapter focuses on the evolution of petal cell shape in Section *Paniculatae*, specifically in the sister pair of species *N.*

cordifolia Phil. (non-conical cells) and *N. solanifolia* Walp. (conical cells). This scenario of a sister pair of species with contrasting states of character (conical vs. non-conical) provides an exceptional opportunity to investigate the molecular changes that have given rise to differences in petal epidermal cell morphology. Moreover, it provides a system to compare to the mechanisms found to potentially be involved in controlling petal cell shape in sister species *N. forgetiana* (conical) and N. *bonariensis* (non-conical) in Section *Alatae* (Chapter 3), and how these mechanisms differ or converge between distantly related clades of *Nicotiana*.

2.2.1 Natural history and pollination of *Nicotiana* Section *Paniculatae*

Nicotiana section *Paniculatae* Goodsp. is one of 13 taxonomic sections within the genus. It is constituted by seven diploid species (chromosome number: n = 12) from Western South America (Table 2.1; Goodspeed, 1954; Knapp *et al.*, 2004; Clarkson *et al.*, 2004, 2010). Species of *N.* section *Paniculatae* are stout herbs or small trees, with long-petiolate leaves, cordate to truncate at the base, and usually with short white pubescence. All the species have long tubular, yellow or greenish yellow flowers with straight corolla tube and small rounded lobes (Goodspeed, 1954; Knapp *et al.*, 2004; Clarkson *et al.*, 2004).

The monophyly of the section is well supported in phylogenetic analyses based on molecular markers and combined data sets (Chase *et al.*, 2003; Knapp *et al.*, 2004; Clarkson *et al.*, 2004). Three sister pairs of geographically close species are also well supported in the phylogenies: *N. paniculata* and *N. knightiana*, *N. benavidesii* and *N. raimondii*, and *N. solanifolia* and *N. cordifolia*. However, the relationships among these three clades is unclear, with phylogenetic analyses based on different markers giving alternative hypotheses of relationship. Analyses of *ADH (Alcohol Dehydrogenase*, Kelly *et al.*, 2010) and *ITS* (*Internal Transcriber Spacing*; Chase *et al.*, 2003) markers place *N. benavidesii* and *N. raimondii* as the basal most clade. On the other hand, plastid (Clarkson *et al.*, 2004) and *Glutamine Synthase* (*GS*; Clarkson *et al.*, 2010) markers put *N. cordifolia* and *N. solanifolia* as the earliest diverging clade of the section. Morphologically, these species pairs are difficult to distinguish from each other both vegetatively and florally, but they are not found sympatrically (Clarkson *et al.*, 2004).

Although field studies of natural pollination of these species are scarce, pollination in the section is thought to be mostly by birds (Goodspeed, 1954; Anderson *et al.*, 2001; Ollerton *et al.*, 2012; Tiedge & Lohaus, 2017).

Table 2.1. Species of *Nicotiana* Section *Paniculatae*: Geographic distribution and some distinctive characteristics.

Species Name	Geographic Distribution	Petal Cell Shape	Flower Colour	Putative Pollinators	Reference
Nicotiana cordifolia Phil.	Chile, Masafuera	Non-conical	Yellow	Birds	Anderson et al., 2001
Nicotiana solanifolia Walp.	N Chile (coast)	Conical	Green	Hummingbirds	Ballester et al., 2016
Nicotiana benavidesii Goodsp.	Peru	Conical	Greenish yellow	Birds	Goodspeed, 1954
Nicotiana raimondii J.F.Macbr.	Peru Urubamba valley	Conical	Greenish yellow	Birds	Goodspeed, 1954
Nicotiana knightiana Goodsp.	S Peru (coast)	Conical	Yellow	Hummingbirds	Tiedge and Lohaus, 2017
Nicotiana paniculata L.	W Peru	Conical	White	Birds, potentially nocturnal moths	Ollerton et al., 2009
Nicotiana cutleri D'Arcy	S Bolivia	Not identified	White?	Birds	D'Arcy, 1976

2.2.2 Evolution of petal cell shape in *Nicotiana* Section *Paniculatae*

Petal cell shape in *Nicotiana* section *Paniculatae* has been characterized for six of the seven species (Taylor, 2015; Figure 2.1) and is predominantly conical except for *N. cordifolia,* which has non-conical petal cells (Figure 1.1). Taylor (2015) mapped petal epidermal cell shape onto the phylogeny of the diploid species of *Nicotiana* (Figure 1.7). This allowed the application of ancestral state reconstruction methods to infer the sequence of transitions that have taken place at ancestral nodes (Taylor, 2015). Ancestral state reconstruction using Parsimony and Maximum Likelihood methods independently, resulted in an ambiguous ancestral state of petal cell shape for the genus. For *Paniculatae*, both methods agreed that the ancestral state for the section is ambiguous. Within *Paniculatae* Maximum Likelihood predicted only losses of conical cells, whereas parsimony suggested possible gains depending on the ancestral states (Taylor, 2015). All species of the sister clade Section *Undulatae* have non-conical cells.

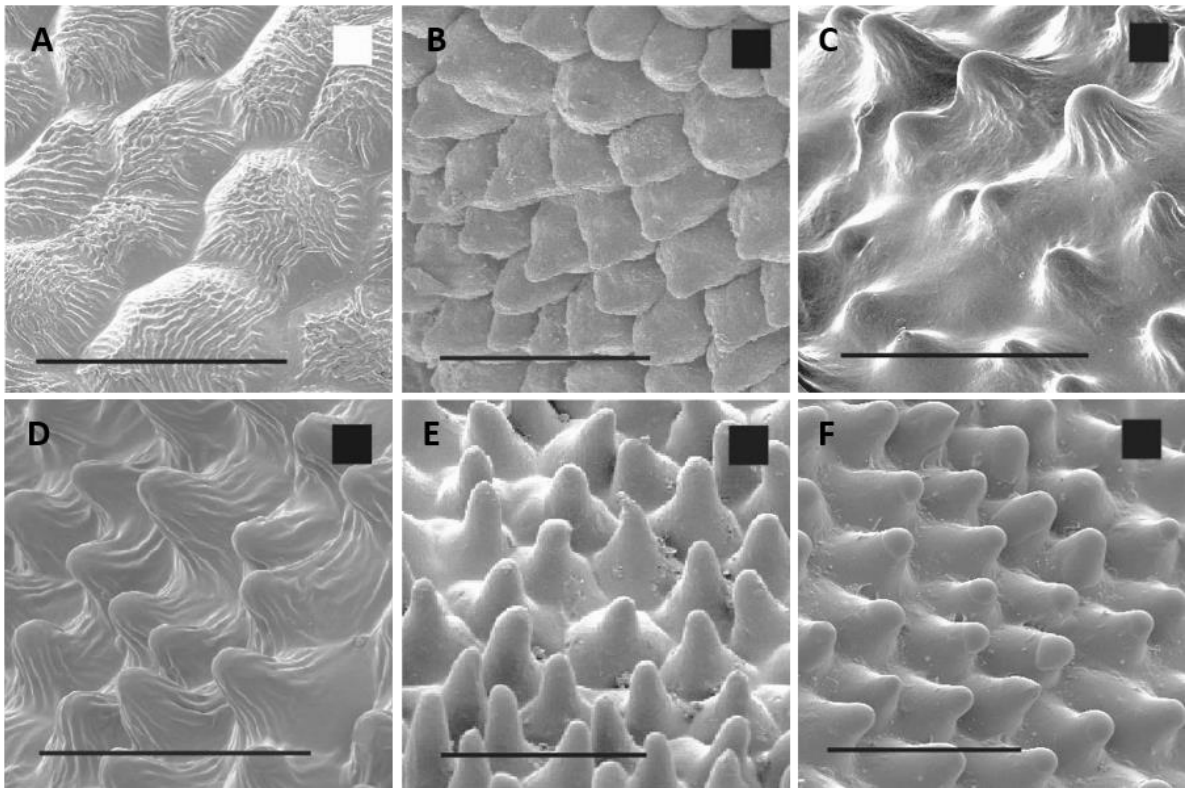

Figure 2.1. Diversity of petal cell shape in *Nicotiana* Section *Paniculatae*
Petal cell shape in *Nicotiana* Section *Paniculatae* ranges from non-conical striated to conical-papillate. A-F. SEM microphotographs of the adaxial surface of the petal of *N. cordifolia* (A); *N. solanifolia* (B); *N. benavidesii* (C); *N. raimondii* (D); *N. knightiana* (E); *N. paniculate* (F). Black and white squares represent conical and non-conical cell shape respectively. Scale bars: 50 µm. Modified from Taylor (2015).

2.2.3 Sister species *N. cordifolia* and *N. solanifolia*

N. cordifolia and *N. solanifolia* are both endemic species of Chile (Figure 2.2). *N. solanifolia* (the conical celled species, Figure 2.3) occurs in the coast of the Atacama Desert in the north of Chile, from the littoral plains to 1000 meters of altitude (Goodspeed, 1954; Ballester *et al.*, 2016). It is commonly found in low elevation zones along interior valleys (Goodspeed, 1954; Dillon, 2005). *N. solanifolia* plants are stocky slow growing shrubs, 0.5-3 m tall, with long petiolate truncate leaves. The surface of the leaf is puberulent with densely packed simple trichomes, composed of from four to many cells in which the basal-most cell of the stalk is modified (round in shape and larger in size, Goodspeed, 1954) (Figure 2.4A-D). Glandular trichomes, with heads consisting of a single cell and long stalked, are also present in this species (Figure 2.4B). The flowers *of N. solanifolia* occur in panicular inflorescences. The corolla is light greenish yellow, 35-50 mm long. Pollination is thought to be by birds, although there are not many field studies on this species, Ballester et al. (2016) have reported sightings of flowering plants, up to 2 m tall, attracting numerous insects and some birds, such as the northern hummingbird (*Rhodopis vesper vesper*)

and the giant hummingbird (*Patagona gigas gigas,* Figure 2.3). *N. solanifolia* has high tolerance for dry and hot conditions with high radiation, however, it has low resistance to frost (Ballester *et al.*, 2016). The common name of these plants in Chile is "tabaco cimarrón" (black tobacco), which may refer to the long history of consumption by humans in the Atacama region, revealed by archeological artifacts and phytoliths dating back to 1500 BC (Carrasco *et al.*, 2015; Ballester *et al.*, 2016).

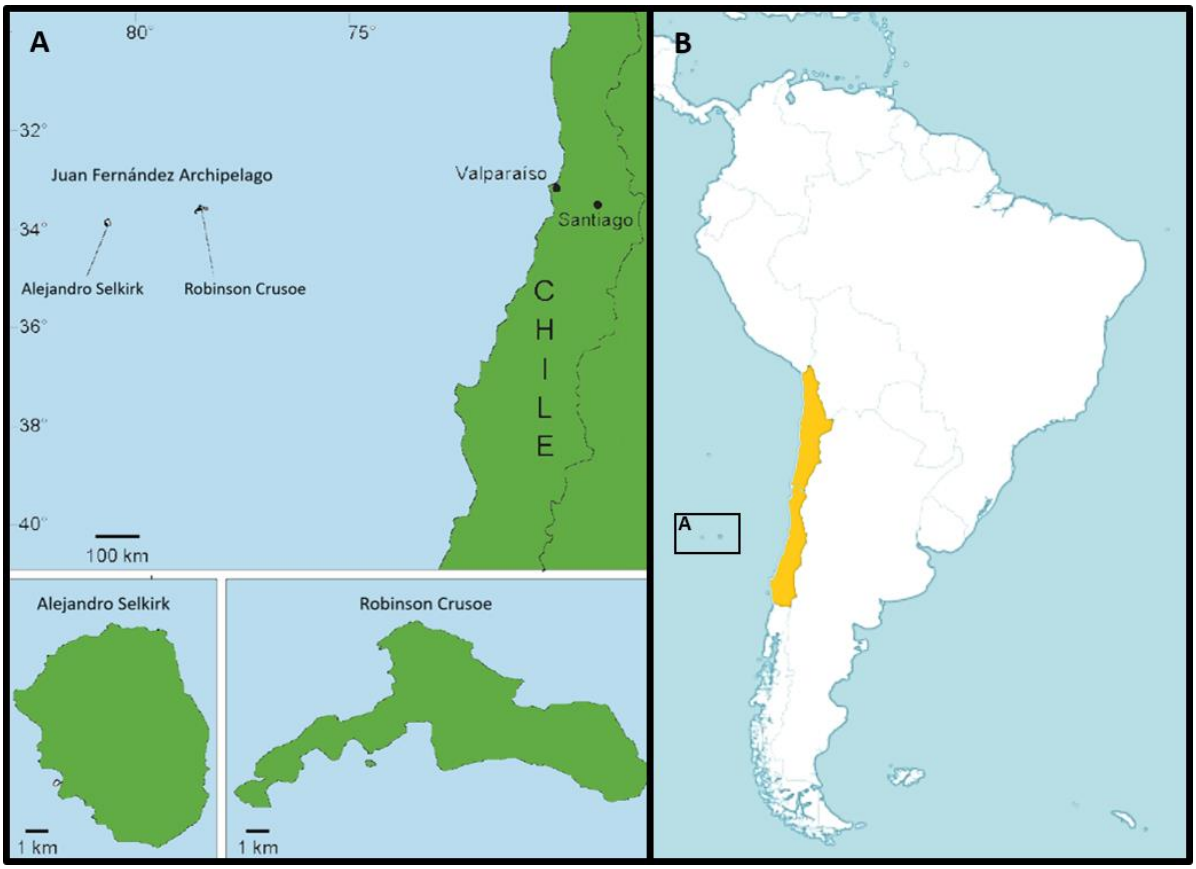

Figure 2.2. Geographic distribution of *N. cordifolia* and *N. solanifolia* (Section *Paniculatae*).
A. Location of the Juan Fernández Archipelago in the Southeastern Pacific Ocean where *N. cordifolia* occurs. Modified from Takayama *et al.* (2018). B. Distribution of *N. solanifolia* in the Atacama Region, north of Chile (yellow area). Inset square (A) in B, shows the location of the Juan Fernandez Archipelago. Map retrieved from RBG-Kew (2016b).

Figure 2.3. *Nicotiana solanifolia* grows in the Atacama Desert of Chile and its putative pollinators are humingbirds.

This species is endemic to the Atacama Desert in the north of Chile. Flowering occurs October-January. A-B. General habit. C. Inflorescence branch. D-E. Flowers in different developmental stages. F-G. Putative pollinators in the wild: northern hummingbird *(Rhodopis vesper vesper*, F) and giant hummingbird (*Patagona gigas gigas,* G). Photo credits: A-E: Gardner et al., 2019; F-G: Ballester et al., 2016.

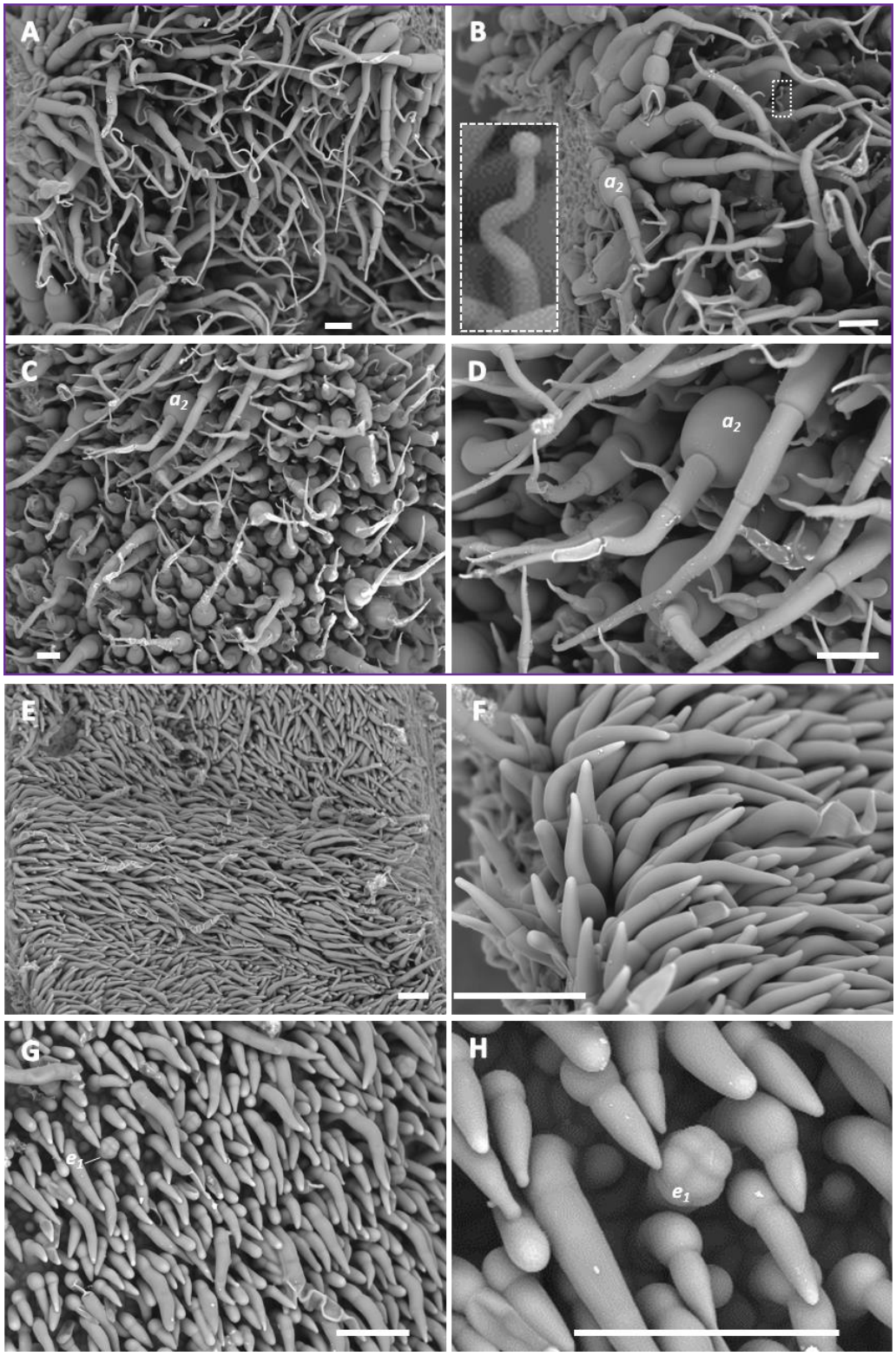

Figure 2.4. Diversity of epidermal features on leaves of *Nicotiana solanifolia* and *Nicotiana cordifolia* (Section *Paniculatae*).

A-D. Lamina of *N. solanifolia*, A-B. Abaxial surface, C-D Adaxial surface. Simple trichomes (a_2) are the most common outgrowth. Glandular trichomes (dashed box in B) are also present. E-G. Lamina of *N. cordifolia.* E-F. Abaxial surface; G. Adaxial surface. Indumenta in *N. cordifolia* is mostly of densely packed simple trichomes. Hydathodes (e_1 in G and H) are also present but not glandular hairs. Cryo-SEM images. Scale bars=100µm.

Nicotiana cordifolia, with non-conical petal cells, is endemic on Masafuera, Juan Fernandez Islands off the northern coast of Chile (Figure 2.2). *N. cordifolia* plants (Figure 2.5) are soft-woody shrubs 1 to 2 m high, inhabiting precipitous rocky walls of marginal quebradas and coastal cliffs (Goodspeed, 1954). The leaves are cordate with long petioles and fine puberulent whitish indumenta on both surfaces (Goodspeed, 1954)(Figure 2.4E-H). Indumenta is mostly of densely packed simple trichomes, composed of from one to three cells. Hydathodes, consisting of single, short, wide stalk cells topped by two to four tiers of cells, each tier consisting of four to eight cells, are also present in this species (Figure 2.4G, H). *N. cordifolia* is distinct from all other species of the genus in the complete absence of glandular trichomes (Goodspeed, 1954). Flowers occur in lax panicles. The corolla is 21-28 mm long with or without purple overlying cream colour. Plants growing on Santa Clara Island are reported to have pale yellow flowers (Danton, 2006). Flowering occurs November to January. Although field studies are lacking for this species, *N. cordifolia* is known to be visited by hummingbirds and other birds for pollination (Anderson *et al.*, 2001). Moreover, local wardens have reported visits by flies and other Diptera (Saez Quintana, pers. comm.). *N. cordifolia* has been reported as critically endangered by the national authorities of Chile (CONAF, 2019). Habitat degradation by large herbivores (goats and rabbits) is the main menace for the species, with wild populations estimated to be as low as 250 mature individuals (CONAF, 2019). Conservation programs are being developed in the islands, including greenhouse propagation of the species (Saez Quintana, pers. comm.). One of the putative pollinators of *N. cordifolia,* the endemic hummingbird *Sephanoides fernandensis,* is considered now extinct, although inaccessible parts of this island may still be a refuge for some individuals (Anderson *et al.*, 2001). Another hummingbird putative pollinator, *S. sephaniodes,* is also considered as important for the reproduction of *N. cordifolia* (Anderson *et al.*, 2001).

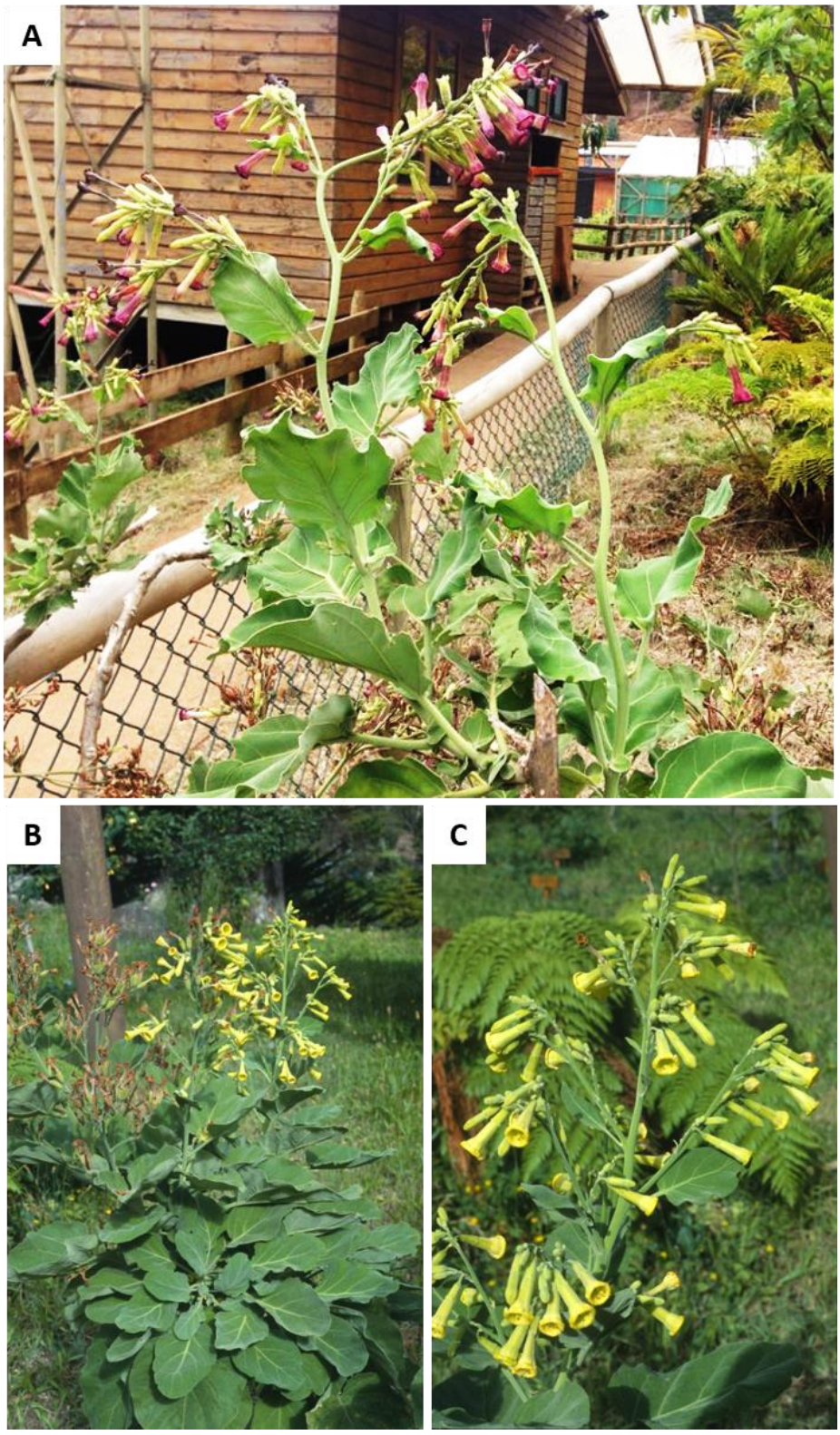

Figure 2.5. *Nicotiana cordifolia* is endemic to the Juan Fernandez Islands (Chile), is visited by hummingbirds and is categorized as endangered for conservation.
A. General habit of plants growing at the conservation plots in CONAF-Robinson Crusoe Island. B-C. Plants from Santa Clara Island growing at San Juan Bautista Botanic Gardens, Valparaiso, Chile. Flowers of *N. cordifolia* are more commonly red-purple (A), but plants from Santa Clara (B-C) usually have yellow flowers (Danton, 2006). Photo credits: A: Constanza Valdivieso, B-C: Gardner et al., 2019.

The divergence of *N. solanifolia* and *N. cordifolia* is estimated to have occurred sometime after the islands' formation, <2.4 million years ago (Goodspeed, 1954). The series of morphological differences between *N. solanifolia* and *N. cordifolia,* including flower colour and epidermal cell morphology (petal cell shape and vegetative organ trichomes), suggests that a suite of developmental changes have occurred in *N. cordifolia*, possibly as a result of co-regulation of different molecular pathways. Petal epidermal shape, flower colour and trichome development have all been linked to the actions of MYB transcription factors, including MYB subgroup 9 genes (Brockington et al., 2013).

2.3 MATERIALS AND METHODS

2.3.1 Isolation of R2R3 MYB Subgroup 9 genes from *Nicotiana* spp.

2.3.1.1 Plant Material

Sources of seed and plant material for petal epidermal cell characterization and nucleic acid extraction for molecular work are detailed in Appendix 4. Plants were grown under glasshouse conditions at 18-25°C in Levington's (UK) compost. During the growth period, plants received supplemental lighting from Osram 400 W high-pressure sodium lamps (Osram, München, Germany), or LED lights, on a 16 h : 8 h, light : dark photoperiod. Wild type plants were grown at the Department of Plant Sciences or at the Plant Growth Facility (PGF) of the University of Cambridge, Cambridge, UK. Conditions in the growing chambers were set to 20°C, 60% humidity, 12 h light/ 8 h darkness. All transgenic plants were grown at the PGF.

2.3.1.2 DNA and RNA Extraction and cDNA Synthesis

Plant tissue was collected in 15 ml Falcon, or 1.5 ml or 2.5 ml Eppendorf tubes, and immediately immersed in liquid nitrogen. The tissue was either used immediately or kept at -80°C until use. Grinding of the tissue was done either in a liquid nitrogen-cooled sterile mortar and pestle, or in a TissueLyser II, QIAGEN. Tissue to be ground in the tissue lyser was moved to 2.5 ml safe-lock Eppendorf tubes including a 5 mm diameter glass bead. The tissue was ground at 300 rpm for 30 seconds. All tissue manipulation was carried out using sterile or autoclaved instruments cooled down with liquid nitrogen.

Extraction of nucleic acids (RNA and/or gDNA) was done using cetylmethylammonium bromide (CTAB; Gambino *et al.*, 2008, Appendix 5), or self-made guanidinium-acid-phenol reagents (similar to commercial TRIzol or TRI; Chomczynski & Sacchi, 1987, 2006, Appendix 5). Quick

genomic DNA extraction buffer (Appendix 5) was used for initial genotyping of transgenic lines (see section 2.3.3.7).

Complementary DNA (cDNA) was synthesized with BioScript retrotranscriptase from RNA using B26 or Generacer oligonucleotides, after DNAase treatment and phenol-chloroform clean up. Yield and impurities of RNA and DNA were assessed using a Nanodrop spectrophotometer (Thermo Scientific) and gel electrophoresis (section 2.3.1.5).

2.3.1.3 Primer Design

Primers were designed in Geneious R9 from alignments of known sequences of R2R3 Subgroup 9 MYB genes of various *Nicotiana* species. Alignments included partial sequences of several *Nicotiana* species including *N. forgetiana*, *N. longiflora* and *N. langsdorfii* (Section *Alatae*), and *N. solanifolia* and *N. cordifolia* (Section *Paniculatae*) from Taylor (2015). Sequences of *Nicotiana* species retrieved from publicly available gene databases were also included. Primers were designed with the aid of the online OligoAnalyzer 3.1 tool from Integrated DNA Technologies. Primers were optimized for melting temperature, GC content, hairpin formation and dimerization as recommended in Dieffenbach et al. (1993), using OligoCalc online calculator (Kibbe 2007). Primers were used to amplify independently different regions of the putative coding sequences of the genes of interest. Primer combinations used to amplify the 5' end, 3' end and intermediate region of *MIXTA-2*, *MIXTA-like*, MYBl7-1 and MYBl7-2 are listed in Appendix 6a. Primer combinations used to amplify the entire putative coding sequence of the genes are listed in Appendix 6b.

2.3.1.4 Polymerase Chain Reaction (RT-PCR) Amplification

RT-PCR was used to amplify R2R3 Subgroup 9 MYB genes from the *Nicotiana* species of interest. One of three polymerase enzymes was used for RT-PCR reactions: EcoTaq was used for testing the presence of inserts in transformed bacteria and plants; PCRBIO® polymerase was used for the amplification of *Nicotiana* MYB subgroup 9 genes yet to be sequenced; and Phusion® High-Fidelity (a polymerase that proofreads sequences as it replicates them) was used when sequence accuracy was important. A standard PCR reaction recipe and program are summarized in Table 2.2.

Table 2.2. Reaction conditions and thermocycling sequence for a standard polymerase chain reaction.

REACTION CONDITIONS		THERMOCYCLING PROFILE		
Reagent concentration	Final concentration	Reaction phase	Temperature (°C)	Time (min)
10X reaction buffer	1X	Initial denaturation	94	5
20mM dNTPs	200µM	Denaturation	94	0.5
100 µM forward primer	200nM - 5µM	Primer annealing	50 – 65	0.5
100 µM reverse primer	200nM - 5µM	Extension	72	15-60 s
5 U/µL Taq polymerase	0.75 – 2µM	Final extension	72	5
gDNA or cDNA template	1-3 µL added	Final hold	4	∞

2.3.1.5 Visualisation of nucleic acids by agarose gel electrophoresis

RT-PCR products were visualized in 2% agarose gels containing 0.2 µg/ml final concentration ethidium bromide. Electrophoresis grade agarose was mixed with 0.5 × TBE buffer (Appendix 5) to a concentration of 0.8-1.5%. The agarose was dissolved by heating for 1.2 minutes in a microwave and allowed to cool by shaking the flask in cold water. The molten agarose was then poured into a gel tray containing ethidium bromide (0.2 µg/ml final concentration) and fitted with a plastic comb to create the desired number of wells. Once set, any combs were removed, and the gel was placed in an electrophoresis tank filled with 0.5 × TBE. Nucleic acid samples (4 – 15 µl for PCR product; 1 µl DNA/RNA) to be loaded onto the gel were mixed with 1 µl loading buffer (Appendix 5) and transferred to the wells by pipette. Up to 3µl of 1 Kb HyperLadder™ or 100 bp Invitrogen™ Ladder was loaded alongside the samples and an electric current of 90 to 110 V was applied to the gel using a Consort E835 power pack (Sigma–Aldrich). DNA/RNA bands were visualised under UV light.

2.3.1.6 Extraction of DNA fragments from agarose gels

DNA extractions of PCR products from gels were done using Invitrogen™ PureLink™ Quick Gel Extraction or Monarch DNA Gel Extraction Kit (New England Biolabs, Inc.) following the manufacturer's instructions. PCR products and gel extracts were stored at -20°C.

2.3.1.7 Ligation of a PCR product into a cloning vector

The replication of DNA sequences of interest was achieved by molecular cloning using plasmids that replicate in *Escherichia coli*. Ligation of DNA fragments of interest was done into one of two plasmid vectors containing the *lacZα* gene (for white-blue colony selection): pGEM®-TEasy, when the overhangs of the amplicon had sticky ends (*e.g*. after amplification with EcoTaq or PCRBIO), or linearised pBluescript SK-, when the amplicon had blunt ends (*e.g*. after amplification with Phusion).

pGEM-T Easy vectors have single 3′ terminal thymidine nucleotides at both ends of the insertion site. This greatly improves the efficiency of ligation of a PCR product into the plasmids by providing a compatible overhang for specific binding of the 3' adenine nucleotides left by some Taq polymerases (*e.g.* PCRBIO). The pGEM®-TEasy plasmid also contains the ß -lactamase gene that confers ampicillin resistance, and the lacZ gene which encodes the alpha-peptide of the ß-galactosidase enzyme. This alpha-peptide coding sequence lies on either side of a multiple cloning site. When bacteria containing the pGEM®-TEasy plasmid are grown with IPTG (Isopropyl β-D-1-thiogalactopyranoside, inducer of the lac operon) and X-gal (5-bromo-4-chloro-3-indolyl-β-D-galactopyranoside, as a substrate for lacZα), if the plasmid has ligated to itself with no insert the IPTG induces expression of the uninterrupted lacZ gene. This produces the β–galactosidase enzyme which then metabolises the colourless X-gal to a bright blue product. When insertion of a fragment into the plasmid disrupts ß-galactosidase activity, X-gal cannot be metabolised and the colony remains white. In this way blue-white screening allows selection of plasmids containing a DNA insert. The pBluescript SK- vector also uses blue/white screening, as described above, as well as conferring ampicillin resistance. The pBluescript SK- vector had been previously linearised using the EcoRV restriction enzyme, which leaves blunt ends. This makes this plasmid suitable for blunt-ended cloning.

T4 DNA ligase (New England Biolabs, Inc.) was used in all ligation reactions. Reaction mixes contained 0.5µl of vector, 0.5 µl of 10X ligase buffer, 0.5µl of enzyme and 2.5-3.5 µl of PCR product or gel extract. Final volume of 5 µl was completed with sterile distilled water. Ligations were left to incubate for 16 h at 16°C for pBluescript SK- and at room temperature for pGEM®-TEasy.

2.3.1.8 *Generation of DH5α* E. coli *competent cells*

Volumes of plasmid DNA were scaled up by transferring them into the fast-growing bacterium *E. coli*. The DH5α strain was treated to enable the passive uptake of plasmid DNA as follows: a 50 µL aliquot of a previous culture was thawed on ice and then added to 10ml of liquid LB (LB, Appendix 5). The culture was incubated overnight at 37°C, shaking at 180 rpm. 1 ml of the culture was then inoculated in each of 4 × 30 ml liquid LB and incubated for three hours in a shaking incubator at 37°C. The remaining steps were all performed on ice or in a centrifuge cooled to 4°C. The cells were pelleted by centrifugation for 5 minutes at 4000 rpm. The supernatant was discarded, and the cells resuspended in 10 ml 100mM $MgCl_2$ (4°C), before being recovered on ice for five minutes. The cells were then isolated by centrifugation at 4000 rpm and the supernatant discarded. Finally, the cells were resuspended in 2 ml of *E. coli* freezing solution containing 60mM $CaCl_2$ and immediately frozen in aliquots of 50 µl using liquid nitrogen. Aliquots of competent *E. coli* were stored at –80°C until required.

2.3.1.9 *Transformation of DH5α* E. coli *with a plasmid vector*

The product of ligation was transformed into chemically competent *E. coli* strain DH5α (section 2.3.1.8) with ampicillin resistance. DH5α *E.coli* strain is ideal for plasmid cloning because it contains the recA gene to prevent homologous recombination, the $endA_1$ mutation to inactivate an endogenous endonuclease that can degrade plasmid DNA, and the lacZ ΔM15 allele as an α receptor to complete the β-galactosidase protein tetramer during blue-white screening using the lacZ gene.

5 µL of the ligation reaction (section 2.3.1.7) was combined with a 50 µL aliquot of competent cells and heat shocked at 42°C for 70 s to promote insertion of the plasmid into the bacterial cells. The mix was then left to recover on ice for 2-5 min and resuspended in 700 µL of liquid LB. The liquid culture was incubated at 37°C for 30-60 min to allow multiplication of the transformed cells. Solid LB (LBA, Appendix 5) plates were prepared containing 100mg/L ampicillin. 100 µL of IPTG and 20 µL of X-Gal were spread out with sterile glass beads on the solid media. 200 µl of the liquid culture were plated on each of the solid media plates. The antibiotic selection (ampicillin) along with lacZα, which the vector contains, allowed for positive selection of the colonies. Successful gene amplification was then confirmed using colony PCR (section 2.3.1.10). Selected positive colonies were picked with sterile wooden toothpicks and 3ml LB cultures with 100 mg/L ampicillin were grown at 37°C, 180 rpm, for 12 h.

2.3.1.10 Screening bacterial colonies using colony PCR

A small amount of each colony to be screened was transferred with a sterile toothpick into 20µl dH_2O. At least five colonies were screened per transformation. The tubes were heated to 95°C for five minutes to burst open the cells, and then 5 µl of the template was used in a PCR reaction, as described in section 2.3.1.4, using primers designed to anneal to either the plasmid or the insert. The PCR products were separated by agarose gel electrophoresis as detailed in section 2.3.1.5. Positively transformed colonies yielded bands that matched the expected size of the amplicon when the insert was present. When a particular orientation of the insert within the plasmid was desired (for example, when the plasmid was intended for plant transformation, (sections 2.3.3, 3.3.3), a combination of plasmid backbone and specific gene primers was used.

2.3.1.11 Plasmid purification, sequencing and analysis of genes in a plasmid vector

The desired plasmid was extracted using a homemade miniprep (alkaline cell lysis method) plasmid preparation protocol. All solutions used are listed in Appendix 5. 1.5 ml of the liquid culture from 2.3.1.9 were transferred into an Eppendorf tube and spun down for 1 min at 13000 rpm. All the LB was removed and 300 µl of SOL1 plus 5 µl of RNAseA (10 mg/ml) were added to the pellet. A short vortex was applied to resuspend the pellet. 300 µl of SOL2 was added and the tube inverted a few times to mix. Following this, 300 µl of SOL3 was added and the tube inverted a few times to mix. The samples were left on ice for 5 min followed by 10 min centrifugation at 13000 rpm. After this centrifugation step the lysed cell components would have been pelleted at the bottom and on the walls of the tube, leaving a clear liquid containing the DNA in the supernatant. The liquid supernatant (around 800 µl) was carefully collected without disturbing the cell debris and recovered in a new tube. 640 µl of isopropanol was added to the collected liquid and spun down for 20 min at 13000 rpm. All the liquid was removed and a small pellet at the bottom of the tube containing the DNA was recovered. 1 ml of 70% ethanol was added and spun down for 3 min at 13000 rpm. All the ethanol was carefully removed and the pellet left to dry for 10 minutes in the flume hood. The plasmid was resuspended in 20 µl of sterile water and the DNA quantified by Nanodrop. 10 µl aliquots of 100 ng/µl DNA plasmids were then sent for Sanger Sequencing at the Department of Biochemistry, University of Cambridge, using appropriate primers to the vector (*e.g.* M13 Forward/Reverse).

2.3.2 DNA and protein sequence analyses

Raw sequences were received as DNA electropherogram files (.ABI file extension). Geneious R9 was used for visualizing, annotating and alignment of the DNA sequences. DNA sequences were

translated to predicted amino acid sequences using Geneious R9 and/or MEGA X software (Kumar *et al.*, 2018). Graphic predictions of the protein structures were made from the amino acid sequences using PredictProtein (Rost *et al.*, 2004) online tool.

2.3.3 Heterologous expression of candidate genes in *Nicotiana tabacum*

Heterologous expression in *Nicotiana tabacum* was used to test the function of selected candidate genes from the *Nicotiana* species of interest for two main reasons: (1) *N. tabacum* is a model species with a well-established *Agrobacterium tumefaciens* mediated transformation protocol, and (2) *N. tabacum* ectopic expression has been used to assess the function of R2R3 SB9 MYB genes across several plant species including members of the Solanaceae family (Baumann *et al.*, 2007). Additionally, *N. tabacum* has been extensively used at the Evolution and Development Laboratory, Department of Plant Sciences, University of Cambridge, to test the funstion of R2R3 Subgroup 9 MYBs from other angiosperm species, which makes it a system suitable for comparative analyses. However, because the genes to be overexpressed are also from *Nicotiana* species, high similarity among sequences would be expected between the orthologues of *N. tabacum* and those from the donor species (*N. cordifolia* and *N. solanifolia*), which needs to be taken into consideration when assessing heterologous expression of the genes in the putative transgenic lines (see section 2.3.3.7).

2.3.3.1 Generation of Nicotiana spp. *expression vectors*

Full length versions of *NcMIXTA-like* and *NsMIXTA-like* were cloned into a pBluescript SK- primary plasmid vector. pGreen II was used as the binary vector. Visualization of plasmid sequences, selection of double digestion restriction enzymes, virtual digestions and virtual ligations for construct building were done using the cloning tools of Geneious R9. For the case of *MIXTA-like* genes from species of section *Paniculatae*, both the empty pGreen II plasmid and the pBluescript plasmid containing the gene were digested in parallel with restriction enzymes PstI and SalI. Enzymes and buffers used in digestions are listed in Appendix 6b. The digestions were incubated at 37°C for two hours. Products of the digestions were run in a 1% agarose gel and the fragments of interest were excised, extracted from the gel with Monarch® DNA Gel Extraction Kit, and quantified using Nanodrop. The inserts were then ligated directionally into the linearized pGREEN plasmid using T4-ligase. The mass of insert required at molar 3:1 insert:vector ratio, in the range needed for typical ligation reaction, was calculated using the NEBioCalculator™ v1.9.0 online. Ligation reactions were incubated for 16 h at 16°C and then stored at -20°C. pGreen II plasmid maps for *NcMIXTA-like* and *NsMIXTA-like* are in Figure 2.6.

2.3.3.2 *Generation of* A. tumefaciens *GV3101 competent cells*

Transformation of *Nicotiana* spp. leaf discs was performed using electrocompetent *Agrobacterium tumefaciens* strain GV3101 (section 2.3.3.3). To obtain numerous copies of these cells to be ready for transformation, a sample from a previous batch of cells was streaked out on a LBA plate with antibiotics (50 µg/L kanamycin, 25 µg/L gentamicin) for 48 h. A single colony was inoculated overnight in 2 mL LB plus antibiotics with shaking (180 rpm) at 28°C. The overnight culture was transferred to 200 mL LB in a sterile 500mL flask and grown at 28°C shaking at 250 rpm until the OD reached values ≥ 0.3 (~4-5 h). The liquid culture was spun for 10 min at 5,000 rpm in sterile 50 mL Falcon tubes at 4°C. The supernatant was discarded, and the pellet resuspended in 20 mL ice-cold 1mM HEPES pH 7 (sterile, filtered). The resulting liquid culture was spun for 10 min at 5,000 rpm at 4°C, followed by additional rounds of discarding supernatant and resuspending the pellet two more times. In the final round, after removing the supernatant, the pellet was resuspended in 2 mL ice-cold 10% glycerol (sterile, filtered). The liquid culture was dispensed in 40 µL aliquots in pre-chilled, sterile Eppendorf tubes, snap frozen in liquid nitrogen and stored at -80°C.

2.3.3.3 *Transformation of* Agrobacterium tumefaciens *competent cells*

Agrobacterium tumefaciens strain GV3101 has a chromosomal rifampicin resistance gene, but is sensitive to kanamycin, making it good for use with binary vectors that confer kanamycin resistance (such as pGREEN). It contains a disarmed Ti plasmid that possesses the virulence genes needed for T-DNA insertion and a gentamicin resistance gene but has no functional T-DNA region of its own. The GV3101 strain used also contains the pSOUP vector, which provides the machinery for pGREEN to replicate inside *Agrobacterium* and confers tetracycline resistance.

A. tumefaciens GV3101 competent cells were transformed to include the plasmid vectors of interest (Figure 2.6) by electroporation. 50 µL of competent cells and 1 µL of the plasmid vector were pipetted into a 0.5 cm BioRad Cuvette. 1.8 V, 400 ohms pulse was applied in a BioRad Gene pulser Xcell. The transformed cells were recovered in 1 ml LB for three hours at 30°C and 180 rpm. For selection of transformed cells, aliquots of the liquid culture (10-100 µL) were pipetted onto LBA plates containing gentamycin 25 mg/L and kanamycin 50 mg/L at 30°C for 48 h. Positive transformants were confirmed by colony PCR (section 2.3.1.10).

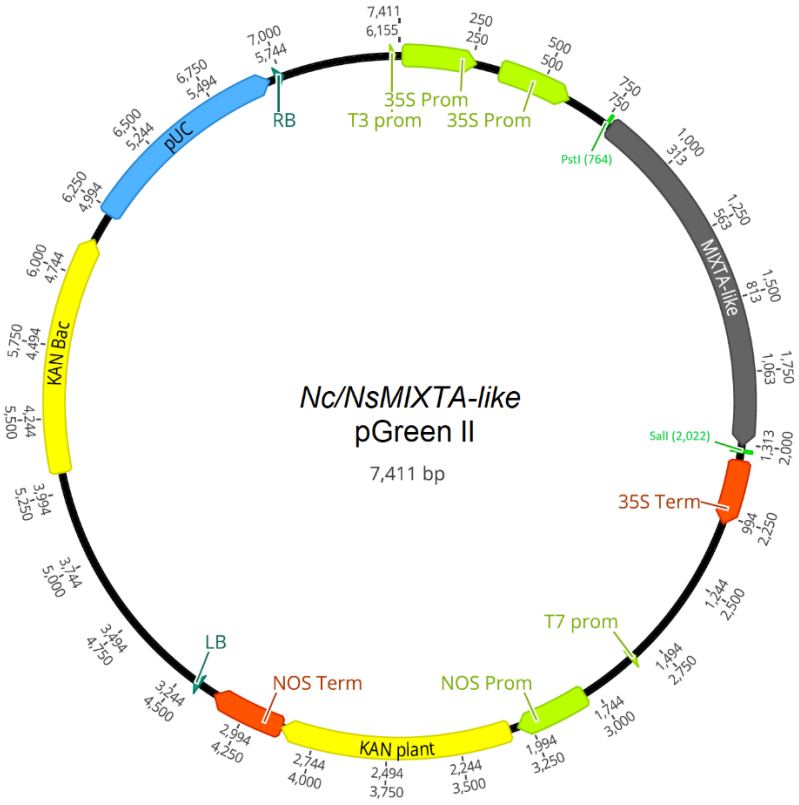

Figure 2.6. Plasmid map of *N. cordifolia/N.solanifolia MIXTA-like* in pGreen II used for stable transformation of *N. tabacum*.
Blue bar represents origin of replication (pUC), light green bars promoters (T3 Prom, 35S Prom, T7 Prom and NOS Prom), orange bars terminators (35S Term and NOS Term), yellow bars kanamycin resistance genes for plant (KAN Plant) and bacteria (Kan Bac), dark green bars regulatory elements (RB, LB) and grey bar the coding sequence of the gene of interest (*Nc/NsMIXTA-like*). Restriction sites used for double digestion are indicated with green arrows (PstI/SalI).

2.3.3.4 *Preparation of* Agrobacterium *liquid cultures*

Cultures of *A. tumefaciens* GV3101 containing the construct of interest were grown from single colonies in liquid LB with kanamycin 50 mg/L and gentamycin 25 mg/L at 28°C, rotating at 180 rpm. 1 ml of liquid culture was sub-cultured in 200 ml LB daily for 72 H. 200 ml *Agrobacterium* cultures were subdivided into four 50ml aliquots in sterile Falcon tubes. *A. tumefaciens* cells were pelleted by centrifugation at 4000 rpm, 10°C for 5 minutes. Supernatant LB was discarded and the cell pellets were resuspended in infiltration buffer (Liquid MS, Table 2.3) and adjusted to an O.D. greater than 0.5.

Table 2.3. Composition of media used for *A. tumefaciens* mediated transformation of *N. tabacum* and *N. benthamiana*.
N. tabacum stable transformation was performed in Chapters 2 and 3. *N. benthamiana* stable transformation in Chapter 3 only. MS = Murashige and Skoog medium including vitamins (Duchefa Biochemie). Sigma Aldrich or Duchefa Biochemie plant agar were used as solidifying agents.

	Leaf discs of *N. tabacum* (MS-Tabac)	**Leaf discs of *N. benthamiana* (MS-Benth)**	**Liquid MS**
MS	4.4 g/L	2.2 g/L	4.4 g/L
Sucrose	20 g/L	20 g/L	20 g/L
Plant Agar	8 g/L	8 g/L	NA

2.3.3.5 Handling of leaf explants for stable transformation

Explants were obtained from young leaves of *Nicotiana tabacum* var. Samsun plants growing in the greenhouse conditions (section 2.3.1.1). The leaves were put in 1 L Duran bottles filled with 10% commercial bleach and shaken for 15 minutes at 120 tilts/minute on a Rocker 25. The bleach solution was removed from the bottle, and the leaves were rinsed with sterile distilled water in the laminar flow hood four times, to remove any bleach residues. All instruments (forceps, blades, scalpels, etc.), liquid and solid media, were previously sterilized by autoclaving at 121°C for 20 minutes at 105 kPa. All tissue handling was carried out in the aseptic laminar flow hood. Leaf explants were infiltrated with *Agrobacterium* cultures by cutting the tissue while immersed in the liquid culture. The midrib and margin of the leaves were removed, and the laminar tissue was sectioned in 0.5 mm^2 squares. After imbibition, the sections of explant were blot dried with sterile filter paper and moved to Petri dishes with growing media (MS-Tabac, Table 2.3) with phytohormones (0.5 mg/L IAA and 1 mg/L BAP) without antibiotics. The leaf discs were put with the abaxial surface in contact with the solid media.

2.3.3.6 Co-cultivation and tissue propagation

To allow infection of the bacteria cells into the leaf explants, the plates without antibiotics were left for co-cultivation at 24°C in the dark for 48 h to 72 h. Explants were then sub-cultured into MS-Tabac with phytohormones (0.5 mg/L IAA and 1 mg/L BAP) and antibiotics (kanamycin 100 mg/L, cefotaxime 500 mg/L and ampicillin 200 mg/L) and kept at 24°C 16 h L/8 h D. Kanamycin acted as selection agent for the plant transformed cells and cefotaxime and ampicillin to deter bacterial growth including overgrowth of *Agrobacterium*. Leaf tissue was sub-cultured to fresh media with phytohormones and antibiotics every 10-14 days. In the case of *N. tabacum*, callus formation usually starts 14-25 days after infiltration and regeneration of transformed plantlets 20-40 days after infiltration. Regenerated plantlets 3-5 cm tall were excised from the original tissue, cut at the base of any remaining callus, and moved to 50 ml Hamilton jars with MS-Tabac with antibiotics, no phytohormones, for rooting. When the root system was well developed (2-5 cm long roots, ramified) the plantlets were moved to soil and kept in growing chambers at the PGF (see section 2.3.1.1).

2.3.3.7 Characterization of putative N. tabacum transgenic lines-Genotyping

Young leaf tissue of putative transgenic lines was collected in liquid nitrogen for gDNA (quick gDNA extraction, section 2.3.1.2) and RNA extraction (guanidinium-acid-phenol extraction, section 2.3.1.2). Bioscript retrotranscriptase was used for cDNA synthesis as explained in section 2.3.1.2. Transgene expression was confirmed with PCR using the DNA polymerase EcoTaq or

PCRBIO (see section 2.3.1.4) with primers specific for the transgene (Appendix 6c). In order to reduce the likelihood of obtaining false positives via PCR amplification of the *N. tabacum* orthologue of the transgene, instead of amplification of the transgene itself, the sequence of the transgene was aligned to the orthologue in *N. tabacum*, retrieved from available public databases NCBI GenBank (http://www.ncbi.nlm.nih.gov/) and SolGenomics (Fernandez-Pozo *et al.*, 2015). Primers were designed to have 100% similarity to the transgene sequence, and less than 92% similarity to the *N. tabacum* sequence (Appendix 6c). Transgene expression was compared to that of *NtUBIQUITIN* (*NtUBQ*) within the same plant. All putative transformants were compared to a *N. tabacum* WT plant.

2.3.3.8 Characterization of putative N. tabacum *transgenic lines-Phenotyping*

Selected putative transgenic lines were characterized morphologically. Macromorphological features were imaged with an 8-megapixel digital camera (iPhone 5s). Photographs were taken of the entire plant, one mature flower and one mature leaf (fourth leaf from the tip of the inflorescence axis). Zeiss EVO HD15 Scanning Electron Microscope (cryo-SEM) was used to image epidermal features on leaf and flower. 5 mm^2 samples were mounted on stubs using conductive graphite paint. Mounted tissues were cryo-preserved in liquid nitrogen. 5 minutes of sublimation at -90°C were applied to enable removal of surface ice. Samples were sputter coated with 4 nm of platinum. SEM photographs were obtained using backscattering. The epidermal surfaces selected for characterization were: abaxial leaf, adaxial leaf, abaxial petal, adaxial petal, anther and carpel.

2.4 RESULTS

2.4.1 Growing *N. cordifolia* and *N. solanifolia* as a source of living tissue for molecular and morphological analyses

Seeds of *N. cordifolia* and *N. solanifolia* were sown in September 2015. Although germination and overall growth of the plants was normal, flowering did not occur during the four years of development of this project. These two species are perennial soft woody-shrubs naturally growing in very specific environmental conditions (see section 2.2.3). Several modifications in the growing conditions were trialled to promote flowering. For *N. solanifolia,* for instance, watering was reduced to a minimum to mimic the very dry natural conditions of the Atacama Desert in which this species grows. Moreover, one specimen was maintained in an outdoors garden at local climate conditions, on average cooler than the greenhouse. For *N. cordifolia*

watering was also reduced and some specimens were located under artificial shade in the greenhouse to mimic the rocky crevasses where this species grows in the Juan Fernandez Islands. Because the limitations in flower material during the experimental phase of this project, only leaf material of *N. cordifolia* and *N. solanifolia* was used for the molecular characterization of the species. Nevertheless, several specimens were kept growing in different locations in Cambridge, including the Department of Plant Sciences and the Cambridge University Botanic Garden (CUBG) greenhouses. In April 2019, after the initial submission of this manuscript, one plant of *N. cordifolia* growing at CUBG flowered. Later that same year, July 2019, a specimen of *N. solanifolia* bloomed at the Department of Plant Sciences. Morphological characterization of the flowers and adaxial petal cell shape, along development, was carried out for these species then, but not further molecular work was performed.

2.4.2 Establishing flower developmental stages in *N. solanifolia* and *N. cordifolia*

The developmental series of the adaxial petal surfaces of *N. cordifolia* (non-conical) and *N. solanifolia* (conical) are shown in Figure 2.7 and Figure 2.8. In both species petal epidermal cells initiate flat with smooth surface. The cells expand and the cell surface becomes wrinkled in *N. cordifolia* early in development (stage 3), whereas the surface of the cells is smooth along all stages of development in *N. solanifolia*. The conical cells of *N. solanifolia* become apparent late in development (stage 4-5).

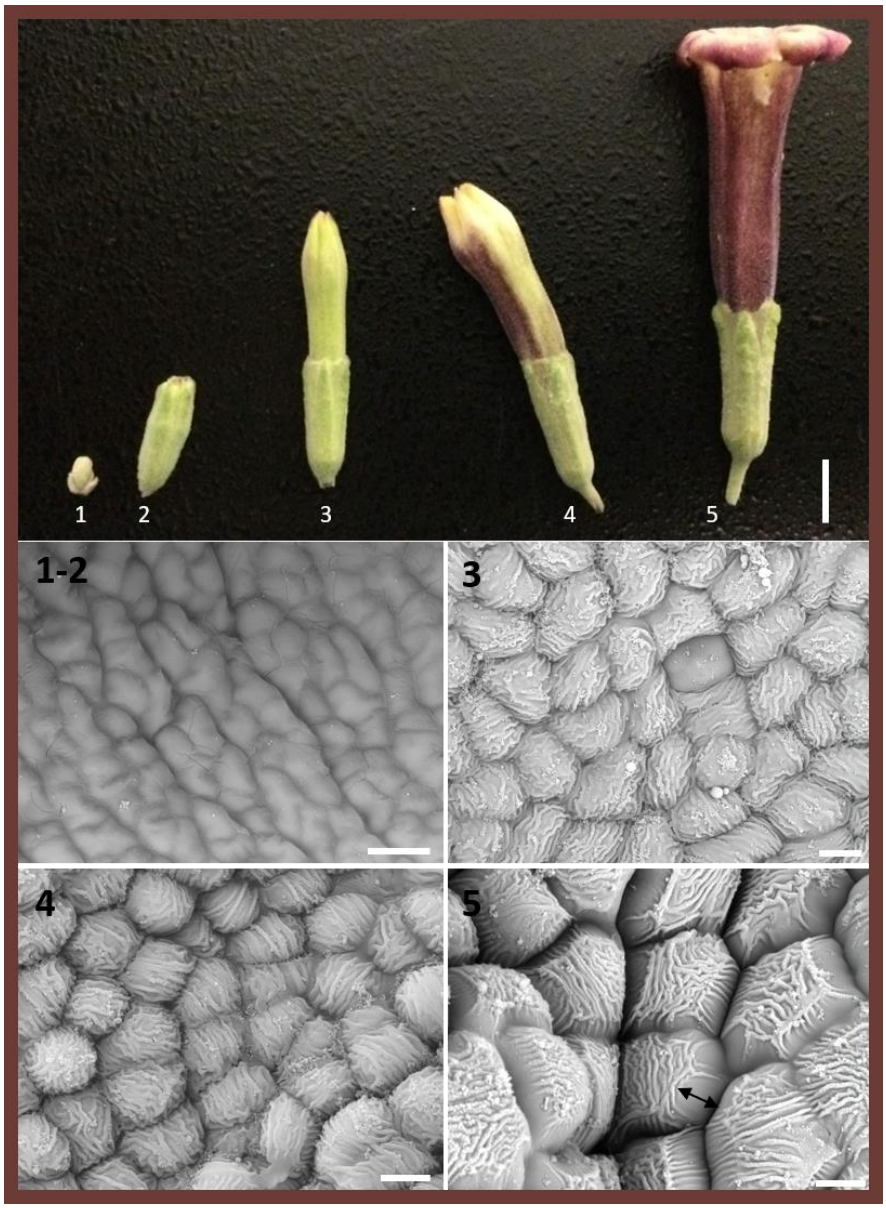

Figure 2.7. Flower and adaxial petal cell shape development in *Nicotiana cordifolia.*
Top panel: Macromorphology of flowers at five developmental stages. Middle and bottom panel: SEM images of adaxial petal cells at the same five developmental stages. Adaxial petal cells in *N. cordifolia* are non-conical across all developmental stages and present conspicuous irregular striations on the surface. Epidermal petal cells at maturity (bottom panel-stage 5) protrude slighty from the surface of the petal (black double headed arrow). Scale bar top panel = 10.0 mm, middle and bottom panel = 10 µm.

Stage 1-2: Flower buds closed; 0.1-20.0 mm long; green calyx surrounding the rest of the flower; tips of the calyx lobes appear closed over the rest of the organs (top panel-1, 2). Adaxial petal cells are irregular in contour with a smooth surface (bottom panel-1-2).

Stage 3: Flower buds open; 20.0-40.0 mm long; petal lobes and tube emerge from the tip of the calyx and corolla tube elongates; corolla lobes closed over the rest of the organs, corolla white-greenish in colour (top panel-3). Adaxial petal cells non-conical, flat in height, polygonal in contour, with wrinkled (irregularly striated) surface (middle panel-3).

Stage 4: Flower buds open; 40.0-50.0 mm long; petal lobes and corolla tube protruding out from the tip of the calyx; corolla lobes closed over the rest of the organs, tube of the corolla dark red in colour, corolla lobes yellowish-pink (top panel-4). Adaxial petal cells non-conical, almost flat in height, polygonal in contour, with wrinkled (irregularly striated) surface (bottom panel-4)

Stage 5: Mature flower; ≥50 mm; petal lobes fully open, corolla tube fully expanded, dark red in colour (top panel-5). Adaxial petal cells polygonal in contour, with wrinkled (irregularly striated) surface, non-conical, slightly extending out the surface in height (up to 10 µm over the petal surface, double headed arrow, bottom panel-5).

Figure 2.8. Flower and adaxial petal cell shape development of *Nicotiana solanifolia* (Section *Paniculatae*).

Top panel: Macromorphology of flowers at five developmental stages. Bottom panel: SEM images of adaxial petal cells at the same five developmental stages. Adaxial petal cells in *N. solanifolia* at maturity are non-conical from stage 1 to 3, conical with rounded tip at stage 4 and conical ending in a papilla (rounded protuberance) at stage 5. Occassionally, flowers at stage 5 presented erect corolla lobes (arrow head). Scale bar top panel = 10.0 mm, bottom panel = 10 µm.

Stage 1-2: Flower buds closed; 0.1-0.5 mm long; green calyx surrounding the rest of the flower; tips of the calyx lobes appear closed over the rest of the organs (top panel-1). Adaxial petal cells are rectangular in contour with a smooth surface (bottom panel-1 and 2).

Stage 3: Flower buds open; 10.0-20.0 mm long; petal lobes emerge from the tip of the calyx; corolla lobes closed over the rest of the organs, corolla green-yellowish in colour (top panel-3). Adaxial petal cells circular in contour with smooth surface, dome-shaped (bottom panel-3).

Stage 4: Flower buds open; 20.0-40.0 mm long; petal lobes and corolla tube protruding out from the tip of the calyx; corolla lobes closed over the rest of the organs, tube of the corolla green-yellowish, corolla lobes green (top panel, 4). Adaxial petal cells conical with rounded tips (bottom panel-4).

Stage 5: Mature flower; ≥40.0 mm; petal lobes fully open, green-yellowish in colour (top panel-5). Adaxial petal cells conical, circular in contour, tip ending in a papilla (rounded protrusion) (bottom panel-5).

2.4.3 Sequencing of R2R3 MYB Subgroup 9 genes in *N. cordifolia* and *N. solanifolia*

gDNA and cDNA from leaf tissue were used for all molecular characterization of *N. cordifolia* and *N. solanifolia*. Nucleotide sequences of the coding regions of the four candidate genes (*MIXTA-2, MIXTA-like, MYBl7-1* and *MYBl7-2*) were initially assembled from DNA fragments cloned independently from different regions of the gene (see primer design 2.3.1.3, Appendix 6a). Assembly was performed using the multiple alignment algorithm to align the cloned DNA fragments to the known sequences of several *Nicotiana* species (Appendix 7). After the initial complete characterization of the gene, primers were designed to amplify the entire coding sequence of each gene in a single RT-PCR reaction. Complete coding sequences cloned into pBluescript SK are listed in Table 2.4 and have been deposited in the lab repository of plasmids where they are stored at -20°C.

Comparisons between DNA and amino acid sequences of the coding regions of the candidate genes were made from pairwise alignments of the consensus sequence of each gene for the two species (Appendix 7, Figure 2.10).

Table 2.4. pBluescript SK plasmids of full coding sequences of R2R2 Subgroup 9 genes of *N. cordifolia* and *N. solanifolia.*

Species	Gene	Code	F Primer	R Primer	Plasmid Nanodrop		
					ng/µl	260/280	260/230
Nicotiana cordifolia	*MIXTA-2*	260.70	Nic_MIXTA-2_F10	Nsola_MIXTA-2_R1	664.70	1.88	2.15
	MIXTA-like	293.40	Nic_ML_F4	Nic_ML_R29	1705.90	1.92	2.31
	MYB17-1	205.11	Nf_MYB17-1_1F	Nic_MYB17-1_R10	44.90	1.90	2.22
	MYB17-2	183.80	Nf_MYB17-2_1F	Nf_MYB17-2_1R	466.70	1.87	2.04
Nicotiana solanifolia	*MIXTA-2*	264.40	Nic_MIXTA-2_F10	Nsola_MIXTA-2_R1	1399.50	1.92	2.42
	MIXTA-like	313.40	Nic_ML_F4	Nic_ML_R29	362.40	1.80	1.80
	MYB17-1	205.12	Nf_MYB17-1_1F	Nic_MYB17-1_R10	968.10	1.95	2.22
	MYB17-2	183.90	Nf_MYB17-2_1F	Nf_MYB17-2_1R	713.30	1.83	1.98

2.4.3.1 Comparison between MIXTA-2 orthologues of N. cordifolia *and* N. solanifolia

Appendix 7A shows multiple alignment of MIXTA-2 (R2R3 MYB Subgroup 9A) orthologues of *Nicotiana* spp. including *N. cordifolia* and *N. solanifolia*. The sequences were found to be highly conserved between the two sister species. Two consecutive base substitutions were detected in positions 1032-1033 (AT in *N. cordifolia* vs. GG in *N. solanifolia*, Figure 2.9). Translated in 'Frame I' these substitutions fall at the end (CCA in *N. cordifolia* vs. CCG in *N. solanifolia*) and the

beginning (TTA in *N. cordifolia* and GTA in *N. solanifolia*) of consecutive codons. The substitution A for G in position three of the respective codon is synonymous, both CCA and CCG code for proline (P). However, the substitution falling in position one of the following codon results in different translated amino acids: TTA codes for valine (V) whereas GTA is translated into leucine (L). To assess the potential effect of this difference between sequences of sister species, the chemical and structural properties of both amino acids were retrieved from the literature, and the substitution leucine for valine was plotted in the corresponding protein prediction (L345V, Figure 2.9). Both L and V are aliphatic, non-polar, hydrophobic amino acids, there is a mutation mass shift of 14 Da between the two amino acids and they can be substituted for each other with 95% confidence (Bordo & Argos, 1991). There are no predicted secondary structures (*e.g.* helices) in position 345 and this region coincides with a disordered region. In terms of solvent accessibility, the amino acid in this position is exposed. The effect of point mutation algorithm predicts a score of -58, which indicates a strong signal for neutral/no effect (Rost *et al.*, 2004). Taking into consideration these properties, the potential effect of the V345L substitution in the protein function was interpreted to be relatively low and the two variants of *MIXTA-2* were not considered for the ectopic expression experiments in *N. tabacum* to further test the effect of sequence differences in protein function (section 2.3.3).

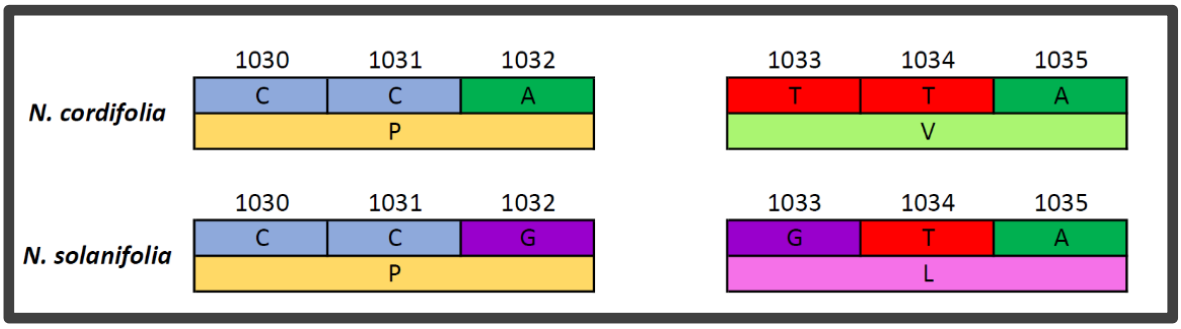

Figure 2.9. Two-nucleotide substitution in position 1032-1033 of *MIXTA-2* and effect on the translated amino acids.
A two-nucleotide difference detected between the sequences of *NcMIXTA-2* and *NsMIXTA-2* was predicted to have neutral or no-effect on the function of the resulting protein. This inference was based on the chemical and structural properties of the amino acids, as well as on their position along the amino acid chain.

2.4.3.2 Comparison between MIXTA-like orthologues of N. cordifolia and N. solanifolia

Figure 2.10 shows pairwise alignment of *MIXTA-like* (R2R3 MYB Subgroup 9A) orthologues of *N. cordifolia* (*NcMIXTA-like*) and *N. solanifolia* (*NsMIXTA-like*). Several differences in the DNA and amino acid sequences were detected between the sister species (Table 2.5). Synonymous nucleotide substitutions occur in positions 24 (8 amino acid residue) and 597 (199 amino acid

residue). Non-synonymous nucleotide substitutions with negative scores of predicted effect of point mutation occur in positions 67 (23 amino acid residue), 134 (45 amino acid residue, 428 (143 amino acid residue) and 694 (232 amino acid residue). Non-synonymous substitutions with positive scores of predicted effect of point mutation occur in position 134 (45 amino acid residue) and 1051 (351 amino acid residue). In *N. solanifolia* a 15-nucleotide deletion occurs in position 1111-1125 (GGA GGC GGA GGC GGA). This deletion removes a 5-glycine amino acid stretch but does not introduce frameshift changes. Figure 2.11 shows the predicted protein secondary structure of MIXTA-like in Section *Paniculatae* and the estimated effect of point mutations detected. Because of the relatively large number of differences identified between the coding sequences of *MIXTA-like* of *N. solanifolia* (conical cells) and *N. cordifolia* (non-conical cells) the two orthologues, *NcMIXTA-like* and *NsMIXTA-like*, were selected for heterologous expression in *N. tabacum* to experimentally asses the effect of such differences on the protein function (Section 2.3.3).

Table 2.5. Nucleotide substitutions and amino acid shifts detected between orthologues of *MIXTA-like* in *N. solanifolia* and *N. cordifolia.*

Nucleotide Position	Nucleotide substitution (*NsMIXTA-like-NcMIXTA-like*)	Position in codon	Effect of the substitution	Amino acid position	Amino acid shift (*NsMIXTA-like-NcMIXTA-like*)	Effect of point mutation score
24	T-C	3	Synonymous	8	D-D	-99
67	C-A	1	Non-synonymous	23	Q-K	-96
134	G-A	2	Non-synonymous	45	G-E	+29
428	C-T	2	Non-synonymous	143	A-V	-37
597	C-G	3	Synonymous	199	G-G	-99
694	A-C	1	Non-synonymous	232	T-P	-7
1051	C-T	1	Non-synonymous	351	L-F	+3
141	T-A	1	Non-synonymous	381	C-S	-8

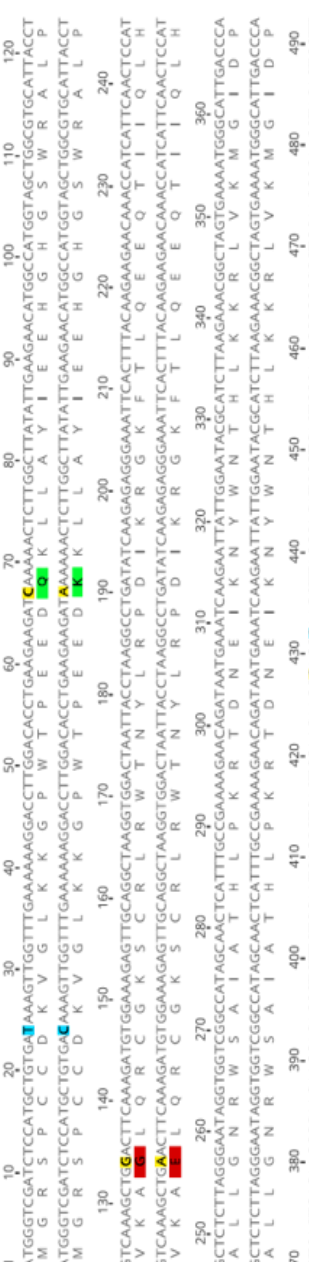

Figure 2.10. DNA and amino acid (aa) alignments of *MIXTA-like*/MIXTA-like sequences of *N. solanifolia* (conical cells) and *N. cordifolia* (non-conical cells) Section *Paniculatae*.

Eight single nucleotide substitutions were detected between *NsMIXTA-like and NcMIXTA-like*. Nucleotide substitutions with synonymous effect on the amino acid sequences are highlighted in blue and those with non-synonymous effect in yellow. Amino acid shifts with neutral or negative score of effect of point mutation are highlighted in green and those with positive scores in red. A five-glycine amino acid stretch (red box) was present in NcMIXTA-like but not in NsMIXTA-like. Numbers on top of the aligment correspond to the nucleotide position.

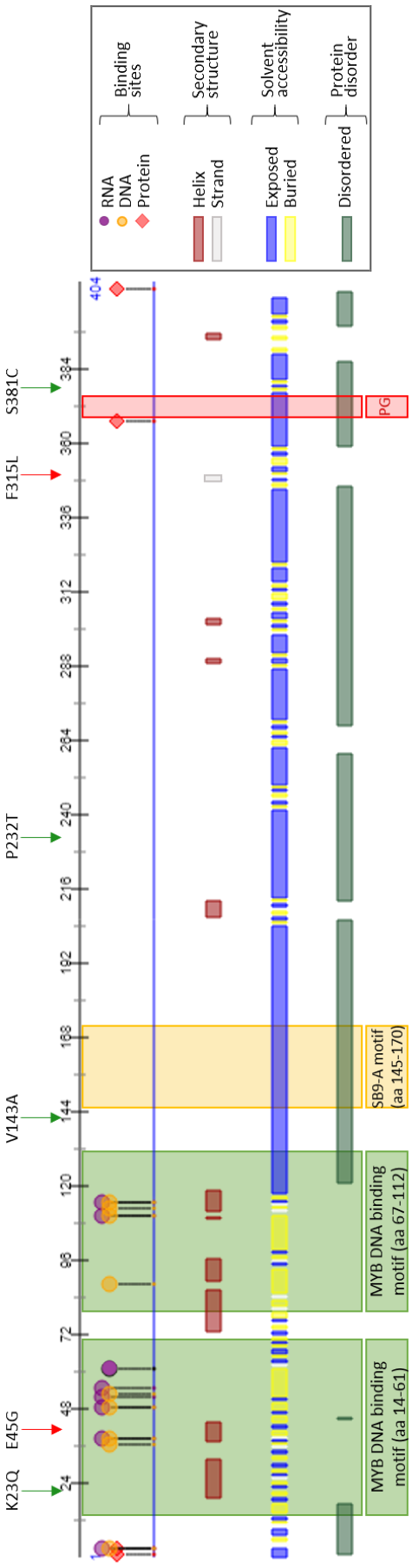

Figure 2.11. Predicted protein properties of MIXTA-like in *N. cordifolia* (Section *Paniculatae*).
Six amino acid substitutions detected when comparing MIXTA-like protein sequences of sister species *N. cordifolia* (non-conical) and *N. solanifolia* (conical) are marked with arrows at the top. Green arrows identify substitutions with negative scores (*e.g.* with no or neutral effect on the resulting protein function), and red arrows indicate substitutions with positive scores (*e.g.* predicted to have an impact on the protein function). Red shaded rectangle indicates the position of a 5-glycyne insertion (amino acid residue 371-375) in *N. cordifolia* not present in *N. solanifolia*.

2.4.3.3 *Comparison between MYB17-1 orthologues of* N. cordifolia *and* N. solanifolia

Appendix 7C shows pairwise alignment of *MYBI7-1* (R2R3 MYB Subgroup 9B) orthologues of *N. cordifolia* (*NcMYBI7-1*) and *N. solanifolia* (*NsMYBI7-1*). No differences in the nucleotide sequences were detected and the orthologues in the two sister species were interpreted as being identical. *MYBI7*-1 genes from species in Section *Paniculatae* were not ectopically expressed in *N. tabacum*.

2.4.3.4 Comparison between MYB17-2 orthologues of N. cordifolia *and* N. solanifolia

Appendix 7D shows alignment of consensus sequences of *MYBI7-2* (R2R3 MYB Subgroup 9B) orthologues of *N. solanifolia* (*NsMYBI7-2*) and *N. cordifolia* (*NcMYBI7-2*) and other *Nicotiana* species. Sequence differences found between *NsMYBI7-2* and *NcMYBI7-2* are listed in Table 2.6. Four synonymous nucleotide substitutions were confirmed in positions 303, 468, 507, 516. The remaining differences coincided with ambiguities in the nucleotide reads of *NsMYBI7-2* (red letters column 2, Table 2.6). Ambiguities in the sequencing reads were detected after amplifying the same fragment from the same species on different occasions. From 19 ambiguous nucleotide reads in *NsMYBI7-2,* 10 have synonymous effects where there is no shift in the translated amino acid compared to *NcMYBI7-2* (*e.g.* position 588). The remaining 9 ambiguities have ambiguous effects on the translated amino acids when compared to *NcMYBI7-2* (*e.g.* position 590). In all cases of ambiguous effect, one of the potential reads of the ambiguity in *NsMYBI7-2* codes for the same amino acid present in the corresponding position in *NcMYBI7-2* (*e.g.* position 590, Figure 2.12). The nucleotide ambiguities detected in *NsMYBI7-2* can be interpreted as derived from the assembly of DNA fragments cloned independently from different individuals. The presence of multiple reads within the same species indicates that there is intraspecific variation in the nucleotide sequence of *NsMYBI7-2*. As there were no variants, at the nucleotide nor at the amino acid level, unique to the conical-celled species *N. solanifolia* compared to the non-conical celled species *N. cordifolia*, the sequence differences detected between *MYBI7-2* orthologues were interpreted as unlikely to be responsible for the differences in the phenotype.

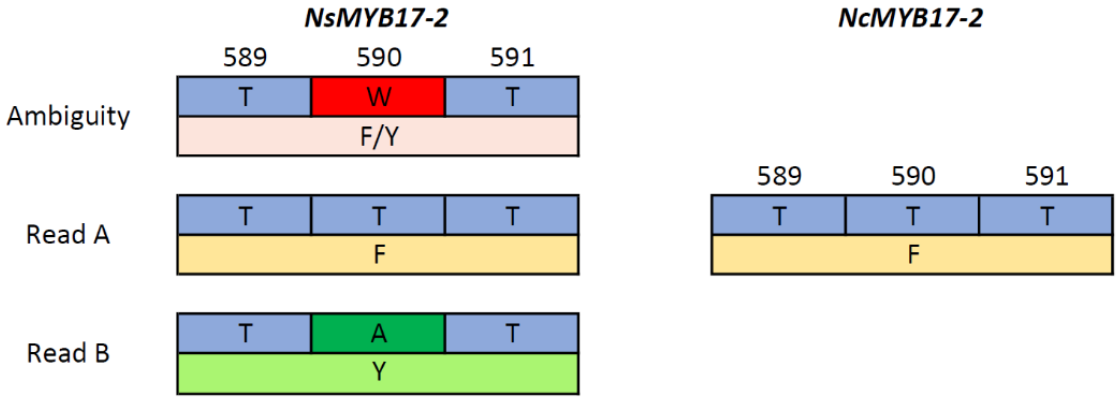

Figure 2.12. Ambiguities in the sequences reads of candidate genes were detected within the same species and coincided with reads in the sister species.

Ambiguities in the sequencing reads were detected after amplifying the same fragment from the same species on different occasions. This figure shows one example of ambiguity in *NsMYB17-2* (position 590), from *N. solanifolia* (conical cells) in which at least one of the potential reads translates to the same amino acid as in *NcMYB17-2,* from *N. cordifolia* (non-conical cells).

Table 2.6. List of nucleotide substitutions detected between *NsMYB17-2* and *NcMYB17-2*.
A. Nucleotide substitutions with their predicted effect in the putative (s) amino acid translation. **B.** Key for nucleotide ambiguities (red letters column 2) listed in A. Ambiguous nucleotide reads in *NsMYB17-2* have either synonymous (no shift in the amino acid, column 6) or ambiguous effect compared to *NcMYB17-2*. In all cases of ambiguous effect, one of the potential reads of the ambiguity in *NsMYB17-2* codes for the same amino acid present in the same position in *NcMYB17-2* (column 6).

A

Nucleotide Position	Nucleotide substitution (*NsMYB17-2-NcMYB17-2*)	Position in codon	Effect of the substitution	Amino acid position	Amino acid shift (*NsMYB17-2-NcMYB17-2*)
303	T-C	3	Synonymous	101	D-D
468	T-C	3	Synonymous	157	L-L
507	A-G	3	Synonymous	169	L-L
516	A-G	3	Synonymous	172	S-S
588	R-G	3	Synonymous	196	K-K
590	W-T	2	Ambiguous	197	Y/F-F
606	R-G	3	Synonymous	202	K-K
651	R-A	3	Synonymous	217	K-K
691	R-G	1	Ambiguous	217	S/G-G
708	S-G	3	Synonymous	236	S-S
714	Y-C	3	Synonymous	238	V-V
723	Y-C	3	Synonymous	241	S-S
755	R-A	2	Ambiguous	252	G/D-D
798	K-G	3	Synonymous	266	S-S
802	W-T	1	Ambiguous	268	S/C-C
805	W-T	1	Ambiguous	269	N/Y-Y
808	R-A	1	Ambiguous	270	A/T-T
884	R-A	2	Ambiguous	295	G/E-E
891	Y-C	3	Synonymous	297	S-S
906	R-A	3	Ambiguous	302	M/I-I
909	Y-T	3	Synonymous	303	Y-Y
921	K-G	3	Ambiguous	307	S/R-R
942	W-A	3	Synonymous	314	P-P

B

IUPAC nucleotide code	Base
R	A or G
Y	C or T
S	G or C
W	A or T
K	G or T

2.4.4 Heterologous expression of *NcMIXTA-like* and *NsMIXTA-like* in *N. tabacum*

2.4.4.1 Molecular characterization of expression of NcMIXTA-like *and* NsMIXTA-like *in* N. tabacum

N. tabacum transformed plants putatively expressing the gene of interest were genotyped using RT-PCR with primers designed as explained in section 2.3.3.7 for both constructs. However, although the primers were designed to minimize the likelihood of amplifying the orthologue of *MIXTA-like* native to *N. tabacum,* still an amplification product might have been present for the wild type. In order to confirm that the amplification product from the putative transgenic lines corresponded to the transgene and not to any orthologue native to *N. tabacum*, the PCR products were sequenced. A multiple sequence alignment (Appendix 8) including the PCR products of the transgenic lines, the sequence of the *NcMIXTA-like* and *NsMIXTA-like* plasmids, the product of amplification from the WT and the sequence for *N. tabacum MIXTA-like* retrieved

from publicly available databases allowed the detection of diagnostic DNA fragments which differentiated the transgene from the *N. tabacum* orthologue. In this way five transformed lines were confirmed for *NcMIXTA-like* (Lines 7, 10, 14, 16 and 19 Figure 2.13) and six for *NsMIXTA-like* (Lines 1, 2, 4, 6, 10, and 11, Figure 2.14).

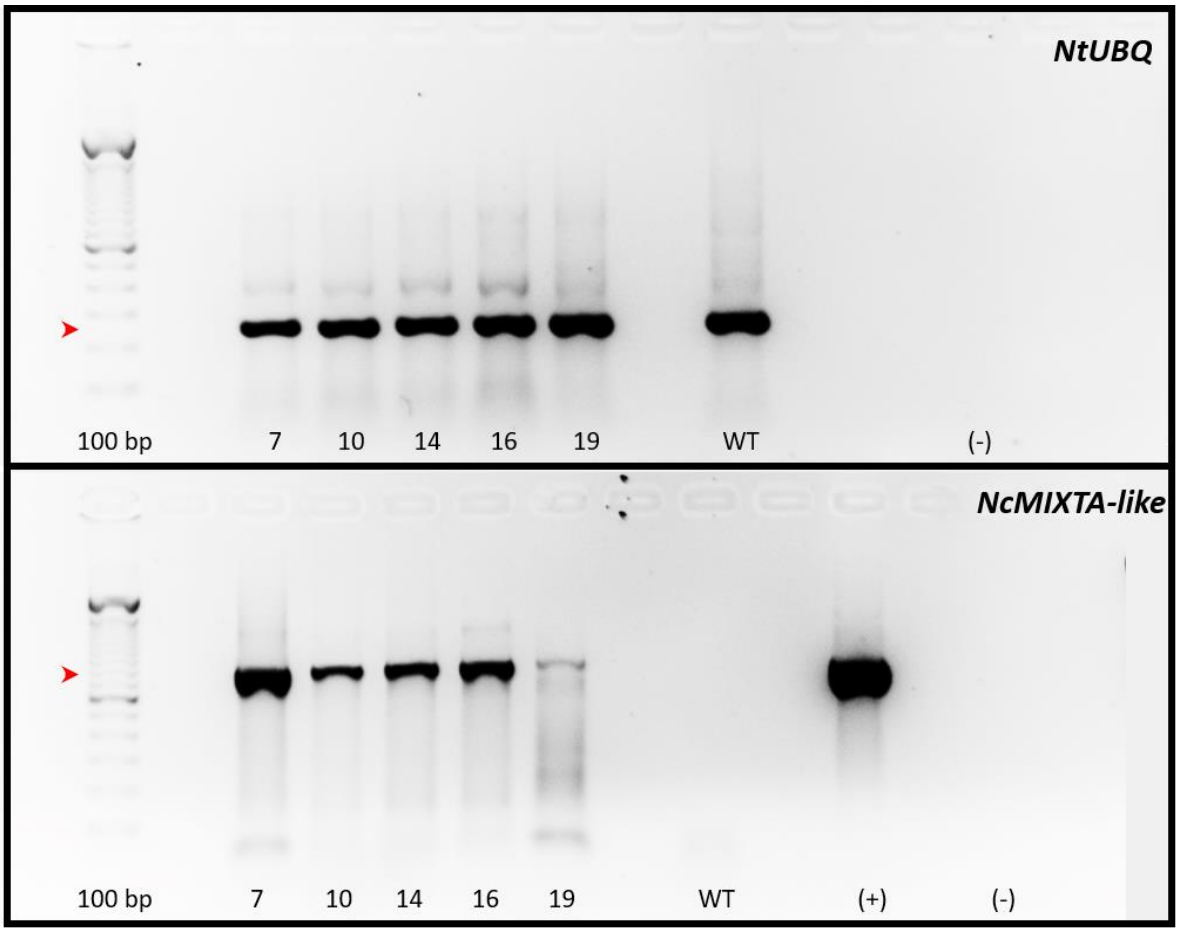

Figure 2.13. PCR screening for expression of transgene *NcMIXTA-like* in putative transgenic lines of *N. tabacum*.

Upper panel shows RT-PCR products of *NtUBQ* (expected size 248 bp, red arrow head) in eight putative transgenic lines and the wild type (WT). Lower panel shows RT-PCR products of *NsMIXTA-like* (expected size 889 bp, red arrow head) in six putative transgenic lines and the WT. Negative control (-) shows the product of water as template in the reaction. Positive control (+) shows the product of 1 µl (1:100 dilution) of a plasmid vector carrying the transgene *NcMIXTA-like.*

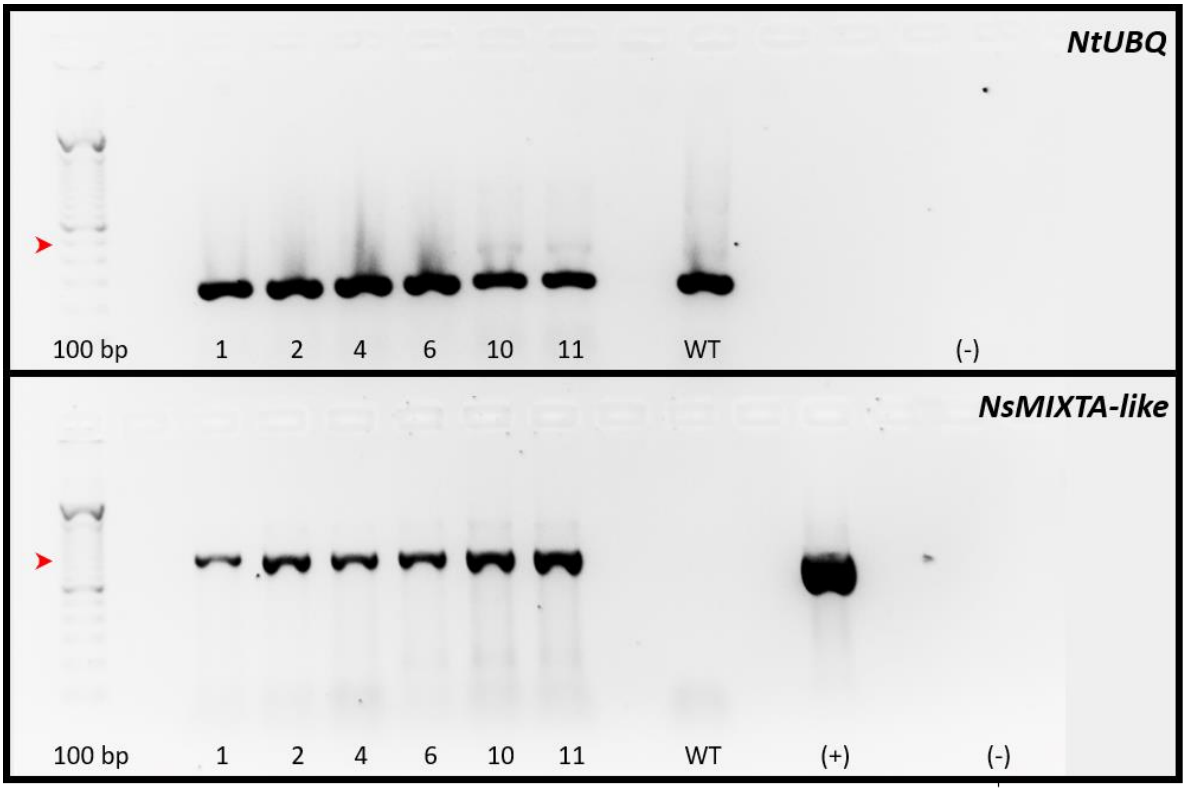

Figure 2.14. PCR screening for expression of transgene *NsMIXTA-like* in putative transgenic lines of *N. tabacum*.

Upper panel shows RT-PCR products of *NtUBQ* (expected size 248 bp, red arrow head) in eight putative transgenic lines and the wild type (WT). Lower panel shows RT-PCR products of *NsMIXTA-like* (expected size 889 bp, red arrow head) in six putative transgenic lines and the WT. Negative control (-) shows the product of water as template in the reaction. Positive control (+) shows the product of 1 µl (1:100 dilution) of a plasmid vector carrying the transgene *NcMIXTA-like*.

2.4.4.2 *Morphological characterization of* NcMIXTA-like *and* NsMIXTA-like *transgenic lines of* N. tabacum

Figure 2.15 shows leaf and flower macromorphology of *N. tabacum* WT compared to selected transgenic lines overexpressing *NcMIXTA-like* (line 14) and *NsMIXTA-like* (line 11). Macromorphological features for other transgenic lines characterized are depicted in Appendix 9. At the macromorphological level no evident differences were detected between the WT and the transgenic lines. Multiple branching in some transgenic lines (compared to the single axis of the WT) is likely an artefact derived from the manipulation of the plantlets during tissue culture (*e.g.* Appendix 9 *NcMIXTA-like* line 17, Plate I and *NsMIXTA-like* line 14, Plate II).

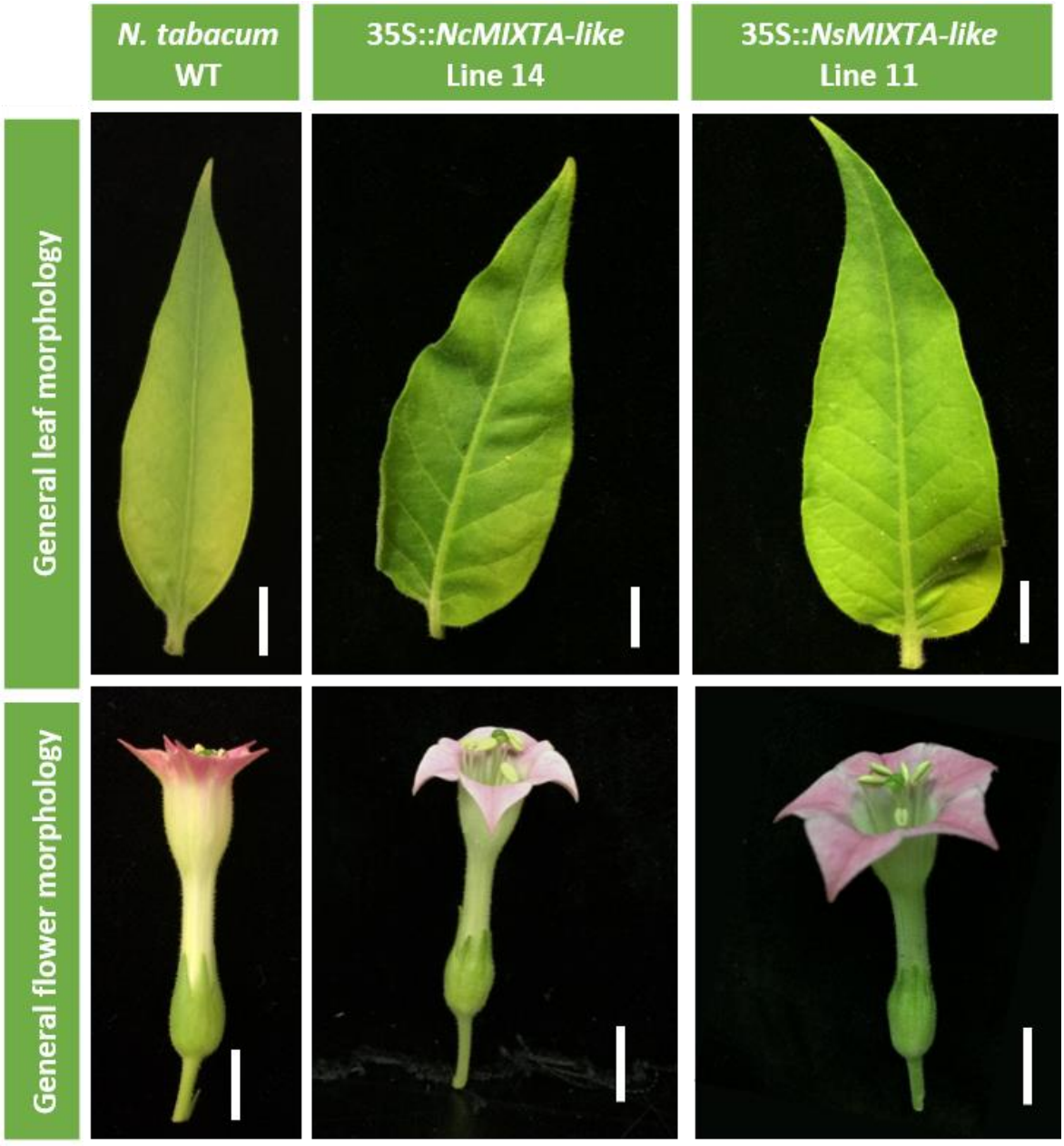

Figure 2.15. Ectopic expression of *NcMIXTA-like* and *NsMIXTA-like* in *N. tabacum* has little effect on the phenotype of macromorphological features.
Top: Transgenic lines sometimes presented partially revolute margins compared to the wild type. Bottom: There were no obvious macromorphological differences between the WT and the transgenics. Scale bars = 10 mm.

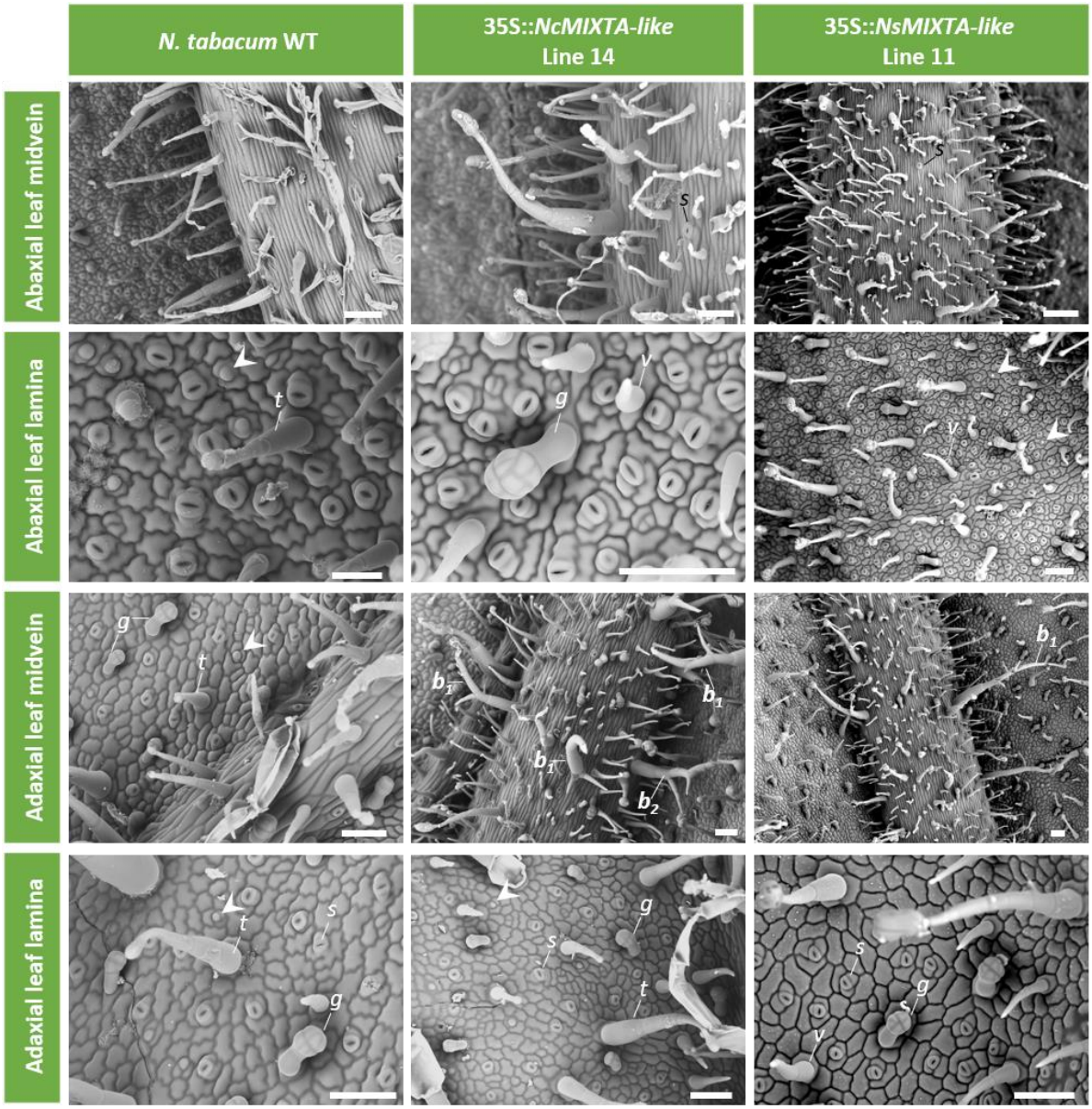

Figure 2.16. Effect of ectopic expression of *NcMIXTA-like* and *NsMIXTA-like* on leaf epidermis of *N. tabacum*.

Branched trichomes (b_1, b_2) are only present on the adaxial surface of the midrib in the transgenic lines. S: stomata; t: simple trichome, g: glandular trichome, arrow heads: epidermal outgrowths in early developmental stages. Scale bars= 100 µm.

Figure 2.16 shows cryo-SEM microphotographs of leaf surfaces of *N. tabacum* WT compared to selected lines overexpressing *NcMIXTA-like* (line 14) and *NsMIXTA-like* (line 11). The abaxial surface of the midvein in both WT and transgenics is covered by simple trichomes (*t*) composed of 1 to 5 cells. The abaxial and adaxial lamina in both the WT and the transgenics present simple trichomes (*t*) and glandular trichomes (*g*). Branched trichomes (*b*) with either vestigial (b_1) or well-developed secondary branches (b_2) are only present on the adaxial surface of the midrib in the transgenic lines. Cryo-SEM images of epidermal surfaces of additional *N. tabacum* WT and

transgenic lines examined are in Appendix 9, Plate III to Plate XXV. Epidermal features of *N. tabacum* lines expressing NsMIXTA-like (line 14).

Comparison of the petal surfaces of *N. tabacum* WT and selected transgenic lines expressing *NcMIXTA-like* (line 14) and *NsMIXTA-like* (line 11) is depicted in Figure 2.17. Simple trichomes are present on the abaxial surfaces of the petal of both the WT and the transgenics, however, in the WT the trichomes are mostly restricted to the zone along the midvein of the petal and the margins of the lobes, whereas in the transgenic lines they are spread around all the surface of the petal. Both the abaxial and the adaxial surface of *N. tabacum* WT have conical cells, which makes it difficult to assess any effect the expression of the candidate genes may have on the morphology of these cells. The adaxial surface of the petal of the transgenic lines also presents conical cells, however, on petals derived from both constructs (*NcMIXTA-like* and *NsMIXTA-like*) some of the cells are clavate (*c*, Figure 2.18, Figure 2.17) in shape rather than papillate (arrow heads, Figure 2.17). Stomata are present on the abaxial petal surfaces of both the WT and the transgenic lines.

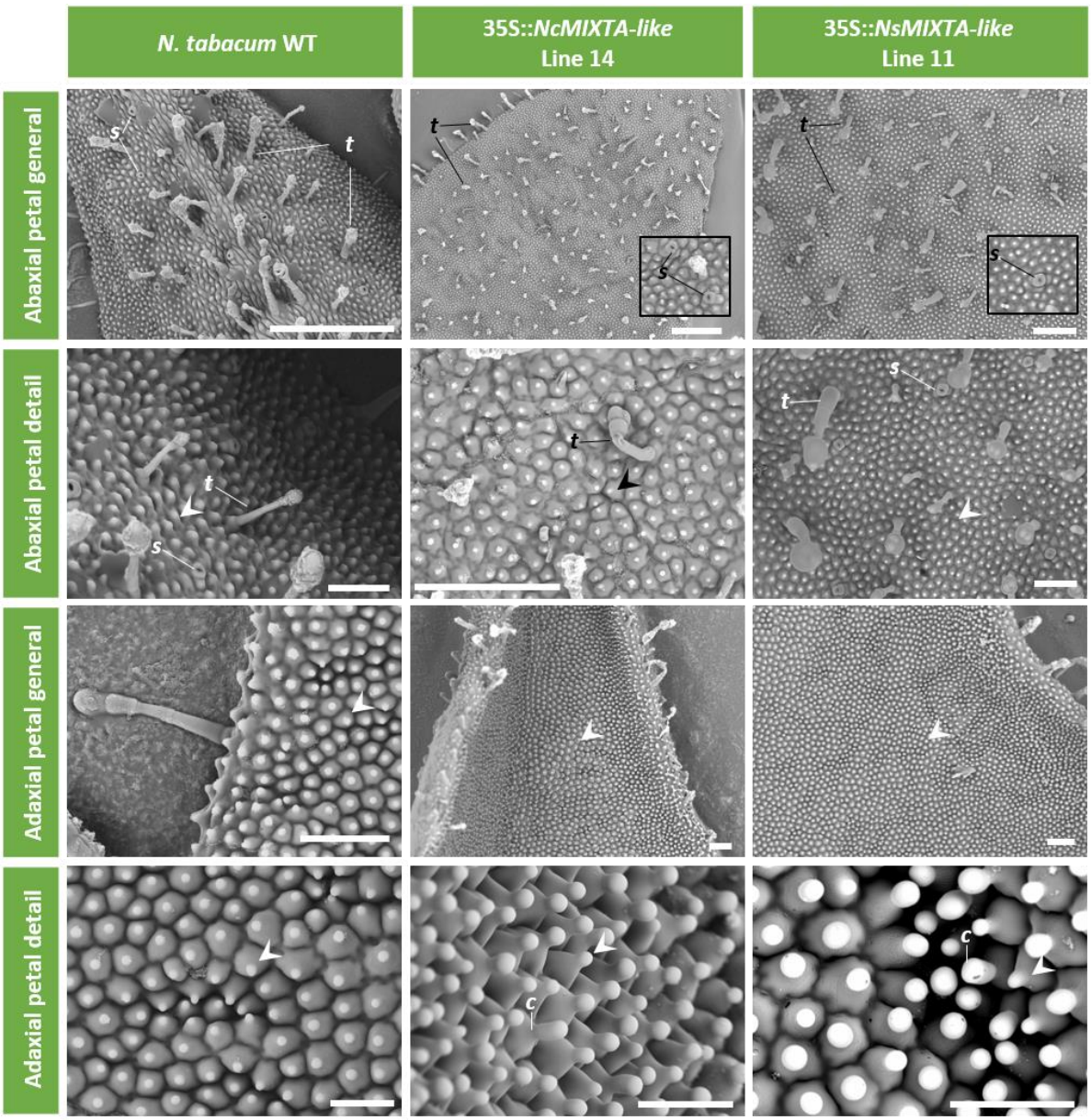

Figure 2.17. Ectopic expression of *NcMIXTA-like* and *NsMIXTA-like* affects the morphology of epidermal cells on petals of *N. tabacum*.

Simple trichomes *(t)* and stomata *(s)* are present on the abaxial surface of both the WT and the transgenics. Conical cells (arrow heads) are present on the abaxial and adaxial surfaces of both the WT and the transgenics, however, some epidermal cells on the adaxial surface of the transgenic lines are clavate *(c)* in shape rather than conical. Scale bars: First row=500µm, second and third row= 100 µm, fourth row= 50 µm.

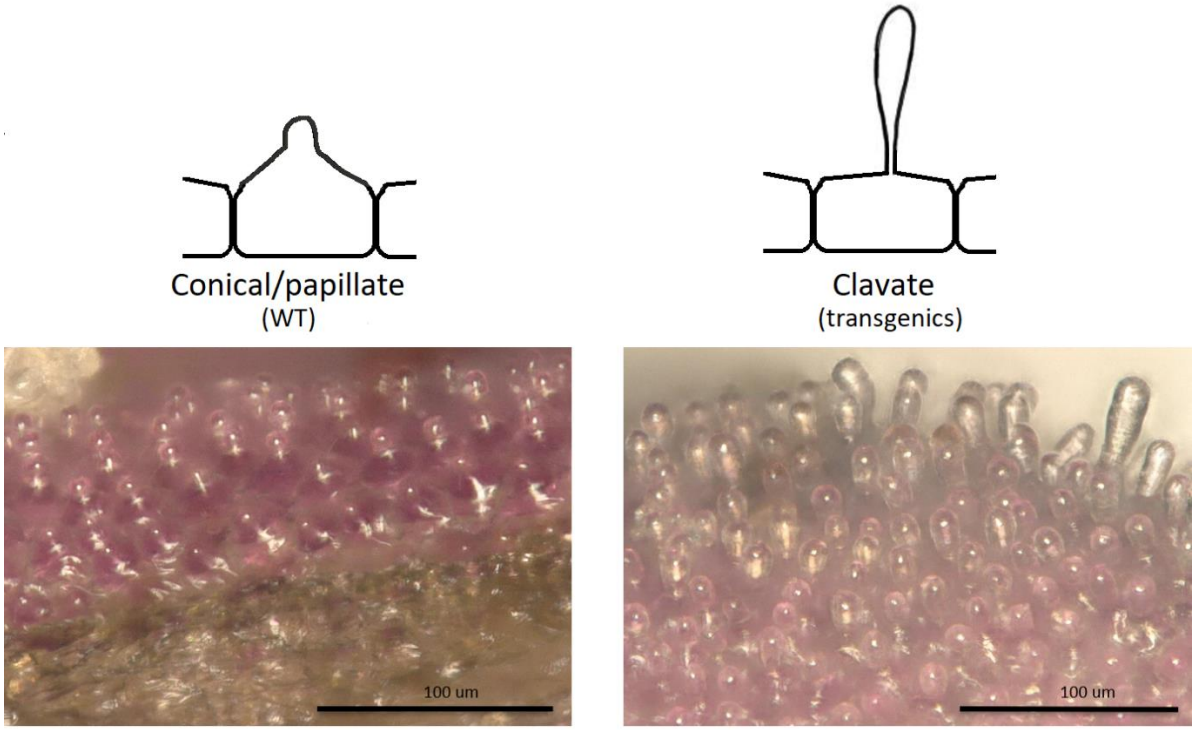

Figure 2.18. Conical/papillate cells are characteristic of the adaxial petal surface of *N. tabacum* WT whereas clavate cells are common in transgenic lines expressing R2R3 MYB gene constructs from other *Nicotiana* species.

Simplified diagrams (top) and digital stero microscope images (bottom) of adaxial epidermal cells of petals of *N. tabacum*. WT (left) and transgenic line overexpressing *NbMYB17-1* (right). Conical cells present a basal width/height ratio between 1.5 and 0.5, papillate is a term refered to conical cells when the tip of the cell ends in a nipple-like projection. Clavate cells present a basal width/height ratio between 0.5 and 0.15 and might represent transitional forms toward trichomes, hair-like epidermal structures with basal height/width ratios lower than 0.15 (*e.g.* **t** in Figure 2.17). Quantitative delimitations of epidermal cell structures adapted from Barthlott & Ehler, 1977.

Anther features for *N. tabacum* WT and transgenic lines of *NcMIXTA-like* and *NsMIXTA-like* are pictured in Figure 2.19. The epidermal cells of the anther in *N. tabacum* WT are in general pyramid shaped striated conical cells (arrow heads, Figure 2.19). Scarce epidermal outgrowths (*e*, Figure 2.19) are sometimes present mostly on the proximal flanks and the base of the anther sacs. Epidermal outgrowths were more common and more pronounced in lines overexpressing either of the constructs (*NcMIXTA-like* or *NsMIXTA-like*) than in the WT. Moreover, the surface of the tip of the filament of some lines presented conical cells (*NsMIXTA-like* Line 11, Figure 2.19) a phenotype not occurring in the WT. Self-pollination occurred spontaneously in all putative lines overexpressing *NcMIXTA-like* and *NsMIXTA-like* which suggest that the epidermal features derived from the expression of the candidate genes did not prevent anther dehiscence.

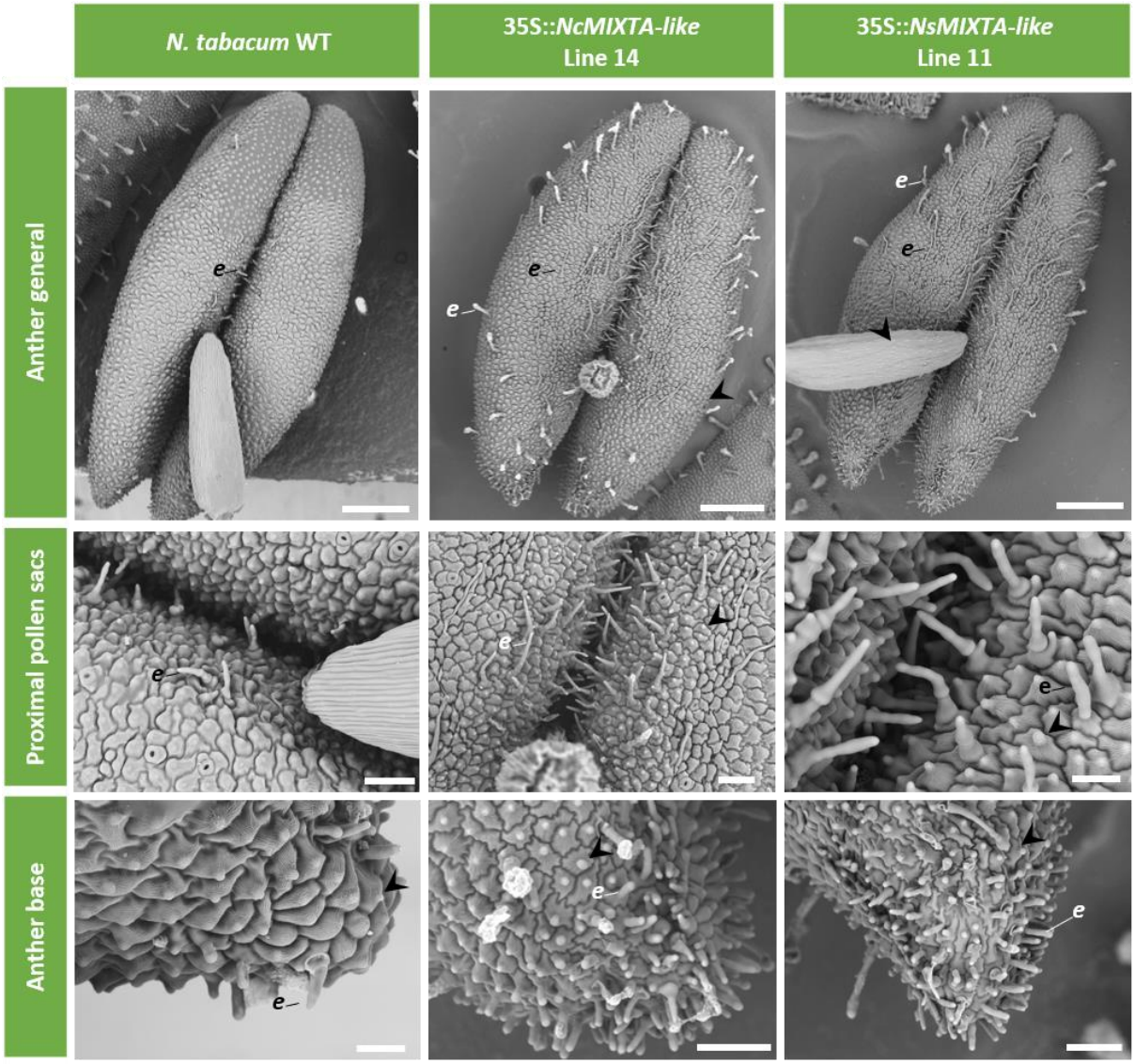

Figure 2.19. Ectopic expression of *NcMIXTA-like* and *NsMIXTA-like* increases the number and size of epidermal features on the anther surface of *N. tabacum* transgenic lines.
Epidermal outgrowths (*e)* and conical cells (arrow heads) are more prominent and abundant in the transgenic lines than in the wild type. Conical cells are present on the filament of the transgenic lines (panel top right) but not on the WT (top left). Scale bars: First row=500µm, second and third row=100 µm.

The surface of the carpel in *N. tabacum* WT is smooth with dome-shaped epidermal cells, this makes it ideal for comparisons of epidermal features between the WT and putative transgenic lines potentially presenting epidermal outgrowths (Figure 2.20). Both groups of lines, those expressing *NcMIXTA-like* and those expressing *NsMIXTA-like*, presented epidermal protrusions on the surface of the carpel (arrow heads Figure 2.20, Appendix 9, Plate VII, Plate IX, Plate XI, Plate XIII, Plate XV, Plate XVII, Plate XXI, Plate XXII, Plate XXV). *NcMIXTA-like* line 14 (Figure 2.20) (Plate IX) and *NsMIXTA-like* line 11 (Figure 2.20)(Appendix 9, Plate XXI) presented the most pronounced phenotype compared to other transgenic lines of the same construct. These lines had conical cells with pointy tips on all the surface of the carpel, being more evident at the

base. Lines with intermediate to strong phenotypes are *NcMIXTA-like* 15 (Plate IX), line 16 (Plate XIII) and line 19 (Plate XV), and *NsMIXTA-like* 10 (Plate XIX), line 11 (Plate XXI) and line 13 (Plate XXIII). Lines with a weaker phenotype had sparse patches of conical cells on the surface and/or at the base of the carpel, these included *NcMIXTA-like* lines 8 (Appendix 9, Plate XVII) and line 10 (Appendix 9, Plate VII). Interestingly, *NsMIXTA-like* line 14 (Appendix 9, Plate XXV) presented numerous stomata at the base of the carpel, a phenotype not present in the WT or in any of the other lines.

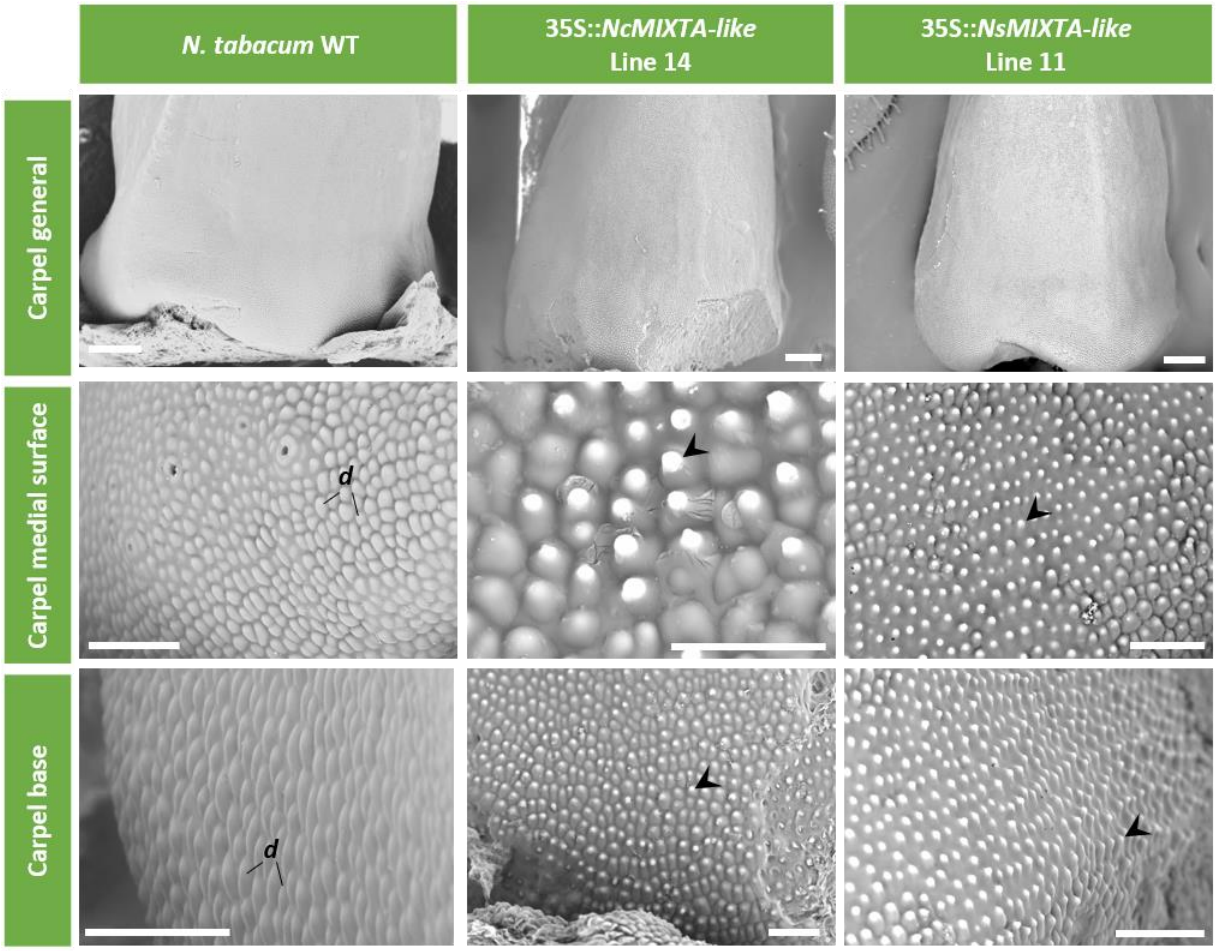

Figure 2.20. Expression of *NcMIXTA-like* and *NsMIXTA-like* promotes ectopic growth of conical cells on the carpel surface of *N. tabacum* transgenic lines.
The presence of pointy conical cells (arrow heads) on the surface of the carpel of the transgenic lines, compared to the smooth dome shaped cells of the wild type (d), is the most striking phenotype derived from the transgene expression. Scale bars: First row=500µm, second and third row= 100 µm.

In general, these results demonstrate that the ectopic expression of both *NcMIXTA-like* and *NsMIXTA-like* in *N. tabacum* promote ectopic epidermal outgrowths. No evident differences were detected between the phenotypes of the transgenic lines overexpressing *NcMIXTA-like*, the *MIXTA-like* orthologue from the non-conical celled species *N. cordifolia*, compared to those

expressing *NsMIXTA-like*, the *MIXTA-like* orthologue from the conical-celled species *N. solanifolia*.

2.5 DISCUSSION

2.5.1 Sequences of R2R3 Subgroup 9 MYB transcription factors in *N. cordifolia* and *N. solanifolia*

Single mutations can have drastic consequences for protein structure, function and associated phenotype. The detailed characterization of R2R3 MYB Subgroup 9 genes in *N. cordifolia* and *N. solanifolia* allowed the detection of differences between the coding sequences of the non-conical and the conical celled species that potentially would have an effect on the function of the native protein. The genes characterized within the R2R3 MYB Subgroup 9A belong to the two different subclades: *MIXTA-2* to the subclade *MIXTA* and *MIXTA-like* to the subclade *MIXTA-like*. These genes presented contrasting patterns when comparing the sequences of orthologues between sister species. *MIXTA-2* was conserved between the species with only two nucleotides (one amino acid) difference between orthologues of sister species. The substitution detected involved a shift from leucine (L) in the conical-celled species *N. solanifolia* to valine (V) in the non-conical celled species *N. cordifolia*. Considering that the chemical properties of these two amino acids are similar, that they lay in an exposed region of the protein, not coinciding with any secondary protein structure, close to the C terminal of the protein, this amino acid shift was interpreted as not likely to promote effects in the protein function.

On the other hand, the orthologues of *MIXTA-like* presented several differences between sister species. The potential effect of each of these differences in the putative protein encoded by the genes varied greatly. Two of the six amino acid changes detected fall in the MYB DNA binding motif (K23Q and E45G, Figure 2.11). Amino acid shifts occurring in key protein motifs are expected to have a stronger effect on the function of the native protein. The effect of point mutation score for the shift from lysine (K) to glutamine (Q) in position 23 is -93 (Figure 2.11). Negative scores are expected to have neutral or no effect on the protein function. K and Q are both acyclic large polar amino acids of surface. The mass shift between K and Q is 0 and they can be substituted for each other with 95% confidence (Bordo & Argos, 1991). In the case of the shift of glutamic acid (E) for glycine (G) the score of point mutation is +29 (Figure 2.11). Mutations with positive scores are predicted to potentially have an effect on the protein function. The chemical properties of these two amino acids are contrasting: E is an acyclic acidic

polar large amino acid, whereas G is an aliphatic neutral small amino acid. The mutation mass shift between E and G is 72 Da, a significative difference in size especially considering that the shift occurs in a buried region of the protein and three residues away from a helix secondary structure (Figure 2.11). The remaining amino acid shifts detected between *NsMIXTA-like* and *NcMIXTA-like* have negative scores (V143A (-37), P232T (-7), S381C (-8)) or low positive scores (F351L (+3)). These point mutations are thus expected to have neutral or no effect on the protein function. A 15-nucleotide deletion was detected in *NsMIXTA-like* compared to *NcMIXTA-like* and *MIXTA-like* orthologues from other *Nicotiana* species (Appendix 7). This deletion corresponds to a polyglycine stretch close to the C terminus of the protein (Figure 2.10 and Figure 2.11). Polyglycine stretches have been demonstrated to play a role in protein-protein interaction and intracellular mobility (Inoue & Keegstra, 2003).

For the R2R3 MYB Subgroup 9B clade, only representatives of the subclade *MYBI7* occur in *Nicotiana* (section 1.4.2). There are no genes of the subclade *MYBI7-like* in *Nicotiana*. Two genes of the *MYBI7* subclade (*MYBI7-1* and *MYBI7-2*) were cloned from *N. solanifolia* and *N. cordifolia*. The coding sequences of *NcMYBI7-1* and *NsMYBI7-1* were found to be highly conserved, with no differences detected between sister species (Appendix 7C). *MYBI7*-2 was also found to be conserved between the two species, however there was variation detected among individuals of *N. solanifolia*. In some individuals the coding sequence of *NsMYBI7-2* was identical to that of *NcMYBI7-2* and in others there were nucleotide substitutions that were mostly synonymous. Although *NsMYBI7-2*, the orthologue from the conical-celled species, was found to be labile in some positions of the nucleotide sequence, the fact that at least some individuals present identical sequence to *NcMYBI7-2*, the orthologue of the non-conical celled species, suggests that the substitutions detected in *MYBI7-2* are not responsible for the differences in the phenotype of the two species.

2.5.2 Heterologous expression of *NcMIXTA-like* and *NsMIXTA-like* in *N. tabacum*

Because of the sequence differences detected between the *MIXTA-like* orthologue of the conical celled species *N. solanifolia* and that of the non-conical celled species *N. cordifolia*, *MIXTA-like* was selected to further explore the protein function of the alternative sequences of each one of the sister species. Ectopic expression of *NcMIXTA-like* and *NsMIXTA-like* in *N. tabacum* allowed us to test whether there was any loss of function of the protein between non-conical and conical celled species. If the sequence differences detected between the orthologues of *MIXTA-like* were solely responsible for the differences in petal cell shape between *N. cordifolia* and *N. solanifolia*,

we would expect major differences between the phenotypes resulting from the overexpression of *NsMIXTA-like* (the orthologue from the conical celled species *N. solanifolia)* compared to the phenotype of lines overexpressing *NcMIXTA-like* (the orthologue from the non-conical celled species *N. cordifolia*). Overexpression of *NsMIXTA-like* (conical-celled species) would be hypothesized to result in the enhanced production of epidermal outgrowths compared to *NcMIXTA-like.* However, heterologous expression in *N. tabacum* under a strong constitutive promoter, (double CaMV 35S) demonstrated that both orthologues function as positive regulators of epidermal outgrowths, including conical cells. In the poliploid *N. tabacum* here may be some redundancy in function between the paralogues, such that their combined expression has effects on cell shape in a dosage-dependent manner (Schranz et al., 2002). However, the phenotypic effects observed in the transgenic lines are considered to be derived from the action of the transgene, under a strong constitutive promoter, and is confirmed by the independent transgenic lines with similar phenotypes, morphologically different from the wild type.

The functions of various R2R3 Subgroup 9 genes have been characterized for several Core Eudicot species, including some in the Order Solanales (Table 2.7, Table 3.5). Ectopic expression of R2R3 Subgroup 9 genes in *N. tabacum* has been extensively used to test the function of these genes. However, the function of R2R3 Subgroup 9 transcription factors from other *Nicotiana* species (including *N. tabacum*) had not been experimentally tested by expression in *N. tabacum* previously. Most of the subgroup 9 genes that have been functionally characterised in angiosperms belong to the subgroup 9A clade, to which *MIXTA-like* belongs. In general, these functional studies have demonstrated that subgroup 9A gene members are positive regulators of epidermal cell projections such as trichomes and conical petal cells (Glover *et al.*, 1998; Perez-Rodriguez *et al.*, 2005; Alcorn, 2013; Reed, 2014; Bailes, 2016). The phenotypes of *N. tabacum* lines overexpressing *NcMIXTA-like* and *NsMIXTA-like* do not differ considerably from each other (section 2.4.3.2.). Table 2.7 shows a comparison of the epidermal features associated with ectopic expression of R2R3 Subgroup 9A genes from different angiosperm species in *N. tabacum*. The characteristic phenotype of *NcMIXTAlike* and *NsMIXTAlike* ectopic expression lines can be considered similar to the phenotypes derived from expressing in tobacco genes belonging to the *MIXTA-like* subclade from other angiosperms: *AmMYBML1, AmMYBML2* and *AmMYBML3* from *Antirrhinum majus* (Glover *et al.*, 1998; Perez-Rodriguez *et al.*, 2005; Jaffé *et al.*, 2007)*; VfML8* and *VfML64* from *Vicia faba* (Bailes, 2016); and *SlML*, *SaML* and *ScML* from several *Solanum* species (Alcorn, 2013). In general, transgenic lines expressing *MIXTA-like* genes have been shown to present weaker phenotype compared to those expressing genes from other subclades

of R2R3 MYB Subgroup 9, including representatives of the *MIXTA* subclade (Glover *et al.*, 1998; Perez-Rodriguez *et al.*, 2005; Alcorn, 2013).

Ectopic expression of R2R3 subgroup 9A genes (*MIXTA* and *MIXTA*-like) from *Solanum* species with contrasting petal cell shape was carried out by Alcorn (2013) and Davis (2016). Both types of constructs including orthologues from non-conical celled species and from conical celled species, were shown to promote ectopic conical cells on the surface of the carpel. This suggests that there is no loss of function between the non-conical and the conical celled species, similarly to the findings for *Nicotiana* in the current work.

2.5.3 Molecular control of petal cell shape in *N. solanifolia* and *N. cordifolia*

Given that the sequences of *MIXTA-2*, *MYBI7-1* and *MYBI7-2* are conserved between the two sister species, and that it was experimentally demonstrated that the sequence differences between *MIXTA-like* orthologues are not likely to be responsible for petal cell shape differences between *N. solanifolia* and *N. cordifolia*, it is necessary to consider alternative mechanisms in which one or more of the four candidate genes might be involved. The results of this work suggest that the *N. cordifolia* (non-conical celled species) MYB subgroup 9 proteins are still functional, and that loss of conical cells in this species is more likely to be due to a change in MYB subgroup 9 expression, or due to a change in another gene upstream or downstream in the same developmental pathway.

Any differential expression may occur between sister species and/or between developmental stages of the petal. To experimentally address these hypotheses, it would be necessary to do a detailed characterization of the development of the petal in both species to assess the precise stage in which conical cells develop in *N. solanifolia*. Molecular characterization of the expression could be then be performed by comparing expression levels of candidate genes in the petals of both species at key developmental stages. Unfortunately, as mentioned in section 2.4.1, no flowering occurred for the specimens of *N. solanifolia* and *N. cordifolia* growing in Cambridge.

2.5.4 Petal cell shape and plant pollinator interactions in Section *Paniculatae*

There are two main questions to address related to petal cell shape and its role in the interaction with the pollinators in Section *Paniculatae*: (1) Why conical cell shape is the prevalent state of

Table 2.7. Phenotypic effect on epidermal features of the heterologous expression of R2R3 MYB Subgroup 9A subclade genes in *N. tabacum*

Species (adaxial petal cell shape)	Gene Clade	Gene Subclade	Gene name	Phenotype of the epidermis in the transgenic lines							Reference
				Ovary	Anther	Stamen filament	Petal abaxial	Petal adaxial	Leaf adaxial	Leaf abaxial	
Cabomba caroliniana (conical in inner whorl tepal tips)	SB9A	Early diverging	*CcSBG9A-1*	Ectopic conical cells, multicellular trichomes	Conical cells protruding further than WT, irregular shaped; multicellular trichomes	Ectopic cell protrusions	Not reported	Longer tip of conical cells; multicellular trichomes	Majority of cells with single central outgrowth; long-stalked, multicellular branched trichomes		Reed, 2014
Thalictrum thalictroides (conical cells on adaxial petaloid sepal)	SB9-A	Early diverging	*TtMYBML2*	Ectopic conical cells				Increased length, tips elongated			
Vicia faba (conical in the wing petals)	SB9-A	MIXTA	*VfMIXTA*	Ectopic conical cells, multicellular trichomes, branched trichomes	Increased trichomes, branched trichomes	Increased trichomes, branched trichomes	Increased trichomes, branched trichomes	Increased trichomes, branched trichomes	Increased trichomes, branched trichomes	Increased trichomes, branched trichomes	Bailes, 2016
		MIXTA-like	*VfML8*	Conical cells	Ectopic conical cells on the slit zone	Ectopic conical cells	WT phenotype	WT phenotype	WT phenotype	WT phenotype	Bailes, 2016
			VfML64	Ectopic (shallow)conical cells	WT phenotype	WT phenotype	WT phenotype	WT phenotype	WT phenotype	WT phenotype	Bailes, 2016
Arabidopsis thaliana (conical in WT)	SB9-A	MIXTA-like	*AtMYB16*	Ectopic conical cells				Increased length, tips elongated			Baumann *et al* ., 2007
Antirrhinum majus (conical in WT)	SB9-A	MIXTA	*AmMIXTA*	Simple and multicellular glandular trichomes, vestigial branches on trichomes and trichome heads				Conical cells developed into trichomes, simple and long stalked glandular trichomes	Majority of cells with single central outgrowth; long-stalked, multicellular branched trichomes (branching type b_1)	Ectopic conical cells	Perez-Rodriguez, 2005; Glover et al., 1998
Antirrhinum majus (conical in WT)		MIXTA-like	*AmMYBML1*	Simple 1-2 celled trichomes, conical cells	Ectopic conical cells			Glandular trichomes	Wild type in appearance	Wild type in appearance	Perez-Rodriguez, 2005
			AmMYBML2	Ectopic conical cells	Ectopic conical cells	Ectopic conical cells		Conical cells longer than in WT	Ectopic conical cells	Ectopic conical cells	Perez-Rodriguez, 2005;Baumann, 2007
			AmMYBML3	Ectopic (shallow)conical cells	WT phenotype	WT phenotype	WT phenotype	Conical cells longer than in WT	Wild type in appearance	Wild type in appearance	Jaffe et al., 2007

Continuation Table 2.7

Species (adaxial petal cell shape)	Gene Clade	Gene Subclade	Gene name	Phenotype of the epidermis in the transgenic lines							Reference
				Ovary	Anther	Stamen filament	Petal abaxial	Petal adaxial	Leaf adaxial	Leaf abaxial	
Petunia hybrida (conical in WT)	SB9-A	MIXTA-like	*PhMYB1*	Ectopic conical cells				Conical cells longer than in WT			Baumann et al., 2007
Solanum laciniatum (conical)	SB9-A	MIXTA-like	*SlML*	Ectopic conical cells (irregular), occasionally stomata	WT phenotype	WT phenotype	WT phenotype	WT phenotype	WT phenotype	WT phenotype	Alcorn, 2013
Solanum aviculare (non-conical)	SB9-A	MIXTA-like	*SaML*	Ectopic conical cells (patches)	WT phenotype	WT phenotype	WT phenotype	WT phenotype	WT phenotype	WT phenotype	
Solanum sisymbriifolium (conical)	SB9-A	MIXTA	SsMx	Conical cells, unicellular to multicellular trichomes	WT phenotype	WT phenotype	WT phenotype	Ectopic stomata and trichomes in the corolla tube	WT phenotype	WT phenotype	
		MIXTA-like	*SsML*	Ectopic conical cells (all cells)	WT phenotype	WT phenotype	WT phenotype	WT phenotype	WT phenotype	WT phenotype	
Solanum capsicoides (non-conical)	SB9-A	MIXTA	*ScMx*	Patchy conical outgrowths, intermittent multicellular glandular trichomes	WT phenotype	WT phenotype	WT phenotype	Ectopic stomata and trichomes in the corolla tube	WT phenotype	WT phenotype	
		MIXTA-like	*ScML*	Ectopic conical cells (tall, in all cells), rarely stomata	WT phenotype	WT phenotype	WT phenotype	WT phenotype	WT phenotype	WT phenotype	
Solanum lycopersicum (conical)	SB9-A	MIXTA	*SlMIXTA-1*	Ectopic conical cells abundant on the surface	Fingerlike epidermal outgrowths on connective, conical cells on anther surface	Conical cells sometimes present, sparce	WT phenotype	Conical cells on the corolla lobes (as in WT), also present on the corolla tube	Conical cells present	Conical cells present	Davis, 2019
			SlMIXTA-2	Ectopic stomata on the carpel surface	Fingerlike outgrowths on the connective			WT phenotype	Branched trichomes on veins	WT phenotype	
			SlMIXTA-3	Incipient conical cells on the carpel surface	Sparce epidermal otgrowths on the connective			WT phenotype on the corolla lobes, incipient conical cells on the corolla tube			
			SlMIXTA-4	Conical cells and sparse fingerlike outgrowths	Glandular trichomes on connective, conical cells on the anther sacs surface		WT phenotype	WT phenotype	WT phenotype	WT phenotype	
	SB9-A	MIXTA-like	*SlMIXTA-like-1*	Conical cells on the carpel surface	Fingerlike outgrowths abundant on the connective and sparce on the anther sacs			WT phenotype on the corolla lobes, conical cells on the corolla tube	Conical cells on the laminar tissue, branched trichomes present	Conical cells on the laminar tissue	
	SB9-B	MYB17	*SlMYB17-1*	Prominent, widespread conical cells on the carpel surface	Long, fingerlike outgrowths on all surfaces, sparce stalked stomata	Fingerlike outgrowths, conical cells		WT phenotype on the corolla lobes, conical cells on the corolla tube		Branched trichome present	
			SlMYB17-2	Long, fingerlike outgrowth abundant on the carpel surface	Fingerlike outgrowths mostly on the connective			WT phenotype on the corolla lobes, trichome on the corolla tube	Branched trichomes present	Conical cells present	
Nicotiana cordifolia (non-conical)	SB9-A	MIXTA-like	*NcMIXTA-like*	Ectopic conical cells	Increased trichomes, branched trichomes present	Ectopic conical cells	Increased trichomes	Conical cells longer than in WT (papillate and clavate)	Branched trichomes on midrib	WT phenotype	This work (Chapter 2)
Nicotiana solanifolia (conical)	SB9-A	MIXTA-like	*NsMIXTA-like*	Ectopic conical cells	Increased trichomes, branched trichomes present	Ectopic conical cells	Increased trichomes	Conical cells longer than in WT (papillate and clavate)	Branched trichomes on midrib	WT phenotype	

character in the Section and (2) What are the evolutionary and/or ecological mechanisms that have resulted in the loss of conical cells in *N. cordifolia*.

As mentioned in section 1.2.2.2, the absence of conical cells on flower petals is thought to be related to the transition from insect to bird pollination. As birds do not experience the surface of the petal, as small insects would do, the function of conical cells in enhancing grip could be lost (Papiorek *et al.*, 2014; Ojeda *et al.*, 2016). However, if pollination in the mainland species of Section *Paniculatae* is thought to be mostly by birds, it is not clear why all the species in the continent have kept conical cells on their petals. Potentially, continental species in Section *Paniculatae* have mixed pollination systems, in which small pollinators that interact with the petal surface still serve as pollinators in addition to birds.

On the other hand, the geographic and ecological distance of *N. cordifolia* from its close relatives on the continent might help to understand why conical cells are absent from the petals of this species. Ojeda *et al.*, (2016) have done pairwise comparisons between angiosperm species in Macronesian oceanic island and their closest continental relatives. They hypothesize that there is a tendency to shift from insect pollination in the continental species to bird pollination in the islands and that this shift might be accompanied by a loss of conical cells on the petals of the island's species. In oceanic islands the diversity and abundance of insects is relatively low (Chamorro *et al.*, 2012). The Juan Fernández Islands insect fauna is small in general and is notably lacking species dedicated to floral visits (Anderson *et al.*, 2001). As there would be no animal pollinators that benefit from the presence of conical cells, and the energetic cost of building conical cells might be higher than that of building non-conical cells, the character might be lost.

The same logic could be applied if the oceanic island species is self-compatible. A high prevalence of self-compatible species (80%) has been reported for the Galápagos Islands (Chamorro *et al.*, 2012)). This reproductive strategy is also common in other oceanic islands and is attributable to the poor insular pollinator faunas compared with those on continents (Barrett, 1996). A similar pattern occurs in the Juan Fernández (Anderson *et al.*, (2001)). Anderson *et al.*, (2001) reports *N. cordifolia* in the group of species endemic to the Juan Fernández Islands that are self-compatible but that are not facultative selfers. Although self-compatible, this species is herkogamous (*i.e.* anthers and stigma spatially separated), and thus requires pollen transfer (Anderson *et al.*, 2001).

Local wardens in the Juan Fernández Archipelago think that the pollination in *N. cordifolia* is by wind (Sáez-Quintana, personal communication, 2018). Although there are no studies to confirm that this is the case, a potential shift to anemophily could be also considered for *N. cordifolia*. Anemophily is thought to occur in low levels in South American oceanic islands such as the Galápagos (Chamorro *et al.*, 2012). Flowering plant species surveyed in these islands were found to not produce large amounts of pollen, and no floral morphologies typically associated with wind pollination (*e.g*. exserted stamens) are common in this flora (Chamorro *et al.*, 2012). The reasons for such a low level of anemophily in the Galápagos are suggested to be related to the abiotic conditions of these islands: in the lowlands, most flowering takes place in the warm rainy season, while in the highlands, many flowers are produced during the cool season and both rain and humidity reduce the efficiency of wind pollination (Chamorro *et al.*, 2012). *N. cordifolia* flowers between the months of November and January and grows on crevasses in rocky cliffs (see section 2.2.3). Pollen production in this species has been assessed by Anderson *et al.*, (2001) at 85,000 pollen grains per flower. This value is relatively high within the range of species of the Juan Fernández islands studied (2,667 to 133,439 pollen grains per flower; Anderson *et al.*, 2001). From this information is not possible to rule out anemophily as a likely pollination mechanism prevailing in natural conditions for *N. cordifolia*.

Local wardens in the island have also reported visits by flies and other Diptera to *N. cordifolia* (Sáez Quintana, personal communication, 2018). Dipterans are important flowering plant pollinators and are reported as the insects that most frequently visited flowers in the humid zone of the Galapagos (Chamorro *et al.*, 2012) and in the Juan Fernández Archipelago itself (Anderson *et al.*, 2001). The dark-red flowers of *N. cordifolia* vaguely resemble the colours of sapromyophilous blossoms (flowers pollinated by carrion flies) that tend to be dark and mimic the substrate associated with their odours (carrion, dung, etc.) (Woodcock *et al.*, 2014). Moreover, there are examples of flies that are frequent visitors to blue-violet, pink or red flowers, often with tubular corollas and hidden nectar (Woodcock *et al.*, 2014). Considering an association with fly pollinators for *N. cordifolia* is interesting. However, given the field observations by Anderson (2001) in which hummingbirds were the predominant visitors of this species, the reported visits by Diptera could represent opportunistic feeding, rather than representing an established plant-pollinator association

Chapter 3.

Evolution and molecular control of petal epidermal cell morphology in Nicotiana *Section* Alatae

3 Evolution and molecular control of petal epidermal cell morphology in *Nicotiana* Section *Alatae*

3.1 SUMMARY

Sister species *Nicotiana bonariensis* and *N. forgetiana*, Section *Alatae*, present contrasting petal cell shape: *N. bonariensis* has non-conical cells whereas *N. forgetiana* has conical cells. This chapter focuses on assessing the role of candidate genes in the R2R3 MYB Subgroup 9 transcription factor family in petal cell shape identity of these sister species. Entire coding sequences of four candidate genes: *MIXTA-2* and *MIXTA-like* (Subgroup 9A) and *MYBI7-1* and *MYBI7-2* (Subgroup 9B) were obtained for both species. The predicted amino acid sequences were found to be conserved between *MIXTA-2*, *MIXTA-like* and *MYBI7-2* when comparing the two species. However, amino acid differences were detected between the predicted sequences of *MYBI7-1* when comparing *N. bonariensis* to *N. forgetiana*. *In silico* comparisons of these sequences allowed an approximation of the potential effect of the differences detected on the function of the putative coded protein. To test the functional effect of these differences, the two orthologues of *MYBI7-1*, one from *N. bonariensis* (*NbMYBI7-1*) and one from *N. forgetiana* (*NfMYBI7-1*), were ectopically expressed in *Nicotiana tabacum* using *Agrobacterium tumefaciens* mediated stable transformation. Both sets of *N. tabacum* transgenic lines, expressing *NbMYBI7-1* or *NfMYBI7-1*, presented ectopic epidermal outgrowths on vegetative and reproductive organs, phenotypes highly contrasting to those of the wild type *N. tabacum*. This confirmed that the two orthologues of *MYBI7-1* are positive regulators of epidermal outgrowths. These results suggest that the sequence differences detected between the genes from the two species cannot be responsible for the conical vs. non-conical phenotype. Semiquantitative RT-PCR (semiq-RT-PCR) gene expression analyses of the four candidate genes suggested higher expression levels of *MIXTA-2* in petals of the conical-celled species (*N. forgetiana*), compared to the non-conical one (*N. bonariensis*). Quantitative RT- PCR (qPCR) confirmed differential expression of *MIXTA-2* between the two species, and improved resolution of the patterns of expression of the other candidate genes. The role of petal cell shape in *Nicotiana* Section *Alatae*, specifically in *N. bonariensis* and *N. forgetiana,* is discussed.

3.2 INTRODUCTION

As has been mentioned previously (sections 1.4.1 and 2.2.2) petal cell shape has been characterized for the majority of the species of *Nicotiana* (Taylor, 2015; this work). A working hypothesis of the evolution of the character petal cell shape in the genus (Taylor, 2015; Figure 1.7) has allowed the detection of sister pairs of species that present contrasting characteristics of petal cell shape. Chapter 2 studies the evolution of petal cell shape in Section *Paniculatae*. The present chapter focuses on the evolution of petal cell shape in Section *Alatae*, specifically in the sister pair of species *N. bonariensis* Lehmann. (non-conical cells) and *N. forgetiana* Hort. Ex Hemsley (conical cells). This scenario of a sister pair of species with contrasting states of character (conical vs. non-conical) provides an exceptional opportunity to investigate the molecular changes that have given rise to differences in petal epidermal cell morphology. Moreover, it provides a system to compare to the mechanisms found to be involved in controlling petal cell shape in sister species *N. cordifolia* (non-conical) and N. *solanifolia* (conical) in Section *Paniculatae*, allowing analyses of how these mechanisms differ or converge between distantly related clades of *Nicotiana*.

3.2.1 Natural history and pollination of *Nicotiana* Section *Alatae*

Nicotiana section *Alatae* Goodsp. is one of 13 taxonomic sections within the genus. It is constituted by seven diploid species (chromosome number: n = 9, 10), distributed in Central and South America, predominantly from the eastern Andes to southeastern Brazil (Table 3.1) (Goodspeed, 1954; Knapp *et al.*, 2004; Clarkson *et al.*, 2004, 2010). Species of *N.* section *Alatae* are herbaceous rosettes with sessile, pubescent leaves. The flowers present a zygomorphic, salveform corolla, with a long, thin tube, that widens suddenly into a flat-faced limb, green, white or pink to red in colour. The corolla tube presents an abrupt dilation at the throat, and the corolla lobes are acute or rounded. Flowering is reported to be usually vespertine with flowers wilting in the day (Goodspeed, 1954; Knapp *et al.*, 2004; Clarkson *et al.*, 2004).

The monophyly of the section is well supported in phylogenetic analyses based on molecular markers and combined data sets (Chase *et al.*, 2003; Knapp *et al.*, 2004; Clarkson *et al.*, 2004). Three clusters of closely related species are supported in the phylogenies: *N. plumbaginifolia* and *N. longiflora* (n = 10), *N. alata* and *N. langsdorfii* (n = 9) and *N. forgetiana* and *N. bonariensis* (n = 9). *N. mutabilis*, one of the most recently described species in the genus, was initially placed in section *Alatae* on the grounds of morphology, habit, distribution and chromosome number

(Stehmann *et al.*, 2002). Phylogenetic analysis that have included *N. mutabilis* support this classification and show this species embedded in the n = 9 clade.

Section *Alatae* is noteworthy for its diversity of floral morphology, blooming phenology and mating systems (Goodspeed, 1954; Ippolito, 2000). Putative pollinators have been proposed for most species in the section (Ippolito, 2000)(Table 3.1).

Table 3.1. Species of *Nicotiana* Section *Alatae*: Geographic distribution and some distinctive characteristics

Species Name	Geographic Distribution	Petal Cell Shape	Flower Colour	Putative Pollinators	Reference
Nicotiana alata Link & Otto	Uruguay-Brazil and Argentina	Conical	White	Hawkmoths	(Ippolito *et al.*, 2004)
Nicotiana langsdorfii Weinm	Uruguay-Brazil-Argentina	Conical	Bright green	Hummingbirds, *Bombus* spp., Halictic bees	(Kaczorowski *et al.*, 2005)
Nicotiana bonariensis Lehm	SE Brazil, Argentina-Uruguay	Non-conical	White	Small perching moths	(Kaczorowski *et al.*, 2005)
Nicotiana forgetiana Hemsl	SE Brazil	Conical	Red	Hummingbirds, small bees, small hawkmoths	(Ippolito *et al.*, 2004)
Nicotiana longiflora Cav.	Uruguay-Brazil and Bolivia	Non-conical	White?	Hawkmoths	(Ippolito *et al.*, 2004)
Nicotiana mutabilis Stehmann & Samir	South Brazil	Conical	White-pink	Hummingbirds, others	(Stehmann *et al.*, 2002)
Nicotiana plumbaginifolia Viv.	Andes-NW Argentina	Non-Conical	White	Self-pollination	(Cocucci, 1988)

3.2.2 Evolution of petal cell shape in *Nicotiana* Section Alatae

Petal cell shape in *Nicotiana* section *Alatae* has been characterized for the seven species in the section (Taylor, 2015). Four species, *N. alata*, *N. langsdorfii, N. mutabilis* and *N. forgetiana,* have conical cells, and three, *N. bonariensis*, *N. longiflora* and *N. plumbaginifolia*, non-conical (Figure 3.1). Taylor (2015) mapped petal epidermal cell shape onto the phylogeny of the diploid species of *Nicotiana* (Figure 1.7)(Clarkson *et al.*, 2004). As mentioned in section 2.2.2, ancestral state for petal cell shape in the genus is ambiguous (Taylor, 2015). For Section *Alatae*, the ancestral state for the section is also ambiguous. Maximum Likelihood predicted a conical-celled ancestor and independent losses of conical cells, whereas parsimony suggested possible gains depending on the ancestral states (Taylor, 2015).

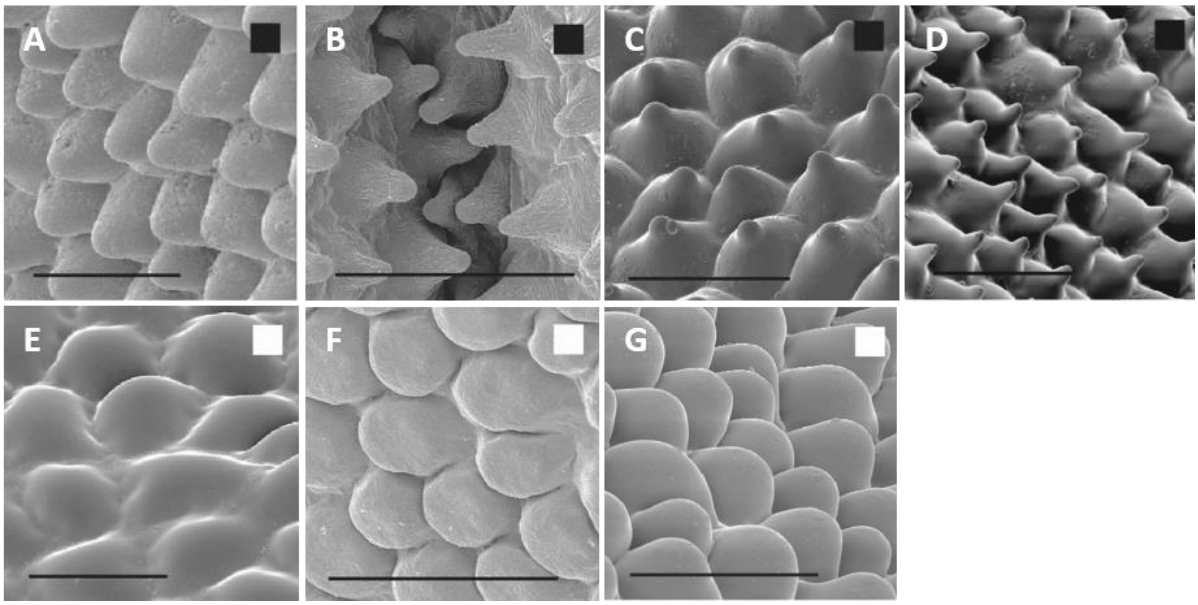

Figure 3.1. Diversity of petal cell shape in *Nicotiana* Section *Alatae*.
Petal cell shape in *Nicotiana* Section *Alatae* ranges from non-conical lenticulate (*e.g.* E) to conical papillate (*e.g.* B, C, D). A-G. SEM microphotographs of the adaxial surface of the petal of A. *N. alata*; B. *N. langsdorfii*; C. *N. forgetiana;* D. *N. mutabilis;* E. *N. bonariensis*; F. *N. longiflora*; G. *N. plumbaginifolia*. Black and white squares represent conical and non-conical respectively. Scale bars:50 µm. Modified from Taylor (2015).

3.2.3 Sister species *N. bonariensis* and *N. forgetiana*

N. bonariensis and *N. forgetiana* occur in the eastern part of Southern South America (Figure 3.2). *N. bonariensis* occurs from South East Brazil to North Eastern Argentina and Uruguay and *N. forgetiana* in South Eastern Brazil (Goodspeed, 1954; RBG-Kew, 2016b).

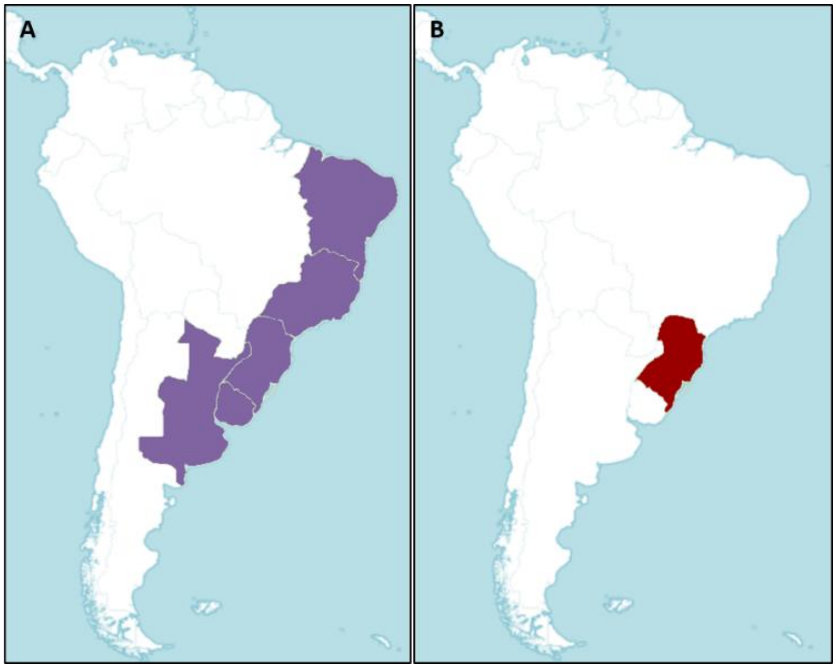

Figure 3.2. Geographic distribution of *N. bonariensis* and *N. forgetiana* (Section *Alatae*)
A. Geographic distribution of *N. bonariensis* (purple) includes South East Brazil, Northern Argentina and Uruguay. B. *N. forgetiana* (red) occurs in South Eastern Brazil. Maps retrieved from RBG-Kew Plants of the World Database (2016b).

Plants of *Nicotiana bonariensis,* the non-conical celled species (Figure 3.3B, D), are annual or biannual herbaceous rosettes, with a main central stem erect. The leaves are sessile or with short winged petiole; ovate in shape, decurrent and pubescent. The flowers occur in paniculate inflorescences. Flowers in a single individual are of the same colour, closing during the time of higher insolation. The corolla is salveiform; the external (abaxial) face is glandular-pubescent, white, pale-green, pinkish-white, pink, or magenta in colour, the adaxial face is white or pink-white. The limb is asymmetric (zygomorphic) and deeply lobate. The stamens are inserted, geniculate (bended), adnate to the lower half of the corolla tube, glandular pubescent at the base and of different lengths; the anthers are purple in colour and the pollen cream. Flowering and fruiting almost simultaneous during the whole year, with a peak during Spring and Summer, *N. bonariensis* inhabits wet to dry terrains, borders of roads and altered areas, behaving frequently as a ruderal species (Goodspeed, 1947; Vignoli-Silva & Auler Mentz, 2005).

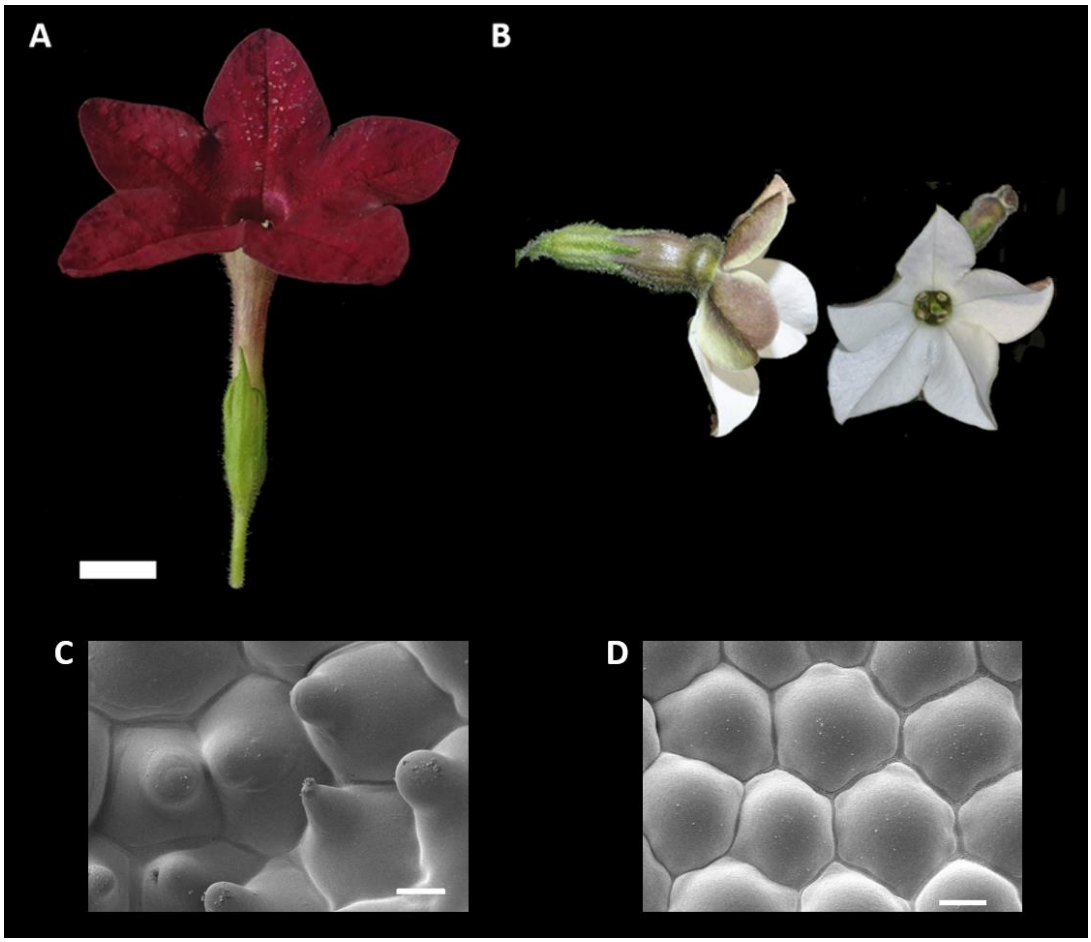

Figure 3.3. Sister species in Section *Alatae* present contrasting petal cell shape: *N. forgetiana* (conical) and *N. bonariensis* (non-conical).
A-B. Macroscopic flower morphology of *N. forgetiana* (A) and *N. bonariensis* (B). C-D. SEM microphotographs of epidermal cells on the adaxial surface of the petal of *N. forgetiana* (C, conical) and *N. bonariensis* (D, non-conical). Scale bars: A-B = 10 mm; C-D = 10 µm.

Small perching moths, which land on the long lower limbs of *N. bonariensis*, are thought to be the predominant pollinators of this species (Kaczorowski *et al.*, 2005). After over 30 h of field observation in four populations of *N. bonariensis,* Kaczorowski *et al.*, (2005), reported that small perching moths visiting the plants had proboscis lengths that matched the short corolla tube length very well, but few such moths (nor any other pollinator) had been observed. Florivorous beetle larvae were also commonly found inside *N. bonariensis* flowers in some populations, but their role in pollination was not apparent (Kaczorowski *et al.*, 2005). Scent chemical profiles of *N. bonariensis* are characteristic of flowers pollinated by noctuid moths, including a 4- to 30-fold excess in nocturnal vs. diurnal emission (Raguso *et al.*, 2003).

N. forgetiana, the species with conical petal cells (Figure 3.3A, C), is a ruderal species that grows in well-drained soil in rock outcrops, roadsides, and disturbed areas. Plants of *N. forgetiana* are herbaceous, annual or biannual, 0.5-1.0 m tall. The basal leaves form a rosette and the rest of the leaves are distributed helicoidally along a central straight axis. The leaves on the basal portion have a short petiole and the rest of the leaves are sessile. The flowers occur in paniculate inflorescences and are pedicellate. Lobes of the corolla are unequal, four shorter or the same length and the fifth exceeding the calyx tube. The corolla is salveiform, glandular-pubescent in the external (abaxial) face, colour varying from cream, white-green, pink, soft pink, magenta, or pink- purple. The limb is slightly asymmetrical, deeply lobed. The adaxial face of the limb is usually described as "purple-red flush" in colour (Ippolito, 2000), and the plants used in this thesis fit that description, however, flowers of natural populations of *N. forgetiana* in southern Brazil are reported to vary between cream, white-green, green, light pink, magenta or pink-purple (Vignoli-Silva & Auler Mentz, 2005). *N. forgetiana* flowers rarely have a detectable odour and poses a short floral tube (Ippolito *et al.*, 2004). Several hummingbird species are thought to pollinate *N. forgetiana* and infrequently solitary bees and small hawkmoths visit the flowers of this species close after sunrise (Ippolito *et al.*, 2004).

3.3 MATERIALS AND METHODS

3.3.1 Cloning of R2R3 MYB Subgroup 9 genes from *Nicotiana* spp.

Plant material was obtained as described in section 2.3.1.1. Details on the sources of seed for *N. bonariensis* and *N. forgetiana* are listed in Appendix 4. Extraction of nucleic acids was as described in section 2.3.1.2. cDNA was synthesized as described in 2.3.1.2. Primers used for sequencing of candidate genes were designed as stated in section 2.3.1.3 and are listed in

Appendix 6a-b. RT-PCR amplification was carried out as described in section 2.3.1.4. Molecular cloning and Sanger sequencing was as described in sections 2.3.1.5 to 2.3.1.11.

3.3.2 DNA and protein sequence analyses

DNA and amino acid sequences were analysed as explained in section 2.3.2. Protein structure predictions were obtained using PredictProtein (Rost *et al.*, 2004) online tool.

3.3.3 Heterologous expression of candidate genes in *N. tabacum* and *N. benthamiana*

Heterologous expression in *N. tabacum* and *N. benthamiana* was used to test the function of selected candidate genes from *N. bonariensis* and *N. forgetiana*. *N. benthamiana* was transformed in addition to *N. tabacum* because this species has non-conical petal epidermal cells, which makes this model system a good option to test the potential effect of overexpressing R2R3 MYB Subgroup 9 genes on petal tissue that does not present conical cells by default. If overexpression of any candidate genes would result in the ectopic appearance of conical cells on the petals of *N. benthamiana,* transgenic lines presenting this phenotype could be used in contrast to the non-conical celled phenotype of the wild type for pollinator behaviour experiments (Chapter 5).

Generation of pGreen II expression vectors (Figure 3.4) was performed as explained in section 2.3.3.1. PstI and SalI restriction enzymes were used for double digestion of the empty pGreen II plasmid and the pBluescript plasmid containing *NbMYBI7-1* and *NfMYBI7-1*. For *Nf/NbMIXTA-2*, the gene of interest was in the opposite orientation in pBluescript than required for assembly into pGreen. Restriction sites were added by PCR amplification using designed primers (Appendix 6c): HindIII at the 5' end and EcoRI at the 3' end. PCR amplification in this case was run from a 1:100 dilution of the original *NfMIXTA-2* pBluescript plasmid.

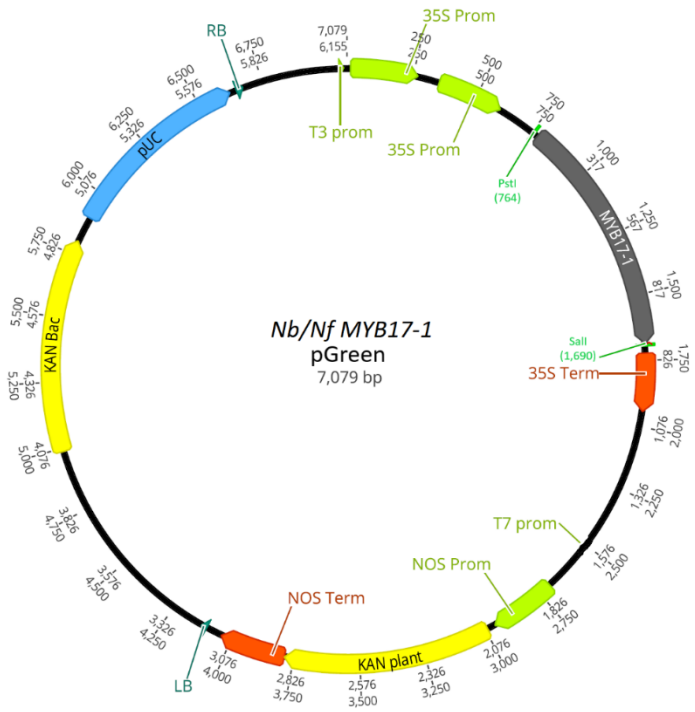

Figure 3.4. Plasmid map of *N. bonariensis/ N. forgetiana MYB17-1* in pGreen II used for stable transformation.
Blue bar represents origin of replication (pUC), light green bars promoters (T3 Prom, 35S Prom, T7 Prom and NOS Prom), orange bars terminators (35S Term and NOS Term), yellow bars kanamycin resistance genes for plant (KAN Plant) and bacteria (Kan Bac), dark green bars regulatory elements (RB, LB) and grey bar the coding sequence of the gene of interest (*NbMYB17-1* or *NfMYB17-1*). Restriction sites (PstI/SalI) used for double digestion are indicated with green arrows. Restriction sites used for double digestion of *NbMIXTA-2* and *NfMIXTA-2* (not shown on figure) were HindIII/EcoRI.

Transformation of *A. tumefaciens* GV3101 competent cells was done by electroporation as described in section 2.3.3.3. Leaf discs of *N. tabacum* WT or *N. benthamiana* WT were infiltrated with transformed *A. tumefaciens* GV3101 liquid cultures as explained in sections 2.3.3.4 and 2.3.3.5). Tissue culture and maintenance of putative transgenic plants was carried out following the protocol in section 2.3.3.6. Media components and hormone combination used for *N. tabacum* and *N. benthamiana* are listed in Table 2.3.

Expression of the transgenes in putative transgenic lines was tested using gDNA and/or cDNA as template via RT-PCR using specific primers as described in section 2.3.3.7. Morphological characterization of putative transgenics was done as described in section 2.3.3.8.

3.3.4 Characterization of petal cell development in *N. bonariensis* and *N. forgetiana*

Developmental stages of the flower of both species were defined by observation and measuring of individual flowers from plants growing in greenhouse conditions at the Department of Plant Sciences, University of Cambridge, Cambridge, UK (section 2.3.1.1). Flowers of each of the developmental stages established by macromorphological analyses were sampled and mounted for micromorphological characterization of the petal epidermis using cryo-SEM (section 2.3.3.8).

3.3.5 Expression analyses of R2R3 MYB Subgroup 9 genes in petal of *N. bonariensis* and *N. forgetiana*

Expression patterns of R2R3 MYB Subgroup 9 MYBs were characterized for sister species in Section *Alatae* using two different methods of quantification: Semiquantitative RT-PCR (semiqRT-PCR, section 3.3.5.4) and Quantitative RT-PCR (qPCR, section 3.3.5.5)

3.3.5.1 Collection of plant tissue

Nicotiana spp. plants were grown under greenhouse conditions as described in section 2.3.1.1. Plants were dissected with clean needles, scalpels and forceps under the stereomicroscope and immediately frozen in liquid nitrogen, before storage at -80°C.

Tissue from flowers in the same stage of development from 1-3 plants, growing at the same time in the same conditions, was collected over a period of several days up to two weeks. Separate tubes were maintained for each tissue type and continually added until reaching a minimum of 100 mg. Three independent biological replicates were collected for each tissue type. Tissue was ground to a fine powder using a tissue lyser (section 2.3.1.2).

3.3.5.2 RNA extraction and cDNA synthesis for gene expression analyses

RNA was extracted using self-made guanidinium-acid-phenol reagents (similar to commercial TRIzol or TRI; Chomczynski & Sacchi, 1987, 2006, section 2.3.1.2). The RNA was run on a gel to inspect the quality, the yield quantified by nanodrop (section 2.3.1.5) and then DNase-treated as detailed in section 2.3.1.2. To test for any genomic DNA contamination residual from the RNA extraction, a RT-PCR reaction (section 2.3.1.4) for a housekeeping gene was run using 0.2 µL of DNase-treated RNA as template. 5 µg of total DNase-treated RNA, confirmed to have been purified, was then used for cDNA synthesis with Bioscript retrotranscriptase (section 2.3.1.2) for semi-quantitative PCR (semiq-PCR) or Superscript™ III retrotranscriptase for quantitative PCR (qPCR).

3.3.5.3 Primer specificity testing for expression analyses

As the *Nicotiana* genes of interest had similarities in their sequences, it was important to ensure the specificity of each set of primers for only the gene they had been designed for (*i.e.* that there was no cross-amplification between genes). To test for this, 1 ng/µL of the most complete pBluescript SK plasmid for each gene (Table 3.2) was used as the template in a PCR reaction (section 2.3.1.4) using PCRBIO polymerase and the gene specific primers for expression analyses

(Appendix 6d) for 35 cycles at an annealing temperature of 60°C. Each set of primers was tested against each of the four plasmid templates for each species, and the PCR products were visualised on an agarose gel. If a set of primers was only able to amplify a product from the gene that they had been designed for, they were deemed to be sufficiently specific to that gene; primers that failed this test were discarded and redesigned.

3.3.5.4 Characterization of gene expression using Semi-quantitative RT-PCR

Semiquantitative RT-PCR was used to establish relative levels of gene expression of the four candidate genes compared to a gene of reference (*Cytochrome Oxidase- 1, COX-1*) and to compare these levels of expression between species and at different developmental stages. *COX-1* was selected as a reference gene because it had been established to be the most stable among nine potential reference genes evaluated by Taylor (2015) to be used in qPCR analyses of *N. forgetiana* (section 3.3.5.5). However, further tests for housekeeping genes stability performed later (section 3.3.5.5.1) showed that *COX-1* was not as stable as other genes selected specifically for qPCR.

5 µg of total DNase-treated RNA, assessed by Nanodrop, from each sample were subject to reverse transcription using Bioscript retrotranscriptase (section 2.3.1.2). Special care was taken to ensure that the same amount of RNA was retrotranscribed for each sample. 1 µL of cDNA was used as template for a 50 µL reaction (Table 2.2). 10 uL were removed from the reaction at 23, 28, 30 and 35 cycles. 5uL of each were run on an electrophoresis gel to visualize the amplification pattern (section 2.3.1.5).

3.3.5.5 Characterization of gene expression using Quantitative PCR (qPCR)

3.3.5.5.1 Primer efficiency testing

A set of primers for qPCR may not be 100% efficient (*i.e.* produce double the amount of PCR product per cycle). In order to control for differences in amplification efficiency, a standard curve was produced for each set of primers as described in Ramakers *et al.*, (2003). Minipreps of plasmids containing the amplicon of interest (created as described in section 2.3.1.11) (Table 3.2) were diluted 10-fold repeatedly over eight samples (resulting in a range of dilutions from 0.1 to 1 x 10^{-8} of the original concentration). 0.3 µL each of these dilutions was used as template in 10µL qPCR reaction mixes with the other components assembled as follows: 4.2 µL Milli Q® autoclaved dH_2O, 5 µL of Luna® Universal qPCR Master Mix 2X, 0.5 µL of each primer (Forward and Reverse, 10 µM concentration). Cycling conditions, plate readings and post PCR melt curve analyses were performed as described in section 3.3.5.5.2.

Ct (cycle threshold) values were exported to an xlsx file and analysed in Microsoft Excel. Standard curves were created by averaging the Ct values for technical replicates and plotting this against Log(N_0), where N_0 is the starting concentration of the reaction template. The PCR efficiency was then calculated from the slope of the standard curve (Efficiency=10 $^{-1/slope}$). PCR efficiencies were used in later calculations of gene expression using the comparative Ct method (see section 3.4.5.2.2). The standard curves also gave the range of Ct values that were valid for interpretation (i.e. that responded in a log-linear fashion to starting template concentrations).

3.3.5.5.2 Reaction and thermocycling conditions for RT-qPCR

For quantification of expression of the candidate genes 1:10 dilutions of the cDNA samples were prepared using Milli Q® autoclaved water just prior to the experiment. 0.3 µL of cDNA dilution was used as template in a 10 µL qPCR reaction mix with the other components assembled as follows: 4.2 µL Milli Q® autoclaved dH_2O, 5 µL of Luna® Universal qPCR Master Mix 2X, 0.5 µL of each primer (Forward and Reverse, 10 µM concentration). 40 cycles of PCR were performed with a CFX384 Touch™ Real-Time PCR Detection System with cycling conditions as follows: 1 min at 95°C, 40 cycles of 15s at 95°C, 15s at 60°C, 15s at 72°C. A plate fluorescence reading was taken once per cycle. A post PCR melt curve analysis was performed from 65°C to 95°C with readings taken at 0.2°C intervals. Relative gene expression was quantified using CFX Maestro™ Software (BioRad Laboratories, Inc). Ct values were analysed with the tool provided by the machine software. All reactions for genes of interest were performed in triplicate alongside no template controls (NTCs).

3.4 RESULTS

3.4.1 Growing *N. bonariensis* and *N. forgetiana* as a source of living tissue for molecular and morphological analyses

N. bonariensis and *N. forgetiana* are herbaceous annuals or biannuals, easy to grow in greenhouse conditions (as described in 2.3.1.1) and a reliable source of living material for experimentation. Flowering in both *N. bonariensis* and *N. forgetiana* occurs ca. 8 weeks after sowing. The production of flowers is constant for up to six months of growing. For the purposes of this research, collection of living tissue and characterization of the plants was carried out between 8 and 15 weeks after sowing.

3.4.2 Sequencing of R2R3 MYB Subgroup 9 genes in *N. bonariensis* and *N. forgetiana*

gDNA and cDNA from leaf, flower and petal tissue was used as template for molecular characterization of *N. bonariensis* and *N. forgetiana*. Nucleotide sequences of the coding regions of the four candidate genes (*MIXTA-2, MIXTA-like, MYBl7-1 and MYBl7-2*) were initially assembled from DNA fragments cloned independently from different regions of the gene (see primer design 2.3.1.3, Appendix 6a). Assembly was performed using the multiple alignment algorithm to align the cloned DNA fragments to the known sequences of several *Nicotiana* species (Appendix 7). After the initial complete characterization of the gene, primers were designed to retrotranscribe the coding sequence of each gene in a single RT-PCR reaction (Appendix 6b). Full sequences of the coding regions cloned into pBluescript SK are listed in Table 3.2 and have been deposited in the laboratory repository of plasmids where they are stored at -20°C.

Comparisons between DNA and amino acid sequences of the coding regions of the candidate genes were made from comparison alignments of the consensus sequence of each gene for the two species (Appendix 7A, Figure 3.5).

Table 3.2. pBluescript SK plasmids containing full coding sequences of R2R2 Subgroup 9 genes of *N. forgetiana* and *N. bonariensis*.

Species	Gene	Code	F Primer	R Primer	Plasmid Nanodrop		
					ng/µl	260/280	260/230
Nicotiana bonariensis	*MIXTA-2*	198.05	Nic_MIXTA-2_F10	Nic_MIXTA-2_1R	1064.3	1.92	2.17
	ML	307.02	Nic_ML_F4	Nic_ML_R29	1113.5	1.88	2.28
	MYB17-1	284.02	Nf_MYB17-1_1F	Nic_MYB17-1_R10	136.4	1.94	2.39
	MYB17-2	183.06	Nf_MYB17-2_1F	Nf_MYB17-2_1R	415.5	1.86	2.00
Nicotiana forgetiana	*MIXTA-2*	198.04	Nic_MIXTA-2_F10	Nic_MIXTA-2_1R	2610.3	1.97	2.34
	ML	307.01	Nic_ML_F4	Nic_ML_R29	599.4	1.86	2.24
	MYB17-1	281.01	Nf_MYB17-1_1F	Nic_MYB17-1_R10	391.8	1.89	2.21
	MYB17-2	183.07	Nf_MYB17-2_1F	Nf_MYB17-2_1R	798.3	1.89	2.25

3.4.2.1 Comparison between MIXTA-2 orthologues of N. bonariensis *and* N. forgetiana

Appendix 7A shows DNA alignment of *MIXTA-2* (R2R3 MYB Subgroup 9A) orthologues of *N. bonariensis* and *N. forgetiana* and other *Nicotiana* species. The sequences were initially found to be identical between the two species. However, additional versions of the sequences cloned from different individuals on different occasions gave a better understanding of the range of

substitutions occurring in these species. When aligning the different versions cloned, for any given variable position at least one individual of each species presents one of the possible nucleotides in that position (Figure 3.5). This suggests that the sequence of *MIXTA-2* is labile and as there are no nucleotide substitutions unique for either of the two species, these substitutions alone cannot explain the differential phenotype of petal cell shape in *N. bonariensis* and *N. forgetiana*. Because of this interpretation, *MIXTA-2* initially was not considered for the heterologous expression in *N. tabacum* experiments (section 3.4.3). However, the outcomes of the gene expression analyses (section 3.4.5.3) suggested that this gene might play an important role in the development of conical cells in *N. forgetiana*. To confirm that *MIXTA-2* is a positive regulator of epidermal outgrowths (including conical cells), heterologous expression in *N. tabacum* and *N. benthamiana* is currently in progress. A version of the sequence that has been found in both *N. bonariensis* and *N. forgetiana* (*Nb/NfMIXTA-2;* Appendix 7A) was used to build the pGreen construct used for transformation (Figure 3.4).

Figure 3.5. (Next page) Clonning of *MIXTA-2* of *N. bonariensis* and *N. forgetiana* resulted in multiple sequence versions non-diagnostic for the species.

Five versions of *NbMIXTA-2* (purple box) and three versions of *NfMIXTA-2* (red box) cloned from different individuals on different occasions. Dots indicate the same nucleotide as the sequence at the top. Yellow bands indicate nucleotide positions that are variable in the alignment. For any given variable position at least one individual of each species presents one of the possible nucleotides in that position.

3.4.2.2 Comparison between MIXTA-like orthologues of N. bonariensis *and* N. forgetiana

Figure 3.6 shows multiple alignment of *MIXTA-like*/MIXTA-like (R2R3 MYB Subgroup 9A) orthologues of *N. bonariensis* (*NbMIXTA-like*) and *N. forgetiana* (*NfMIXTA-like*). The sequences included in Figure 3.6 show the variation detected in several versions of *MIXTA-like* cloned from different individuals of the two species. Nucleotide substitutions that result in shifts in the amino acid can be detected. For instance, a substitution of A for C in position 67 in one version of *NfMIXTA-like* (cloned from petal tissue of *N. forgetiana,* Version 1 in Figure 3.6), results in a shift from lysine (K) to glutamine (Q). Similarly, a substitution of A by G in position 274 in a different version of *NfMIXTA-like* (cloned from petal tissue of *N. forgetiana,* Version 2 in Figure 3.6), results in a shift from isoleucine (I) to methionine (M), potentially inducing an alternative start codon. However, in both cases at least one of the other versions of *NfMIXTA-like* cloned presents the same nucleotide in the correspondent position compared to the two versions of *NbMIXTA-like*. Given the high degree of identity among the different versions of the two species, and that there were no diagnostic features in the sequence of *NfMIXTA-like* compared to *NbMIXTA-like*, the differences detected were not considered as good candidates to explain the differences in phenotype of the two species (conical vs. non conical petal cells) and *MIXTA-like* was not included in the heterologous expression experiments (section 3.4.3).

Figure 3.6. (Next page) *MIXTA-like*/MIXTA-like sequences of *N. forgetiana* (conical cells) and *N. bonariensis* (non-conical cells) Section *Alatae*.
Nucleotide and amino acid sequences of MIXTA-like were considered highly conserved between sister species in Section *Alatae,* despite some single nucleotide polymorphisms detected when comparing multiple versions. Nucleotide substitutions with synonymous effect on the amino acid sequences are highlighted in blue and those with non-synonymous effect in yellow. Amino acid shifts with predicted neutral or no effect of point mutation (negative scores) are highlighted in green and those with an expected effect on the protein function (positive scores) in red.

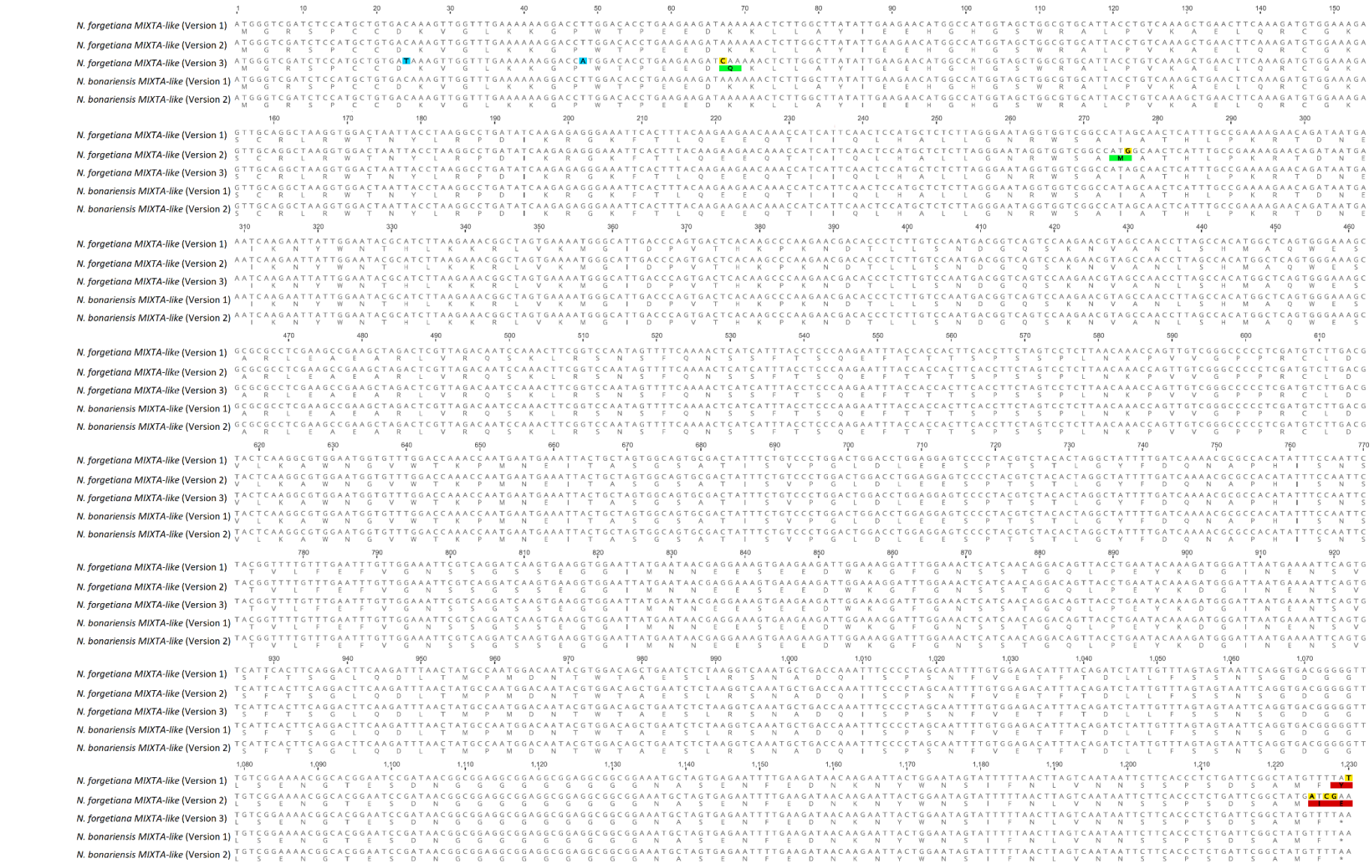
N. forgetiana MIXTA-like (Version 1)
N. forgetiana MIXTA-like (Version 2)
N. forgetiana MIXTA-like (Version 3)
N. bonariensis MIXTA-like (Version 1)
N. bonariensis MIXTA-like (Version 2)

3.4.2.3 *Comparison between MYB17-1 orthologues of* N. bonariensis *and* N. forgetiana

Figure 3.7 shows pairwise alignment of *MYB17-1*/MYB17-1 (R2R3 MYB Subgroup 9B) orthologues of *N. bonariensis* (*NbMYB17-1*) and *N. forgetiana* (*NfMYB17-1*). Several differences in the DNA and amino acid sequences were detected between the sister species (Figure 3.7, Figure 3.8, Table 3.3). Synonymous nucleotide substitutions are common (14 detected in the pairwise analysis) and in all cases are due to substitutions in the nucleotide at position three of the respective codon. Non-synonymous nucleotide substitutions with negative scores of predicted effect of point mutation occur in position 646 (215 amino acid residue, threonine for alanine, T-A, score -7) and 868 (289 amino acid residue, isoleucine for leucine, I-L, score -46). Non-synonymous substitutions with positive scores of predicted effect of point mutation occur in position 383 (127 amino acid residue, proline for histidine, P-H, score +18), 619 (215 amino acid residue, isoleucine for valine, I-V, score +20) and 679 (226 amino acid residue, phenylalanine for leucine, F-L, score +19). The potential effect on the protein of these amino acid substitutions is discussed in section 3.5.1. Figure 3.8 shows the predicted protein secondary structure of MYB17-1 in Section *Alatae* and the estimated effect of point mutations detected. Because of the relatively large number of differences identified between the coding sequences of *MYB17-1* of *N. forgetiana* (conical cells) and *N. bonariensis* (non-conical cells) the two orthologues, *NfMYB17-1* and *NbMYB17-1*, were selected for heterologous expression in *N. tabacum* to experimentally asses the effect of such differences in the protein function (section 2.3.3).

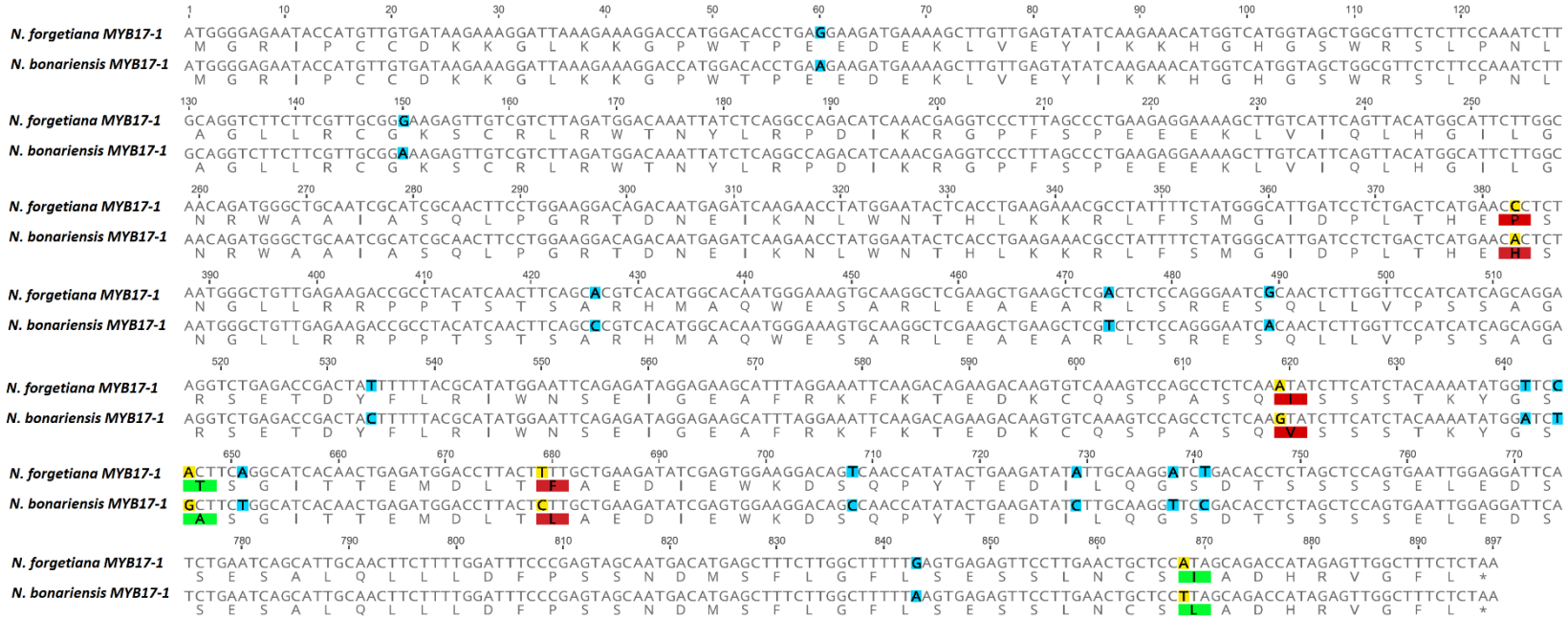

Figure 3.7. Pairwise aligments of *MYB17-1*/MYB17-1 sequences of *N. forgetiana* (conical cells) and *N. bonariensis* (non-conical cells).
Nineteen single nucleotide substitutions were detected between *NfMYB17-1* and *NbMYB17-1*. Nucleotide substitutions with synonymous effect on the amino acid sequences are highlighted in blue and those with non-synonymous effect in yellow. Amino acid shifts with predicted neutral or no effect of point mutation (negative scores) are highlighted in green and those with an expected effect on the protein function (positive scores) in red.

Table 3.3. Nucleotide substitutions and amino acid shifts detected between orthologues of *MYB17-1* in *N. forgetiana* and *N. bonariensis*.

Nucleotide Position	Nucleotide substitution (NfMYB17-1-*NbMYB17-1*)	Position in codon	Effect of the substitution	Amino acid position	Amino acid shift (NfMYB17-1-NbMYB17-1)	Effect of point mutation score
60	A-G	3	Synonymous	19	E-E	-99
150	G-A	3	Synonymous	49	G-G	-99
383	C-A	2	Non-synonymous	127	P-H	+18
426	A-C	3	Synonymous	141	A-A	-99
474	A-T	3	Synonymous	157	R-R	-99
489	G-A	3	Synonymous	162	S-S	-99
534	T-C	3	Synonymous	177	Y-Y	-99
619	A-G	1	Non-synonymous	206	I-V	+20
642	T-A	3	Synonymous	213	G-G	-99
645	C-T	3	Synonymous	214	S-S	-99
646	A-G	1	Non-synonymous	215	T-A	-7
651	A-T	3	Synonymous	216	S-S	-99
679	T-C	1	Non-synonymous	226	F-L	+19
708	T-C	3	Synonymous	235	S-S	-99
729	A-C	3	Synonymous	242	I-I	-99
738	A-T	3	Synonymous	246	G-G	-99
741	T-C	3	Synonymous	247	S-S	-99
843	G-A	3	Synonymous	280	L-L	-99
868	A-T	1	Non-synonymous	289	I-L	-46

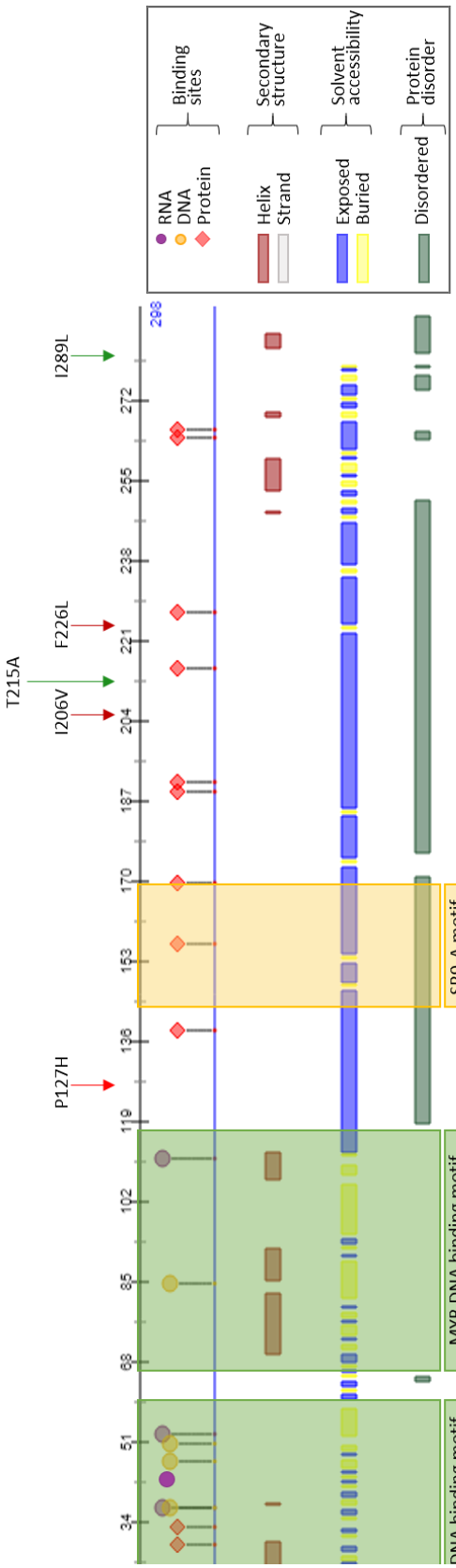

Figure 3.8. Predicted protein properties of MYB17-1 in *N. forgetiana* (Section *Alatae*).
Five amino acid substitutions detected when comparing MYB17-1 protein sequences of sister species *N. forgetiana* (conical) and *N. bonariensis* (non conical) are marked with arrows. Amino acid residues are annotated using the one letter nomenclature. The amino acid to the left is the one present in *N. forgetiana* and the one to the right in *N. bonariensis*. Number on top rows refer to the position of the substitution detected. Green arrows identify substitutions with negative scores (*e.g.* with no or neutral effect on the resulting protein function), and red arrows indicate substitutions with positive scores (*e.g.* predicted to have an impact on the protein function). Green and yellow shaded boxes indicate the positions of the diagnostic motifs. Protein properties depicted in the prediction are listed in the legend box to the right.

3.4.2.4 *Comparison between MYB17-2 orthologues of* N. bonariensis *and* N. forgetiana

Appendix 7D shows multiple alignment of *MYBI7-2* (R2R3 MYB Subgroup 9B) orthologues of *Nicotiana spp.* including *N. bonariensis* and *N. forgetiana*. No differences in the nucleotide sequences were detected and the orthologues in the two sister species were interpreted as being identical. *MYBI7-2* genes from species in Section *Alatae* were not overexpressed in *N. tabacum*.

3.4.3 Heterologous expression of *NbMYB17-1* and *NfMYB17-1*in *N. tabacum*

3.4.3.1 *Molecular characterization of expression of* NbMYB17-1 *and* NfMYB17-1 *in* N. tabacum

N. tabacum transformed plants expressing the gene of interest were identified for both constructs. Five transformed lines were confirmed for *NbMYBI7-1* (lines 21-1, 24-2,25-2, 29-2 and 29-3; Figure 3.9) and five for *NfMYBI7-1* (lines 5, 8, 10, 11 and 12; Figure 3.10). Semiquantitative PCR was used to compare expression of the transgene in contrast to the wild type. As was mentioned in section 2.4.3, amplification of the native orthologues of *N. tabacum* would be expected. In the case of putative transgenics expressing *NbMYBI7-1* and *NfMYBI7*-1, amplification of the transgene was detected from cycle 23 and clearly defined strong bands were visible in cycles 28 and 35, whereas in the wild type a faint band only appeared in cycle 28 of amplification. This confirms heterologous expression of the gene of interest in the transgenic lines. Semiquantitative PCR also allowed the comparison of relative levels of expression of the transgene among putative transgenic lines. In the case of *NbMYBI7-1* a stronger band in line 29-2 suggested higher levels of expression in this line (Figure 3.16). In contrast line 25-2 presents a fainter band at cycle 23 and the band at cycles 28 and 35 looks thiner than for other lines (Figure 3.9). Differential patterns of relative expression of the transgene for putative transgenic lines expressing *NfMYBI7-1* are not evident from the electrophoresis gel images (Figure 3.10).

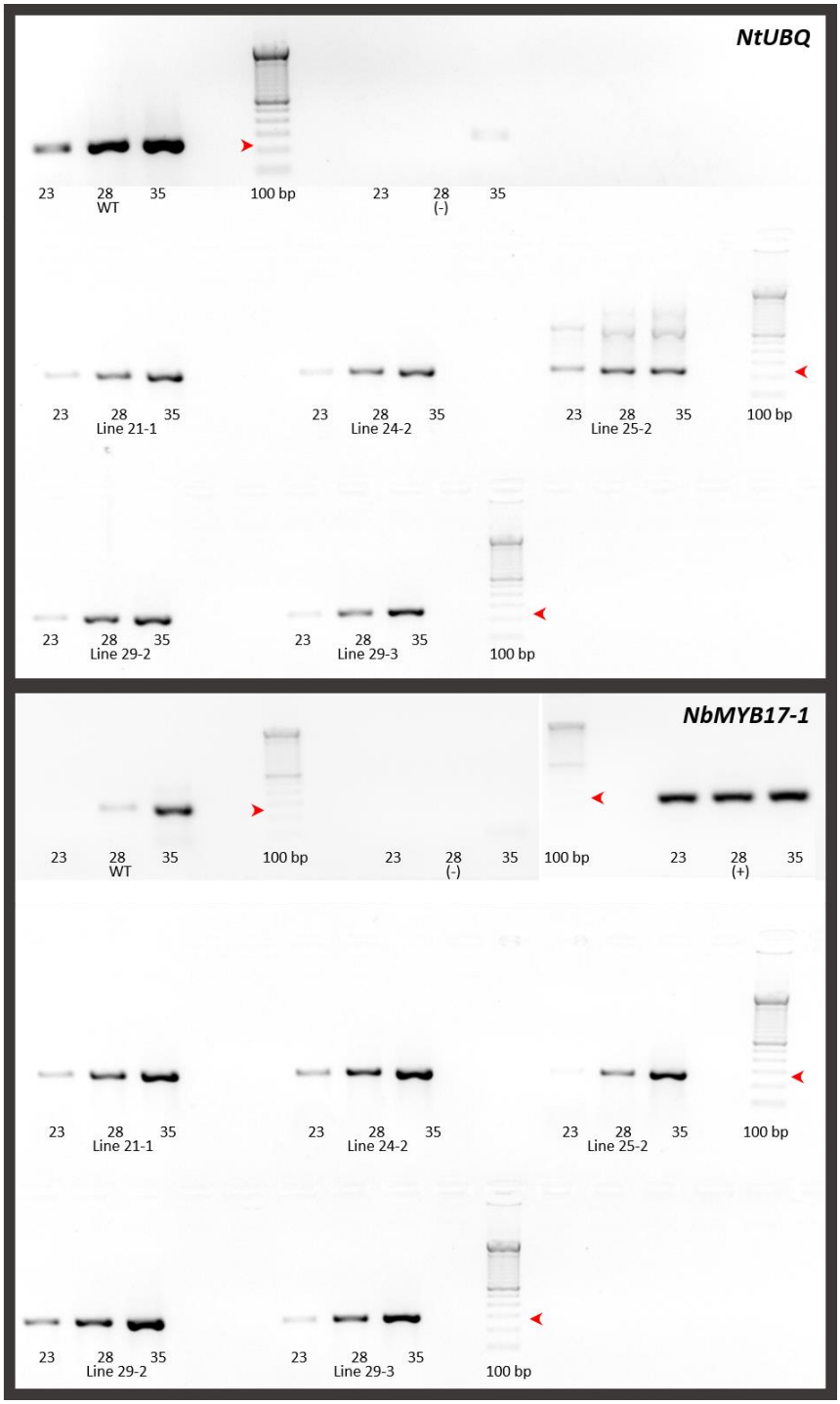

Figure 3.9. Expression levels of *NbMYB17-1* in putative transgenic lines of *N. tabacum*.
The transcript level of *NbMYB17-1* in wild type *N. tabacum* and putative transgenic lines was examined by semi-quantitative PCR. *NtUBQ* was used as an internal reference gene. 1 µL of cDNA from leaf tissue was used as template for each 50 µL PCR reaction. Upper panel shows semiquantitative RT-PCR products of *NtUBQ* (expected size 248 bp, red arrow head) in five putative transgenic lines (21-1, 24-2, 25-2, 29-2 and 29-3) and the wild type (WT). Lower panel shows semiquantitative RT-PCR products of *NbMYB17-1* (expected size 280 bp, red arrow head) in the same five putative transgenic lines and the WT. Negative control (-) shows the product of water as template in the reaction. Positive control (+) shows the product of 1 µl (1:100 dilution) of *NbMYB17-1* pBluescript plasmid. Products of the amplification were sampled at 23, 28 and 35 cycles.

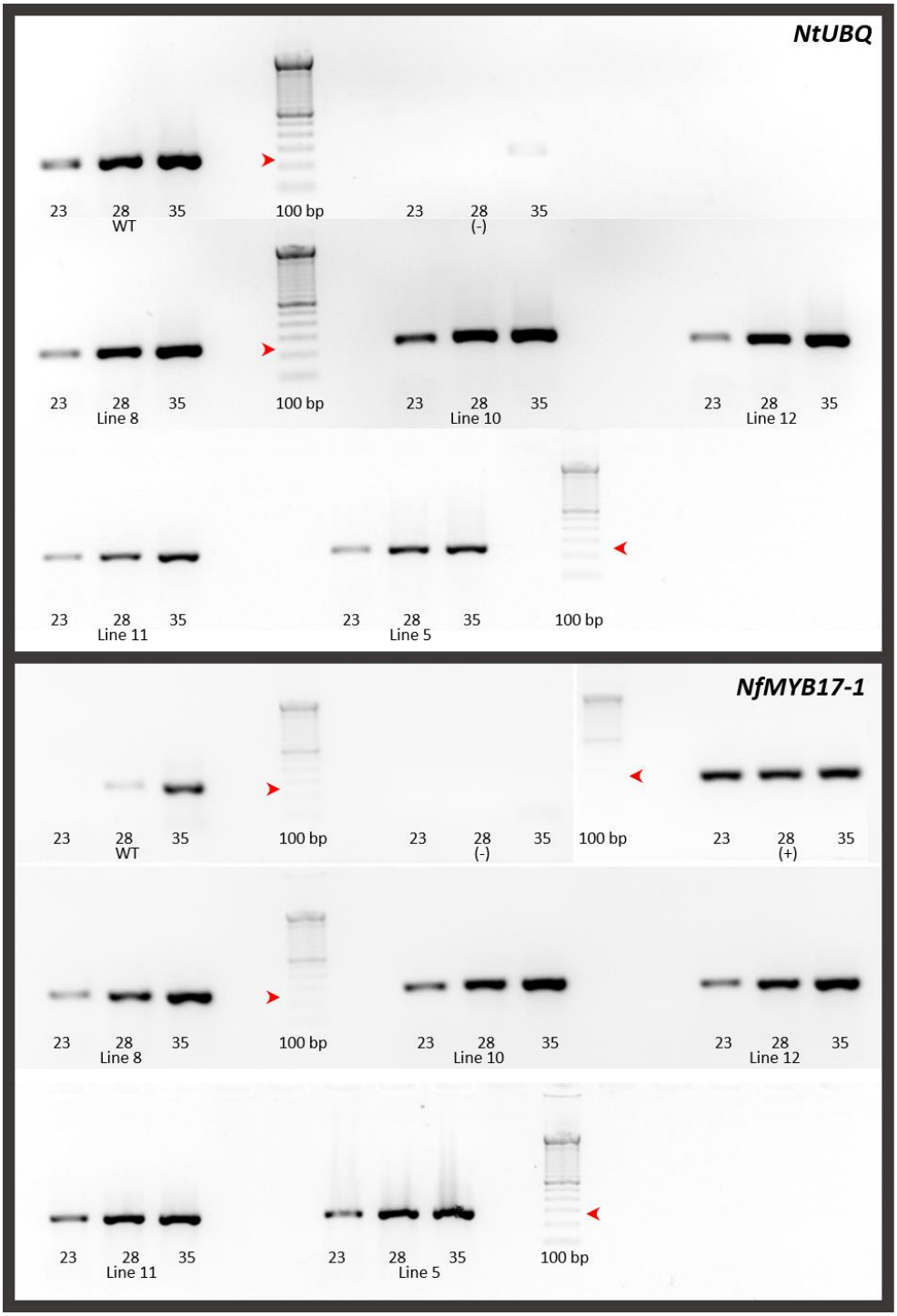

Figure 3.10. Expression of *NfMYB17-1* in putative transgenic lines of *N. tabacum.*

The transcript level of *NfMYB17-1* in wild type *N. tabacum* and putative transgenic lines was examined by semi-quantitative PCR. *NtUBQ* was used as an internal reference gene. 1 µL of cDNA from leaf tissue was used as template for each 50 µL PCR reaction. Upper panel shows semiquantitative RT-PCR products of *NtUBQ* (expected size 248 bp, red arrow head) in five putative transgenic lines (8, 10, 12, 11, 5) and the wild type (WT). Lower panel shows semiquantitative RT-PCR products of *NfMYB17-1* (expected size 280 bp, red arrow head) in the same five putative transgenic lines and the WT. Negative control (-) shows the product of water as template in the reaction. Positive control (+) shows the product of 1 µl (1:100 dilution) of *NfMYB17-1* pBluescript plasmid. Products of the amplification were sampled at 23, 28 and 35 cycles.

3.4.3.2 *Morphological characterization of* NbMYB17-1 *and* NfMYB17-1 *transgenic lines of* N. tabacum

Figure 3.11 shows leaf and flower macromorphology of *N. tabacum* WT compared to selected transgenic lines overexpressing *NbMYB17-1* (line 29-2) and *NfMYB17-1* (line 5). Macromorphological features for other transgenic lines characterized are depicted in appendices. At the macromorphological level no evident differences were detected between the WT and the transgenic lines.

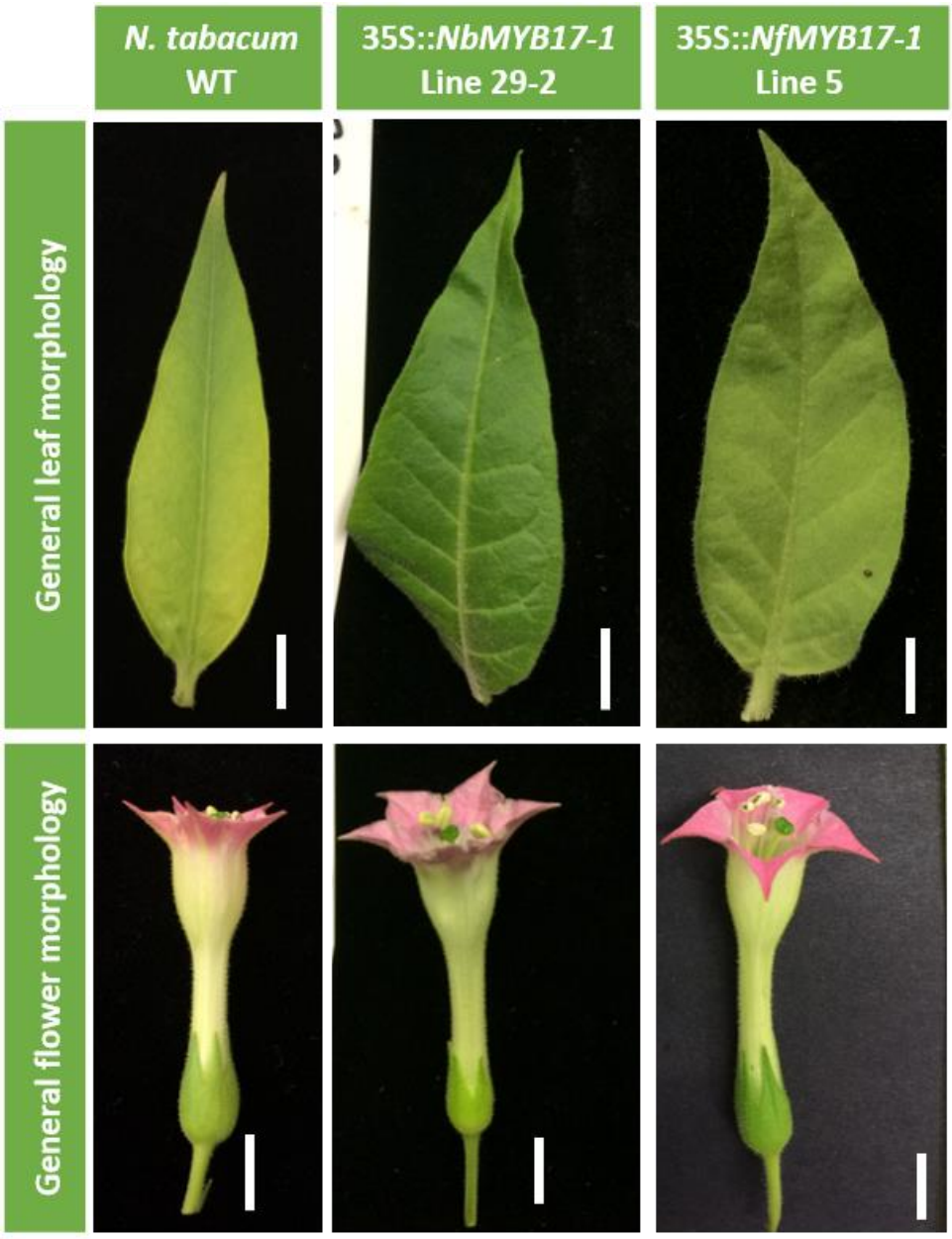

Figure 3.11. Ectopic expression of *NbMYB17-1* and *NfMYB17-1* in *N. tabacum* has little effect on the phenotype of macromorphological features.
Top: Transgenic lines sometimes presented partially revolute margins compared to the wild type. Bottom: There were no obvious macromorphological differences between the WT and the transgenics. Scale bars = 10 mm.

Figure 3.12 shows cryo-SEM microphotographs of leaf surfaces of *N. tabacum* WT compared to selected lines expressing *NbMYB17-1* (line 29-2) and *NfMYB17-1* (line 5). Trichome density appears to be higher in the transgenic lines than in the WT. In the transgenics, both abaxial and adaxial surfaces of the lamina and the midvein present pointy-short epidermal outgrowths similar to conical petal epidermal cells. Branched trichomes with up to three orders of branching occur in the abaxial and adaxial surfaces of the lamina and midvein of the transgenic lines. Cryo-SEM images of epidermal surfaces of additional *N. tabacum* WT and transgenic lines examined are in Appendix 10.

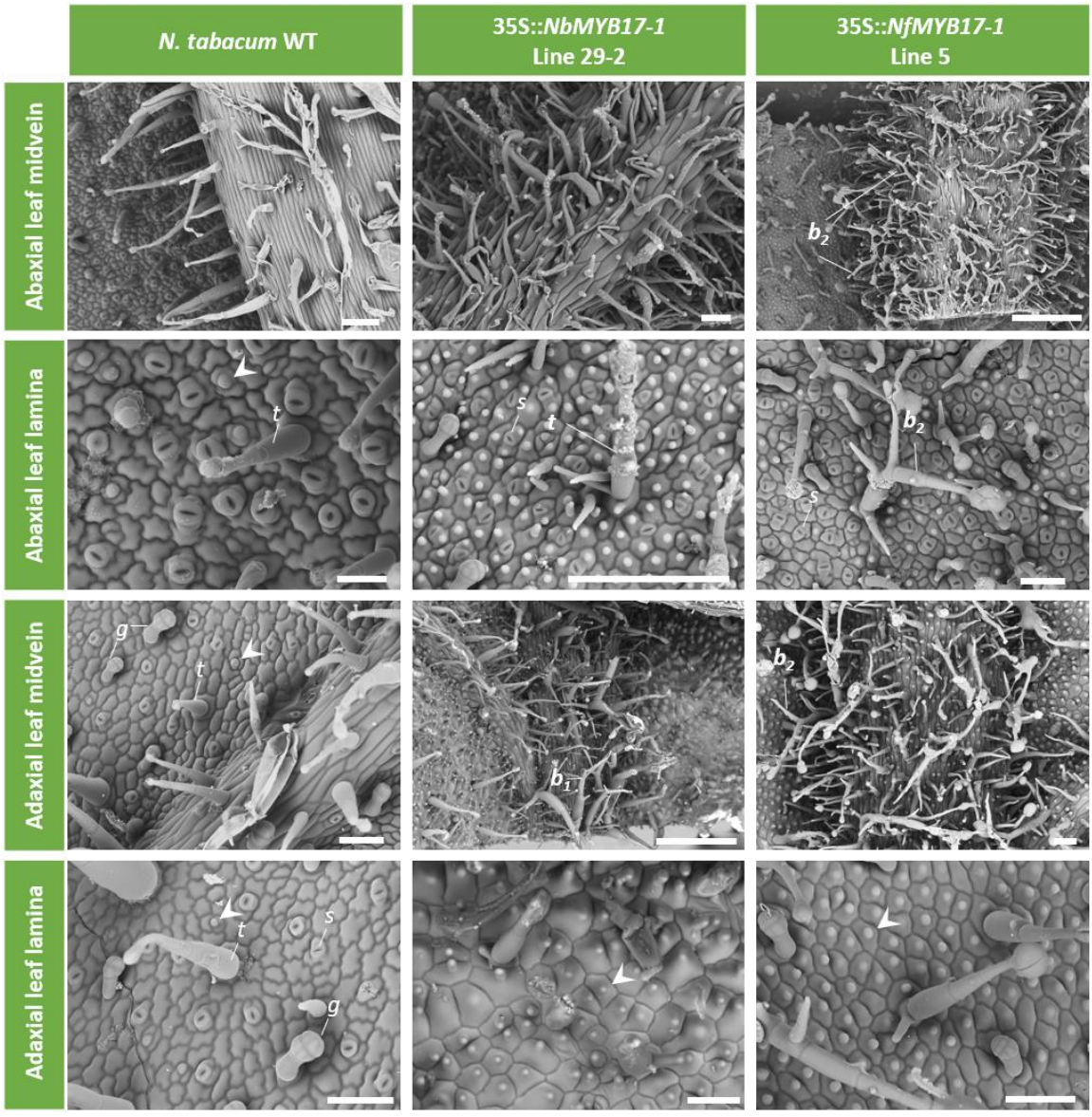

Figure 3.12. Effect of ectopic expression of *NbMYB17-1* and NfMYB17-1 on leaf epidermis of *N. tabacum*.

Branched trichomes (b_1, b_2) and conical cells (arrow heads in the images for transgenics) are present on the abaxial and adaxial surfaces of the midrib and the lamina in the transgenic lines, but absent from the WT. *t*: simple trichome, *g*: glandular trichome, arrow heads: conical cells. Scale bars= 100 µm.

Comparison of the petal surfaces of *N. tabacum* WT and selected transgenic lines expressing *NbMYBI7-1* (line 29-2) and *NfMYBI7-1* (line 5) is depicted in Figure 3.13. Simple trichomes are present on the abaxial surfaces of the petal of both the WT and the transgenics, however, in the WT the trichomes are mostly restricted to the zone along the midvein of the petal and the margins of the lobes, whereas in the transgenic lines they are spread around all the surface of the petal. As mentioned in section 2.4.3.2 both the abaxial and the adaxial surface of *N. tabacum* WT have conical cells, however, the cell features of the transgenic lines expressing the two versions of *MYBI7-1* (*NbMYBI7-1* and *NfMYBI7-1*) are clearly distinguishable from the WT, presenting almost exclusively clavate cells on both abaxial and adaxial surfaces, instead of the typical papillate cells of the WT (Figure 2.18). More complex epidermal outgrowths (*e* in Figure 3.13) can also be present on the adaxial surface of the petal of the transgenic lines with stronger phenotypes.

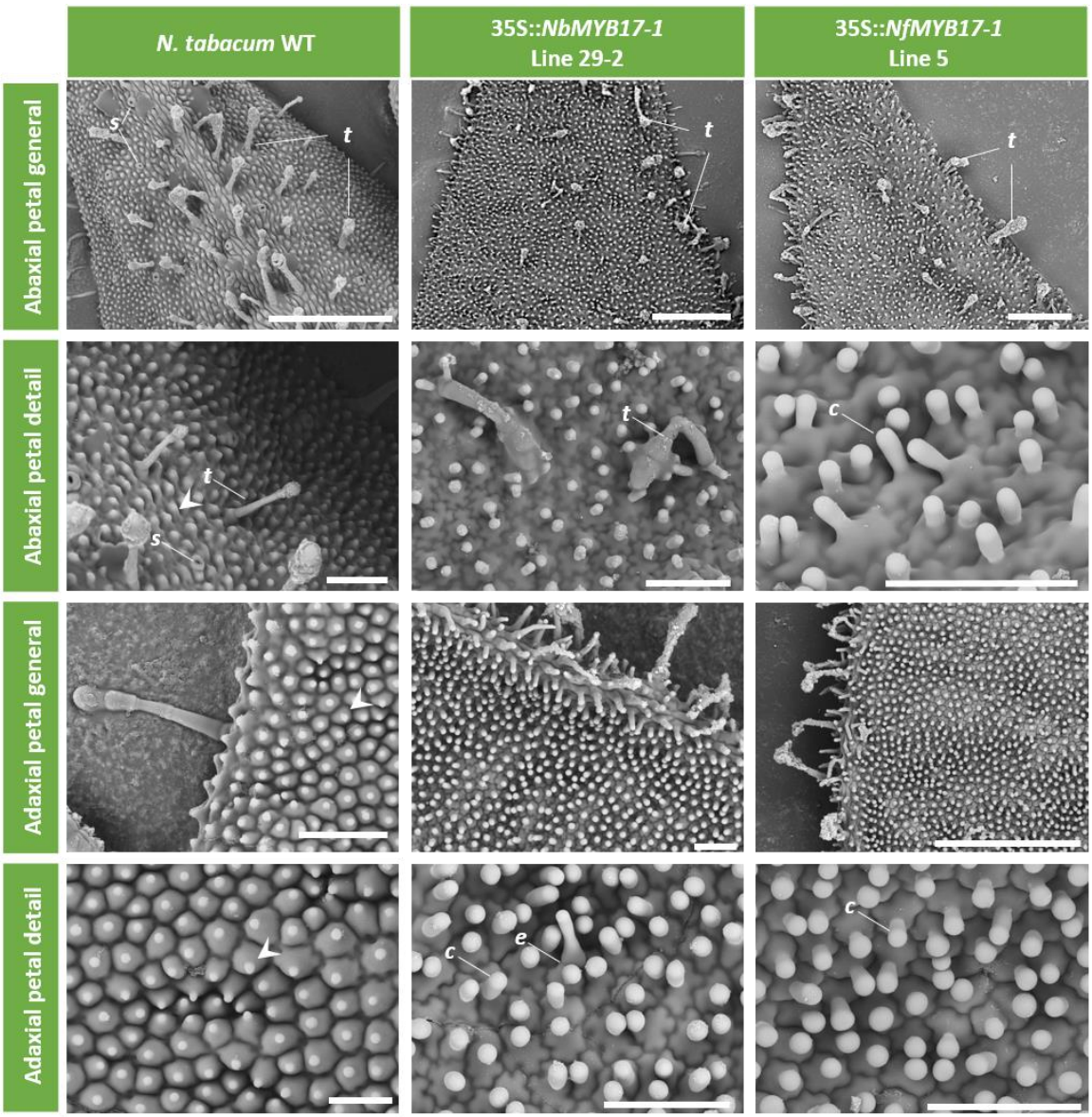

Figure 3.13 Ectopic expression of *NbMYB17-1* and *NfMYB17-1* affects the morphology of epidermal cells on petals of *N. tabacum*.

Simple trichomes *(t)* and stomata *(s)* are present on the abaxial surface of both the WT and the transgenics. Conical cells (arrow heads) are present on the abaxial and adaxial surfaces of the WT. In the transgenic lines the petal epidermal cells on the abaxial and adaxial surfaces are clavate *(c)* in shape rather than conical. Scale bars: First row=500µm, second and third row= 100 µm, fourth row= 50 µm.

Anther features for *N. tabacum* WT and transgenic lines of *NbMYBI7-1* and *NfMYBI7-1* are pictured in Figure 3.14. Epidermal outgrowths on the anthers of the transgenic lines expressing either of the constructs (*NbMYBI7-1* or *NfMYBI7-1*) had morphology extremely different to the WT. Densely arranged, finger-like epidermal outgrowths were present all over the pollen sacs. The typical pyramidal shaped cells of the WT were mostly absent, and when present they occurred on the distal surface of the pollen sacs and had enlarged and/or globose tips (Appendix 10, *NbMYBI7-1* line 24-2, Plate VIII). Simple and branched trichomes were occasionally present

on the anther surface (Appendix 10, *NfMYBI7-1* line 10, Plate XXVIII and *NfMYBI7-1* line 12, Plate XXXII). The surface of the filament presented conical cells and/or simple trichomes, a phenotype not occurring in the WT. Self-pollination was limited or completely absent in several transgenic lines (*NbMYBI7-1* line 29-2, Plate XIII, and *NfMYBI7-1* line 8, Plate XXV), this might be due to the dense occurrence of trichomes along the dehiscence zone of the anthers of these lines.

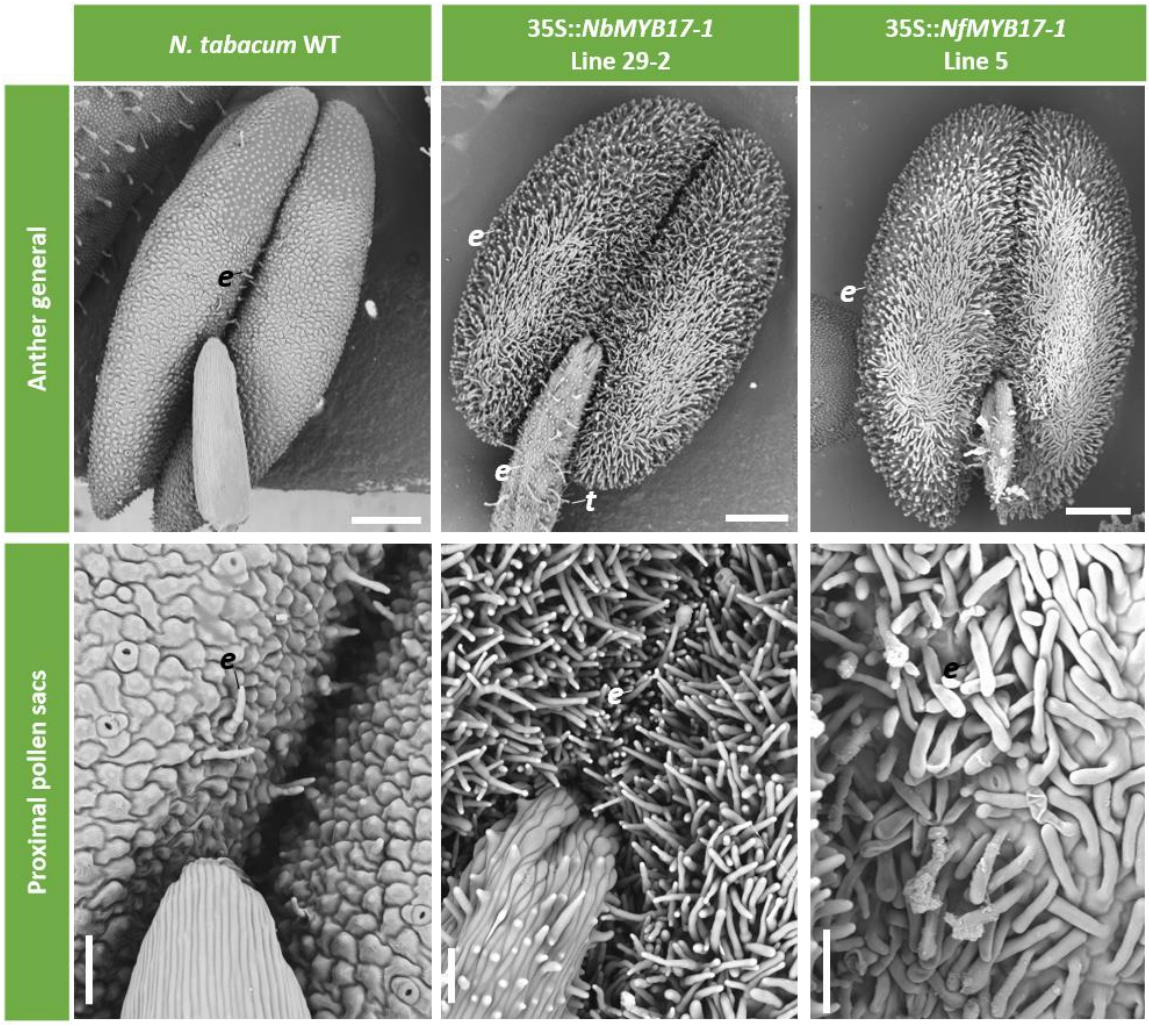

Figure 3.14. Ectopic expression of *NbMYB17-1* and *NfMYB17-1* increases the number and size of epidermal features on the anther surface of *N. tabacum* transgenic lines.
The transgenic lines present long tubular epidermal outgrowths (*e*) densely packed on all surfaces of the anther. The apical filament in the transformed lines has epidermal outgrowths of different lengths including simple trichomes (*t*). Scale bars = 500 µm top row, 100 µm bottom row.

Comparisons of epidermal features on carpel between the WT and putative transgenic lines are depicted in Figure 3.15. Both groups of lines, those expressing *NbMYBI7-1* and those expressing *NfMYBI7-1,* presented striking epidermal protrusions on the surface of the carpel.

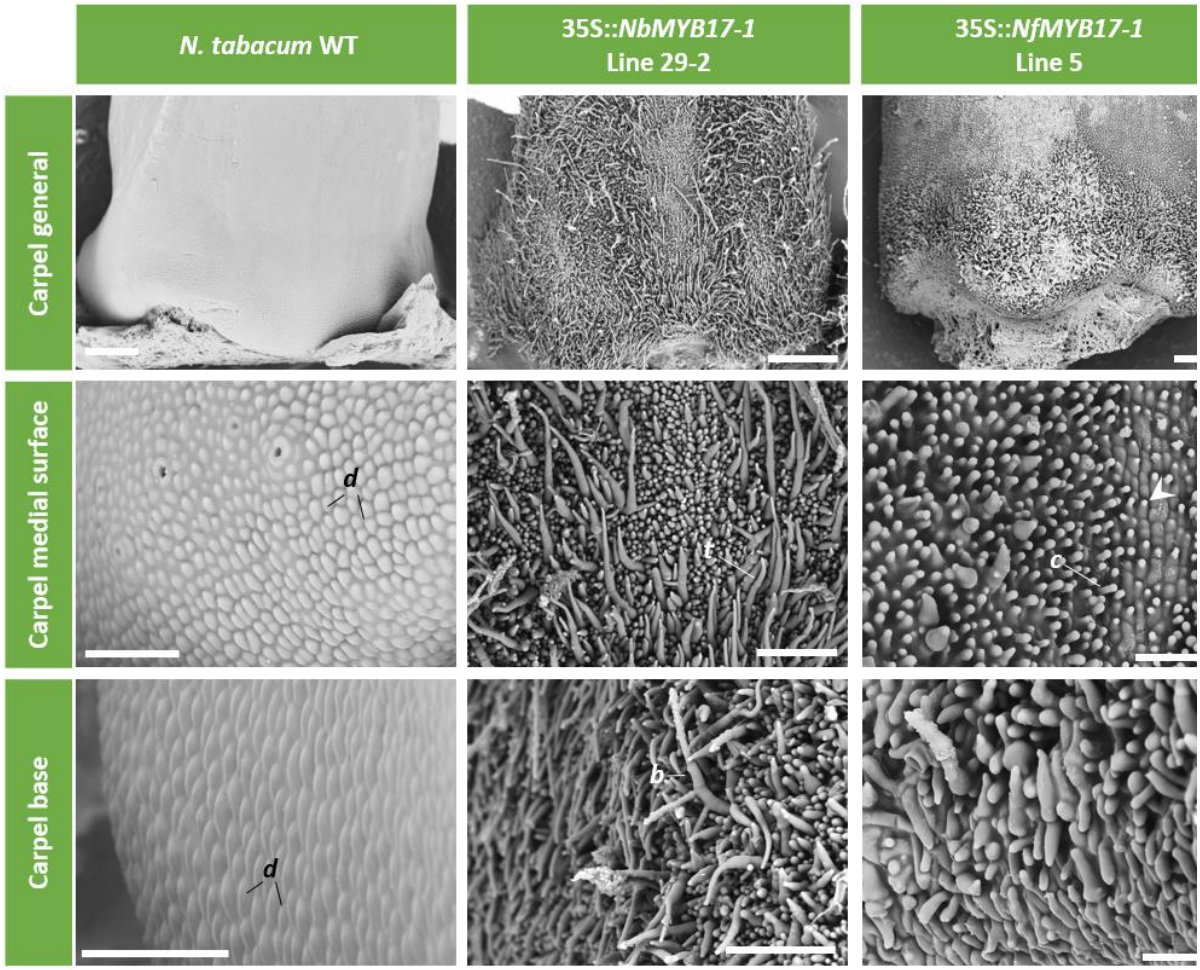

Figure 3.15. Expression of *NbMYB17-1* and *NfMYB17-1* promotes ectopic growth of epidermal outgrowths including conical cells and trichomes on the carpel surface of *N. tabacum* transgenic lines.

The presence of a range of densely packed epidermal outgrowths from conical (arrow heads) and clavate (c) cells to simple (t) and branched trichomes (b), compared to the smooth dome shaped cells (d) of the WT, is the most striking phenotype derived from the transgene expression. Scale bars = 500 µm first row, 100 µm second and third rows.

Compared to the smooth dome-shaped epidermal cells on the surface of the carpel of *N. tabacum* WT, lines ectopically expressing *NbMYBI7-1* or *NfMYBI7-1* (Figure 3.15) present phenotypes that are very different. All lines analysed had clearly defined epidermal outgrowths on all areas of the ovary. There was a clear zonation of the epidermal outgrowths along different regions of the ovary, for instance, the base of the ovary in general had longer, more complex and more densely arranged epidermal outgrowths than the rest of the organ. Moreover, in some lines the suture line between the two carpels that form the ovary, had five or more lines of cells with contrasting characteristics to the rest of the surface (shorter and more loosely arranged), resulting in a clear band along the suture (Figure 3.15, *NbMYBI7-1* line 25-2, Appendix 10, Plate X). Ectopic epidermal outgrowths on the carpel of the transgenic lines ranged from simple conical (arrowheads in Figure 3.15) or clavate (*cl* in Figure 3.15) cells (Appendix 10, *NbMYBI7-1*

line 25-2, Plate X), to single trichomes formed from one to many cells, to branched trichomes, and single cells with multiple outgrowths in different directions (Appendix 10, *NbMYBI7-1* line 29-3, Plate XVII, panel D). Stomata were also detected on the surface of the carpel of some transgenic lines (Appendix 10, *NfMYBI7-1* line 11, Plate XXXI and *NfMYBI7-1* line 12, Plate XXXIII).

3.4.4 Establishing flower developmental stages in *N. bonariensis* and *N. forgetiana*

The developmental series of the adaxial petal surfaces of *N. bonariensis* (Figure 3.16) and *N. forgetiana* (Figure 3.17) showed that similar stages of cell development are reached at similar stages of floral development in both species. In both species epidermal cells initiate flat. These cells expand and become more rounded. By stage 4, the cells of both species are rounded and dome shaped. The final cell shapes of these two species do not become apparent until late on in floral development: *N. forgetiana* cells only acquire their conical shape between stages 4 and 5, whilst the *N. bonariensis* cells remain non-conical between stages 4 and 5.

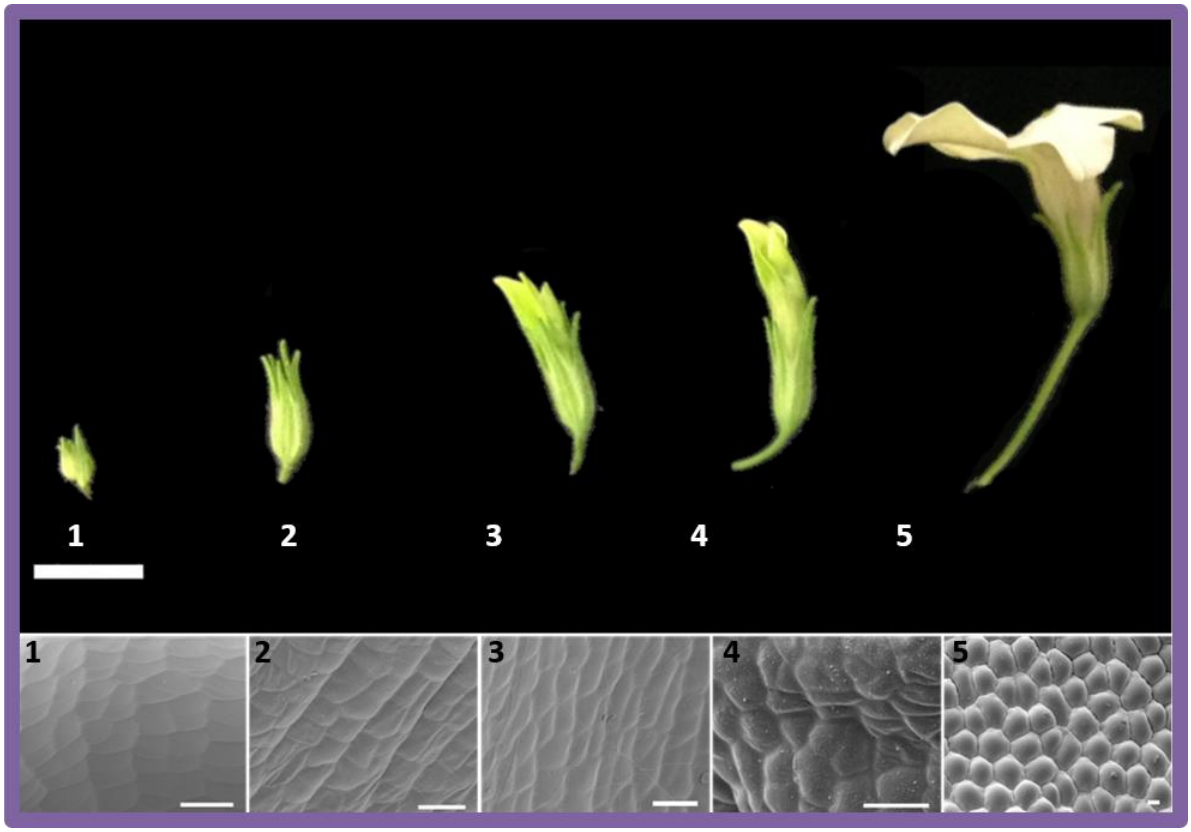

Figure 3.16. Flower and adaxial petal cell development of *N. bonariensis* (Section *Alatae*).
Top panel: Macromorphology of flowers at five developmental stages. Bottom panel: SEM images of adaxial petal cells at the same five developmental stages. Adaxial petal cells in *N. bonariensis* are non-conical across all developmental stages. Scale bar top panel = 10.0 mm, bottom panel = 10 µm.
Stage 1: Flower buds closed; 0.1-0.5 mm long; green calyx surrounding the rest of the flower; tips of the calyx lobes appear closed over the rest of the organs (top panel-1). Adaxial petal cells are rectangular in contour with a smooth surface (bottom panel-1).
Stage 2: Flower buds closed; 0.6-10.0 mm long; green calyx surrounding the rest of the flower; tips of the calyx lobes open slightly relative to the rest of the organs (top panel-2). Adaxial petal cells angular in contour with smooth surface (bottom panel-2).
Stage 3: Flower buds open; 10.0-20.0 mm long; petal lobes emerge from the tip of the calyx; corolla lobes closed over the rest of the organs, corolla white-greenish in colour (top panel-3). Adaxial petal cells rhomboidal in contour with smooth surface, lenticulate (bottom panel-3).
Stage 4: Flower buds open; 20.0-25.0 mm long; petal lobes and corolla tube protruding out from the tip of the calyx; corolla lobes closed over the rest of the organs, corolla white-purplish in colour (top panel-4). Adaxial petal cells dome shaped with smooth surface (bottom panel-4).
Stage 5: Mature flower; ≥25 mm; petal lobes fully open, white on the adaxial surface, white-purple-greenish on the abaxial surface (top panel-5). Adaxial petal cells rounded in contour, slightly dome shaped, non-conical (bottom panel-5).

Figure 3.17. Flower and adaxial petal cell shape development of *N. forgetiana* (Section *Alatae*).
Top panel: Macromorphology of flowers at five developmental stages. Bottom panel: SEM images of adaxial petal cells at the same five developmental stages. Adaxial petal cells in *N. forgetiana* are non-conical from stage 1 to 4, and become conical between stages 4 and 5. Scale bars top panel = 10.0 mm, bottom panel = 10 µm.
Stage 1: Flower buds closed; 0.1-0.5 mm long; green calyx surrounding the rest of the flower; tips of the calyx lobes appear closed over the rest of the organs (top panel-1). Adaxial petal cells are rectangular in contour with a smooth surface (bottom panel-1).
Stage 2: Flower buds closed; 0.6-10.0 mm long; green calyx surrounding the rest of the flower; tips of the calyx lobes open slightly relative to the rest of the organs (top panel-2). Adaxial petal cells slightly undulate in contour with smooth surface (bottom panel-2).
Stage 3: Flower buds open; 10.0-20.0 mm long; petal lobes emerge from the tip of the calyx; corolla lobes closed over the rest of the organs, corolla light green in colour (top panel-3). Adaxial petal cells circular in contour, lenticular, with smooth surface (bottom panel-3).
Stage 4: Flower buds open; 20.0-40.0 mm long; petal lobes and corolla tube protruding out from the tip of the calyx; corolla lobes closed over the rest of the organs; corolla lobes tip light to dark red; corolla throat and tube light green in colour (top panel-4). Adaxial petal cells dome shaped with smooth surface (bottom panel-4).
Stage 5: Mature flower; ≥40.0 mm; petal lobes fully open, dark red on the adaxial and abaxial surface of the petal lobes, green with red lines on the abaxial surface of the corolla throat and tube (top panel-5). Adaxial petal cells rounded in contour, with clearly defined pointy tips, conical (bottom panel-5).

3.4.5 Expression analyses of R2R3 MYB Subgroup 9 candidate genes in *N. bonariensis* and *N. forgetiana*

Taylor (2015) characterized expression patterns of R2R3 Subgroup 9 MYBS in *N. forgetiana* (conical cells) using qPCR. At the time of Taylor's investigation, no flower material was available for *N. bonariensis*, the non-conical celled sister species of *N. forgetiana*, so she used for comparison a close relative with non-conical cells, *N. longiflora*, which is also a member of Section *Alatae*. For these two species, Taylor (2015) compared expression patterns by pooling together tissue from petals in stages 1-2 to petals fully mature (stage 5). In the present investigation expression patterns of R2R3 MYB subgroup 9 MYBs are characterized for *N. forgetiana* (conical cells) and its sister species *N. bonariensis* (non-conical cells). The pool of tissue at earlier stages of development selected for this characterization is similar to that of Taylor (2015), by pooling together tissue from petals at stages 1 and 2 of development. However, for the later stages, a pool of petal tissue from stages 3 and 4 was selected for the analyses. Stages 3-4 of development were preferred over stage 5 (fully mature flower) as the expression of the genes involved in the morphogenesis of conical cells is likely to be more evident before the phenotype is detected.

3.4.5.1 Semiquantitative RT-PCR expression analyses of R2R3 Subgroup 9 MYB genes in N. bonariensis *and* N. forgetiana

Figure 3.18 shows semiquantitative RT-PCR products for four R2R3 Subgroup 9 MYB genes, *MIXTA-2, MIXTA-like, MYBI7-1* and *MYBI7-2,* in *N. forgetiana* and *N. bonariensis* at two developmental stages, at 23, 28 and 35 cycles. *COX-1* (cytochrome oxidase 1) was used as a reference gene in this experiment.

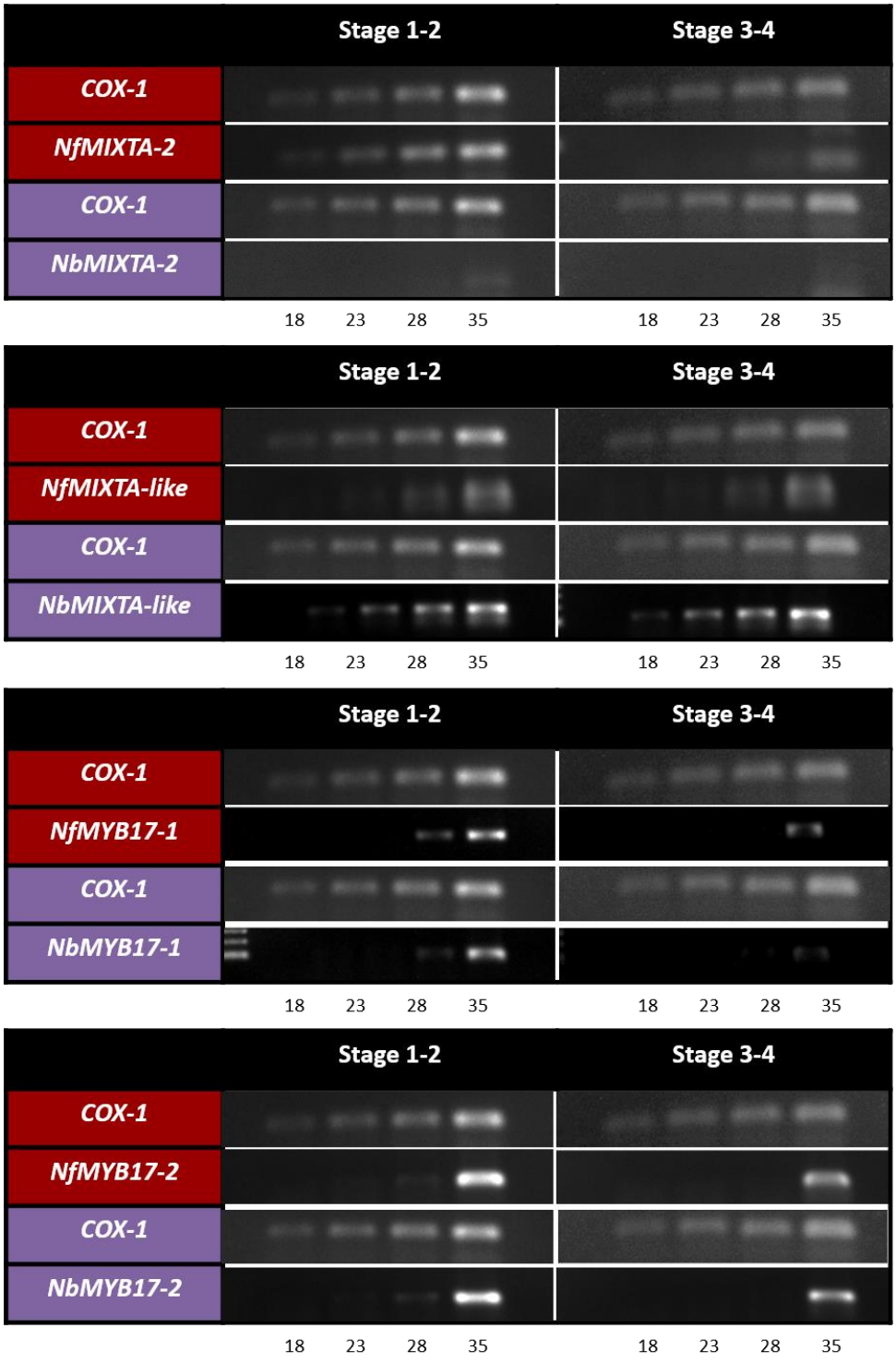

Figure 3.18. Expression of R2R3 Subgroup 9 MYB candidate genes in petals of *N. forgetiana* and *N. bonariensis* assessed by semi-qPCR.

The expression of R2R3 Subgroup 9 candidate genes (*MIXTA*-2, *MIXTA-like, MYB17-1* and *MYB17-2)* in petals of *N. forgetiana* (conical cells, red blocks) and *N. bonariensis* (non-conical cells, purple blocks) was assessed at two developmental stages (stage 1-2 and stage 3-4). *COX-1* was used as a reference gene. *MIXTA-2* was found to be differentially expressed in the two sister species. Expression of *MIXTA-2* in *N. bonariensis* (non-conical) is reduced in stages 1-2 and stages 3-4 compared to *N. forgetiana* (conical). 1 µL of cDNA from petal tissue was used as templeate for each 5 µL RT-PCR reaction. Products of the amplification were sampled at 18, 23, 28 and 35 cycles.

3.4.5.2 *qPCR expression analyses of R2R3 Subgroup 9 MYB genes in* N. bonariensis *and* N. forgetiana

3.4.5.2.1 Identification of stable reference genes for *N. bonariensis* and *N. forgetiana*

Three genes were considered for use as reference genes for qPCR expression analyses. *COX-1* (cytochrome oxidase-1) had been characterized by Taylor (2015) as the most suitable among nine genes analysed according to its relative stability in *N. forgetiana* and *N. longiflora*. *COX-1* was also the gene of reference used for the semiquantitative RT-PCR expression analyses in this chapter (Figure 3.18). The other two genes considered were *EF1α* (*Elongation factor 1 α*) and *L25* (*L25* ribosomal protein) which had been demonstrated to have the highest expression stability in qPCR in model species *Nicotiana tabacum* (Schmidt & Delaney, 2010) and had been used as reference genes for this kind of gene expression analyses in non-model species *N. attenuata* (Groten *et al.*, 2015).

3.4.5.2.2 Amplification efficiencies of primers used for qPCR expression analyses

Amplification efficiencies were calculated for reference gene primers using standard curves. These values represent the factor by which the amount of PCR product increases per cycle, *e.g.* an amplification efficiency of 1.0 (2.0 efficiency Pfalff definition) corresponds to a doubling of product per cycle. Primer efficiencies for each set of primers used in this chapter are shown in Table 3.4. These values were factored into the final calculation of relative gene expression. *COX-1* was not considered in the final assessment of relative expression of the genes of interest because the primer efficiency was higher than 1.10 for *N. forgetiana*. Recommended values for reaction efficiency range between 0.90 and 1.10 (90-110%).

Table 3.4. Amplification efficiencies for qPCR primers used in this chapter

R2R3 Subgroup 9 Genes

Primer Pair	Efficiency	Efficiency Pfalff definition
MIXTA-2	0.97	1.97
MIXTA-like	0.93	1.93
MYB17-1	1.04	2.04
MYB17-2	0.98	1.98

Reference Genes

Primer pair	*N. forgetiana*		*N. bonariensis*	
	Efficiency	Efficiency Pfalff definition	Efficiency	Efficiency Pfalff definition
COX-1	1.22	2.22	0.94	1.94
EF-1α	1.05	2.05	1.03	2.03
L25	1.09	2.09	0.94	1.94

Figure 3.19 shows expression patterns for *MIXTA-2, MIXTA-like* and *MYB17-1* genes in petals at two developmental stages (stage 1-2 and stage 3-4) of *N. bonariensis* and *N. forgetiana*.

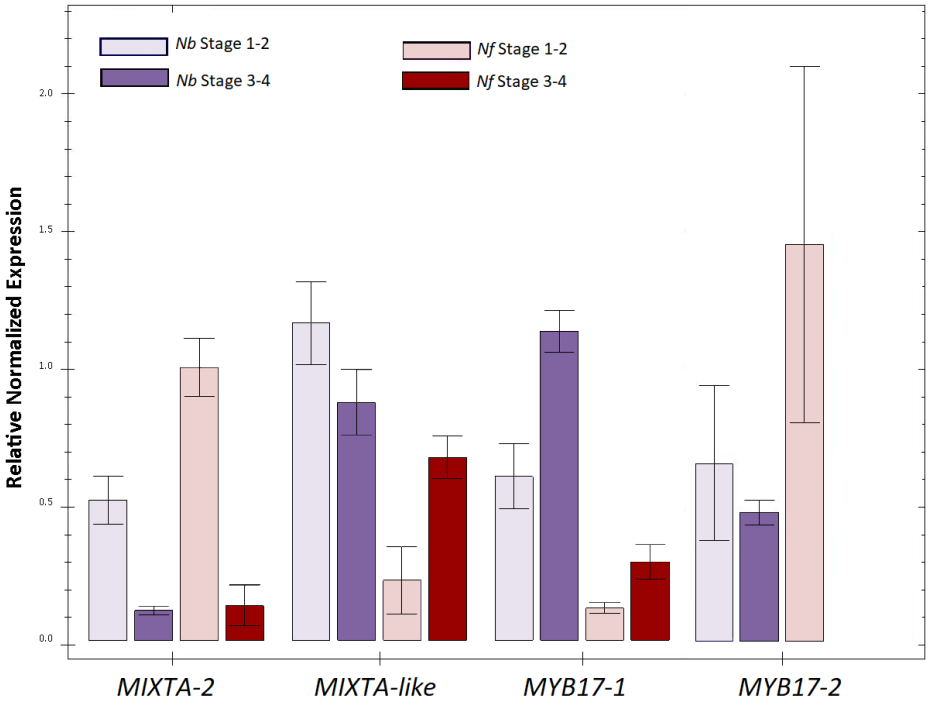

Figure 3.19. Differential expression of R2R3 MYB Subgroup 9 genes, between sister species *N. bonariensis* (non-conical) and *N. forgetiana* (conical), across developmental stages.
Relative normalized expression of R2R3 Subgroup 9 MYB genes in *N. bonariensis* and *N. forgetiana*. Expression of *MIXTA-2*, *MIXTA-like*, *MYB17-1* and *MYB17-2* in petals of *N. bonariensis* (Nb, purple) and *N. forgetiana* (Nf, red) at stages 1-2 (lighter shades) and 3-4 (darker shades) of development, relative to the reference genes EF1α and L25. n=3, error bars show the standard error of the mean. All values are the mean of three biological replicates with three technical replicates.

3.4.5.3 *Gene expression patterns of* MIXTA-2 *in* N. bonariensis *and* N. forgetiana

Relative expression levels of *MIXTA-2* assessed by qPCR (Figure 3.19) were higher in stage 1-2 than in stage 3-4 for both species. When comparing between species, expression levels of this gene were higher in *N. forgetiana* (conical cells) than in *N. bonariensis* (non-conical cells). This pattern is consistent with the results from the semiquantitative RT-PCR characterization of expression (Figure 3.18, first panel), although the qPCR detected a higher level of expression in *N. bonariensis* than did the semiquantitative analysis. The pattern is also consistent with the comparison between *N. forgetiana* and *N. longiflora* (non-conical cells) by Taylor (2015).

3.4.5.4 *Gene expression patterns of* MIXTA-like *in* N. bonariensis *and* N. forgetiana

Relative expression of *MIXTA-like* assessed by qPCR (Figure 3.19) is higher in stage 1-2 in *N. bonariensis* compared to stage 3-4 of the same species. In contrast, *MIXTA-like* levels of expression are lower in the earlier stages (1-2) of *N. forgetiana* compared to the later stages (3-4). When comparing between species, *MIXTA-like* levels of expression are higher at the two

developmental stages assessed in the non-conical celled *N. bonariensis*. The differential pattern of expression between species was similar in the semiquantitative RT-PCR assessment (Figure 3.18, second panel), however the resolution between developmental stages within each species was improved with the qPCR. The patterns detected are partially consistent with the findings by Taylor (2015). In that case, *MIXTA-like* gene expression levels were also higher in the non-conical celled species *N. longiflora*, but the patterns of expression between developmental stages within species were different. For the non-conical celled *N. longiflora*, levels of expression were still higher at the earlier stage (1-2) but the expression at the later stage (stage 5) was much reduced. For the conical celled-species *N. forgetiana* expression levels were higher at the earlier stages (1-2) compared to the later (stage 5). It is important to notice that the developmental stages assessed in this work are not the same as the ones evaluated by Taylor (2015), so the results are not necessarily contradictory but might be adding improved resolution to the gene expression profile of these species.

3.4.5.5 Gene expression patterns of MYB17-1 *in* N. bonariensis *and* N. forgetiana

For both species, levels of expression assessed by qPCR of *MYBI7-1* (Figure 3.19) were lower at the early stages (1-2). When comparing between species, the non-conical celled *N. bonariensis* presented higher expression of *MYBI7-1* than the conical celled *N. forgetiana*. Differential expression between developmental stages was detected for both species in the semiquantitative RT-PCR assessment (Figure 3.18, third panel), however differential expression between the two species was not detected through this method. Compared to the assessment of Taylor (2015) these results are congruent with the pattern reported for *N. longiflora* and *N. forgetiana*, in which *MYB-17-1* presented higher levels of expression in the non-conical celled species. Differences between developmental stages are once again difficult to interpret as different stages were evaluated in each work. However, levels of expression for *MYBI7-1* in the non-conical celled species *N. longiflora* present a marked contrasting pattern from stage 1-2 to stage 5, being clearly higher at early stages. On the contrary, levels of expression of this gene in *N. forgetiana* assessed by Taylor (2015) appear to be equally low at both stages of development.

3.4.5.6 Gene expression patterns of MYB17-2 *in* N. bonariensis *and* N. forgetiana

Quantification of expression levels of *MYBI7-2* coincide with the pattern detected in the semiquantitative PCR exploration (Figure 3.18, fourth panel). Higher levels of expression are detected in the earlier stages of development in petals of both species. With the qPCR analysis differential expression patterns between the conical and the non-conical celled species can be noticed. In *N. bonariensis* (non-conical celled species), levels of expressions in earlier

developmental stages (stge 1-2) are lower relative to *N. forgetiana* (conical celled species). However, during the later stages of development (stage 3-4), expression of *MYBI7-2* is undetectable in the conical celled species *N. forgetiana.* Taylor (2015) found overall low levels of expression for *MYBI7-2* in *N. longiflora* and *N. forgetiana*, but the gene presented higher expression in the conical celled species *N. forgetiana*.

3.5 DISCUSSION

3.5.1 Sequences of R2R3 Subgroup 9 MYB transcription factors in *N. bonariensis* and *N. forgetiana*

The detailed characterization of R2R3 MYB Subgroup 9 genes in *N. bonariensis* and *N. forgetiana* allowed the detection of differences between the coding sequences of the non-conical and the conical celled species that potentially could have an effect on the function of the native protein. The genes characterized within the R2R3 MYB Subgroup 9A belong to the two different subclades: *MIXTA-2* to the subclade *MIXTA* and *MIXTA-like* to the subclade *MIXTA-like*. These genes presented similar patterns when comparing the sequences of orthologues between sister species. For both genes, differences in the coding sequences were detected within individuals of the same species for both *N. bonariensis* and *N. forgetiana.* However, for any given variable position at least one individual of each species presented one of the possible nucleotides in that position (Figure 3.5, Figure 3.6). This suggests that the sequence of *MIXTA-2* and *MIXTA-like* in *N. forgetiana* and *N. bonariensis* is labile, with multiple alleles present, and that the substitutions detected cannot explain the differential phenotype of petal cell shape in these species.

For the R2R3 MYB Subgroup 9B clade two genes of the *MYBI7* subclade (*MYBI7-1* and *MYBI7-2*) were cloned from *N. bonariensis* and *N. forgetiana.* The coding sequences of *NbMYBI7-1* and *NfMYBI7-1* were found to be highly divergent, with several differences detected between sister species (Figure 3.7, Figure 3.8, Table 3.3). Non-synonymous substitutions with positive scores of predicted effect of point mutation were detected, and in consequence this gene was selected to test the idea that sequence differences might be involved in defining differential phenotypes of petal cell shape. On the contrary, coding sequences for *NbMYBI7-2* and *NfMYBI7-2* were found to be highly conserved.

3.5.1.1 *Potential effect of amino acid differences detected between* NbMYB17-1 *and* NfMYB17-1

As listed in section 3.4.2.3, several amino acid substitutions were detected when comparing the sequences of NbMYB17-1 and NfMYB17-1. Two of those substitutions were predicted to have no or neutral effect on the protein function: threonine for alanine, (T-A, amino acid residue 215, score -7) and isoleucine for leucine (I-L, amino acid residue 289, score -46). On the other hand, three amino acid substitutions were predicted to have an effect on the protein function: amino acid residue 127, proline for histidine (P-H, score +18), amino acid residue 215, isoleucine for valine (I-V, score +20) and amino acid residue 226, phenylalanine for leucine (F-L, score +19).

Position 127 of the amino acid chain corresponds to a disordered exposed region of the protein (Figure 3.8). Histidine and proline are chemically and structurally different. First, there is a considerable 40 Da mutation shift between the two amino acids (Bordo & Argos, 1991). Histidine is generally considered to be a polar amino acid, however it is unique with regard to its chemical properties, which means that it does not substitute particularly well with any other amino acid (Betts & Russell, 2007). Histidine is structurally flexible, being relatively easy to move protons on and off of the side chain (*i.e.* changing the side chain from neutral to positive charge) (Betts & Russell, 2007). This flexibility means that there is ambiguity about whether H prefers to be buried in the protein core or exposed to solvent. Also, that H it is an ideal residue for protein functional centres (Betts & Russell, 2007). Proline, on the other hand, is one of the few very small amino acids, it is unique in that it is the only amino acid where the side chain is connected to the protein backbone twice, forming a five-membered ring. P is unable to occupy many of the main-chain conformations easily adopted by all other amino acids and is often found in very tight turns in protein structures (Betts & Russell, 2007). It can also function to introduce kinks into α-helices since it is unable to adopt a normal helical conformation. Despite being aliphatic the preference for turn structure means that prolines are usually found on the protein surface. The proline side chain is very non-reactive. This, together with its difficulty in adopting many protein main-chain conformations, means that it is very rarely involved in protein active or binding sites (Betts & Russell, 2007; Choi et al., 2012). The chemical and structural differences between H and P, account for the positive score predicted for the effect of the substitution on the protein function.

Position 215 of the MYB17-1 protein lays on a disordered, exposed region. Both I and V are aliphatic, non-polar, hydrophobic amino acids, there is a mutation mass shift of 14 Da between the two amino acids and they can be substituted for each other with 95% confidence (Bordo & Argos, 1991). Moreover, whereas most amino acids contain only one non-hydrogen substituent

attached to their beta (Cβ carbon), I and V contain two (are Cβ branched), this means that there is a lot more bulkiness near to the protein backbone and that these amino acids are more restricted in the conformations the main chain can adopt. In spite of the overall chemical similarities between these two molecules, substitutions of valine for isoleucine have been shown to result in more compact protein structure at high pH, which would reduce the electrophoretic mobility of the protein (Keating & Cronan, 1996). These likelihood of changes under specific cellular environmental conditions may account for the positive score predicted for the substitution.

Residue 226 also corresponds to a disordered, exposed region of the protein. Leucine is an aliphatic, hydrophobic, non-polar amino acid. Phenylaniline is aromatic, hydrophobic and non-polar. There is a mutation mass shift of 34 Da between the two amino acids and they can be substituted for each other with 95% confidence (Bordo & Argos, 1991). Leucine side chain is very non-reactive and is thus rarely directly involved in protein functions like catalysis, although it can play a role in substrate recognition (Betts & Russell, 2007). The aromatic side chain of phenylalanine could be involved in stacking interactions with other aromatic side chains (Betts & Russell, 2007). The differences in the potential interactions of these two amino acids is probably influencing the positive score predicted for this substitution in the protein function.

3.5.2 Heterologous expression of *NbMYB17-1* and *NfMYB17-1* in *N. tabacum*

Because of the sequence differences detected between the *MYBl7-1* orthologue of the conical celled species *N. forgetiana* and that of the non-conical celled species *N. bonariensis*, *MYBl7-1* was selected to further explore the protein function of the alternative sequences of each one of the sister species. Ectopic expression of *NbMYBl7-1* and *NfMYBl7-1* in *N. tabacum* allowed us to test whether there was any loss of function of the protein between non-conical and conical celled species. If the sequence differences detected between the orthologues of *MYBl7-1* were solely responsible for the differences in petal cell shape between *N. bonariensis* and *N. forgetiana*, we would expect major differences between the phenotypes resulting from the overexpression of *NbMYBl7-1* (the orthologue from the non-conical celled species *N. bonariensis)* compared to the phenotype of lines overexpressing *NfMYBl7-1* (the orthologue from the conical celled species *N. forgetiana*). However, heterologous expression in *N. tabacum* demonstrated that both orthologues function as positive regulators of epidermal outgrowths, including conical cells. However, compared to the phenotypes resulting from heterologous expression in *N. tabacum* of *MIXTA-like* orthologues of *N. cordifolia* and *N. solanifolia* (section 2.4.3.2*)*, the type, relative

abundance and size of the epidermal outgrowths resulting from ectopically expressing *MYB17-1* suggest a stronger effect of the sequence of *MYB17-1* in epidermal outgrowth regulation than the sequence of *MIXTA-like*.

Few R2R3 MYB Subgroup 9B genes have been characterized via ectopic expression in *N. tabacum* (Table 3.5). Brockington *et al.*, (2013) ectopically expressed a *MYB17-like* clade gene from *Lotus japonicus* (Fabaceae, Rosidae). Epidermal cells on the abaxial and adaxial surfaces of leaves of *N. tabacum* lines expressing *LjMYB17-like* are predominantly papillate with reduction in the occurrence of stomata. Similarly to this work, Brockington et al., (2013) detected long thin epidermal cells with occasional papillae and short and long simple trichomes on the anther filaments. On the ovary walls the cells of the transgenics were predominantly papillate, and on the petals elongated papillate cells and simple trichomes occurred (Brockington, 2013).

Along with other R2R3 MYB Subgroup 9 genes (Table 2.7), Bailes (2016) characterized two Subgroup 9B genes for *Vicia faba* (Fabaceae, Rosidae): *VfMYB17* in clade MYB17 and *VfMYB17-like* in clade MYB17-like. Through ectopic expression of both genes in *N. tabacum,* Bailes (2016) confirmed that they were positive regulators of epidermal outgrowths. The phenotype was stronger in lines expressing *VfMYB17-like*, but both constricts were shown to produce conical cells with varying degrees of protrusion on the ovaries of *N. tabacum* (Bailes, 2016).

Davis (2019) characterized the function of two genes of *Solanum lycopersicum* (Solanaceae, Asteridae) in the *MYB17* clade (*SlMYB17-1* and *SlMYB17-2*). As has been mentioned, there are no representatives of the MYB17-like clade in Solanales (section 1.4.2). Heterologous expression of both *SlMYB17-1* and *SlMYB17-2* in *N. tabacum* resulted in ectopic epidermal outgrowths on anthers carpel and stigma. Moreover, branched trichomes were detected on the leaves for both constructs. The phenotype of putative transgenic lines expressing *SlMYB17* genes (Davis, 2019; Table 3.5) strongly resembles the phenotype reported in this work for the heterologous expression of *MYB17-1* genes of sister species in *Nicotiana* Section *Alatae*.

Table 3.5. Phenotypic effect on epidermal features of the heterologous expression of R2R3 MYB Subgroup 9B subclade genes in *N. tabacum*

Species (adaxial petal cell shape)	Gene Clade	Gene Subclade	Gene name	Phenotype of the epidermis in the transgenic lines							Reference
				Ovary	Anther	Stamen filament	Petal abaxial	Petal adaxial	Leaf adaxial	Leaf abaxial	
Lotus japonica	SB9-B	MYB17-like	*LjMYB17-like*	Epidermal cells predominantly papillate (conical)		Long thin epidermal cells with occasional papillae and short and long simple trichomes		Conical cells on the petal surface are now mostly elongated into long glandular trichomes	Epidermal cells predominantly papillate with reduction in the occurrence of sto- mata	Epidermal cells predominantly papillate with reduction in the occurrence of stomata	Brockington *et al* ., 2013
Vicia faba	SB9-B	MYB17	*VfMYB17*	Conical cells with varying degrees of protrusion		Moe bumpy texture than WT, sometimes cells protruding	WT phenotype	WT phenotype	Ectopic conical cells	Ectopic conical cells	Bailes, 2016
		MYB17-like	*VfMYB17-like*	Conical cells with varying degrees of protrusion	Pyramidal cells protruding away with cylindrical elongation and spherical bulge at the top top	Conical cell-like projections of varying lengths	Elongated conical cells, trichomes more abundant than in WT	Elongated conical cells, trichomes present	Ectopic conical cells	Ectopic conical cells	
Solanum lycopersicum (conical)	SB9-B	MYB17	*SlMYB17-1*	Prominent, widespread conical cells on the carpel surface	Long, fingerlike outgrowths on all surfaces, sparce stalked stomata	Fingerlike outgrowths, conical cells		WT phenotype on the corolla lobes, conical cells on the corolla tube		Branched trichome present	Davis, 2019
			SlMYB17-2	Long, fingerlike outgrowth abundant on the carpel surface	Fingerlike outgrowths mostly on the connective			WT phenotype on the corolla lobes, trichome on the corolla tube	Branched trichomes present	Conical cells present	
Nicotiana bonariensis (non-conical)	SB9-B	MYB17	*NbMYB17-1*	Abundant ectopic epidermal outgrowths from conical cells to branched trichomes	Long tubular epidermal outgrowths densely packed on all surfaces of the anther	Epidermal outgrowths of different lengths including simple trichomes	Increased trichomes, clavate epidermal cells	Conical cells longer than in WT (papillate and clavate)	Conical cells and branched trichomes present, higher abundance of trichomes	Conical cells and branched trichomes present, higher abundance of trichomes	This work (Chapter 3)
Nicotiana forgetiana (conical)	SB9-A	MYB17	*NfMYB17-1*	A range of densely packed epidermal outgrowths from conical and clavate cells to simple and branched trichomes	Long tubular epidermal outgrowths densely packed on all surfaces of the anther	Epidermal outgrowths of different lengths including simple trichomes	Increased trichomes, clavate epidermal cells	Conical cells longer than in WT (papillate and clavate)	Conical cells and branched trichomes present, higher abundance of trichomes	Conical cells and branched trichomes present, higher abundance of trichomes	

3.5.3 Gene expression patterns of R2R3 Subgroup 9 MYB transcription factors in *N. bonariensis* and *N. forgetiana*

The developmental series of *N. bonariensis* (Figure 3.16) and *N. forgetiana* (section Figure 3.17) showed that the development of the adaxial petal epidermal cells in the two species roughly coincide. The only distinction is between stages 4 and 5 (pre- and post- anthesis) when the cells of *N. forgetiana* acquire their characteristic pointy tips.
The characterization of gene expression of R2R3 9 MYBs in *N. bonariensis* and *N. forgetiana* by semiquantitative RT-PCR gave an initial idea of the differential expression of the genes between the two sister species. Using this method, a striking pattern of reduced expression of the *MIXTA-2* gene in the petals of *N. bonariensis* (non-conical cells) compared to *N. forgetiana* (conical cells), was evident. However, the results lack resolution to interpret finer features of the gene expression patterns, for example, to identify differences within species at consecutive developmental stages. Nevertheless, semiquantitative RT-PCR is a technique easy to perform and of low cost that could be used as an initial exploration of gene expression, complementary to q-PCR.

q-PCR assessment of relative gene expression in sister species of *Nicotiana* Section *Alatae* provided improved resolution of the expression patterns detected with semiquantitative RT-PCR. Differential expression in *MIXTA-2* between *N. forgetiana* and *N. bonariensis* was confirmed with the q-PCR experiment. *MIXTA-2* also presented higher levels of expression in the conical-celled species *N. forgetiana.* This suggests that differential levels of expression of this gene may play a role in the differentiation of conical cells in this species. The expression of *MIXTA-2* in *N. forgetiana,* as quantified by q-PCR, is higher during the earlier stage of development (1-2), but during stage 3-4 the levels of expression are very similar to *MIXTA-2* in *N. bonariensis* at stage 3-4. This suggests that the gene activity in earlier stages of development might be involved in the development of conical cells even though these epidermal structures only are apparent at the later stages (stage 5, Figure 3.17).

MYBl7-2 expression levels assessed by q-PCR present a similar pattern to *MIXTA-2* of higher expression levels at the earlier developmental stage (1-2) in the conical-celled species, *N. forgetiana,* compared to the levels of expression during the late stage (3-4) of the same species. These levels of expression during stage 1-2 are also higher compared to the expression in the non-conical celled species (*N. bonariensis*) during the early stages. *NfMYBl7-2* then, is a good

candidate to further explore its involvement in the development of conical cells on the petals of *N. forgetiana*.

It is also interesting that *MIXTA-like* and *MYBI7-1* are more highly expressed in the petals of the species with non-conical cells, *N. bonariensis*. As has been shown in this thesis, both *MIXTA-like* and *MYBI7-1* genes of *Nicotiana* species are positive regulators of epidermal outgrowths so it is not clear why they would they be more highly expressed in the non-conical celled species. In *Arabidopsis thaliana* the expression of a MYB subgroup 9B gene (*AtMYBI7*) has been associated with the vegetative to floral meristem identity transition, through interactions with *LEAFY* (*LFY*) (Pastore *et al.*, 2011). *AtMYBI7* is most highly expressed in young *Arabidopsis* floral primordia and in the stamens and carpels of older flowers. Expression was not reported in the petal. The role of MYBI7 subclade genes with respect to cell outgrowth is not known. Their only characterised function is an involvement with the developing petals. The *Nicotiana LFY* homologues, *NFLI* and *NFL2*, are expressed in floral and vegetative meristems (Kelly *et al.*, 1995), although their expression in developing petals was not assessed.

3.5.4 Molecular control of petal cell shape in *N. bonariensis* and *N. forgetiana*

Given that the sequences of *MIXTA-2*, *MIXTA-like* and *MYBI7-2*, in spite of some interspecific variation, can be considered conserved between the two sister species, and that it was experimentally demonstrated that the sequence differences between *MYBI7-1* orthologues are not likely to be responsible for petal cell shape differences between *N. bonariensis* and *N. forgetiana*, differential expression of the candidate genes in the petals is a mechanism likely to be involved in the contrasting phenotype of these two species. The results of this work suggest that the *N. bonariensis* (non-conical celled species) MYB subgroup 9 proteins are still functional, and that loss of conical cells in this species is more likely to be due to a change in MYB subgroup 9 expression, or due to a change in another gene upstream or downstream in the same developmental pathway.

The details on how R2R3 Subgroup 9 MYB transcription factors are involved in regulatory networks controlling epidermal cell patterning, including conical cells, is not well understood. However, from investigations in other angiosperms some inferences can be made (see section 6.1.4 for further discussion). Characterisations of the regulatory regions of R2R3 Subgroup 9 MYB genes in sister species of *Nicotiana* that differ in their cell morphologies, would allow the identification of potential *cis*-regulatory elements in regions immediately upstream and

downstream of these genes. Putative promoters could be fused to reporter genes, and subsequently transformed into a model (such as *N. tabacum*) to determine their spatiotemporal expression patterns. Similarly, selective deletion of promoter regions in these constructs would allow precise identification of motifs that are important for R2R3 Subgroup 9 MYB gene regulation (Taylor, 2015).

In this chapter experimental evidence for differential expression of R2R3 subgroup 9 MYBs has been provided. *MIXTA-2* and *MYBI7-2*, being more highly expressed in the petals of the conical celled species *N. forgetiana,* are good candidates to be involved in the regulation of petal cell development in this species. Confirming the role of *Nb/NfMIXTA-2* and *Nb/NbMYBI7-2* as positive regulators of epidermal outgrowth (including conical cells) is then crucial to continue this line of work. Heterologous expression of *Nb/NfMIXTA* in *N. tabacum* and *N. benthamiana* was attempted at the end of this project, however, the putative putative transgenic lines for both model species did not grow further than in the sapling stage and genotyping and phenotyping of these lines was not possible. A next step in this line of investigation would be to genetically manipulate the expression of *MIXTA-2* and *MYBI7-2* in *N. forgetiana* itself. With the progress that has been made in the establishment of an *Agrobacterium* mediated stable transformation protocol for *N. forgetiana* (Chapter 4), this kind of experiment should be possible to perform in the future.

3.5.5 Petal cell shape and plant pollinator interactions in Section *Alatae*

In a different manner to species in Section *Paniculatae*, where most species have conical cells and only one has non-conical (section 2.2.2), there is a more "even" distribution of petal cell shape (conical vs. non-conical) among the species in Section *Alatae* (section 3.2.2). However, in a similar manner to Section *Paniculatae*, and the genus *Nicotiana* in general (Taylor, 2015), there do not seem to be consistent associations between pollinator identity and petal cell shape in Section *Alatae*. *N. forgetiana*, *N. langsdorfii* and *N. mutabilis* are thought to be primarily hummingbird pollinated (Raguso *et al.*, 2003; Ippolito *et al.*, 2004) and all have conical cells, which contradicts the idea that bird pollinated flowers tend to have non-conical cells to deter small pollinators as visitors (as discussed in sections 1.2.2.2 and 2.5.4). On the other hand, *N. alata* (conical), *N. longiflora* (non-conical) and *N. plumbaginifolia* (non-conical) all have been reported to be pollinated by hawkmoths (Ippolito *et al.*, 2004), hovering pollinators which in theory would not benefit from the flowers having conical cells, so these would have a tendency to be lost from the petals of hawkmoth pollinated flowers.

Sister species *N. bonariensis* and *N. forgetiana* present contrasting features, not only in petal cell shape, but in colour (white vs. red), overall size, length of the tube, corolla symmetry (Figure 3.3) and scent profiles (Raguso *et al.*, 2006). This may represent a case of niche partitioning driven by differential pollinator systems. *N. bonariensis* would represent a case of specialization towards pollination by moths, and *N. forgetiana* a tendency towards a hummingbird pollination system. However, the limited field observations for these species (Ippolito, 2000; Ippolito *et al.*, 2004; Raguso *et al.*, 2006) (Table 3.1) in which visits by various putative pollinators have been recorded, suggest that these species might still present mixed pollination systems. The presence of conical cells in *N. forgetiana* and spectral properties of the petals of these species as characterized in Chapter 5, might give support to the idea of bees being also pollinating visitors for these species.

Alternatively, the presence or absence of conical cells might not necessarily be directed by flower-pollinator interaction. For instance, petal cell shape may be influenced by factors other than pollination, such as petal wettability or thermoregulation (Whitney *et al.*, 2011c) (section 1.2.2.3). Even more, there may be no selection for or against the trait at all, and it may simply be evolving under genetic drift.

Chapter 4

Establishing an Agrobacterium *tumefaciens mediated transformation system for non-model* Nicotiana *species as a tool to study petal cell shape development*

4 Establishing an *Agrobacterium tumefaciens* mediated transformation system for non-model *Nicotiana* species as a tool to study petal cell shape development

4.1 INTRODUCTION

Agrobacterium tumefaciens mediated transformation is an important tool in plant sciences and plant biotechnology (Gelvin, 2003). For species with an established stable transformation protocol, the ability to regulate individual genes provides a valuable method to explore the function of such genes. Most of the commonly transformable species are crops or model species such as *Arabidopsis thaliana* (*e.g.* Chang *et al.*, 1994) and *Nicotiana tabacum* (*e.g.* Horsch *et al.*, 1985). However, stable transformation protocols for non-model plant species are still scarce. Having the possibility to transform non-model species is crucial to address ecological and evolutionary questions that cannot be resolved using model species (Krügel *et al.*, 2002). This chapter explores the potential to transform non-model species of *Nicotiana* (Section *Alatae* and *Paniculatae*) aiming to generate a tool to investigate gene regulation of petal cell shape. A stable transformation protocol would allow further exploration of the molecular evolution of conical cells by inserting R2R3 MYB Subgroup 9 genes potentially responsible for cell shape in conical-celled species into the genomes of the non-conical-celled species, or knocking out the genes in the species with conical epidermal cells using RNA interference (RNAi) or genome editing (CRISPR) methods. Plant lines obtained through transformation could be used to explore how animal pollinators (*e.g.* bumblebees, hawkmoths) respond to conical and non-conical celled lines of the same species in controlled behaviour set-ups, and even, potentially, in field settings. A good example of the scope of this kind of experimental biological tools in relation to pollination biology is the work carried out with the Grand Basin Desert of North America native *N. attenuata* (Section *Petunioides*). An *A. tumefaciens* stable transformation protocol has been established for this non-model *Nicotiana* (Krügel *et al.*, 2002). This tool has been used extensively to perform transformations with genes coding for key enzymes and to address ecological questions such as the role of certain genes in plant-mycorrhizal association for this species (Krügel *et al.*, 2002; Groten *et al.*, 2015). Interestingly, *N. attenuata* transgenic lines in which the expression of biosynthetic genes of floral attractants and repellents had been blocked via *A. tumefaciens* transformation, were used in a series of field experiments to assess the influences of non-pigment floral chemistry on nectar removal by animals, floral visitation, florivory, rates of outcrossing, and fitness through both male and female functions (Kessler *et al.*, 2008).

4.1.1 *Agrobacterium tumefaciens* as a tool for gene transfer

A. tumefaciens is a naturally occurring soil bacterium causing crown gall disease in numerous species of eudicots. The molecular mechanisms of *A. tumefaciens* pathogenicity are well known and are the basis of *Agrobacterium*-mediated plant transformation. *Agrobacterium* has the exceptional ability to transfer a particular DNA segment (T-DNA) of a tumor inducing (Ti) plasmid into the nucleus of infected plant cells. T-DNA is then stably integrated into the host genome and transcribed (Schell & Van Montagu, 1977; de la Riva *et al.*, 1998; Gelvin, 2003; Nester *et al.*, 2003). The Ti plasmid carries virulence (vir) genes that are involved in the processing of the T-DNA and its subsequent export from the bacterium to the plant cell. The T-DNA includes genes to produce phytohormones (auxins and cytokinins) which stimulate cell proliferation and gall formation. It also includes genes for opines that serve as a food source for *Agrobacterium*. To the right and left ends of the T-DNA there are repeated DNA sequences (25 bp), called T-DNA borders, that can be physically separated from the remainder of the Ti-plasmid. The tumor promoting and the opine-synthesis genes in the T-DNA are not required for its transfer to the plant cell, thus, it is possible to remove these genes from the T-DNA and replace them with a gene of interest and/or a selection marker (Hoekema *et al.*, 1983).

Binary vector systems are frequently used to generate transgenic plants. In these systems the binary vector (Ti vector) contains T-DNA border sequences between which foreign DNA can be cloned to be transferred to the plant genome (e.g. pGreen; Hellens *et al.*, 2000). Binary vectors are based on plasmids stable in both *Escherichia coli* and *Agrobacterium*. Because the Ti vectors are usually "disarmed", the host *Agrobacterium* contains a Ti helper plasmid with the functions necessary for gene transfer to plant cells but lacking a T-DNA. A number of *Agrobacterium* strains containing non-oncogenic vir helper plasmids have been developed, including GV3101 (Holsters *et al.*, 1980) and LBA4404 (Hoekema *et al.*, 1983).

4.1.2 Green Fluorescence Protein (GFP) as a reporter gene in plant transformation

When establishing an *A. tumefaciens* mediated plant transformation protocol, the use of visual markers, which enable direct observation of transformation events, results in a more precise and easier evaluation of various treatments and procedures. Several marker genes (β-glucuronidase, GUS; luciferase, LUC; or β-galactosidase, LacZ) have been successfully used in plant genetic

transformation (Helmer *et al.*, 1984; Ow *et al.*, 1986; Jefferson *et al.*, 1987; Hraška *et al.*, 2006; Malabadi *et al.*, 2008). The Green Fluorescent Protein (GPF) is widely used as a reporter in plant transformation. GFP occurs in nature in the Pacific jellyfish *Aequorea victoria* (Shimomura *et al.*, 1962; Prasher *et al.*, 1992; Shimomura, 2005). GFP transforms the luminescent blue light emitted by another jellyfish protein, aequorin, into green light. Its use has many advantages in plant transformation studies compared to other visual markers (Haseloff *et al.*, 1997; Elliott *et al.*, 1999; Hraška *et al.*, 2006; Malabadi *et al.*, 2008). GFP screening is non-destructive and does not require the addition of any interfering substances like exogenous substrates or enzymes. It allows monitoring transgenic expression from early stages of transformation through the recovery of living transgenic plants without the need to sacrifice valuable, sometimes sparse, transgenic material. Considering these advantages, GFP was selected as a reporter gene for assessing genetic transformation of *N. forgetiana*, *N. bonariensis*, *N. cordifolia* and *N. solanifolia*.

4.1.3 Regeneration of transgenic plants via tissue culture

In the *A. tumefaciens* mediated transformation process, tissue culture techniques are crucial to obtain and propagate putative transgenic tissues and plants. Explants to be inoculated with *Agrobacterium* can be taken from different parts of the plant (e.g. leaves, hypocotyls), or from many types of mature cells provided they are able to de-differentiate into totipotent cells. Tissue culture techniques involve growing the explants in sterilized nutrient media under controlled aseptic conditions. The nutrient medium must provide a carbon source (e.g. sucrose), inorganic salts, vitamins, amino acids and growth regulators like auxins and cytokinins (Smith, 2012). Given the appropriate combination of nutrients and hormone regulators, tissue culture has the potential to promote growth and differentiation through the main stages of the transformation protocol: (1) inoculation of the *A. tumefaciens* into the plant explant, (2) callus induction, (3) regeneration and shoot production, and (4) rooting. In this chapter, a broad spectrum of tissue culture media compositions was trialed looking for the optimal conditions for transformation of the four species of interest.

4.1.4 *Agrobacterium* mediated transformation in the genus *Nicotiana*

Nicotiana tabacum and *N. benthamiana* are two major model species for genetic transformation due to their high susceptibility to *A. tumefaciens* and high regeneration capacity of leaf explants through shoot organogenesis (Clemente, 2006). *N. tabacum* was the first plant species to be transformed with *A. tumefaciens*. *N. benthamiana* is susceptible to a vast number of plant viruses

(>500) and has become a cornerstone for the study of host/virus interactions in plants. *N. plumbaginifolia* has been widely used for *A. tumefaciens* mediated transformations mostly from protoplasts (Horsch *et al.*, 1984) and *N. sylvestris* (Section *Sylvestris*) has been used as a diploid alternative for its allotetraploid descendant *N. tabacum* in investigations on plasmid transformation (Maliga & Tungsuchat-Huang, 2014). Other *Nicotiana* species with readily available stable transformation protocols are the polyploids *N. debneyi* (Section Suaveolentes; Duan *et al.*, 2016) and *N. clevelandii* (Section Polydicliae; Tavazza *et al.*, 1988; Duan *et al.*, 2016), and the diploids *N. glutinosa* (Section Undulatae; Duan *et al.*, 2016), and *N. attenuata* (Section *Petunioides*; Krügel *et al.*, 2002). *N. clevelandii,* for instance, is used as a propagation host for many plant viruses. *A. tumefaciens* mediated transformation of this species has been aimed at conferring engineered protection against viruses (Tavazza *et al.*, 1988). *N. attenuata* as mentioned before (section 4.1) is becoming a model species for ecological studies and the ability to genetically transform this species has become an important tool in these studies (Baldwin & Karb, 1995; Kessler *et al.*, 2008, 2010; Groten *et al.*, 2015; Luu *et al.*, 2017).

The main objectives of this chapter were:

- Identifying the most suitable species for *A. tumefaciens* mediated stable transformation among the four species of interest
- Trialling a broad spectrum of conditions to optimize a transformation protocol for the species identified as most suitable

4.2 MATERIALS AND METHODS

4.2.1 *Agrobacterium tumefaciens* strains and plasmid vector

Most assays for transformation of *Nicotiana* spp. referred to in this section were performed using electrocompetent *Agrobacterium tumefaciens* strain GV3101. This strain has a chromosomal rifampicin resistance gene, but is sensitive to kanamycin, making it good for use with binary vectors that confer kanamycin resistance (such as pGREEN). More details on GV3101 are given in sections 2.3.3 and 2.3.3.2. *A. tumefaciens* strain LBA4404, which includes pSoup, rifampicin, tetracycline and streptomycin resistance, was used in parallel to GV3101 in one assay (section 4.3.1) during this investigation.

The binary vector used in all assays, pEM009_eGFP_pGREEN, contains two copies of the cauliflower mosaic virus (CaMV) 35S promoter, confers kanamycin resistance and contains an

enhanced Green Fluorescent Protein (eGFP) gene that functions as a reporter gene (Figure 4.1). The CaMV 35S is the most widely used promoter in plant biotechnology derived from the common plant virus CaMV. CaMV is considered to be a strong constitutive promoter, and it facilitates high level of RNA transcription in a wide variety of plants (Odell *et al.*, 1985).

4.2.2 *Agrobacterium tumefaciens* transformation by electroporation

A. tumefaciens competent cells (obtained as explained in section 2.3.3.2) were transformed to include pEM009_eGFP_pGREEN by electroporation. 50 µL of competent cells and 1 µL of the plasmid vector were pipetted in a 0.5 cm BioRad Cuvette. 1.8 V, 400 ohms pulse was applied in a BioRad Gene pulser Xcell. The transformed cells were recovered in 1 ml LB (Appendix 5) for three hours at 30°C and 180 rpm, before selection on LBA (Appendix 5) containing gentamycin 25 mg/L and kanamycin 50 mg/L at 30°C for 48 H. Positive transformants were confirmed by colony PCR (section 2.3.1.10).

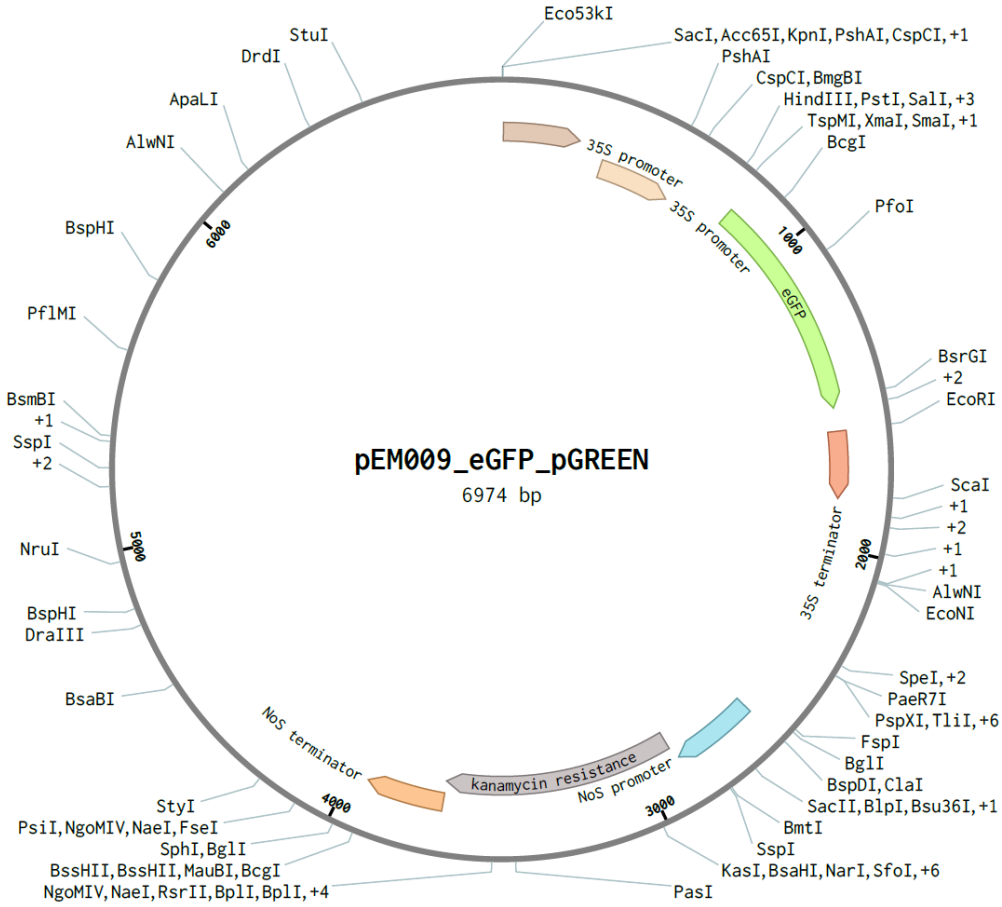

Figure 4.1. Plasmid used in stable transformation assays of four species of Nicotiana.
pEM009_eGFP_pGreen includes a double 35S promoter, coding sequence for eGFP reporter protein and confers kanamycin resistance.

4.2.3 Preparation of *Agrobacterium* liquid cultures

Cultures of *A. tumefaciens* (strain GV3101 or LBA4404) containing the construct were grown from single colonies in liquid LB (Appendix 5) with kanamycin 50 mg/L and gentamycin 25 mg/L at 28°C, rotating at 180 rpm. 1 ml of liquid culture was sub-cultured in 200 ml LB daily for 72 H. *Agrobacterium* cultures were pelleted at 10°C for 5 min at 4000 rpm, resuspended in Murashige-Skoog (liquid MS, Table 2.3) infiltration buffer, and adjusted to an O.D. greater than 0.5.

4.2.4 Handling of explants

Explants were obtained from either young leaf of *Nicotiana* spp. plants growing in glasshouse conditions, or from hypocotyls obtained aseptically on growing media (as explained in section 4.2.5). No sterilization was required for the hypocotyls grown *in vitro*. The leaves were put in 1 L Duran bottles filled with 10% commercial bleach and shaken for 15 minutes at 180 rpm on a

Rocker 25. The bleach solution was removed from the bottle, and the leaves were rinsed with sterile distilled water in the laminar flow hood four times, to remove any bleach residues. All instruments (forceps, blades, scalpels, etc.), liquid and solid media, were previously sterilized by autoclaving at 121˚C for 20 minutes at 105 kPa. All tissue handling was carried out in the aseptic laminar flow hood. Explants (leaf discs or hypocotyls) were infiltrated with *Agrobacterium* cultures by cutting the tissue while immersed in the liquid culture. For leaves, the midrib and margin were removed, and the laminar tissue was sectioned in 0.5 mm^2 squares. After imbibition, the sections of explant were blot dried with sterile filter paper and moved to Petri dishes with media (as listed in Table 4.1, Table 4.2 and Table 4.4) without antibiotics. The leaf discs were put with the abaxial surface in contact with the solid media. Handling of explants for hypocotyls is described in section 4.3.2.2.

4.2.5 Co-cultivation and tissue propagation

For co-cultivation the plates were left at 24°C in the dark for 48 h to 72 h. Explants were then sub-cultured into callus induction media (MS-L or MS-Hyp, Table 4.1) with antibiotics and kept at 24°C 16 h light/8 h darkness. Tissue was sub-cultured to fresh media every 10-14 days.

Table 4.1. Media composition used for stable transformation assays from leaf discs and hypocotyls.

	Media composition for assays with leaf discs (MS-L)	Media composition for assays with hypocotyls (MS-Hyp)
MS	4.4 g/L	4.4 g/L
Sucrose	20 g/L	30 g/L
Ascorbic acid	NA	20 mg/L
L-cysteine	NA	60 mg/L
Solidifying agent	8 g/L (plant agar)	2.5 g/L (Gelrite)

4.2.6 Seed sterilization and germination

For transformation assays using hypocotyls as explants, seeds of *Nicotiana forgetiana* harvested from plants growing in greenhouse conditions were used (see section 4.3.2.1). Seeds in *Nicotiana* spp. are very small (1-2 mm length) and numerous. Between 40 and 100 seeds of *N. forgetiana* were sterilized at a time. Seeds were placed in a 1.5 ml autoclaved Eppendorf tube. 1 ml of the sterilizing agent (10% bleach, 5% bleach or 70% ethanol) was poured into the tube to cover the seeds. The tube was vortexed for 1 minute and incubated at room temperature. Time of incubation varied depending on the substance used as sterilizing agent and was adjusted

according to the results obtained (5-15 minutes). The sterilizing agent was removed in the flow hood by pipetting, and the seeds rinsed with 1 ml sterile water three times with 1-minute vortex between washes. All liquid was removed, and 10 to 20 seeds per plate were placed on sterile tissue culture media (MS-Hyp, Table 4.1) without hormones or antibiotics. Plated seeds were left to germinate at 24°C under different light regime treatments (16 h light/8 h dark; 24 h dark, or alternating regimes; see 4.3.2.2).

4.2.7 Imaging

A Leica M165 FC fluorescent stereo microscope was used to obtain bright field and fluorescence microscope images. GFP-2 filter cube with UV source was used to assess expression of GFP by fluorescence in putative transgenic tissues and plants.

4.3 RESULTS

4.3.1 Assays using leaf discs as explants

4.3.1.1 Stage I: Assays using leaf discs of four non-model Nicotiana *species*

In the first stage of this investigation, leaf discs of the four *Nicotiana* species of interest*: N. forgetiana* and *N. bonariensis* (Section *Alatae*) and *N. cordifolia* and *N. solanifolia* (Section *Paniculatae*), were used as explants to trial stable transformation of these species. *A. tumefaciens* strain GV3101 was used for this set of assays. The phytohormone combination used in this assay was selected as it is widely used for stable transformation of *N. tabacum* (see section 2.3.3). In the case of *N. tabacum* the same combination of hormones (1 mg/L BAP, 0.5 mg/L IAA; "Leaf A" in Table 4.2) is used during the tissue culture stages of co-cultivation, callus induction and regeneration. This first set of assays resulted in very scarce induction of callus for *N. forgetiana* (Figure 4.2). Because of malfunctioning of the controlled conditions of the tissue culture room, the *Agrobacterium* overgrew the culture and GFP fluorescence was difficult to establish (Figure 4.2 A-B). By day 60 after inoculation, the callus had turned brown and dry (Figure 4.2 C-F). No callus formation or regeneration was detected for the other three species.

Table 4.2. Phytohormone composition of media used for stable transformation of *Nicotiana* spp. using leaf discs as explant.

Treatments	BAP (mg/L)	IAA (mg/L)	NAA (mg/L)	Auxin:Cytokinin Ratio	Reference
Leaf A	1	0.5	NA	1:2	E&D Lab Protocol
Leaf B	1	0.25	NA	1:4	
Leaf C	1	0.1	NA	1:10	
Leaf D	1	0.02	NA	1:50	Krügel et al., 2002
Leaf E	1	NA	0.1	1:10	Clemente, 2006

A subsequent assay, also using leaf discs of the four species, was carried out trying two different combinations of hormones: 1 mg/L BAP, 0.02 mg/L IAA ("Leaf D" in Table 4.2; Krügel et al., 2002); and 1 mg/L BAP, 0.01 NAA ("Leaf E" in Table 4.2, Clemente, 2006). For all species a low proportion of leaf discs produced calli under both treatments. These calli were mostly brown and slow growing (Figure 4.3). Some GFP fluorescence was detected although it was difficult to differentiate from auto-fluorescence characteristic of wounded or unhealthy tissue. Only one event of plant regeneration occurred for the species *N. bonariensis* growing under treatment "Leaf D" conditions (1 mg/L BAP, 0.02 mg/L IAA; Figure 4.4). The callus surrounding this regenerated plantlet was clearly fluorescent (cl in Figure 4.4B), however, only some of the differentiated epidermal cells and trichomes presented fluorescence on the cell membranes (Figure 4.4 C-D). This plantlet was excised from the contiguous callus and moved to a Hamilton jar with basal media (MS-L, Table 4.1) with antibiotics (hormones removed) to promote rooting. There was no production of roots and the health of the plant decreased. After 25 days the senescent plant was discarded.

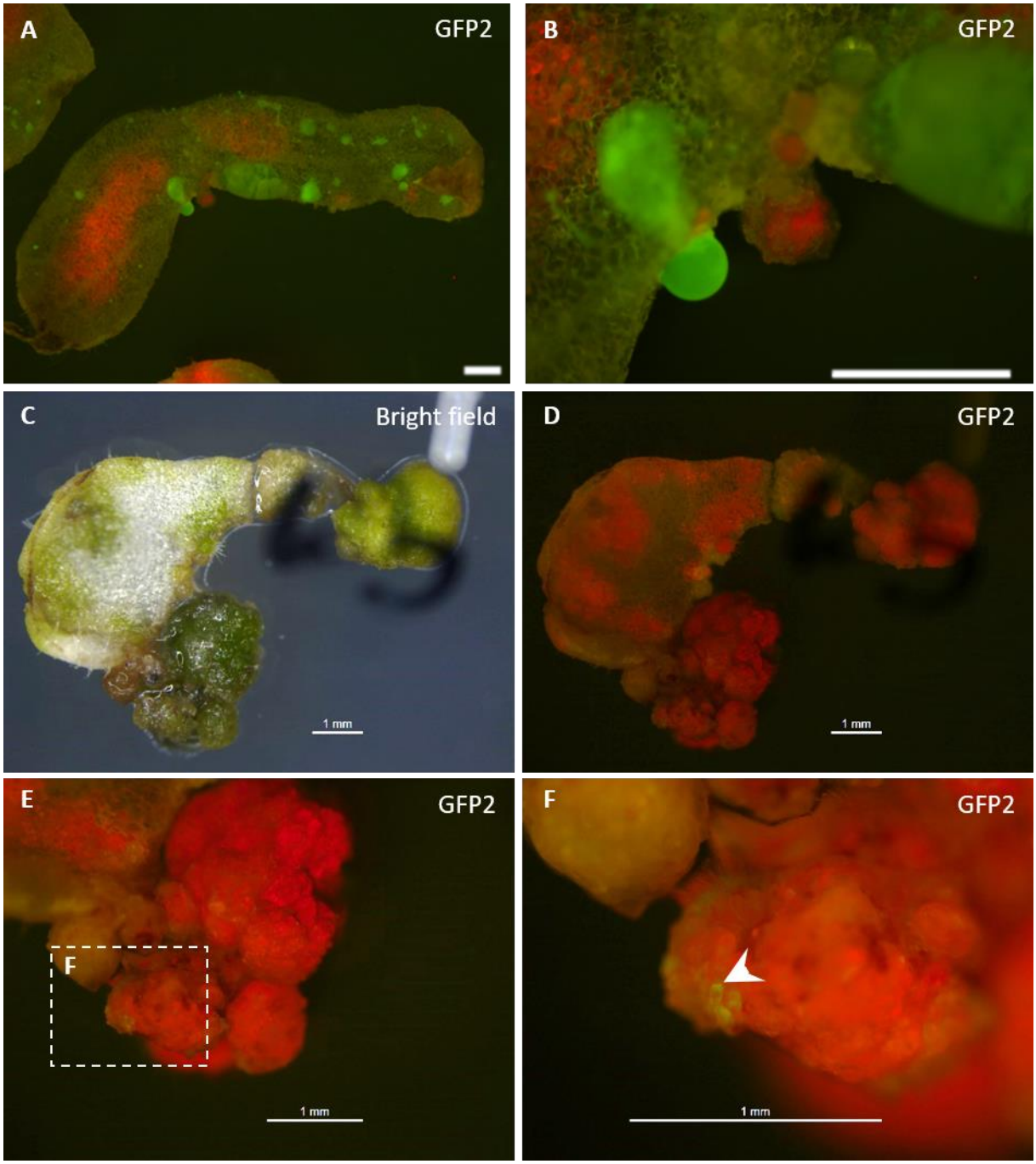

Figure 4.2. Callus formation but no regeneration of differentiated tissue, resulted from stable transformation assays of *N. forgetiana* leaf discs using a hormone combination previously used for model species *N. tabacum*.

Leaf discs of *Nicotiana forgetiana* after 40 days (A-B) and 60 days (C-F) of inoculation with *A. tumefaciens* strain GV3101. Green fluorescent blobs in A and B correspond to accumulation of *A. tumefaciens* bacterial cells on the plant tissue. Arrowhead in F shows GFP fluorescent transformed callus cells. Callus induction media: 1 mg/L BAP, 0.5 mg/L IAA ("Leaf A", Table 4.2). A-B, D-F: GFP-2 fluorescence cube applied. C. Bright field microphotograph. Scale bars= 1.0 mm.

4.3.1.2 Stage II: Assays using leaf discs of Nicotiana *species in Section Alatae*

For the following set of assays, only the species in Section *Alatae* were used as they were recognized to be the most reliable source of living material and flower production under

greenhouse conditions. A new round of transformation of leaf discs from *N. forgetiana* and *N. bonariensis* with treatments "Leaf A" (1 mg/L BAP, 0.5 mg/L IAA) and "Leaf D" (1 mg/L BAP, 0.02 mg/L IAA) was carried out. Two additional treatments were included keeping constant the concentration of cytokinin BAP (1 mg/L) and varying the concentration of auxin IAA ("Leaf B": 0.25 mg/L IAA and "Leaf C": 0.10 mg/L IAA; Table 4.2). As the auxin/cytokinin interaction has been demonstrated to regulate *in vitro* organogenesis (Skoog and Miller, 1957; Su et al., 2011), these four treatments were considered to encompass a wide variation of auxin:cytokinin ratios to be evaluated (Table 4.2). In this case, all treatments were successful at promoting callus formation in *N. forgetiana* (Figure 4.5), however, regeneration only occurred for *N. forgetiana* under treatment "Leaf B" (1 mg/L BAP, 0.25 mg/L IAA; Figure 4.5D-F, Figure 4.6). The plantlets produced were sub-cultured periodically to media of the same characteristics (Figure 4.6). Although the callus surrounding these plantlets was in general GFP positive, the plantlets were either lacking GFP (Figure 4.5E-F) or presented fluorescence more likely consistent with wound response or poor health of the tissue (Figure 4.6). No callus formation or regeneration occurred for *N. bonariensis*.

Given the initial results of "Stage II", a subsequent set of assays used the hormone combination of treatment "Leaf B" (1 g/L BAP, 0.25 g/L IAA) to assess if a different strain of *A. tumefaciens* would improve the efficiency of the transformation. Strain LBA4404 was used in parallel with GV3101 to transform leaf discs of *N. forgetiana* and *N. bonariensis*. For *N. bonariensis* few events of callus induction were detected for both strains. These calli were brownish in colour and did not present GFP fluorescence. For *N. forgetiana* the results were similar to *N. bonariensis*, with relatively more callus formation with LBA4404 than with GV3101, however, unlike the previous round, no regeneration occurred in this round of transformation.

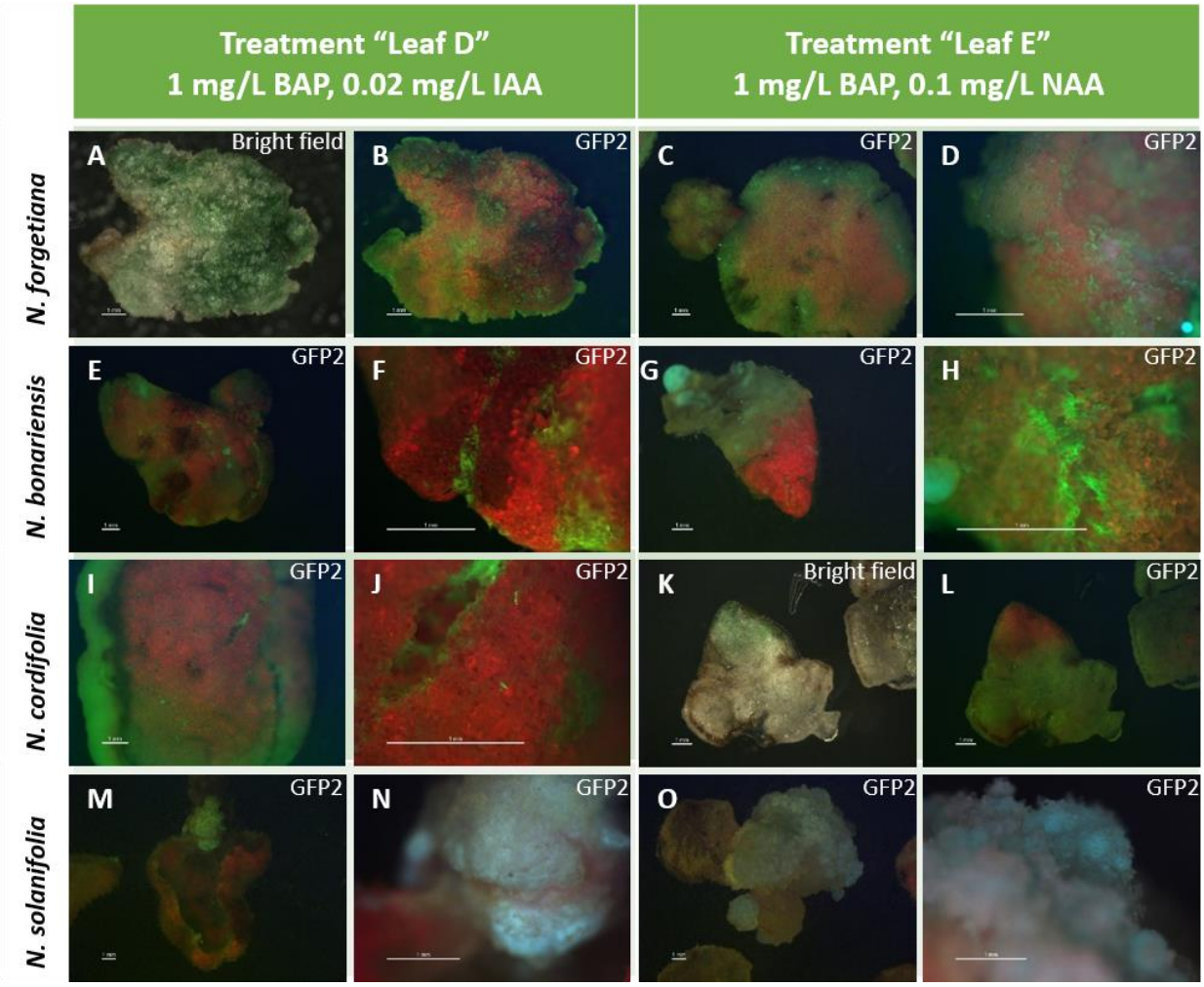

Figure 4.3. Production of transformed callus but no regeneration resulted from leaf discs of four non-model *Nicotiana* species treated with two callus induction/regeneration hormone combinations.
Examples of the production of transformed (GFP fluorescent) callus can be odserved for *N. forgetiana* under treatment "Leaf E" (C-D), *N. bonariensis* under treatment "Leaf E" (G-H) and *N. solanifolia* under treatments "Leaf D" (M-N) and "Leaf E" (O-P). GFP fluorescent tissue along the edges of the leaf discs (*e.g.* B, I, J) correspond to cell areas impregnated with *Agrobacterium* but with no callus production. Photographs were taken 60 days after inoculation with *A. tumefaciens* GV3101. All images are GFP2 fluorescence photographs, except A and K that are bright field photographs. Scale bars: 1.0 mm

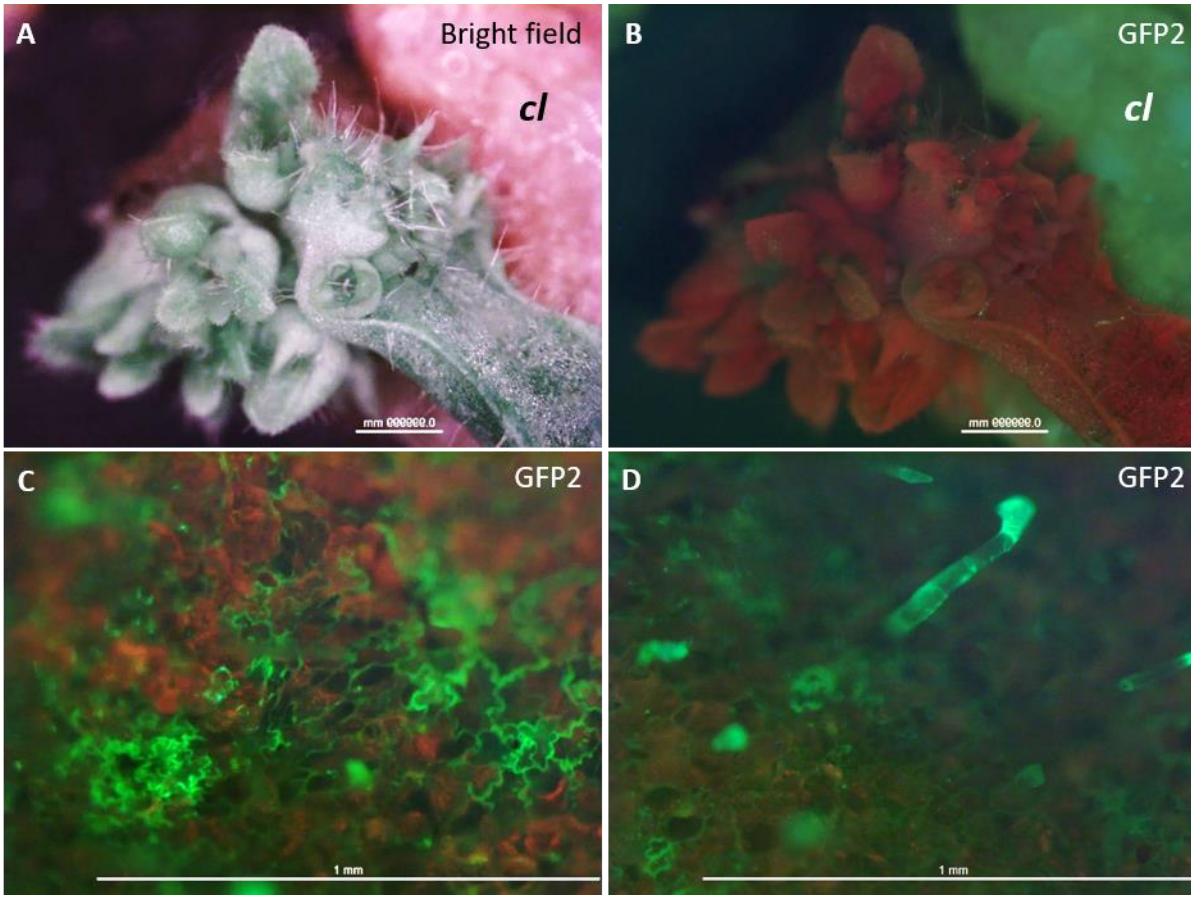

Figure 4.4. *Nicotiana bonariensis* plantlet regenerated from leaf discs using the transformation conditions established by Krügel et al., (2002) for *N. attenuata*.

A single event of regeneration occurred for *N. bonariensis* leaf discs treated with 1.0 mg/L BAP and 0.02 mg/L IAA ("Leaf D" treatment). A-B. General morphology of the plantlet. C-D. Close-up on the surface of the leaf. GFP fluorescence is detected in the cell-membranes (C) and leaf trichomes (D). cl: callus. A. Bright field photograph. B-D. GFP2 fluorescence filter. Scale bars: 1.0 mm

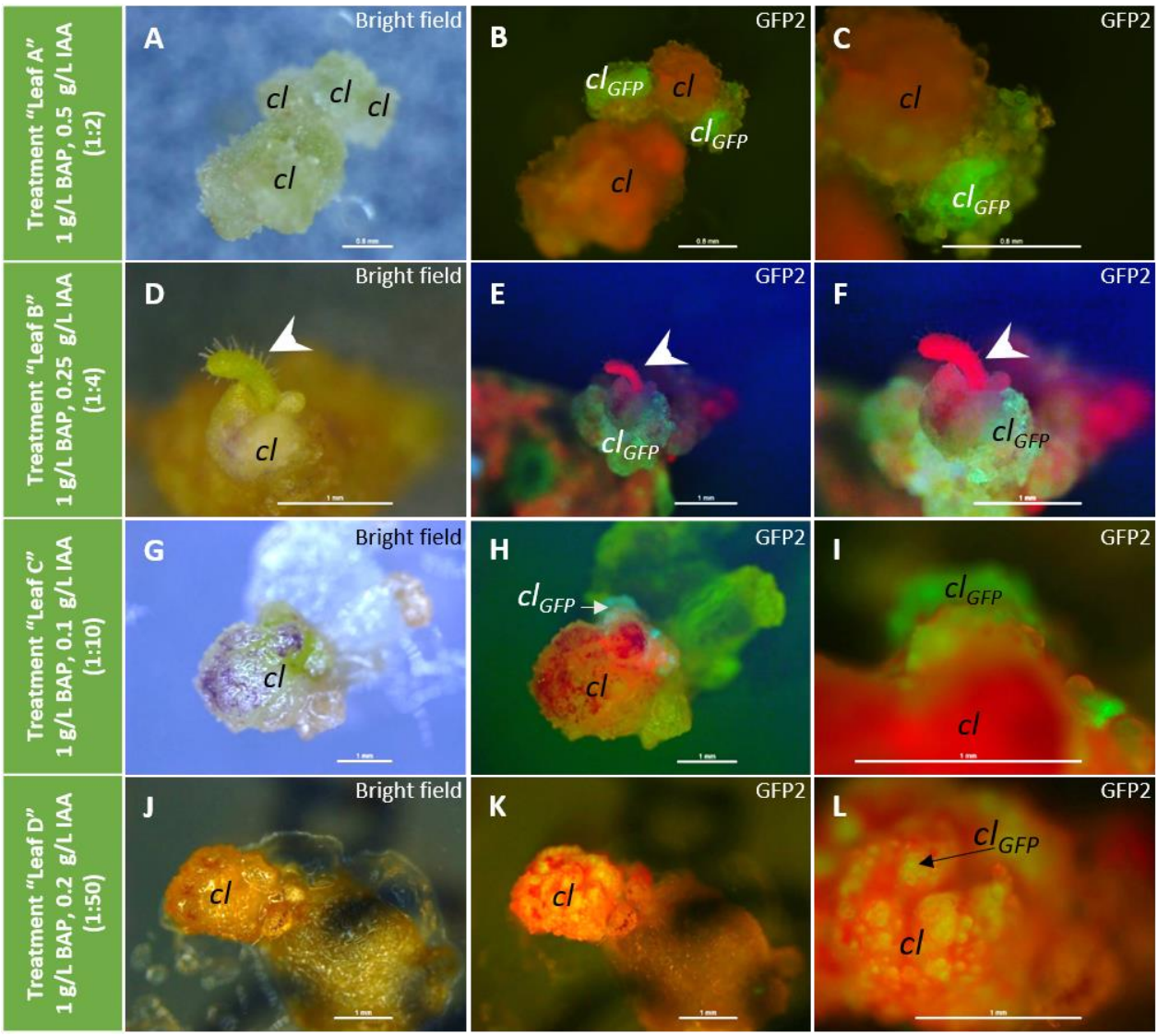

Figure 4.5. *N. forgetiana* leaf discs treated with different auxin:cytokinin ratios generally presented callus formation, but only sporadically events of regeneration.

For all hormone combinations a mix of non-transformed callus (cl) and transformed/GFP fluourescent callus (cl_{GFP}) was observed. A single regeneration event occurred for leaf discs treated with 1:4 auxin:citokinine ratio (Leaf B, second row in the figure). However, the regenerated plantled (arrow head) did not present GFP fluorescence. Photographs were taken 60 days after inoculation with *A. tumefaciens* GV3101. A, D, G, J are bright field microphotographs, all other panels are GFP2 fluorescence microphotographs. Auxin:cytokinin ratios are listed in parentheses next to each treatment name (left column). Scale bars: 1 mm.

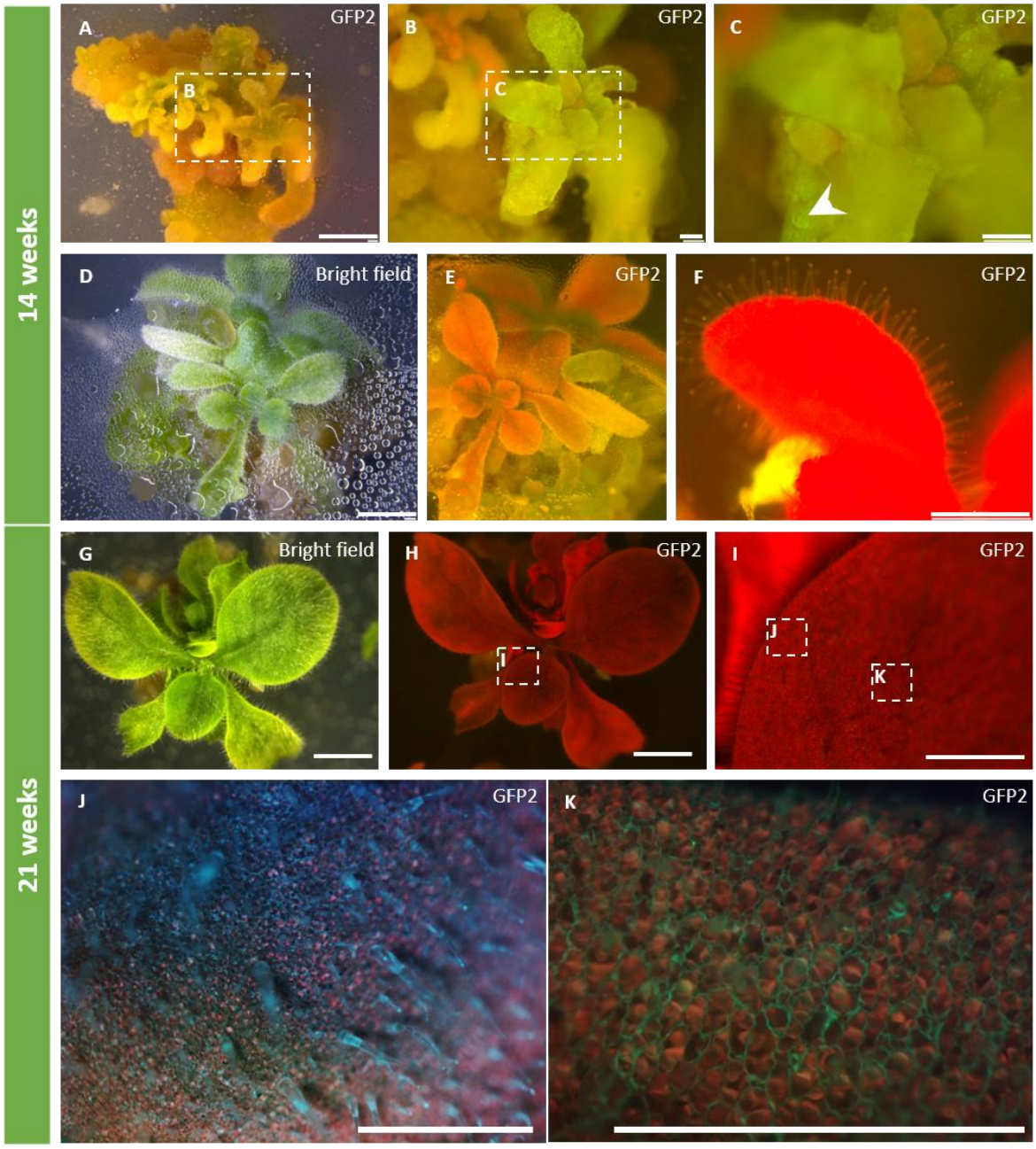

Figure 4.6. Plantlets of *N. forgetiana* regenerated from leaf discs after treatment "Leaf B" (1 mg/L BAP; 0.25 mg/L IAA) 14 and 21 weeks after inoculation.

Treatment "Leaf B" (1:4 auxin:cytokinin ratio) was the most effective for plant regeneration from leaf discs of *N. forgetiana.* However, regenerated plantlets expressing GFP (A-C) were small and brittle with short shoots. Arrowheads in C indicate zones were GFP is clearly identified. Plantlets not expressing or with low expression of GFP (D-K) had bigger, healthier looking leaves and longer shoots (D, E, G, H). In this kind of plantlets GFP was only detected in the leaf trichomes (J) and the cell-membranes (H). Scale bars: A, D, E, G-H: 5mm; B-C, F, I-K: 1 mm.

4.3.2 Hypocotyls as an alternative source of explants for stable transformation

In parallel to the transformation assays with leaf discs, the reliability of seed production to obtain hypocotyls was assessed for both *N. forgetiana* and *N. bonariensis*.

4.3.2.1 Obtaining a reliable source of seeds from N. forgetiana *and* N. bonariensis

As *N. forgetiana* and *N. bonariensis* species are self-incompatible in nature, manual pollination was attempted for both. In each case three plants were used, and five individual flowers marked as receptors of either pollen from the same flower (self-pollination) or from pollen of marked flowers from the other two plants (crosses). For the receptor flowers used in crosses all stamens were removed before maturation. For the donor flowers individual mature dehiscent stamens were removed with tweezers and rubbed against the receptive stigma of the receptor flowers. When donor and receptor flowers were the same, stamens were left to mature and removed after manual pollination. The success of manual pollination was assessed by touching the ovaries of the receptor flowers after 2-3 weeks. Fertilized flowers presented hardened ovaries and the senescent corolla would dehisce from the flower easily. The ovaries of non-fertilized flowers felt soft to the touch and the senescent corolla remained attached to the flower. All fertilized flowers were left to develop into fruit (dehiscent capsules) and all seeds from each capsule were collected and stored. For *N. bonariensis* no flowers were successfully fertilized for any of the crosses or self-pollination attempted (zero out of 45 flowers, Table 4.3). For *N. forgetiana* the success of fertilization was high (41 out of 45 flowers, Table 4.3). The flowers pollinated with their own pollen were as successful as the flowers receiving foreign pollen. Although self-pollination does not occur naturally in the greenhouse for *N. forgetiana*, from the results obtained via manual pollination, this species was considered as a reliable source of seeds to be used in transformation assays using hypocotyls.

Table 4.3. Self- and cross-pollination experiments with *N. forgetiana* and *N. bonariensis*.
The number of flowers fertilized after 3 weeks is reported. For each plant five flowers were self-pollinated and ten received pollen from other plants of the same species.

N. forgetiana WT				
	Plant 1 Donor	**Plant 2 Donor**	**Plant 3 Donor**	**Total per plant**
Plant 1 Receptor	5	4	5	14
Plant 2 Receptor	4	5	5	14
Plant 3 Receptor	5	3	5	13
Total	14	12	15	41

N. bonariensisWT				
	Plant 1 Donor	**Plant 2 Donor**	**Plant 3 Donor**	**Total per plant**
Plant 1 Receptor	0	0	0	0
Plant 2 Receptor	0	0	0	0
Plant 3 Receptor	0	0	0	0
Total	0	0	0	0

4.3.2.2 Seed handling and germination of N. forgetiana

Different methods of seed sterilization were evaluated for *N. forgetiana*. Initially 10% bleach with 15 minutes incubation resulted in no germination of the seeds sterilized, which suggested that the concentration of bleach and/or the time of incubation were detrimental for the seeds. Two different treatments were trialled to overcome this problem: (1) reducing the incubation time of 10% bleach to 5 minutes and (2) replacing the bleach with 70% ethanol as sterilizing agent. Seeds cleaned with ethanol did not germinate. Seeds cleaned with 10% bleach, 5 minutes incubation, presented germination rates higher than 50%. For the following steps this last sterilizing protocol was preferred.

10-20 sterile seeds were left on sterile media without hormones or antibiotics to germinate (Figure 4.7A). The same medium composition was used for germination and the following stages of tissue culture (MS-Hyp, Table 4.1). Several variations in medium composition were adopted for the assays with hypocotyls (MS-Hyp) compared to the assays with leaves (MS-L): (1) sugar composition was increased to 30 g/L sucrose, (2) 20 mg/L ascorbic acid and 60 mg/L L-cysteine were added to the media to neutralize potential reactive oxygen species (ROS), and (3) Gelrite® was used as a gelling agent rather than agar. These changes were adopted based on reports from the literature of successful stable transformation from hypocotyls in other *Nicotiana* species and other flowering plants (Krügel *et al.*, 2002).

Hypocotyls from germinating seeds grown under 16 h light/8 h dark daily regimes were very short (0.5-4 mm, Figure 4.7B) and difficult to manipulate as a source of explant for transformation. In consequence, several variations in light regimes and temperature were trialled to obtain longer, healthy hypocotyls, suitable to use in the following stages of the protocol. Germination rate was low (30%) in seeds under 24 h dark conditions, either at 24°C or 30°C. Hypocotyls grown under these conditions were longer but very thin and the cotyledons were small and chlorotic (pale green in colour). Alternatively, a set of seeds under 16 h light/8 h dark daily regimes at 24°C were left to germinate (2-4 days) and then moved to 24 h dark at 24°C. This promoted elongation of healthy hypocotyls reaching up to 15 mm in 10 days (Figure 4.7C). These germination and hypocotyl elongation conditions were preferred to obtain explants for the following steps of the transformation assays.

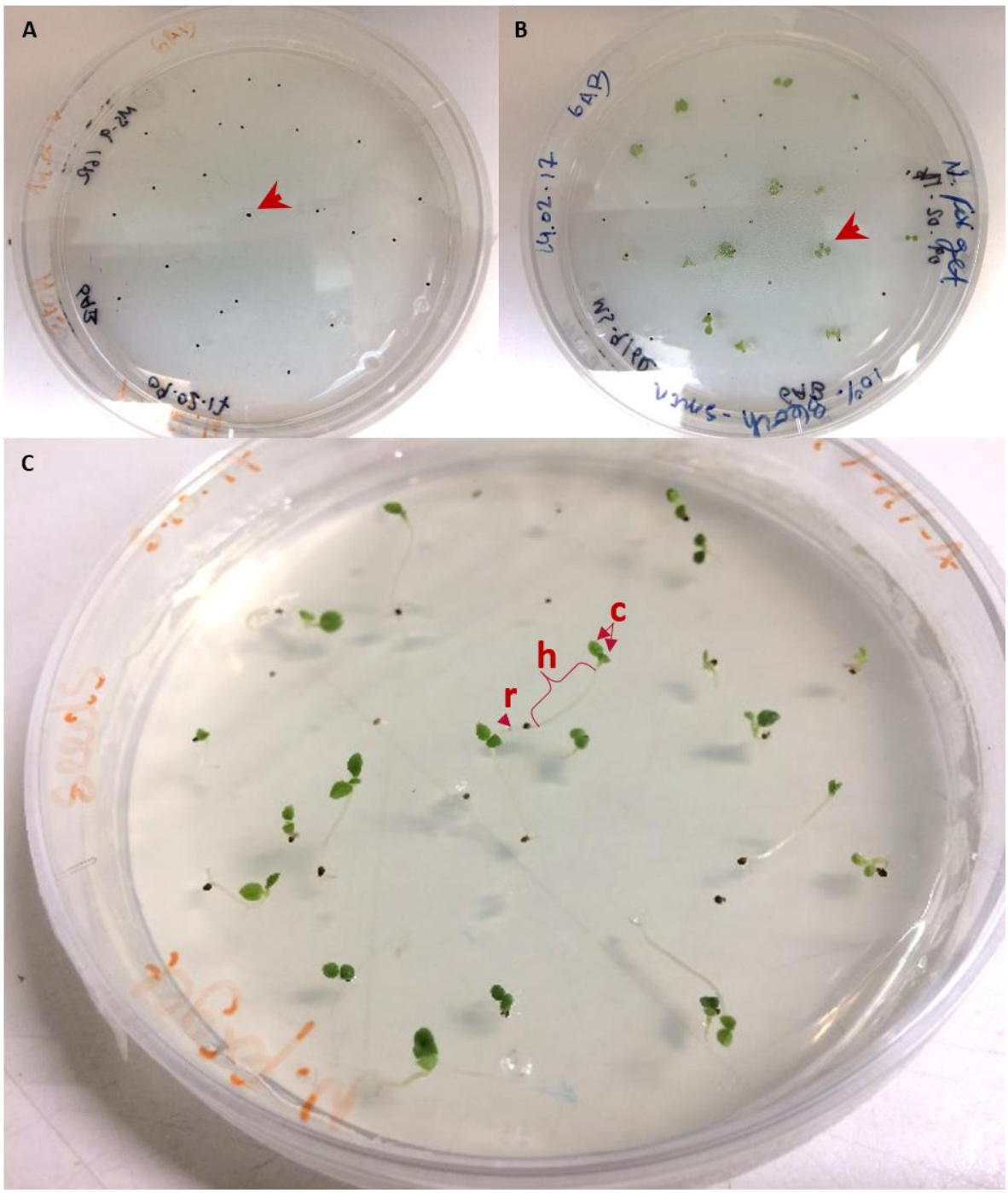

Figure 4.7. Steps to obtain healthy hypocotyls of *N. forgetiana* to be used as explants for transformation.

A. Sterile seeds (arrow head) are placed on growing media for germination. B. Germinated seeds with short hypocotyls (arrow head), 3-8 days after germination. Up to this point seeds were kept at 16 h light/8 h dark, 24°C conditions. After B, plates with germinating seeds were moved to 24 h dark, 24°C conditions for 10-15 days. C. Germinated seeds with long hypocotyls. Red brace indicates the hypocotilar zone, to be excised and used for transformation. c: cotyledons; h: hypocotyl; r: radicle.

4.3.2.3 *Optimizing tissue culture from hypocotyls of* N. forgetiana

Handling of explants

Hypocotyls of *N. forgetiana* were dissected with sterile scalpels while submerged in *A. tumefaciens* liquid culture. The radicle and the cotyledons were discarded and only the hypocotyl tissue was used as explant for transformation (Figure 4.7C). 200 µM acetosyringone was added to both the *Agrobacterium* liquid culture and the co-cultivation medium. Acetosyringone is a natural wound response molecule (flavonoid) that induces the *Agrobacterium* vir-Genes, and its use has been reported to enhance transformation efficiency in several plant species (Sheikholeslam & Weeks, 1987; Park, 2006). The time the explant was kept submerged in the liquid culture varied between 5 to 60 minutes, no major differences in transformation success can be attributed to time of imbibition only, but times between 30 and 60 minutes were preferred to allow complete impregnation of the explant. To increase penetration of liquid culture into the hypocotyl, a subset of explants was treated with 2 minutes vacuum exposure while submerged in the liquid culture. This treatment resulted in physical damage of the explants and is not recommended for handling material of this species.

The most important factor in handling explants was found to be the health of the tissue. Longer, healthy hypocotyls (as discussed in section 4.3.2.2) were shown to be easier to handle and gave better results in the following steps of the transformation.

After imbibition, the sections of explant were blot dried with sterile filter paper and moved to petri dishes with callus induction media (see section below for details on the composition) without antibiotics. For co-cultivation the plates were left at 24°C and dark for 72 H. Explants were then sub-cultured into callus induction media with antibiotics and kept at 24°C 16 h light/8 h dark. Tissue was sub-cultured to fresh media every 10-14 days.

Promoting callus formation

An initial assay used the same hormone composition as reported for transformation of hypocotyls of *N. attenuata* (Callus A: 0.02 mg/L IAA; Krügel *et al.*, 2002). This treatment resulted in callus formation at ca. 5 weeks after inoculation. Callus appeared mainly along the cut edges of the explants (Figure 4.8A-E). Unexpectedly, regeneration also occurred almost simultaneously to callus formation with this treatment (Figure 4.8E-F). Calli and regenerating plantlets were moved to fresh media of the same composition every 10-14 days. This resulted in abundant regeneration of plantlets that were small, brittle, with tiny leaves in tight rosettes,

positive for GFP in a mosaic like pattern (Figure 4.9). Subsets of these plantlets were moved to shoot induction media as described in the section "Shoot induction" below.

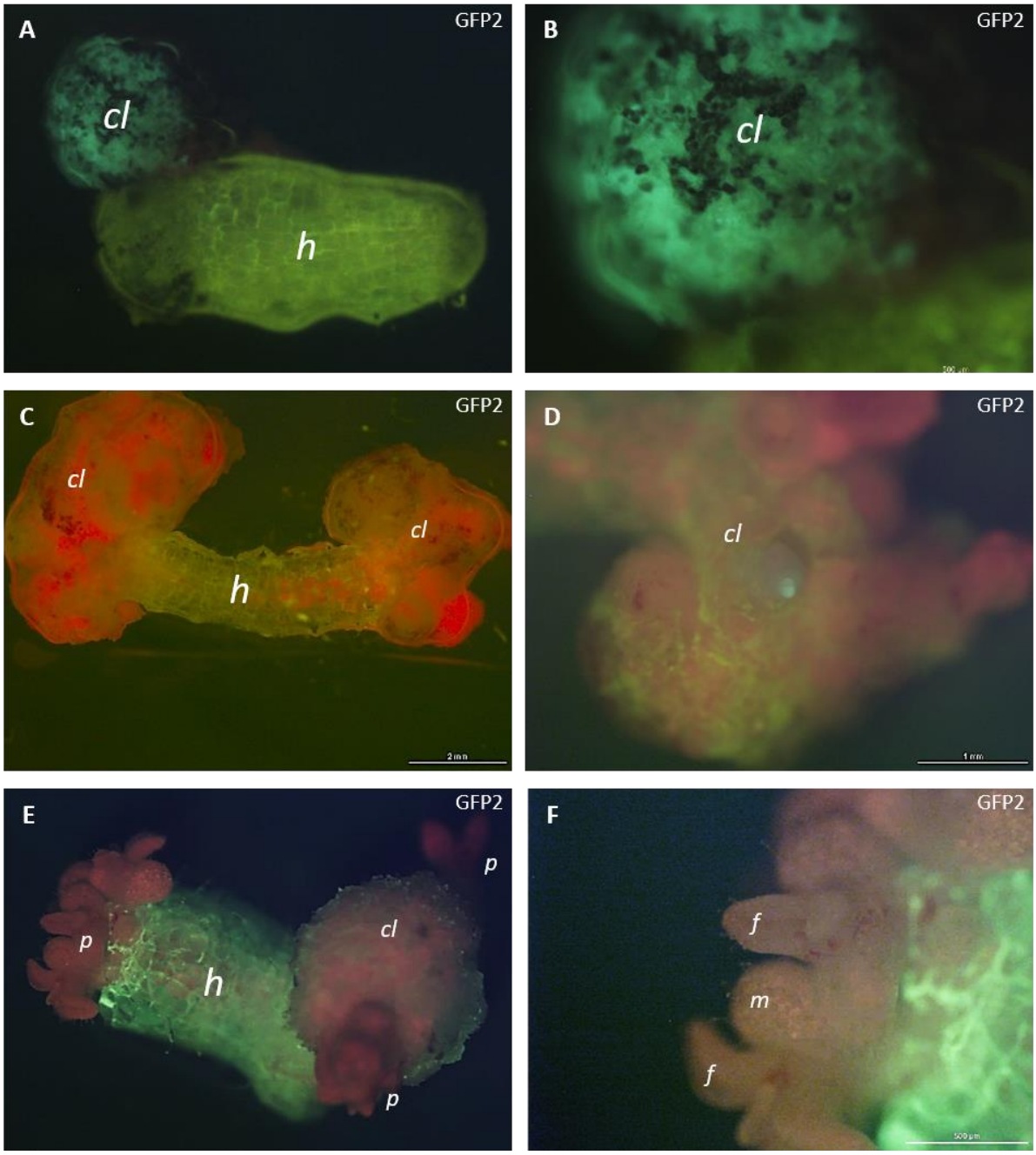

Figure 4.8. Transformation assays using hypocotyls of *N. forgetiana* as explant were successful in promoting callus initiation and early plantlet regeneration.
A-B. Hypocotyl with callus expressing GFP ca. 25 days after inoculation. C-D. Hypocotyl with non-transformed callus after ca. 25 days after inoculation. E-F. Hypocotyl with non-transformed callus and newly regenerated plantlets ca. 40 days after inoculation. h: hypocotyl; cl: callus; p: plantlet; m: apical meristem of the plantlet; f: leaf primordia. Scale bar: 1 mm

In a second set of assays, three additional media compositions were trialled for callus formation from hypocotyls of *N. forgetiana* (Callus B-D, Table 4.2). These media were selected from the literature as they had been shown to promote callus formation in other *Nicotiana* species

(Tavazza *et al.*, 1988; Krügel *et al.*, 2002; Li *et al.*, 2003). There were no significant differences between treatments. All three media were successful in promoting callus formation from healthy hypocotyls. Moreover, events of regeneration occurred in all three treatments. Plantlets presented phenotypes similar to those described for the "Callus A" treatment.

Table 4.4. Phytohormone composition of media used for stable transformation of *Nicotiana forgetiana* hypocotyls.

Stage of the Transformation	Treatment	BAP (mg/L)	IAA (mg/L)	Kinetin (mg/L)	NAA (mg/L)	Reference
Callus Induction	**Callus A**	1.0	0.0	NA	NA	Krügel et al. 2002
	Callus B	1.0	2.0	NA	NA	Tavazza et al., 1993
	Callus C	2.58	0.89	NA	NA	Li et al. 2003
Regeneration and shoot promotion	**Shoot A**	0.5	NA	NA	NA	Krügel et al. 2002
	Shoot B	2.0	1.0	0.5	NA	Geethalaskshmi et al., 2016
	Shoot C	No hormones				
Rooting	**Root A**	0.5	1.0	2.0	NA	Geethalaskshmi et al., 2016
	Root B	NA	NA	NA	0.1	Clemente, 2006
	Root C	No hormones				Krügel et al. 2002, E&D Lab Protocol

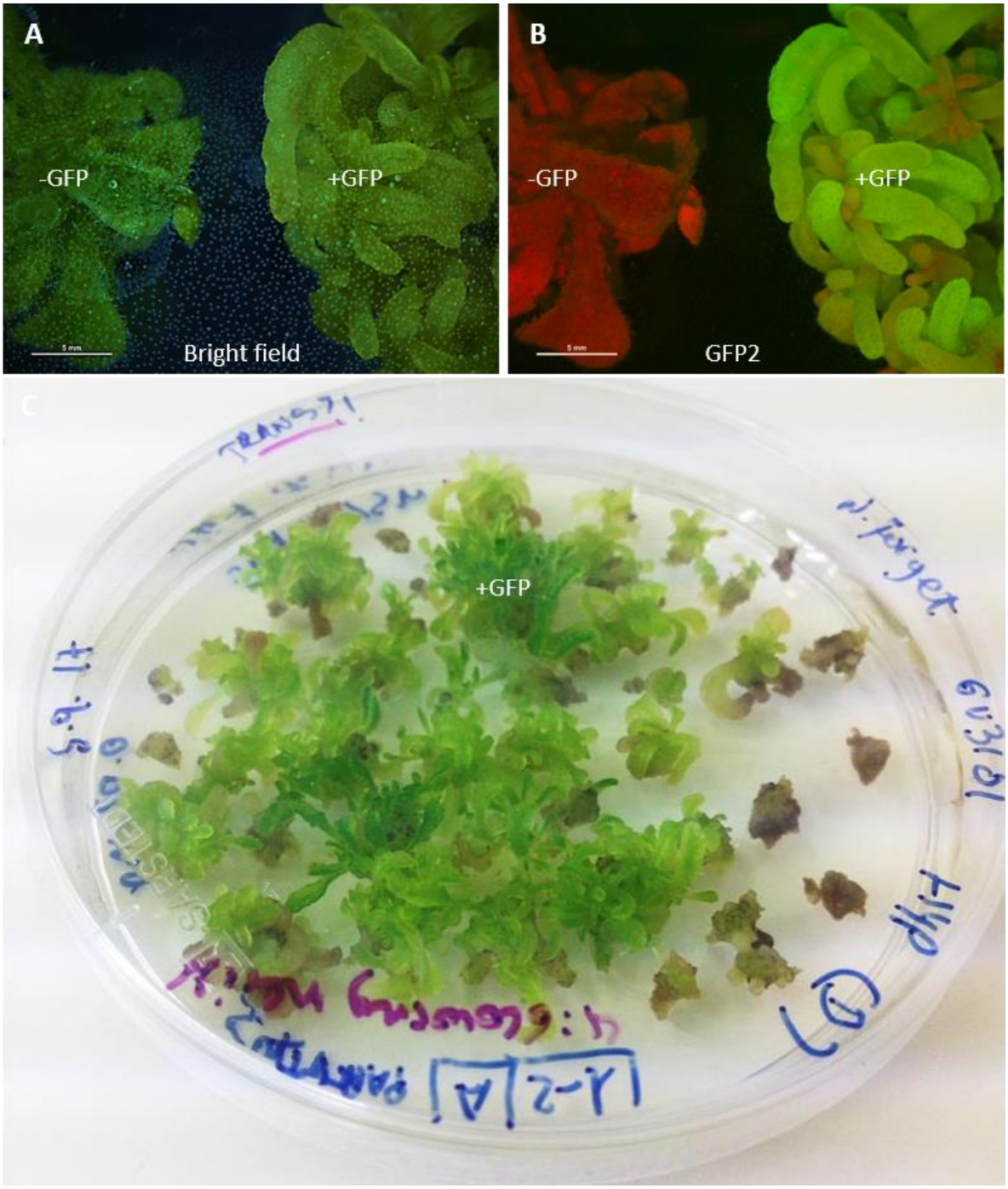

Figure 4.9. Plantlets were regenerated of *N. forgetiana* from hypocotyls, but plant elongation and maturity were not achieved for GFP transformed plantlets.

A and B are bright field (A) and GFP2 fluorescence (B) microphotographs of the same two plantlets. The plantlet on the left, is a non-expressing GFP plantlet (-GFP), and the one on the right is expressing GFP (+GFP). The plants not expressing GFP are bigger and healthy looking, and do not present green fluorescence. The transformed plantlets expressing GFP are small and brittle, with short shoots and leaves arranged in tight rosettes. C. Petri dish with the typical GFP expressing regenerating plantlets of *N. forgetiana*. Light green spots on A are artifacts derived from water condensation on the Petri dish through which the photos were taken.

Shoot induction

In general, for *Nicotiana* species with established *A. tumefaciens* mediated stable transformations, different media compositions are required for shoot induction compared to callus production (Krügel et al., 2002; Clemente, 2006; Geethalakshmi et al., 2016). It was surprising that for *N. forgetiana* the callus formation media trialled had the ability to promote regeneration as well. Given the phenotype of the regenerated plantlets (short and brittle), taller plants with well-developed organs were desired to continue with the following stages of tissue culture and propagation into soil of the transgenic lines. Looking to reach this level of plant development, three different shoot induction media were trialed (Table 4.2). Subsets of both callus or regenerated plantlets from the three callus induction media attempted were distributed into the three shoot induction alternatives. All media resulted in regeneration from callus and further regeneration from plantlets, but the new plants persistently had very short shoots and small organs (Figure 4.10). In an attempt to promote growth of the regenerating plantlets by etiolation, a subset was moved to 24 h dark for ten days. Elongation of the small leaves occurred, but they were thin and chlorotic. There was no elongation of shoots in these plantlets and GFP fluorescence was lost.

Rooting

Three different media compositions were trialled in order to promote rooting of the transformed plantlets. None of the treatments resulted in rooting of the small, brittle plantlets typical of *N. forgetiana*. However, a single plant, with no GFP fluorescence, longer flexible leaves and well differentiated shoots, produced roots when treated with 0.1 g/L NAA with antibiotics.

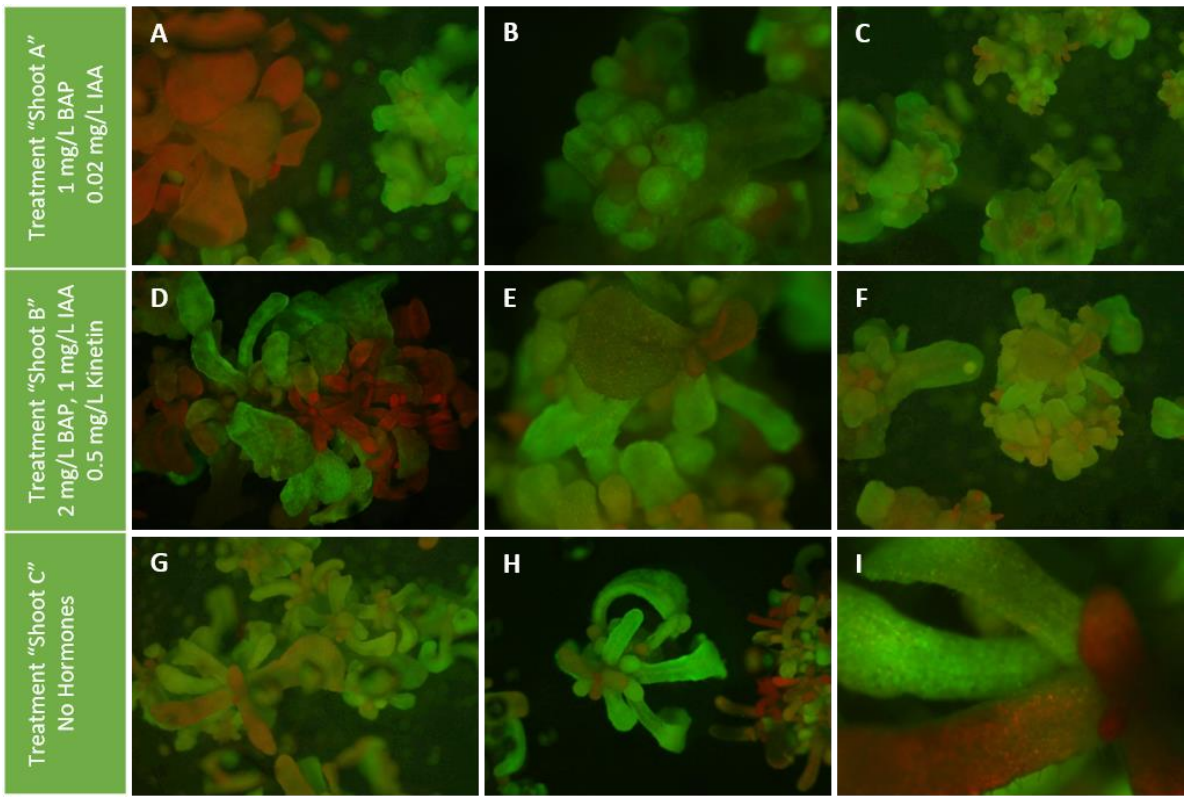

Figure 4.10. Different shoot induction treatments on GFP-expressing plantlets of *N. forgetiana* resulted in increased plantlet regeneration but not plant elongation.
A-I. Examples of *N. forgetiana* plantlets, regenerated from hypocotyl, exposed to three different shoot induction treatments. Left column indicates the treatment applied. Most regenerated plantlets presented a mosaic pattern of GFP expression, with areas expressing GFP appearing green, and areas non-expressing GFP appearing red. GFP2 photographs taken 120 days after inoculation with *A. tumefaciens* GV3101.

4.4 DISCUSSION

4.4.1 Using *Nicotiana* spp. leaves as explants for *A. tumefaciens* mediated transformation

Agrobacterium tumefaciens mediated transformation of plants is intended as a robust tool for determining gene function by having the ability to silence or over-express individual genes (Márton *et al.*, 1979; Horsch *et al.*, 1985). Several model plant systems, including *Nicotiana tabacum,* are currently readily transformable and are widely used in various lines of research (section 4.1.4). As a starting point in this chapter, trials with a previously established protocol for *A. tumefaciens* transformation of *N. tabacum* were performed for leaf explants of *N. forgetiana* and *N. bonariensis* in Section *Alatae*, and *N. cordifolia* and *N. solanifolia* in Section *Paniculatae* (section 4.3.1.1). These initial trials demonstrated the difficulties to promote callus formation from inoculated leaves in these species.

Transformation protocols for *Nicotiana* species other than *N. tabacum* are available in the literature (Krügel *et al.*, 2002; Clemente, 2006). Selectable markers, explants, media and cultivation conditions were shown to be crucial in the design of the *A. tumefaciens* transformation protocol for *N. attenuata* (Krügel *et al.*, 2002). In this species only explants from the hypocotyls of germinating seeds (and not leaves, cotyledons or roots) provided reliable material for transformation. The exposure to auxins and antibiotics was also important in defining the transformation protocol for this species. As the initial transformation assays of species in Section *Alatae* and *Paniculatae* using the protocol for *N. tabacum* were unsuccessful, variations on the protocol (type of explant, hormone and/or antibiotic concentrations) were tested.

For subsequent trials, the two species in Section *Alatae*, *N. forgetiana* and *N. bonariensis* were established as the best candidates for transformation because of their short life cycles and reliable production of flowers. *N. cordifolia* and *N. solanifolia* (Section *Paniculatae*) are not optimal for this kind of experimentation because of their life cycles (perennials or biannual shrubs) and particular life history (see sections 2.2.3). The leaves in these species are highly pubescent (Figure 2.4) and of relatively hard texture (coriaceous). Moreover, the time of maturation and the specific time and conditions for flowering, are difficult to control in greenhouse conditions (2.4.1).

The results from the assays using leaf explants of *N. bonariensis* and *N. forgatiana* and different media composition and hormone combinations (Figure 4.4, Figure 4.5, Figure 4.6) indicated that the *Agrobacterium tumefaciens* strain GV3101 is efficient in delivering T-DNA to leaf tissue of both species. Both *N. forgetiana* and *N. bonariensis* then have potential to be transformed from leaf but finding an optimal hormone combination is crucial. Transformation from leaves of these sister species was trialled in parallel, meaning that the explants had the same age, and the transformation and tissue culture parameters were identical. Although callus induction occurred in the two species, only *N. forgetiana* produced transformed explants under one treatment. This suggests that optimal regeneration medium is species/genotype-dependent.

4.4.2 Using *N. forgetiana* hypocotyls as explants for *A. tumefaciens* mediated transformation

The results indicate that the protocols described enable efficient transformation of *N. forgetiana* from hypocotyl and have potential application for transformation of this species. The most

persistent difficulty in the process has been the development of plantlets in appropriate conditions to be moved to soil and grown into adult plants. The nature of the phenotype of the regenerated plants could be due to toxicity of GFP (Malabadi *et al.*, 2008). In *A. tumefaciens* mediated transformation of *Arabidopsis thaliana,* using GFP as a reporter gene, regeneration of fertile plants from the brightest transformants has been shown to be difficult (Malabadi *et al.*, 2008). The use of alternative reporter genes or attempt transformation with candidate genes directly should be considered.

In this chapter, the bases of a successful transformation for *N. forgetiana* from hypocotyls are established. As the wild type of this species has conical cells, downregulating candidate R2R3 Subgroup 9 MYB genes would allow us to test their role in the development of conical cells. R2R3 MYB Subgroup 9 genes that have been transgenically repressed or knocked out include: *AmMIXTA* in *A. majus* (Noda *et al.*, 1994), *GhMYB25* (Machado et al., 2009) and *GhMYB25-like* (Walford *et al.*, 2011) in *Gossypium hirsutum*, *PhMYBI* in *Petunia hybrida* (Baumann *et al.*, 2007), *AtMyb106* in *Arabidopsis thaliana* (Gilding & Marks, 2010) and *SlMIXTA*-like in *Solanum lycopersicum* (Lashbrooke *et al.*, 2015). All these studies presented strong knock out or repression phenotypes, including loss of conical cells on petals (Noda *et al.*, 1994) and fruits (Lashbrooke *et al.*, 2015), dramatic reduction in trichomes (Machado et al., 2009) and loss of seed fibres (Walford *et al.*, 2011). Obtaining transgenic lines with non-conical cells on the petals of *N. forgetiana* would be an excellent step that would provide an important tool to be used in further experimentation including the use of transformed plants in pollination behaviour experiments in the field and the laboratory.

Chapter 5

The effect of petal cell shape in the perception of red and white flowers by Bombus terrestris

5 The effect of petal cell shape in the perception of red and white flowers by *Bombus terrestris*

5.1 INTRODUCTION

This chapter explores the effect of petal cell shape as an enhancer of colouration framed in the scenario of sister species in *Nicotiana* Section *Alatae*, *N. forgetiana* (red colour, conical cell shape) and *N. bonariensis* (white colour, non-conical cell shape)(Chapter 3). A series of experiments using artificial flowers were run to test whether flowers of the same colour but contrasting cell shape were perceived differentially by model pollinator *Bombus terrestris*.

5.1.1 Petal cell shape as an enhancer of petal colouration

As previously discused (sections 1.2.1 and 1.2.2), epidermal cell shape determines several physical aspects of the petals. For instance, petal cell shape influences floral temperature (Comba *et al.*, 2000; Whitney *et al.*, 2011a), the wettability of floral surfaces (Whitney *et al.*, 2011c) and floral scent release and dispersal (Whitney *et al.*, 2011a). All these are features that have the potential to affect the attractiveness of flowers towards animal pollinators. Moreover, petal cell shape can act as a direct tactile clue for pollinators (Kevan & Lane, 1985) and has a significant impact for insect pollinators due to its effect on grip (Whitney *et al.*, 2009b, a; Rands *et al.*, 2011; Alcorn *et al.*, 2012; Papiorek *et al.*, 2014; Pattrick, 2017).

Petal cell shape also alters the refraction and reflection of light from the petals, changing the intensity of floral colour (Noda *et al.*, 1994; Gorton & Vogelmann, 1996; Glover & Martin, 1998). Isogenic lines of the snapdragon *Antirrhinum majus*, that only differ in the loss of function of the *MIXTA* gene in the mutant line compared to the wild type (Figure 1.1), clearly exemplify the contrasting appearance (at least to the human eye) resulting from differential cell shapes on these lines (Noda *et al.*, 1994; Glover & Martin, 1998).

Several works have experimentally addressed questions related to the effect of petal cell shape as an enhancer of petal colouration and its role in pollination (Glover & Martin, 1998; Comba *et al.*, 2000; Dyer *et al.*, 2007; Alcorn *et al.*, 2012). As discussed in section 1.3.2, molecular development of conical cells in *A. majus* has been characterized in detail (Noda *et al.*, 1994; Glover *et al.*, 1998; Perez-Rodriguez *et al.*, 2005; Jaffé *et al.*, 2007). Lines of the *mixta* mutant with non-conical cells have been readily available for researchers to compare to the wild type

with conical cells on the adaxial surface of the petals (Figure 1.1). Petal pigmentation in *A. majus* is also well understood. The magenta colour of the wild type is given by the accumulation of flavonoid pigments (cyanidin) in the vacuole of the petal epidermal cells (Martin *et al.*, 1991). A single gene *NIVEA* codes for the enzyme (chalcone synthase) that catalyses the first step in the biosynthetic pathway of these pigments. A mutation at the *NIVEA* locus results in plants with white flowers, lacking not only the purple anthocyanins visible to the human eye but also all of the flavonoid pigments capable of absorbing light of any wavelength, including ultraviolet (UV) A radiation (Noda *et al.*, 1994; Glover & Martin, 1998). *A. majus* wild type (pigmented/conical cells), the *mixta* mutant (pigmented/non-conical cells), the *nivea* mutant (non-pigmented/conical cells) and the *mixta*/*nivea* double mutant (non-pigmented/non-conical cells) have been used to test the theory that conical cells increase the attractiveness of a flower, and to compare the contribution of conical cells with the contribution of pigmentation in the pollination of *Antirrhinum* (Glover & Martin, 1998; Comba *et al.*, 2000; Dyer *et al.*, 2007).

In a series of experiments with open pollinated plants, Glover and Martin (1998) found that emasculated mutant lines of *mixta* and *nivea* produced significantly fewer fruit than the wild type. For any particular plot at a particular time, non-conical-celled pigmented flowers were pollinated less than conical-celled pigmented flowers, and non-conical-celled white flowers were also pollinated less than conical-celled white flowers. From these data the authors proposed that petal cell shape in *A. majus* is a significant factor which affects the chances of a flower being visited by a pollinator. Those flowers with conical cells were more attractive to bees at all times, irrespective of whether they were pigmented or not (Glover & Martin, 1998). Further field experiments showed that wild bumblebees presented with arrays of different flowers were more likely to reject *nivea* and *mixta* mutant flowers than wild type ones, both before and after landing on the flower (Comba et al. 2000).

Whitney *et al.*, (2009a) also used isogenic lines of *A. majus* to test ideas on the role of petal cell shape in pollination. These authors also used biomimetic artificial flowers replicating the colour and cell shape of wild type and *mixta* mutant *A. majus*. They showed that foraging bumblebees are able to discriminate between different surfaces via tactile cues alone. These authors found that bumblebees use color cues to discriminate against flowers that lack conical cells, but only when flower surfaces are presented at steep angles, making them difficult to manipulate.

Using artificial flowers mimicking the reflectance spectra of both *A. majus* wild-type and the *mixta* mutant, Dyer et al., (2007) showed that when *Bombus terrestris* were trained to associate

a food reward with the wild-type biomimetic flower, they were able to discriminate this flower type over the mutant with 69.2% accuracy. This demonstrated that bees were able to discriminate between wild-type and *mixta* mutant flowers by their colour alone, as these artificial flowers did not differ in surface texture.

Alcorn *et al* (2012) explored whether conical petal cells would make handling moving flowers of *Petunia hybrida* easier for pollinators. The wildtype of *P. hybrida* has conical cells on the adaxial surface of the petal. A line of *P. hybrida* in which *PhMYB1*, a gene responsible for the formation of conical cells, is disrupted by insertion of the dTph1 transposon, has non-conical cells. The *phmyb1* mutant, a revertant wild type line from which the transposon has excised germinally, and has conical cells, and the V26 line that also has conical cells but has darker colouration, were used in these experiments. In a laboratory setup, these authors used these three lines to test *Bombus terrestris* preference for conical- or non-conical-celled flowers under different conditions of motion, and to explore how colour and visibility interact with tactile cues to form a pollinator's preference. They found that the bumblebees preferred to visit conical-celled *Petunia* flowers except when the conical-celled flowers were harder to detect visually (darker colouration). The bees then favoured flowers that were easier to detect. But when flowers were moving and more difficult to handle, bees always learned to favour conical-celled flowers, irrespective of visual difficulty (Alcorn *et al.*, 2012; Alcorn, 2013).

These experiments with isogenic lines and artificial flowers have demonstrated independently that bees can discriminate between flowers based on cell shape only. The cited works on *A. majus* and *P. hybrida* clearly show the tactile component (enhanced grip) of the discrimination between flowers of different textures. However, whether or not bees can discriminate between conical and non-conical celled flowers of the same pigment background from visual clues alone (ie without touching the flowers) is still not clear.

5.1.2 Bee perception and pollination

Bees are very flexible with their learning behaviour and can be trained to associate a wide variety of traits such as surface texture (Kevan & Lane, 1985; Pattrick, 2017), volatile composition (Bailes, 2016; Groen *et al.*, 2016), temperature (Whitney et al. 2008), colouration (Glover & Martin, 1998; Dyer *et al.*, 2007) and other visual clues (Reed, 2014; Whitney *et al.*, 2016; Moyroud *et al.*, 2017) with a reward, making them a good model species for studying learning behaviour in pollinating insects.

Pollinators often sequentially visit one flower type while bypassing other equally rewarding flower types in the process. This pattern of flower choice in pollinators is known as flower constancy (Chittka *et al.*, 1999; Gegear & Laverty, 2005). Floral constancy is thought to be driven by the cognitive limitations of the pollinators, and is affected by floral parameters, such as inter-plant distances, nectar rewards, flower morphology, and floral colour (Chittka *et al.*, 1999).

Bees have three simple eyes, or ocelli, and two compound eyes constituted of repeated units called ommatidia. Ommatidia are located on an almost hemispherical surface on the head, and each one points in a slightly different direction, offering a wide angle of sight. Bee vision is trichromatic, having UV, blue and green receptors with maximum sensitivities near 340, 430, and 535 nm (Daumer, 1956; Chittka, 1992; Peitsch *et al.*, 1992). The image a bee sees is a combination of the inputs of all their ommatidia, each one having a different type or combination of receptors (Skorupski & Chittka, 2010).

The bee colour hexagon (Chittka, 1992) is a colour space model that allows researchers to predict the bee-subjective appearance of object colours and present this information in a graphical format. In colour space, a coloured stimulus occupies a single locus depending on the photoreceptor excitation signals. The distance between two loci is representative of the perceptual difference between two coloured stimuli when viewed by a bee, with more dissimilar colours positioned further apart than similar ones (Chittka, 1992; Armold *et al.*, 2010). The central point of the diagram marks the locus of all uncoloured stimuli in the hexagon (Chittka, 1992).

A bee returning to the feeding site in search of a flower, be it natural or artificial, must first detect the target from a distance. Once the flower has been detected, the bee will approach it up to a distance at which it is able to recognize whether or not the flower is similar to that stored in memory (Giurfa & Lehrer, 2009). At greater distances, bees also rely on the contrast between flowers and green vegetation (Chittka & Raine, 2006; Dyer *et al.*, 2015). Thus, an additional component important for flower recognition by bees is “green contrast”: the specific contrast between stimulus and background in the green photoreceptor type (Giurfa *et al.*, 1996; Papiorek *et al.*, 2013).

5.1.3 Red flowers, white flowers and bee vision

Colour constitutes one of the main traits considered in pollination syndrome theory (Faegri & Van Der Pijl, 1979). According to this theory, unrelated plant species adapted to the same pollinators should show convergence of floral traits, including colour. For example, bee pollinated flowers are expected to be brightly coloured, with yellow and blue being considered classic bee colours (Faegri & Van Der Pijl, 1979). As bees do not have receptors that perceive much red light, the idea that bees cannot see red flowers is widespread among pollination biologists (Chittka & Waser, 1997). This has led many workers to assume that red colouration is an adaptation by which flowers exclude bees as visitors. However, many bee-pollinated flowers are red or pink. It has been shown that the spectral sensitivity curve of the green receptor in bees has an extended tail, and reaches around 650 nm, well beyond the orange/red boundary (Chittka & Waser, 1997). Moreover, it has been demonstrated empirically that bees can discriminate reflectance patterns over a range of 550-650 nm, since these patterns would occupy different loci in bee colour space (Chittka & Waser, 1997). Most red blossoms also contain a blue component, so they will appear blue or ultraviolet to a bee (Faegri & Van Der Pijl, 1979). The petal lobes of *N. forgetiana* appear red to the human eye (Figure 3.3). Although it is thought to be pollinated by various hummingbird species, *N. forgetiana* is occasionally visited by Halictid bees and small hawkmoths (Goodspeed, 1954; Ippolito, 2000; Ippolito *et al.*, 2004)(section 3.2.3).

White flowers are generally associated with nocturnal pollinators, particularly moths (Faegri & Van Der Pijl, 1979). Nocturnal moths' visual sense is sensitive to colours at night and these animals have a strong olfactory sense (Faegri & Van Der Pijl, 1979). Thus, according to classic pollination syndrome theory, flowers pollinated by nocturnal moths are expected to be mostly white or faintly coloured, presenting instead a strong aroma at night (Faegri & Van Der Pijl, 1979). The interpretation of how bees perceive white flowers visually varies. The hexagon model of colour vision predicts that white flowers which reflect ultraviolet light resemble green foliage to a bee's eye, whereas, according to other models of bee colour vision, UV- reflecting white is discriminable from foliage green (Waser & Chittka, 1998; Vorobyev *et al.*, 1999). Most white flowers do not reflect UV light but absorb it, so they would appear green to a bee.The petal lobes of *N. bonariensis* on the adaxial surface are white (Figure 3.3), and the pollination of this species is thought to be by small perching moths (Ippolito, 2000)(section 3.2.3).

The epidermal cell structures on floral petals are exceedingly fine-grained: conical cells have a diameter across the base in the range of 10 μm, and it is thought that bees discriminate these structures with the sensilla trichodea on the tips of the antennae (Kevan & Lane, 1985; Whitney *et al.*, 2009b). It has been considered that the angular resolution of a bee's eye is far too coarse for it to visually detect the optical effect produced by conical cells as intensifiers of petal pigments (Dafni *et al.*, 1997; Waser & Chittka, 1998). However, further investigations have shown that bee foragers possess significantly better resolution than previously reported or estimated behaviourally (Rigosi *et al.*, 2017).

5.1.4 The effect of petal cell shape on bumblebee perception in the floral systems of *N. forgetiana* and *N. bonariensis*

Considering the colour characteristics associated with classical pollination syndromes alone, the predicted natural pollinators of *N. forgetiana* and *N. bonariensis* would probably not be bees. *N. bonariensis,* with 'human white' flowers, would likely fit in the moth pollination syndrome, and *N. forgetiana,* with 'human red' flowers, would attract birds or butterflies. Moreover, as discussed in section 5.1.3, both colours may potentially fall in the "invisible" zone of the bee vision hexagon.

In this chapter, petal colour, as perceived by bees, was characterized for *N. forgetiana* and *N. bonariensis* (Section 5.3). This information in addition to the known petal cell shape of these species, was used as a starting point in the design of artificial flowers that would mimic the potential range of combinations of colour/petal cell shape of the sister pair. These artificial flowers were used to assess the effect of these combinations on the perception of the flowers by *B. terrestris*.

To test if *B. terrestris* was able to visually discriminate between flowers with conical vs. non-conical textures on the same (white or red) pigment background, a differential conditioning experiment was run (sections 5.2.4 and 5.3.3). In this experiment, individual bumblebees were presented with a set of vertically oriented flowers with the same pigment background, in which half of the flowers were conical and half were non-conical in texture. Flowers of contrasting texture were filled with either reward or punishment. If the bumblebees were able to visually identify flowers with contrasting cell shape, we would expect individual bees to stop drinking from the type of flower carrying the punishment and visit only flowers loaded with the reward. On the other hand, to test if the presence of conical cells would have a positive effect on the way bumblebees perceive the flower compared to non-conical cells, a foraging speed experiment was

run (sections 5.2.5 and 5.3.4). In this experiment, individual bumblebees were presented with a set of horizontally oriented flowers of identical characteristics (same pigment background and cell shape), arranged at regularly spaced intervals. If the shape of the cells would influence the ease with which bumblebees detect flowers from the green background, we would expect to find quantifiable differences in the time of flight between flowers of conical texture compared to those with non-conical texture.

The differential conditioning experiments demonstrated that bumblebees can learn to identify flowers with conical cells from flowers with non-conical cells on both red and white pigment backgrounds, using only visual cues. However, foraging speed experiments showed that there were no significative differences in the velocity in which bumblebees moved from one rewarding flower to the next, when comparing experiments using flowers of the same colour and contrasting texture. The implications of these findings in the context of pollination biology of *N. forgetiana* and *N. bonariensis* are discussed.

5.2 MATERIALS AND METHODS

5.2.1 Petal colour and cell shape characterization of *N. forgetiana* and *N. bonariensis*

In order to accurately replicate petal colour and cell shape of *N. forgetiana* and *N. bonariensis* in artificial flowers, a detailed characterization of these features was necessary. Plants used for petal colour and petal cell shape characterisation were grown in greenhouses at the Department of Plant Science, University of Cambridge (see 2.3.1.1 for plant growth conditions). For petal colour characterization, petals were sampled from flowers from three different plants of the same age growing at the same time. Individual petal lobes were dissected with razor blades and put on black cardboard with the adaxial surface facing up. Measurements were taken of at least six petals of each species, using an Ocean Optics S2000 spectrophotometer (Dundedin, FL, USA), relative to a white reflection standard. The spectrophotometer was connected to a computer running SpectraSuite (Ocean Optics). The light spectrum analysed ranged from 300 to 700 nm, and the spectrometer sensor was fixed at an angle of 90° from the measuring area. Three independent measurements from each petal were recorded. Spectrophotometer reads were quantified using the PAVO 2.0 package in RStudio (Version 1.1.463) to obtain reflectance spectra, and to plot the spectral signature of each sample in the bee colour hexagon (Chittka, 1992).

Artificial flowers used in the experiments were coloured epoxy resin discs (see 5.2.2 for further details on fabrication). Several pigment combinations were tried to obtain spectrophotometric signatures and bee colour hexagon loci values for the artificial flowers close to the ones measured for the petals of *N. forgetiana* and *N. bonariensis*. Spectrophotometer measurements were taken from the discs and the data were processed as explained above. Reflectance spectra and the bee vision hexagon loci of potential pigment combinations were compared to those of the petals.

5.2.2 Reproducing conical and non-conical petal cell shape in artificial flowers

Artificial flowers used for the bumblebee behavior experiments were 58 mm diameter coloured epoxy resin discs, replicating either conical or non-conical cell surfaces along the entire area. To mimic the *N. forgetiana-N. bonariensis* natural scenario, ideally petal cell shape of these species would be replicated. However, petal lobe area in these species is relatively small compared to the minimum surface required to construct artificial flowers for the bumblebee behavior experiments. 58 mm size discs are preferred as this ensures that to reach the reward located at the centre of the disc the bumblebees cannot use any edges nearby to hold onto. Alternative surfaces with the desired characteristics were explored in petals and other organs of several angiosperm species growing in the Cambridge University Botanic Garden (*e.g*. *Rosa* spp., *Paeonia mascula* ssp. *arietina*, *Tulipa* 'Negrita', *Magnolia* x *soulangeana*, *Magnolia liliflora* 'Nigra', *Zanthedeschia aethiopica*). From this exploration, the spathe (inflorescence bract) of *Zanthedeschia aethiopica 'Crowborough'* (Araceae, cultivar of garden origin) was found to be ideal to use as a template to replicate both conditions of cell shape because of its size, and because it presents conical cells on the adaxial surface and non-conical cells on the abaxial (Figure 5.1).

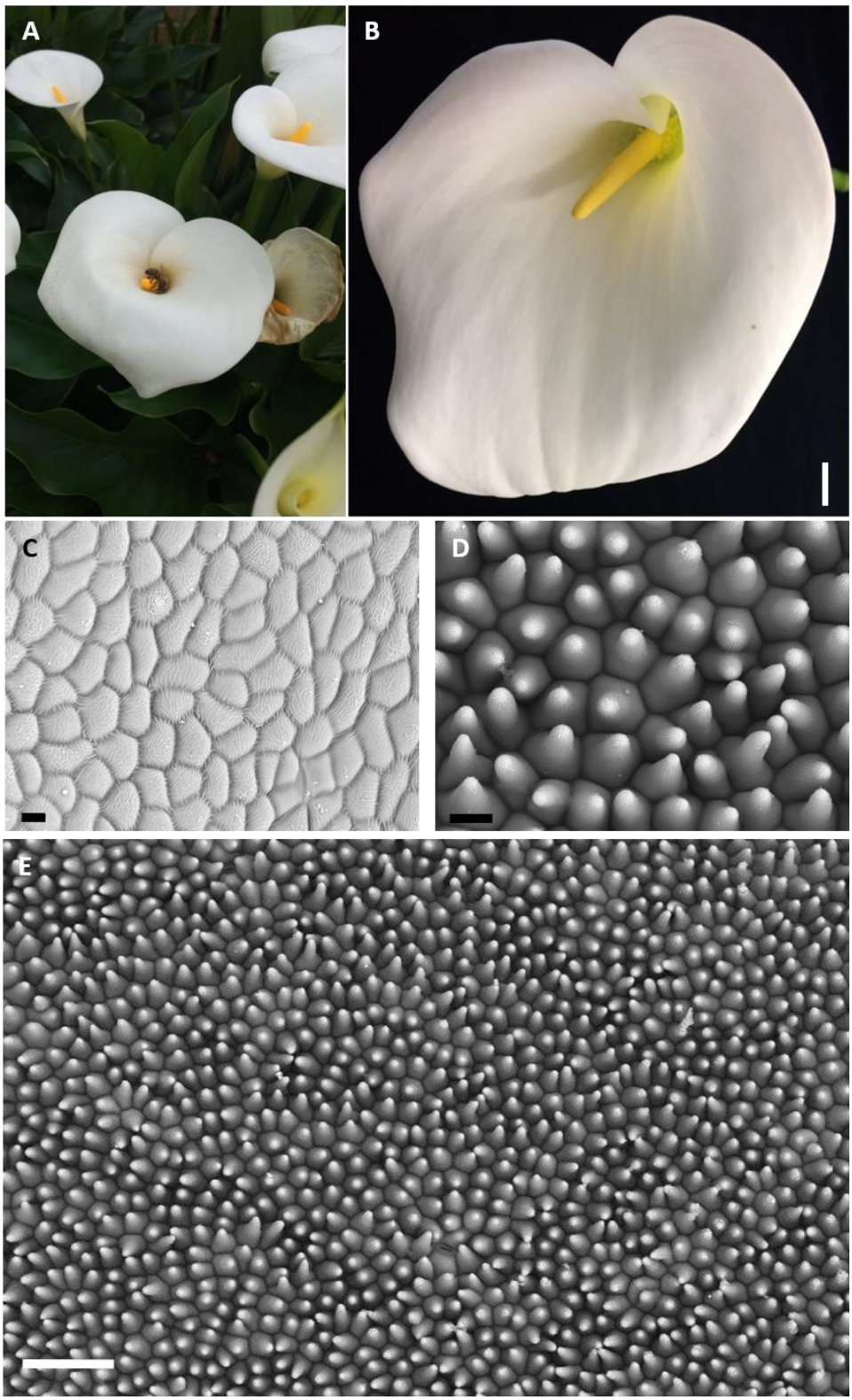

Figure 5.1. Surfaces of the spathe of *Zantedeschia aethiopica* (Araceaea) were selected as models of conical and non-conical cells to create moulds for the artificial flowers used in bee experiments.

A-B. General morphology of the inflorescence of *Z. aethiopica*: White petal-like spathe surrounding the yellow spike-like spadix. C. Non-conical epidermal cells on the abaxial surface of the spathe. D-E. Conical epidermal cells on the adaxial surface of the spathe. C-E. Cryo-SEM images. Scale bars: B = 1 cm, C-D = 20 µm, E = 100 µm.

Z. aethiopica spathes were carefully dissected and flattened to make casts that were at least as big as the desired discs. Moulds of both surfaces of the spathe were obtained with two-part dental wax (dental impression mould Elite HD+ light body, normal set, Zhermack). The shape of the disc was obtained by creating a higher relief contour following the periphery of a 58 mm circular Petri dish lid with additional dental wax. The epoxy discs were created from the dental wax moulds using two-part epoxy resin (Pebeo Gedeo Crystal Resin). Powder pigments were weighed, added to the resin pre-polymer in a glass vase and mixed for ten minutes with a magnetic stirrer at high speed. The mixes were stirred for an additional 10 minutes after adding the hardener. 9 ml of the coloured liquid resin mix was poured onto each individual mould. Filled moulds were degassed by applying five rounds of one-minute vacuum followed by one-minute recovery. The samples were left to set for a minimum of 24 H.

To confirm the quality of the epoxy replicates, all the discs used for bumblebee behavior experiments were scanned using a Keyence SBL, VHX-5000 microscope. Any discs that did not have homogeneous distribution of cells or presented any bubbles, were discarded.

5.2.3 *Bombus terrestris* maintenance and wellbeing

Bombus terrestris audax bees were obtained from Biobest (supplied by Agralan, Ashton Keynes, UK) and housed in plastic nest boxes of approximate size 292 x 225 x 240 (L x W x H) mm. These were connected via a gated transparent tube (15 mm diameter, 30 cm long) to a wooden flight arena (100 × 70 × 30 cm) constructed with a clear UV-transparent Perspex lid (Figure 5.2). The gates in the connecting tube could be used to control which bees enter and leave the arena. The base of the arena was painted green with Plasit-Kote fast-drying enamel, B9 “Garden Green”. The room temperature was kept constant at 21 °C. Illumination was provided for fourteen hours a day using Sylvania professional Activa 172 58 W fluorescent tubes on the ceiling of the room. The frequency of these lights was kept at over 200 Hz (above the bee-flicker fusion frequency) using Philips HF-B 236 TLD ballasts. Adjustable lamps with a frequency of over 200 Hz, fitted with daylight bulbs, were placed above the colony entrance to control flower illumination. The colony was fed with fresh 30% sucrose solution daily and pollen grains were supplied two times a week. Foragers were either hand-marked with water-based Thorne queen marking paint in various colour combinations, or with numbered tags (queen marking kit from Abelo, Full Sutton, York, UK) attached with glue, to distinguish individuals during experimentation. For each experiment, foragers from two to three colonies were used.

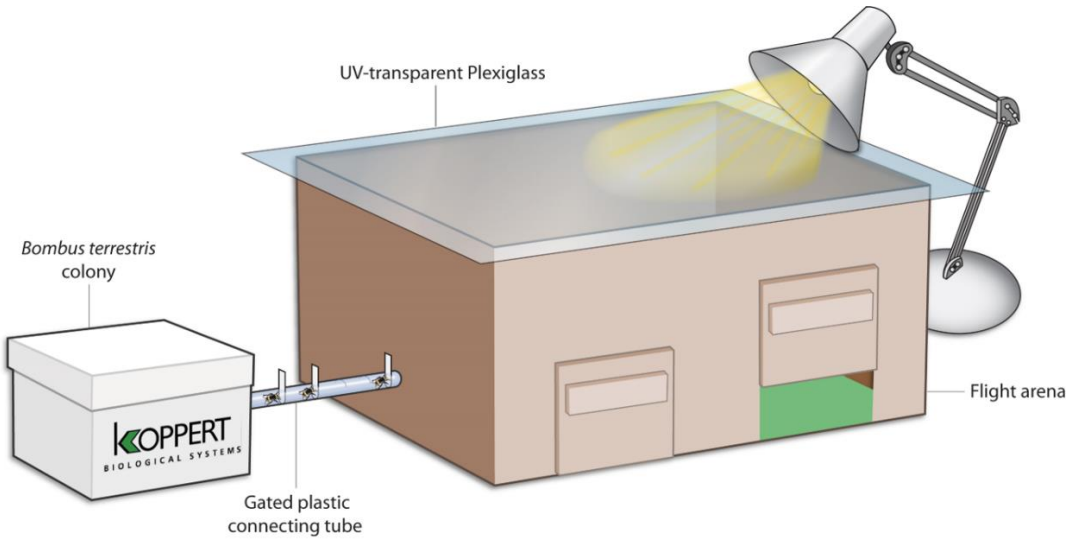

Figure 5.2. Experimental setup of the bee arena for behavioural studies.
A colony of *Bombus terrestris* is connected to a wooden flight arena via a gated plastic tube. The lid is made from UV-transparent Plexiglas. Diagram from Reed (2014).

5.2.4 Differential conditioning experiments

5.2.4.1 General experimental setup for differential conditioning

Experimental flowers for this set of experiments were single discs in a vertical position. To hold the discs vertically, they were attached using adhesive Velcro tape to a support stand consisting of a 58 mm petri dish lid glued to two wooden sticks (length approx. 150 mm), held vertically in a Hamilton jar (60 x 39 mm, height x diameter) using a foam bung/stopper Figure 5.3).

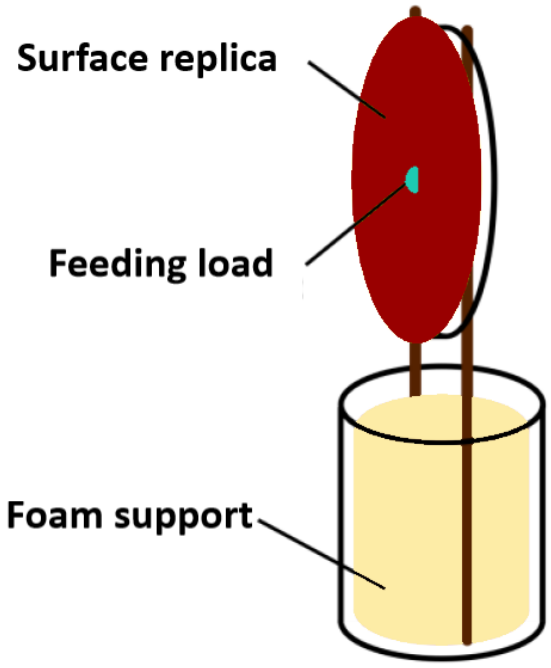

Figure 5.3. Feeder used for the attachment of the differential conditioning experiment.
The feeding load would be either 15 µl of 30% sucrose or 0.12% quinine. Figure modified from (Pattrick, 2017).

5.2.4.2 Training phase for differential conditioning experiments

Training flowers were either sets of four PCR tubes, similar to the day to day feeders the bees were used to, put on the holders in a vertical position, or cardboard spectrally grey discs in a vertical position. During the training phase, each individual was allowed to familiarize itself with the vertical feeding set-up using PCR training flowers. Three PCR training flowers with 15 µl of 30% sucrose solution were randomly positioned in the arena; an individual bee was introduced into the arena and allowed to feed. When it had fed on the three flowers a large reward (100 µL of 30% sucrose solution) was offered to the bee to allow it to fill up and encourage it to return to the hive. In the following bouts, training disc flowers were used instead of PCR flowers to familiarize the bee with the discs in a vertical position. A bee was considered trained after it had completed three successful bouts of foraging.

5.2.4.3 Experimental test for differential conditioning

During the test phase, six differential conditioning artificial flowers of the same colour were randomly positioned in the arena. Three flowers presented conical cells with 15 µL of 0.12% quinine solution and three flowers displayed non-conical cells with 15 µL of 30% sucrose solution (or vice versa). An individual trained bee was released into the arena, and the flowers that it successively visited were recorded. After each visit, the flower was refilled with sucrose or quinine solution and moved to a new position in the arena; the positions of the non-visited flowers were also randomized. Consequently, the position of the six flowers changed constantly throughout the experiment. The flowers were cleaned with distilled water and 20% ethanol solution between each foraging bout and between individual bees (to remove scent marks). Visits were categorized in three groups: “Drink”, when the bee landed on the disk and tasted (or drank) the feeding load; “touch”, when the bee landed or touched the flower with its legs or other body parts without drinking or tasting the feeding load; and “hover”, when the bee approached the flower and touched it with its antennae. If the bee approached the flower without touching it, it was not considered as a visit. The type of visit was noted as the kind of interaction with respect to the type of disc surface as follows: Drink on conical (DC), touch on conical (TC), hover on conical (HC), drink on non-conical (DNC), touch on non-conical (DNC) and hover on non-conical (HNC)(Table 5.1).

Table 5.1. Type of visits considered in differential conditioning experiments.

Abbreviation	Type of visit
DC	Drink on conical
TC	Touch on conical
HC	Hover on conical
DNC	Drink on non-conical
TNC	Touch on non-conical
HNC	Hover on non-conical

To control for the potential effect of aroma and/or UV fluorescence of quinine in differentiating flowers with sugar from flowers with quinine, the experiment was run for one bee using six identical flowers (red conical), three with 30% sugar and three with 0.12% quinine. The proportion of visits to flowers with quinine and to flowers with sugar for the control was close to 50:50 (Table 5.2). Moreover, it has previously been demonstrated that bumblebees are unable to discriminate between the two solutions prior to landing (Whitney *et al.*, 2008; Moyroud *et al.*, 2017), and quinine is widely used in differential conditioning experiments with bees (*e.g.* Whitney *et al.*, 2009d; Moyroud *et al.*, 2017; Lawson *et al.*, 2018)

Table 5.2. Control bee for differential conditioning experiments.
Proportion of visits to sugar and quinine loaded flowers per bout. The control bee was presented with a series of flowers of the same colour and texture, half of them loaded with sugar, half with quinine.

Bout No.	Proportion of visits to sugar	Proportion of visits to quinine
1	0.41	0.59
2	0.44	0.57
3	0.59	0.41
4	0.45	0.55
5	0.53	0.47
Average	0.48	0.52

For the pairwise comparison red conical versus red non-conical, nine bees were tested. Ten bees were tested for the white conical versus white non-conical pairwise comparison. Each bee was tested for a minimum of 100 choices. Four sets of experiments were considered, defined by the colour of the disc (white or red) and by on which disc texture (conical or non-conical) the reward (sugar) had been allocated. Five bees were tested for the white/sugar on conical, white/sugar on non-conical, red/sugar on non-conical experimental sets, and four for the red/sugar on conical experimental set.

To summarize all the observations from each colour in a single comparison, and for further statistical analyses, drinking visits to conical in the "sugar on conical" datasets, and drinking visits to non-conical in the "sugar on non-conical" datasets, were scored as "correct choice".

5.2.4.4 Statistical analyses for differential conditioning experiments

Statistical analyses were run in RStudio (Version 1.1.463) and Jupyter Notebooks (Kluyver *et al.*, 2016)(running in Anaconda Navigator Version 1.9.6).

The change in the proportion of visits to conical, and of correct choices, were calculated for each colour dataset and for all the datasets combined. Learning curves were estimated from the proportion of correct choices at any given visit per bee. Because the number of visits recorded per bee varied, the bee with the smallest number of observations was considered to define the extent of the curves (experience, approx. 100 visits/choices). Bins of 10 visits each were generated for the analyses. A generalised linear logistic binomial regression model was calculated.

In the binomial logistic regression, the following fixed effect model is fitted to the data:

$$log\left(\frac{pi}{1-pi}\right) = \alpha_0 + \alpha_1(i)$$

where p_i is the probability of a specific choice (*e.g.* correct choice) in the i_{th} choice and where α_0 and α_1 are the parameters to be estimated. α_1 controls how the logit of the probability of choosing correctly increases with i, positive values of α_1 indicate that foragers are learning over time.

The probability for the model is calculated as the mean of the probability of a correct choice at any given visit (from 1 to 100) calculated from the values of all the bees in the dataset. The null hypothesis considered is that there is no effect of the experience (number of choices or visits) in the probability of any given bee to make a correct choice ($H_o = \alpha_1 = 0$). Alternatively, if bees can learn to discriminate between flowers with punishment from flowers with reward, as experience increases, the probability of any given bee to make a correct choice would increase with the number of choices/visits ($H_o = \alpha_1 \geq 0$). The fit of the data to the model was assessed by comparing the single parameter Wald test statistic against the chi-square distribution($\chi 2$).

5.2.5 Foraging speed experiments

5.2.5.1 General experimental setup for foraging speed

Experimental flowers for this set of experiments (refered also as foraging speed flowers) were single discs in a horizontal position on the flight arena's floor, set 30 cm apart from one another (Figure 5.4).

Figure 5.4. Horizontal setup of artificial flowers used in foraging speed experiments.
Three identical foraging speed flowers were set in a horizontal position 30 cm apart from each other. Reward load was put on the center of the disc.

5.2.5.2 Training phase for foraging speed experiments

Training flowers used were disks made in the same way as the ones used for the experiment but using cardboard as a mould for texture. Training flowers had colouration spectra falling in the grey zone of the bee colour hexagon.

During the training phase, each bee was allowed to forage freely on three training foraging speed flowers containing 15 µl of 30% sucrose solution. A bee was considered trained after it had completed at least three successful bouts of foraging.

5.2.5.3 Experimental test for foraging speed

During the test phase, three foraging speed flowers, displaying identical colour (white or red) and cell shape (conical or non-conical) and offering 15 µL of 30% sucrose solution, were set 30 cm apart from one another in the arena. An individual bee was introduced to the arena and its foraging bout (from the time it landed on the first flower until it landed on the third flower) was recorded with an iPhone 5s 8 Megapixel digital camera. A large reward (100 µL of 30% sucrose solution) was offered to the bee at the end of the foraging bout to allow it to fill up and encourage it to return to the hive. Parts of the flowers with which the bees came into contact were cleaned with distilled water and 20% ethanol to remove scent marks. A new set of flowers with the alternative petal cell shape was set 30 cm apart from one another in a new location. The experiment was repeated with the same bee, but with flowers in the new position. Bouts were run alternating cell shape and moving the flowers between five different locations in the bee arena. Ten complete foraging bouts on each of the two flower types were recorded for each individual bee. This routine allowed us to control for the variability in foraging speed between foragers (as each bee performed the experiment on each type of flower) and any potential effect of the position of the flowers in the arena. Ten individuals for each flower colour were independently tested in total. The time taken for each bee to travel between each flower was extracted from the recordings using Adobe Premiere Pro Video or DaVinci Resolve Video Software.

5.2.5.4 Statistical analyses for foraging speed experiments

For statistical analyses the time values extracted from the video software in format HH:MM:SS:ss were converted to integers in "Units of time" (1 unit of time = 1/60 seconds). The different combinations of background pigment and surface texture were considered as treatments: White-conical (WC), white-non-conical (WNC), red-conical (RC) and red-non-conical (RNC). Statistics were run in RStudio (Version 1.1.463). 0.01 and 0.99 quantiles were considered to remove extreme outliers from the data.

Welch two-sample t-test was applied to allow general comparisons of the data without discriminating into treatments. The mean of the time of flight between Flower 1 and Flower 2 was compared to the mean time of flight between Flower 2 and Flower 3, for all the treatments, and the mean of the time of flight between discs with conical surfaces was compared to the time of flight between flowers with non-conical surfaces. A single-factor ANOVA and a post hoc Tukey's HSD test were conducted to compare the differences among the four treatments.

5.3 RESULTS

5.3.1 Petal colour and cell shape characterization of *N. forgetiana* and *N. bonariensis*

Reflectance spectra and loci in the bee colour hexagon plots for *N. bonariensis* and *N. forgetiana* petals are shown in Figure 5.5 and Figure 5.6. The white petals of *N. bonarienis* present an increase in absorbance at 400 nm (violet), followed by a plateau (Figure 5.5A). The spectral curve of the petals of *N. forgetiana* (Figure 5.6A) is characterised by a low peak between 400 and 500 nm (violet) and a steep rise between 600 and 700 nm (orange-red).

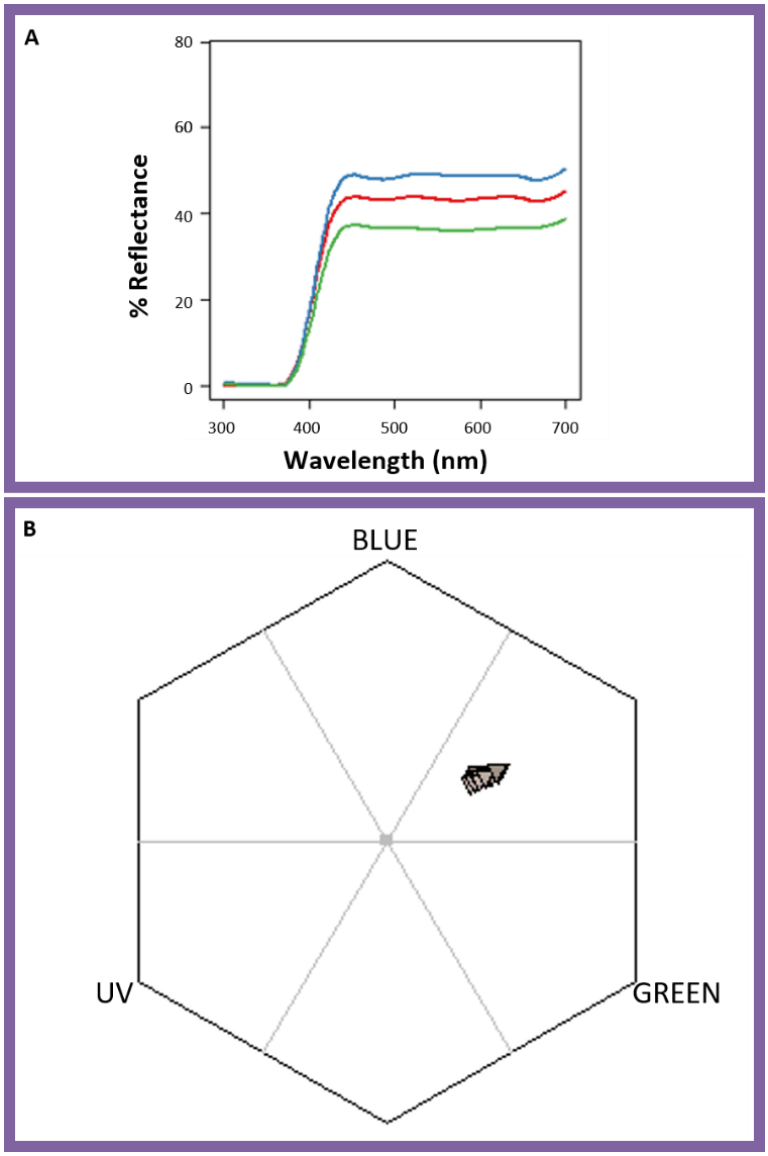

Figure 5.5. Reflectance spectra and bee hexagon loci for petals of N. *bonariensis*.
A. Representative reflectance spectra of the adaxial surface of the petal of *N. bonariensis*. The graph corresponds to three independent measurements of the same petal (coloured lines). **B.** Bee hexagon loci of *N. bonariensis* petals (grey triangles). Loci values were calculated for each independent measurement of reflectance (coloured lines in A, 18 in total, from six different petals of three independent plants).

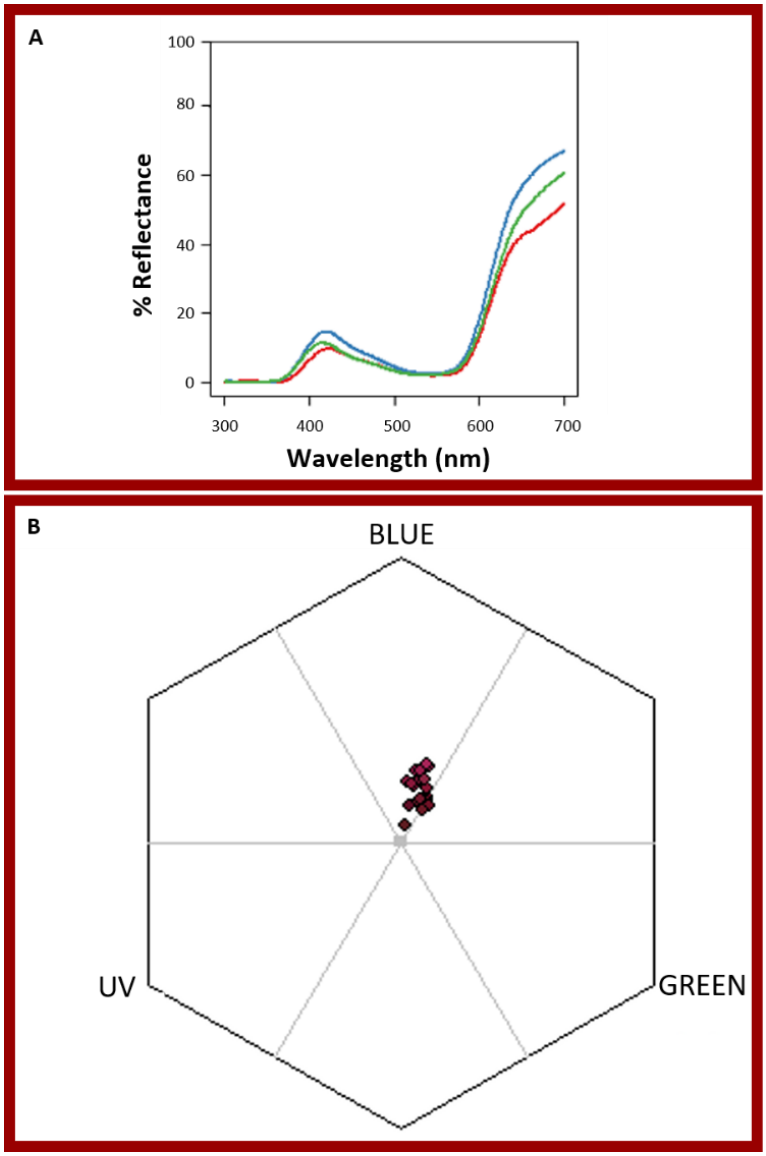

Figure 5.6. Reflectance spectra and bee hexagon loci for petals of *N. forgetiana.*
A. Representative reflectance spectra of the adaxial surface of the petal of *N. forgetiana*. The graph corresponds to three independent measurements of the same petal (coloured lines). B. Bee hexagon loci of *N. forgetiana* petals (red diamonts). Loci values were calculated for each independent measurement of reflectance (coloured lines in A, 18 in total, from six different petals of three independent plants).

5.3.2 Reproducing petal colour of *N. forgetiana* and *N. bonariensis* in artificial flowers

To accurately match colouration of both, white and red flowers, several pigment combinations were assesed. In the case of the white colouration of *N. bonariensis*, from two different white pigments trialled, titanium white (PW6, L. Cornelissen & Son Ltd.) and zinc white (PW4, L. Cornelissen & Son Ltd.), the reflectance spectra of titanium white matched in great proportion the curve of *N. bonariensis* (Figure 5.7). Similarly to the petals, titanium white discs presented an increase in absorbance at 400 nm (violet), followed by a plateau. The values of the discs on the bee vision hexagon partially overlapped or were close to the petal ones. The addition of pigments of other colours to the mix did not improve the pattern, so titanium white was selected as the single pigment component for the white discs. The pigment combination formulae

selected to build the white discs to be used in the bumblebee experiments are listed in Table 5.3. Microscopic features of the final discs are depicted in Figure 5.8.

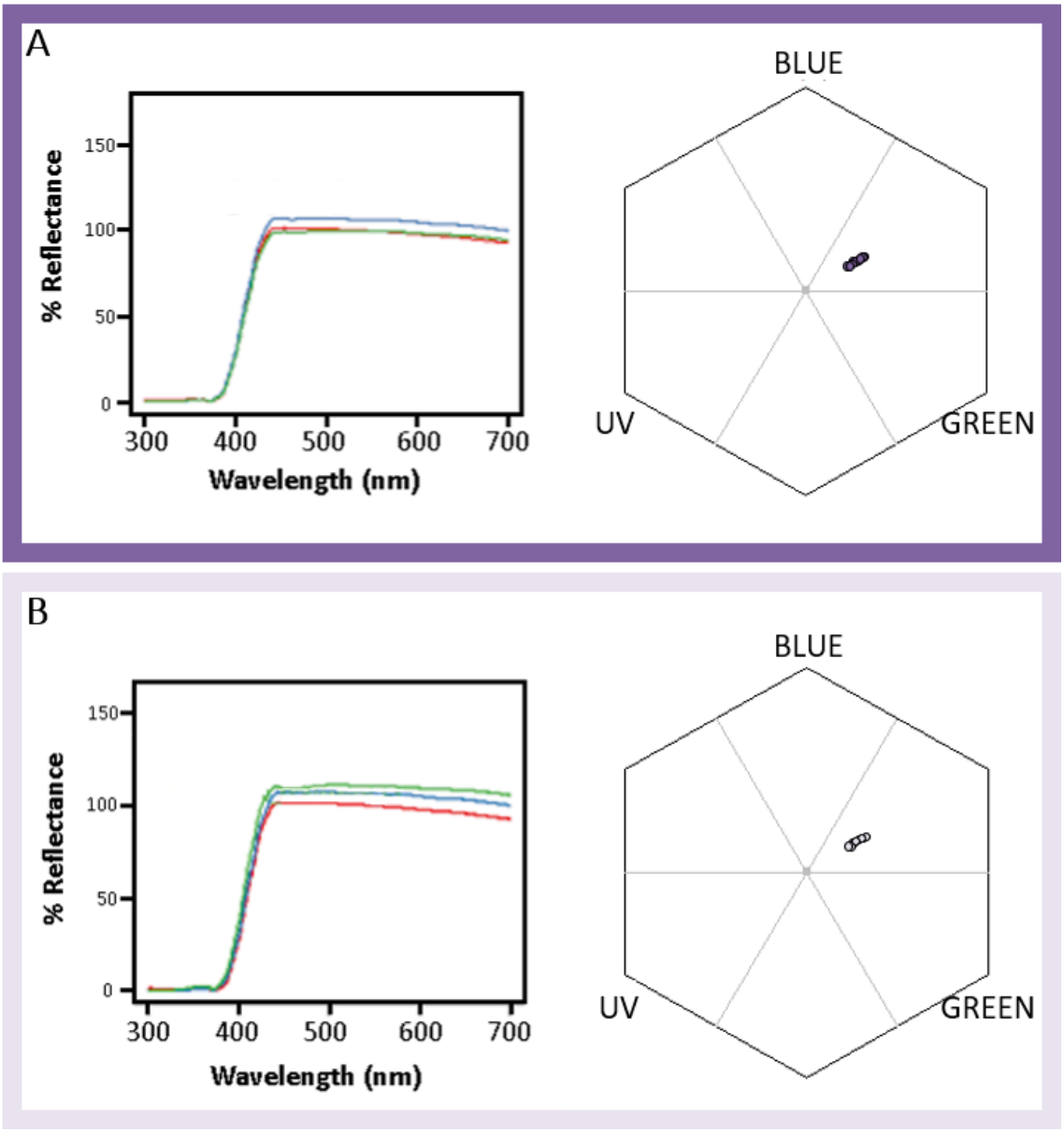

Figure 5.7. Reflectance spectra and bee hexagon loci for white discs, with conical and non-conical surfaces, used in pollinator behaviour experiments mimic the optical characteristics of *N. bonariensis* petals.
A. Reflectance spectra (left) off three independent measurements (coloured lines) of a single white disc with conical-celled surface; and bee hexagon loci (right) of four white discs with conical texture (three values per disc). B. Reflectance spectra (left) off three independent measurements (coloured lines) of a single white disc with non-conical-celled surface; and bee hexagon loci (right) of three white discs with non-conical texture (three values per disc).

Obtaining a pigment mix that accurately resembled the spectral pattern of the red flowers of *N. forgetiana* was challenging. The pigment combination that best resembled the reflectance spectra of the petal was quinacrinadone magenta (PR122, L. Cornelissen & Son Ltd.) with manganese violet (PV 16, L. Cornelissen & Son Ltd.; Figure 5.8), presenting a low peak between

400 and 500 nm and a steep rise between 600 and 700 nm. However, the percentage of reflectance obtained from this and other pigment combinations was always low (close to the black values), and when the pigment concentration was reduced attempting to increase reflectance, the discs were translucent instead of opaque. Opaque discs were preferred for bumblebee behaviour experiments as they would reduce any stimulus to the bee vision resulting from light passing through the disc. The loci occupied by the pigment combination that better resembled the reflectance spectrum of *N. forgetiana* petals (Figure 5.9) does not overlap with the values measured for the flowers in the bee colour hexagon (Figure 5.6). However, these values for the discs are close to the values of the "darkest" flowers measured, including the value calculated for the reflectance spectrum of *N. forgetiana* reported in the Flower Reflectance Database (Arnold et al., 2010). These points (for the "darkest" flowers and for the discs) also are close to the grey central point in the visual space for bees. Importantly, the loci values for discs replicating conical celled surfaces and the ones with non-conical celled surfaces were very similar, which would make a good case for the main objective of the experiment of testing the effect produced by differential cell shape in otherwise identical discs in terms of pigment background. The pigment combination formulae selected to build the red discs to be used in the bumblebee experiments are listed in Table 5.3.

Table 5.3. Pigment combinations used in artificial flowers used for bumblebee pollination behaviour experiments.

The pigment combinations listed in this table were selected from a range of pigment mixes trialled and characterized with the spectrophotometer. These combinations were found to best match the reflectance spectra and bee hexagon loci of the petals of *N. bonariensis* and *N. forgetiana*.

Colour	Pigment Combination
Red/*N. forgetiana*	2.8 mg/mL quinacridone magenta (PR122) 2.8 mg/mL manganese violet (PV 16)
White/*N. bonariensis*	22.2 mg/mL titanium white (PW 6)

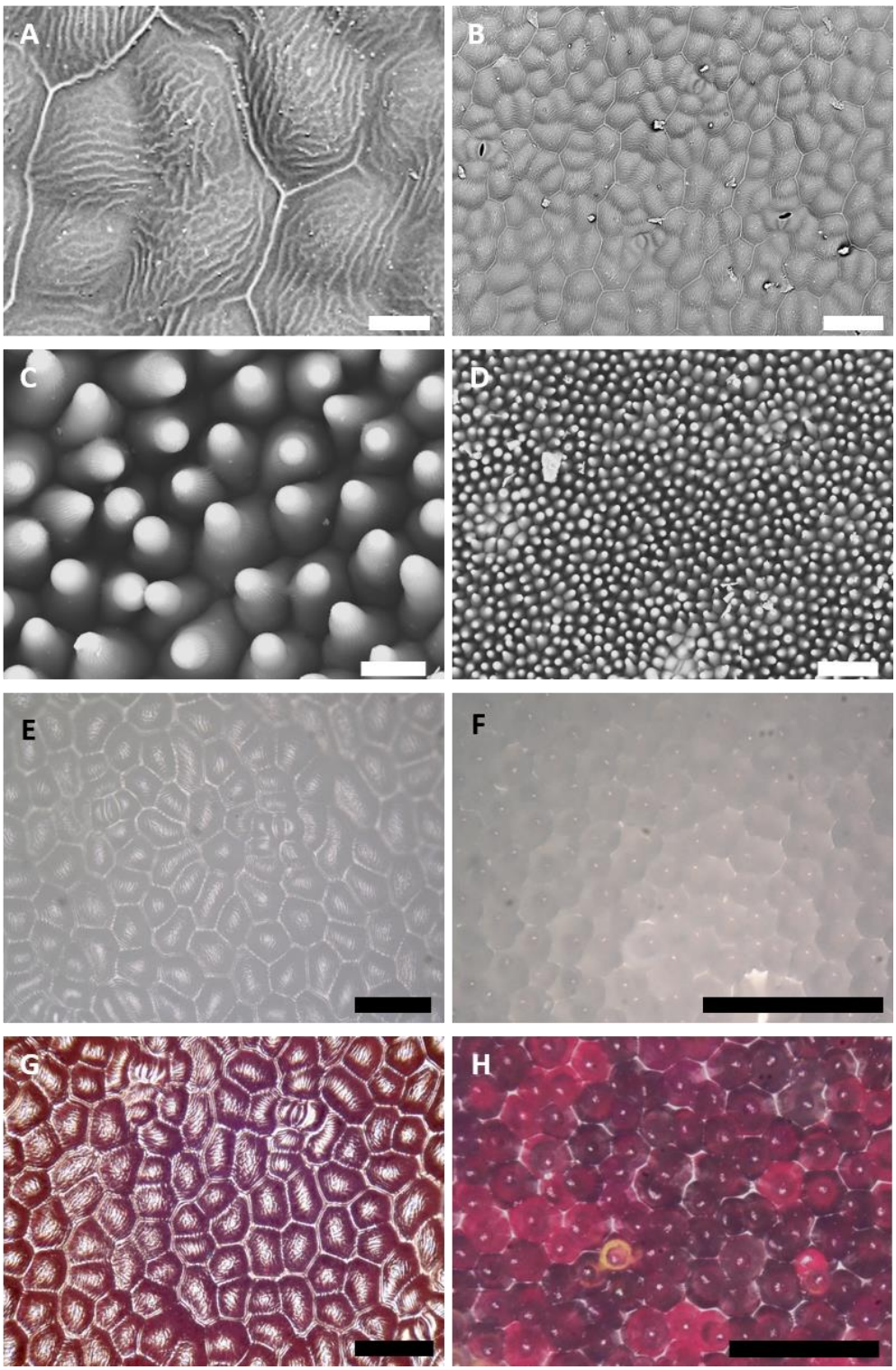

Figure 5.8. Petal cell shape (conical and non-conical) was replicated with high resolution on the surface of the biomimetic coloured epoxy resin discs used for the bumblebee behavior experiments.
Adaxial (conical) and abaxial (non-conical) epidermal surfaces of the spathe of *Z. aethipica* were replicated with high resoulution epoxy resin on the surface of the artificial flowers. A-D. SEM microphotographs of the surface of epoxy resin replicates of non-conical (A-B) and conical (C-D) epidermal surfaces (compare to Figure 5.1C for non-conical and Figure 5.1D-E for conical cells of the living plant). E-H Bright field digital microphotographs (Keyence microscope) of coloured epoxy resin discs. E-D. White pigmented discs with non-conical (E) and conical (F) surfaces. G-H. Red discs with non-conical (G) and conical (H) surfaces. Scale bars: A, C = 20 µm; B, D, E-H = 100 µm.

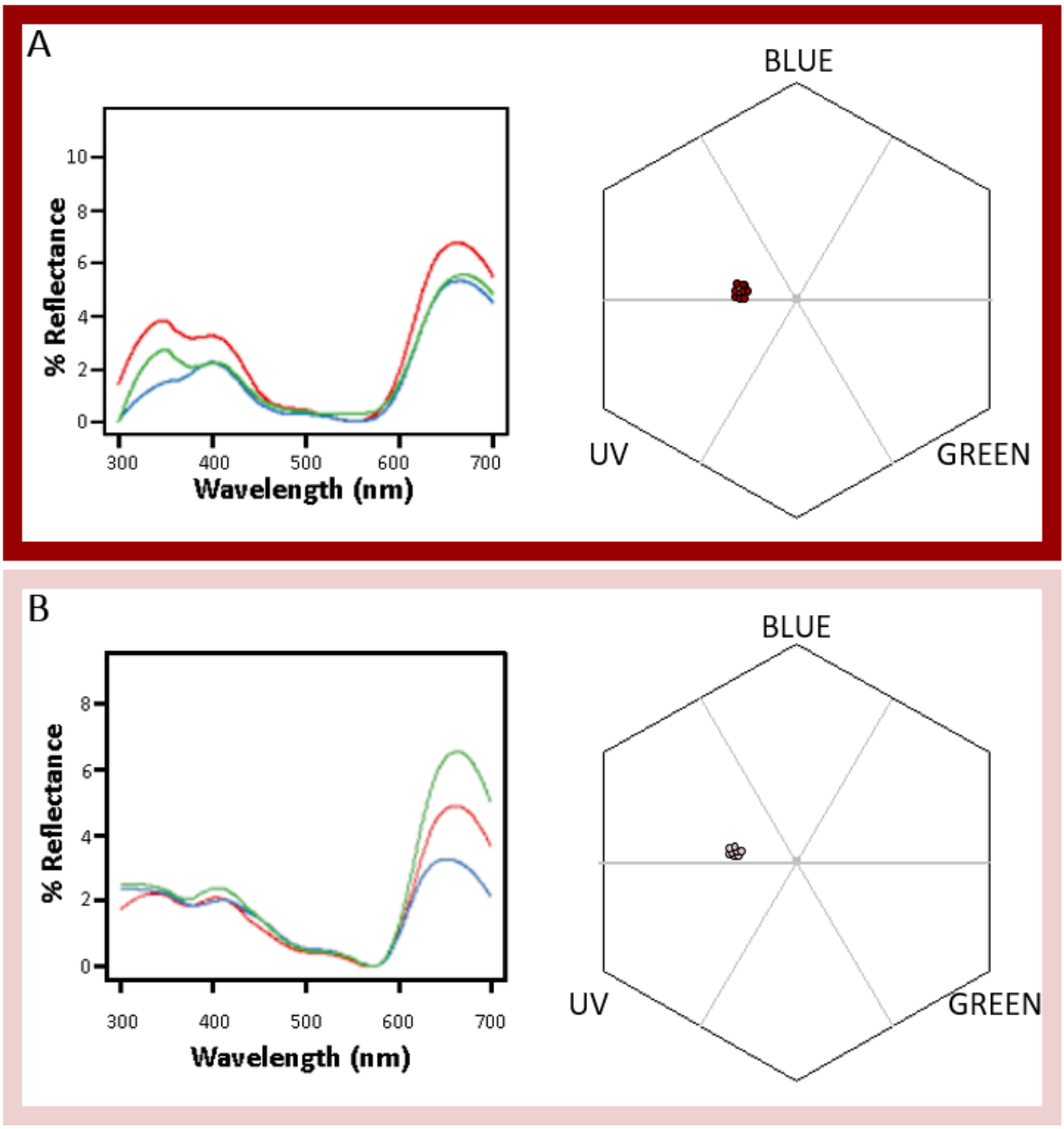

Figure 5.9. Reflectance spectra and bee hexagon loci for red discs, with conical and non-conical surfaces, used in pollinator behaviour experiments resemble the optical characteristics of *N. forgetiana* petals.

A. Reflectance spectra (left) off three independent measurements (coloured lines) of a single red disc with conical-celled surface; and bee hexagon loci (right) of three red discs with conical texture (three values per disc). B. Reflectance spectra (left) off three independent measurements (coloured lines) of a single red disc with non-conical-celled surface; and bee hexagon loci (right) of three red discs with non-conical texture (three values per disc).

5.3.3 Differential conditioning experiments

5.3.3.1 There are no innate preferences for disc texture in the bumblebees

Pollinators often have an innate bias to particular values of some traits (Lunau & Maier 1995; Raine & Chittka 2007). In order to test if the bumblebees had any innate preference to visit either the conical or the non-conical celled surface discs, a logistic regression of the probability to visit a conical celled disc was fit to the first 50 visits of the ten bees doing experiments on white discs, the nine bees doing experiments on red discs and a combined dataset of all bees. The number of visits initially reflects any innate preference of the bee for conical or non-conical celled flowers if three were any and will subsequently change as the bee learns to associate the combination of reward (sucrose) and surface texture. In this case all types of visits to a conical celled surface were accounted for the test (*i.e.* drink on conical -DC, touch on conical -TC and hover on conical -HC,Table 5.1), and the proportion was calculated in reference to the total number of visits up to each consecutive bout of 10 visits. The null hypothesis to be tested was:

H_o: Probability of visiting a conical celled disc during the first 50 visits = 0.5

The statistical tests accepted the null hypothesis, which means that the probability of visiting either type of surface (conical or non-conical) was the same (0.5), demonstrating that the bumblebees had no innate preference for any type of surface (Table 5.4).

Table 5.4. Statistical test to asses innate preferences for flower disc surfaces by bumblebees.
The null hypotheses (H_o) of the probability of a bumblebee visiting a conical celled disc during the first 50 visits being the same as the probability of visiting a non-conical celled flower, during the first 50 visits, were accepted for all datasets tested.

Dataset	χ2 (1)	P value	Decision to H_0
White discs	0.79	0.35	Accept
Red discs	0.75	0.39	Accept
Combined	2.1e-3	0.96	Accept

5.3.3.2 Bumblebees can learn to discriminate between flowers of contrasting texture and differential reward through experience

The probability of choosing a conical celled flower was used to explore the patterns of progression of each experimental set (Figure 5.10A-D for experiments with white flowers and Figure 5.10A-D for experiments with red flowers). This probability was calculated per bout of 10 visits for each bee, relative to the total number of visits recorded

(DC+TC+HC+DNC+TNC+HNC, Figure 5.10A, C; Figure 5.10A, C), and to the number of drinking visits (DC+DNC, Figure 5.10B, D; Figure 5.10B, D), up to 100 visits. Generalised binomial logistic models were fit to the data as described in 5.2.5.4. For both sets of experiments, run with white discs and run with red discs, a trend towards increased of visits to conical is observed for the "sugar on conical" datasets (Figure 5.10A, B, Figure 5.10A, B). This trend is more evident when only "drinking visits" are considered to calculate the proportion (Figure 5.10B, Figure 5.10B). The opposite tendency, towards decreasing the proportion of visits to conical, is observed in the "sugar on non-conical" datasets (Figure 5.10C, D; Figure 5.10C, D).The final analyses in Figure 5.10 and Figure 5.11 bring together the data from the experiment with sugar on conical and the experiment with sugar on on-conical, for each of the white and red flowers datasets, respectively. In these analyses a correct choice is defined as either DC (drink on conical) for the "sugar on conical" bees or DNC (drink on non-conical) in the "sugar on non-conical" bees. The proportion of correct choices, for both datasets, shows a tendency to increase with the number of visits and with the number of drinking visits (Figure 5.10E, F; Figure 5.11E, F). This is the expected tendency if the bees could discriminate flowers with conical from flowers from non-conical surfaces with the same pigment background. The Wald test statistic for all sets of data resulted in positive values and the calculated P-values indicated slopes significantly different from 0
(reject the null hypothesis $H_o = \alpha_1 = 0$) in all cases.

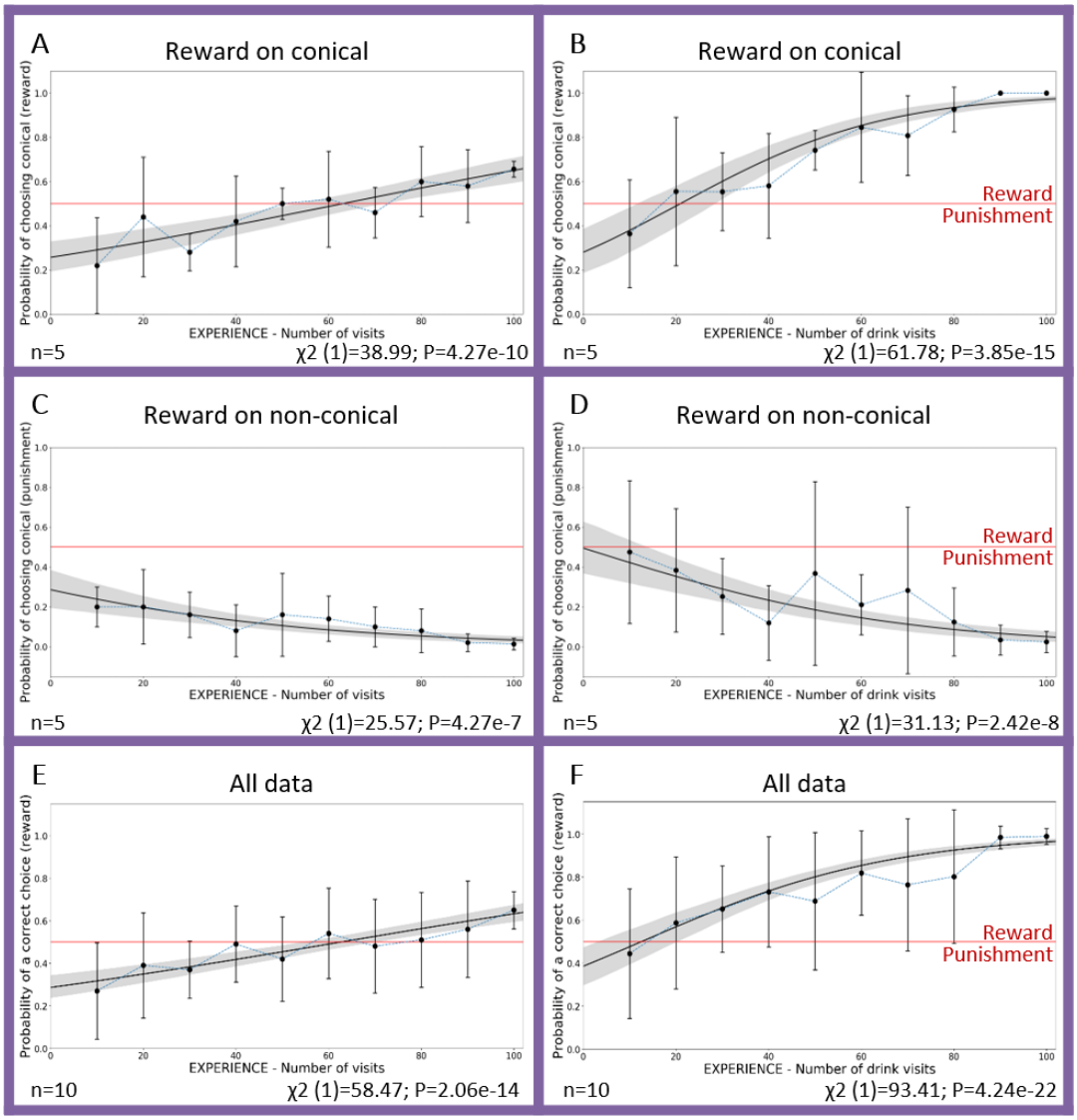

Figure 5.10. Bumblebees can learn to discriminate between white artificial flowers of contrasting texture and differential reward through experience.

Bumblebees can be trained by differential conditioning (using solutions of 30% sucrose as a "reward" versus 0.12% quinine as "punishment") to distinguish between white artificial flowers that only differ on the shape of the cells on the surface. In graphs A to D, the probability of choosing a conical celled flower was used to explore the patterns of progression of the experimental sets. In A and B, the "reward" is on the conical celled flowers and a trend towards increasing visits to "rewarding" flowers is evident. In C and D, the conical celled flowers are loaded with "punishment" and a tendency towards decreasing visits to "punishing" flowers is visible. In E and F, datasets of all the experiments run with white flowers are pooled together. For these plots, a correct choice is defined as a drink visit on a "rewarding" flower. Increasing success of choice is indicated by a rising learning curve. The plots to the left (A, C and E) include data for all the bee visits to a flower in an experiment, whereas the plots to the right (B, D and F) include only the visits in which a bee drinks from a loaded flower. The slopes of the curves are more pronounced in the graphs including "drink visits" only (right). For all plots: Bees were choosing from six discs, three with conical-celled texture and three with non-conical celled texture. Black dots (joined by dashed blue line) are the mean of the proportion of correct choices, every 10 choices, for all the bees for 100 consecutive choices. The black solid line is the fitted generalized binomial logistic model. The grey shading corresponds to 95% confidence intervals on the fitted response. The red line indicates the 0.5 probability value. The number of bees for each dataset (n), calculated chi-square statistic (χ2; the number in brackets indicates degrees of freedom) and p-value (P) are reported at the bottom of each plot.

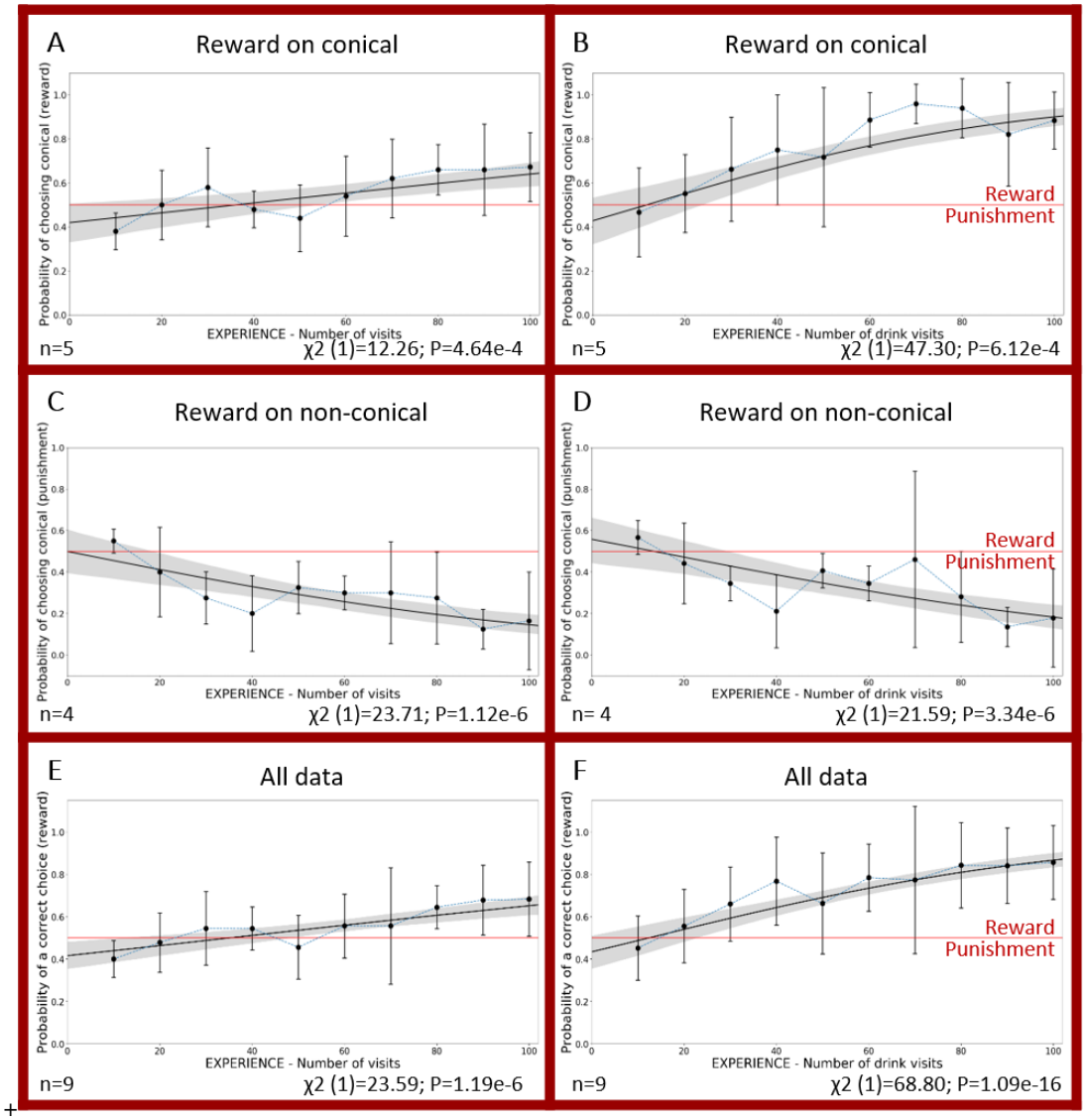

Figure 5.11. Bumblebees can learn to discriminate between red artificial flowers of contrasting texture and differential reward through experience.

Bumblebees can be trained by differential conditioning (using solutions of 30% sucrose as a "reward" versus 0.12% quinine as "punishment") to distinguish between red artificial flowers that only differ on the shape of the cells on the surface. In graphs A to D, the probability of choosing a conical celled flower was used to explore the patterns of progression of the experimental sets. In A and B, the "reward" is on the conical celled flowers and a trend towards increasing visits to "rewarding" flowers is evident. In C and D, the conical celled flowers are loaded with "punishment" and a tendency towards decreasing visits to "punishing" flowers is visible. In E and F, datasets of all the experiments run with red flowers are pooled together. For these plots, a correct choice is defined as a drink visit on a "rewarding" flower. Increasing success of choice is indicated by a rising learning curve. The plots to the left (A, C and E) include data for all the bee visits to a flower in an experiment, whereas the plots to the right (B, D and F) include only the visits in which a bee drinks from a loaded flower. The slopes of the curves are more pronounced in the graphs including "drink visits" only (right). For all plots: Bees were choosing from six discs, three with conical-celled texture and three with non-conical celled texture. Black dots (joined by dashed blue line) are the mean of the proportion of correct choices, every 10 choices, for all the bees for 100 consecutive choices. The black solid line is the fitted generalized binomial logistic model. The grey shading corresponds to 95% confidence intervals on the fitted response. The red line indicates the 0.5 probability value. The number of bees for each dataset (n), calculated chi-square statistic (χ^2; the number in brackets indicates degrees of freedom) and p-value (P) are reported at the bottom of each plot.

Figure 12 shows the fitted generalized binomial logistic models for experiments with white flowers and red flowers pooled together (n = 19 bees). As mentioned before, correct choice is defined as either DC (drink on conical) for the "sugar on conical" bees or DNC (drink on non-conical) in the "sugar on non-conical" bees. InFigure 5.12A the probability of a correct choice is calculated relative to all the visits in an experimental bout of 10 for each of the 19 bees (10 bees executing the experiment with white discs, 9 with red discs). In Figure 5.12B only "drink visits" are considered to calculate the probability of a correct choice. The pattern of increased probability of a correct choice is evident in the slopes of the learning curves for the three sets of experiments: with white flowers (Figure 5.10E-F), with red flowers (Figure 5.11E-F) and pooled data (Figure 5.12A-B). The Wald test statistic for all sets of data resulted in positive values and the calculated p values are significant to reject the null hypotheses ($H_o = \alpha_1 = 0$). These results indicate that the bumblebees can be trained to discriminate between identical flowers, pigmented red or white, that only differ on the texture of the surface (conical or non-conical).

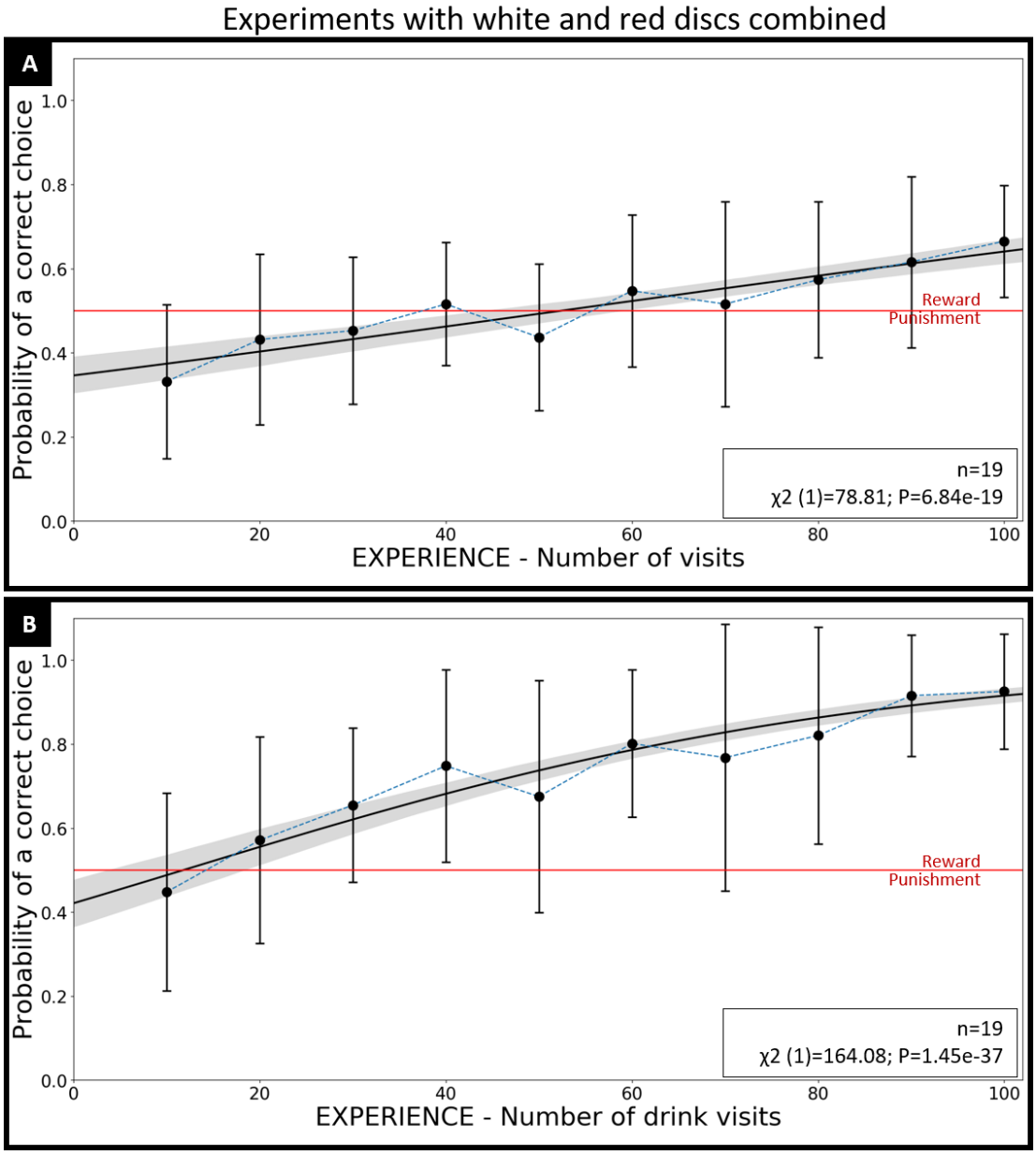

Figure 5.12. Learning curves showing that bumblebees can learn to discriminate between artificial flowers (red or white) of contrasting texture and differential reward through experience.
Bumblebees can be trained by differential conditioning (using solutions of 30% sucrose as a "reward" versus 0.12% quinine as "punishment") to distinguish between artificial flowers (red or white) that only differ on the shape of the cells on the surface. Datasets of all the experiments run with white (n=10) and red (n=9) flowers are pooled together. A correct choice is defined as a drink visit on a "rewarding" flower. Increasing success of choice is indicated by a rising learning curve. A includes data for all the bee visits to a flower in the experiments. B includes only the visits in which a bee drinks from a loaded flower. The slope of the curve is (continuation from previous page) more pronounced in the graph including "drink visits" only (B). For both plots: Bees were choosing from six discs, three with conical-celled texture and three with non-conical celled texture. Black dots (joined by dashed blue line) are the mean of the proportion of correct choices, every 10 choices, for all the bees for 100 consecutive choices. The black solid is the fitted generalized binomial logistic model. The grey shading corresponds to 95% confidence intervals on the fitted response. The red line indicates the 0.5 probability value. The number of bees for each dataset (n), calculated chi-square statistic (χ2; the number in brackets indicates degrees of freedom) and p-value (P) are reported at the bottom of each plot.

5.3.3.3 *Assesing the use of tactile clues by bumblebees to discriminate between conical and non-conical celled flowers*

To assess for the use of tactile cues by the bees in discriminating between flowers of different texture, type of visits (Table 5.2) were scored by whether they could be considered as a "tactile cue" to reject a punishing flower. For the "sugar on conical" datasets, touch on non-conical (TNC) and hover on non-conical (HNC) were scored as tactile clues. Similarly, for the "sugar on non-conical" datasets, touch on conical (TC) and hover on conical (HC) were considered as a use of this type of cues. If the bees only could discriminate between flowers with conical and non-conical textures from tactile cues, the frequency of tactile cue visits to the punishment flowers would be expected to be as high as the frequency of visits to the reward flowers (50:50). Alternatively, if the bees were able to discriminate between both types of flowers from visual cues only (without the need to touch the flower), the frequency of tactile cue visits to punishing flowers would be expected to be smaller compared to that of visits to reward flowers. To test these hypotheses, statistics were applied as explained for the insect learning curves (section 5.2.4). This is a novel statistical approach trying to increase our understanding of the different levels at which bees can discriminate flowers based on the physical effect derived from differential cell shape.

Figure 5.13 shows the average proportion for all bees (n=19) of tactile cues used to reject a punishment flower, every 10 choices, and a generalised linear regression model to fit the observations as the number of visits increases. A tendency towards decreasing the frequency of tactile cues as experience (number of visits) increases is observed. Wald statistics (χ^2) values exceed the critical values of the distribution. The null hypothesis of 0.5 probability ($H_o = \alpha_1 = 0$) of rejecting a punishment flower was rejected, indicating that the bumblebees can be trained to discriminate between conical and non-conical celled flowers using visual clues only in addition to tactile clues.

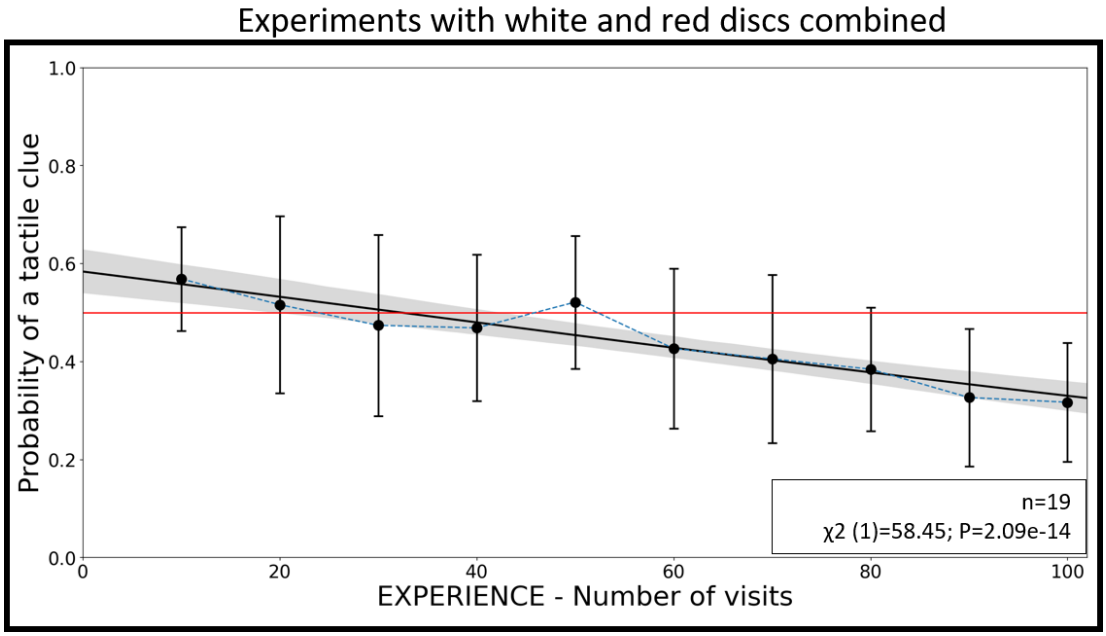

Figure 5.13. As experience increases, bumblebees reduce the use of tactile clues to discriminate between artificial flowers of contrasting textures.
Bumblebees trained by differential conditioning (using solutions of 30% sucrose as a "reward" versus 0.12% quinine as "punishment") to distinguish between artificial flowers (red or white) that only differ in the shape of the cells on the surface, initially use tactile clues to discriminate between different textures. As the experiment progresses, the use of tactile clues is reduced significatively. Datasets of all the experiments run with white (n=10) and red (n=9) flowers are pooled together. Tactile clues include all types of visits in which any part of the insect contacts the flower (drink, touch, hover, Table 5.1). Decreasing use of tactile clues is indicated by a negative slope curve. In the differential conditioning experiments, bees were choosing from six discs, three with conical-celled texture and three with non-conical celled texture. Black dots (joined by dashed blue line) are the mean of the proportion of tactile clue visits, every 10 choices, for all the bees for 100 consecutive choices. The black solid line is the fitted generalized binomial logistic model. The grey shading corresponds to 95% confidence intervals on the fitted response. The red line indicates the 0.5 probability value. The number of bees (n), calculated chi-square statistic (χ2; the number in brackets indicates degrees of freedom) and p-value (P) are reported at the bottom of the plot.

5.3.4 Foraging speed experiments

Average foraging speed time, calculated for all bees, was 2.91 s., from flower 1 to flower 2, 2.895 s., and from flower 2 to flower 3, 2.873 s (Figure 5.14). Average time of flight for bees performing the experiment on white discs was 3.24 s., for the rounds on conical discs 3.08 s. and for the rounds on non-conical discs 3.40 s. For the bees on red discs, average foraging speed was 2.59 s., for those on red conical, 2.51 s., and those on red non-conical 2.66 s. The average speed for all bees flying between conical discs (white or red) was 2.86 s., and between non-conical discs 2.90 s (Figure 5.15). Descriptive statistics for foraging speed experiments are listed in Appendix 11. Time values in the tables and used for statistic analyses are given in "units of time", where each unit of time corresponds to 1/60 seconds.

There were no significant differences between measurements of flight time from flower 1 to flower 2 compared to flight time from flower 2 to flower 3 (Figure 5.14A). Thus, the entire dataset was compiled for further analyses. An initial exploration bringing together sets of experiments run with conical surfaces of both colours compared to sets run with non-conical celled flowers, suggested that there were no significative differences between the two sets of measurements (Figure 5.14B). However, when analyzing each set of data independently, ANOVA identified significant differences between the means of different treatments (Appendix 11B, panel C). Tukey multiple comparison of means test (Appendix 11B, panel D) p adjusted values suggest that the significant differences detected in the ANOVA can be attributed specifically to the comparisons between the two sets with non-conical cells (WNC-RNC, Figure 5.15).

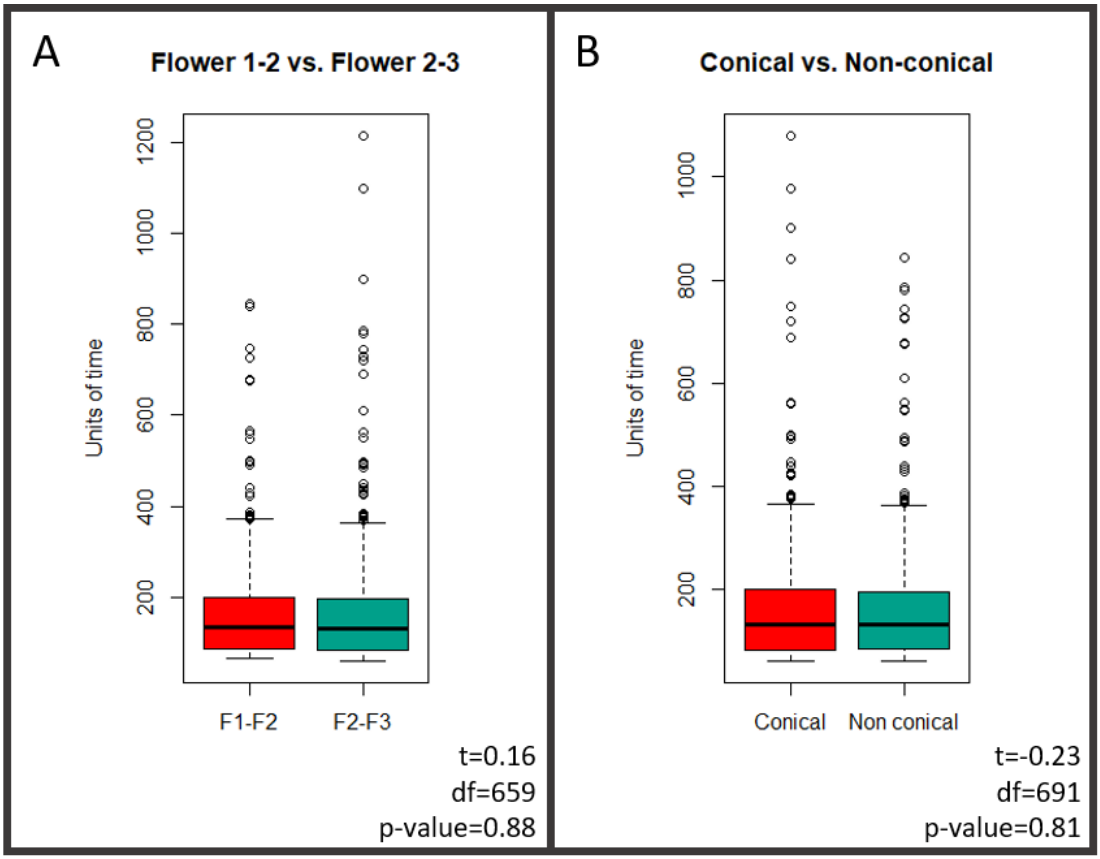

Figure 5.14. Bumblebee foraging speed between artificial flowers with the same texture is not affected by the texture of the flower.

As conical cells have optical properties that have been shown to enhance petal colouration and the detectability of flowers by pollinators (see sections 1.2.2.1 and 5.1.1), foraging time between flowers with conical cells was expected to be reduced compared to foraging time between non-conical celled flowers. Time of flight was measured between three identical artificial flowers on a horizontal position, 30 cm apart from each other loaded with 10 µL of 30% sucrose (Figure 5.4). **A.** Comparisons of the flight times between "Flower 1-2" (F1-F2) and "Flower 2-3" (F2-F3). There are no significative differences between the time of flight from the first to the second flower and the time of flight from the second to the third flower. **B.** Comparisons of the times of flight between "Conical" and the times of flight between "Non-conical" flowers. There are no significative differences between the time of flight measured in experimental bouts using conical celled flowers and those using non-conical celled ones. Both comparisons include all the observations from all the treatments combined. Median flight time (thick black line), quartile values (boxes) and total range of flight time are represented. Empty circles mean outliers foraging times of individuals. Welch two-sample t-test statistics reported at the bottom of each plot.

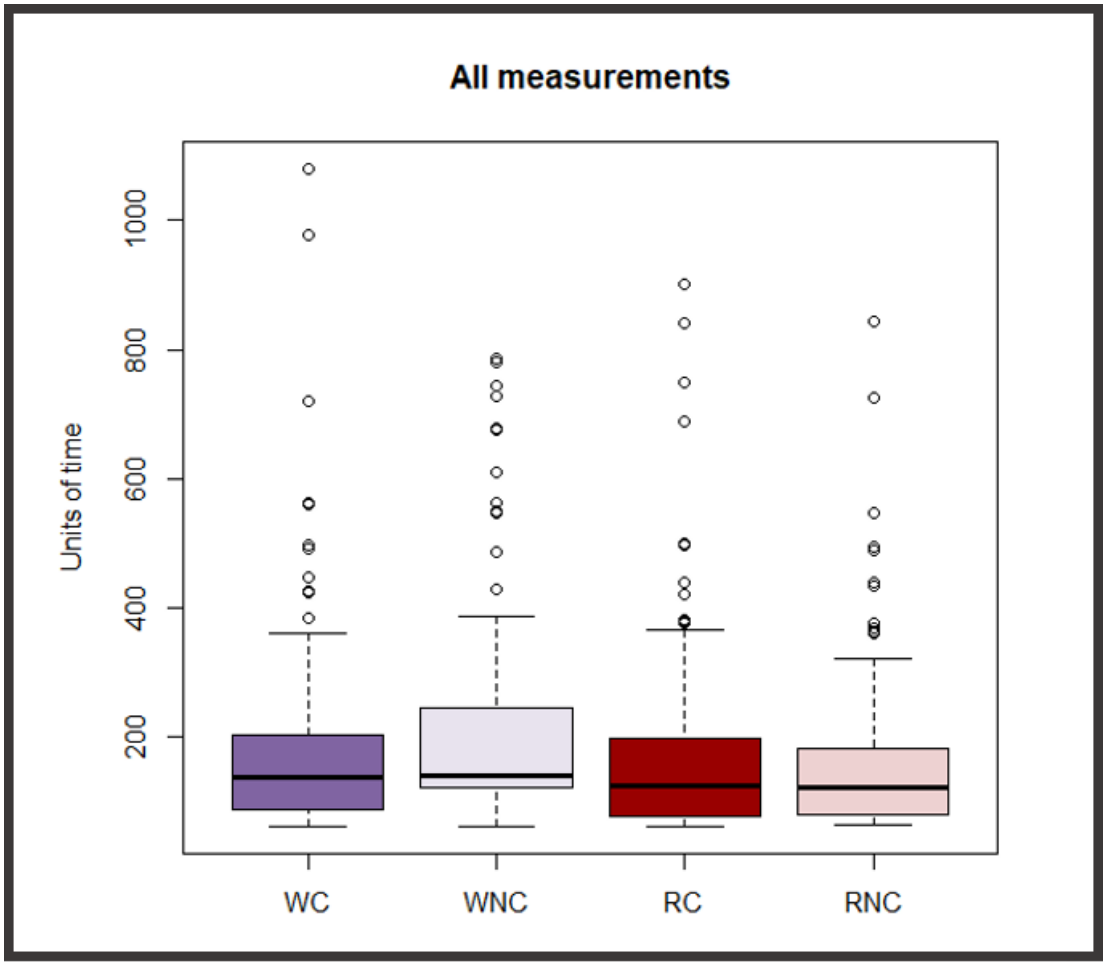

Figure 5.15. Bumblebee foraging speed between artificial flowers with the same texture is not affected by the combination of colour and texture of the flower.

As the optical properties of petals are derived from the interaction between pigment colouration and petal cell shape (see sections 1.2.2.1 and 5.1.1), combinations of conical and non-conical celled flowers on a white or on a red pigment background were used to test the idea that conical cells would increase the detectability of flowers by bumblebees. Time of flight was measured between three identical artificial flowers on a horizontal position, 30 cm apart from each other, loaded with 10 µL of 30% sucrose (Figure 5.4). Comparisons discriminate sets of data of four different treatments (combinations of colour and texture of the flower): White-conical (WC, dark purple), white-non-conical (WNC, light purple), red-conical (RC, dark red) and red-non-conical (RNC, light red). A one-way between subjects ANOVA was conducted to compare the effect of the treatments on foraging speed There are no significative differences between the time of flight of different treatments. There was not a significant effect of the treatments on foraging speed at the $p<0.05$ level for the three conditions [$F(3,689) = 5.43$, $p = 0.00108$]. Median flight time (thick black line), quartile values (boxes) and total range of flight time are represented. Empty circles mean outliers foraging times of individuals.

5.4 DISCUSSION

This chapter focused on assessing the effect of petal cell shape on the discrimination of flowers by *Bombus terrestris,* using artificial flowers which mimicked the attributes of sister species *N. forgetiana* and *N. bonariensis*.

5.4.1 Are the white flowers of *N. bonariensis* and the red flowers of *N. forgetiana* "invisible"to bees?

A thorough characterization of petal cell shape and colouration of both species was carried out as a first step in the design of the artificial flowers (section 5.3.1.). Colour reflectance measurements allowed for loci calculations for the bee colour hexagon. These loci confirm that *N. forgetiana* (red flowers) and *N. bonariensis* (white flowers) occupy different colour spaces as perceived by bees (Figure 5.4). Both colours, as perceived by humans, have been claimed to be "invisible" to bees (Section 5.1.3).

The white petals of *N. bonariensis* reflect wavelengths from 400 nm and occupy loci of excitation in the blue receptor of bees (Figure 5.7). These flowers do not have reflectance in the UV band, which has been associated with the sensory exclusion of bees by white UV-reflecting flowers (Lunau *et al.*, 2011; de Camargo *et al.*, 2018). 40 from 44 species with white flowers, known to be pollinated by bees, did not present reflectance in the UV band in a community level analysis by DeCamargo *et al.* (2018) in Southeastern Brazil.

The reflectance spectrum of the red flowers of *N. forgetiana* is mostly UV absorbing, presents a small peak of reflectance (up to 20%) in the violet-blue range of the spectrum, and displays main wavelengths reflected in the 600-700 nm (orange-red) interval. The bee colour loci for the petals sampled of this species appeared closer to the center of the hexagon. The measurements obtained here overlap with the reflectance spectrum of *N. forgetiana* reported in the Floral Reflectance Database (Armold *et al.*, 2010). These features coincide with characterizations for red flowers pollinated by hummingbirds, which are mostly UV-absorbing and probably achromatic for bees (Lunau *et al.*, 2011; de Camargo *et al.*, 2018).

From these results it could be deduced that the colour profile of the white flowers of *N. bonariensis* presents characteristics typical of bee-pollinated flowers. On the other hand, the

profile of the red flowers of *N. forgetiana* suggests that the colour of these flowers might be difficult to detect by the visual system of bees. However, the natural variation of colour in these species is not entirely represented in these measurements. For instance, a range of colouration "between cream, white-green, green, light pink, magenta or pink-purple" has been reported for *N. forgetiana* in its natural habitat (Vignoli-Silva & Auler Mentz, 2005). Moreover, petal cell shape might be playing a part in the perception of these petals by bees.

5.4.2 Can bumblebees discriminate between red flowers and white flowers with contrasting surface texture?

Differential conditioning experiments run with artificial red and white flowers were used to test the ability of bumblebees to distinguish between flowers that were identical except for type of cells on their surface (conical vs. non-conical). The results show that experienced foragers are more likely to choose rewarding flowers than are naïve foragers (Figure 5.10, Figure 5.10, Figure 5.12). They can discriminate between conical and non-conical celled flowers in both white and red pigment backgrounds. This confirms a pattern that has been previously demonstrated through experimentation with real and artificial flowers in other colours (Glover & Martin, 1998; Comba *et al.*, 2000; Dyer *et al.*, 2007; Whitney *et al.*, 2009a; Alcorn *et al.*, 2012; Alcorn, 2013) (sections 5.1 and 5.1.2).

Similarly to this work, Whitney *et al.* (2009a) tested whether bumblebees could recognise conical-celled from non-conical celled artificial flowers on a pigment background mimicking that of *Antirhinum majus*. Flowers that differed only in having conical or non-conical celled surfaces, were used in differential conditioning experiments. They found that bumblebees can identify and learn rewarding surfaces by touch alone (Whitney *et al.*, 2009a). They suggest that a difference in the shape of petal epidermal cells, distinguishable only by touch, is sufficient to provide a tactile cue to bees (Whitney *et al.*, 2009a).

The system used in this investigation to record the type of interaction of the bumblebee with the visited flower (section 5.2.4, Table 5.1) allowed us to further explore the nature of the cues involved in the discrimination of the two different types of flowers. The quantification of the use of tactile cues to identify non-rewarding flowers (Figure 5.13) suggests that trained bumblebees can discriminate flowers with conical cells from flowers with non-conical surfaces using visual cues alone as well as tactile cues alone.

5.4.3 Do conical cells facilitate the recognition of white and red flowers by bumblebees?

Because of their optical properties, conical cells might be expected to increase flower detectability. Using isogenic lines of *A. majus* (section 5.1.1) for bumblebee experiments under controlled laboratory conditions, Dyer *et al.* (2007) found that although bees could discriminate the flowers from different lines, inexperienced bees exhibited no preference for either type, and that the flowers did not differ in their detectability in a Y-maze (Dyer *et al.*, 2007).

The foraging speed experiments in this chapter do not show significant differences among the times of flight of bumblebee between artificial flowers with different texture (conical or non-conical) and identical pigment background (red or white) (Figure 5.14, Figure 5.15).

The visual effect of conical cells might depend on factors such as vertical position and motion of the flower (Chittka & Raine, 2006; Alcorn *et al.*, 2012). With the horizontal setup used for the foraging speed experiments those variables were reduced to a minimum, and the point of view of the bees was always from the top on to a still object. For instance, Alcorn *et al.*, (2012) showed that bees preferred to visit conical-celled *Petunia* flowers except when the conical-celled flowers were harder to detect visually. The bees then favoured flowers that were easier to detect. But when flowers were moving and more difficult to handle, bees always learned to favour conical-celled flowers, irrespective of visual difficulty (Alcorn *et al.*, 2012).

The alternative to quantify foraging time between discs in a vertical setup was explored. When visiting the conical flowers in a vertical position, it was evident that the effect of conical cells in improving grip on the respective surfaces was very significant. Visiting bees would easily hold on the conical surface disks and would drink the entire volume of reward, then flying to the next flower. In contrast, when facing the non-conical flowers in a vertical position, foragers would experience extreme difficulties to handle the discs and, on most occasions, would not finish the entire volume of reward from one flower before moving to the next one. In many cases, the bee would visit the three vertical non-conical flowers, drinking only small amounts of the reward from each flower, and coming back to the colony with a half empty stomach. This inconsistency in the pattern, derived from the difficulty of obtaining the reward from the non-conical celled flowers, made running this experiment unviable. The time of flight between non-conical celled flowers after partial feed would not be comparable to the time of flight between conical celled

ones after complete feed of the reward load, and would not be used to test the hypotheses that conical cells increase the detectability of flowers by the bumblebees.

5.4.4 The potential for pollination behaviour experiments with real flowers of sister species *N. bonariensis* and *N. forgetiana*

An ideal experiment to test the effect of petal cell shape in combination with petal colouration of *N. bonariensis* and/or *N. forgetiana* would be to undertake pairwise comparisons of real flowers that were identical in all respects except for the presence of conical cells.

Understanding the genetic mechanisms involved in the regulation of petal cell shape in these species (Chapter 3) is crucial in this regard. As discussed in section Chapter 4, *Agrobacterium tumefaciens* mediated transformation is a powerful tool to genetically manipulate plants to obtain genotypes of interest. Some progress has been made in understanding the role of candidate regulatory transcription factors, R2R3 Subgroup 9 MYBs, in *N. bonariensis* and *N. forgetiana*. Moreover, an *A. tumefaciens* transformation protocol is being established for *N. forgetiana.*

Further investigation in the field is necessary to fully understand pollination of these species. The natural variation of *N. forgetiana* and *N. bonariensis* also would offer opportunities to explore the role of petal cell shape in the interaction between plant and pollinator through pollinator behaviour experiments. As mentioned above, several variants of floral colour have been reported in the natural range of *N. forgetiana*. Assessing petal cell shape of these variants and having a better understanding of their pollination biology in the field, would open the possibilities to explore the role of petal cell shape in association with colour for this species.

Chapter 6

General Discussion

6 GENERAL DISCUSSION

The overall objective of this project was to further understand character evolution of petal cell shape in the genus *Nicotiana* (Solanaceae) and its implications for the interaction between flowers and their animal pollinators, using a combination of molecular, morphological and pollinator behavior methodologies.

6.1 Molecular mechanisms potentially involved in petal cell shape evolution in *Nicotiana* Sections *Alatae* and *Paniculatae*

First, in Chapters II and III, a candidate gene approach was used to explore the role of R2R3 Subgroup 9 transcription factors in determining petal cell shape identity in two distantly related pairs of sister species of *Nicotiana* with contrasting phenotypes of petal cell shape: *N. cordifolia* (non-conical) and *N. solanifolia* (conical, Section *Paniculatae*) and *N. bonariensis* (non-conical) and *N. forgetiana* (conical, Section *Alatae*).

6.1.1 Sequence differences in R2R3 Subgroup 9 MYBs are not solely responsible for petal cell shape

Obtaining the complete coding sequences of four candidate R2R3 MYB Subgroup 9 genes in each species allowed us to determine whether there were any differences between the gene orthologues in sister species. Any differences between sequences were first evaluated to assess whether they caused a substitution of amino acid, and if so, the potential effect of amino acid substitutions on the function of the encoded protein. Interestingly, in each section a different gene was found to be a good candidate to test the effect of sequence substitutions between orthologues in the protein function. *MIXTA-like* (R2R3 MYB Subgroup 9A) was found to have amino acid differences potentially altering the function of the coded protein for sister species in Section *Paniculatae*. On the other hand, *MYBI7-1* (R2R3 MYB Subgroup 9B) was the best candidate for this type of analyses in sister species from Section *Alatae*. Since all R2R3 MYB Subgroup 9 proteins have been shown to have the ability to induce conical cell outgrowth in some other species (*e.g. Antirrhinum majus,* Perez-Rodriguez *et al.*, 2005*, Vicia faba,* Bailes, 2016) it was considered possible that mutations to different members of the family might potentially result in morphologically convergent loss or change to conical cell form.

The two versions of each of these genes, one from the species with non-conical cells and one from the species with conical cells, were then ectopically expressed in model species *Nicotiana tabacum* via *Agrobacterium tumefaciens* stable transformation under control of a double CaMV 35S promoter, following a well-established protocol that has been used previously to analyse the function of Subgroup 9 R2R3 MYBs (sections 2.4.3, 3.4.3). Ectopic expression in *N. tabacum* allowed us to (1) test if the proteins of interest would promote the formation of epidermal outgrowths in the recipient plant, and (2) test if there were any differences in the phenotype of transgenic lines expressing alternative versions of the same gene. The results showed that all the genes ectopically expressed in *N. tabacum*, regardless of the phenotype of the species of origin (conical or non-conical petal cell shape), had the ability to promote epidermal outgrowths. The differences in the coding sequences detected between sister pairs of species were then not proved to be solely responsible for the presence or absence of conical petal epidermal cells.

Even though the two versions of the same gene coming from sister species induced similar phenotypes after ectopic expression in *N. tabacum,* when comparing the phenotypes resulting from the two different genes (*MIXTA-like* and *MYBI7-1*) major differences in the type, morphology and relative abundance of the ectopic epidermal outgrowths were detected. In general, alternative versions of *MYBI7-1* resulted in more extreme phenotypes consisting of multiple types of epidermal outgrowths on all organs analysed, usually relatively large and densely packed (Figures 3.16, 3.17, 3.18 and 3.19), whereas the ectopic expression of different versions of *MIXTA-like* resulted in more subtle phenotypes (Figure 2.16, Figure 2.17, Figure 2.19, Figure 2.20). This could be an effect of intrinsic differences in the effectiveness of individual experiments related to the health of the explant tissue to be transformed, the health of the *Agrobacterium* inoculation culture used for transformation, or variations in the growing conditions during the development of the transformation. However, variation in these factors was designed to be minimal, and the differences detected were consistent across multiple transgenic lines. These differences could therefore demonstrate how different proteins within the same small family may have different abilities to induce cell outgrowth, as has been demonstrated for R2R3 Subgroup 9 MYBs in *A. majus* (section 1.3.2).

Ectopic expression of *MIXTA* in *A. majus* (Martin *et al.*, 2002) results in the formation of two distinct cell types on leaves. *AmMYBML1* controls trichome formation in the corolla tube, conical epidermal and mesophyll cell morphogenesis in ventral petals, and hinge formation (Perez-Rodriguez *et al.*, 2005). *AmMYBML2* is responsible for cone elongation in conical cells (Baumann *et al.*, 2007) and *AmMYBML3* can induce conical cell outgrowth and is expressed in

trichomes (Jaffé *et al.*, 2007). All the genes studied in *A. majus* belong to the Subgroup 9A of R2R3 MYBs. However, the presence of genes from the Subgroup 9B cannot be ruled out in this species, and the complete genome assembly of *A. majus* cultivar JI7 that is currently available (Li *et al.*, 2019) might provide an opportunity to evaluate wether or not additional R2R3 Subgroup 9 MYBs are present in *Antirrhinum.* Other species in which the function of multiple R2R3 Subgroup 9 MYBs has been assessed include *Arabidopsis thaliana* (Baumann *et al.*, 2007; Gilding & Marks, 2010; Pastore *et al.*, 2011), *Vicia faba* (Bailes, 2016), *Gossypium hirsutum* (Machado et al., 2009; Walford et al., 2011) and *Solanum* spp. (Alcorn, 2013; Davis, 2019) (Appendix 1).

An interesting system to compare to *Nicotiana* is that of the closely related genus *Solanum,* for which petal cell shape has also been mapped to the phylogeny of the group and multiple independent losses of conical cells have been detected (Alcorn, 2013). Similarly to this work, closely related *Solanum* species with contrasting conical/non-conical petal epidermal morphologies were selected to test the protein function of the R2R3 MYB subgroup 9A genes from each species via *A. tumefaciens* mediated transformation of *N. tabacum* (Alcorn, 2013). Despite the changes observed between the protein sequences of R2R3 Subgroup 9A genes in *Solanum* species pairs, each gene identified was capable of directing conical cell fate following heterologous expression in tobacco (Alcorn, 2013). When comparing species with contrasting cell shape, it was not the change in R2R3 MYB Subgroup 9A protein itself that caused the change in petal cell morphology (Alcorn, 2013). In comparison with the *Solanum* work that compared selected R2R3 Subgroup 9A MYBs only, in species in the same part of the phylogeny but not sister species, the present investigation represents a tighter analysis of molecular evolution of petal cell shape. First, R2R3 MYB Subgroup 9 transcription factors were characterized for two pairs of sister species in *Nicotiana,* which allowed us to focus further on the molecular mechanisms underlying the divergence between the most closely related species. Second, members of all Subgroup 9 clades known to be present in *Nicotiana* (and in Solanales) were analysed in the current work.

6.1.2 Differential expression among R2R3 Subgroup 9 MYBs might be defining petal cell shape in *Nicotiana* spp.

To test the alternative idea that differential expression of candidate genes was then responsible for the contrasting phenotypes, gene expression was assessed via semiquantitative RT-PCR and qPCR for sister species *N. forgetiana* and *N. bonariensis* (Section *Alatae*). Unfortunately, no living flower material was available for the species in *Section Paniculatae*. In spite of being

conserved in terms of its sequence, both semiquantitative RT-PCR and qPCR analyses showed a clear pattern of differential expression in the gene *MIXTA-2* between sister species *N. forgetiana* and *N. bonariensis*. *MIXTA-2* presents higher levels of expression in petal tissue of *N. forgetiana* during early (1-2) and late (3-4) stages of flower development compared to petals of *N. bonariensis*. *MIXTA-2* is then a good candidate to explain the differences in morphology of petal epidermis between these two species. The ability of *MIXTA-2* to promote epidermal outgrowths is currently being tested by *A. tumefaciens* stable transformation of *N. tabacum* and *N. benthamiana*. Ectopic epidermal outgrowths are expected to be present in the transgenics expressing the conserved *MIXTA-2* sequence from sister species in Section *Alatae*. Genes in the *MIXTA* clade from several plant species have been demonstrated to be positive regulators of epidermal outgrowths via heterologous expression in *N. tabacum*. These include *AmMIXTA* from *A. majus* (Noda *et al.*, 1994), *VfMIXTA* from *Vicia faba* (Bailes, 2016), *ScMx* from *Solanum capsicoides* and *SsMx* from *S. sisymbrifolium* (Alcorn, 2013) (Table 2.7).

A similar pattern was again detected in *Solanum*. When comparing expression of the candidate gene *MIXTA-like* among *Solanum* species with conical and non-conical cells, Alcorn (2013) found that the conical celled species *S. laciniatum* showed the highest expression levels of the gene compared to non-conical celled species *S. capsicoides* and *S. aviculare*, suggesting that reduced expression of *MIXTA-like* in the two non-conical celled species might be responsible for the loss of conical cells on their petals.

In order to test whether the same gene expression patters are involved in regulating petal cell shape in sister species in Section *Paniculatae*, *N. cordifolia* and *N. solanifolia*, a reliable source of flower tissue material is needed. As shown in Chapter II flowering of these two species under cultivation is inconsistent. Alternatively, sampling of floral tissue, fixed for *a posteriori* extraction of RNA, could be attempted in the field (Yang *et al.*, 2017).

6.1.3 Regulatory changes rather than mutations in the coding sequence might be directing epidermal cell development in *Nicotiana* spp.

The results of this investigation on the molecular control of petal cell shape in sister pairs of species of *Nicotiana* fit one of the most important and widely accepted paradigms of evo-devo in evolutionary theory: the idea that alterations in gene regulation represent the most significant causal basis of phenotypic change and evolution (Carroll, 2000, 2008; Wray, 2007; Rodríguez-Mega *et al.*, 2015) (section 1.3). This paradigm suggests that coding sequence mutations are rarely the cause of morphological evolution. Instead, it is proposed that changes in gene

regulation, regulatory networks and regulatory sequences are the source of morphological variation and diversity (Carroll, 2008).

Comparative studies of gene expression in diverse animals and plants, across all taxonomic levels, have revealed a general association between the gain, loss, or modification of morphological traits and changes in gene regulation during development (Carroll, 2005). Changes in the expression of an individual gene may evolve through alterations in *cis*-regulatory sequences or in the deployment and activity of the transcription factors that control gene expression, or both (Carroll, 2005, 2008). Progress toward elucidating the mechanisms governing the evolution of specific traits and genes has required the study of models in which genetic and molecular methods enable the identification and dissection of functional differences among populations or species. Traits in plants for which such detailed analysis has been possible include flower coloration in *Ipomea* (Durbin *et al.*, 2003), plant architecture in *Arabidopsis* (Yoon & Baum, 2004), and branching patterns in *Zea mays* (Wang *et al.*, 1999).

While the coding sequences of structural and regulatory proteins are constrained by pleiotropy, modular *cis*-regulatory regions enable a great diversity of patterns to arise from alterations in regulatory circuits through the evolution of novel combinations of sites for regulatory proteins in *cis*-regulatory elements (Gompel *et al.*, 2005). The frequency of functional sequence changes in proteins that affect form is relatively low. Mutations in a coding region are usually poorly tolerated and eliminated by purifying selection (Stern, 2000). For example, a mutation in the coding region of a transcription factor that functions in multiple tissues may directly affect all of the genes which the protein regulates. In contrast, a mutation in a single *cis*-regulatory element will affect gene expression only in the domain governed by that element. On the contrary, even complete loss-of-function mutations in regulatory elements are possible because the compartmentation created by the modularity of *cis*-regulatory elements limits the effects of mutations to individual body parts (Carroll, 2005). If R2R3 Subgroup 9 MYB genes affect multiple downstream pathways involved with cuticle biosynthesis and trichome development (see section 6.1.4), changes in protein structure may be more likely to produce a detrimental effect on the plant than changes in regulation.

6.1.4 Potential involvement of R2R3 Subgroup 9 MYB transcription factors in regulatory networks controlling epidermal cell patterning

As has been demonstrated in this work and in multiple investigations, R2R3 Subgroup 9 MYBs are key regulators of epidermal cell differentiation across multiple plant species. However, how

these transcription factors are involved in regulatory networks controlling epidermal cell patterning, including conical cells, is not well understood.

Very little is known about the genes that are upstream of the subgroup 9 gene pathway. Based on the understanding of epidermal cell fate control in *A. majus,* Martin *et al.*, (2002) suggested that the floral homeotic B class MADs genes, *DEFICIENS* (*DEF*) and *GLOBOSA (GLO),* may be upstream of *AmMIXTA*, and may form complexes with intermediate MADs box proteins (such as *DEFH72*, *DEFH84* and *DEF200*) to activate its expression late in petal development. One observation that supports this hypothesis is that if *DEF* function is restored in *A. majus deficiens* mutants late in petal development, flat epidermal cells are transformed to conical cells (Coen & Carpenter, 1992), suggesting a close link between *DEF* expression and conical cell formation. Additionally, the *AmMIXTA* promoter region contains binding sites for MADs box proteins, and *DEF*, *DEFH72* and *DEFH200* genes are all expressed in overlapping regions with *AmMIXTA*, late in petal development (Davies *et al.*, 1996).

Additional information stems from research in the model plant *Arabidopsis thaliana.* Zhang *et al.*, (2009) suggested that the meristem identity regulator LEAFY (LFY) and the MADS domain protein AGL15 regulate the expression of the MYB subgroup 9 gene *AtMYB17*. The *AtMYB17* promoter contains several binding sites for both proteins, and promoter-GUS fusion experiments showed that the LFY protein may be able to fine-tune *AtMYB17* expression during flower development. Additionally, *AtMYB17* is up-regulated in plants that overexpress *AGL15*. Yeast-two-hybrid and bimolecular fluorescence complementation (BiFC) have suggested that LFY and AtMYB17 proteins interact directly *in vitro* and *in vivo* to form heterodimers (Pastore *et al.*, 2011).

Information about downstream targets for R2R3 Subgroup 9 MYB genes is also scarce. Transgenic and microarray experiments in *A. thaliana* have revealed that *AtMYB16* and *AtMYB106* form part of a regulatory cascade alongside the *WAX INDUCER 1/SHINE 1* gene to activate pathways involved with wax and cutin biosynthesis (Oshima *et al.*, 2013). Experiments with mutant plants have suggested that the other *Arabidopsis* subgroup 9 protein, AtMYB17, directly upregulates the *API* transcription factor, which in turn signals commitment to flower formation (Pastore *et al.*, 2011).

Further insights have bene provided by investigations in *Solanum lycopersicum.* The characterization of SlSHN3 activity in tomato suggested that this transcription factor may exert

its influence on epidermal cell patterning through HD-ZIP IV and/or MIXTA transcription factors (Shi *et al.*, 2013). Later findings showed that SlMIXTA-like not only promotes conical epidermal cell development in tomato fruit but is a major positive regulator of cuticular lipids, more specifically cutin monomer biosynthesis as well as cuticle assembly (Lashbrooke *et al.*, 2015). This is apparent from the wide range of down-regulated cutin biosynthetic genes in tomato lines silenced for *SlMIXTA-like* expression as well as the notable correlation between *SlMIXTA-like* expression and the deposition of cuticle on tomato fruits (Lashbrooke *et al.*, 2015). A link between cuticle synthesis and cell outgrowth pathways is not surprising, as wax and cutin composition, secretion and synthesis occur during cell expansion (Suh *et al.*, 2005).

Little is known about the downstream developmental pathway involved with cell fate and shape change. Up regulation of a Poplar subgroup 9 gene, *PtaMYB186,* correlates with increased transcript abundance of genes previously implicated in trichome development in *Arabidopsis* (including *KAKTUS* and *AtMYB4*) (Plett *et al.*, 2010). However, a suite of other genes are also down-regulated, including those implicated in circadian rhythm, cell wall biosynthesis, cell division, photosynthetic functions and hormone signalling. This suggests that subgroup 9 genes can act as activators and repressors in multiple downstream developmental pathways.

In recent years the development of a live-confocal imaging approach for the quantitative study of conical cell morphogenesis in *A. thaliana* has allowed further exploration of the molecular mechanisms involved (Ren *et al.*, 2017; Dang *et al.*, 2018). Ren et al. (2017) showed through genetic screens that *A. thaliana KTN1*, *ROP GTPases*, and *SPIKE1* are required for conical cell shaping. The loss of *KTN1* prevented random microtubule networks from shifting into well-ordered microtubule arrays at later developmental stages, which is correlated with the tip sharpening of conical cells (Ren *et al.*, 2017). In connected research, also through genetic screen of *A. thaliana,* Dang *et al.*, (2018) demonstrated that loss-of-function mutations in A*NGUSTIFOLIA* (*AN*), which encodes a homolog of mammalian *CtBP*/*BARs*, resulted in swollen conical cells, correlating with increased accumulation of reactive oxygen species (ROS). *CtBP*/*BARs* has been shown to function in microtubule organization, vesicle budding from the Golgi, leaf pavement cell morphogenesis, and trichome branching (Kim *et al.*, 2002). Furthermore, through enhancer screening, they demonstrated that mutations in *KTN1* enhanced conical cell phenotypes of the AN knockout (*an-t1*) mutants. Genetic analyses showed that *AN* acted in parallel with *KTN1* to control conical cell shaping. This showed that the AN-ROS pathway jointly functioned with KTN1 to modulate microtubule organization, correlating with

the tip sharpening of conical cells (Dang *et al.*, 2018). The precise molecular interactions that bring about cell shape change, including petal conical cells, are yet to be investigated.

6.2 Differential drivers of petal cell shape related to pollination in *Nicotiana* Sections *Alatae* and *Paniculatae*

Different evolutionary drivers might be directing the transition from conical to non-conical cells in *Nicotiana* Section *Paniculatae* when compared to *N.* Section *Alatae* as discussed in Chapters 2 and 3. In the case of *Paniculatae,* as discussed in section 2.5.4., the loss of the character in *N. cordifolia* might be associated with the radiation of the clade to an oceanic island. *N. solanifolia* and the other continental species, in spite of being interpreted as being more likely pollinated by birds, might conserve conical cells and have in fact mixed pollination systems, in which crawling insect pollinators might still benefit from the traction provided by the presence of conical cells. It has been hypothesized that there is a tendency to shift from insect (or mixed) pollination in continental species to bird pollination in islands and that this shift might be accompanied by a loss of conical cells on the petals of island-dwelling species (Ojeda et al. 2016). As birds do not have foot structures that interact with the surface of the petal, as small insects would do, the function of conical cells in enhancing grip could be lost (Ojeda et al., 2016).

In the case of the loss of conical cells in *N. bonariensis* compared to *N. forgetiana,* because of their morphological characteristics and colouration features, these two species can easily be typified as corresponding to traditional pollination syndromes. *N. forgetiana* with long tubular red flowers, would be a typical bird pollinated flower. On the other hand, *N. bonariensis,* with white asymmetric vespertine flowers, presents as a typical case of pollination by nocturnal moths. However, as shown in Chapter 5, flower colouration of these species when plotted on the bee colour hexagon might not necessarily be excluding bees from the potential range of visitors of these species, specially *N. bonariensis*. So, the loss of conical cells in this case may be in fact deterring "unwanted" visitors such as bees, that would be negatively affected by the absence of conical cells to grip on. This seems more plausible given that the flowers of *N. bonariensis* are generally pendant and therefore difficult for bees to grip (Alcorn, 2013). The presence of conical cells in *N. forgetiana* might also be a sign of mixed pollination by birds and insect in this species.

Alternatively, there may be no selection for or against petal cell shape at all, and it may simply be evolving under genetic drift. In order to test these and other ideas more field investigations and pollinator behaviour experiments are needed.

In both cases, information on pollination systems for these species is limited. So, the plausible evolutionary drivers of petal cell shape proposed are speculative. Our understanding of the relative importace of different factors involved in petal cell identity in *Nicotiana* would benefit from a reconstruction of evolutionary history of pollination shifts in the genus (Taylor, 2015). This would require comprehensive field studies of taxa where pollinator identity is unknown or ambiguous, as is the case for *N. cordifolia, N. solanifolia, N. bonariensis* and *N. forgetiana*. Although some progress has been made for *N. cordifolia* (Anderson *et al.*, 2001), *N. forgetiana* (Ippolito, 2000; Ippolito *et al.*, 2004; Raguso *et al.*, 2006) and *N. bonariensis* (Raguso *et al.*, 2006; Kaczorowski *et al.*, 2008), pollination ecology studies to identify which animal visits, feed from the flowers, and transfer pollen, and in which frequencies, is needed for these species.

6.3 Experimental potential of a stable transformation protocol for *N. forgetiana*

In Chapter 4, I demonstrated that non-model species *Nicotiana forgetiana* has the potential to be transformed using *Agrobacterium tumefaciens*. Callus formation and regeneration of plantlets was possible from leaves, but more efficient from hypocotyls. However, the plants regenerated were small and brittle and major complications in the process were faced for the establishment of plantlets in appropriate conditions to be moved to soil and grown into adult plants. The initial protocol for hypocotyl transformation established in Chapter 4 closely follows the protocol optimized for t *N. attenuata* (Krügel *et al.*, 2002), a diploid species of *Nicotiana* in Section *Petunioides* (sister section to *Alatae*). The media conditions used for the initial step of callus formation for *N. attenuata* successfully resulted in callus formation and even plant regeneration in *N. forgetiana*. However, for the following steps of plant establishment the conditions could not be transferred between the two species. In the case of the genus *Nicotiana* we have the case of the "easily" transformable polyploids *N. tabacum* and *N. benthamiana* (Clemente, 2006). However, the principle difficulty of the transformation and regeneration of *Nicotiana* species has been shown to be their taxonomically- determined proclivity to rapidly 'habituate' and grow vigorously for long periods of time without shoot or root differentiation after a short exposure to exogenous hormones (Bogani *et al.*, 1997). This exemplifies how different species, even those closely related, have different potentials of transformability.

Optimizing the experimental protocol for *A. tumefaciens* mediated transformation of *N. forgetiana* would open the possibilities to further explore the molecular mechanisms involved in epidermal cell differentiation in this species. Through the sequence comparisons and expression analyses in *N. bonariensis* and *N. forgetiana* (Chapter 3), the number of candidate genes that might be involved in the regulation of petal cell shape differentiation in these species has been narrowed down. It would be possible now, by using a transformation protocol, to manipulate individual genes in *N. forgetiana.* For instance, the expression of *MIXTA-2*, which has been demonstrated to be highly expressed in the petals of *N. forgetiana* compared to *N. bonariensis,* could be experimentally reduced in *N. forgetiana* by downregulating the gene using RNA interference (RNAi; Younis *et al.*, 2014)) or genome editing (CRISPR; Woo *et al.*, 2015) methods. This not only would allow us to assess the role of individual genes in petal cell shape differentiation, but also, the plant lines derived from such experiments, given that they would potentially present differences in petal cell shape phenotypes, could be used in pollinator behavior experiments like those shown in Chapter 5 with artificial flowers.

6.4 Future directions to explore the evolution of petal cell shape in *Nicotiana:* Allopolyploids

The species of *Nicotiana* in Australia all represent a derived, monophyletic (with the addition of *N. africana* from Namibia) allopolyploid lineage, the section Suaveolentes (Knapp *et al.*, 2004). Most of the species in this clade have white petals, are mostly nocturnally flowering and presumably moth-pollinated (Knapp, 2010; Marks *et al.*, 2011; Ladiges *et al.*, 2011). *Nicotiana africana* has yellowish green, tubular flowers, suggesting bird pollination, but no field observations have been made for this or other species (Knapp, 2010). The survey of the morphology of petal epidermal cells has shown that the character is homogeneous within the group with all species characterized to date having non-conical petal epidermal cells (Taylor, 2015; this work). This group presents an interesting system in which to understand how macro morphological variation directs pollination in the absence of variation in micromorphological features and colouration. Pollination by nocturnal moths has been deduced based on the white colouration and on the volatile profiles of some species (Raguso *et al.*, 2006). However, the wide variety of floral symmetries, corolla lobe morphologies, size, anther presentation and other morphological characters (Marks *et al.*, 2011), may suggest that there is further specialization for pollination among the species.

Besides a potential intricate evolutionary history of pollination in Section *Suaveolentes*, the molecular mechanisms involved in petal cell shape identity in this clade may also be interesting. The model species *N. benthamiana,* widely used in research in plant sciences, belongs to Section *Suaveolentes. N. benthamiana* has a well-established *Agrobacterium tumefaciens* stable transformation protocol. This species, as most others in Section *Suaveolentes,* has white petals and non-conical epidermal cells. During my investigations for this project, after confirming by heterologous expression in *N. tabacum* that several R2R3 Subgroup 9 candidate genes from *Nicotiana* species in Section *Paniculatae* and Section *Alatae* were able to produce ectopic epidermal outgrowths in floral organs including petals, I selected the gene for which ectopic expression produced the strongest phenotype in *N. tabacum* (*NbMYBI7-1*) to attempt stable transformation in *N. benthamiana.* The rationale behind this was that heterologous expression of *NbMYBI7-1* under a strong constitutive promoter *in N. benthamiana* might result in transgenic lines that would have conical cells on the petals instead of non-conical, but otherwise would be identical to the wild type. These plant lines with contrasting characteristics of petal cell shape would provide a potential tool to be used in pollinator behaviour experiments with bumblebees or other model pollinators (*e.g.* hawkmoths). However, ectopic expression of *NbMYBI7-1* in *N. benthamiana* did not result in the production of conical cells on the petal of this species, although the transgenic plants did present strong phenotypes for ectopic epidermal outgrowths on the ovary (Appendix 12). Molecular characterization has not been fully completed for this series of transgenics, and transgene expression in the petals has not been formally confirmed. However, given the constitutive nature of the promoter used it is highly likely that the transgene is petal-expressed. The differential morphological pattern in the phenotype of individual organs suggests that mechanisms other than the expression of the transcription factor are limiting the formation of conical cells on the petals of *N. benthamiana*. It could be the case that a partner gene or genes of the transcription factor are not expressed in the petal but are in the carpel, or that other mechanisms, such as gene silencing, would be restricting the action of the transcription factor in a tissue specific fashion. One of the progenitor lineages of Section *Suaveolentes* is thought to be a close relative to *N. sylvestris* but the other is uncertain (Clarkson *et al.*, 2010, 2017). Petal cell shape in *N. sylvestris* is conical and the basal most species of section *Suaveolentes*, *N. africana* has non-conical cells as the rest of the species. This suggests that conical cells were lost early in the evolution of the *Suaveolentes* Section. The genetic mechanisms involved in petal cell morphology are probably deeply established in the evolution of this clade of Australian *Nicotianas*. Having *N. benthamiana* as a powerful genetic tool within this group opens the possibilities to explore further these mechanisms.

Another allopolyploid lineage with potential to explore the role of petal cell shape in the evolution of differential pollination systems and the molecular mechanisms involved, is the American Section *Repandae*. Close relatives of the parental lineages of *Repandae* are thought to be in Section *Sylvestres* (*N. sylvestris*) and Section *Trigonophylla* (*N. obtusifolia, N. palmeri*). *N. sylvestris*, as mentioned before, has typical conical petal epidermal cell shape, whereas *N. obtusifolia* and *N. palmeri* have non-conical cells. Interestingly, three of the four species in Section *Repandae*, *N. repanda*, *N. nesophila* and *N. stocktonii*, have non-conical cells, like species in *Trigonoplylla,* and their pollination has been described as adapted for nocturnal hawkmoths. On the contrary, *N. nudicaulis* has conical cells like *N. sylvestris,* and is reported as adapted for bee pollination during the day (Chase *et al.*, 2010). This pattern of distribution of the character makes Section *Repandae* a good candidate group in which to explore the evolution of petal epidermal morphology following allopolyploidy events in *Nicotiana*.

6.5 FINAL REMARKS

This project used a combination of tools of molecular biology, morphology and pollinator behaviour experiments to further understand character evolution of petal cell shape in the genus *Nicotiana.* I explored in parallel the molecular mechanisms involved in petal cell shape in two distantly related clades of *Nicotiana*.: sister species *N. cordifolia* and *N. solanifolia* (Section *Paniculatae*, Chapter 2) and *N. bonariensis* and *N. forgetiana* (Section Alatae, Chapter 3), which have contrasting petal cell shape (conical vs. non-conical). This system provided an exceptional opportunity to explore independent evolutionary pathways leading to the same phenotype.

This is the most complete characterization of R2R3 Subgroup 9 MYB of transcription factors, thought to be involved in the identity of petal cell shape, in sister species with contrasting morphologies. The establishement of an *Agrobacterium tumefaciens* plant transformation protocol for non-model species *Nicotiana forgetiana* provides a novel tool to explore the molecular control of petal cell shape in *Nicotiana* and opens the possibilities to experimentally obtain plant lines to be used in pollinator behaviour experiments. Behaviour experiments with model pollinator *Bombus terrestris* and carefully designed artificial flowers mimicking the features of sister species *N. bonariensis* and *N. forgetiana* provided new insight on the functional aspects of petal cell shape in the context of the interaction between flower and pollinator. The progress made with this work in understanding the mechanisms behind the variation of a single floral trait in a specific group of plants, the genus *Nicotiana,* opens new possibilities for further

research with this model system and contributes to the overarching question of the mechanisms of diversification and radiation of flowering plants.

References

REFERENCES

Abdelaziz M, Bakkali M, Gómez JM, Olivieri E, Perfectti F. **2019**. Anther rubbing, a new mechanism that actively promotes selfing in plants. *The American Naturalist* **193**: 140–147.

Alcorn K. **2013**. Pollinator behaviour and the evolutionary genetics of petal surface texture in the Solanaceae. *PhD Thesis, University of Cambridge*.

Alcorn K, Whitney HM, Glover BJ. **2012**. Flower movement increases pollinator preference for flowers with better grip. *Functional Ecology* **26**: 941–947.

Anderson GJ, Bernardello G, Stuessy TF, Crawford DJ. **2001**. Breeding System and pollination of selected plants endemic to Juan Fernandez Islands. *American Journal of Botany* **88**: 220–233.

Antoniou Kourounioti RL, Band LR, Fozard JA, Hampstead A, Lovrics A, Moyroud E, Vignolini S, King JR, Jensen OE, Glover BJ. **2013**. Buckling as an origin of ordered cuticular patterns in flower petals. *Journal of the Royal Society, Interface* **10**: 20120847.

Aoki S, Ito M. **2000**. Molecular phylogeny of *Nicotiana* (Solanaceae) based on the nucleotide sequence of the matK gene. *Plant Biology* **2**: 316–324.

APG. **2009**. An update of the Angiosperm Phylogeny Group classification for the orders and families of flowering plants: APG III. *Botanical Journal of the Linnean Society* **161**: 105–121.

APG. **2016**. An update of the Angiosperm Phylogeny Group classification for the orders and families of flowering plants: APG IV. *Botanical Journal of the Linnean Society* **161**: 105–121.

Armbruster WS. **2014**. Floral specialization and angiosperm diversity: Phenotypic divergence, fitness trade-offs and realized pollination accuracy. *AoB PLANTS* **6**: 1–24.

Armold SEJ, Faruq S, Savolainen V, McOwan PW, Chittka L. **2010**. FReD: The floral reflectance database - a web portal for analyses of flower colour (M Giurfa, Ed.). *PLoS ONE* **5**: 1–9.

Bailes EJ. **2016**. Improving the pollination of the field bean *Vicia faba* L. *PhD Thesis, University of Cambridge*.

Baldwin IT. **1998**. Jasmonate-induced responses are costly but benefit plants under attack in native populations. *Proceedings of the National Academy of Sciences* **95**: 8113–8118.

Baldwin IT, Karb MJ. **1995**. Plasticity in allocation of nicotine to reproductive parts in *Nicotiana attenuata*. *Journal of Chemical Ecology* **21**: 897–909.

Ballester B, Carrasco C, Desierto AC del. **2016**. Nicotianas litorales del desierto de Atacama: Historia de registro y consumo de tabaco cimarrón (*Nicotiana solanifolia* Warp.). *Revista Taltalia*: 69–87.

Barrett SCH. **1996**. The reproductive biology and genetics of island plants. *Philosophical Transactions of the Royal Society of London. Series B: Biological Sciences* **351**: 725–733.

Barthlott W, Ehler N. **1977**. Raster-Elektronemmikroskopie der Epidermis-Oberflächen von Spermatophyten. *Tropische und subtropische Planzenwelt* **19**: 367–467.**Baumann K, Perez-Rodriguez M, Bradley D, Venail J, Bailey P, Jin H, Koes R, Roberts K, Martin C**. **2007**. Control of cell and petal morphogenesis by R2R3 MYB transcription factors. *Development* **134**: 1691–1701.

Bawa KS. **1990**. Plant-pollinator interactions in tropical rain Forests. *Annual Review of Ecology and*

Systematics **21**: 399–422.

Bäzinger H, Sun H, Luo Y-B. **2005**. Pollination of a slippery lady slipper orchid in south-west China: *Cypripedium guttatum* (Orchidaceae). *Botanical Journal of the Linnean Society* **148**: 251–264.

Bedon F, Ziolkowski L, Walford SA, Dennis ES, Llewellyn DJ. **2014**. Members of the MYB MIXTA-like transcription factors may orchestrate the initiation of fiber development in cotton seeds. *Frontiers in Plant Science* **5**: 179.

Bell CD, Soltis DE, Soltis PS. **2010**. The age and diversification of the angiosperms re-revisited. *American Journal of Botany* **97**: 1296–1303.

Betts MJ, Russell RB. **2007**. Amino-Acid properties and consequences of substitutions. In: Bioinformatics for Geneticists: A Bioinformatics Primer for the Analysis of Genetic Data: Second Edition. 311–342.

Bogani P, Liò P, Intrieri MC, Buiatti M. **1997**. A physiological and molecular analysis of the genus *Nicotiana*. *Molecular phylogenetics and evolution* **7**: 62–70.

Bolinder K, Norbäck Ivarsson L, Humphreys AM, Ickert-Bond SM, Han F, Hoorn C, Rydin C. **2015**. Pollen morphology of *Ephedra* (Gnetales) and its evolutionary implications. *Grana* **55**: 24–51.

Bordo D, Argos P. **1991**. Suggestions for 'safe' residue substitutions in site-directed mutagenesis. *Journal of molecular biology* **217**: 721–9.

Brockington SF, Alvarez-Fernandez R, Landis JB, Alcorn K, Walker RH, Thomas MM, Hileman LC, Glover BJ. **2013**. Evolutionary analysis of the *MIXTA* gene family highlights potential targets for the study of cellular differentiation. *Molecular Biology and Evolution* **30**: 526–540.

Bruce TJA. **2015**. Interplay between insects and plants: dynamic and complex interactions that have coevolved over millions of years but act in milliseconds. *Journal of Experimental Botany* **66**: 455–465.

Buggs RA. **2017**. The Deepening of Darwin's Abominable Mistery. *Nature Ecology & Evolution* **1**: 0169.

de Camargo MGG, Lunau K, Batalha MA, Brings S, DeBrito VLG, Morellato LPC. **2018**. How flower colour signals allure bees and hummingbirds: a community-level test of the bee avoidance hypothesis. *New Phytologist* **222**: 1112–1122.

Carrasco C, Echeverría J, Ballester B, Niemeyer HM. **2015**. De pipas y sustancias: Costumbres fumatorias durante el Periodo Formativo en el Litoral del Desierto de Atacama (Norte de Chile). *Latin American Antiquity* **26**: 143–161.

Carroll SB. **2000**. Endless forms: The evolution of gene regulation and morphological diversity. *Cell* **101**: 577–580.

Carroll SB. **2005**. Evolution at two levels: on genes and form. *PLoS Biology* **3**: 1159–1179.

Carroll SB. **2008**. Evo-devo and an expanding evolutionary synthesis: A genetic theory of morphological evolution. *Cell* **134**: 25–36.

Chamorro S, Heleno R, Olesen JM, McMullen CK, Traveset A. **2012**. Pollination patterns and plant breeding systems in the Galapagos: A review. *Annals of Botany* **110**: 1489–501.

Chanderbali AS, Berger BA, Howarth DG, Soltis PS, Soltis DE. **2016**. Evolving ideas on the origin and evolution of flowers: New perspectives in the genomic era. *Genetics* **202**: 1255–1265.

Chang SS, Park SK, Kim BC, Kang BJ, Kim DU, Nam HG. **1994**. Stable genetic transformation of

Arabidopsis thaliana by *Agrobacterium* inoculation in planta. *The Plant Journal* **5**: 551–558.

Chase MW, Knapp S, Cox A V, Clarkson JJ, Butsko Y, Joseph J, Savolainen V, Parokonny AS. **2003**. Molecular systematics, GISH and the origin of hybrid taxa in *Nicotiana* (Solanaceae). *Annals of Botany* **92**: 107–27.

Chase MW, Paun O, Fay MF. **2010**. Hybridization and speciation in angiosperms: A role for pollinator shifts? *BMC biology* **8**: 45.

Chen K, Rajewsky N. **2007**. The evolution of gene regulation by transcription factors and microRNAs. *Nature Reviews Genetics* **8**: 93–103.

Chittka L. **1992**. The colour hexagon: A chromaticity diagram based on photoreceptor excitations as a generalized representation of colour opponency. *Journal of Comparative Physiology A* **170**: 533–543.

Chittka L, Raine NE. **2006**. Recognition of flowers by pollinators. *Current Opinion in Plant Biology* **9**: 428–435.

Chittka L, Thomson JD. **2002**. *Cognitive ecology of pollination. Animal behavior and floral evolution*. Cambridge, UK: Cambridge University Press.

Chittka L, Thomson JD, Waser NM. **1999**. *Flower constancy, insect psychology, and plant evolution*. Springer-Verlag.

Chittka L, Waser NM. **1997**. Why red flowers are not invisible to bees. *Israel Journal of Plant Sciences* **45**: 169–183.

Choi Y, Sims GE, Murphy S, Miller JR, Chan AP. **2012**. Predicting the functional effect of amino acid substitutions and indels. *PloS one* **7**: e46688.

Chomczynski P, Sacchi N. **1987**. Single-step method of RNA isolation by acid guanidinium thiocyanate-phenol-chloroform extraction. *Analytical Biochemistry* **162**: 156–9.

Chomczynski P, Sacchi N. **2006**. The single-step method of RNA isolation by acid guanidinium thiocyanate-phenol-chloroform extraction: Twenty-something years on. *Nature Protocols* **1**: 581–585.

Clarkson JJ, Dodsworth S, Chase MW. **2017**. Time-calibrated phylogenetic trees establish a lag between polyploidisation and diversification in *Nicotiana* (Solanaceae). *Plant Systematics and Evolution* **303**: 1001–1012.

Clarkson JJ, Kelly LJ, Leitch AR, Knapp S, Chase MW. **2010**. Nuclear glutamine synthetase evolution in *Nicotiana*: Phylogenetics and the origins of allotetraploid and homoploid (diploid) hybrids. *Molecular Phylogenetics and Evolution* **55**: 99–112.

Clarkson JJ, Knapp S, Garcia VF, Olmstead RG, Leitch AR, Chase MW. **2004**. Phylogenetic relationships in *Nicotiana* (Solanaceae) inferred from multiple plastid DNA regions. *Molecular phylogenetics and evolution* **33**: 75–90.

Clemente T. **2006**. Nicotiana (Nicotiana tabaccum, Nicotiana benthamiana). In: *Agrobacterium* Protocols. 143–154.

Cocucci AA. **1988**. Polinización en Solanáceas Neotropicales. *PhD Thesis, Universidad Nacional de Córdoba*: 1–233.

Coen E, Carpenter R. **1992**. The power behind the flower. *New Scientist* **134**: 24–27.

Coen ES, Meyerowitz EM. **1991**. The war of the whorls: genetic interactions controlling flower

development. *Nature* **353**: 31–37.

Comba L, Corbet SA, Hunt H, Outram S, Parker JS, Glover BJ. **2000**. The role of genes influencing the corolla in pollination of *Antirrhinum majus*. *Plant, Cell and Environment* **23**: 639–647.

Crepet WL. **1984**. Advanced (constant) insect pollination mechanisms: Pattern of evolution and implications vis-a-vis angiosperm diversity. *Annals of the Missouri Botanical Garden* **71**: 607.

Crepet WL, Niklas KJ. **2009**. Darwin's second "abominable mystery": Why are there so many angiosperm species? *American Journal of Botany* **96**: 366–381.

Crepet WL, Nixon KC, Gandolfo MA. **2004**. Fossil evidence and phylogeny: The age of major angiosperm clades based on mesofossil and macrofossil evidence from cretaceous deposits. *American Journal of Botany* **91**: 1666–1682.

Culley TM, Weller SG, Sakai AK. **2002**. The evolution of wind pollination in angiosperms. *Trends in Ecology & Evolution* **17**: 361–369.

D'Arcy WG. **1976**. New names and taxa in the Solanaceae. *Annals of the Missouri Botanical Garden* **63**: 363.

Dafni A, Lehrer M, Kevan PG. **1997**. Spatial flower parameters and insect spatial vision. *Biological Reviews of the Cambridge Philosophical Society* **72**: 239–282.

Damerval C, Nadot S. **2007**. Evolution of perianth and stamen characteristics with respect to floral symmetry in Ranunculales. *Annals of Botany* **100**: 631–640.

Dang X, Yu P, Li Y, Yang Y, Zhang Y, Ren H, Chen B, Lin D. **2018**. Reactive oxygen species mediate conical cell shaping in *Arabidopsis thaliana* petals (GP Copenhaver, Ed.). *PLoS Genetics* **14**: e1007705.

Danton P. **2006**. Contribution à la flore de l'archipel Juan Fernández (Chili). Description de deux taxons nouveaux: *Nicotiana cordifolia* subsp. *sanetaclarae subsp. nov.* (Solanaceae), *Robinsonia saxatilis sp. nov.* (Asteraceae). *Acta Botanica Gallica* **153**: 249–255.

Daumer K. **1956**. Reizmetrische Untersuchung des Farbensehens der Bienen. *Zeitschrift für vergleichende Physiologie* **38**: 413–478.

Davies B, Egea-Cortines M, de Andrade Silva E, Saedler H, Sommer H. **1996**. Multiple interactions amongst floral homeotic MADS box proteins. *EMBO journal* **15**: 4330–43.

Davis G V. 2019. Male form and function in *Solanum*. *PhD Thesis, University of Cambridge*.

Dellinger AS, Chartier M, Fernández-Fernández D, Penneys DS, Alvear M, Almeda F, Michelangeli FA, Staedler Y, Armbruster WS, Schönenberger J. **2019**. Beyond buzz-pollination – departures from an adaptive plateau lead to new pollination syndromes. *New Phytologist* **221**: 1136–1149.

Dillon MO. **2005**. The Solanaceae of the Lomas Formations of coastal Peru and Chile. *Monographs in Systematic Botany* **104**: 131–156.

Doebley J. **1993**. Genetics, development and plant evolution. *Current Opinion in Genetics and Development* **3**: 865–872.

Doebley J, Lukens L. **1998**. Transcriptional regulators and the evolution of plant form. *Plant Cell* **10**: 1075–1082.

Doyle JA. **2012**. Molecular and fossil evidence on the origin of angiosperms. *Annual Review of Earth and Planetary Sciences* **40**: 301–326.

Doyle JA, Endress PK. **2002**. Morphological phylogenetic analysis of basal angiosperms: comparison and combination with molecular data. *International Journal of Plant Sciences* **161**: S121–S153.

Du H, Feng B-R, Yang S-S, Huang Y-B, Tang Y-X. **2012**. The R2R3-MYB transcription factor gene family in maize. *PLoS ONE* **7**: e37463.

Duan W, Wang LS, Song GQ. **2016**. Agrobacterium tumefaciens-mediated transformation of wild tobacco species *Nicotiana debneyi*, *Nicotiana clevelandii*, and *Nicotiana glutinosa*. *American Journal of Plant Sciences* **7**: 1–7.

Dubos C, Stracke R, Grotewold E, Weisshaar B, Martin C, Lepiniec L. **2010**. MYB transcription factors in *Arabidopsis*. *Trends in Plant Science* **15**: 573–581.

Durbin ML, Lundy KE, Morrell PL, Torres-Martinez CL, Clegg MT. **2003**. Genes that determine flower color: the role of regulatory changes in the evolution of phenotypic adaptations. *Molecular Phylogenetics and Evolution* **29**: 507–518.

Dyer AG, Garcia JE, Shrestha M, Lunau K. **2015**. Seeing in colour: a hundred years of studies on bee vision since the work of the Nobel laureate Karl von Frisch. *Proceedings of the Royal Society of Victoria* **127**: 66.

Dyer AG, Whitney HM, Arnold SEJ, Glover BJ, Chittka L. **2007**. Mutations perturbing petal cell shape and anthocyanin synthesis influence bumblebee perception of *Antirrhinum majus* flower colour. *Arthropod-Plant Interactions* **1**: 45–55.

Elliott AR, Campbell JA, Dugdale B, Brettell RIS, Grof CPL. **1999**. Green-fluorescent protein facilitates rapid in vivo detection of genetically transformed plant cells. *Plant Cell Reports* **18**: 707–714.

Endress PK. **2010**. The evolution of floral biology in basal angiosperms. *Philosophical transactions of the Royal Society of London. Series B, Biological sciences* **365**: 411–21.

Endress PK, Steiner-Gafner B. **1996**. *Diversity and Evolutionary Biology of Tropical Flowers*. Cambridge University Press.

Erber J, Kierzek S, Sander E, Grandy K. **1998**. Tactile learning in the honeybee. *Journal of Comparative Physiology A: Sensory, Neural, and Behavioral Physiology* **183**: 737–744.

Erber J, Pribbenow B, Grandy K, Kierzek S. **1997**. Tactile motor learning in the antennal system of the honeybee (*Apis mellifera* L.). *Journal of Comparative Physiology - A Sensory, Neural, and Behavioral Physiology* **181**: 355–365.

Faegri K, Van Der Pijl L. **1979**. *The principles of pollination ecology*. Oxford: Pergamon Press.

FAO. **2017**. *FAOSTATS- Food and Agriculture Organization of the United Nations*.

Fenster CB, Armbruster WS, Wilson P, Dudash MR, Thomson JD. **2004**. Pollination syndromes and floral specialization. *Annual Review of Ecology, Evolution, and Systematics* **35**: 375–403.

Fernandez-Pozo N, Menda N, Edwards J, Saha S, Tecle I, Strickler S, Bombarely A, Fisher-York T, Pujar A, Foerster H, *et al.* 2015. The Sol Genomics Network (SGN) from genotype to phenotype to breeding. *Nucleic Acids Research* **43**.

Folkers U, Berger J, Hülskamp M. **1997**. Developmental and hormonal regulation of the *Arabidopsis* <i>cer2<i> gene that codes for a nuclear-localized protein required for the normal accumulation of cuticular waxes. *Development* **124**: 3779–86.

Friedman WE. **2009**. The meaning of Darwin's "abominable mystery". *American Journal of Botany* **96**: 5–21.

Friedman J, Barrett SCH. **2009**. Wind of change: New insights on the ecology and evolution of pollination and mating in wind-pollinated plants. *Annals of Botany* **103**: 1515–1527.

Friis EM, Crane PR, Pedersen KR. **2011**. *Early flowers and angiosperm evolution*. Cambridge: Cambridge University Press.

Friis EM, Crane PR, Pedersen KR, Bengtson S, Donoghue PCJ, Grimm GW, Stampanoni M. **2007**. Phase-contrast X-ray microtomography links Cretaceous seeds with Gnetales and Bennettitales. *Nature* **450**: 549–552.

Friis EM, Pedersen KR, Crane PR. **2006**. Cretaceous angiosperm flowers: Innovation and evolution in plant reproduction. *Palaeogeography, Palaeoclimatology, Palaeoecology* **232**: 251–293.

Friis EM, Pedersen KR, Crane PR. **2009**. Early Cretaceous mesofossils from Portugal and eastern North America related to the Bennettitales-Erdtmanithecales-Gnetales group. *American Journal of Botany* **96**: 252–283.

Gambino G, Perrone I, Gribaudo I. **2008**. A rapid and effective method for RNA extraction from different tissues of grapevine and other woody plants. *Phytochemical Analysis* **19**: 520–525.

Garcia VF, Olmstead RG. **2003**. Phylogenetics of Tribe Anthocercideae (Solanaceae) Based on ndhF and trnL/F Sequence Data. *BioOne* **28**: 609–615.

Geethalakshmi S, Hemalatha B, Saranya N. **2016**. Optimization of media formulations for callus induction, shoot regeneration and root induction in Nicotiana benthamiana. *Journal of Plant Science and Research* **3**: 1–4.

Gegear RJ, Laverty TM. **2005**. Flower constancy in bumblebees: A test of the trait variability hypothesis. *Animal Behaviour* **69**: 939–949.

Gelvin SB. **2003**. *Agrobacterium*-mediated plant transformation: the biology behind the 'gene-jockeying' tool. *Microbiology and Molecular Biology Reviews : MMBR* **67**: 16–37, table of contents.

Gilding EK, Marks MD. **2010**. Analysis of purified *glabra3-shapeshifter* trichomes reveals a role for *NOECK* in regulating early trichome morphogenic events. *Plant Journal* **64**: 304–317.

Giurfa M, Lehrer M. **2009**. Honeybee vision and floral displays: From detection to close-up recognition. In: Chittka L, Thomson JD, eds. Cognitive Ecology of Pollination. 61–82.

Giurfa M, Vorobyev M, Kevan P, Menzel R. **1996**. Detection of coloured stimuli by honeybees: Minimum visual angles and receptor specific contrasts. *Journal of Comparative Physiology A: Sensory, Neural, and Behavioral Physiology* **178**: 699–709.

Givnish TJ. **2010**. Ecology of plant speciation. *TAXON* **59**: 1326–1366.

Glover BJ, Airoldi CA, Brockington SF, Fernández-Mazuecos M, Martínez-Pérez C, Mellers G, Moyroud E, Taylor L. **2015**. How have advances in comparative floral development influenced our understanding of floral evolution? *International Journal of Plant Sciences* **176**: 307–323.

Glover BJ, Martin C. **1998**. The role of petal cell shape and pigmentation in pollination success in *Antirrhinum majus*. *Heredity* **80**: 778–784.

Glover BJ, Perez-Rodriguez M, Martin C. **1998**. Development of several epidermal cell types can be

specified by the same MYB-related plant transcription factor. *Development* **125**: 3497–3508.

Glover BJ, Whitney HM. **2010**. Structural colour and iridescence in plants: The poorly studied relations of pigment colour. *Annals of Botany* **105**: 505–511.

Gomez B, Daviero-Gomez V, Coiffard C, Martín-Closas C, Dilcher DL. **2015**. *Montsechia*, an ancient aquatic angiosperm. *Proceedings of the National Academy of Sciences of the United States of America* **112**: 10985–8.

Gompel N, Prud'Homme B, Wittkopp PJ, Kassner VA, Carroll SB. **2005**. Chance caught on the wing: cis-regulatory evolution and the origin of pigment patterns in *Drosophila*. *Nature* **433**: 481–487.

Goodspeed TH. **1947**. On the evolution of genus *Nicotiana*. *Proceedings of the National Academy of Sciences* **33**: 158–171.

Goodspeed TH. **1954**. *The genus* Nicotiana. Waltham, MA: Cronica Botanica Co.

Gorton HL, Vogelmann TC. **1996**. Effects of epidermal cell shape and pigmentation on optical properties of *Antirrhinum* petals at visible and ultraviolet wavelengths. *Plant physiology* **112**: 879–888.

Grant V. **1994**. Modes and origins of mechanical and ethological isolation in angiosperms. *Proceedings of the National Academy of Sciences of the United States of America* **91**: 3–10.

Groen SC, Jiang S, Murphy AM, Cunniffe NJ, Westwood JH, Davey MP, Bruce TJA, Caulfield JC, Furzer OJ, Reed A, *et al.* 2016. Virus infection of plants alters pollinator preference: A payback for susceptible hosts? (A Whitfield, Ed.). *PLoS Pathogens* **12**: e1005790.

Groten K, Nawaz A, Nguyen NHT, Santhanam R, Baldwin IT. **2015**. Silencing a key gene of the common symbiosis pathway in *Nicotiana attenuata* specifically impairs arbuscular mycorrhizal infection without influencing the root-associated microbiome or plant growth. *Plant Cell and Environment* **38**: 2398–2416.

Grotewold E. **2006**. The genetics and biochemistry of floral pigments. *Annual review of plant biology* **57**: 761–780.

Haag ES, True JR. **2001**. Perspective: From mutants to mechanisms? Assessing the candidate gene paradigm in evolutionary biology. *Evolution; international journal of organic evolution* **55**: 1077–84.

Haseloff J, Siemering KR, Prasher DC, Hodge S. **1997**. Removal of a cryptic intron and subcellular localization of green fluorescent protein are required to mark transgenic *Arabidopsis* plants brightly. *Proceedings of the National Academy of Sciences of the United States of America* **94**: 2122–7.

Haverkamp A, Li X, Hansson BS, Baldwin IT, Knaden M, Yon F. **2019**. Flower movement balances pollinator needs and pollen protection. *Ecology* **100**: e02553.

Hellens RP, Edwards EA, Leyland NR, Bean S, Mullineaux PM. **2000**. pGreen: a versatile and flexible binary Ti vector for *Agrobacterium*-mediated plant transformation. *Plant Molecular Biology* **42**: 819–832.

Helmer G, Casadaban M, Bevan M, Kayes L, Chilton M-D. **1984**. A new chimeric gene as a marker for plant transformation: The expression of *Escherichia coli* β-galactosidase in sunflower and tobacco cells. *Nature Biotechnology* **2**: 520–527.

Herendeen PS, Friis EM, Pedersen KR, Crane PR. **2017**. Palaeobotanical redux: Revisiting the age of the angiosperms. *Nature Plants* **3**: 17015.

Hoekema A, Hirsch PR, Hooykaas PJJ, Schilperoort RA. **1983**. A binary plant vector strategy based on

separation of vir- and T-region of the *Agrobacterium tumefaciens* Ti-plasmid. *Nature* **303**: 179–180.

Holsters M, Silva B, Van Vliet F, Genetello C, De Block M, Dhaese P, Depicker A, Inzé D, Engler G, Villarroel R, *et al.* 1980. The functional organization of the nopaline *A. tumefaciens* plasmid pTiC58. *Plasmid* **3**: 212–230.

Horsch RB, Fraley RT, Rogers SG, Sanders PR, Lloyd A, Hoffmann N. 1984. Inheritance of functional foreign genes in plants. *Science (New York, N.Y.)* **223**: 496–8.

Horsch RB, Fry JE, Hoffmann NL, Eichholtz D, Rogers SG, Fraley RT. 1985. A simple and general method for transferring genes into plants. *Science* **227**: 1229–31.

Houston K, McKim SM, Comadran J, Bonar N, Druka I, Uzrek N, Cirillo E, Guzy-Wrobelska J, Collins NC, Halpin C, *et al.* 2013. Variation in the interaction between alleles of *HvAPETALA2* and microRNA172 determines the density of grains on the barley inflorescence. *Proceedings of the National Academy of Sciences* **110**: 16675–16680.

Hraška M, Rakouský S, Čurn V. 2006. Green fluorescent protein as a vital marker for non-destructive detection of transformation events in transgenic plants. *Plant Cell, Tissue and Organ Culture* **86**: 303–318.

Inoue K, Keegstra K. 2003. A polyglycine stretch is necessary for proper targeting of the protein translocation channel precursor to the outer envelope membrane of chloroplasts. *The Plant journal : for cell and molecular biology* **34**: 661–9.

Ippolito A. 2000. Systematics, floral evolution and speciation in *Nicotiana*. *PhD thesis, University of Missouri, Columbia MO*.

Ippolito A, Fernandes GW, Holtsford TP. 2004. Pollinator preferences for *Nicotiana alata*, *N. forgetiana*, and their F1 hybrids. *Evolution* **58**: 2634–44.

Jaffé FW, Tattersall A, Glover BJ. 2007. A truncated MYB transcription factor from *Antirrhinum majus* regulates epidermal cell outgrowth. *Journal of Experimental Botany* **58**: 1515–1524.

Jakoby MJ, Falkenhan D, Mader MT, Brininstool G, Wischnitzki E, Platz N, Hudson A, Hülskamp M, Larkin J, Schnittger A. 2008. Transcriptional profiling of mature *Arabidopsis* trichomes reveals that *NOECK* encodes the *MIXTA-like* transcriptional regulator MYB106. *Plant physiology* **148**: 1583–602.

Jefferson RA, Kavanagh TA, Bevan MW. 1987. GUS fusions: beta-glucuronidase as a sensitive and versatile gene fusion marker in higher plants. *EMBO journal* **6**: 3901–7.

Jin H, Martin C. 1999. Multifunctionality and diversity within the plant MYB-gene family. *Plant Molecular Biology* **41**: 577–85.

Johnson SD, Steiner KE. 2000. Generalization versus specialization in plant pollination systems. *Trends in Ecology and Evolution* **15**: 140–143.

Kaczorowski RL, Gardener MC, Holtsford TP. 2005. Nectar traits in *Nicotiana* section *Alatae* (Solanaceae) in relation to floral traits, pollinators, and mating system. *American Journal of Botany* **92**: 1270–1283.

Kaczorowski RL, Juenger TE, Holtsford TP. 2008. Heritability and correlation structure of nectar and floral morphology traits in *Nicotiana alata*. *Evolution* **62**: 1738–1750.

Kay QON, Daoud HS, Stirton CH. 1981. Pigment distribution, light reflection and cell structure in petals. *Botanical Journal of the Linnean Society* **83**: 57–83.

Kay KM, Sargent RD. **2009**. The role of animal pollination in plant speciation: Integrating ecology, geography, and genetics. *Annual Review of Ecology, Evolution, and Systematics* **40**: 637–656.

Keating DH, Cronan JE. **1996**. An isoleucine to valine substitution in *Escherichia coli* acyl carrier protein results in a functional protein of decreased molecular radius at elevated pH. *Journal of Biological Chemistry* **271**: 15905–15910.

Kelly AJ, Bonnlander MB, Meeks-Wagner DR. **1995**. NFL, the tobacco homolog of *FLORICAULA* and *LEAFY*, is transcriptionally expressed in both vegetative and floral meristems. *The Plant cell* **7**: 225–34.

Kelly LJ, Leitch AR, Clarkson JJ, Hunter RB, Knapp S, Chase MW. **2010**. Intragenic recombination events and evidence for hybrid speciation in *Nicotiana* (Solanaceae). *Molecular Biology and Evolution* **27**: 781–799.

Kessler D, Baldwin IT. **2007**. Making sense of nectar scents: The effects of nectar secondary metabolites on floral visitors of *Nicotiana attenuata*. *Plant Journal* **49**: 840–854.

Kessler D, Diezel C, Baldwin IT. **2010**. Changing pollinators as a means of escaping herbivores. *Current biology : CB* **20**: 237–42.

Kessler D, Gase K, Baldwin IT. **2008**. Field experiments with transformed plants reveal the sense of floral scents. *Science (New York, N.Y.)* **321**: 1200–2.

Kevan PG, Lane MA. **1985**. Flower petal microtexture is a tactile cue for bees. *Proceedings of the National Academy of Sciences of the United States of America* **82**: 4750–2.

Kim G, Shoda K, Tsuge T, Cho K, Uchimiya H, Yokoyama R, Nishitani K, Tsukaya H. **2002**. The ANGUSTIFOLIA gene of Arabidopsis, a plant *CtBP* gene, regulates leaf-cell expansion, the arrangement of cortical microtubules in leaf cells and expression of a gene involved in cell-wall formation. *EMBO Journal* **21**: 1267–1279.

Kluyver T, Ragan-Kelley B, Pérez F, Granger B, Bussonnier M, Frederic J, Kelley K, Hamrick J, Grout J, Corlay S, *et al.* 2016. Jupyter Notebooks-a publishing format for reproducible computational workflows.

Knapp S. **2010**. On 'various contrivances': Pollination, phylogeny and flower form in the Solanaceae. *Philosophical transactions of the Royal Society of London. Series B, Biological sciences* **365**: 449–60.

Knapp S, Chase MW, Clarkson JJ. **2004**. Nomenclatural changes and a new sectional classification in *Nicotiana* (Solanaceae). *Taxon* **53**: 73–82.

Kramer EM. **2007**. Understanding the genetic basis of floral diversity. *BioScience* **57**: 479–487.

Krügel T, Lim M, Gase K, Halitschke R, Baldwin IT. **2002**. *Agrobacterium*-mediated transformation of *Nicotiana attenuata*, a model ecological expression system. *Chemoecology* **12**: 177–183.

Kumar S, Stecher G, Li M, Knyaz C, Tamura K. **2018**. MEGA X: Molecular evolutionary genetics analysis across computing platforms. *Molecular Biology and Evolution* **35**: 1547–1549.

de la Riva GA, Gonzalez-Cabrera J, Vazquez-Padron R, Ayra-Pardo C. **1998**. Agrobacterium tumefaciens : A natural tool for plant transformation. *Electronic Journal of Biotechnology* **1**: 118–113.

Labandeira CC, Currano ED. **2013**. The fossil record of plant-insect dynamics. *Annual Review of Earth and Planetary Sciences* **41**: 287–311.

Ladiges PY, Marks CE, Nelson G. **2011**. Biogeography of Nicotiana section *Suaveolentes* (Solanaceae)

reveals geographical tracks in arid Australia. *Journal of Biogeography* **38**: 2066–2077.

Lashbrooke J, Adato A, Lotan O, Alkan N, Tsimbalist T, Rechav K, Fernandez-Moreno J-P, Widemann E, Grausem B, Pinot F, *et al.* 2015. The tomato MIXTA-Like transcription factor coordinates fruit epidermis conical cell development and cuticular lipid biosynthesis and assembly. *Plant Physiology* **169**: 2553–71.

Lawson DA, Chittka L, Whitney HM, Rands SA. **2018**. Bumblebees distinguish floral scent patterns, and can transfer these to corresponding visual patterns. *Proceedings of the Royal Society B: Biological Sciences* **285**: 20180661.

Leitch IJ, Hanson L, Lim KY, Kovarik A, Chase MW, Clarkson JJ, Leitch AR. **2008**. The ups and downs of genome size evolution in polyploid species of *Nicotiana* (Solanaceae). *Annals of Botany* **101**: 805–814.

Li B, Huang W, Bass T. **2003**. Shoot production per responsive leaf explant increases exponentially with explant organogenic potential in *Nicotiana* species. *Plant Cell Reports* **22**: 231–238.

Li M, Zhang D, Gao Q, Luo Y, Zhang H, Ma B, Chen C, Whibley A, Zhang Y, Cao Y, *et al.* 2019. Genome structure and evolution of *Antirrhinum majus* L. *Nature Plants* **5**: 174–183.

Lunau K. **2004**. Adaptive radiation and coevolution - Pollination biology case studies. *Organisms Diversity and Evolution* **4**: 207–224.

Lunau K, Maier EJ. 1995. Innate colour preferences of flower visitors. *Journal of Comparative Physiology* A 177: 1–19.

Lunau K, Papiorek S, Eltz T, Sazima M. **2011**. Avoidance of achromatic colours by bees provides a private niche for hummingbirds. *Journal of Experimental Biology* **214**: 1607–1612.

Luu VT, Weinhold A, Ullah C, Dressel S, Schoettner M, Gase K, Gaquerel E, Xu S, Baldwin IT. **2017**. O-acyl sugars protect a wild tobacco from both native fungal pathogens and a specialist herbivore. *Plant physiology* **174**: 370–386.

Machado A, Wu Y, Yang Y, Llewellyn DJ, Dennis ES. **2009**. The MYB transcription factor GhMYB25 regulates early fibre and trichome development. *Plant Journal* **59**: 52–62.

Magallón S, Gómez-Acevedo S, Sánchez-Reyes LL, Hernández-Hernández T. **2015**. A metacalibrated time-tree documents the early rise of flowering plant phylogenetic diversity. *New Phytologist* **207**: 437–453.

Malabadi RB, Teixeira Da Silva JA, Nataraja K. **2008**. Green fluorescent protein in the genetic transformation of plants. *Transgenic Plant Journal* **2**: 86–109.

Maliga P, Tungsuchat-Huang T. **2014**. Plastid transformation in *Nicotiana tabacum* and *Nicotiana sylvestris* by biolistic DNA delivery to leaves. In: Methods in Molecular Biology. 147–163.

Marks CE, Newbigin E, Ladiges PY. **2011**. Comparative morphology and phylogeny of *Nicotiana* Section *Suaveolentes* (Solanaceae) in Australia and the South Pacific. *Australian Systematic Botany* **24**: 61.

Martin C, Bhatt K, Baumann K, Jin H, Zachgo S, Roberts K, Schwarz-Sommer Z, Glover BJ, Perez-Rodriguez M. **2002**. The mechanics of cell fate determination in petals. *Philosophical transactions of the Royal Society of London. Series B, Biological sciences* **357**: 809–13.

Martin C, Paz-Ares J. **1997**. MYB transcription factors in plants. *Trends in genetics : TIG* **13**: 67–73.

Martin C, Prescott A, Mackay S, Bartlett J, Vrijlandt E. **1991**. Control of anthocyanin biosynthesis in

flowers of *Antirrhinum majus*. *Plant Journal* **1**: 37–49.

Martins TR, Barkman TJ. **2005**. Reconstruction of Solanaceae Phylogeny Using the Nuclear Gene SAMT. *Systematic Botany* **30**: 435–447.

Martins DJ, Johnson SD. **2007**. Hawkmoth pollination of aerangoid orchids in Kenya, with special reference to nectar sugar concentration gradients in the floral spurs. *American Journal of Botany* **94**: 650–659.

Márton L, Wullems GJ, Molendijk L, Schilperoort RA. **1979**. *In vitro* transformation of cultured cells from *Nicotiana tabacum* by *Agrobacterium tumefaciens*. *Nature* **277**: 129–131.

McCarthy EW, Arnold SEJ, Chittka L, Le Comber SC, Verity R, Dodsworth S, Knapp S, Kelly LJ, Chase MW, Baldwin IT, *et al.* 2015. The effect of polyploidy and hybridization on the evolution of floral colour in *Nicotiana* (Solanaceae). *Annals of Botany* **115**: 1117–1131.

Mintz-Oron S, Mandel T, Rogachev I, Feldberg L, Lotan O, Yativ M, Wang Z, Jetter R, Venger I, Adato A, *et al.* 2008. Gene expression and metabolism in tomato fruit surface tissues. *Plant Physiology* **147**: 823–51.

Mitchell RJ, Irwin RE, Flanagan RJ, Karron JD. **2009**. Ecology and evolution of plant-pollinator interactions. *Annals of Botany* **103**: 1355–1363.

Mitchell PJ, TjiAN R. **1989**. Transcriptional regulation in mammalian cells by sequence-specific DNA binding proteins. *Science* **245**: 371–378.

Moghbel N, Ryu BM, Ratsch A, Steadman KJ. **2017**. Nicotine alkaloid levels, and nicotine to nornicotine conversion, in Australian *Nicotiana* species used as chewing tobacco. *Heliyon* **3**: e00469.

Moyroud E, Glover BJ. **2017**. The evolution of diverse floral morphologies. *Current Biology* **27**: R941–R951.

Moyroud E, Wenzel T, Middleton R, Rudall PJ, Banks H, Reed A, Mellers G, Killoran P, Westwood MM, Steiner U, *et al.* 2017. Disorder in convergent floral nanostructures enhances signalling to bees. *Nature* **550**: 469–474.

Nester EW, Gordon MP, Amasino RM, Yanofsky MF. **2003**. Crown gall: A molecular and physiological analysis. *Annual Review of Plant Physiology* **35**: 387–413.

Noda K, Glover BJ, Linstead P, Martin C. **1994**. Flower colour intensity depends on specialized cell shape controlled by a Myb-related transcription factor. *Nature* **369**: 661–664.

Odell JT, Nagy F, Chua N-H. **1985**. Identification of DNA sequences required for activity of the cauliflower mosaic virus 35S promoter. *Nature* **313**: 810–812.

Oelschlägel B, Gorb S, Wanke S, Neinhuis C. **2009**. Structure and biomechanics of trapping flower trichomes and their role in the pollination biology of *Aristolochia* plants (Aristolochiaceae). *New Phytologist* **184**: 988–1002.

Ojeda I, Francisco-Ortega J, Cronk QCB. **2009**. *Evolution of petal epidermal micromorphology in Leguminosae and its use as a marker of petal identity*. Oxford University Press.

Ojeda I, Santos-Guerra A, Caujapé-Castells J, Jaén-Molina R, Marrero Á, C. B. Cronk Q. **2012**. Comparative micromorphology of petals in Macaronesian *Lotus* (Leguminosae) reveals a loss of papillose conical cells during the evolution of bird pollination. *International Journal of Plant Sciences* **173**: 365–374.

Ojeda DI, Valido A, Fernández De Castro AG, Ortega-Olivencia A, Fuertes-Aguilar J, Carvalho JA, Santos-Guerra A. **2016**. Pollinator shifts drive petal epidermal evolution on the Macaronesian Islands bird-flowered species. *Biology Letters* **12**: 20160022.

Ollerton J, Alarcon R, Waser NM, Price M V., Watts S, Cranmer L, Hingston A, Peter CI, Rotenberry J. **2009**. A global test of the pollination syndrome hypothesis. *Annals of Botany* **103**: 1471–1480.

Ollerton J, Watts S, Connerty S, Lock J, Parker L, Wilson I, Schueller S, Nattero J, Cocucci AA, Izhaki I, *et al.* 2012. Pollination ecology of the invasive tree tobacco *Nicotiana glauca*: comparisons across native and non-native ranges. *Journal of Pollination Ecology* **9**.

Olmstead RG, Bohs L, Migid HA, Santiago-Valentin E, Garcia VF, Collier SM. **2008**. A molecular phylogeny of the Solanaceae. *Taxon* **57**: 1159–1181.

Olmstead RG, Sweere JA, Spangler RE, Bohs L, Palmer JD, Olmstead RG, Sweere JA, Spangler RE, Palmer JD. **1999**. Phylogeny and provisional classification of the Solanaceae based on chloroplast DNA. In: Nee M, Symon D, Lester R, Jessop J, eds. Solanaceae IV. London: Royal Botanic Gardens, Kew, 111–137.

Oshima Y, Shikata M, Koyama T, Ohtsubo N, Mitsuda N, Ohme-Takagi M. **2013**. MIXTA-Like transcription factors and WAX INDUCER1/SHINE1 coordinately regulate cuticle development in *Arabidopsis* and *Torenia fournieri*. *Plant Cell* **25**: 1609–1624.

Ow DW, De Wet JR, Helinski DR, Howell SH, Wood K V., Deluca M. **1986**. Transient and stable expression of the firefly luciferase gene in plant cells and transgenic plants. *Science* **234**: 856–859.

Owens JN, Takaso T, Runions CJ. **1998**. Pollination in conifers. *Trends in Plant Science* **3**: 479–485.

Pabo CO, Sauer RT. **2003**. Transcription factors: Structural families and principles of DNA recognition. *Annual Review of Biochemistry* **61**: 1053–1095.

Papiorek S, Junker RR, Lunau K, Osorio D. **2014**. Gloss, colour and grip: multifunctional epidermal cell shapes in bee-and bird-pollinated flowers. *PLoS ONE* **9**: e112013.

Papiorek S, Rohde K, Lunau K. **2013**. Bees' subtle colour preferences: How bees respond to small changes in pigment concentration. *Naturwissenschaften* **100**: 633–643.

Park S. **2006**. *Agrobacterium tumefaciens*-mediated transformation of tobacco (*Nicotiana tabacum* L.) leaf disks: Evaluation of the co-cultivation conditions to increase B-glucuronidase gene activity. *PhD Thesis, Louisiana State University*: 1–67.

Pastore JJ, Limpuangthip A, Yamaguchi N, Wu M-F, Sang Y, Han S-K, Malaspina L, Chavdaroff N, Yamaguchi A, Wagner D. **2011**. *LATE MERISTEM IDENTITY2* acts together with *LEAFY* to activate *APETALA1*. *Development* **138**: 3189–98.

Pattrick JG. **2017**. Grip, slip, petals, and pollinators: Linking the biomechanics, behaviour and ecology of interactions between bees and plants.

Peitsch D, Fietz A, Hertel H, de Souza J, Ventura DF, Menzel R. **1992**. The spectral input systems of hymenopteran insects and their receptor-based colour vision. *Journal of Comparative Physiology A* **170**: 23–40.

Pellmyr O. **1992**. Evolution of insect pollination and angiosperm diversification. *Trends in ecology & evolution* **7**: 46–9.

Perez-Rodriguez M, Jaffé FW, Butelli E, Glover BJ, Martin C, Jaffe FW, Butelli E, Glover BJ, Martin

C. **2005**. Development of three different cell types is associated with the activity of a specific MYB transcription factor in the ventral petal of Antirrhinum majus flowers. *Development* **132**: 359–370.

Peterson ML, Miller TJ, Kay KM. **2015**. An ultraviolet floral polymorphism associated with life history drives pollinator discrimination in *Mimulus guttatus*. *American Journal of Botany* **102**: 396–406.

Plett JM, Wilkins O, Campbell MM, Ralph SG, Regan S. **2010**. Endogenous overexpression of *Populus MYB186* increases trichome density, improves insect pest resistance, and impacts plant growth. *Plant Journal* **64**: 419–432.

Prasher DC, Eckenrode VK, Ward WW, Prendergast FG, Cormier MJ. **1992**. Primary structure of the *Aequorea victoria* green-fluorescent protein. *Gene* **111**: 229–33.

Proctor MCF, Yeo P, Lack A. **1996**. *The natural history of pollination*. Timber Press.

Purugganan MD. **1998**. The molecular evolution of development. *BioEssays* **20**: 700–711.

Qiu Y, Lee J, Bernasconi-Quadroni F, Soltis DE, Soltis PS, Zanis M, Zimmer EA, Chen Z, Savolainen V, Chase MW. **2002**. Phylogeny of basal angiosperms: Analyses of five genes from three genomes. *International Journal of Plant Sciences* **161**: S3–S27.

Raguso RA, Levin RA, Foose SE, Holmberg MW, Mcdade LA. **2003**. Fragrance chemistry, nocturnal rhythms and pollination "'syndromes"' in *Nicotiana*. *Phytochemistry* **63**: 265–284.

Raguso RA, Schlumpberger BO, Kaczorowski RL, Holtsford TP. **2006**. Phylogenetic fragrance patterns in *Nicotiana* sections *Alatae* and *Suaveolentes*. *Phytochemistry*: 1931–1942.

Raine NE, Chittka L. 2007. The adaptive significance of sensory bias in a foraging context: Floral colour preferences in the bumblebee *Bombus terrestris* (S Rands, Ed.). *PLoS ONE* 2: e556.

Ramakers C, Ruijter JM, Lekanne Deprez RH, Moorman AFM. **2003**. Assumption-free analysis of quantitative real-time polymerase chain reaction (PCR) data. *Neuroscience Letters* **339**: 62–66.

Rands SA, Glover BJ, Whitney HM. **2011**. Floral epidermal structure and flower orientation: Getting to grips with awkward flowers. *Arthropod-Plant Interactions* **5**: 279–285.

RBG-Kew. **2016a**. *The State of the World's Plants Report – 2016. Royal Botanic Gardens, Kew*.

RBG-Kew. **2016b**. *Nicotiana* L. | Plants of the World Online | Kew Science.

Reed A. **2014**. Petal epidermal patterning and pollination attraction. *PhD Thesis, University of Cambridge*.

Ren H, Dang X, Cai X, Yu P, Li Y, Zhang S, Liu M, Chen B, Lin D. **2017**. Spatio-temporal orientation of microtubules controls conical cell shape in *Arabidopsis thaliana* petals (D Oppenheimer, Ed.). *PLoS Genetics* **13**: e1006851.

RHS. **2019**. Royal Horticultural Society / RHS Gardening.

Riffell JA, Alarcón R, Abrell L. **2008**. Floral trait associations in hawkmoth-specialized and mixed pollination systems: Datura wrightii and *Agave* spp. in the Sonoran Desert. *Communicative & integrative biology* **1**: 6–8.

Rigosi E, Wiederman SD, O'Carroll DC. **2017**. Visual acuity of the honey bee retina and the limits for feature detection. *Scientific Reports* **7**: 45972.

Rodríguez-Mega E, Piñeyro-Nelson A, Gutierrez C, Sánchez MDLP, García-Ponce B, Zluhan-Martínez E, Álvarez-Buylla ER, Garay-Arroyo A. **2015**. Role of transcriptional regulation in the evolution of plant phenotype: A dynamic systems approach. *Developmental Dynamics* **244**: 1074–1095.

Ronse De Craene LP. **2007**. Are petals sterile stamens or bracts? The origin and evolution of petals in the core eudicots. *Annals of Botany* **100**: 621–630.

Ronse De Craene LP, Brockington SF. **2013**. Origin and evolution of petals in angiosperms. *Plant Ecology and Evolution* **146**: 5–25.

Rosas-Guerrero V, Aguilar R, Martén-Rodríguez S, Ashworth L, Lopezaraiza-Mikel M, Bastida JM, Quesada M. **2014**. A quantitative review of pollination syndromes: Do floral traits predict effective pollinators? *Ecology Letters* **17**: 388–400.

Rost B, Yachdav G, Liu J. **2004**. The PredictProtein server. *Nucleic Acid Research*: 321–326.

Särkinen T, Bohs L, Olmstead RG, Knapp S. **2013**. A phylogenetic framework for evolutionary study of the nightshades (Solanaceae): A dated 1000-tip tree. *BMC evolutionary biology* **13**: 214.

Sauquet H, Von Balthazar M, Magallón S, Doyle JA, Endress PK, Bailes EJ, Barroso De Morais E, Bull-Hereñu K, Carrive L, Chartier M, *et al.* 2017. The ancestral flower of angiosperms and its early diversification. *Nature Communications* **8**: 16047.

Savolainen V, Chase MW, Hoot SB, Morton CM, Soltis DE, Bayer C, Fay MF, de Bruijn AY, Sullivan S, Qiu YL. **2000**. Phylogenetics of flowering plants based on combined analysis of plastid *atpB* and *rbcL* gene sequences. *Systematic Biology* **49**: 306–62.

Schell J, Van Montagu M. **1977**. The Ti-plasmid of *Agrobacterium tumefaciens*, a natural vector for the introduction of NIF genes in plants? In: Genetic Engineering for Nitrogen Fixation. Boston, MA: Springer US, 159–179.

Schmidt GW, Delaney SK. **2010**. Stable internal reference genes for normalization of real-time RT-PCR in tobacco (*Nicotiana tabacum*) during development and abiotic stress. *Molecular Genetics and Genomics* **283**: 233–241.

Schranz ME, Quijada P, Sung S-B, Lukens L, Amasino R, Osborn TC. 2002. Characterization and effects of the replicated flowering time gene FLC in *Brassica rapa*. *Genetics* 162, 1457–1468.

Schwarz-Sommer Z, Davies B, Hudson A. **2003**. An everlasting pioneer: The story of Antirrhinum research. *Nature Reviews Genetics* **4**: 655–664.

Scoville AG, Barnett LL, Bodbyl-Roels S, Kelly JK, Hileman LC. **2011**. Differential regulation of a MYB transcription factor is correlated with transgenerational epigenetic inheritance of trichome density in Mimulus guttatus. *New phytologist* **191**: 251–63.

Sheikholeslam SN, Weeks DP. **1987**. Acetosyringone promotes high efficiency transformation of *Arabidopsis thaliana* explants by *Agrobacterium* tumefaciens. *Plant Molecular Biology* **8**: 291–298.

Shi JX, Adato A, Alkan N, He Y, Lashbrooke J, Matas AJ, Meir S, Malitsky S, Isaacson T, Prusky D, *et al.* 2013. The tomato SlSHINE3 transcription factor regulates fruit cuticle formation and epidermal patterning. *New Phytologist* **197**: 468–480.

Shimomura O. **2005**. The discovery of aequorin and green fluorescent protein. *Journal of Microscopy* **217**: 3–15.

Shimomura O, Johnson FH, Saiga Y. **1962**. Extraction, purification and properties of aequorin, a bioluminescent protein from the luminous Hydromedusan, *Aequorea*. *Journal of Cellular and Comparative Physiology* **59**: 223–239.

Skorupski P, Chittka L. 2010. Photoreceptor spectral sensitivity in the bumblebee, *Bombus impatiens* (Hymenoptera: Apidae). *PLoS ONE* **5**: 12049.

Smith RH. 2012. *Plant tissue culture : Techniques and experiments*. Elsevier/AP.

Soltis DE, Smith SA, Cellinese N, Wurdack KJ, Tank DC, Brockington SF, Refulio-Rodriguez NF, Walker JB, Moore MJ, Carlsward BS, *et al.* 2011. Angiosperm phylogeny: 17 genes, 640 taxa. *American Journal of Botany* **98**: 704–730.

Soltis PS, Soltis DE. 2004. The origin and diversification of angiosperms. *American Journal of Botany* **91**: 1614–1626.

Soltis PS, Soltis DE. 2014. Flower diversity and angiosperm diversification. In: Methods in Molecular Biology. Humana Press, New York, NY, 85–102.

Stebbins GL. 1970. Adaptive radiation of reproductive characteristics in angiosperms, I: Pollination mechanisms. *Annual Review of Ecology and Systematics* **1**: 307–326.

Stebbins GL. 2006. Why are there so many species of flowering plants? *BioScience* **31**: 573–577.

Stehmann JR, Semir J, Ippolito A. 2002. *Nicotiana mutabilis* (Solanaceae), a new species from Southern Brazil. *Kew Bulletin* **57**: 639.

Stern D. 2000. Perspective: Evolutionary developmental biology and the problem of variation. *Evolution* **54**: 1079–1091.

Di Stilio VS, Martin C, Schulfer AF, Connelly CF. 2009. An ortholog of *MIXTA-like2* controls epidermal cell shape in flowers of *Thalictrum*. *New Phytologist* **183**: 718–728.

Stockey RA, Rothwell GW. 2009. Distinguishing angiophytes from the earliest angiosperms: A Lower Cretaceous (Valanginian-Hauterivian) fruit-like reproductive structure. *American Journal of Botany* **96**: 323–335.

Stracke R, Werber M, Weisshaar B. 2001. The R2R3-MYB gene family in *Arabidopsis thaliana*. *Current Opinion in Plant Biology* **4**: 447–56.

Suárez-Baron H, Alzate JF, González F, Ambrose BA, Pabón-Mora N. 2019. Genetic mechanisms underlying perianth epidermal elaboration of *Aristolochia ringens* Vahl (Aristolochiaceae). *Flora* **253**: 56–66.

Suh MC, Samuels AL, Jetter R, Kunst L, Pollard M, Ohlrogge J, Beisson F. 2005. Cuticular lipid composition, surface structure, and gene expression in *Arabidopsis* stem epidermis. *Plant Physiology* **139**: 1649–65.

Swinnen G, Goossens A, Pauwels L. 2016. Lessons from domestication: Targeting *cis*-regulatory elements for crop improvement. *Trends in Plant Science* **21**: 506–515.

Takayama K, Crawford DJ, López-Sepúlveda P, Greimler J, Stuessy TF. 2018. Factors driving adaptive radiation in plants of oceanic islands: a case study from the Juan Fernández Archipelago. *Journal of Plant Research* **131**: 469–485.

Tavazza R, Ordas RJ, Tavazza M, Ancora G, Benvenuto E. 1988. Genetic transformation of Nicotiana clevelandii using a Ti plasmid derived vector. *Journal of Plant Physiology* **133**: 640–644.

Taylor L. 2015. The evolution of cell shape in plants. *PhD Thesis, University of Cambridge*: 224.

Taylor EL, Taylor TN. 2009. Seed ferns from the late Paleozoic and Mesozoic: Any angiosperm ancestors

lurking there? *American Journal of Botany* **96**: 237–251.

Tiedge K, Lohaus G. **2017**. Nectar sugars and amino acids in day- and night-flowering Nicotiana species are more strongly shaped by pollinators' preferences than organic acids and inorganic ions (RM Borges, Ed.). *PLoS ONE* **12**: e0176865.

Vignoli-Silva M, Auler Mentz L. **2005**. O gênero *Nicotiana* L. (Solanaceae) no Rio Grande do Sul, Brasil. *IHERINGIA, Sér. Bot.* **60**: 151–173.

Vignolini S, Davey MP, Bateman RM, Rudall PJ, Moyroud E, Tratt J, Malmgren S, Steiner U, Glover BJ. **2012a**. The mirror crack'd: Both pigment and structure contribute to the glossy blue appearance of the mirror orchid, *Ophrys speculum*. *New Phytologist* **196**: 1038–1047.

Vignolini S, Moyroud E, Hingant T, Banks H, Rudall PJ, Steiner U, Glover BJ. **2015**. Is floral iridescence a biologically relevant cue in plant-pollinator signalling? A response to van der Kooi et al. (2014b). *New Phytologist* **205**: 21–2.

Vignolini S, Thomas MM, Kolle M, Wenzel T, Rowland AV, Rudall PJ, Baumberg JJ, Glover BJ, Steiner U. **2012b**. Directional scattering from the glossy flower of *Ranunculus*: how the buttercup lights up your chin. *Journal of The Royal Society Interface* **9**: 1295–1301.

Vogel S, Martens J. **2000**. A survey of the function of the lethal kettle traps of *Arisaema* (Araceae), with records of pollinating fungus gnats from Nepal. *Botanical Journal of the Linnean Society* **133**: 61–100.

Vorobyev M, Hempel De Ibarra N, Brandt R, Giurfa M. **1999**. Do 'white' and 'green' look the same to a bee? *Naturwissenschaften* **86**: 592–594.

Walford S-A, Wu Y, Llewellyn DJ, Dennis ES. **2011**. GhMYB25-like: a key factor in early cotton fibre development. *Plant Journal* **65**: 785–797.

Wang R-L, Stec A, Hey J, Lukens L, Doebley J. **1999**. The limits of selection during maize domestication. *Nature* **398**: 236–239.

Wang Y, Zhang D, Renner SS, Chen Z. **2004**. A new self-pollination mechanism. *Nature* **431**: 39–40.

Waser N, Chittka L. **1998**. Evolutionary ecology: Bedazzled by flowers. *Nature* **394**: 835–836.

Whitney HM, Bennett KM V., Dorling M, Sandbach L, Prince D, Chittka L, Glover BJ. **2011a**. Why do so many petals have conical epidermal cells? *Annals of Botany* **108**: 609–616.

Whitney HM, Chittka L, Bruce TJA, Glover BJ. **2009a**. Conical epidermal cells allow bees to grip flowers and increase foraging efficiency. *Current Biology* **19**: 948–53.

Whitney HM, Dyer A, Chittka L, Rands SA, Glover BJ. **2008**. The interaction of temperature and sucrose concentration on foraging preferences in bumblebees. *Naturwissenschaften* **95**: 845–850.

Whitney HM, Federle W, Glover BJ. **2009b**. Grip and slip. *Communicative and Integrative Biology* **2**: 505–508.

Whitney HM, Glover BJ. **2007**. Morphology and development of floral features recognised by pollinators. *Arthropod-Plant Interactions* **1**: 147–158.

Whitney HM, Glover BJ, Walker RH, Ellis AG. **2011b**. The contribution of epidermal structure to flower colour in the South African flora. *Curtis's Botanical Magazine* **28**: 349–371.

Whitney HM, Kolle M, Alvarez-Fernandez R, Steiner U, Glover BJ. **2009c**. Contributions of iridescence to floral patterning. *Communicative and Integrative Biology* **2**: 230–232.

Whitney HM, Kolle M, Andrew P, Chittka L, Steiner U, Glover BJ. **2009d**. Floral iridescence, produced by diffractive optics, acts as a cue for animal pollinators. *Science (New York, N.Y.)* **323**: 130–3.

Whitney HM, Poetes R, Steiner U, Chittka L, Glover BJ. **2011c**. Determining the contribution of epidermal cell shape to petal wettability using isogenic *Antirrhinum* lines (J Stout, Ed.). *PLoS ONE* **6**: 1–5.

Whitney HM, Reed A, Rands SA, Chittka L, Glover BJ. **2016**. Flower iridescence increases object detection in the insect visual system without compromising object identity. *Current Biology* **26**: 802–808.

Wikström N, Savolainen V, Chase MW. **2001**. Evolution of the angiosperms: Calibrating the family tree. *Proceedings of the Royal Society B: Biological Sciences* **268**: 2211–2220.

Wilkins O, Nahal H, Foong J, Provart NJ, Campbell MM. **2008**. Expansion and diversification of the *Populus* R2R3-MYB family of transcription factors. *Plant Physiology* **149**: 981–993.

Wing SL, Strömberg CAE, Hickey LJ, Tiver F, Willis B, Burnham RJ, Behrensmeyer AK. **2012**. Floral and environmental gradients on a Late Cretaceous landscape. *Ecological Monographs* **82**: 23–47.

Woo JW, Kim J, Kwon S Il, Corvalán C, Cho SW, Kim H, Kim S-G, Kim S-T, Choe S, Kim J-S. **2015**. DNA-free genome editing in plants with preassembled CRISPR-Cas9 ribonucleoproteins. *Nature Biotechnology* **33**: 1162–1164.

Woodcock TS, Larson BMH, Kevan PG, Inouye DW, Lunau K. **2014**. Flies and flowers II: Floral attractants and rewards. *Journal of Pollination Ecology* **12**: 91–99.

Wray GA. **2007**. The evolutionary significance of *cis*-regulatory mutations. *Nature Reviews Genetics* **8**: 206–216.

Wright SI, Kalisz S, Slotte T. **2013**. Evolutionary consequences of self-fertilization in plants. *Proceedings of the Royal Society B: Biological Sciences* **280**: 20130133.

Wu H, Tian Y, Wan Q, Fang L, Guan X, Chen J, Hu Y, Ye W, Zhang H, Guo W, *et al.* 2018. Genetics and evolution of *MIXTA* genes regulating cotton lint fiber development. *New Phytologist* **217**: 883–895.

Yang Y, Moore MJ, Brockington SF, Timoneda A, Feng T, Marx HE, Walker JF, Smith SA. **2017**. An Efficient Field and Laboratory Workflow for Plant Phylotranscriptomic Projects. *Applications in Plant Sciences* **5**: 1600128.

Yoon H-S, Baum DA. **2004**. Transgenic study of parallelism in plant morphological evolution. *Proceedings of the National Academy of Sciences of the United States of America* **101**: 6524–9.

Younis A, Siddique MI, Kim CK, Lim KB. **2014**. RNA interference (RNAi) induced gene silencing: A promising approach of hi-tech plant breeding. *International Journal of Biological Sciences* **10**: 1150–1158.

Yuan Y-W, Byers KJ, Bradshaw H. **2013**. The genetic control of flower–pollinator specificity. *Current Opinion in Plant Biology* **16**: 422–428.

Zhang Y, Cao G, Qu LJ, Gu H. **2009**. Characterization of Arabidopsis MYB transcription factor gene *AtMYB17* and its possible regulation by LEAFY and AGL15. *Journal of Genetics and Genomics* **36**: 99–107.

Zhang Y, Sun T, Xie L, Hayashi T, Kawabata S, Li Y. **2015**. Relationship between the velvet-like texture of flower petals and light reflection from epidermal cell surfaces. *Journal of Plant Research* **128**: 623–632.

Appendices

APPENDICES

Appendix 1. R2R3 Subgroup 9 MYB genes functionally charcterised in land plants.

Summary of the subgroup 9 genes that have been functionally characterised. Figure adapted from Brockington et al., 2013 with recent additions.

Clade	Species	Gene name	Function	Reference
Subgroup 9	*Marchantia polymorpha*	*MpSbg9*	Positive regulator of epidermal conical cells	Taylor, 2015
Subgroup 9A	*Antirrhinum majus*	*AmMIXTA*	Positive regulator of epidermal conical cells	Noda et al., 1994
		AmMYBML1	Positive regulator of epidermal conical cells and trichomes	Perez-Rodriguez et al., 2005
		AmMYBML2	Positive regulator of epidermal conical cells	Baumann et al., 2007
		AmMYBML3	Regulator of epidermal conical cells	Jaffe et al., 2007
	Petunia hybrida	*PhMYB1*	Positive regulator of epidermal conical cells	Baumann et al., 2007
	Mimulus guttatus	*MgMYBML8*	Negative regulator of trichome density	Scoville et al., 2011
	Arabidopsis thaliana	*AtMYB16*	Positive regulator epidermal conical cells	Baumann et al., 2007
		AtMYB106	Positive and negative regulator of trichome development	Gilding and Marks, 2010
	Gossypium hirsutum	*GhMYB25*	Regulator of cotton fiber elongation and trichome density	Machado et al., 2009
		GhMYB25-like	Early regulator of cotton fiber initiation	Walford et al., 2011
	Medicago truncatula	*MtMYBML3*	Positive regulator of trichome development	Gilding and Marks, 2010
	Populus trichopoda	*PtMYB186*	Positive regulator of trichome density	Plett et al. 2010
	Thalictrum thalictroides	*TtMYBML2*	Positive regulator epidermal conical cells	Di Stilio et al. 2009
	Dendrobium crumenatum	*DcMYBML1*	Positive regulator of trichome development	Gilding and Marks, 2010
	Cabomba caroliniana	*CaboMIXTA*	Positive regulator of epidermal conical cells and trichomes	Reed, 2014
	Solanum spp.	*MIXTA* and *MIXTA-like*	Positive regulators of epidermal conical cells and trichomes	Alcorn, 2013; Davis, 2019
	Solanum lycopersicum	*SlMIXTA-like*	Positive regulator of epidermal conical cells on the tomato fruit	Lashbrooke et al., 2015
	Vicia faba	*VfML64*	Positive regulator of epidermal conical cells and trichomes	Bailes, 2016
		VfML8	Positive regulator of epidermal conical cells and trichomes	Bailes, 2016
		VfMIXTA-1	Positive regulator of epidermal conical cells and trichomes	Bailes, 2016
Subgroup 9B	*Arabidopsis thaliana*	*AtMYB17*	Involved in flowering commitment, epidermal analyses not reported	Pastore et al., 2011
	Lotus japonicus	*LjMYB17-like*	Positive regulator of epidermal conical cells	Brockington et al. 2013
	Solanum lycopersicum	*MYB17-1* and *MYB17-2*	Positive regulator of epidermal outgrowths	Davis, 2019
	Vicia faba	*VfMYB17*	Positive regulator of epidermal conical cells and trichomes	Bailes, 2016
		VfMYB17-like	Positive regulator of epidermal conical cells and trichomes	Bailes, 2016

Appendix 2. New data for characterisation of petal cell shape in *Nicotiana*.

The species listed in this appendix had not been characterized for petal cell shape previously (*e.g. Taylor, 2015*). In addition to the adaxial surface of the petal, other features were explored. All the images are SEM microphotographs.

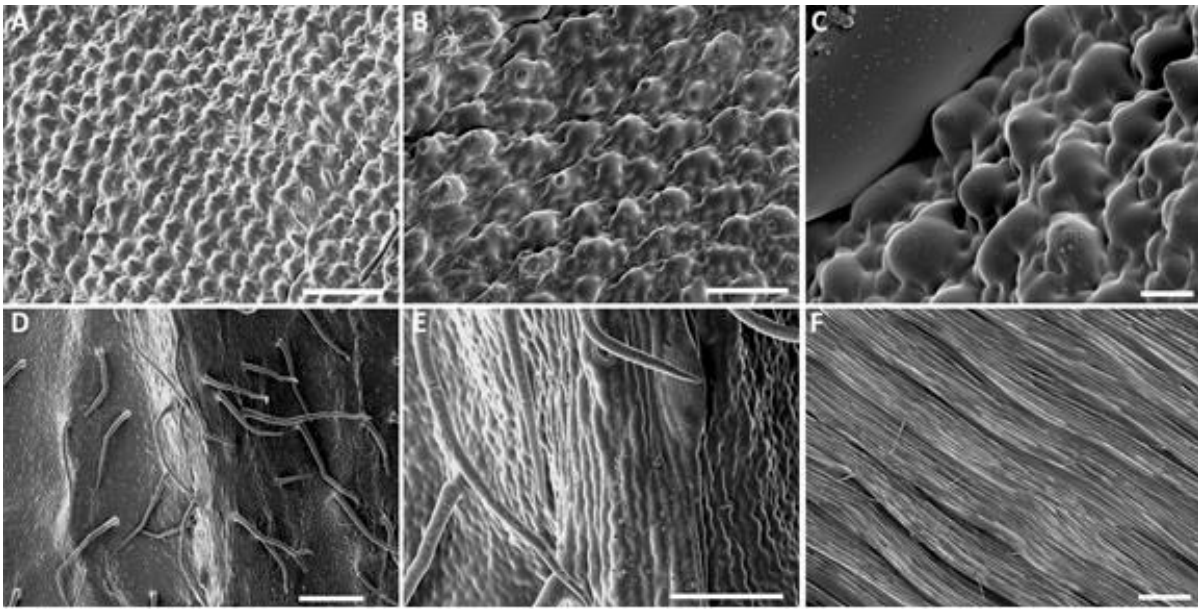

Epidermal cell morphology of petals of *Nicotiana nesophila* (Section *Repandae*). A-C. Rounded tip cells on the adaxial surface of the corolla limb (non-conical). D-E. Multicellular trichomes and undulate epidermal surface on the abaxial corolla limb. F. Fine epidermal striations on the abaxial corolla tube. D-E. Scale bars: A, E= 100µm, B= 50µm, C, F= 20µm, D= 200µm.

(Next page bottom) Epidermal cell morphology of petal of *Nicotiana occidentalis* (Section *Suaveolentes*). A. Dome-shaped cells in the adaxial limb (non-conical). B. Multicellular trichomes on the margins of the adaxial limb. C. Multicellular trichome and jigsaw shaped epidermal cells on the abaxial surface of the limb. D. Striations on the epidermis of the adaxial corolla tube. E. Multicellular trichomes and striate epidermis of the abaxial corolla tube. F. Stamen adnate to the adaxial corolla tube. Scale bars: A and D= 20µm, B and E= 100µm, C= 50µm, F= 300µm. a: anther, f: filament, p: pollen grains.

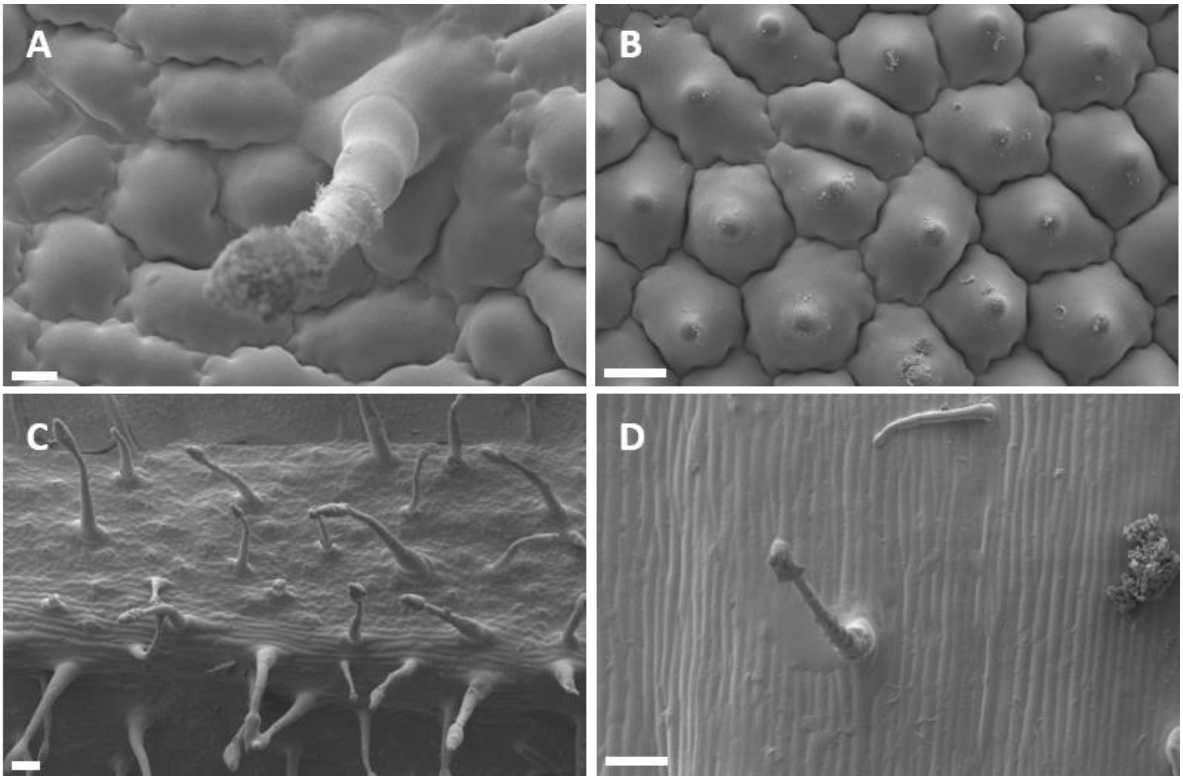

Epidermal cell morphology of petals of *Nicotiana forsterii* Roem. & Schult. (Section *Suaveolentes*). A-B. Petal lobes: A. Abaxial surface with simple trichomes. B. Adaxial surface with papillae (cf. conical). C-D. Tube C. Abaxial surface. D. Adaxial surface. Scale bars: A-B= 20µm, B = 20µm, C-D = 100µm.

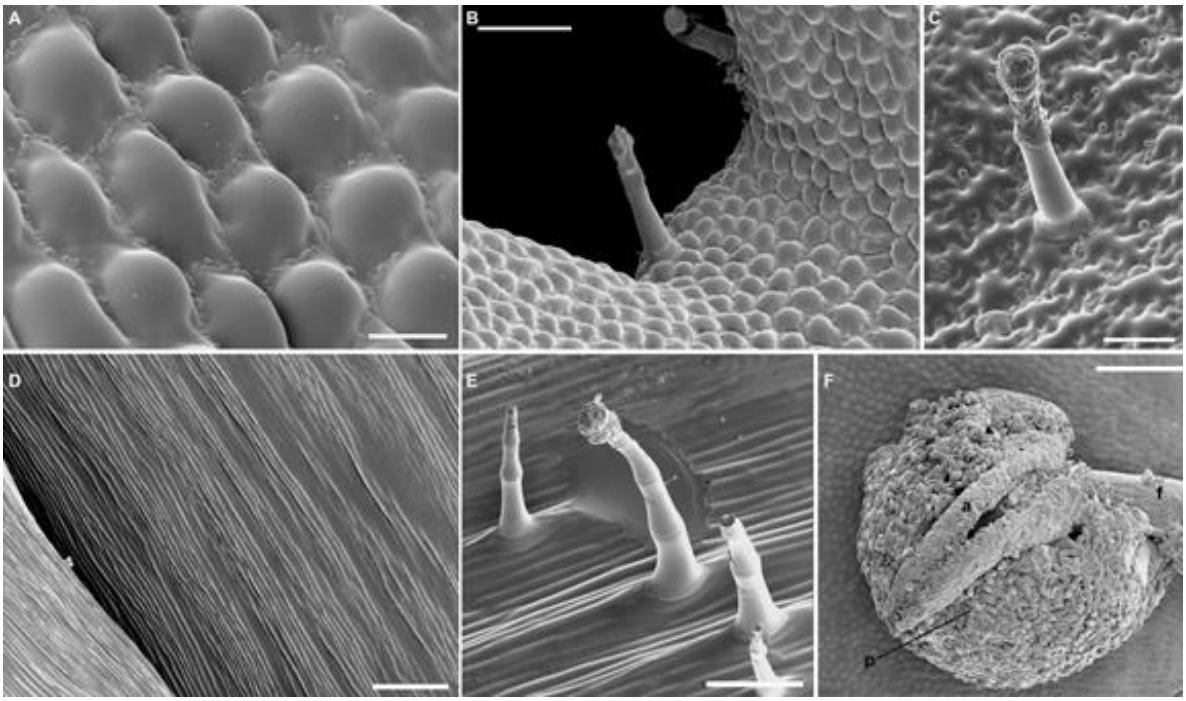

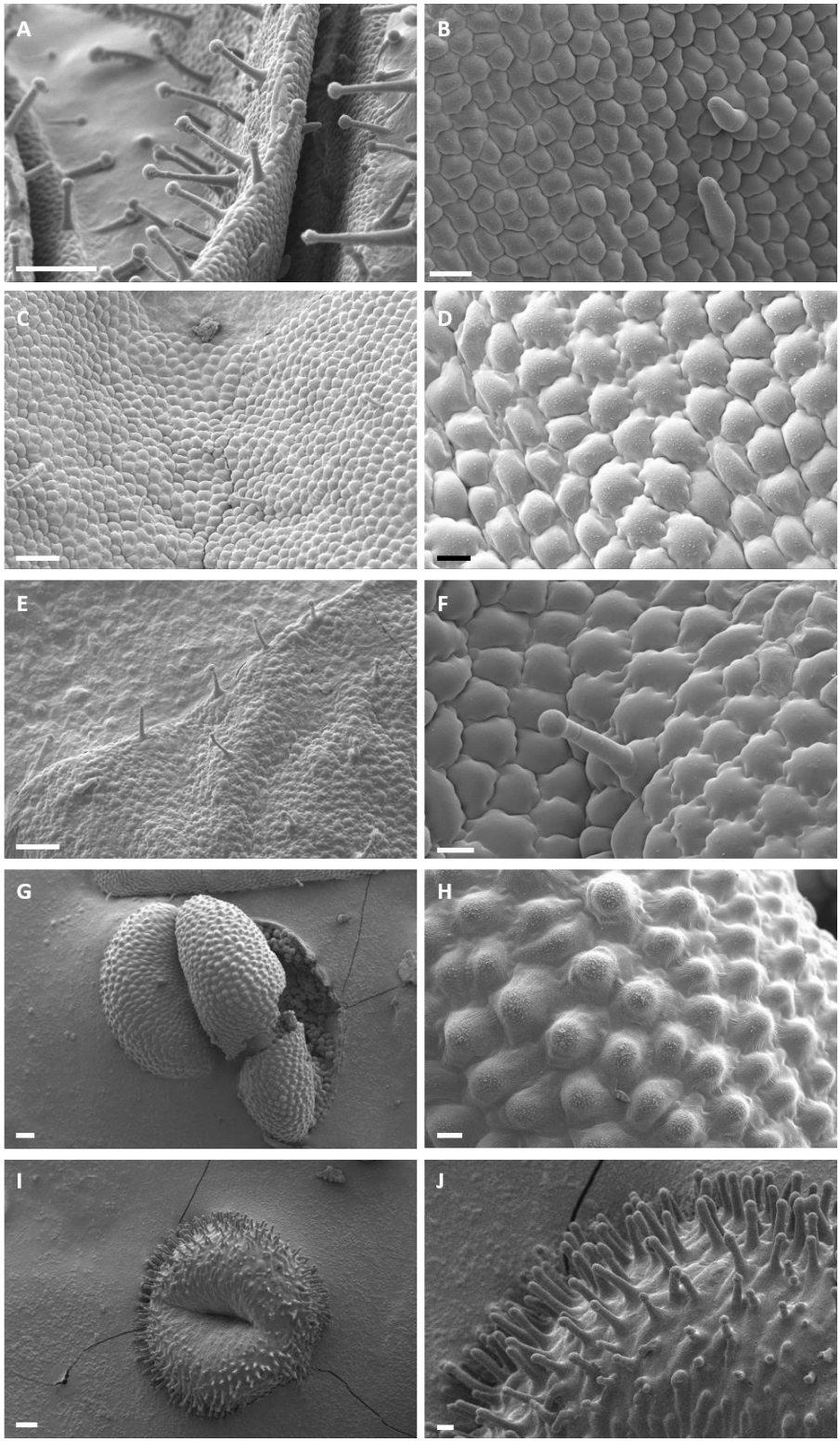

Epidermal cell morphology of *Nicotiana simulans* N. Burb. (Section *Suaveolentes*). A. Young petal still folded. Simple trichomes on the abaxial surface. B. Detail on the adaxial surface of young petal, non-conical cells and short simple trichomes originating. C-D. Adaxial surface of mature petal. E-F. Abaxial surface of mature petal. G-H. Anther with pyramidal shaped cells. I-J. Stigma with long papillae. Scale bars: A, C, E, G, I = 100µm, B, D, F, H, K = 20µm

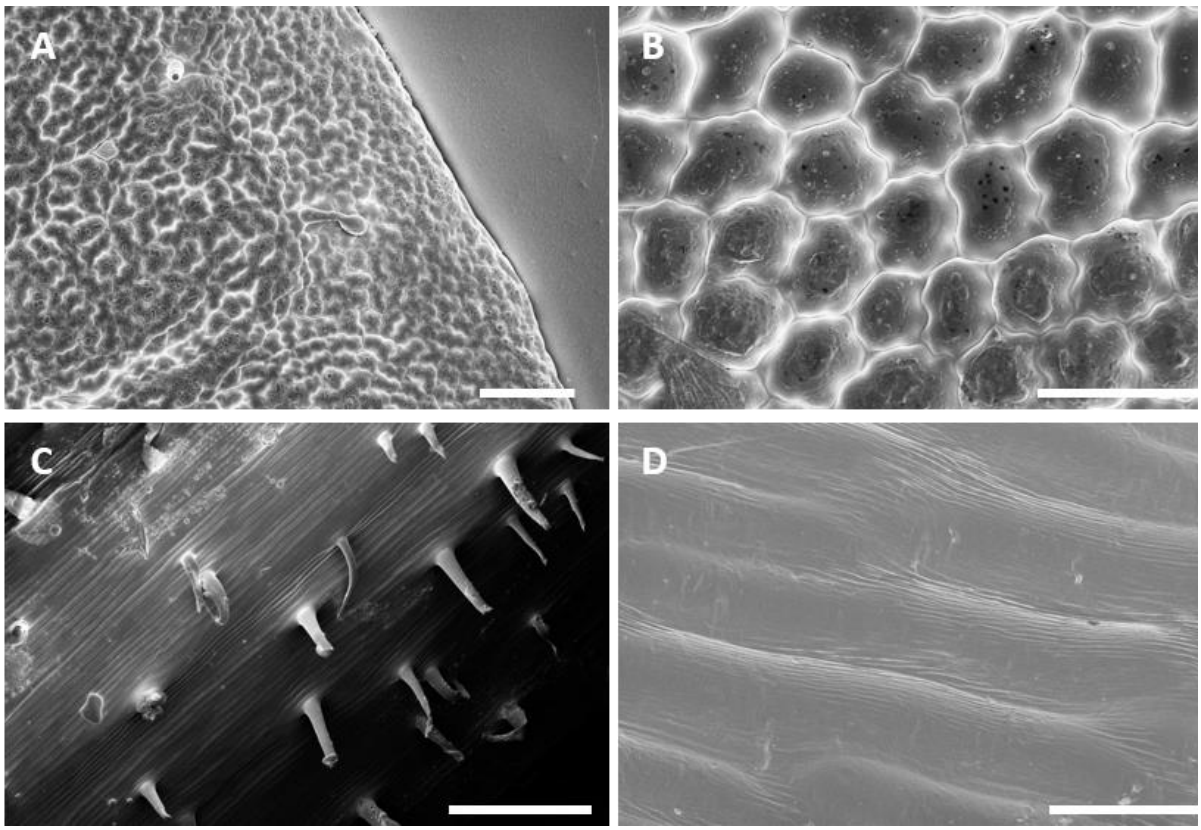

Petal epidermal cell morphology of *Nicotiana umbratica* N. Burb. (Section *Suaveolentes*). A-B. Petal lobes: A. Abaxial with scattered simple trichomes, B. Adaxial surface with flat cells (non-conical). C-D. Tube: C. Abaxial surface, D. Adaxial surface. Scale bars: A= 100µm, B = 20µm, C = 300µm, D = 20µm.

Appendix 3. Phylograms of the R2R3 Subgroup 9 MYB family.

Additional putative sequences of R2R3 Subgroup 9 MYBs from members of the Solanales retrieved from publicly available datasets, and *Nicotiana* spp. sequences obtained by Taylor (2015) for *N. langsdorfii* and *N. longiflora,* and in this work for *N. bonariensis, N. cordifolia, N. forgetiana* and *N. solanifolia*, were added to the original dataset for the angiosperms reported by Brockington *et al.*, (2013).
Analyses were run in Geneious R9. The predicted amino acid sequences were aligned using the Muscle algorithm. Approximately-maximum-likelihood phylogenetic trees were built using FastTree with the Jones-Taylor-Thornton (JTT) model of amino acid evolution.

(Next page) Phylogram of the R2R3 Subgroup 9A MYB transcription factors including additional sequences of the Solanales. Clade MIXTA is represented in green and MIXTA-like in red. Putative sequences analogous to *N. tabacum* MIXTA-1 are highlighted in orange. Newly included sequences from this work are highlighted in purple.

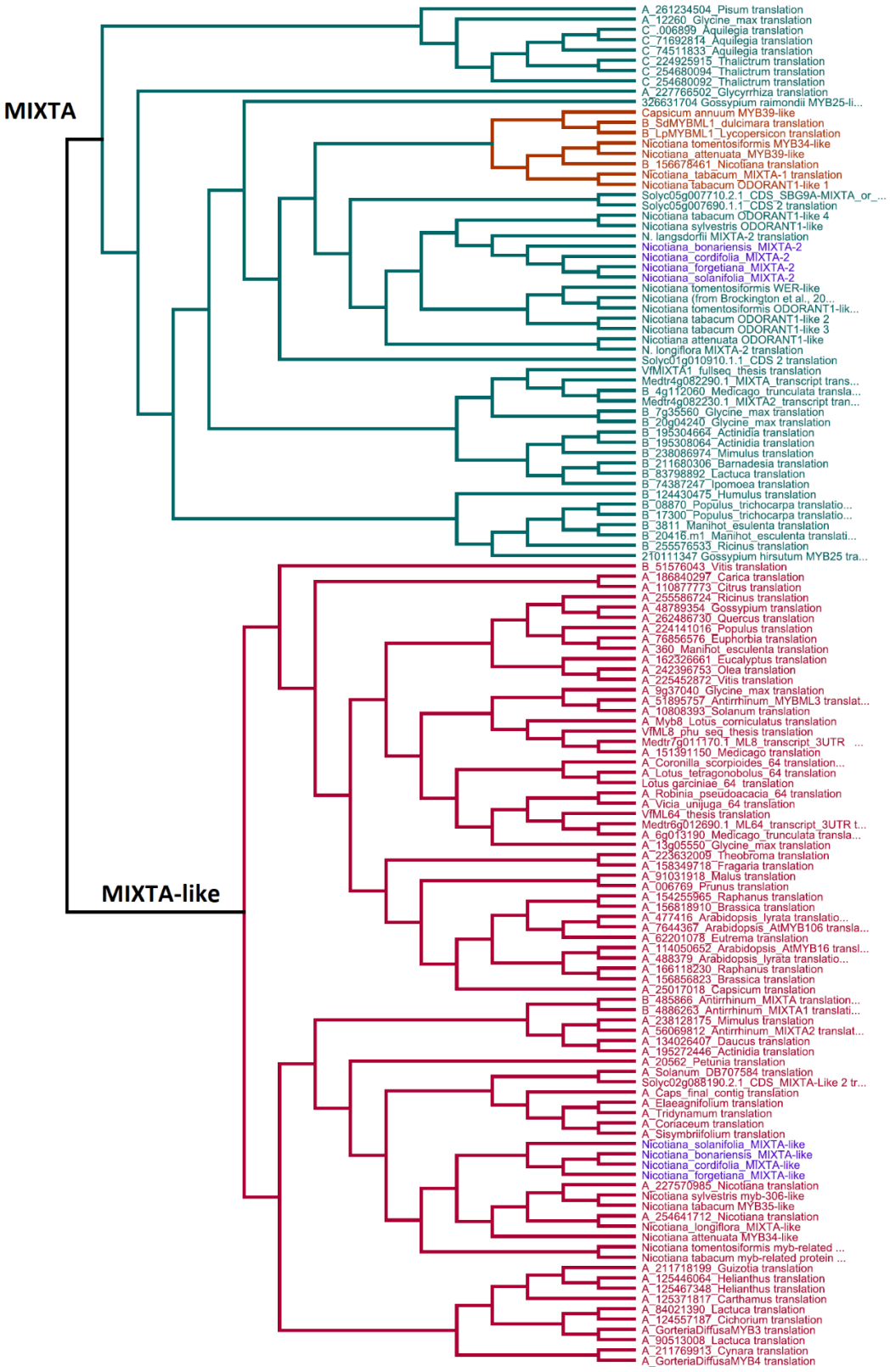
MIXTA
MIXTA-like
A_261234504_Pisum translation
A_12260_Glycine_max translation
C_006899_Aquilegia translation
C_71692814_Aquilegia translation
C_74511833_Aquilegia translation
C_224925915_Thalictrum translation
C_254680094_Thalictrum translation
C_254680092_Thalictrum translation
A_227766502_Glycyrrhiza translation
326631704 Gossypium raimondii MYB25-li...
Capsicum annuum MYB39-like
B_SdMYBML1_dulcimara translation
B_LpMYBML1_Lycopersicon translation
Nicotiana tomentosiformis MYB34-like
Nicotiana_attenuata_MYB39-like
B_156678461_Nicotiana translation
Nicotiana_tabacum_MIXTA-1 translation
Nicotiana tabacum ODORANT1-like 1
Solyc05g007710.2.1_CDS_SBG9A-MIXTA_or_...
Solyc05g007690.1.1_CDS 2 translation
Nicotiana tabacum ODORANT1-like 4
Nicotiana sylvestris ODORANT1-like
N. langsdorfii MIXTA-2 translation
Nicotiana_bonariensis_MIXTA-2
Nicotiana_cordifolia_MIXTA-2
Nicotiana_forgetiana_MIXTA-2
Nicotiana_solanifolia_MIXTA-2
Nicotiana tomentosiformis WER-like
Nicotiana (from Brockington et al., 20...
Nicotiana tomentosiformis ODORANT1-lik...
Nicotiana tabacum ODORANT1-like 2
Nicotiana tabacum ODORANT1-like 3
Nicotiana attenuata ODORANT1-like
N. longiflora MIXTA-2 translation
Solyc01g010910.1.1_CDS 2 translation
VfMIXTA1_fullseq_thesis translation
Medtr4g082290.1_MIXTA_transcript trans...
B_4g112060_Medicago_truncatula transla...
Medtr4g082230.1_MIXTA2_transcript tran...
B_7g35560_Glycine_max translation
B_20g04240_Glycine_max translation
B_195304664_Actinidia translation
B_195308064_Actinidia translation
B_238086974_Mimulus translation
B_211680306_Barnadesia translation
B_83798892_Lactuca translation
B_74387247_Ipomoea translation
B_124430475_Humulus translation
B_08870_Populus_trichocarpa translatio...
B_17300_Populus_trichocarpa translatio...
B_3811_Manihot_esculenta translation
B_20418.m1_Manihot_esculenta translati...
B_255576533_Ricinus translation
210111347 Gossypium hirsutum MYB25 tra...
B_51576043_Vitis translation
A_186840297_Carica translation
A_110877773_Citrus translation
A_255586724_Ricinus translation
A_48789354_Gossypium translation
A_262486730_Quercus translation
A_224141016_Populus translation
A_76856576_Euphorbia translation
A_360_Manihot_esculenta translation
A_162326661_Eucalyptus translation
A_242396753_Olea translation
A_225452872_Vitis translation
A_9g37040_Glycine_max translation
A_51895757_Antirrhinum_MYBML3 translat...
A_10808393_Solanum translation
A_Myb8_Lotus_corniculatus translation
VfML8_phu_seq_thesis translation
Medtr7g011170.1_ML8_transcript_3UTR ...
A_151391150_Medicago translation
A_Coronilla_scorpioides_64 translation...
A_Lotus_tetragonobolus_64 translation
Lotus garciniae_64 translation
A_Robinia_pseudoacacia_64 translation
A_Vicia_unijuga_64 translation
VfML64_thesis translation
Medtr6g012690.1_ML64_transcript_3UTR t...
A_6g013190_Medicago_truncatula transla...
A_13g05550_Glycine_max translation
A_223632009_Theobroma translation
A_158349718_Fragaria translation
A_91031918_Malus translation
A_006769_Prunus translation
A_154255965_Raphanus translation
A_156818910_Brassica translation
A_477416_Arabidopsis_lyrata translatio...
A_7644367_Arabidopsis_AtMYB106 transla...
A_62201078_Eutrema translation
A_114050652_Arabidopsis_AtMYB16 transl...
A_488379_Arabidopsis_lyrata translatio...
A_166118230_Raphanus translation
A_156856823_Brassica translation
A_25017018_Capsicum translation
B_485866_Antirrhinum_MIXTA translation...
B_4886263_Antirrhinum_MIXTA1 translati...
A_238128175_Mimulus translation
A_56069812_Antirrhinum_MIXTA2 translat...
A_134026407_Daucus translation
A_195272446_Actinidia translation
A_20562_Petunia translation
A_Solanum_DB707584 translation
Solyc02g088190.2.1_CDS_MIXTA-Like 2 tr...
A_Caps_final_contig translation
A_Elaeagnifolium translation
A_Tridynamum translation
A_Coriaceum translation
A_Sisymbriifolium translation
Nicotiana_solanifolia_MIXTA-like
Nicotiana_bonariensis_MIXTA-like
Nicotiana_cordifolia_MIXTA-like
Nicotiana_forgetiana_MIXTA-like
A_227570985_Nicotiana translation
Nicotiana sylvestris myb-306-like
Nicotiana tabacum MYB35-like
A_254641712_Nicotiana translation
Nicotiana_longiflora_MIXTA-like
Nicotiana attenuata MYB34-like
Nicotiana tomentosiformis myb-related ...
Nicotiana tabacum myb-related protein ...
A_211718199_Guizotia translation
A_125446064_Helianthus translation
A_125467348_Helianthus translation
A_125371817_Carthamus translation
A_84021390_Lactuca translation
A_124557187_Cichorium translation
A_GorteriaDiffusaMYB3 translation
A_90513008_Lactuca translation
A_211769913_Cynara translation
A_GorteriaDiffusaMYB4 translation

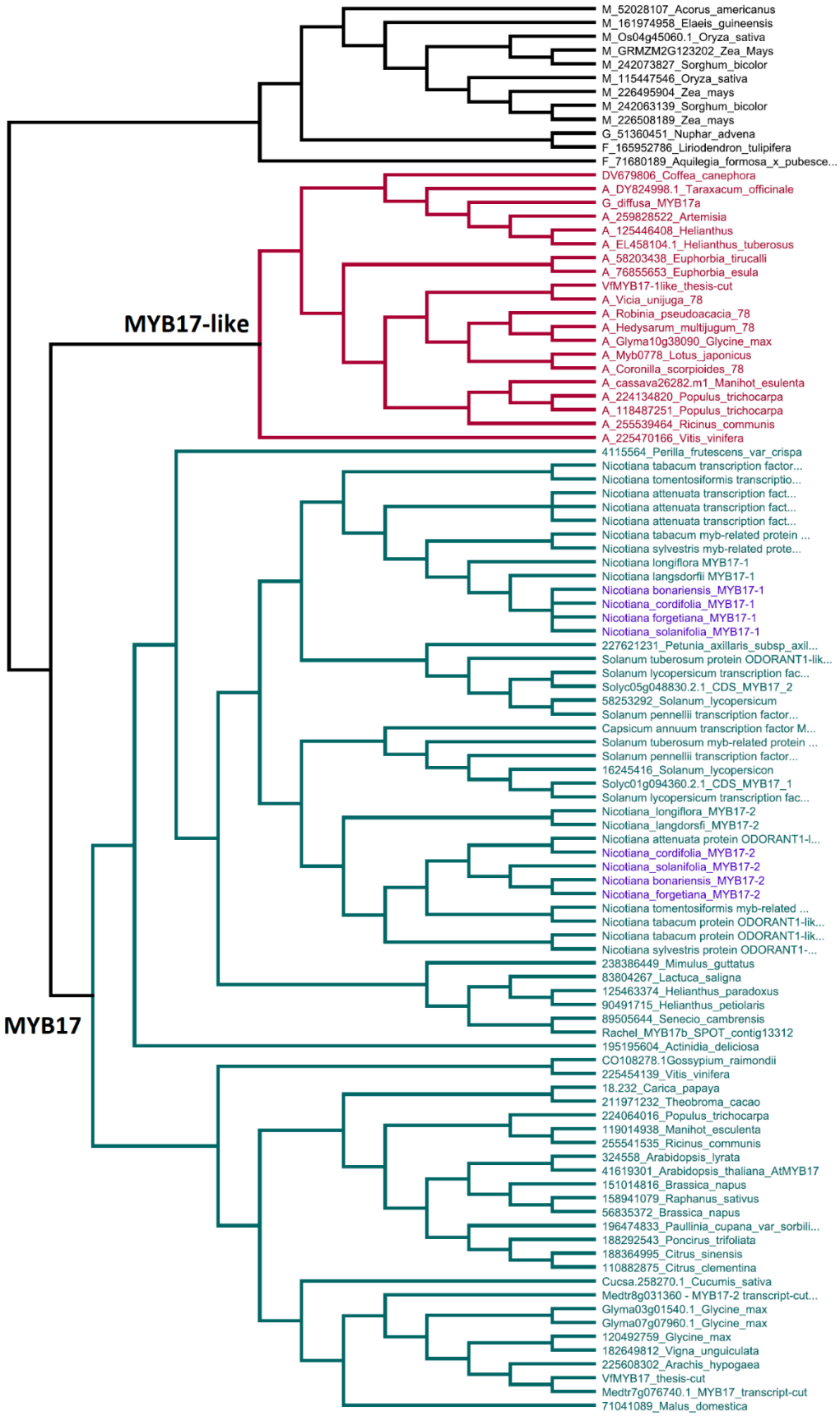

Phylogram of the R2R3 Subgroup 9B MYB transcription factors including additional sequences of the Solanales. Clade MYB17 is represented in green and MYB17-like in red. Newly included sequences from this work are highlighted in purple.

Appendix 4. Plant sources and accessions.

Section	Species	Material type	Source	Accession number
Alatae	*Nicotiana forgetiana*	Seed	GRIN- USDA	TW50
	Nicotiana bonariensis	Seed	GRIN- USDA	TW28
Paniculatae	*Nicotiana cordifolia*	Seed	Jean-Lous Verrier (Imperial Tobacco Inc., France)	
	Nicotiana solanifolia	Seed	GRIN- USDA	TW 123
Repandae	*Nicotiana nesophila*	Seed	GRIND-USDA	TW 87
Suaveolentes	*Nicotiana forsteri*	Seed	GRIN- USDA	TW 43
	Nicotiana occidentalis	Seed	Unconfirmed	??A247?0140
	Nicotiana simulans	Seed	GRIN- USDA	TW 122
	Nicotiana umbratica	Seed	GRIN-USDA	TW 144

GRIN-USDA = US *Nicotiana* Germplasm Collection, Department of Crop Sciences, North Carolina State University, US

Appendix 5. Recipes

CTAB buffer (autoclaved)

2% CTAB powder

100mM Tris HCl pH 8

20mM EDTA pH 8

1.4M NaCl

After autoclave: 2% PVP 40

TRIZOL (guanidinium-acid-phenol reagents)

4M guanidine isothiocyanate

25mM sodium citrate pH7.0

0.5% sarkosyl

2M sodium acetate pH 4

Quick DNA extraction buffer

10mL 1M Tris-HCl pH 7.5

2.5mL 5M NaCl

2.5mL 0.5M EDTA pH 7.5

2.5mL 10% SDS

33.75mL ddH2O

10 × TBE buffer (autoclaved)

880mM Tris base

880mM Boric acid

40mM EDTA pH 8.0

6 x DNA loading dye

For 10 mL:

25 mg Bromophenol blue

25 mg Xylene cyanol FF

1.5 g Ficoll 400

LB (autoclaved)

10gL^{-1} tryptone

5gL^{-1} yeast extract

5gL^{-1} NaCl

LBA (autoclaved)

10gL^{-1} tryptone

5gL^{-1} yeast extract

5gL^{-1} NaCl

12gL^{-1} Bacto Agar

Miniprep Sol1

50mM glucose

25mM TrisHCl (pH 8.0)

10mM EDTA (pH 8)

Miniprep Sol2

0.2M NaOH

1% SDS

Miniprep Sol 3

60mL 5M potassium acetate

11.5mL glacial acetic acid

28.5mL dH_2O

Appendix 6. Lists of primers

A. Primers used to amplify different gene regions

Gene	Region amplified	Direction of primer	Primer Name	Sequence	Expected Fragment (bp)
MIXTA-2	5' END	Forward	Nic_MIXTA-2_F0	TGGGAAGGTCCAAGTGCTGTG	310
		Reverse	NfNc_5'_MIXTA-2_GW_Rnest	TCTCGTTGTCTGTTCTGCTAGGC	
	3' END	Forward	Nbona_MIXTA-2_1F	CACAAACAACATTAATGGTAGCTCAAATG	672
		Reverse	Nf_MIXTA-2_1R	GGAGATCCAATTGGTGAAGTGACC	
	Intermediate	Forward	Nic_MIXTA_F6	AACCTTAGTCATATGGCTGAATGG	252
		Reverse	Nicotiana_forgetiana_MIXTA-2_R1	AGCAAAACCATCAACAAGAATAGAA	
MIXTA-like	5' END	Forward	Nic_ML_F4	ATGGGTCGATCTCCATGCTG	639
		Reverse	Nic_ML_R3	AACACCATTCCACGCCTTGAG	
	3' END	Forward	Nforget_ML_Nest_2_1F	CAATACGTGGACAGCTGAATCTCTAAG	259
		Reverse	Nic_ML_R5	TTAAAACATAGCCGAATCAGAGGGTG	
	Intermediate	Forward	Nicotiana forgetiana MIXTA-LIKE F1	CTTCACCTTCTAGTCCTCTTAACAA	496
		Reverse	Nic_ML_R2	GTCTCCACAAAATTGCCAGGGG	
MYB17-1	5' END	Forward	Nf_MYB17-1_1F	ATGGGGAGAATACCATGTTGTGA	292
		Reverse	Nicotiana_forgetiana_MYB17-1_R1	CAGGAAGTTGCGATGCGATT	
	3' END	Forward	Nbona_MYB17-1_F2	TGGGCTGTTGAGAAGACCGC	837
		Reverse	Nbona_MYB17-1_1R	GCCAAGAAAGCTCATGTCATTG	
	Intermediate	Forward	Nicotiana_forgetiana_MYB17-1_F1	CCAAACGAGGTCCCTTTAGC	439
		Reverse	Nic_MYB17-1_R6	GCAGATGAAGATACTTGAGAGGC	
MYB17-2	5' END	Forward	Nf_MYB17-2_1F	ATGGGGAGAATACCATGTTGTGA	502
		Reverse	Nicotiana_forgetiana_MYB17-2_R1	GTCTTTCCAGAGAGTCCCAAC	
	3' END	Forward	Nbona_MYB17-2_1F	CAGAGATAGGAGAGACATTTAGG	407
		Reverse	Nic_MYB17-2_R2	GAACATGCAGTCTGCTTCCTC	
	Intermediate	Forward	Nicotiana_forgetiana_MYB17-2_F1	TGAACCATCCTCTGCCTCTAA	256
		Reverse	Nic_MYB17-2_R3	TTGAGAAGCTCGACTTTGAGAATC	

B. Primers used to amplify entire coding sequences

Gene of interest	Primer		Sequence	Phusion Tm (°C)	Phusion Tm (°C) for pair	Expected fragment (bp)	Plasmid Digestion
MIXTA-2	**Forward**	Nic_MIXTA-2_F10	ATGGGAAGGTCCAAGTGCTGTG	69.7	68	1041	HindIII HF/EcoRI HF (Cutsmart Buffer)
	Reverse	Nsola_MIXTA-2_R1	TCAGAATAATGGAGATCCAATTGG	65			
MIXTA-like	**Forward**	Nic_ML_F4	ATGGGTCGATCTCCATGCTG	67.7	67.7	1251	PstI/SalI HF (NEB Buffer 3.1)
	Reverse	Nic_ML_R5	TTAAAACATAGCCGAATCAGAGGGTG	68.6			
MYB17-1	**Forward**	Nf_MYB17-1_1F	ATGGGGAGAATACCATGTTGTGA	66.5	62.5	897	PstI/SalI HF (NEB Buffer 3.1)
	Reverse	Nic_MYB17-1_R10	TTAGAGAAAGCCAACTCTATGG	59.5			
MYB17-2	**Forward**	Nf_MYB17-2_1F	ATGGGGAGAATACCATGTTGTGA	66.5	69.5	973	NA
	Reverse	Nic_MYB17-2_R11	TCAGAGGAAGCAGACTGCATGTTC	69.1			

C. Primers used to test expression of transgenes in putative *Nicotiana tabacum* transgenic lines

Overexpressing gene	Primer Name	Sequence	Expected Fragment (bp)	Tranferred similarity to species of interest (%)	Transferred similarity to *N. tabacum* (%)
MIXTA-2	NTrans_MIXTA-2_F1	CCAAAAACTCTTGTCTTGCATTG	716	100	91.3
	NTrans_MIXTA-2_R1	GATCACCAACTCTTGTCATACT		100	<50
MIXTA-like	NTrans_ML_F2	GGTGGACTAATTACCTAAGGCC	889	100	90.9
	NTrans_ML_R2	CCCCTAGCAATTTTGTGGAGAC		100	90.9
MYB17-1	Nbona_MYB17-1_1F	GATAGGAGAAGCATTTAGGAAATTC	280	100	84
	Nbona_MYB17-1_1R	CAATGACATGAGCTTTCTTGGC		100	90.9

D. Primers used in semiquantitative and qRT-PCR expression analyses

Primer Name	Description	Sequence	Applications
NtUBQF	Forward primer for Nicotiana ubiquitin (UBQ) genes	GAGCTCTGACACCATCGACA	cDNA and gDNA test control gene
NtUBQF	Reverse primer for Nicotiana ubiquitin (UBQ) genes	ACATCACGACCACAACCAGA	cDNA and gDNA test control gene
Nic_COX-1_F1	Forward primer for *Nicotiana* cytochrome oxidase I (COX-1) genes	TAAGAAACGACAAATCCCAACT	Used in semiquantitative PCR and RTqPCR
Nic_COX-1_R1	Reverse primer for *Nicotiana* cytochrome oxidase I (COX-1) genes	TCTTAGGGCTTTCGGGTATG	Used in semiquantitative PCR and RTqPCR
Nic_Gt_F1	Forward primer for Nicotiana glutamyl transferase (Gt) genes	ATGCTGAGGAAGGAGAGGAATT	Used in RTqPCR
Nic_Gt_R1	Reverse primer for Nicotiana glutamyl transferase (Gt) genes	GACACTTGGGTCATCAGCTGA	Used in RTqPCR

E. Primers for housekeeping genes used in semiquantitative and qPCR expression analyses

Primer Name	Description	Sequence	Applications
NtUBQF	Forward primer for Nicotiana ubiquitin (UBQ) genes	GAGCTCTGACACCATCGACA	cDNA and gDNA test control gene
NtUBQF	Reverse primer for Nicotiana ubiquitin (UBQ) genes	ACATCACGACCACAACCAGA	cDNA and gDNA test control gene
Nic_COX-1_F1	Forward primer for *Nicotiana* cytochrome oxidase I (COX-1) genes	TAAGAAACGACAAATCCCAACT	Used in semiquantitative PCR and qPCR
Nic_COX-1_R1	Reverse primer for *Nicotiana* cytochrome oxidase I (COX-1) genes	TCTTAGGGCTTTCGGGTATG	Used in semiquantitative PCR and qPCR
Nt_EF1α_F	Forward primer for Nicotiana elongation factor 1 alfa (EF1α) genes	TGAGATGCACCACGAAGCTC	Used in qPCR
Nt_EF1α_R	Reverse primer for Nicotiana elongation factor 1 alfa (EF1α) genes	CCAACATTGTCACCAGGAAGTG	Used in qPCR
Nt_L25_F	Forward primer for Nicotiana ribosomal protein L25 (L25) genes	CCCCTCACCACAGAGTCTGC	Used in qPCR
Nt_L25_R	Reverse primer for Nicotiana ribosomal protein L25 (L25) genes	AAGGGTGTTGTTGTCCTCAATCTT	Used in qPCR

Appendix 7. DNA sequence alignments for R2R3 Subgroup 9 genes in Nicotiana spp.

Appendix 7A. DNA alignment for putative *MIXTA-2* sequences in *Nicotiana* spp. including sequences of *N. bonariensis, N. cordifolia, N. forgetiana* and *N. solanifolia* obtained in this work.

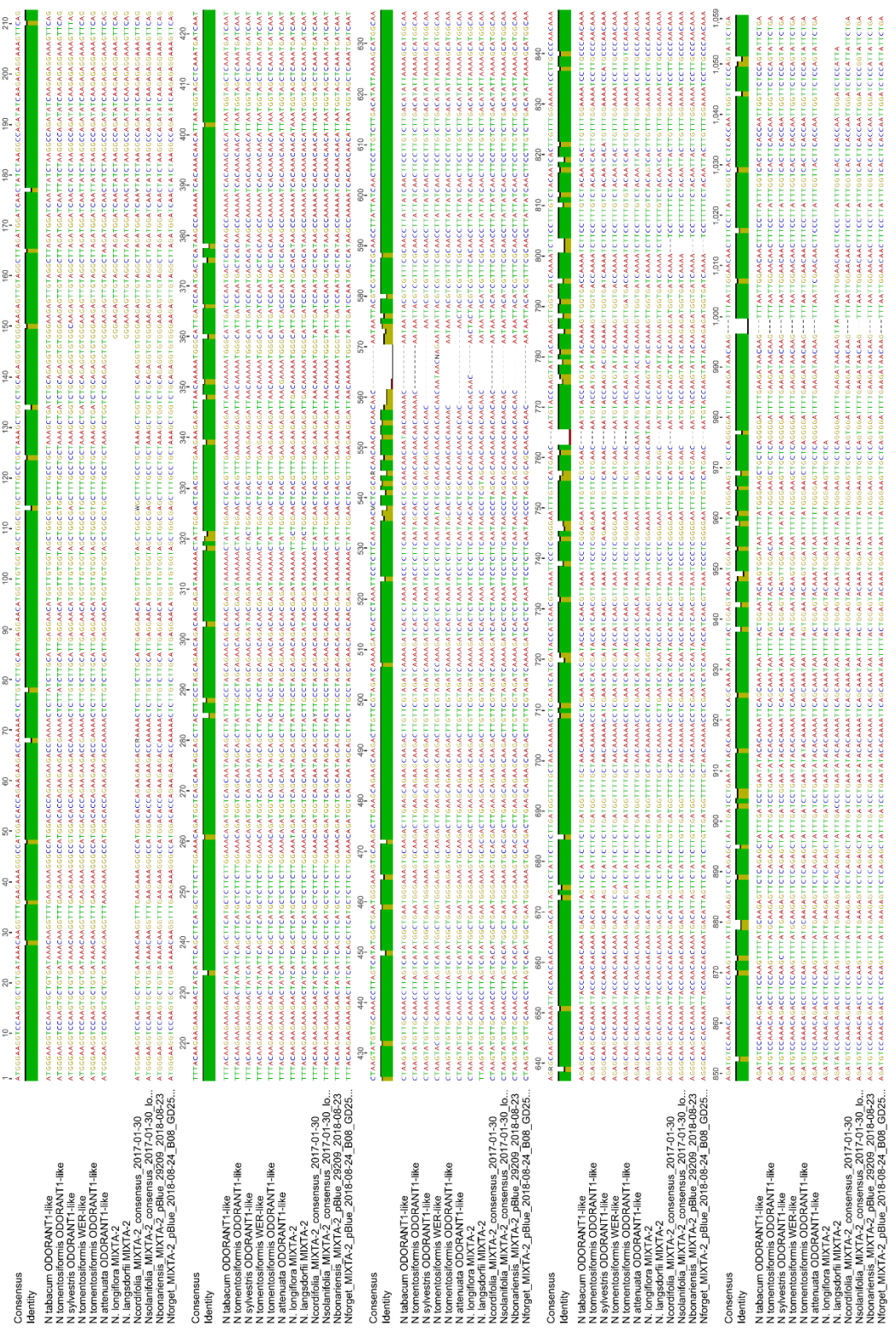

Appendix 7B. DNA alignment for putative *MIXTA-like* sequences in *Nicotiana* spp. including sequences of *N. bonariensis, N. cordifolia, N. forgetiana* and *N. solanifolia* obtained in this work.

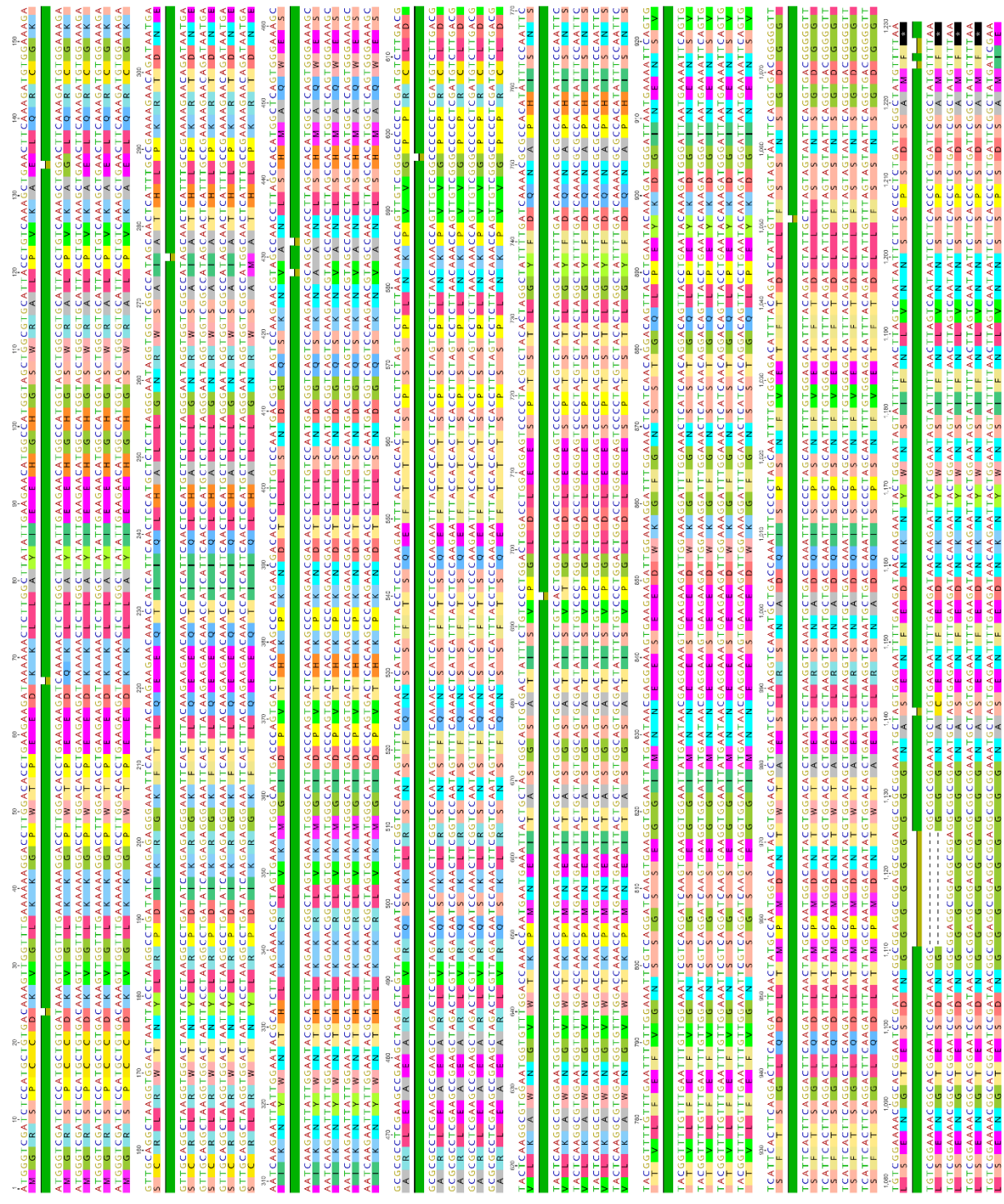

Appendix 7C. DNA alignment for putative *MYB17-1* sequences in *Nicotiana* spp. including sequences of *N. bonariensis, N. cordifolia, N. forgetiana* and *N. solanifolia* obtained in this work.

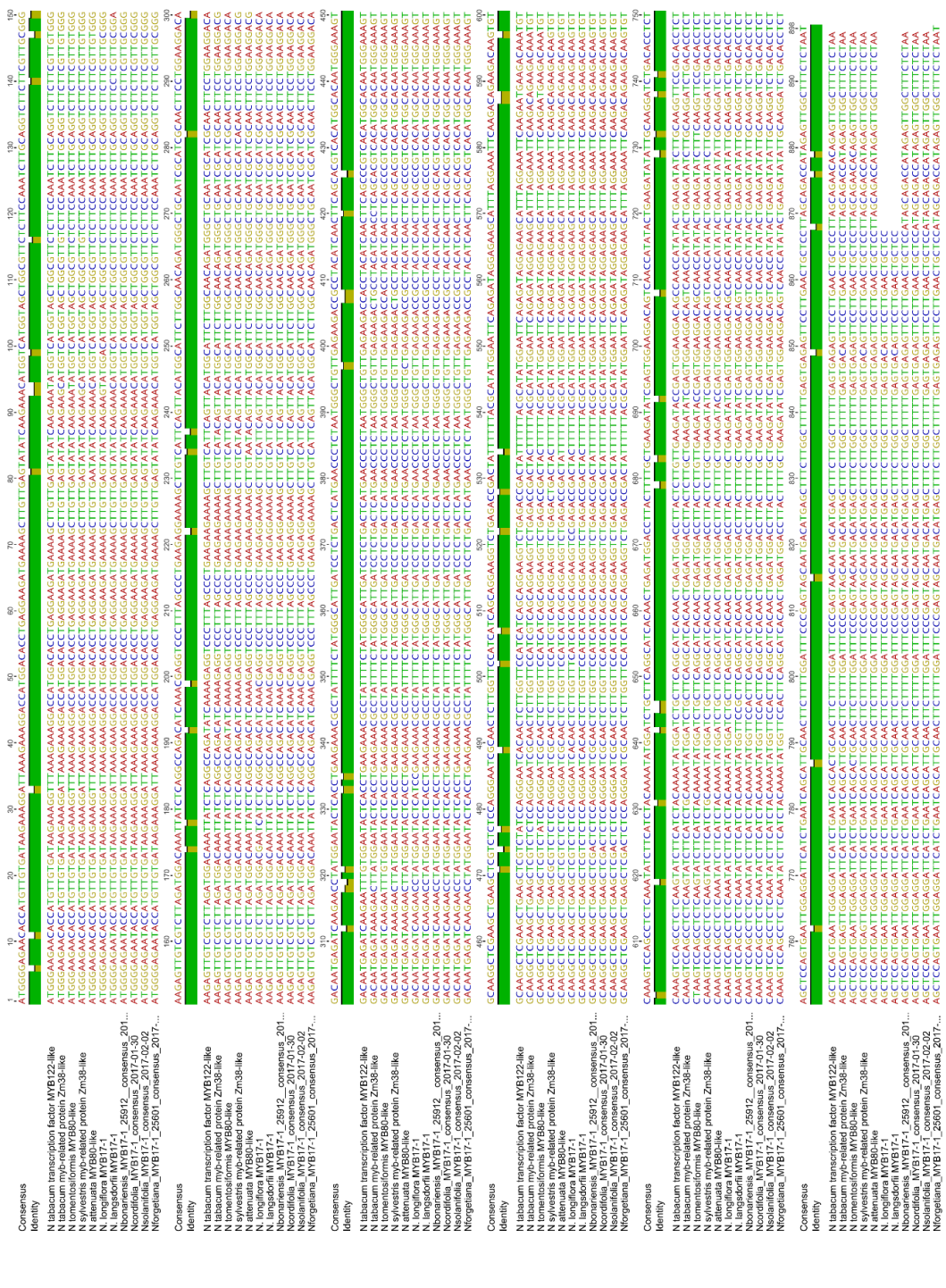

Appendix 7D. DNA alignment for putative *MYB17-2* sequences in *Nicotiana* spp. including sequences of *N. bonariensis, N. cordifolia, N. forgetiana* and *N. solanifolia* obtained in this work.

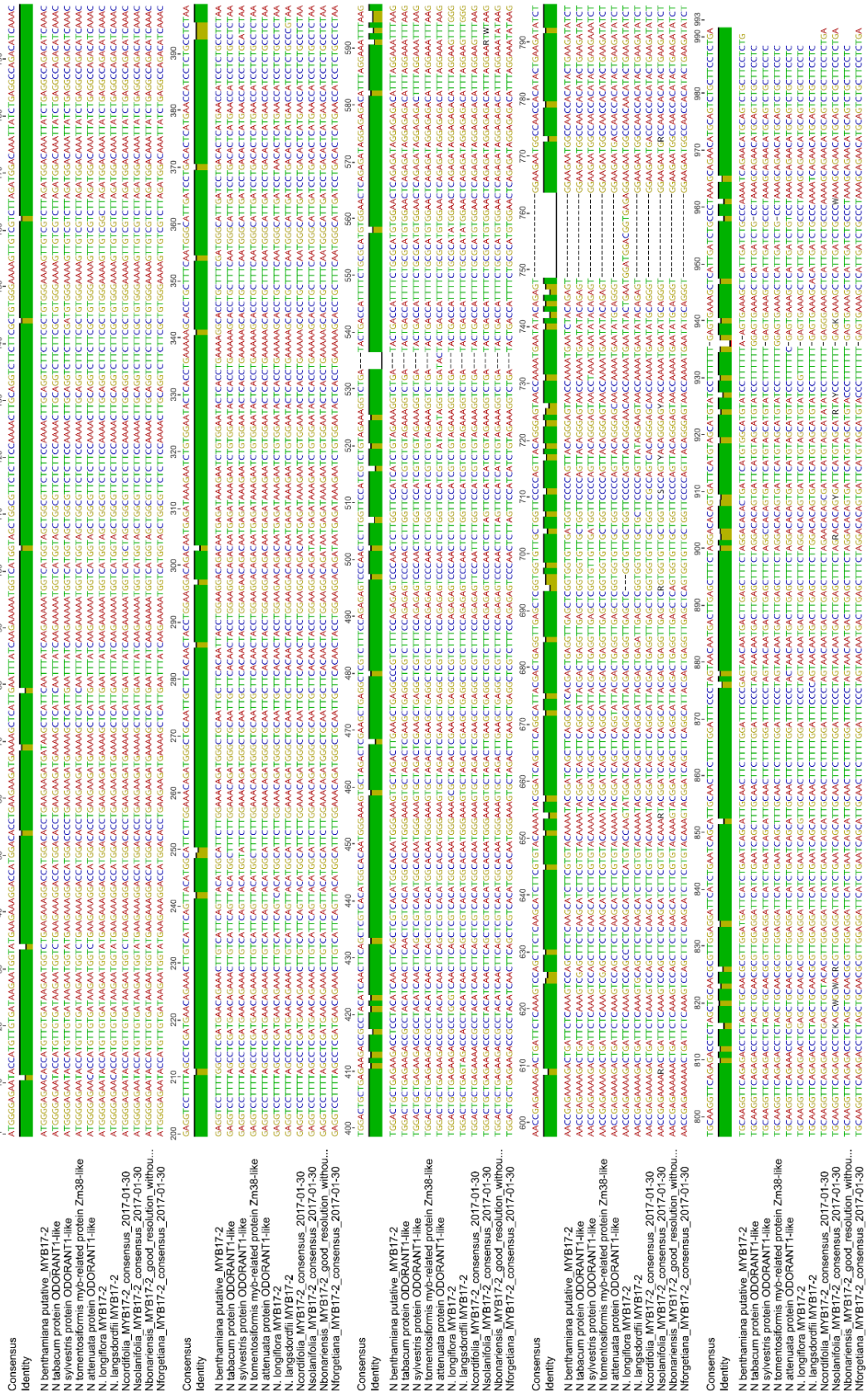

Appendix 8. PCR confirmation of *N. tabacum* lines expressing *NcMIXTA-like* and *NsMIXTA-like*.

RT-PCR products of *NcMIXTA-like* and *NsMIXTA-like* resulting from amplification of cDNA from leaves from putative *N. tabacum* transgenic lines, were sequenced to confirm the identify the origin of the amplicon: native sequence of *N. tabacum* or positive expression of the transgene. The alignment includes the putative sequence of *MIXTA-like* in *N. tabacum* from a BLAST search, a sequence of *NcMIXTA-like* cloned in pBlue, the product of amplification in *N. tabacum* WT, and the product of amplification of four putative transgenic lines expressing *NcMIXTA-like,* and eight putative transgenic lines expressing *NsMIXTA-like.* Primers specific for the transgene are indicated with pink bands. A 24 bp insertion (yellow shade) present only in *NcMIXTA-like* and *NsMIXTA-like* (not shown) and not in *N. tabacum* was considered as a diagnostic feature to identify expression of the transgene. Four lines were identified as positively expressing *NcMIXTA-like* and six *NsMIXTA-like.*

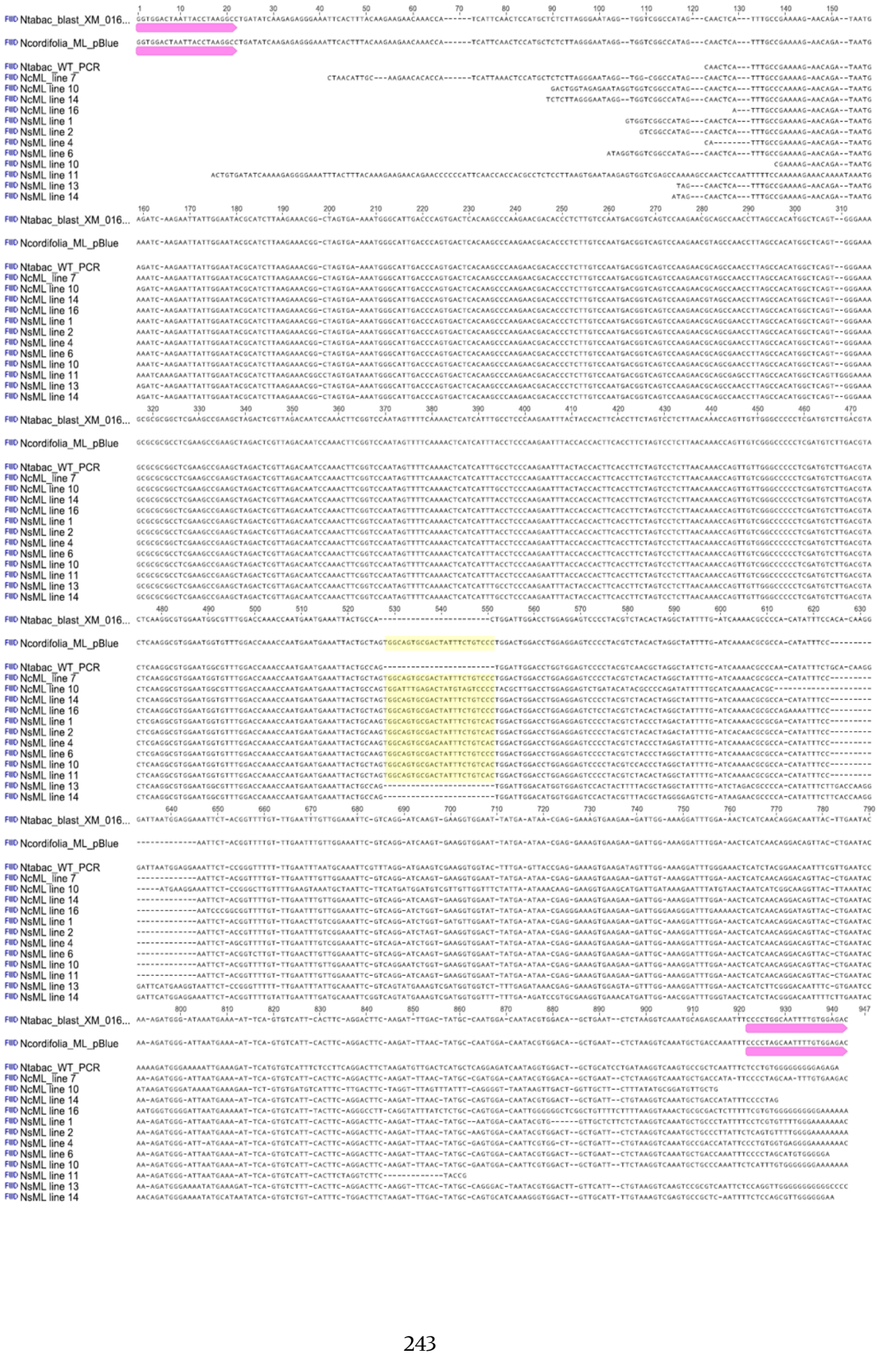
Ntabac_blast_XM_016...
Ncordifolia_ML_pBlue
Ntabac_WT_PCR
NcML_line 7
NcML_line 10
NcML_line 14
NcML_line 16
NsML_line 1
NsML_line 2
NsML_line 4
NsML_line 6
NsML_line 10
NsML_line 11
NsML_line 13
NsML_line 14

Appendix 9. Additional images of transgenics expressing genes from Section *Paniculatae*

LIST OF PLATES

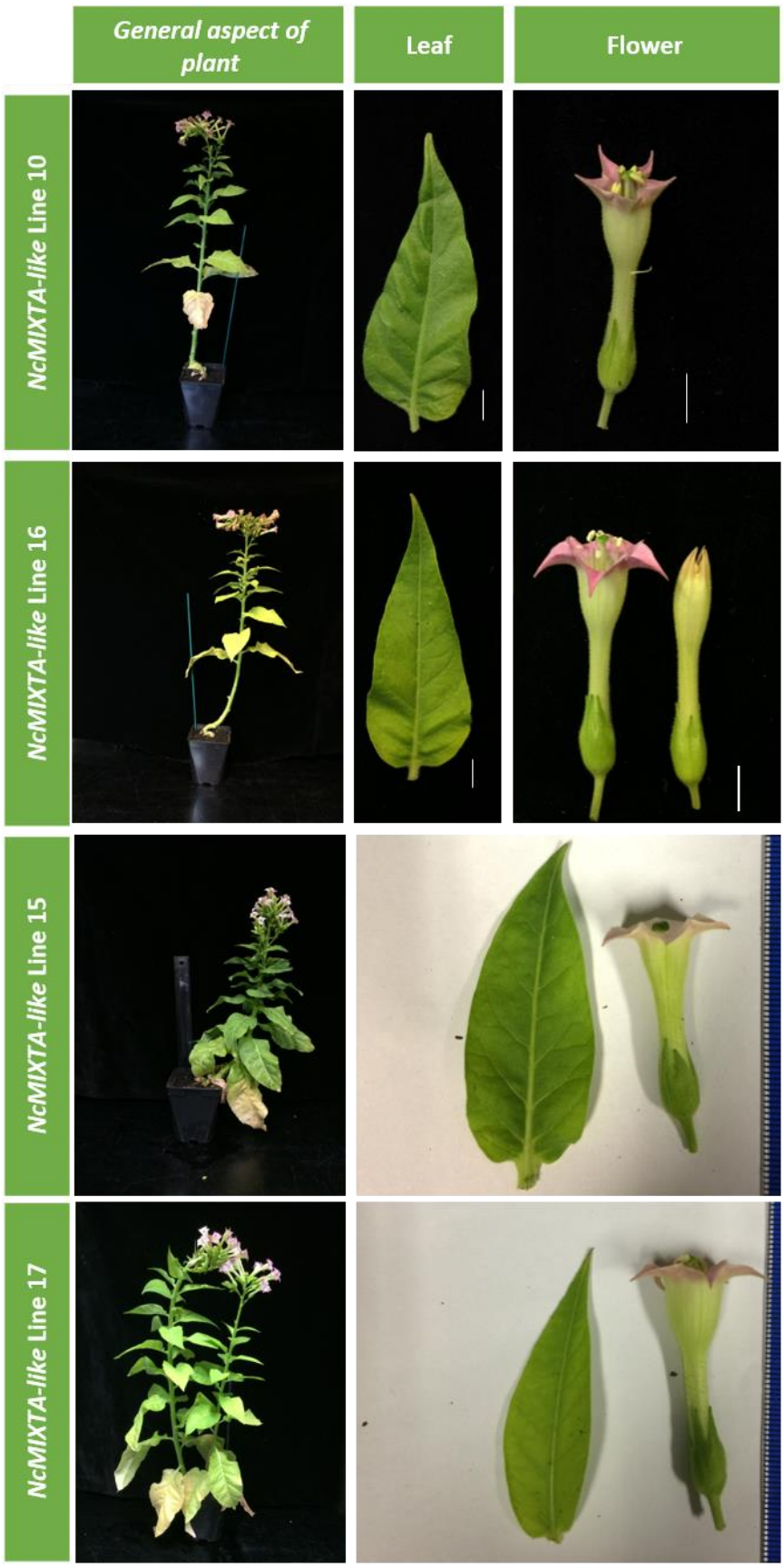

Plate I. Macromorphology of *N. tabacum* transgenic lines expressing *NcMIXTA-like*.
Scale bars= 1 cm

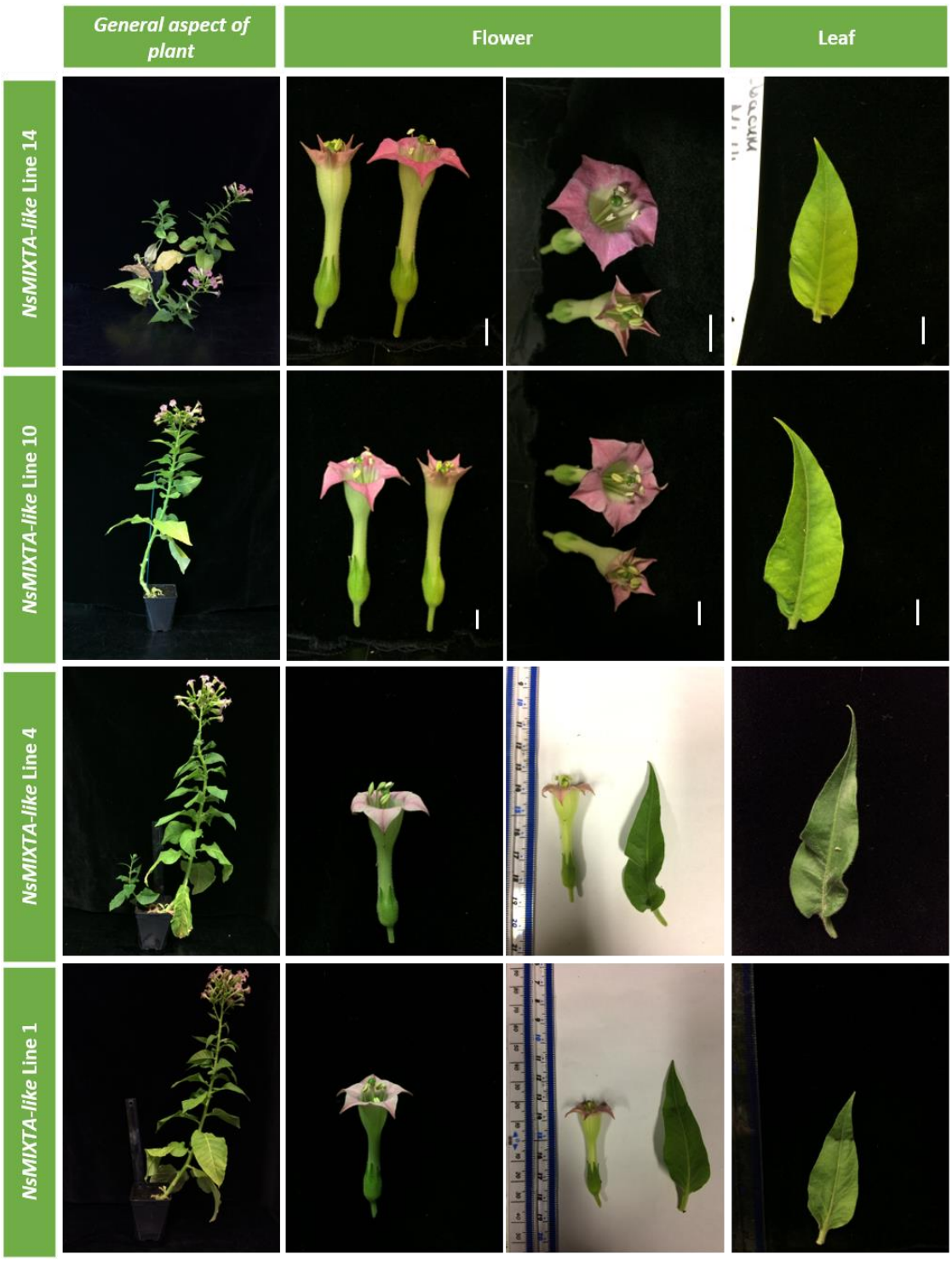

Plate II. Macromorphology of *N. tabacum* transgenic lines expressing *NsMIXTA-like*.
Scale bars= 1cm

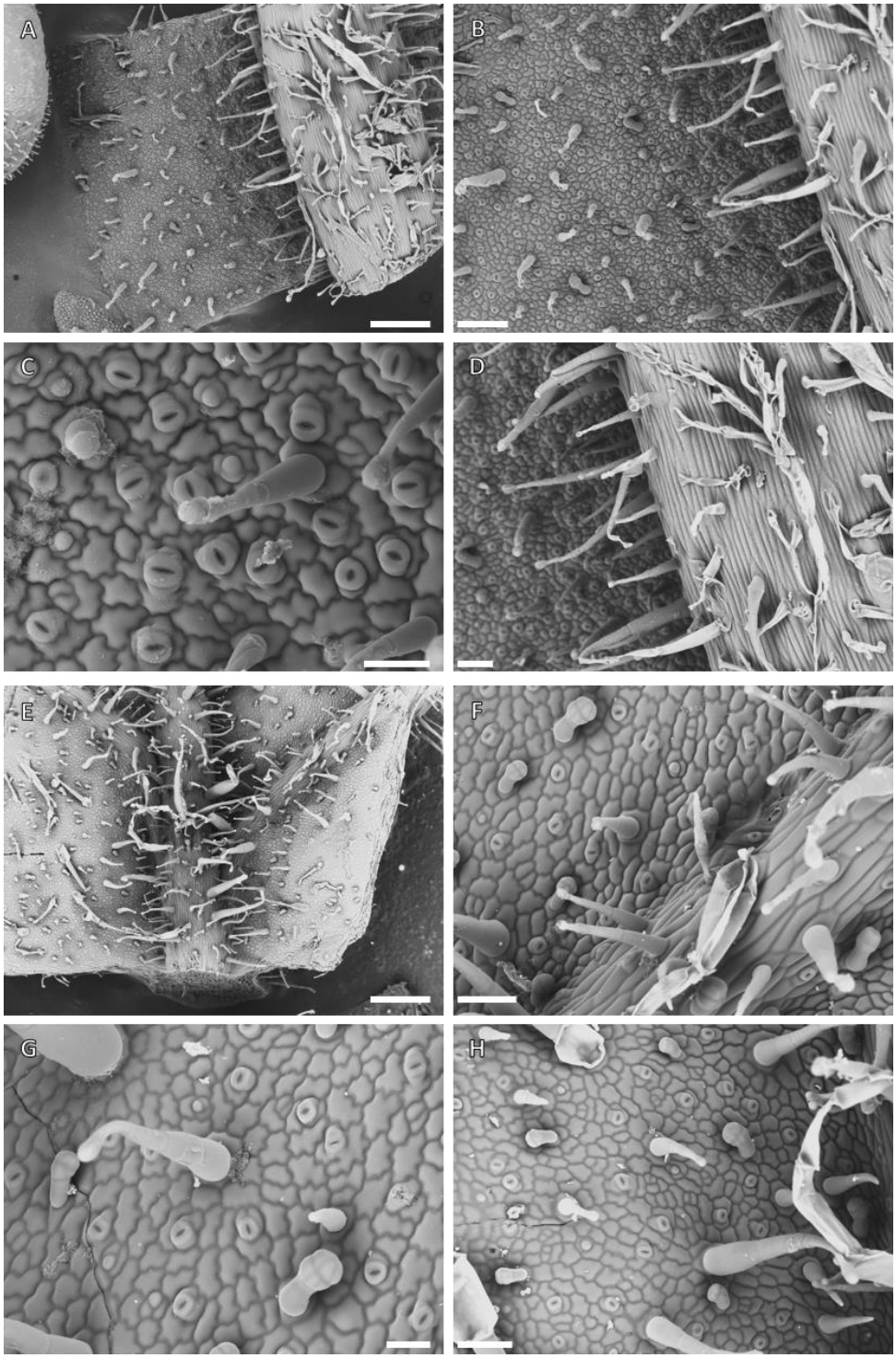

Plate III. Epidermal features on leaf of *N. tabacum* WT.
Cryo-SEM microphotographs of epidermal features on leaf of *N. tabacum* WT. A-D. Abaxial leaf; E-H. Adaxial leaf. Scale bars: A, E=500µm, B=200µm, C, D, F, H=100µm, G=50µm.

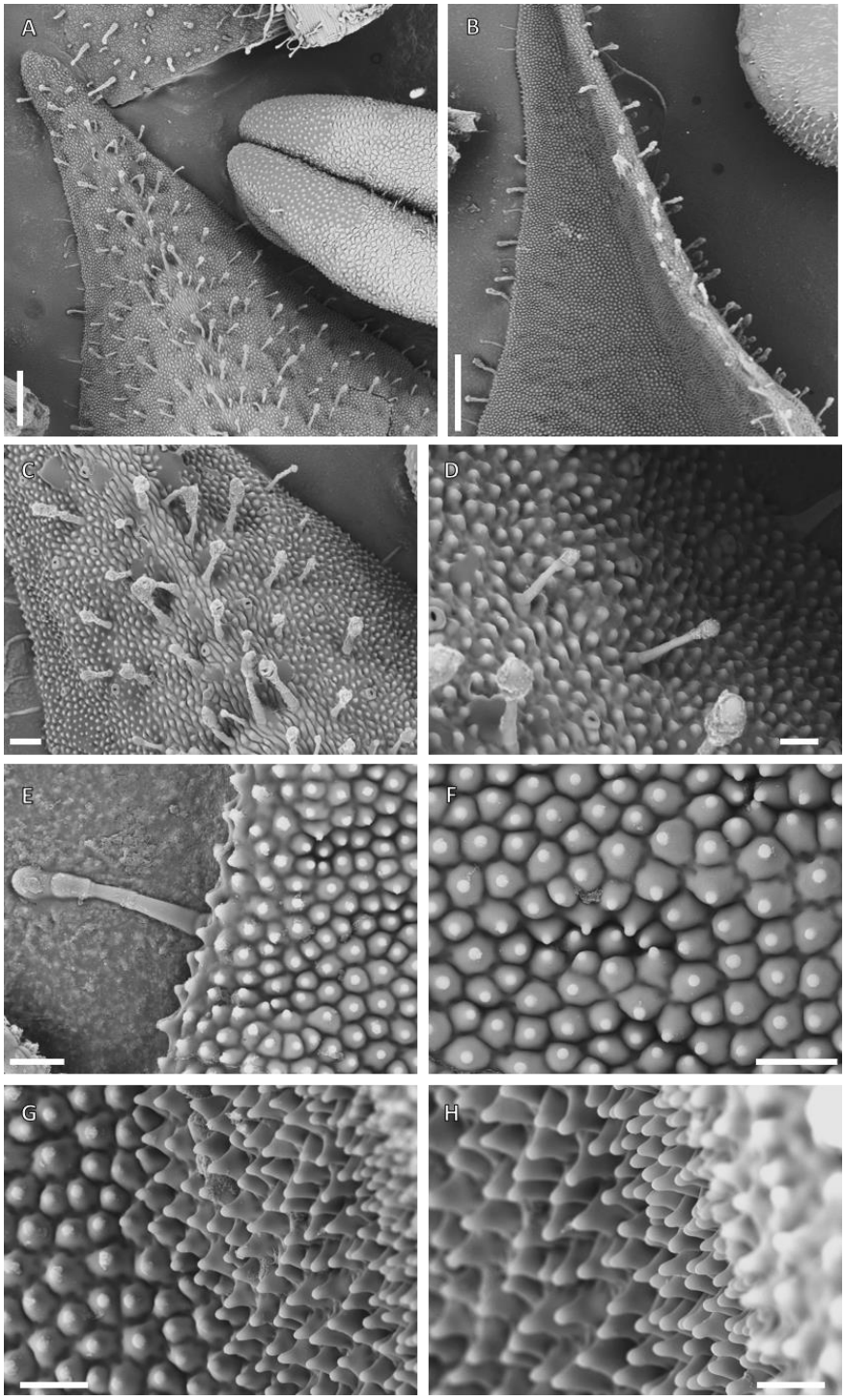

Plate IV. Epidermal features on petal of *N. tabacum* WT.
Cryo-SEM microphotographs of epidermal features on petal of *N. tabacum* WT. A, C-D. Abaxial petal; B, E-H. Adaxial petal. Scale bars: A-B=500µm, C=100µm, D-H=50µm

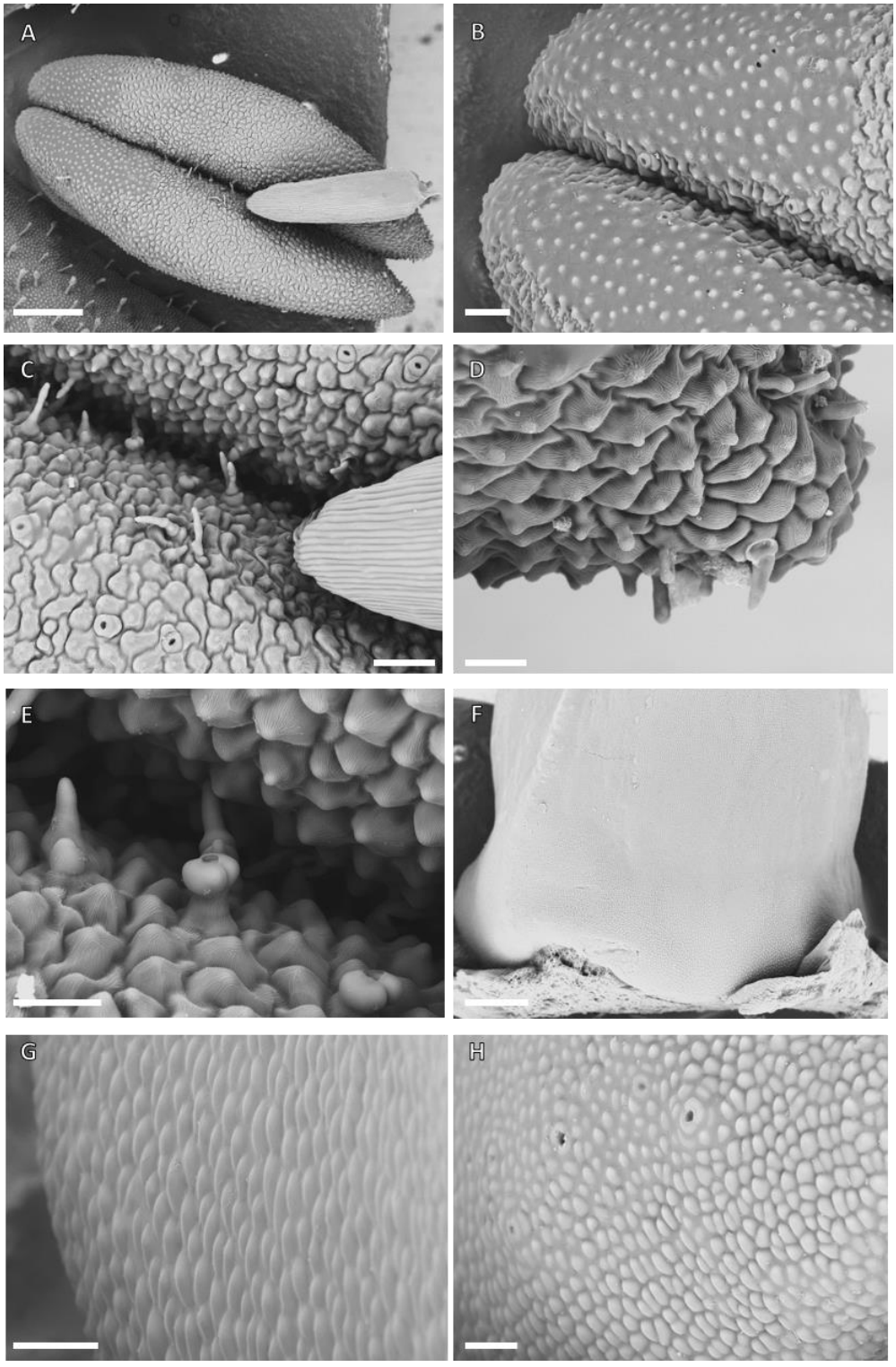

Plate V. Epidermal features on anther and carpel of *N. tabacum* WT.
Cryo-SEM microphotographs of epidermal features on anther and carpel of *N. tabacum* WT. A-E. Anther; F-H. Carpel. Scale bars: A, F=500µm, B-C=100µm, D-E, G-H=50µm

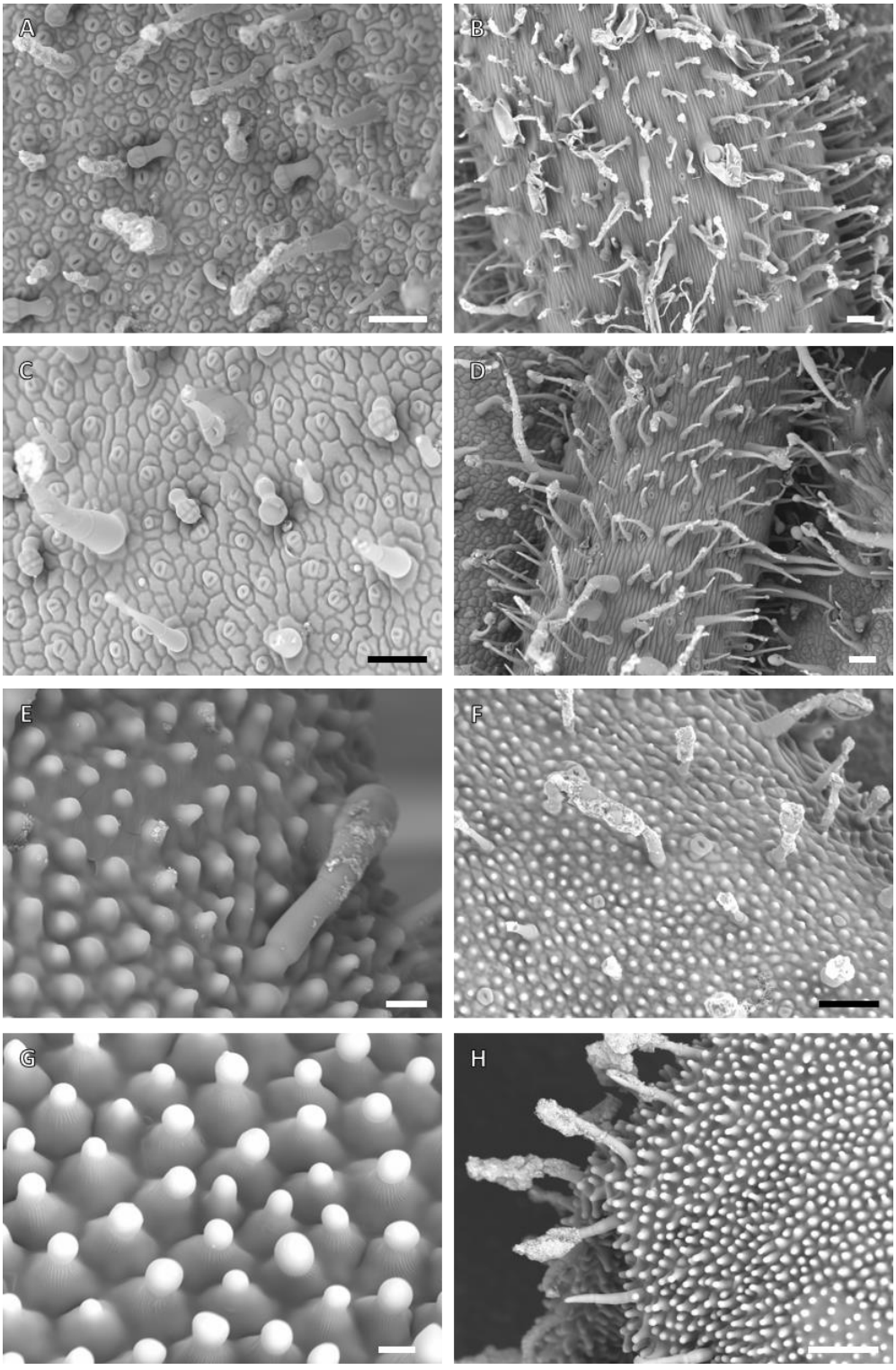

Plate VI. Epidermal features on *N. tabacum* lines expressing *NcMIXTA-like* (line 10).
Cryo-SEM microphotographs of epidermal features in *N. tabacum* 35S:*NcMIXTA-like*, Line 10. A-B. Abaxial leaf; C-D. Adaxial leaf; E-F. Abaxial petal; G-H. Adaxial petal. Scale bars: A-D, F, H=100µm, E=20µm, G=10µm

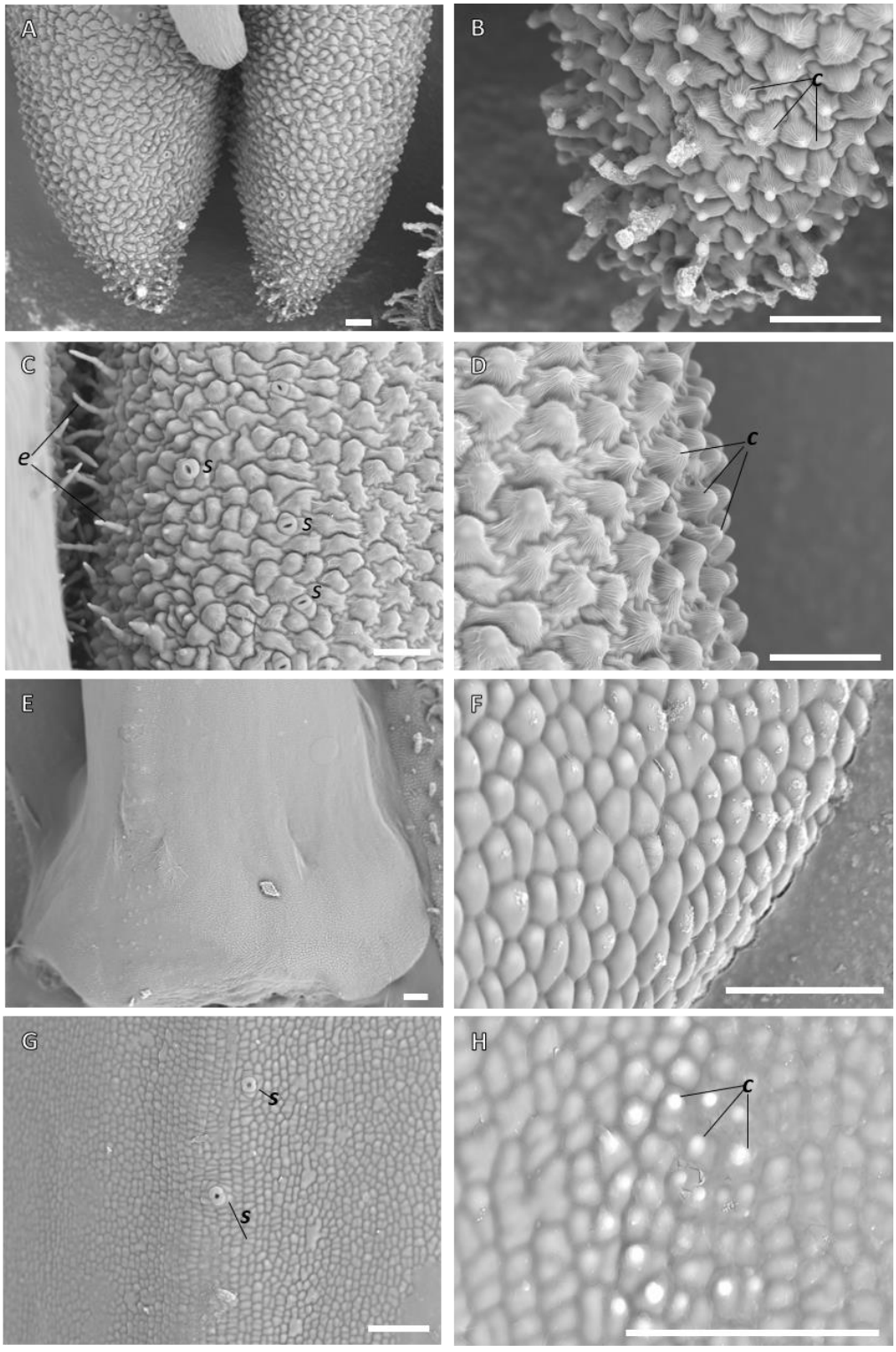

Plate VII. Epidermal features on *N. tabacum* lines expressing *NcMIXTA-like* (line 10).

Cryo-SEM microphotographs of epidermal features in anther and carpel of *N. tabacum* 35S:*NcMIXTA-like*, Line 10. A-D. Anther. A. Anther base; B. Detail on pollen sac basal tip. C. Detail on the proximal surface relative to the filament. D. Detail on the distal surface relative to the filament. E-H. Carpel. E. General aspect of the carpel base. F. Detail on the cells at the base. G. Epidermal cells and stomata along the medial zone of the carpel. H. Conical cells on the medial zone of the carpel. O=Epidermal outgrowths, c=conical cell, s: stomata. Scale bars: A=200µm, B-H=100µm

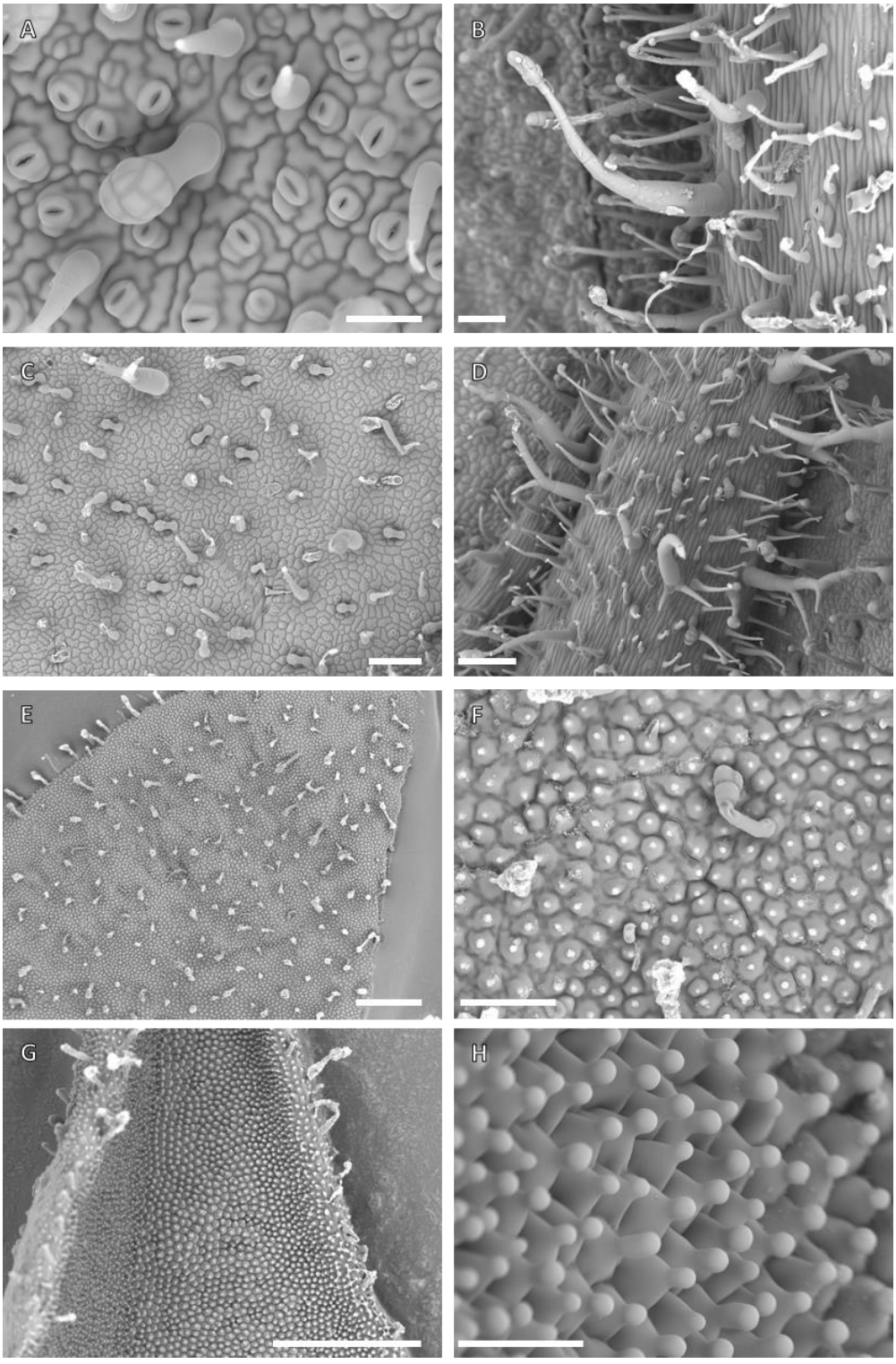

Plate VIII. Epidermal features of *N. tabacum* lines expressing *NcMIXTA-like* (line 14).
Cryo-SEM microphotographs of epidermal features on leaf and petal of *N. tabacum* 35S::*NcMIXTA-like*, Line 14. A-B. Abaxial leaf; C-D. Adaxial leaf; E-F. Abaxial petal; G-H. Adaxial petal. Scale bars: A, F, H=50µm, B=100µm, C-D=200µm, E, G=500µm

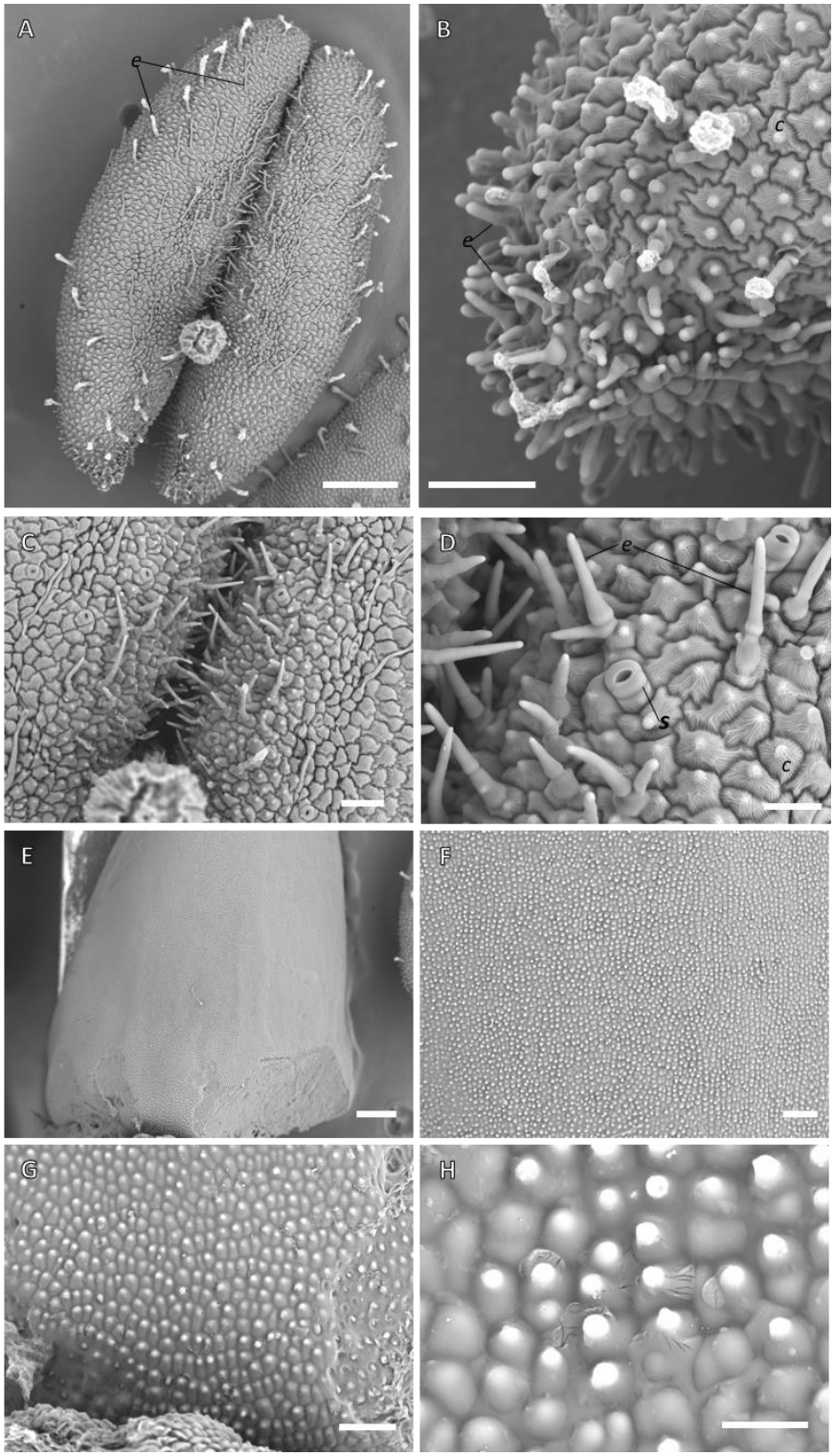

Plate IX. Epidermal features of *N. tabacum* lines expressing *NcMIXTA-like* (line 14).

Cryo-SEM microphotographs of epidermal features on anther and carpel of *N. tabacum* 35S::*NcMIXTA-like*, Line 14. A-D. Anther; E-H. Carpel. A. Anther base; B. Detail on pollen sac basal tip. C. Detail on the proximal pollen sac. D. Close-up on C. E. General aspect of the carpel base. F. Conical cells on the medial zone of the carpel. G. Conical cells at the base of the carpel. H. Close-up on conical cells on the medial zone of the carpel. e=epidermal outgrowths, c=conical cell, s: stomata. Scale bars: A, E=500µm; B-C, F-G=100µm; D, H=50µm

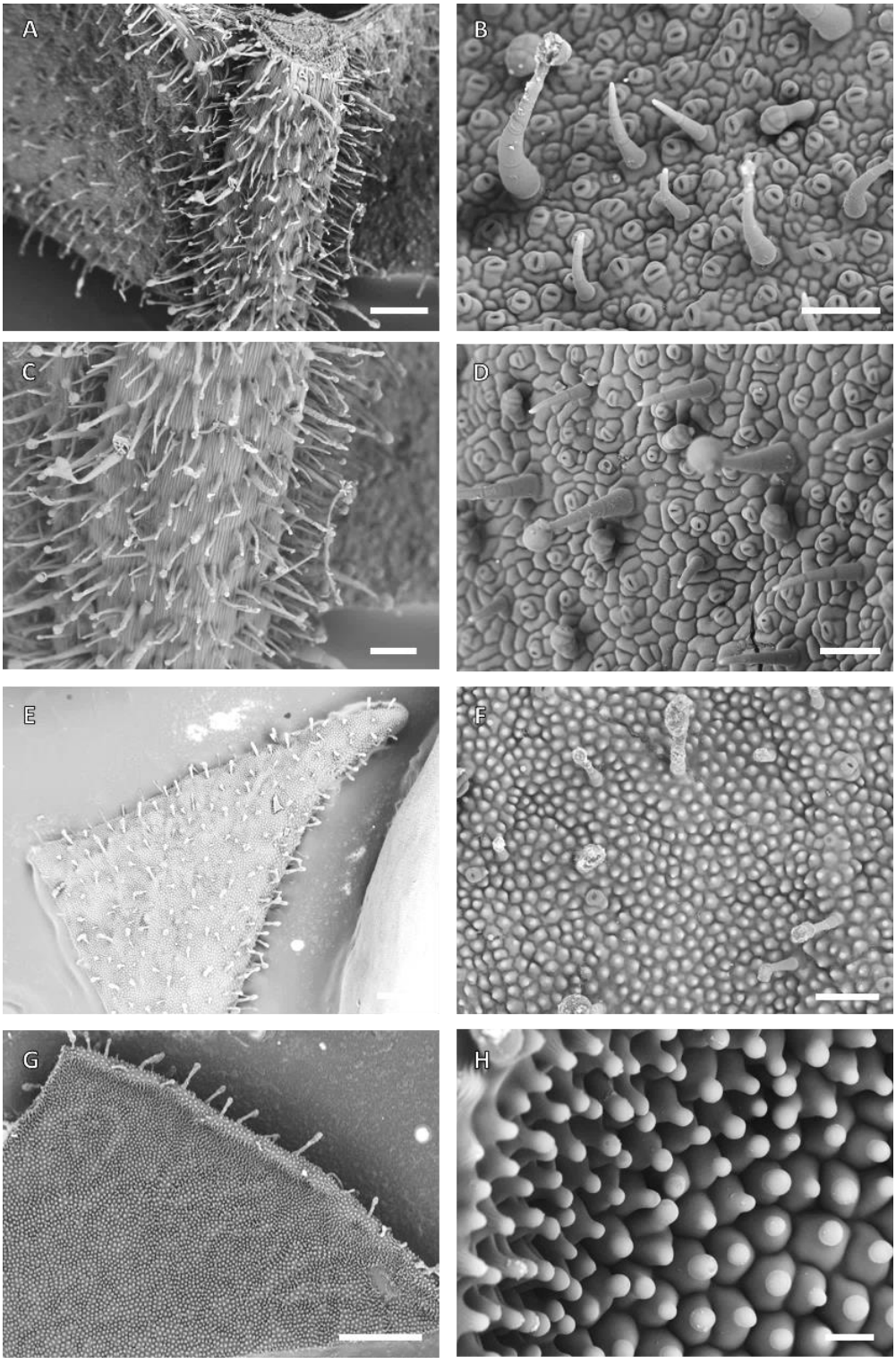

Plate X. Epidermal features of *N. tabacum* lines expressing *NcMIXTA-like* (line 15).

Cryo-SEM microphotographs of epidermal features on leaf and petal of *N. tabacum* 35S::*NcMIXTA-like*, Line 15. A-B. Abaxial leaf; C-D. Adaxial leaf; E-F. Abaxial petal; G-H. Adaxial petal. Scale bars: A, E, G=500µm, B, D,F=100µm, C=200µm, H=20µm

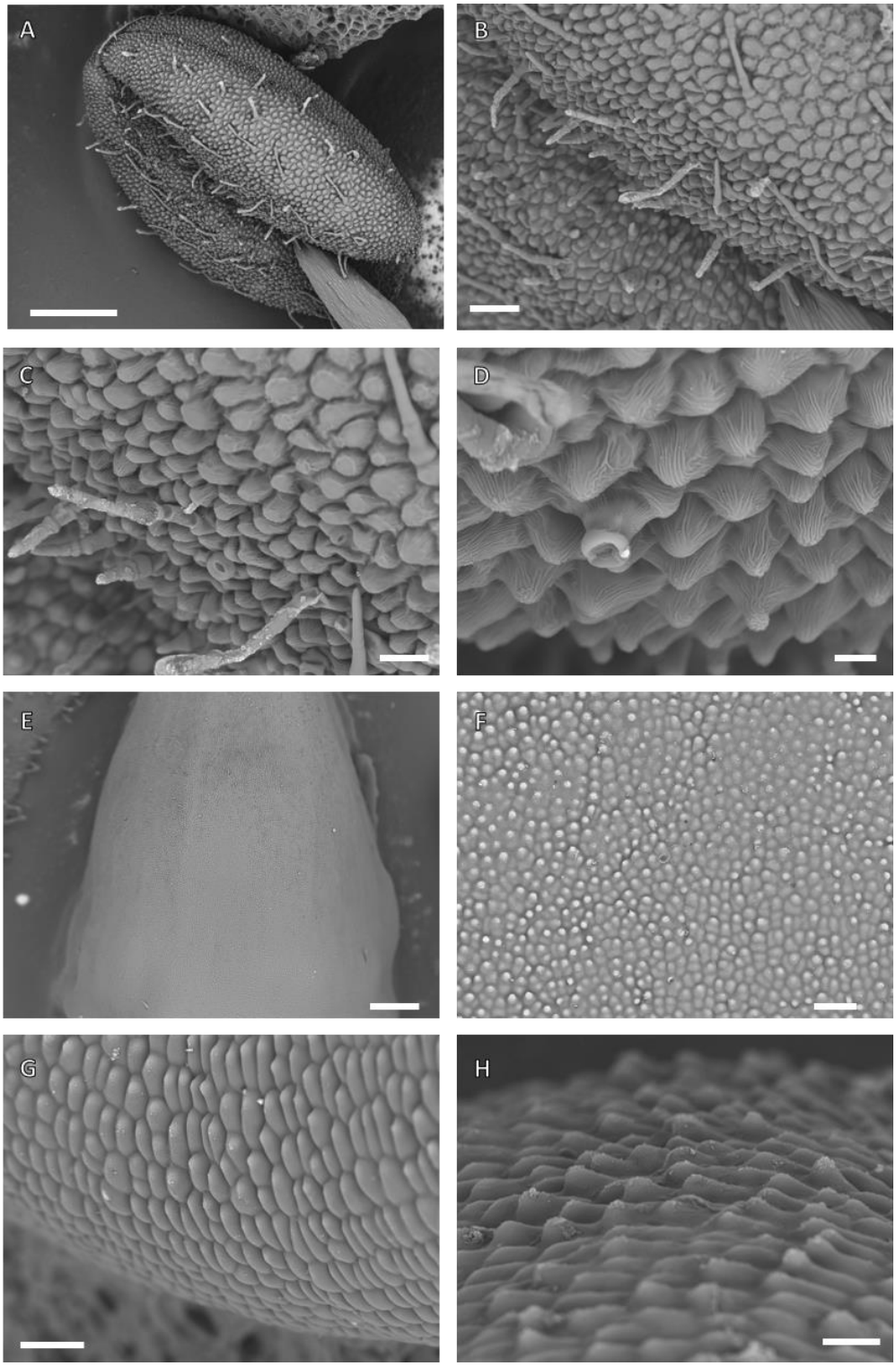

Plate XI. Epidermal features of *N. tabacum* lines expressing *NcMIXTA-like* (line 15).

Cryo-SEM microphotographs of epidermal features on anther and carpel of *N. tabacum* 35S::*NcMIXTA-like*, Line 15. A-D. Anther; E-H. Carpel. A. Anther base; B. Detail on pollen sac basal tip. C. Detail on the proximal pollen sac. D. Close-up on C. E. General aspect of the carpel base. F. Conical cells on the medial zone of the carpel. G. Conical cells at the base of the carpel. H. Close-up on conical cells on the medial zone of the carpel. e=epidermal outgrowths, c=conical cell, s: stomata. Scale bars: A, E=500µm; B=100µm; C, F, G=50µm; D, H=20µm.

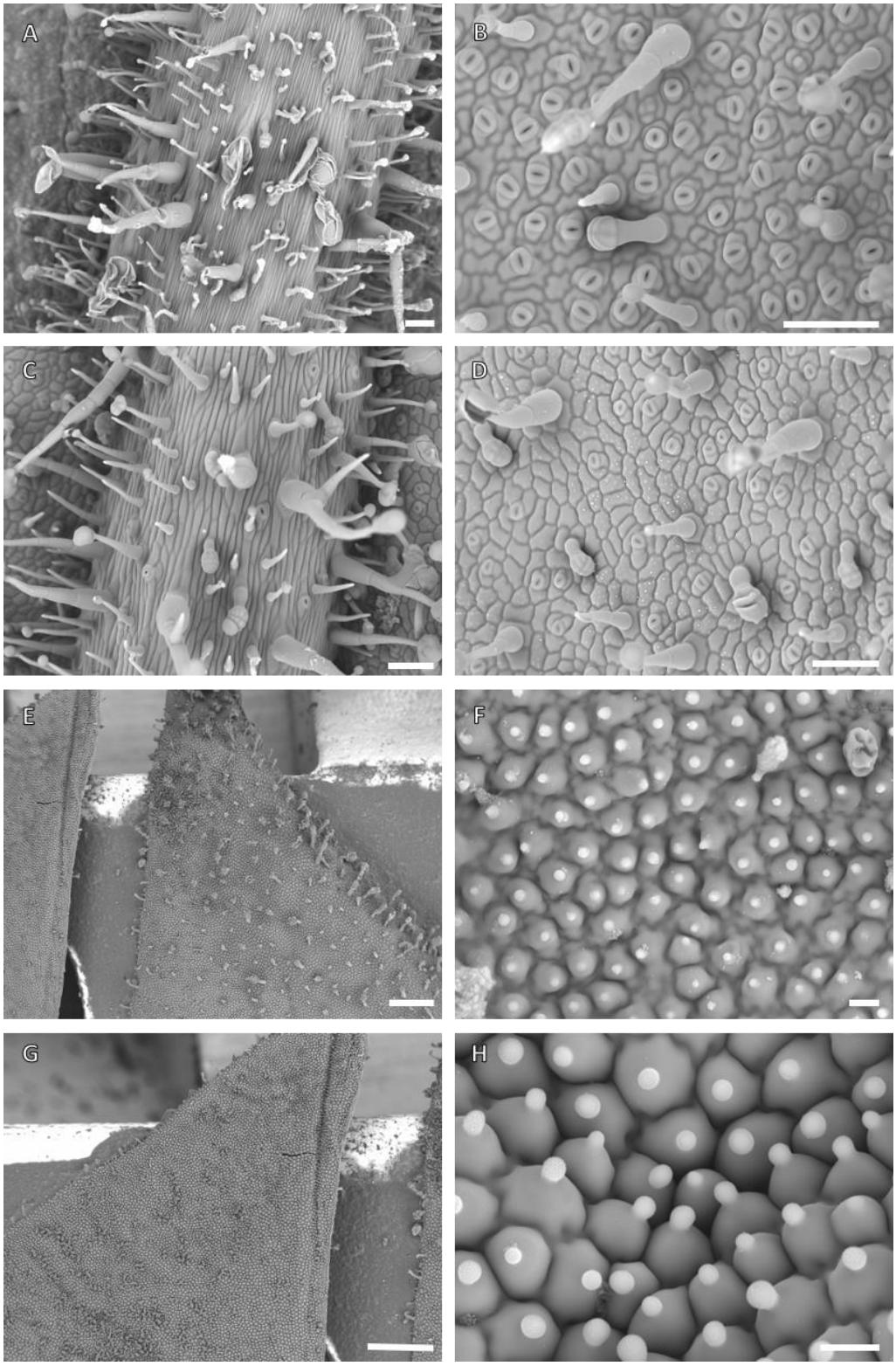

Plate XII. Epidermal features of *N. tabacum* lines expressing *NcMIXTA-like* (line 16).

Cryo-SEM microphotographs of epidermal features on leaf and petal of *N. tabacum* 35S::*NcMIXTA-like*, Line 16. A-B. Abaxial leaf; C-D. Adaxial leaf; E-F. Abaxial petal; G-H. Adaxial petal. Scale bars: A-D=100µm, F, H=20µm, E, G=500µm

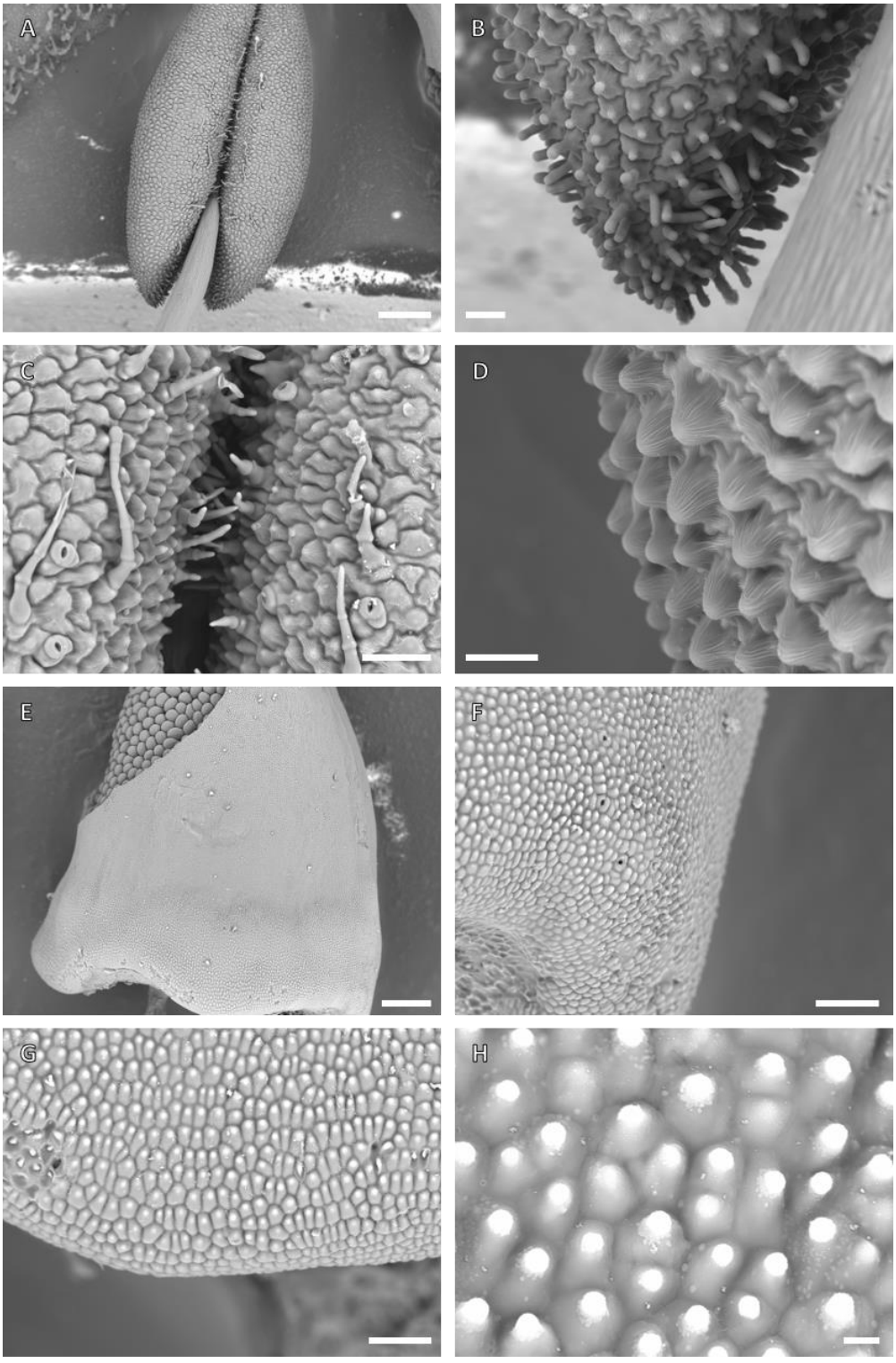

Plate XIII. Epidermal features of *N. tabacum* lines expressing *NcMIXTA-like* (line 16).

Cryo-SEM microphotographs of epidermal features on anther and carpel of *N. tabacum* 35S::*NcMIXTA-like*, Line 16. A-D. Anther; E-H. Carpel. A. Anther base; B. Detail on pollen sac basal tip. C. Detail on the proximal pollen sac. D. Close-up on C. E. General aspect of the carpel base. F. Conical cells on the medial zone of the carpel. G. Conical cells at the base of the carpel. H. Close-up on conical cells on the medial zone of the carpel. e=epidermal outgrowths, c=conical cell, s: stomata. Scale bars: A, E=500µm; B-C, F-G=100µm; D, H=50µm

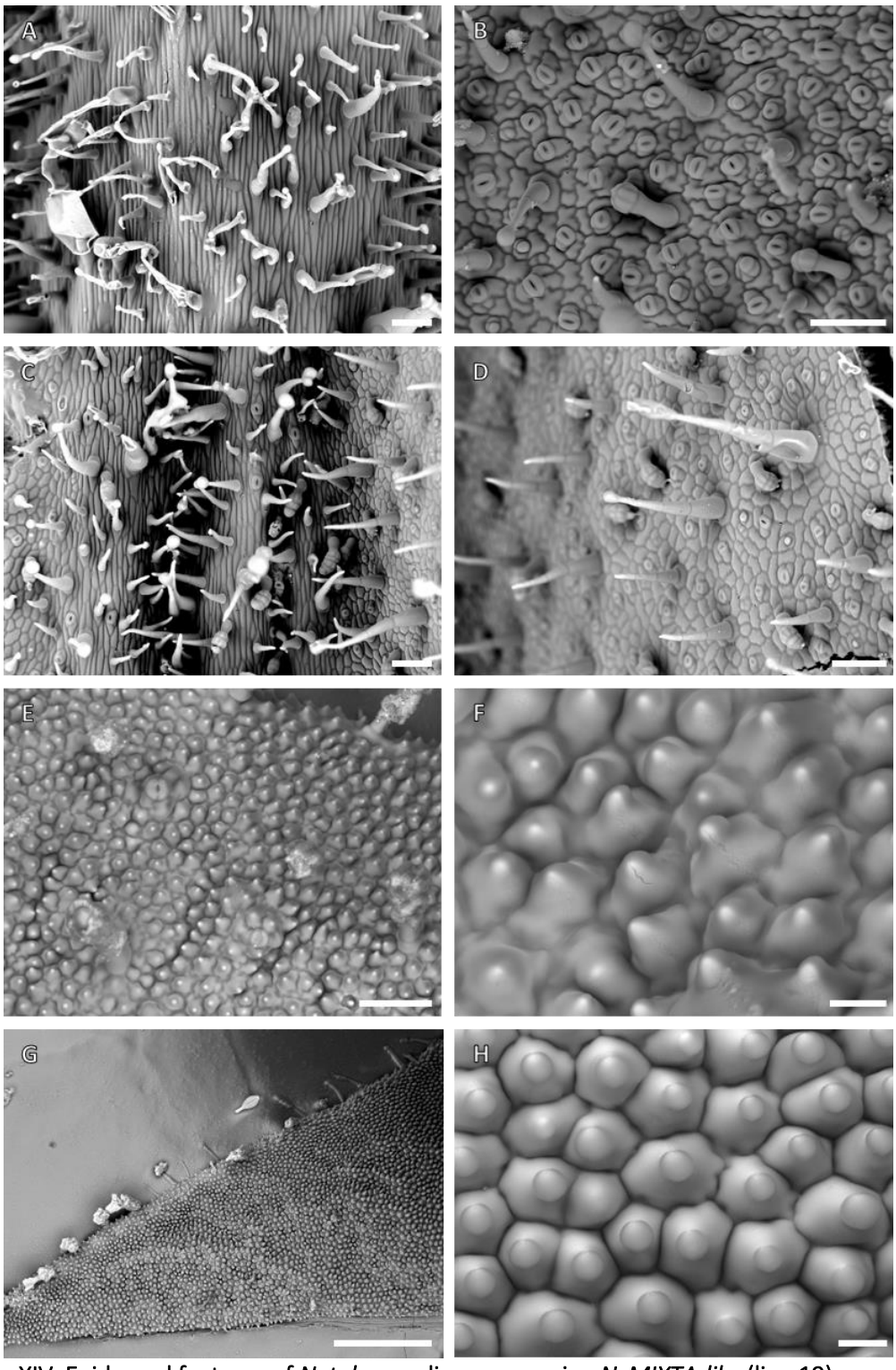

Plate XIV. Epidermal features of *N. tabacum* lines expressing *NcMIXTA-like* (line 19).
Cryo-SEM microphotographs of epidermal features on leaf and petal of *N. tabacum* 35S::*NcMIXTA-like*, Line 19. A-B. Abaxial leaf; C-D. Adaxial leaf; E-F. Abaxial petal; G-H. Adaxial petal. Scale bars: A-E=100µm, F,H=20µm, G=500µm

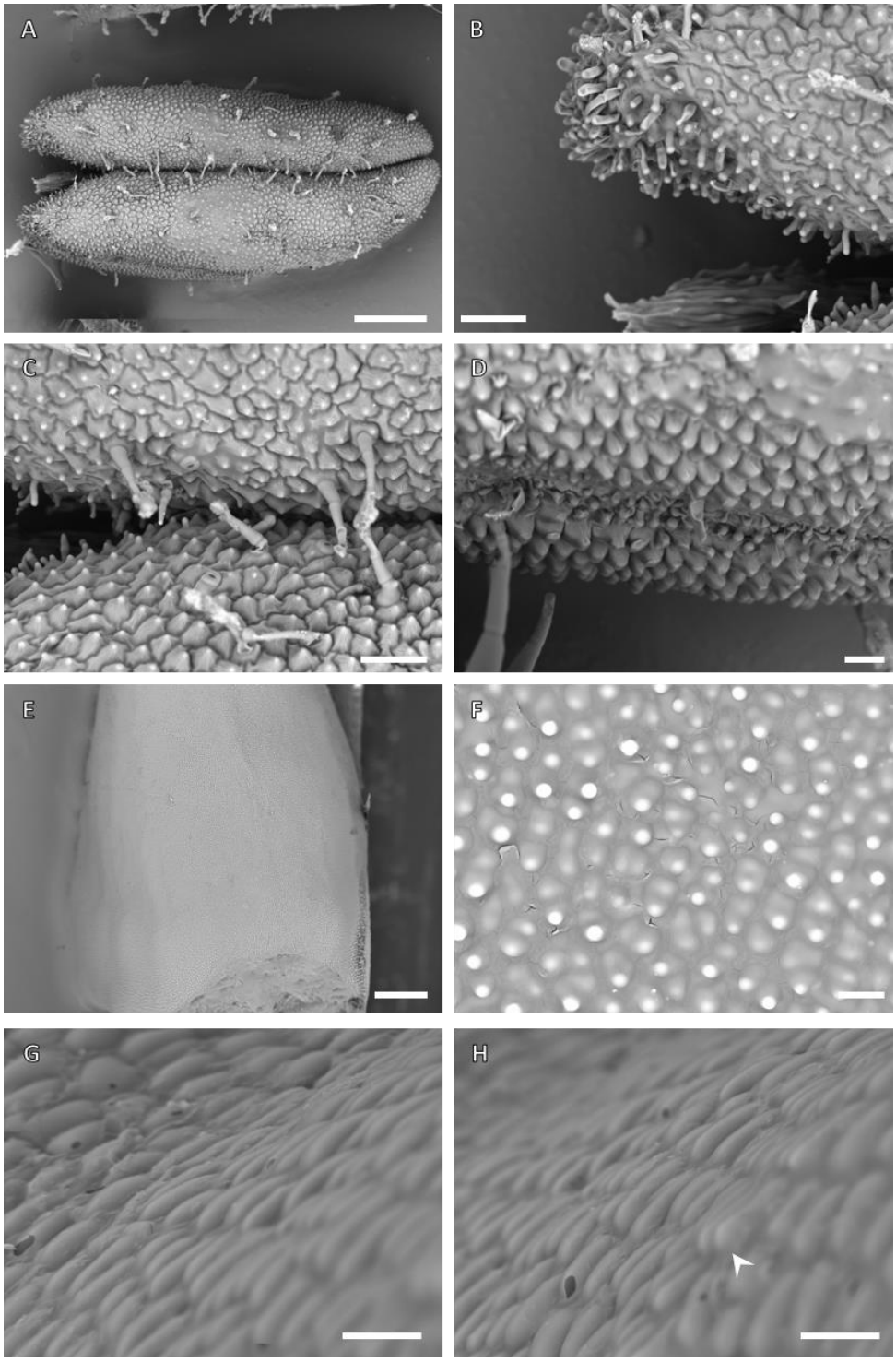

Plate XV. Epidermal features of *N. tabacum* lines expressing *NcMIXTA-like* (line 19).
Cryo-SEM microphotographs of epidermal features on anther and carpel of *N. tabacum* 35S::*NcMIXTA-like*, Line 19. A-D. Anther; E-H. Carpel. A. Anther base; B. Detail on pollen sac basal tip. C. Detail on proximal pollen sac. D. Slit zone. E. General aspect of the carpel. F. Conical cells on the medial zone of the carpel. G-H. Mostly dome shaped cells at the base of the carpel, arrow head shows a cell with a slight pointy protrusion. Scale bars: A, E=500µm; B-C= 100µm, D, F-H=20µm.

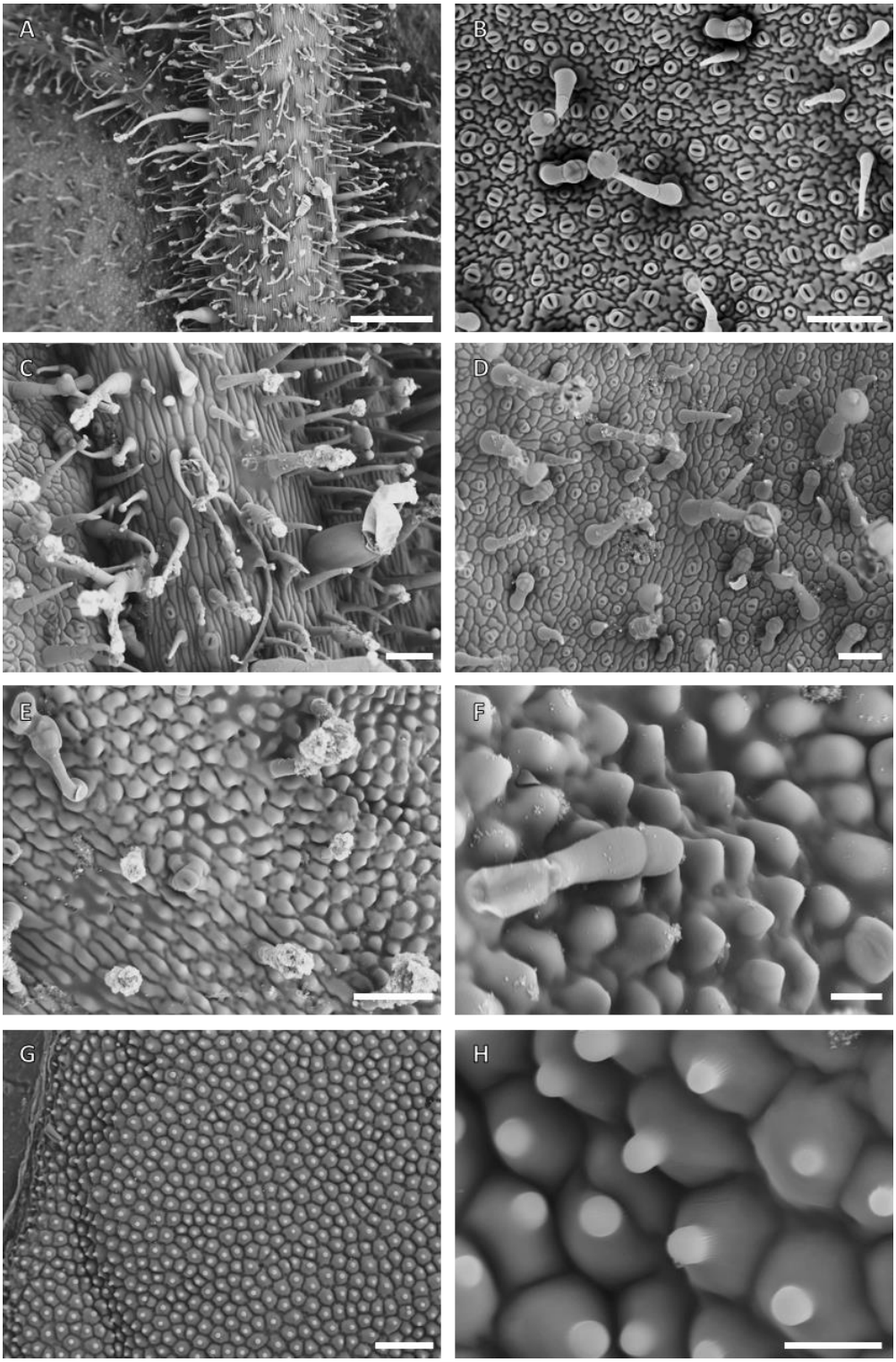

Plate XVI. Epidermal features of *N. tabacum* lines expressing *NcMIXTA-like* (line 8).
Cryo-Cryo-SEM microphotographs of epidermal features on leaf and petal of *N. tabacum* 35S::*NcMIXTA-like*, Line 8. A-B. Abaxial leaf; C-D. Adaxial leaf; E-F. Abaxial petal; G-H. Adaxial petal. Scale bars: A=500µm, B-E, G=100µm, F, H=20µm

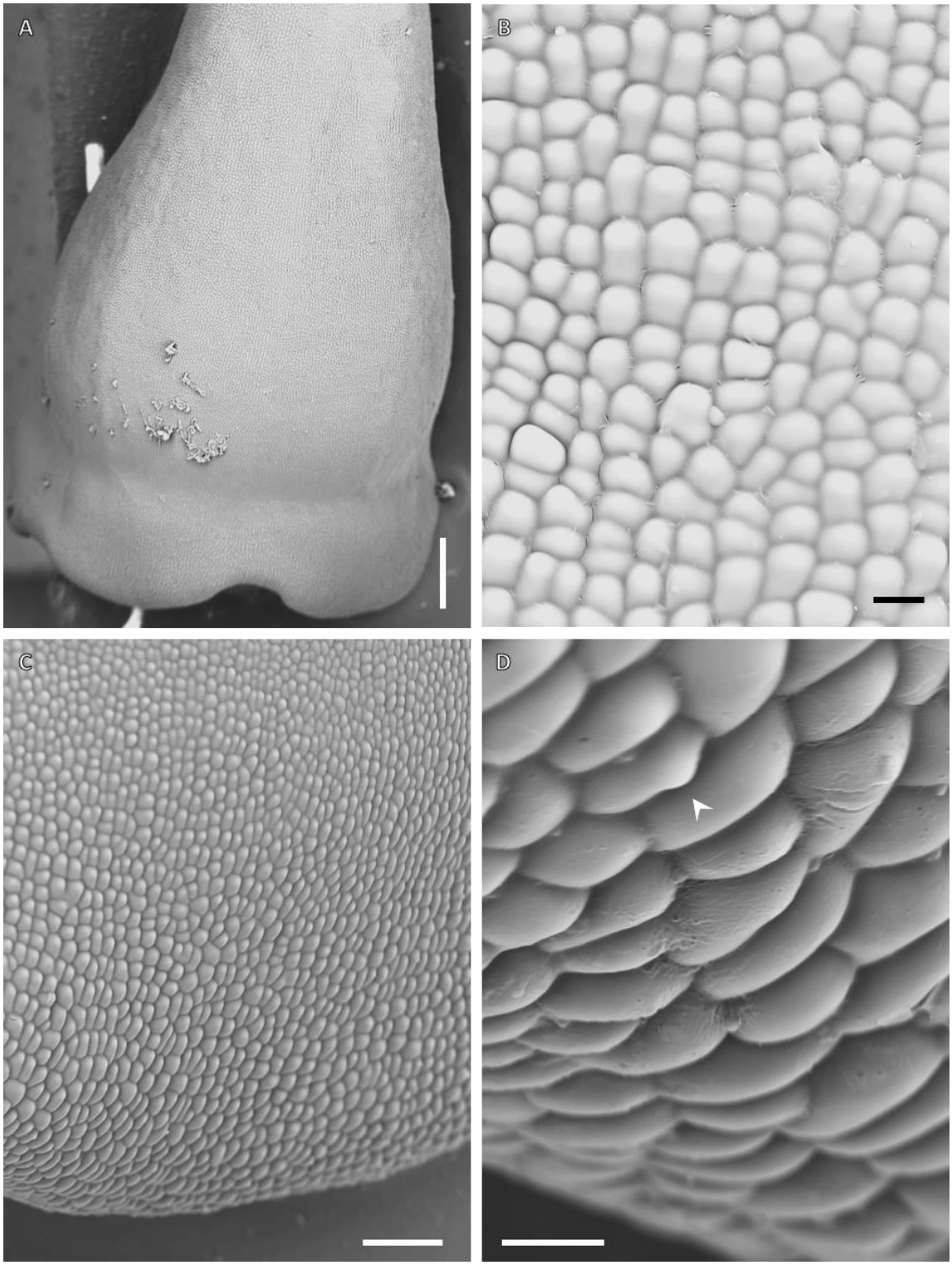

Plate XVII. Epidermal features of *N. tabacum* lines expressing *NcMIXTA-like* (line 8).
Cryo-SEM microphotographs of epidermal features on carpel of *N. tabacum* 35S::*NcMIXTA-like*, Line 8. A-D. A. General aspect of the carpel. B. Dome shaped cells on the medial zone of the carpel. G. Base of the carpel. H. Close-up on cells at the base of the carpel, arrow head points to a initiating conical cell. Scale bars: A=500µm; B, D=20µm; C=100µm

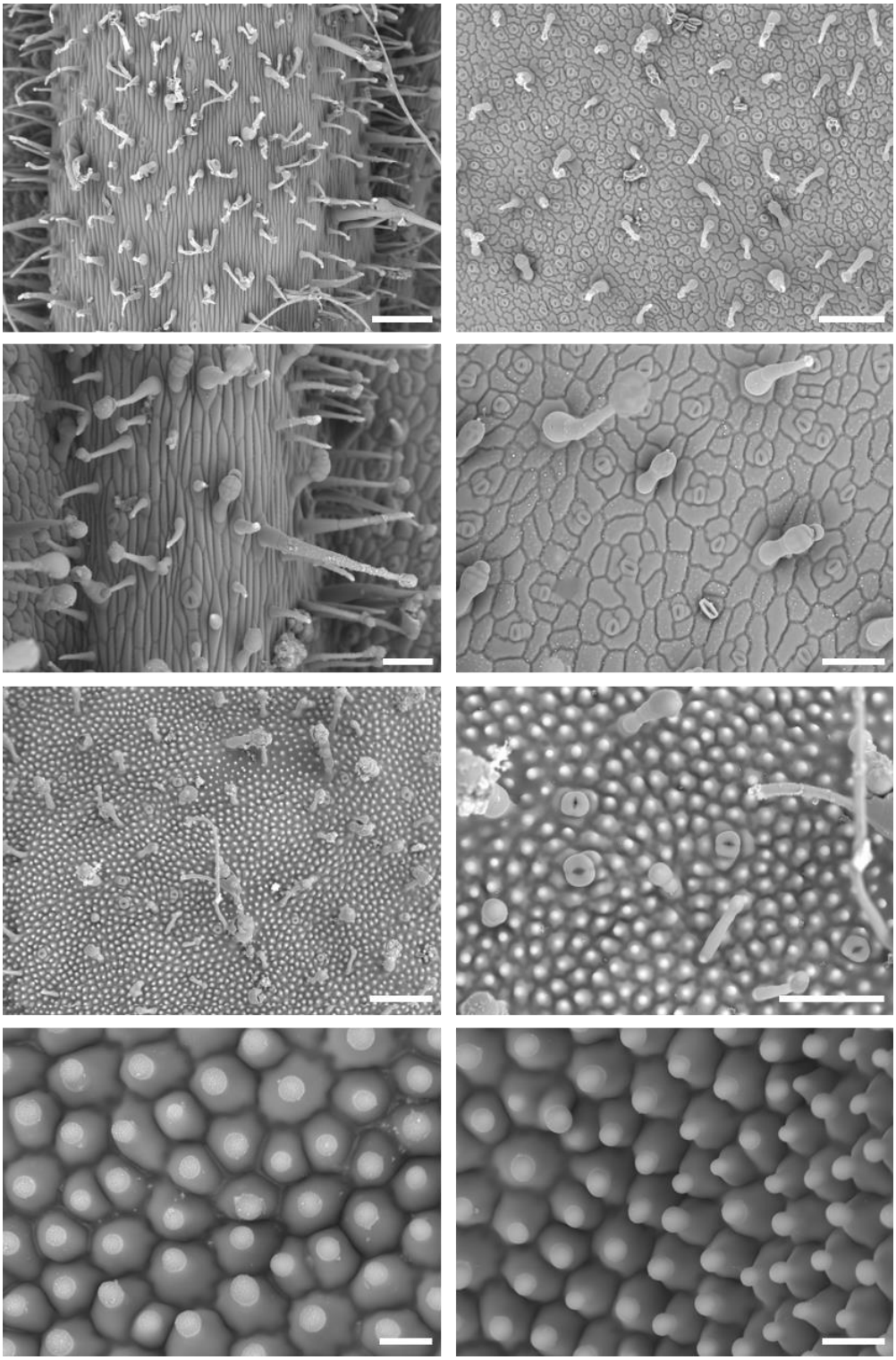

Plate XVIII. Epidermal features of *N. tabacum* lines expressing *NsMIXTA-like* (line 10).
Cryo-SEM microphotographs of epidermal features on leaf and petal of *N. tabacum* 35S::*NSMIXTA-like*, Line 10. A-B. Abaxial leaf; C-D. Adaxial leaf; E-F. Abaxial petal; G-H. Adaxial petal. Scale bars: A-B=200µm, C-F=100µm, G-H=20µm

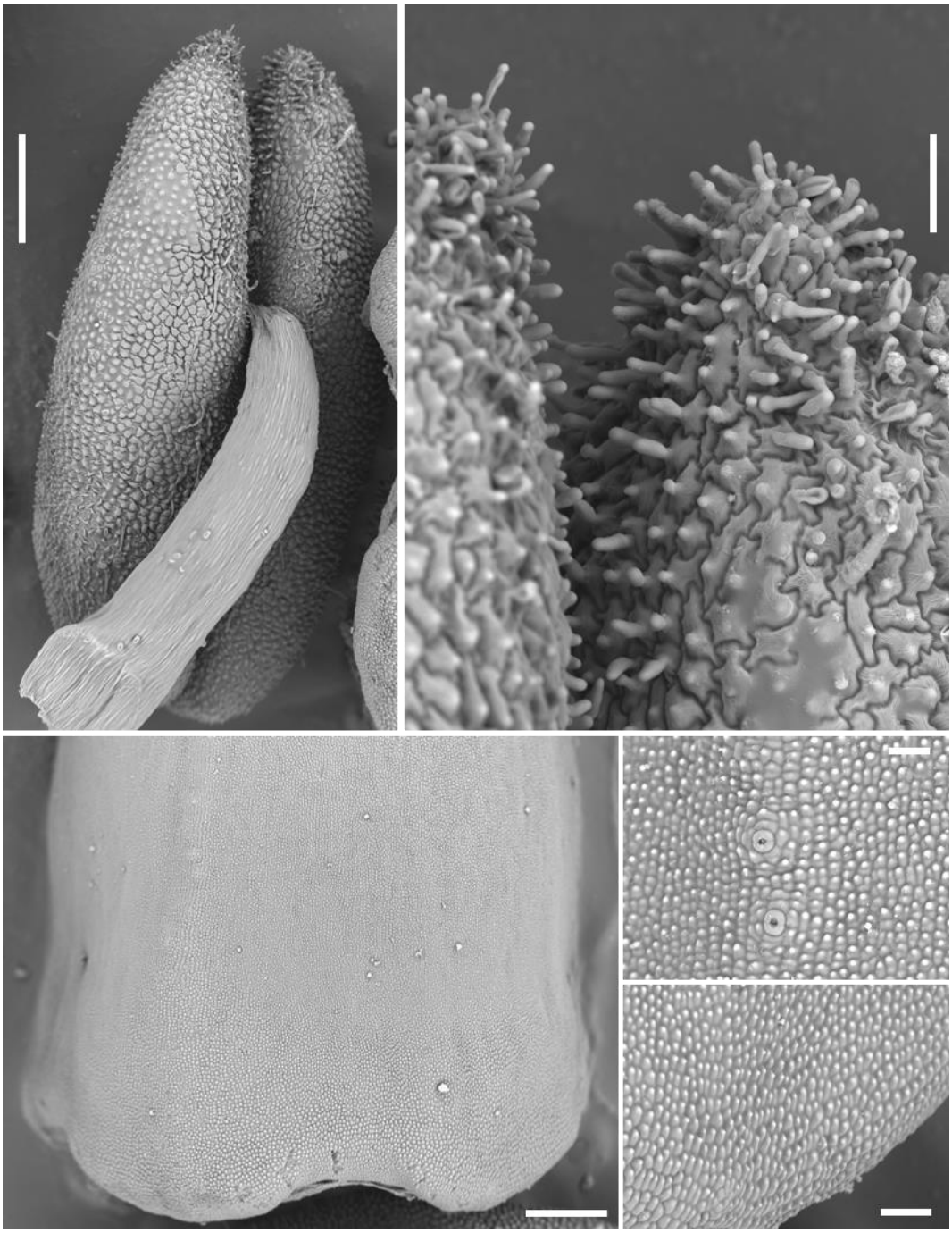

Plate XIX. Epidermal features of *N. tabacum* lines expressing *NsMIXTA-like* (line 10).
Cryo-SEM microphotographs of epidermal features on anther and carpel of *N. tabacum* 35S::*NsMIXTA-like*, Line 10. A-B. Anther; C-E. Carpel. Scale bars: A, C=500µm, B, D=100µm, E=50µm

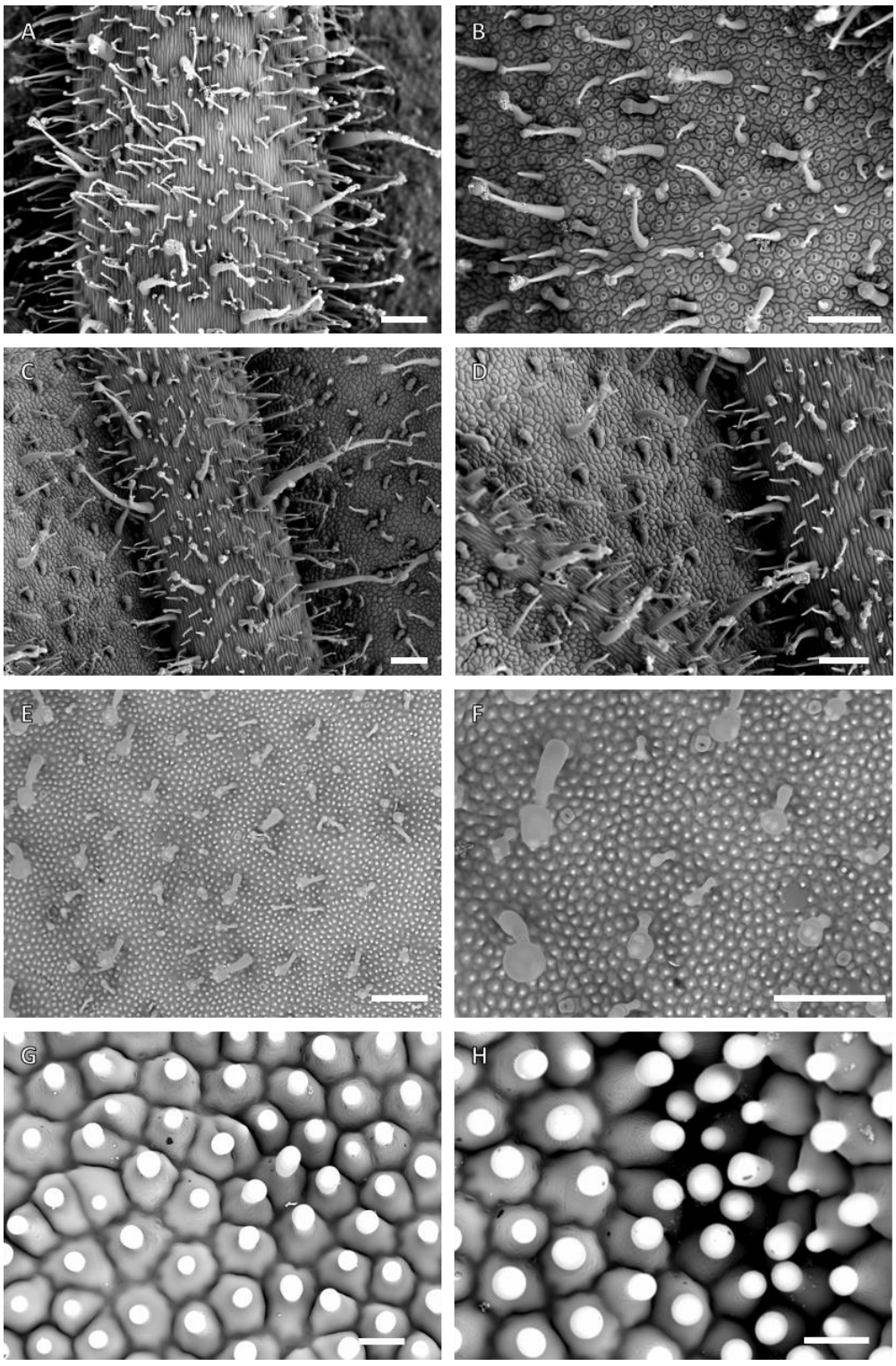

Plate XX. Epidermal features of *N. tabacum* lines expressing *NsMIXTA-like* (line 11).

Cryo-SEM microphotographs of epidermal features on leaf and petal of *N. tabacum* 35S::*NsMIXTA-like*, Line 11. A-B. Abaxial leaf; C-D. Adaxial leaf; E-F. Abaxial petal; G-H. Adaxial petal. Scale bars: A-F=200µm, G-H=20µm

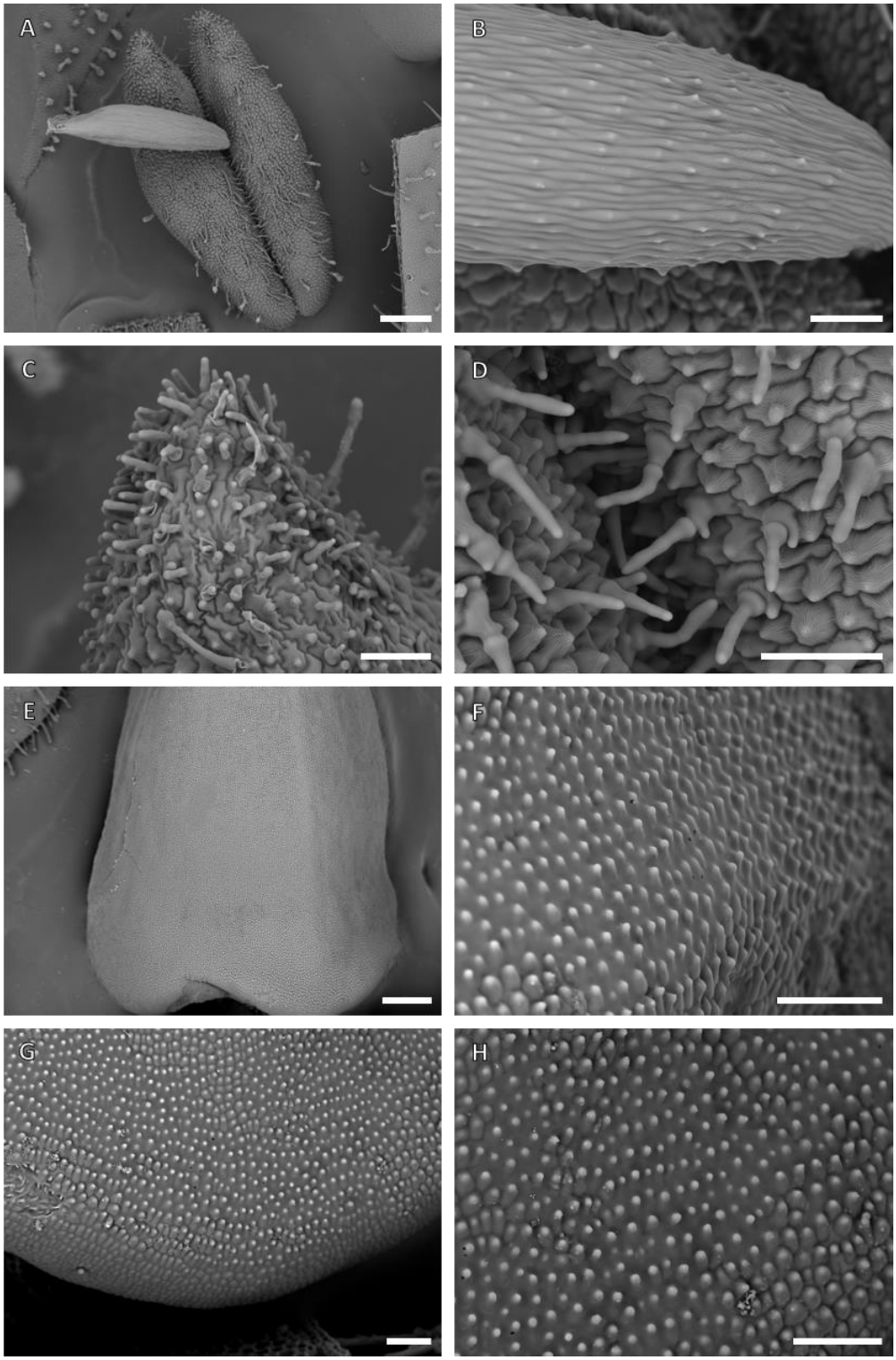

Plate XXI. Epidermal features of *N. tabacum* lines expressing *NsMIXTA-like* (line 11).
Cryo-SEM microphotographs of epidermal features on leaf and petal of *N. tabacum* 35S::*NsMIXTA-like*, Line 11. A-B. Abaxial leaf; C-D. Adaxial leaf; E-F. Abaxial petal; G-H. Adaxial petal. Scale bars: A, E=500µm, B-D, F-H=100µm, C-D=200µm, E,G=500µm

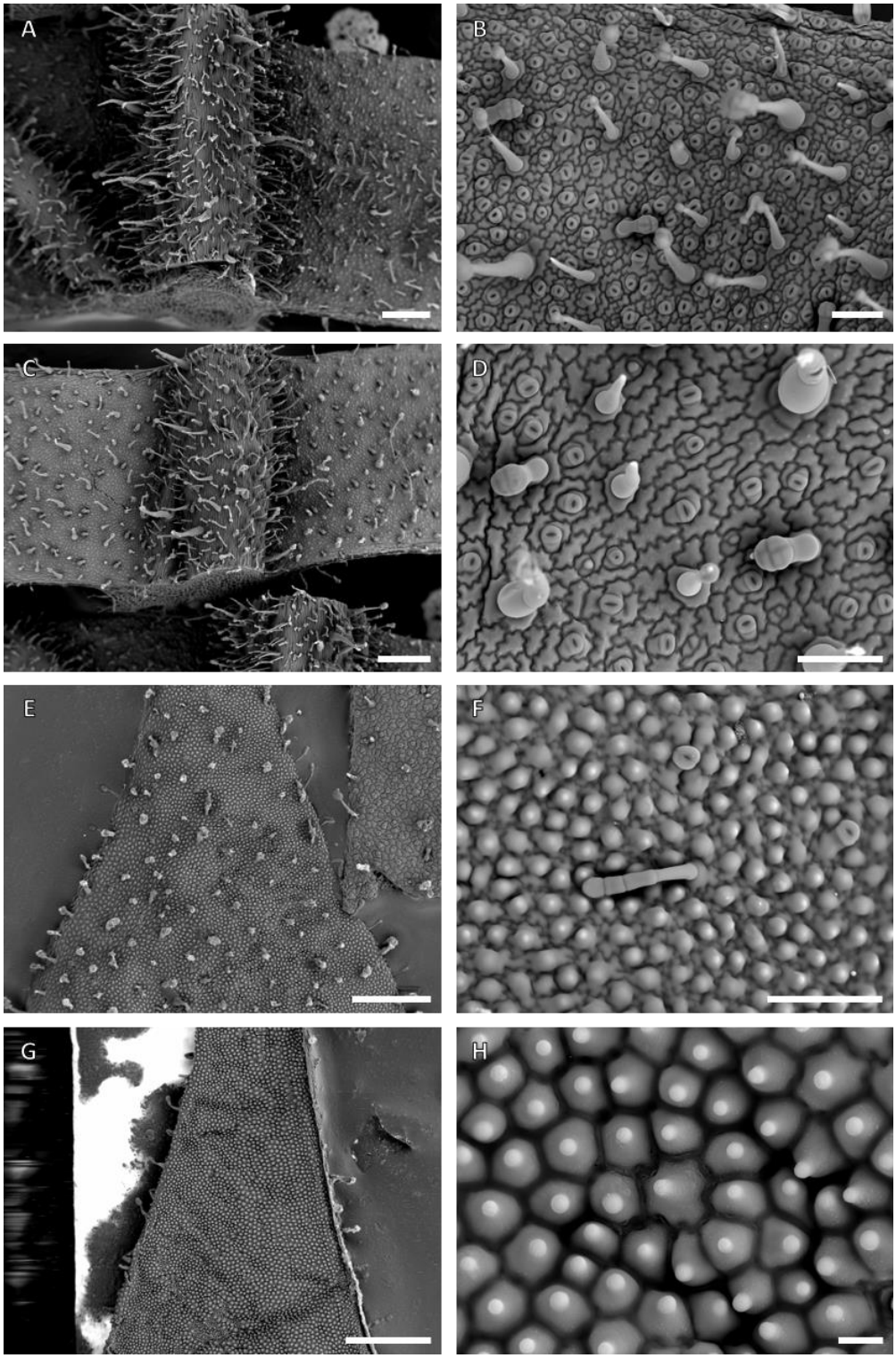

Plate XXII. Epidermal features of *N. tabacum* lines expressing *NsMIXTA-like* (line 13).
Cryo-SEM microphotographs of epidermal features on leaf and petal of *N. tabacum* 35S::*NsMIXTA-like*, Line 13. A-B. Abaxial leaf; C-D. Adaxial leaf; E-F. Abaxial petal; G-H. Adaxial petal. Scale bars: A, C, E, g=500µm, B, D, F=100µm, H=20µm

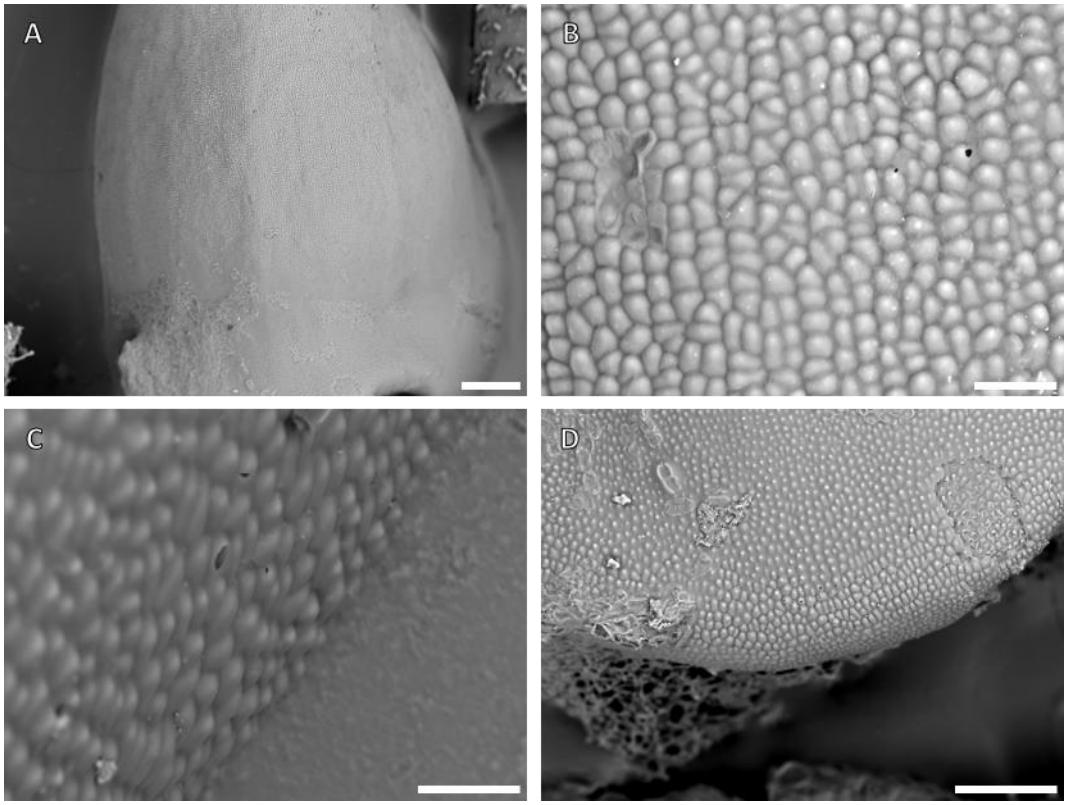

Plate XXIII. Epidermal features of *N. tabacum* lines expressing *NsMIXTA-like* (line 13).
Cryo-SEM microphotographs of epidermal features on carpel of *N. tabacum* 35S::*NsMIXTA-like*, Line 13. Scale bars: A=500µm, B, C=50µm, D=200µm

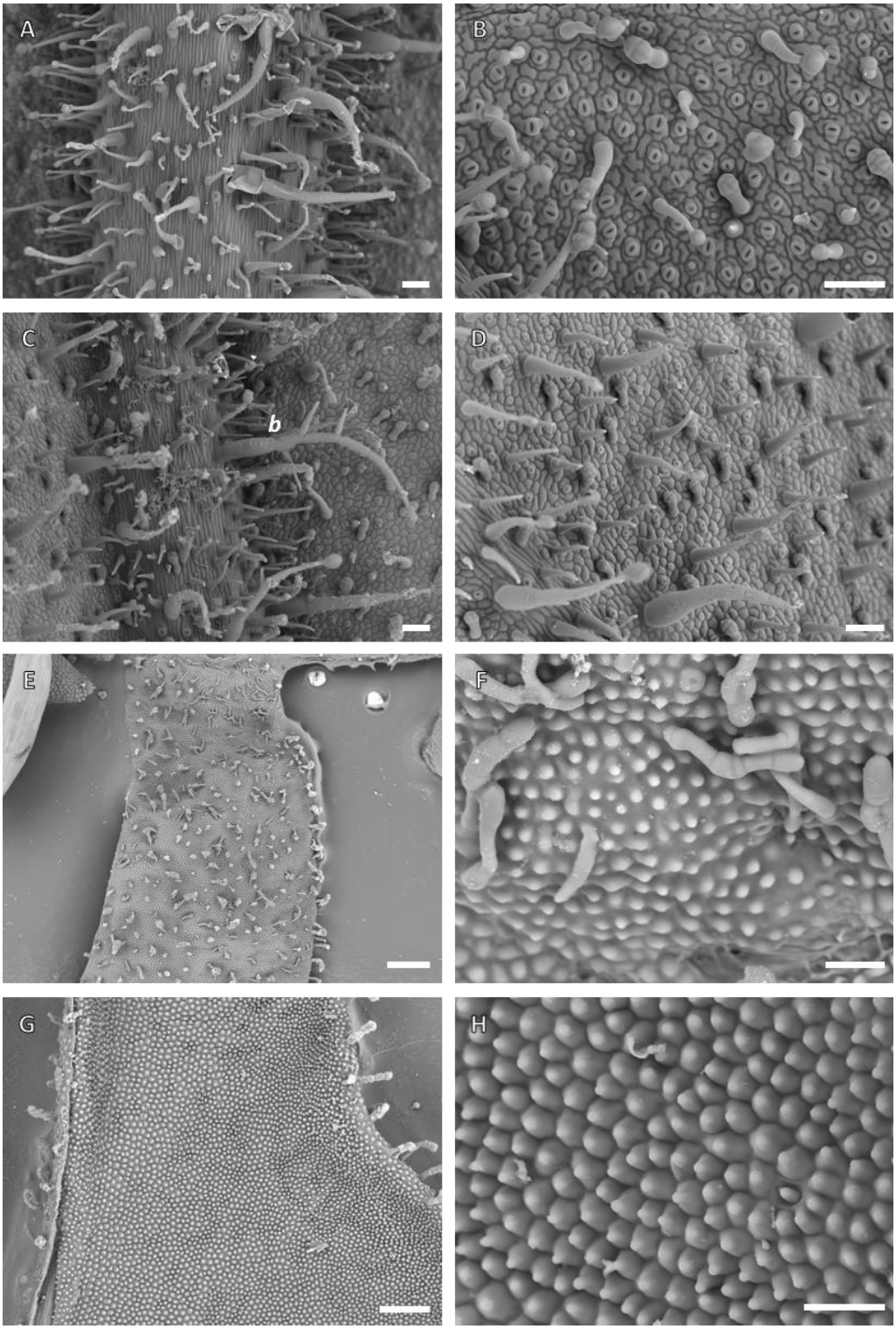

Plate XXIV. Epidermal features of *N. tabacum* lines expressing *NsMIXTA-like* (line 14).
Cryo-SEM microphotographs of epidermal features on leaf and petal of *N. tabacum* 35S::*NsMIXTA-like*, Line 14. A-B. Abaxial leaf; C-D. Adaxial leaf; E-F. Abaxial petal; G-H. Adaxial petal. Branched trichome (b) is pointed out in C. Scale bars: A-D=100µm, E, G=500µm, F, H= 50µm

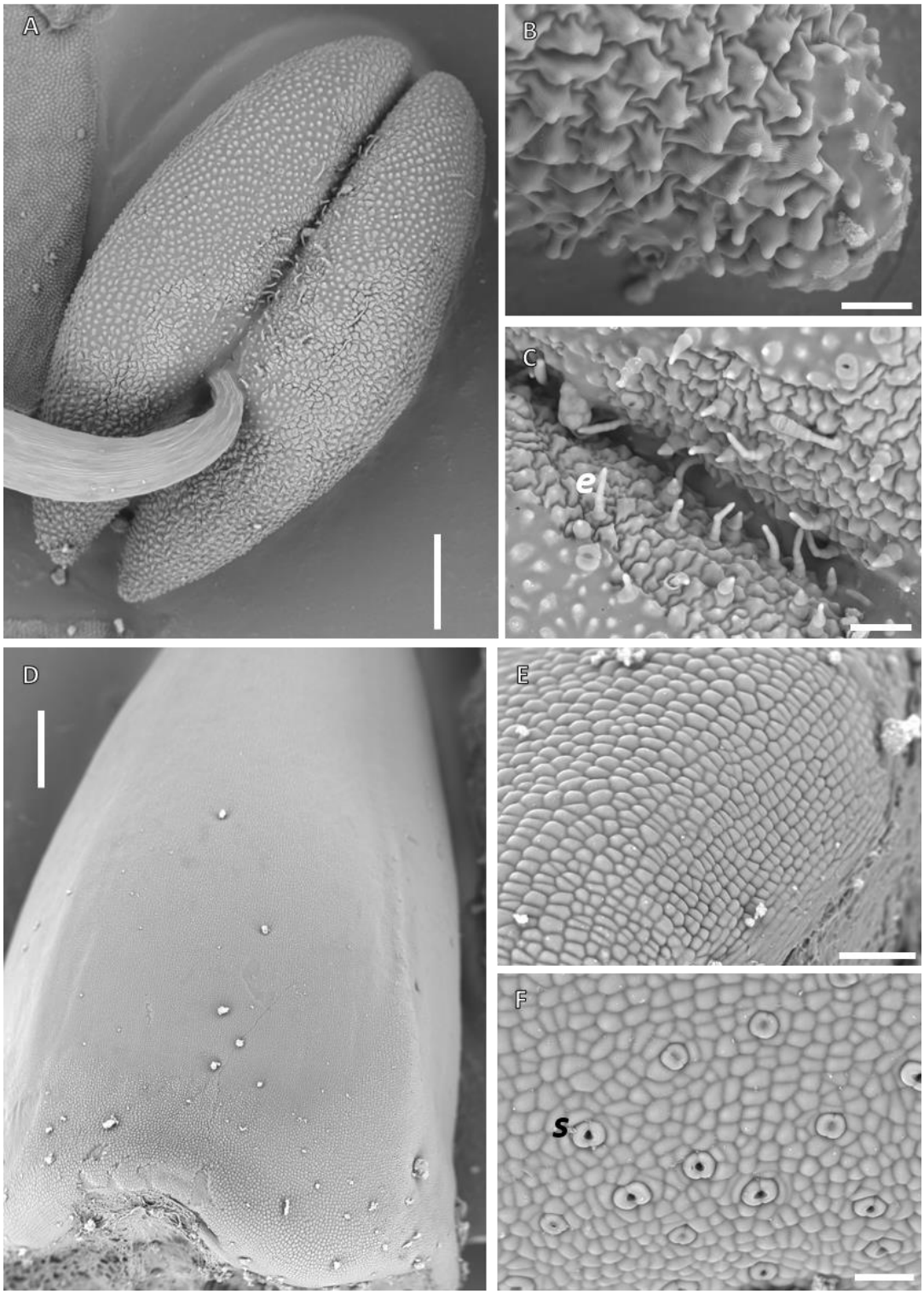

Plate XXV. Epidermal features of *N. tabacum* lines expressing NsMIXTA-like (line 14).
Cryo-SEM microphotographs of epidermal features on anther and carpel of *N. tabacum* 35S::*NcMIXTA-like*, Line 14. A-C. Anther; D-F. Carpel. A. Anther general aspect; B. Base of the anther. C. Detail on the proximal pollen sac. D. General aspect of the carpel. E. Carpel base. F. Stomata at the base of the carpel. e=epidermal outgrowths, c=conical cell, s: stomata. Scale bars: A, D=500µm; B, E= 50µm, C, F=100µm.

Appendix 10. Additional images of transgenics expressing genes from Section *Alatae*

LIST OF PLATES

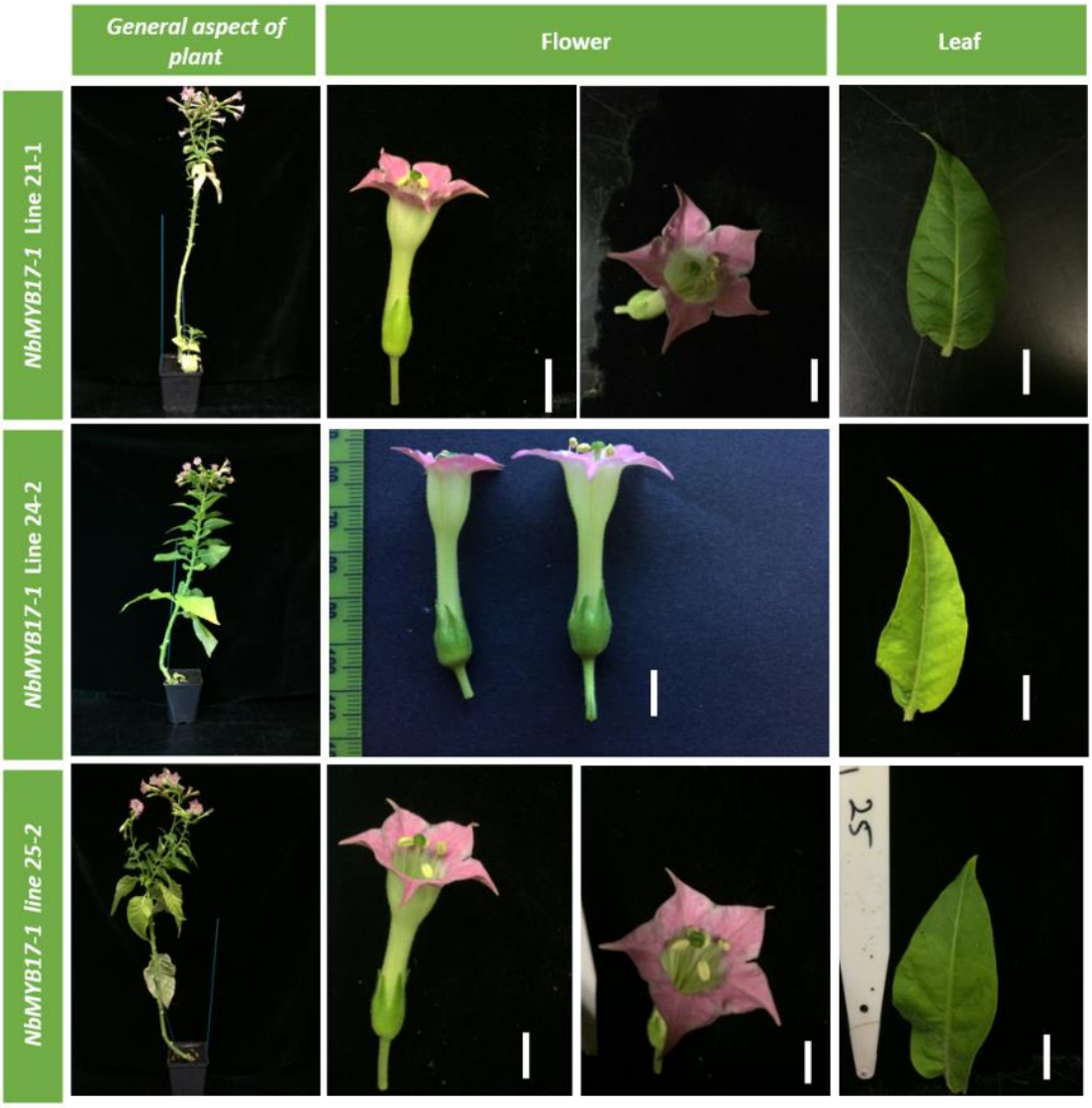

Plate I. Macromorphology of *N. tabacum* transgenic lines expressing *NcMIXTA-like.*
Scale bars= 1 cm.

Plate II. Macromorphology of *N. tabacum* transgenic lines expressing *NsMIXTA-like*.
Scale bars= 1cm

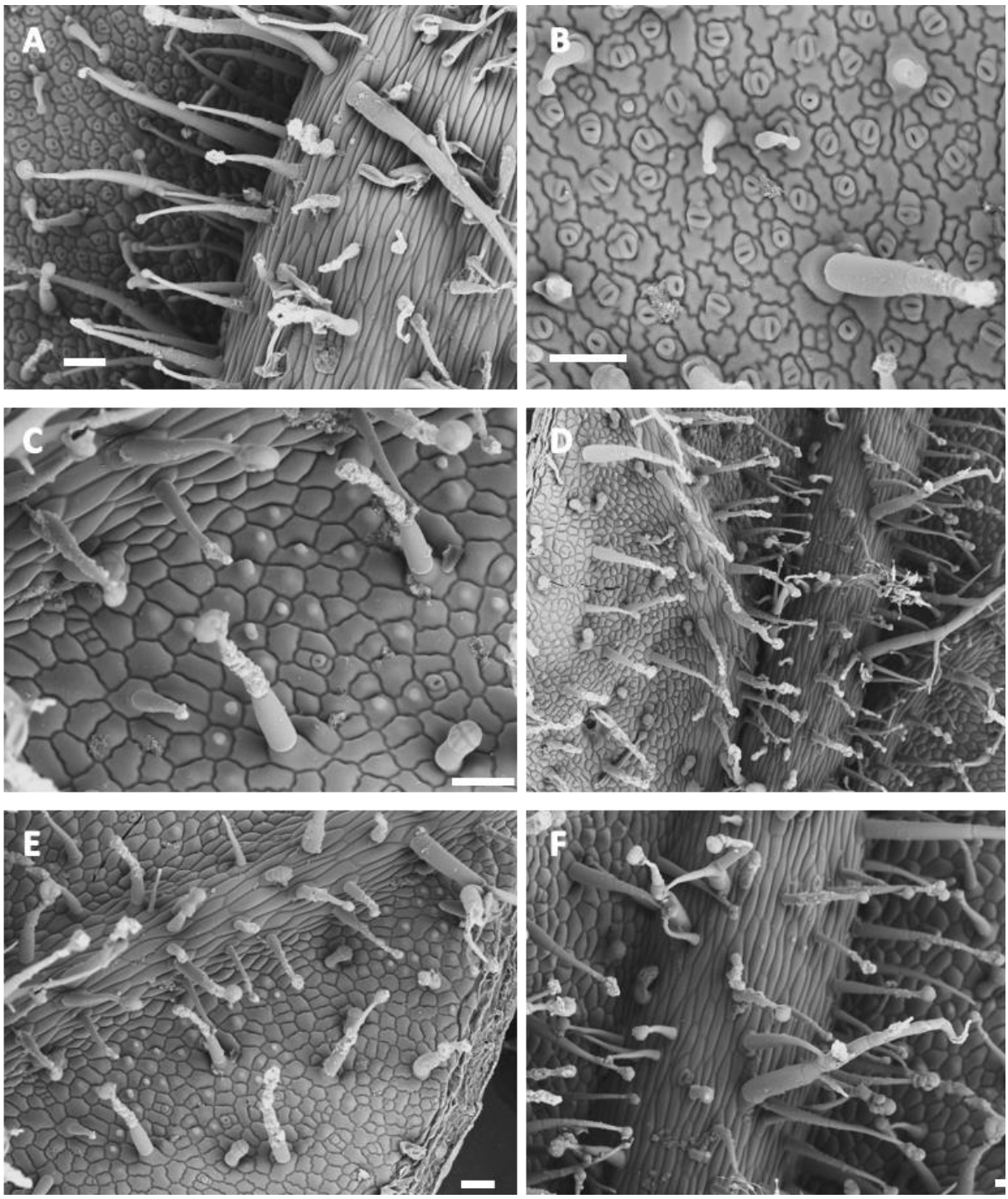

Plate III. Epidermal features of *N. tabacum* lines expressing *NbMYB17-1* (line 21-1).
Cryo-SEM microphotographs of epidermal features on leaf of *N. tabacum* 35S:*NbMYB17-1*, Line 21-1. A-C. Abaxial leaf; D-F. Adaxial leaf. Scale bars: A-F = 100µm.

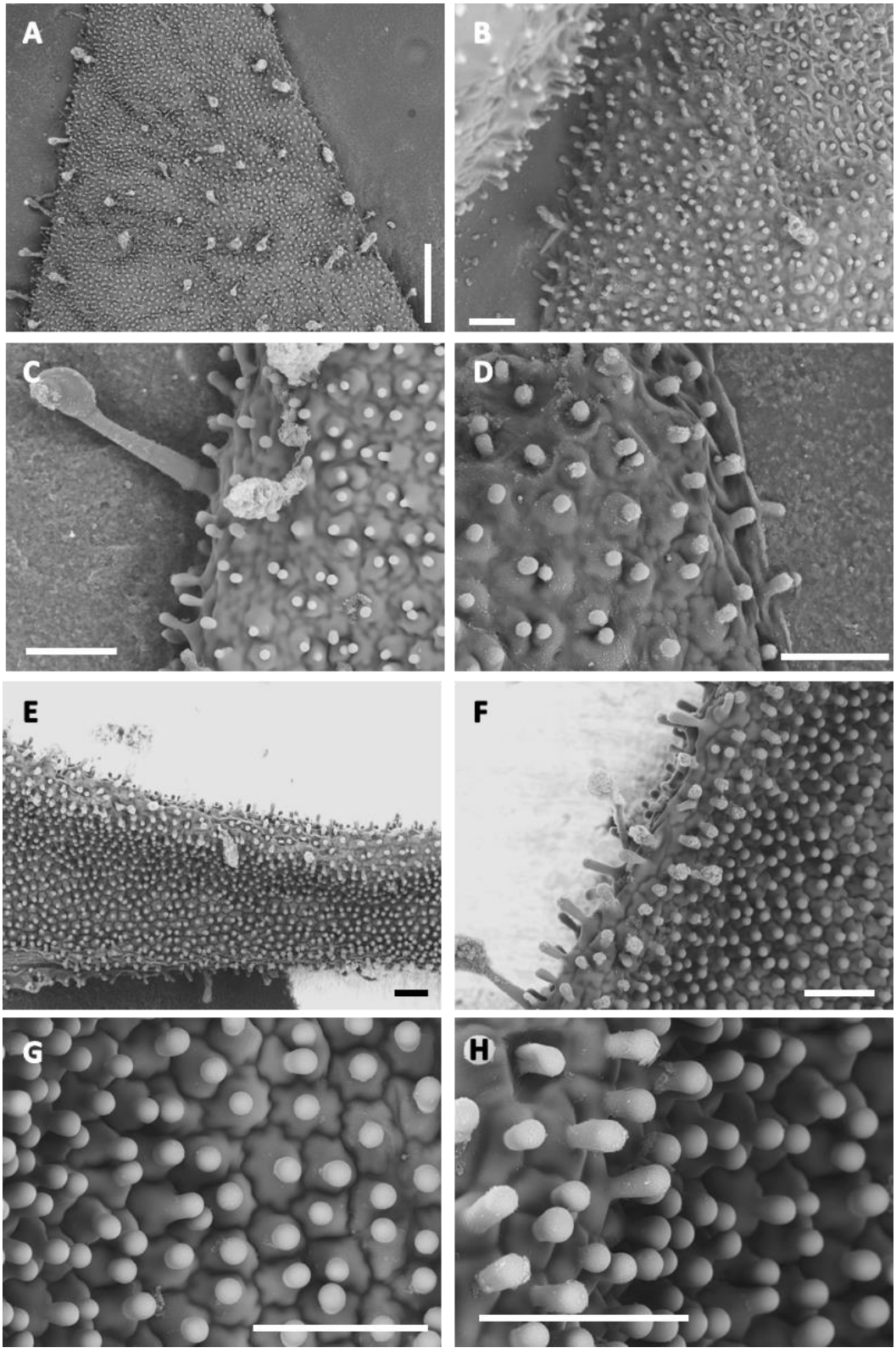

Plate IV. Epidermal features of *N. tabacum* lines expressing *NbMYB17-1* (line 21-1).
Cryo-SEM microphotographs of epidermal features on petal of *N. tabacum* 35S:*NbMYB17-1*, Line 21-1. A-D. Abaxial petal; E-H. Adaxial petal. Scale bars: A = 500µm; B-H = 100µm.

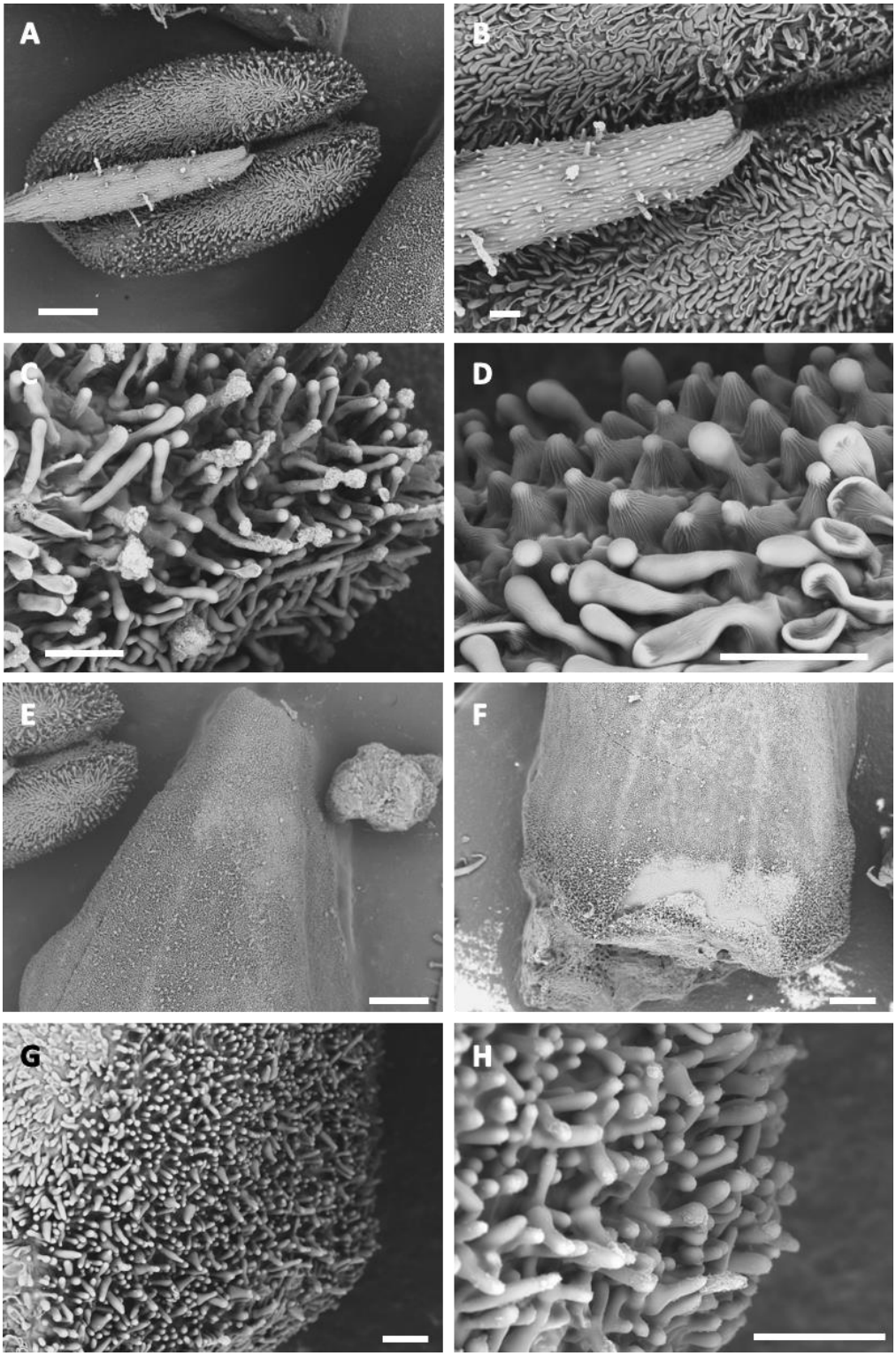

Plate V. Epidermal features of *N. tabacum* lines expressing *NbMYB17-1* (line 21-1).
Cryo-SEM microphotographs of epidermal features on anther and carpel of *N. tabacum* 35S:*NbMYB17-1*, Line 21-1. A-D. Anther; E-H. Carpel. Scale bars: A, E, F = 500µm; B-D, G-H = 100µm.

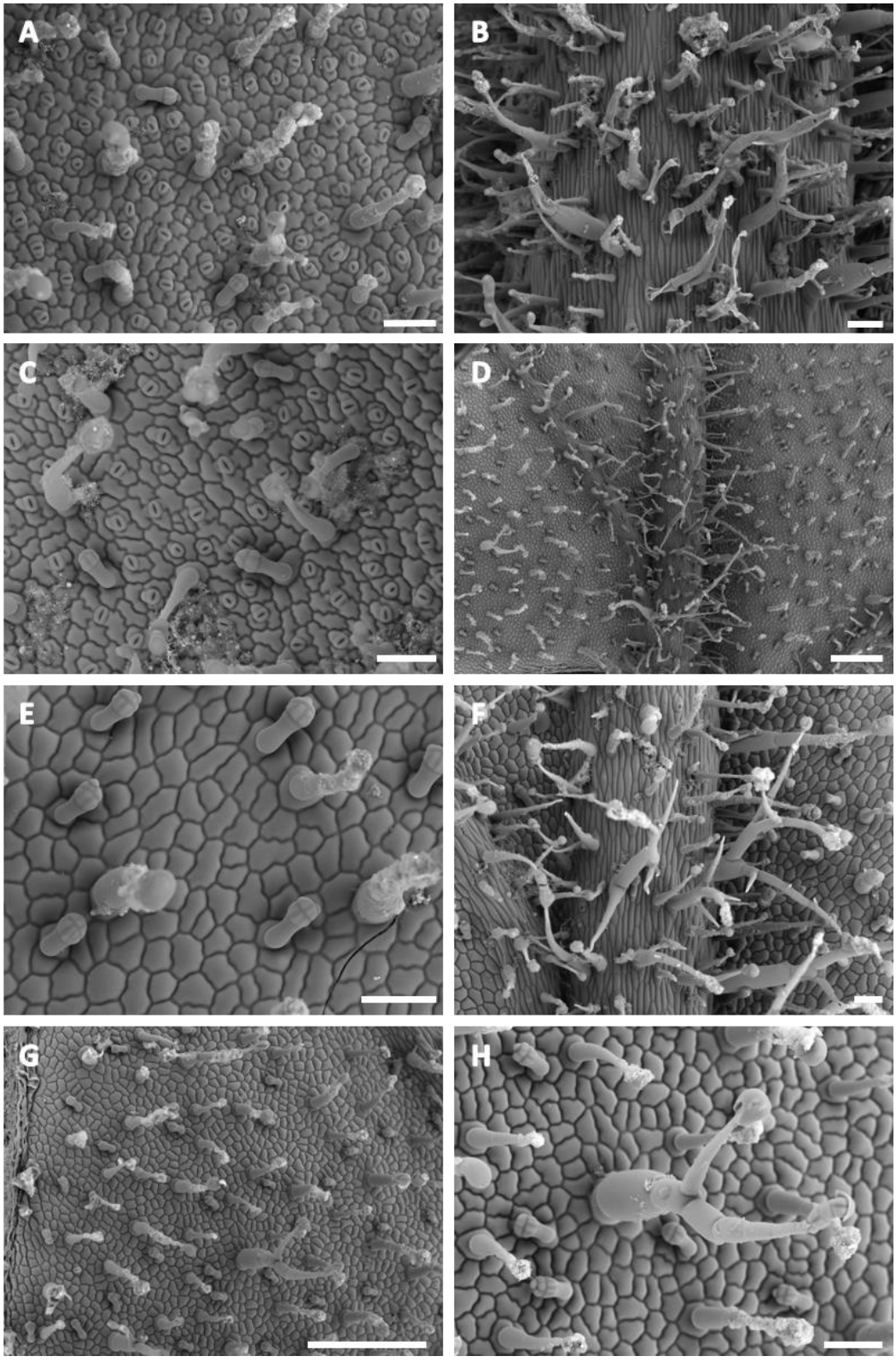

Plate VI. Epidermal features of *N. tabacum* lines expressing *NbMYB17-1* (line 24-2).
Cryo-SEM microphotographs of epidermal features on leaf of *N. tabacum* 35S:*NbMYB17-1*, Line 24-2. A-D. Abaxial leaf; D-H. Adaxial leaf -F. Scale bars: A-C, E-F, H=100µm, D, G=500µm.

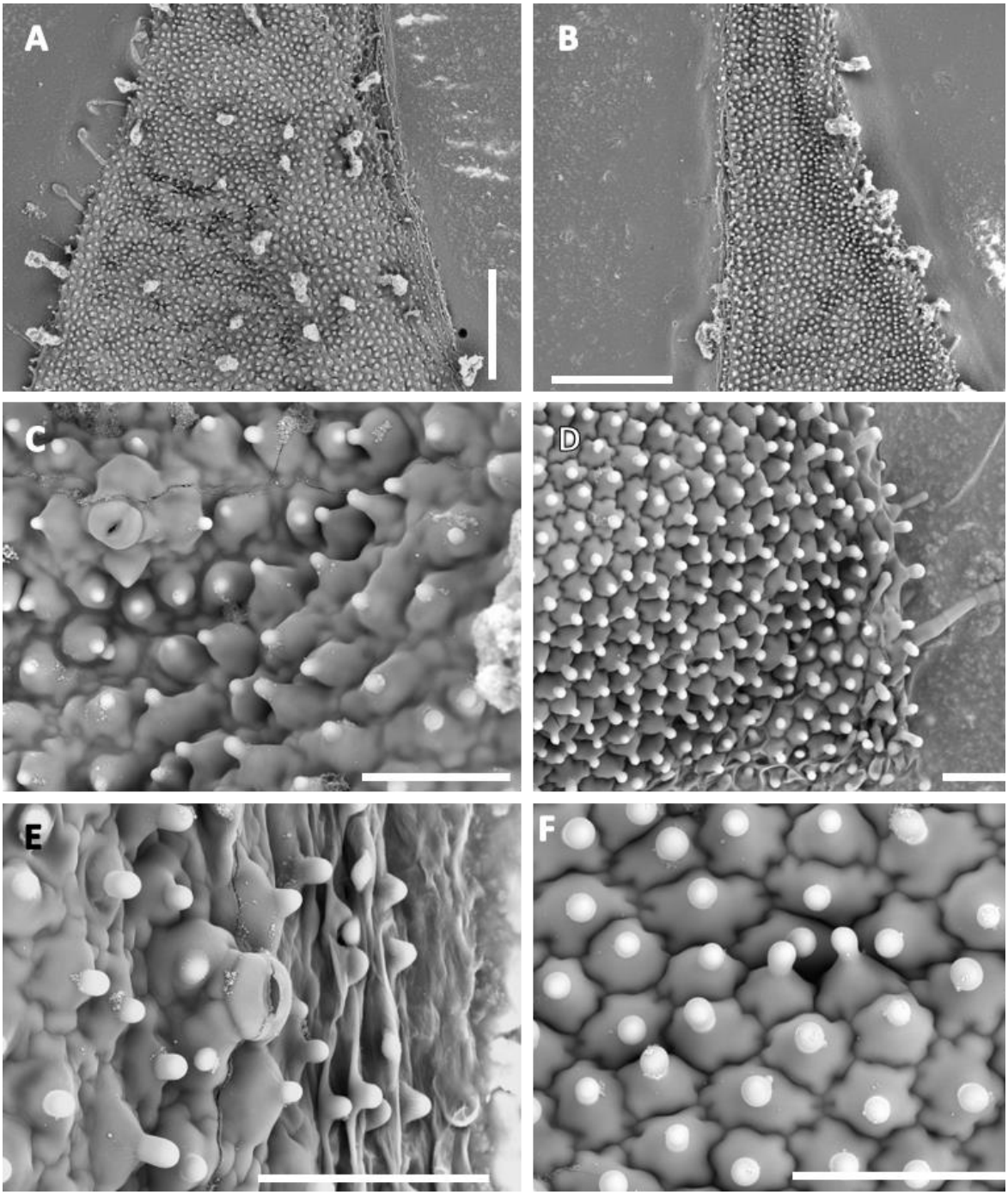

Plate VII. Epidermal features of *N. tabacum* lines expressing *NbMYB17-1* (line 24-2).

Cryo-SEM microphotographs of epidermal features on petal of *N. tabacum* 35S:*NbMYB17-1*, Line 24-2. A, C, E. Abaxial petal; B, D, F. Adaxial petal. Scale bars: A-B = 500µm; C-F = 100µm.

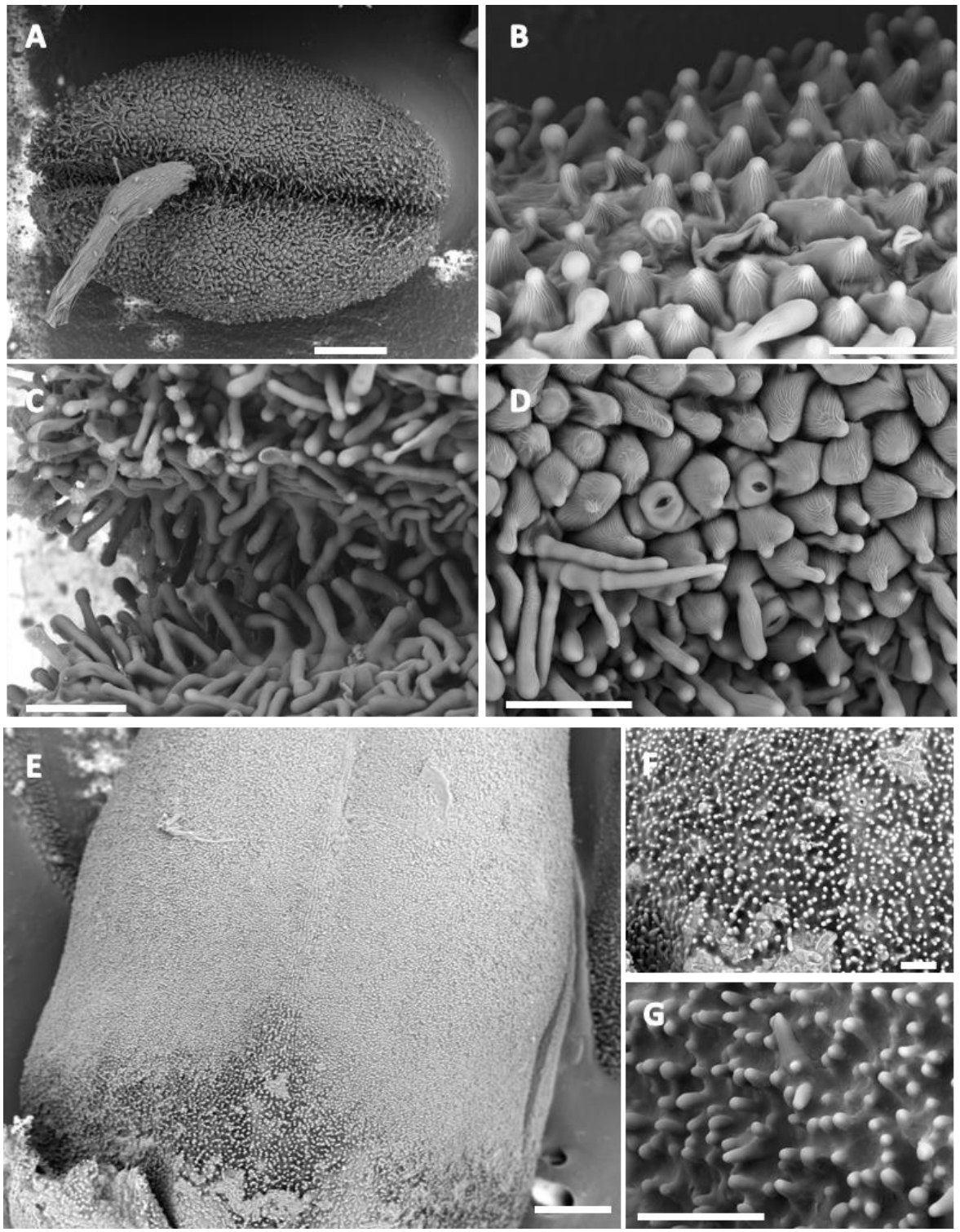

Plate VIII. Epidermal features of *N. tabacum* lines expressing *NbMYB17-1* (line 24-2).
Cryo-SEM microphotographs of epidermal features on anther and carpel of *N. tabacum* 35S:*NbMYB17-1*, Line 24-2. A-D. Anther; E-G. Carpel. Scale bars: A, E = 500µm; B-D, F-G = 100µm.

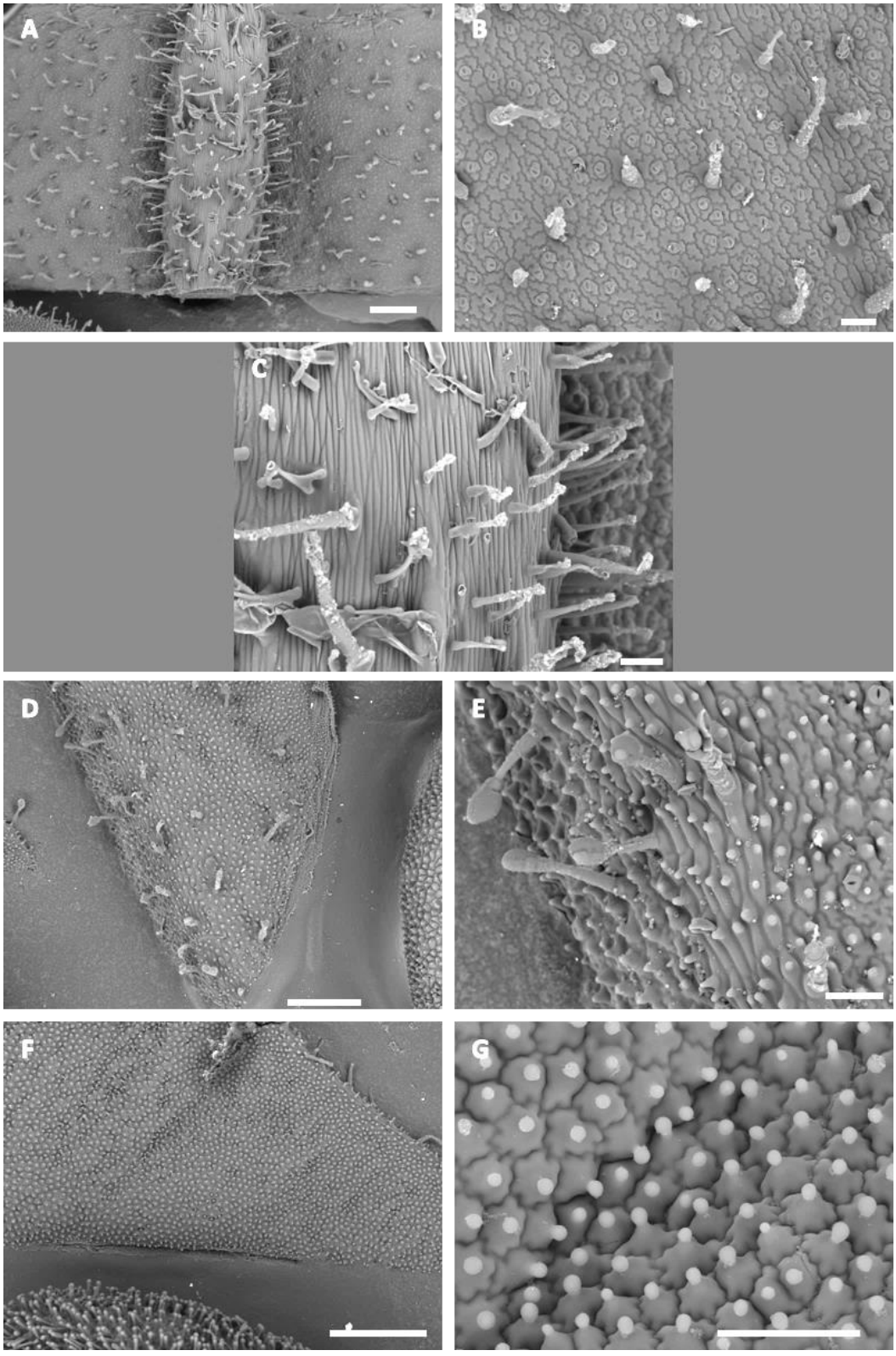

Plate IX. Epidermal features of *N. tabacum* lines expressing *NbMYB17-1* (line 25-2).

Cryo-SEM microphotographs of epidermal features on leaf and petal of *N. tabacum* 35S:*NbMYB17-1*, Line 25-2. A-C. Abaxial leaf; D-E. Abaxial petal. F-G. Adaxial petal -F. Scale bars: A, D, F = 500 µm; B-C, E, G. = 100µm.

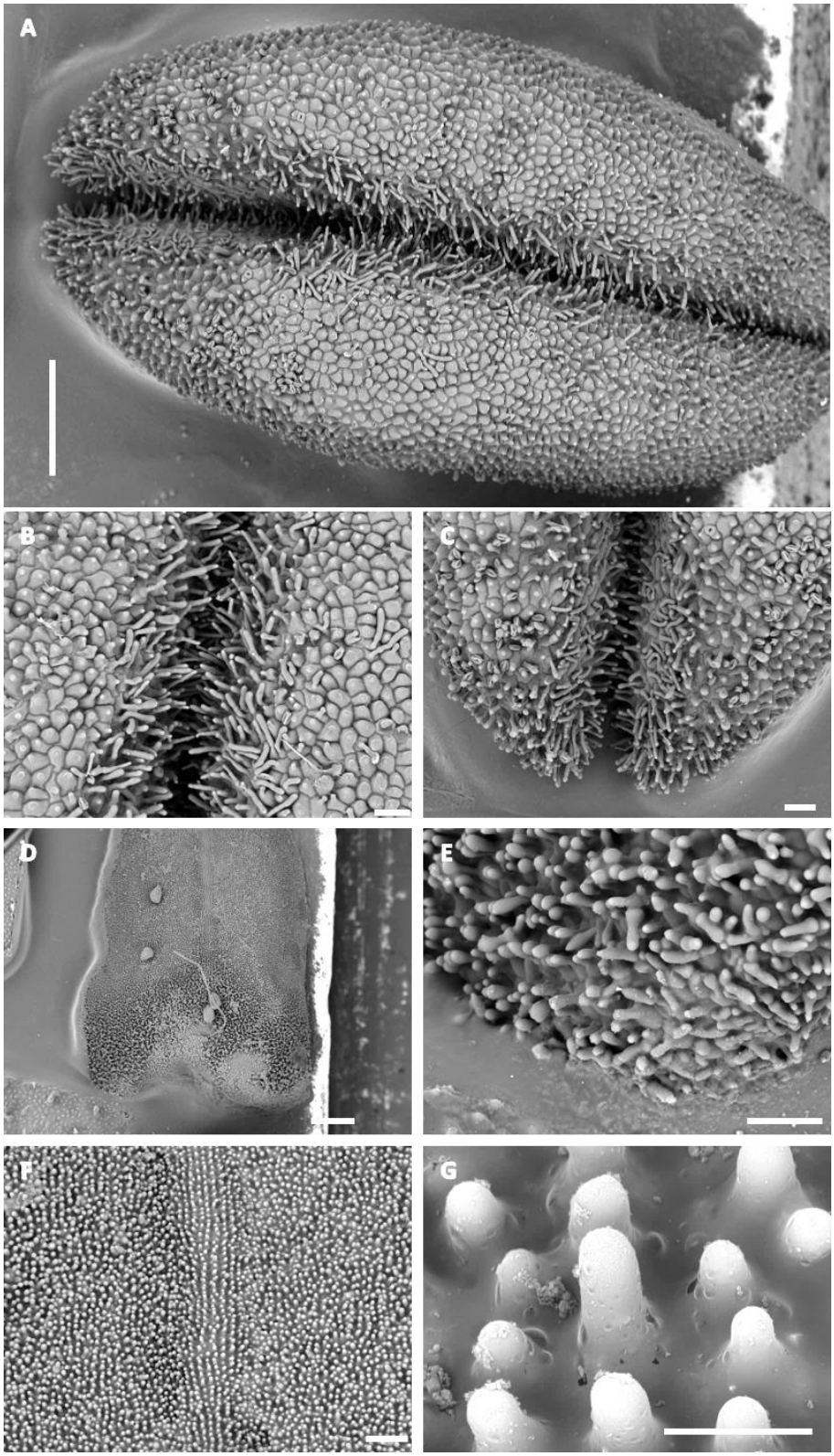

Plate X. Epidermal features of *N. tabacum* lines expressing *NbMYB17-1* (line 25-2).

Cryo-SEM microphotographs of epidermal features on anther and carpel of *N. tabacum* 35S:*NbMYB17-1*, Line 25-2. A-C. Anther; D-G. Carpel. Scale bars: A, D = 500µm; B-C, E-F = 100µm, G = 20µm .

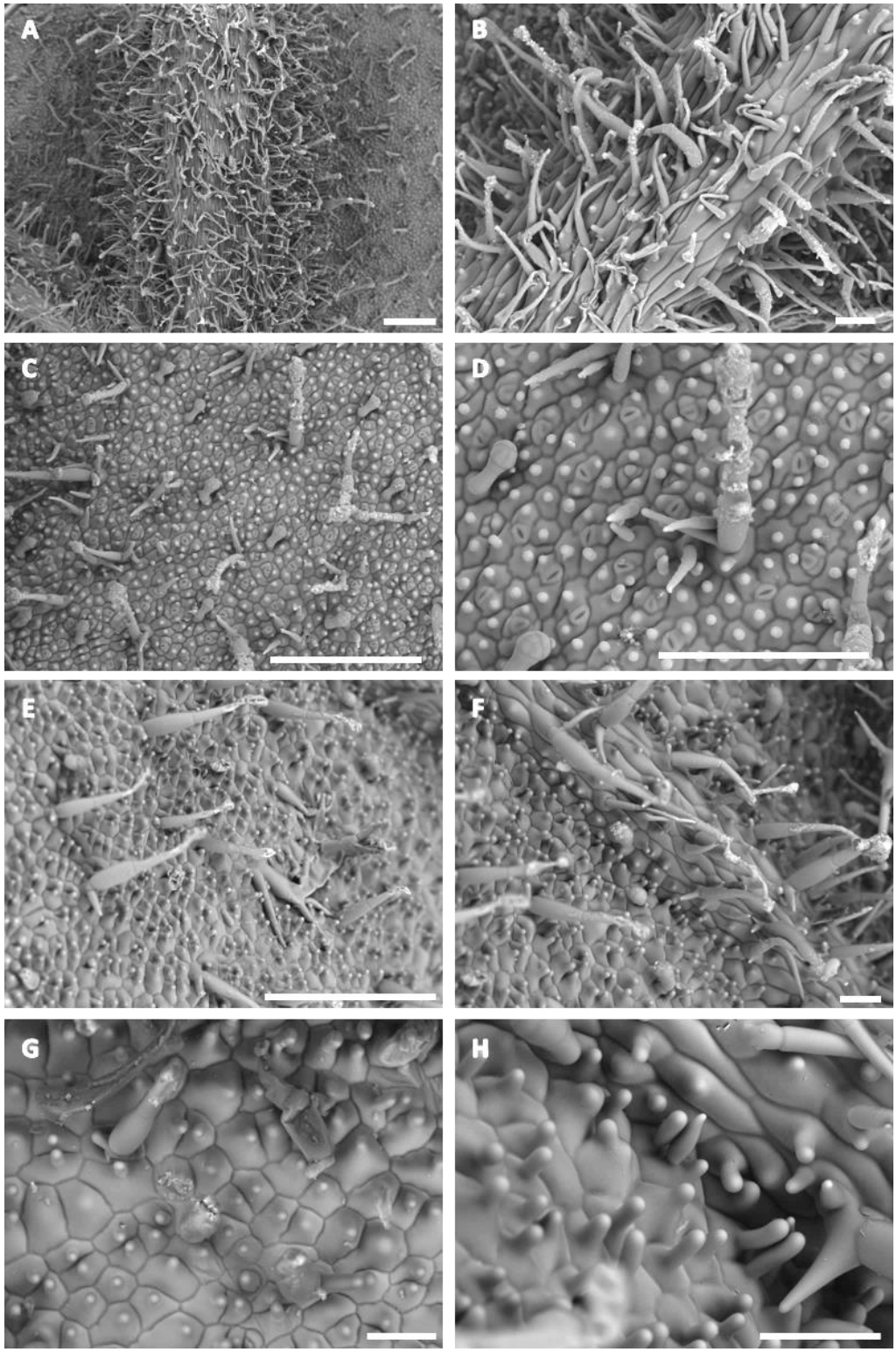

Plate XI. Epidermal features of *N. tabacum* lines expressing *NbMYB17-1* (line 29-2).
Cryo-SEM microphotographs of epidermal features on leaf of N. tabacum 35S:NbMYB17-1, Line 29-2. A-D. Abaxial leaf; E-H. Adaxial leaf . Scale bars: A, C, E = 500 µm; B, D, F-H = 100µm.

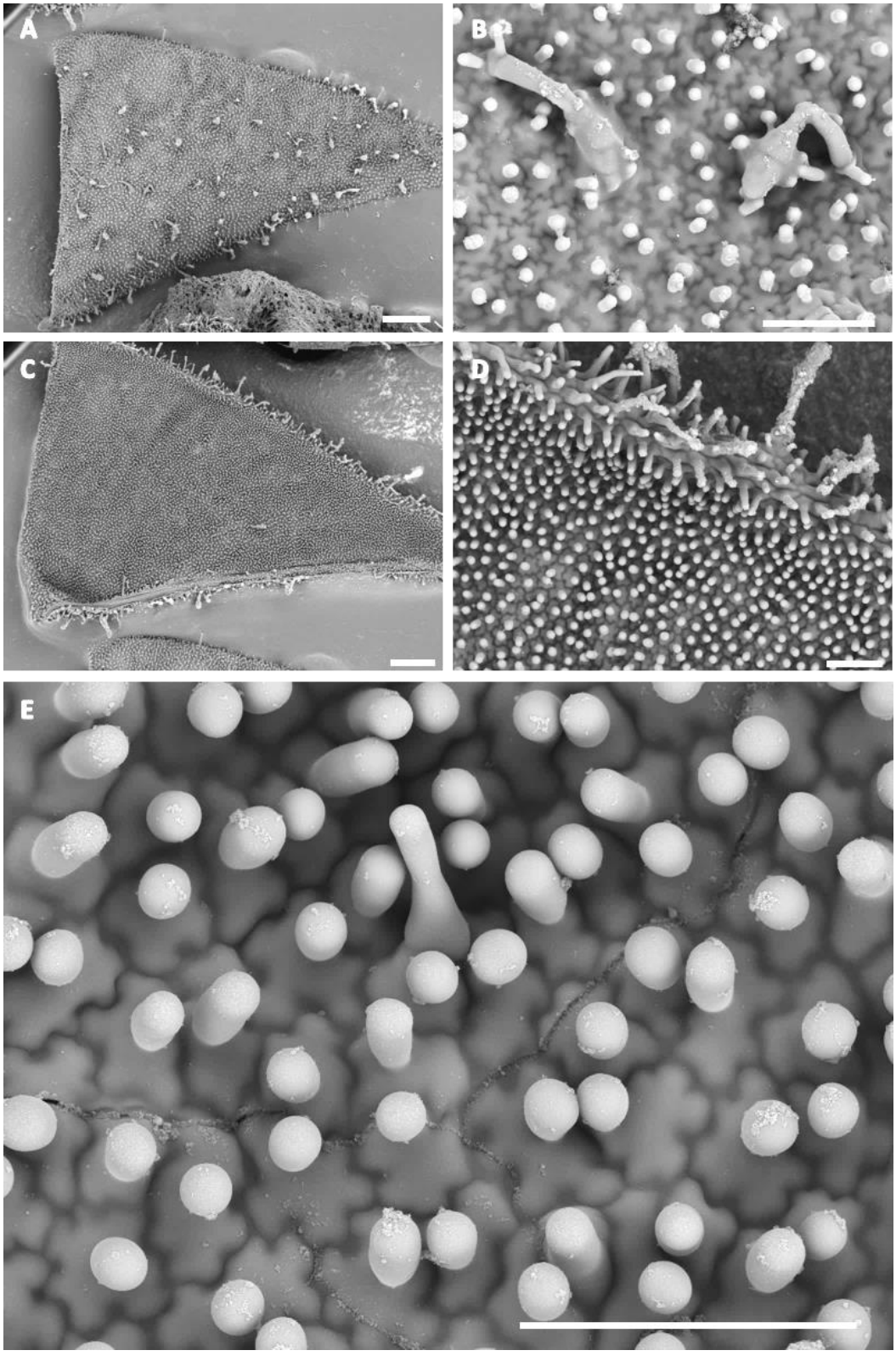

Plate XII. Epidermal features of *N. tabacum* lines expressing *NbMYB17-1* (line 29-2).
Cryo-SEM microphotographs of epidermal features on petal of *N. tabacum* 35S:*NbMYB17-1*, Line 29-2. A-B. Abaxial petal; C-E. Adaxial petal. Scale bars: A, C = 500µm; B, D, E = 100µm.

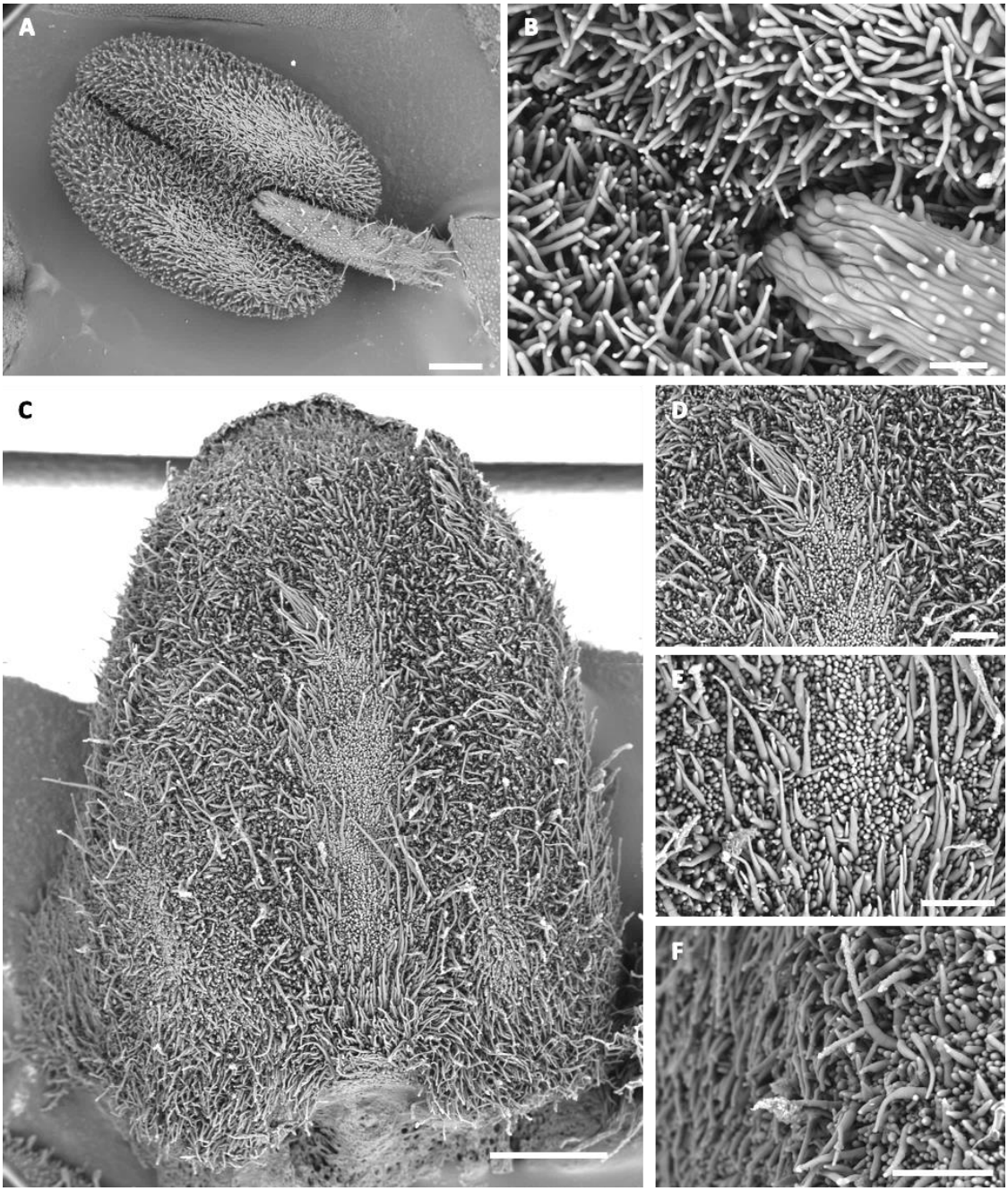

Plate XIII. Epidermal features of *N. tabacum* lines expressing *NbMYB17-1* (line 29-2).
Cryo-SEM microphotographs of epidermal features on anther and carpel of *N. tabacum* 35S:NbMYB17-1, Line 29-2. A-B. Anther; C-F. Carpel. Scale bars: A, C = 500µm; B = 100µm, D-F = 200µm .

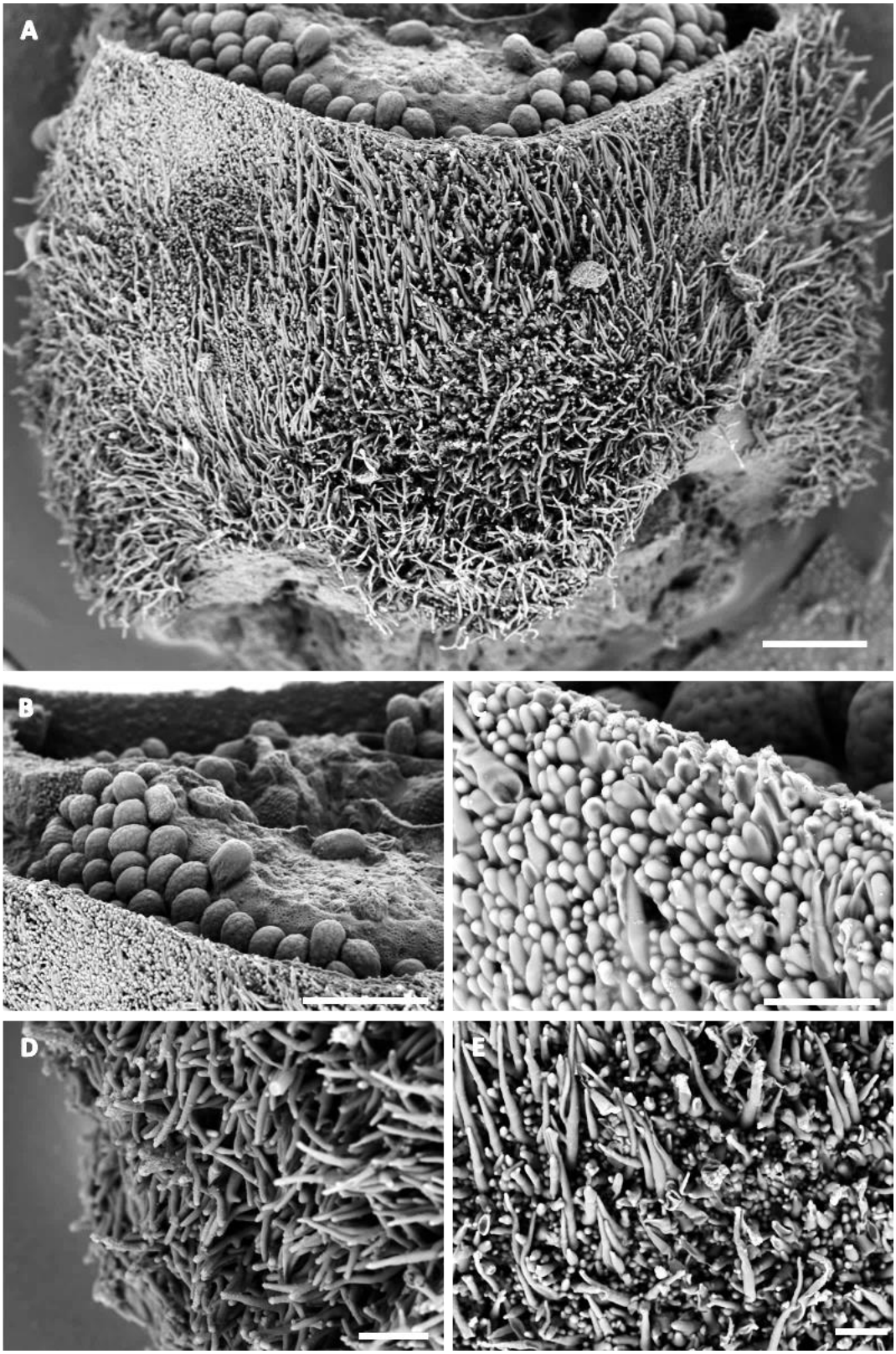

Plate XIV. Epidermal features of *N. tabacum* lines expressing *NbMYB17-1* (line 29-2)
Cryo-SEM microphotographs of epidermal features on carpel of *N. tabacum* 35S:*NbMYB17-1*, Line 29-2. Scale bars: A-B = 500µm; C-E = 100µm.

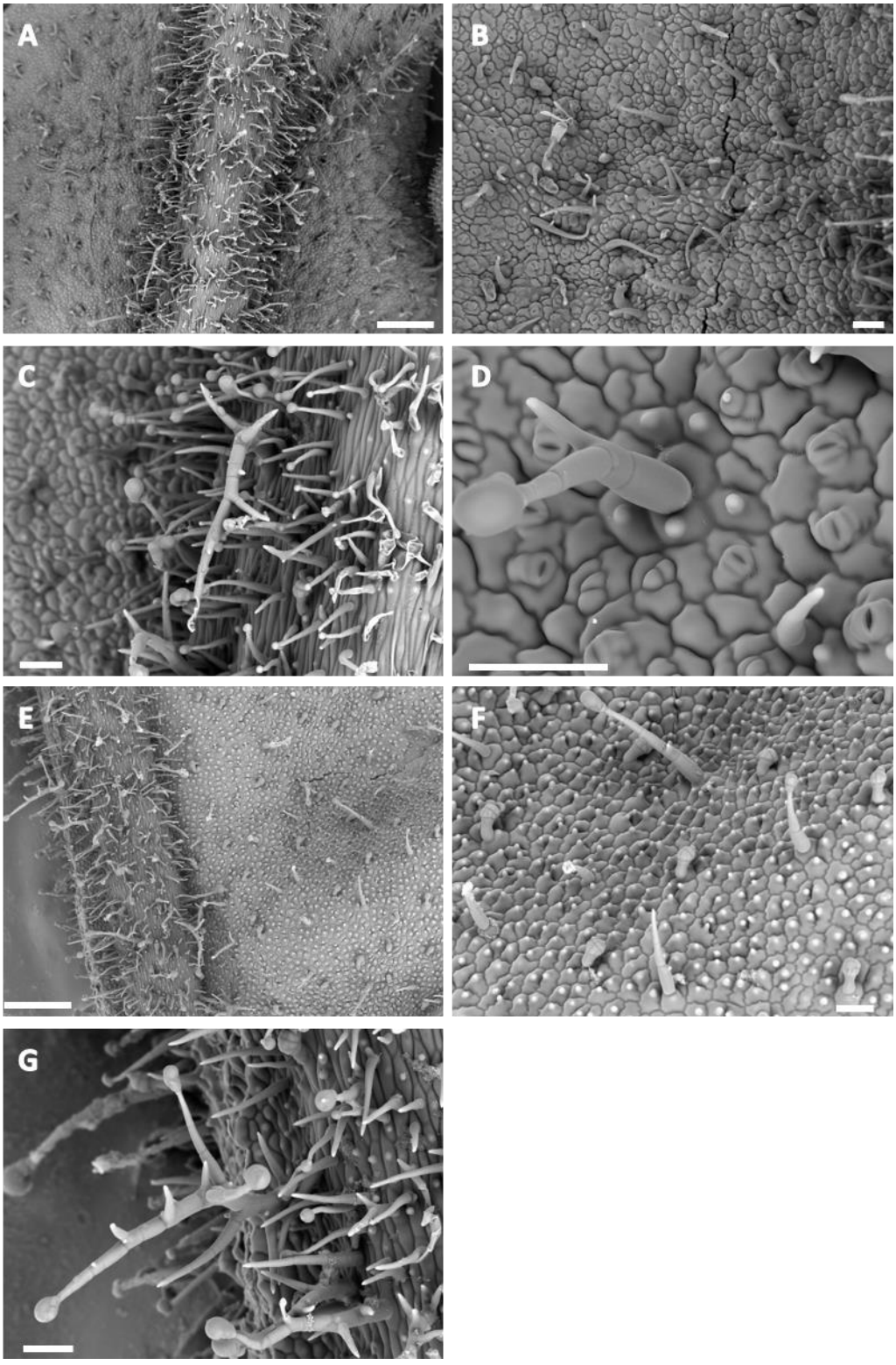

Plate XV. Epidermal features of *N. tabacum* lines expressing *NbMYB17-1* (line 29-3).
Cryo-SEM microphotographs of epidermal features on leaf of N. tabacum 35S:NbMYB17-1, Line 29-3. A-D. Abaxial leaf; D-G. Adaxial leaf -F. Scale bars: A, E = 500 µm; B-D, F-G = 100µm.

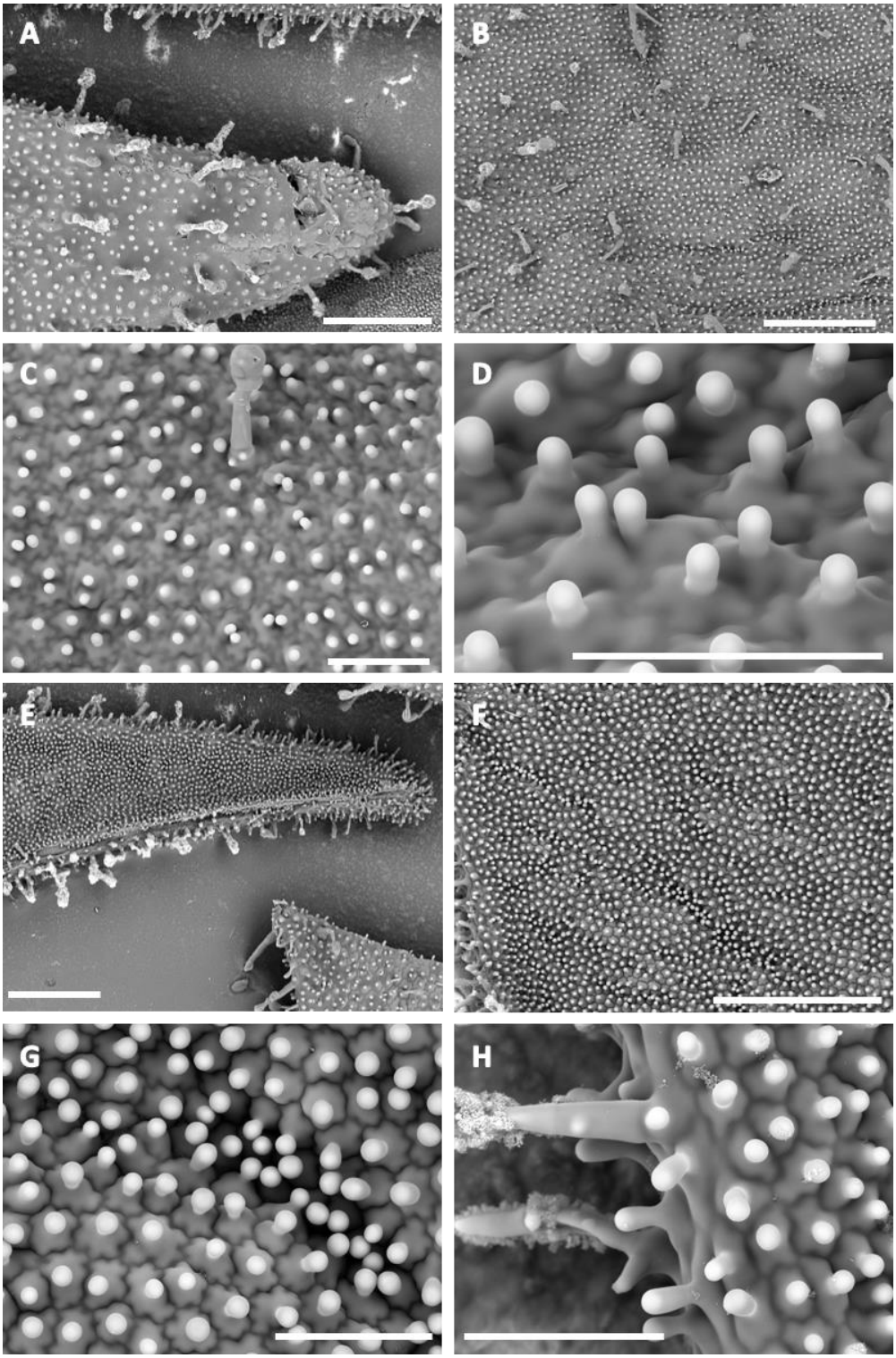

Plate XVI. Epidermal features of *N. tabacum* lines expressing *NbMYB17-1* (line 29-3).
Cryo-SEM microphotographs of epidermal features on petal of *N. tabacum* 35S:*NbMYB17-1*, Line 29-3. A-D. Abaxial petal; E-H. Adaxial petal. Scale bars: A-B, E-F = 500µm; C-D, G-H = 100µm.

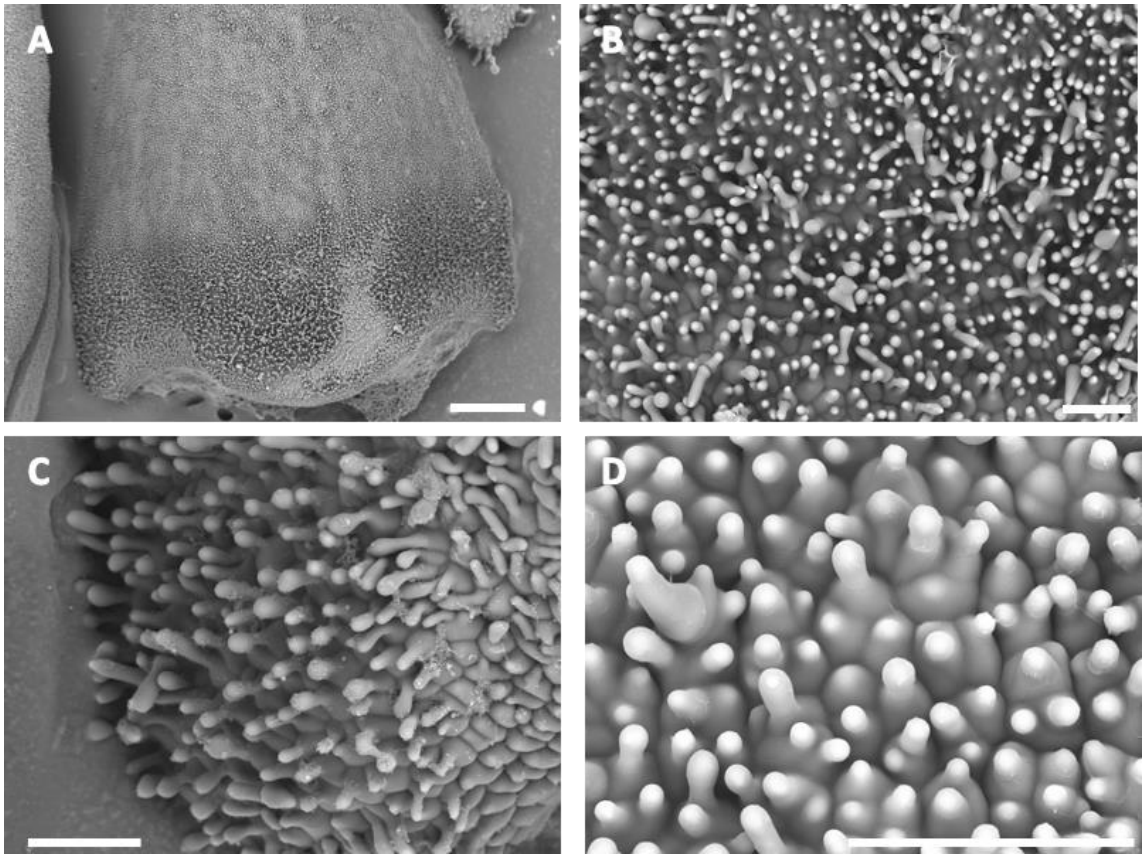

Plate XVII. Epidermal features of *N. tabacum* lines expressing *NbMYB17-1* (line 29-3).
Cryo-SEM microphotographs of epidermal features on carpel of *N. tabacum* 35S:*NbMYB17-1*, Line 29-3. A-D. Carpel. Scale bars: A,= 500µm; B-D = 100µm

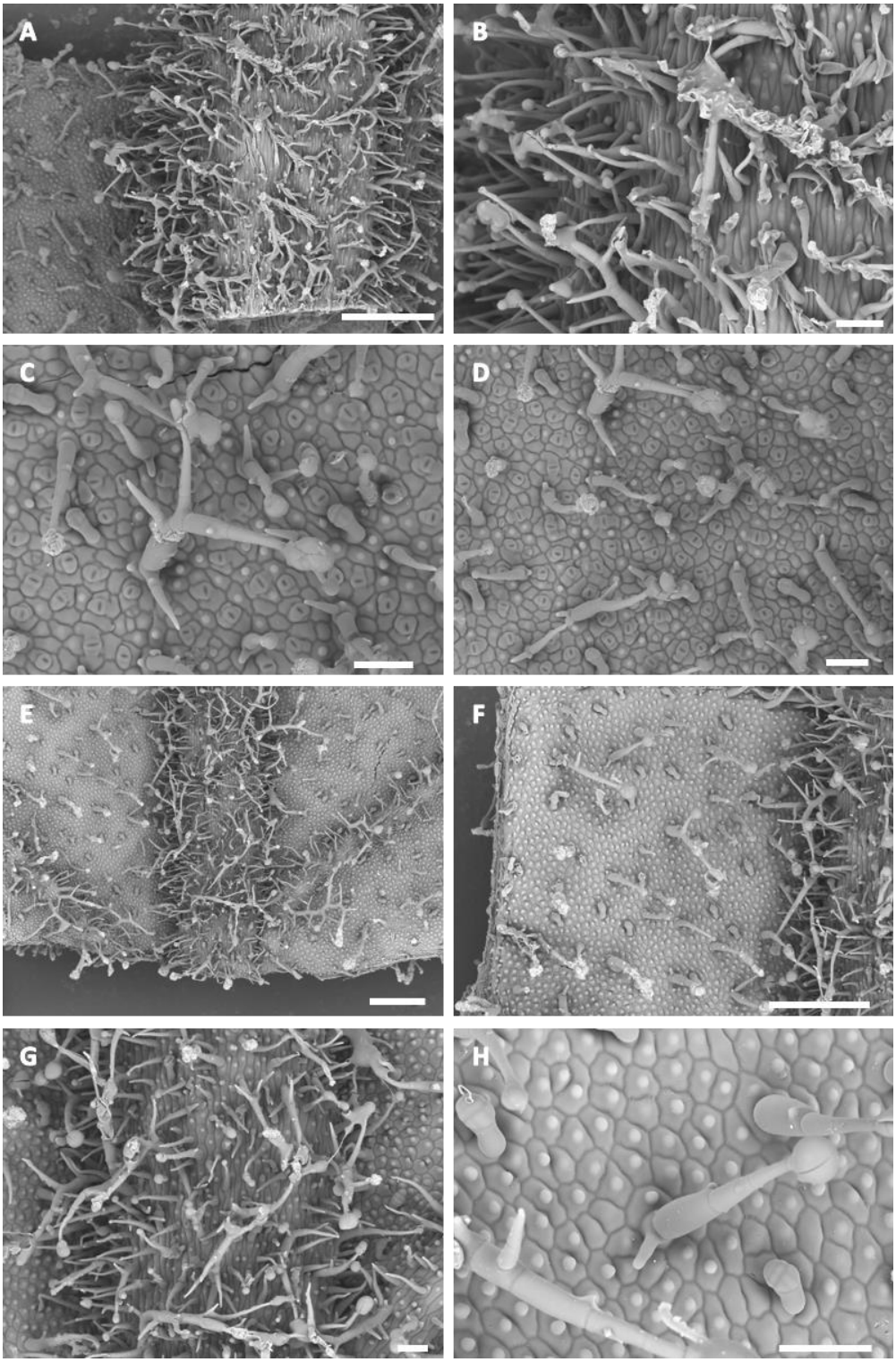

Plate XVIII. Epidermal features of *N. tabacum* lines expressing *NfMYB17-1* (line 5).
Cryo-SEM microphotographs of epidermal features on leaf of *N. tabacum* 35S:*NfMYB17-1*, Line 5. A-D. Abaxial leaf; D-H. Adaxial leaf. Scale bars: A, E-F =500µm, B-D, G-H=100µm

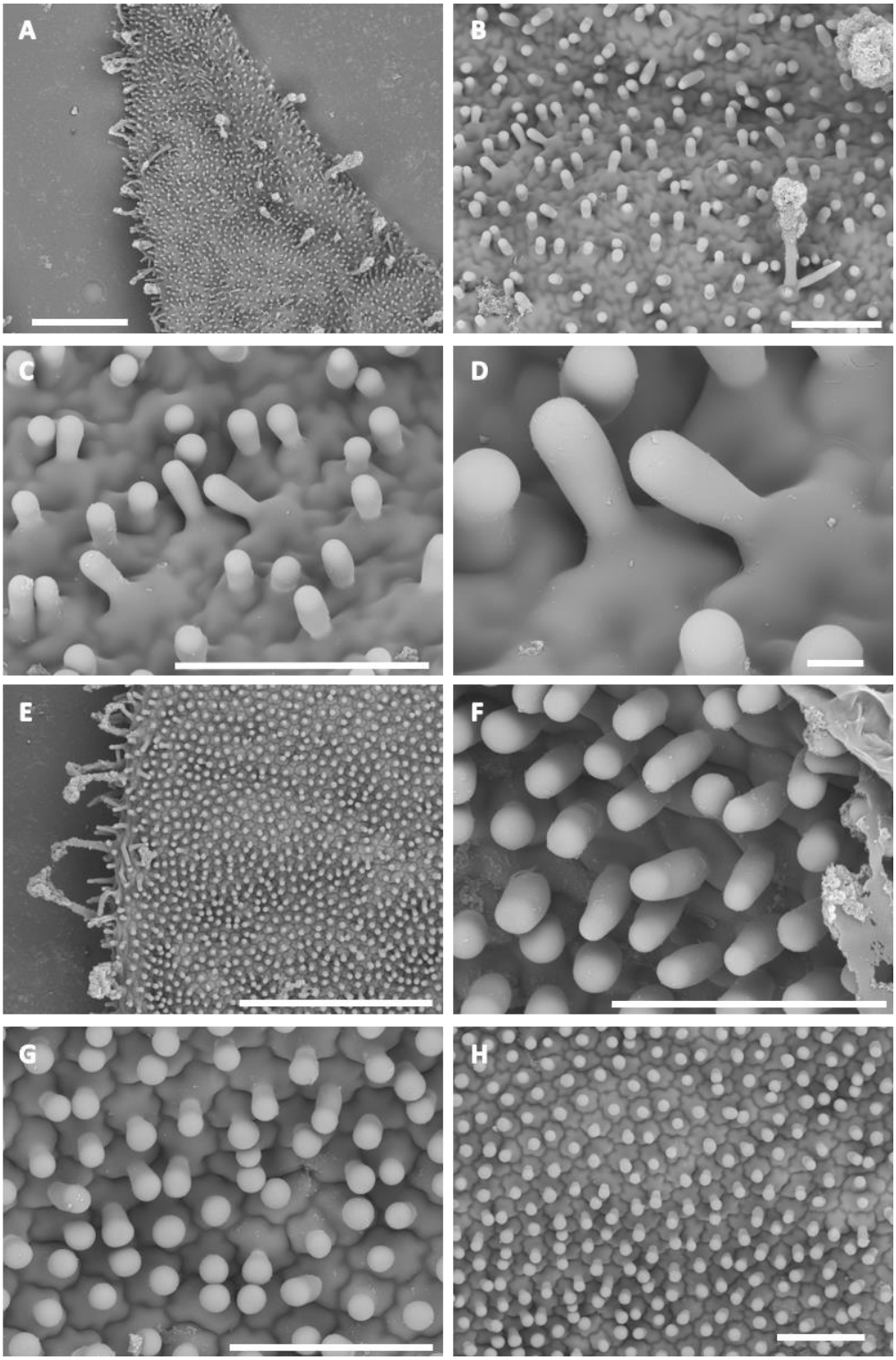

Plate XIX. Epidermal features of *N. tabacum* lines expressing *NfMYB17-1* (line 5).
Cryo-SEM microphotographs of epidermal features on petal of *N. tabacum* 35S:*NfMYB17-1*, Line 5. A-d. Abaxial petal; E-F. Adaxial petal. Scale bars: A, E = 500µm; B-C, F-H = 100µm, D = 10µm.

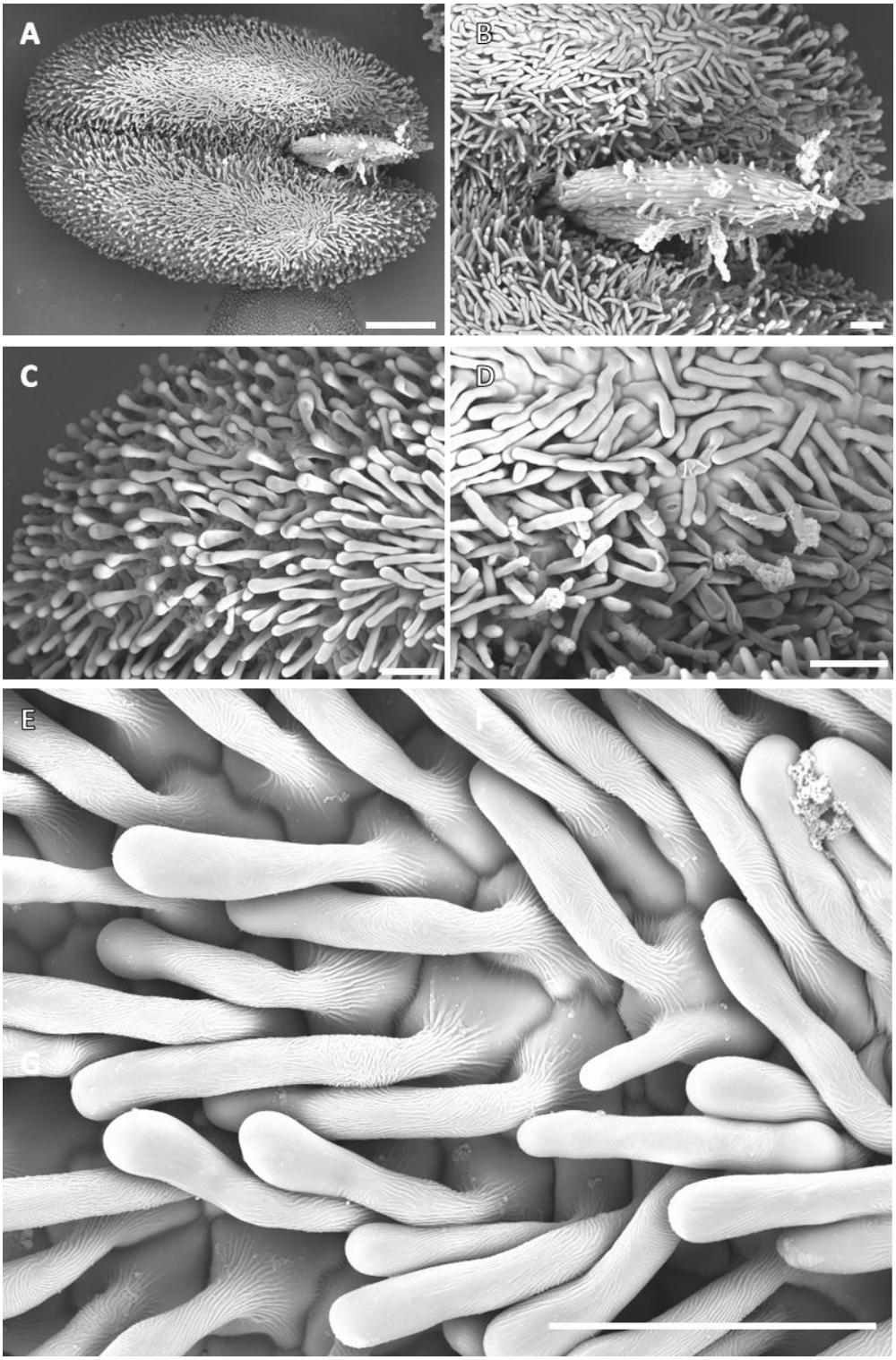

Plate XX. Epidermal features of *N. tabacum* lines expressing *NfMYB17-1* (line 5).
Cryo-SEM microphotographs of epidermal features on anther of *N. tabacum* 35S:*NfMYB17-1*, Line 5. Scale bars: A= 500µm; B-H = 100µm.

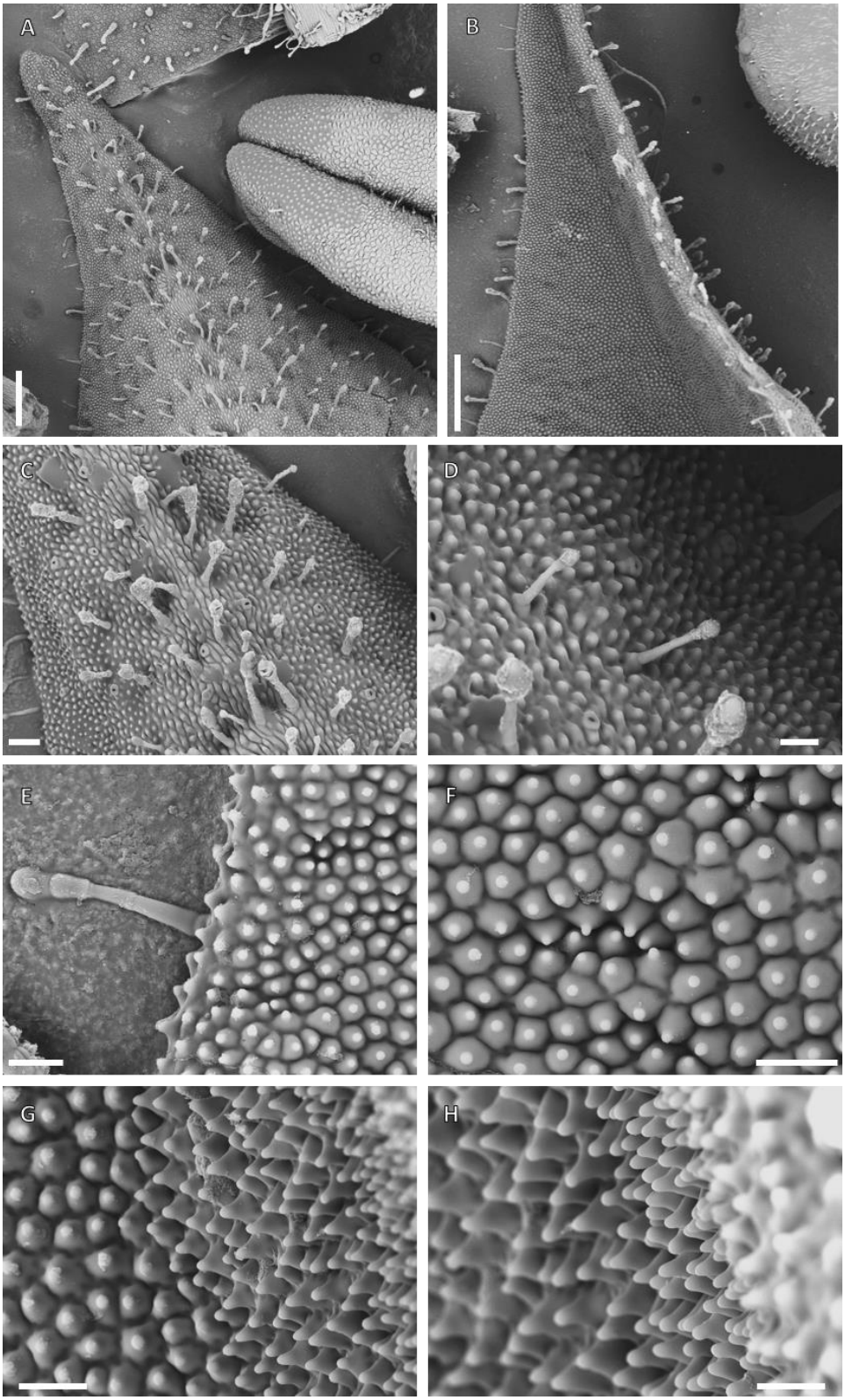

Plate XXI. Epidermal features on petal of *N. tabacum* WT.

Cryo-SEM microphotographs of epidermal features on petal of *N. tabacum* WT. A, C-D. Abaxial petal; B, E-H. Adaxial petal. Scale bars: A-B=500µm, C=100µm, D-H=50µm

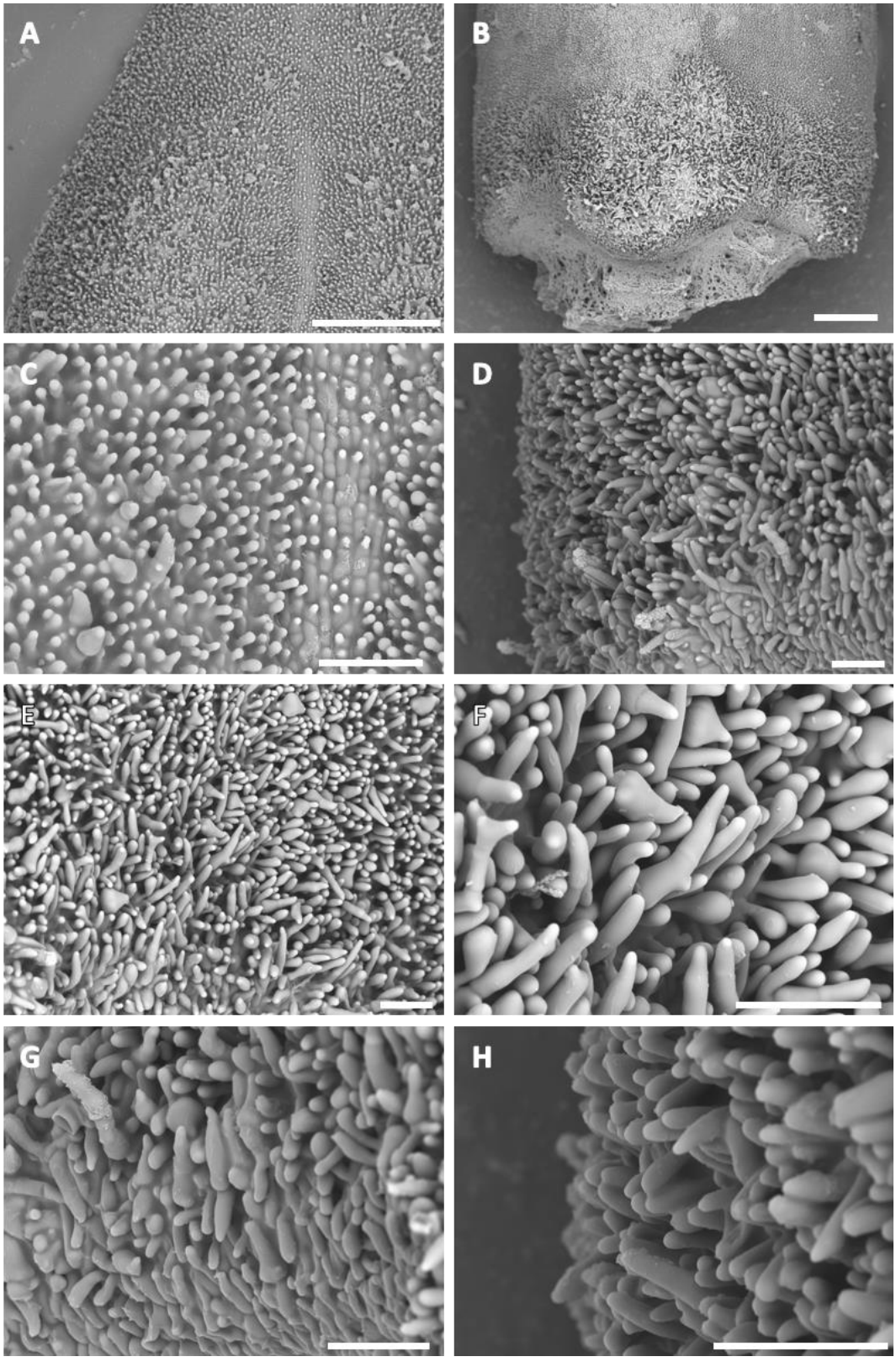

Plate XXII. Epidermal features of *N. tabacum* lines expressing *NfMYB17-1* (line 5).
Cryo-SEM microphotographs of epidermal features on carpel of *N. tabacum* 35S:*NfMYB17-1*, Line 5
Scale bars: A-B= 500µm; C-H = 100µm.

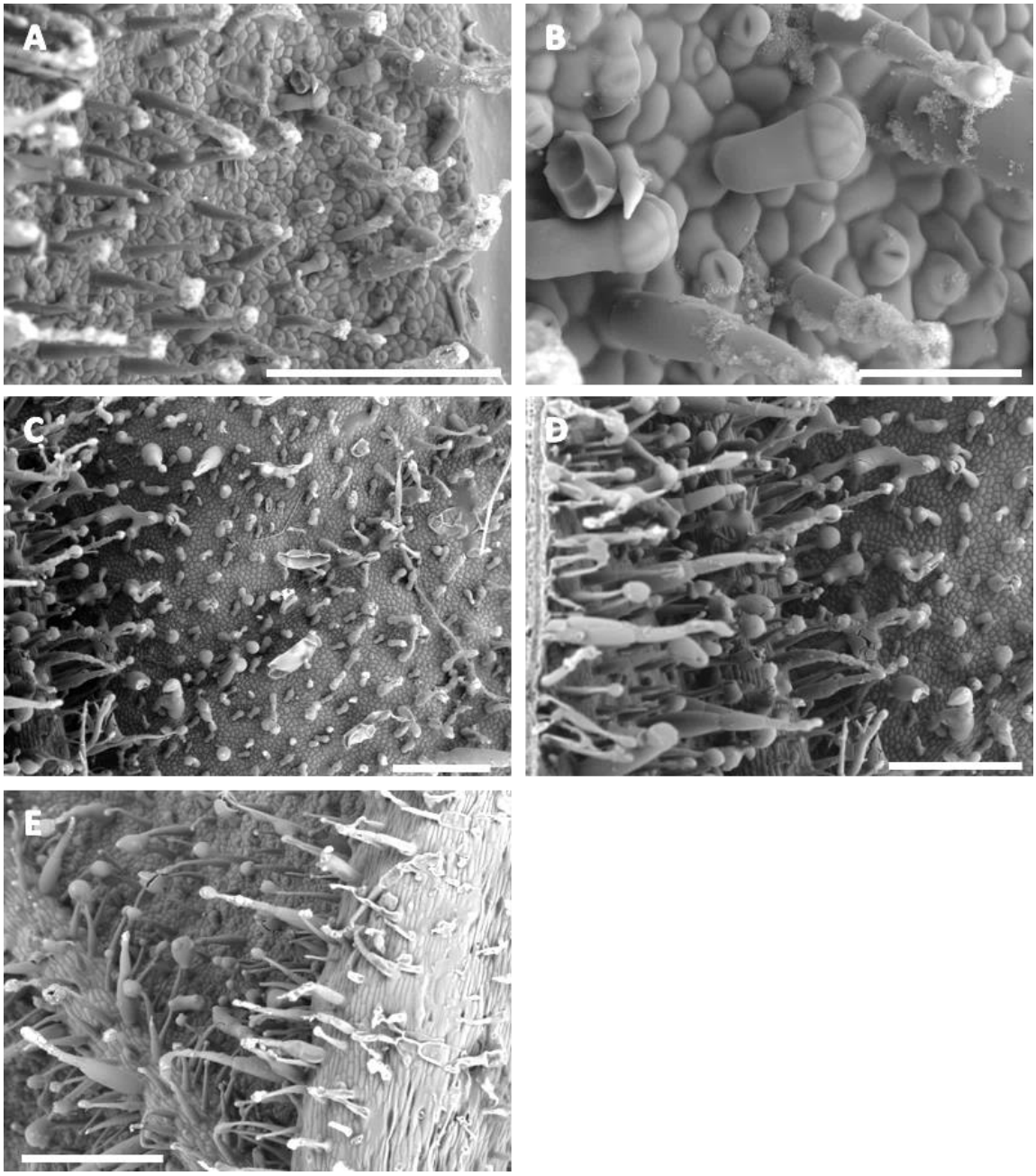

Plate XXIII. Epidermal features of *N. tabacum* lines expressing *NfMYB17-1* (line 8).
Cryo-SEM microphotographs of epidermal features on leaf of *N. tabacum* 35S:*NfMYB17-1*, Line 8. A-B. Abaxial leaf; C-E. Adaxial leaf. Scale bars: A, C-E =500µm, B = 100µm.

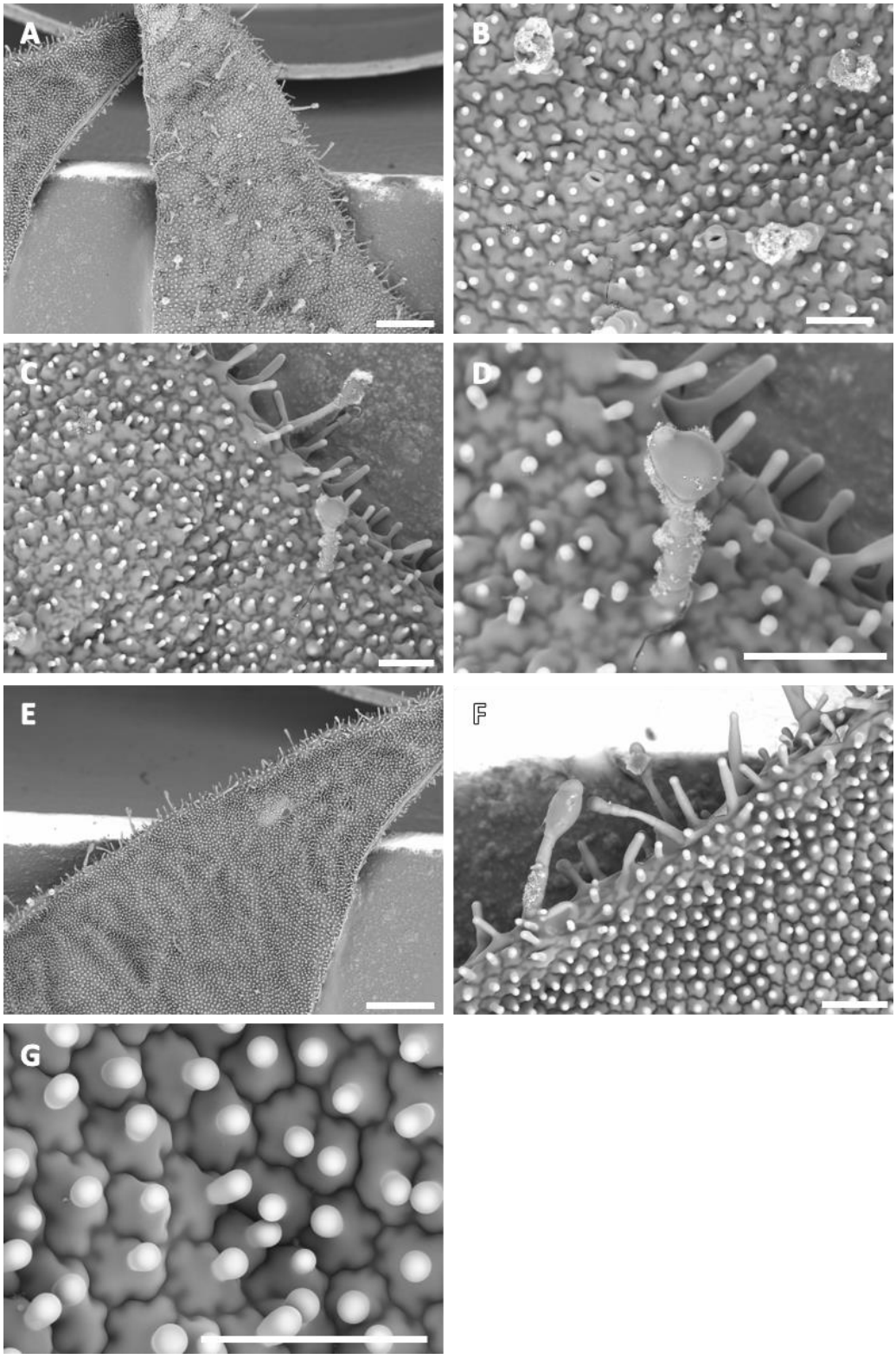

Plate XXIV. Epidermal features of *N. tabacum* lines expressing *NfMYB17-1* (line 8).
Cryo-SEM microphotographs of epidermal features on petal of *N. tabacum* 35S:*NfMYB17-1*, Line 8. A-D. Abaxial petal; E-G. Adaxial petal. Scale bars: A, E = 500µm; B-D, F-G = 100µm.

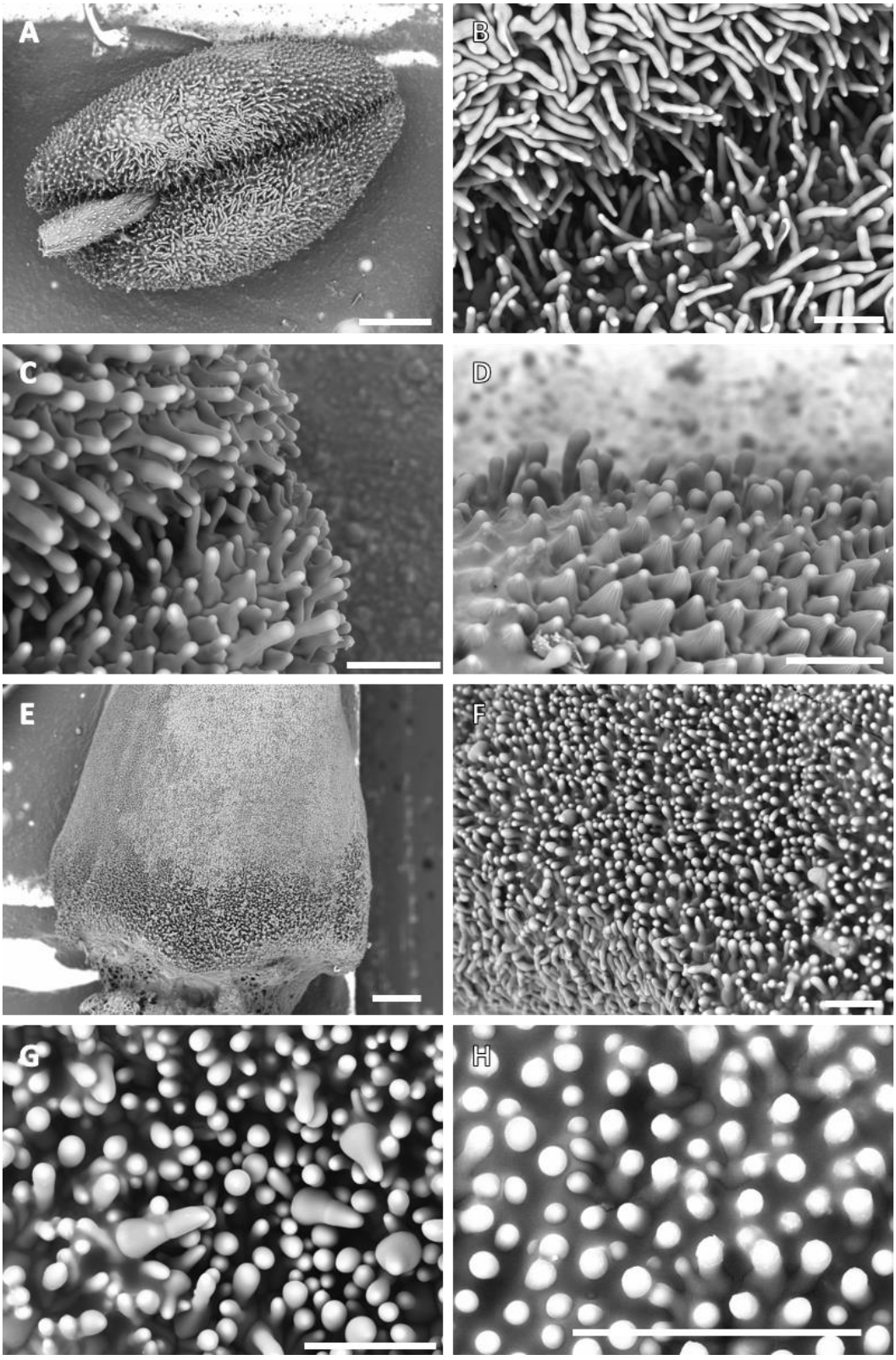

Plate XXV. Epidermal features of *N. tabacum* lines expressing *NfMYB17-1* (line 8).
Cryo-SEM microphotographs of epidermal features on anther and carpel of *N. tabacum* 35S:*NfMYB17-1*, Line 8. A-D. Anther; E-H. Carpel. Scale bars: A, E = 500µm; B-D, F-H = 100µm .

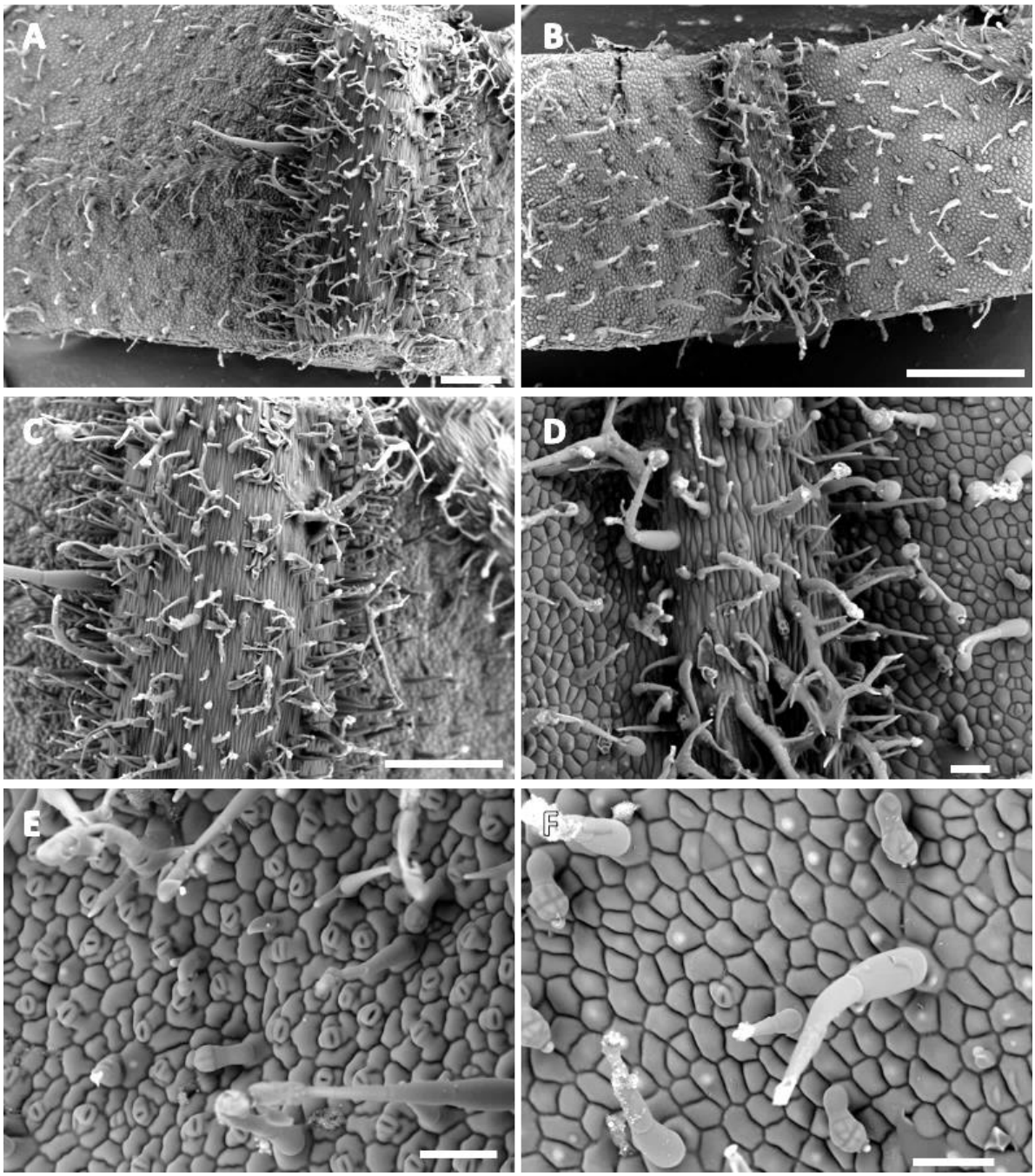

Plate XXVI. Epidermal features of *N. tabacum* lines expressing *NfMYB17-1* (line 10).
Cryo-SEM microphotographs of epidermal features on leaf of *N. tabacum* 35S:*NfMYB17-1*, Line 10. A, C, F. Abaxial leaf; B, D, E. Adaxial leaf. Scale bars: A-C =500µm, D-F = 100µm.

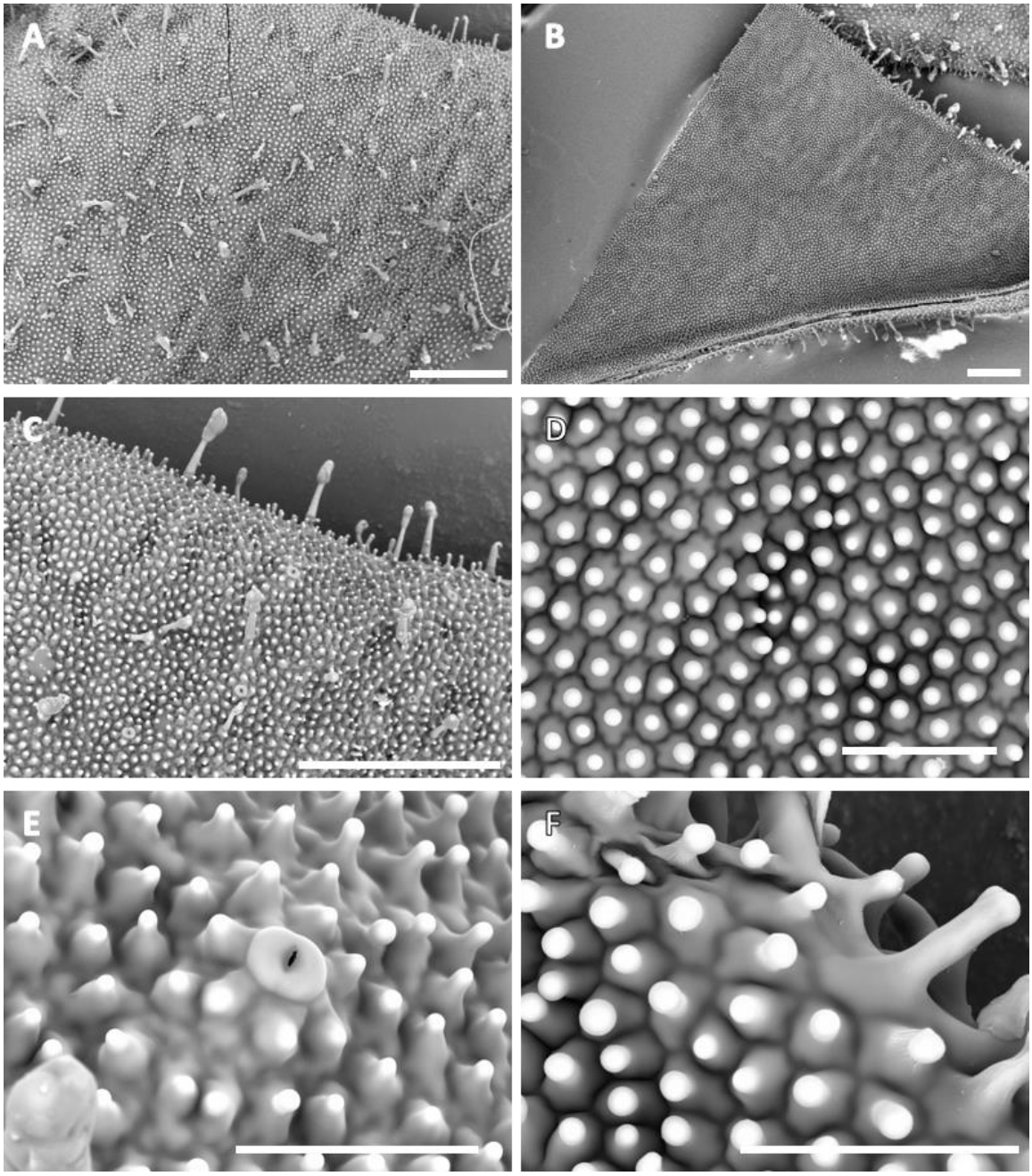

Plate XXVII. Epidermal features of *N. tabacum* lines expressing *NfMYB17-1* (line 10).
Cryo-SEM microphotographs of epidermal features on petal of *N. tabacum* 35S:*NfMYB17-1*, Line 10. A, C, E. Abaxial petal; B, D, F. Adaxial petal. Scale bars: A-C = 500µm; D-F = 100µm.

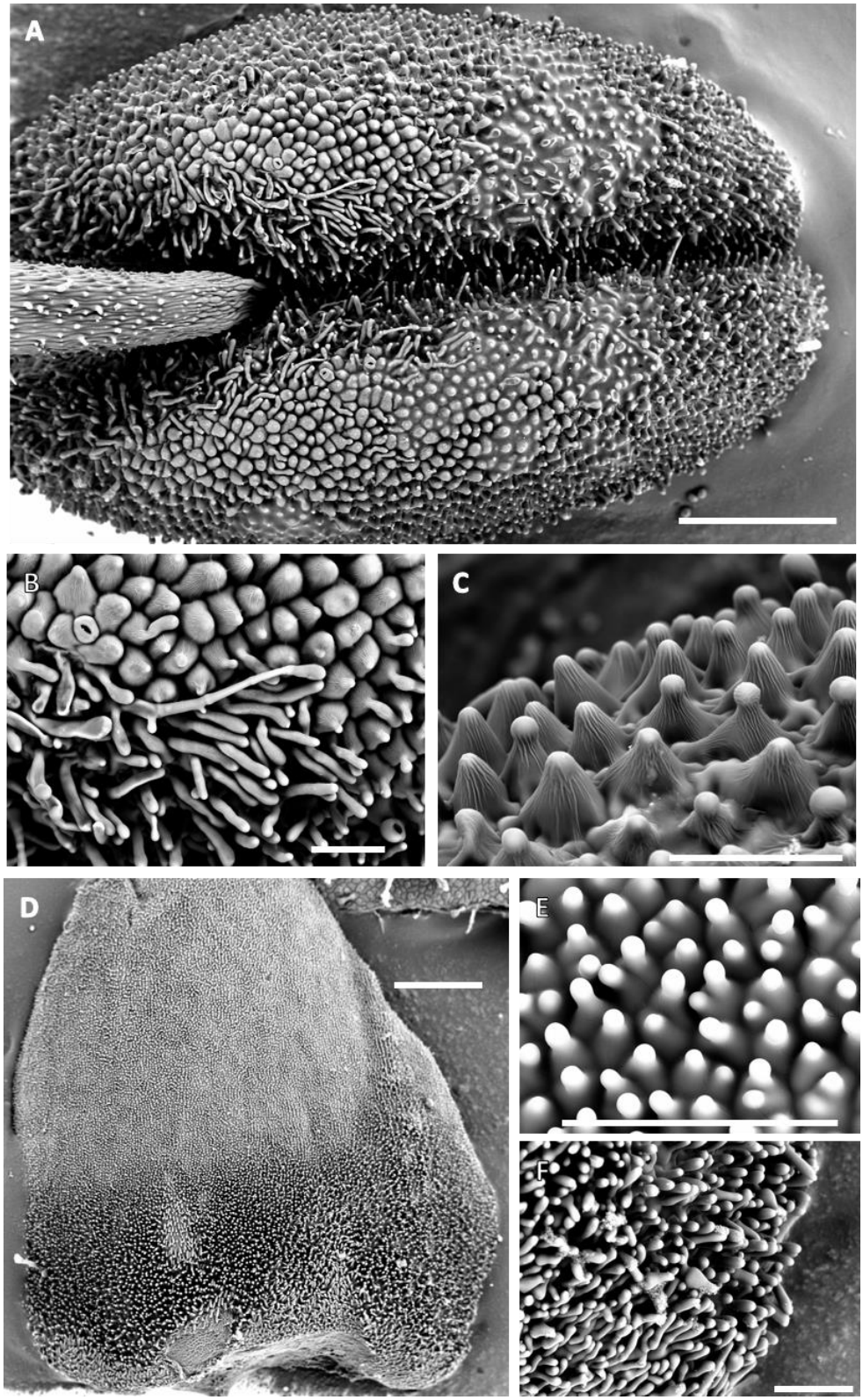

Plate XXVIII. Epidermal features of *N. tabacum* lines expressing *NfMYB17-1* (line 10).
Cryo-SEM microphotographs of epidermal features on anther and carpel of *N. tabacum* 35S:*NfMYB17-1*, Line 10. A-C. Anther; D-F. Carpel. Scale bars: A, D = 500µm; B-C, E-F = 100µm .

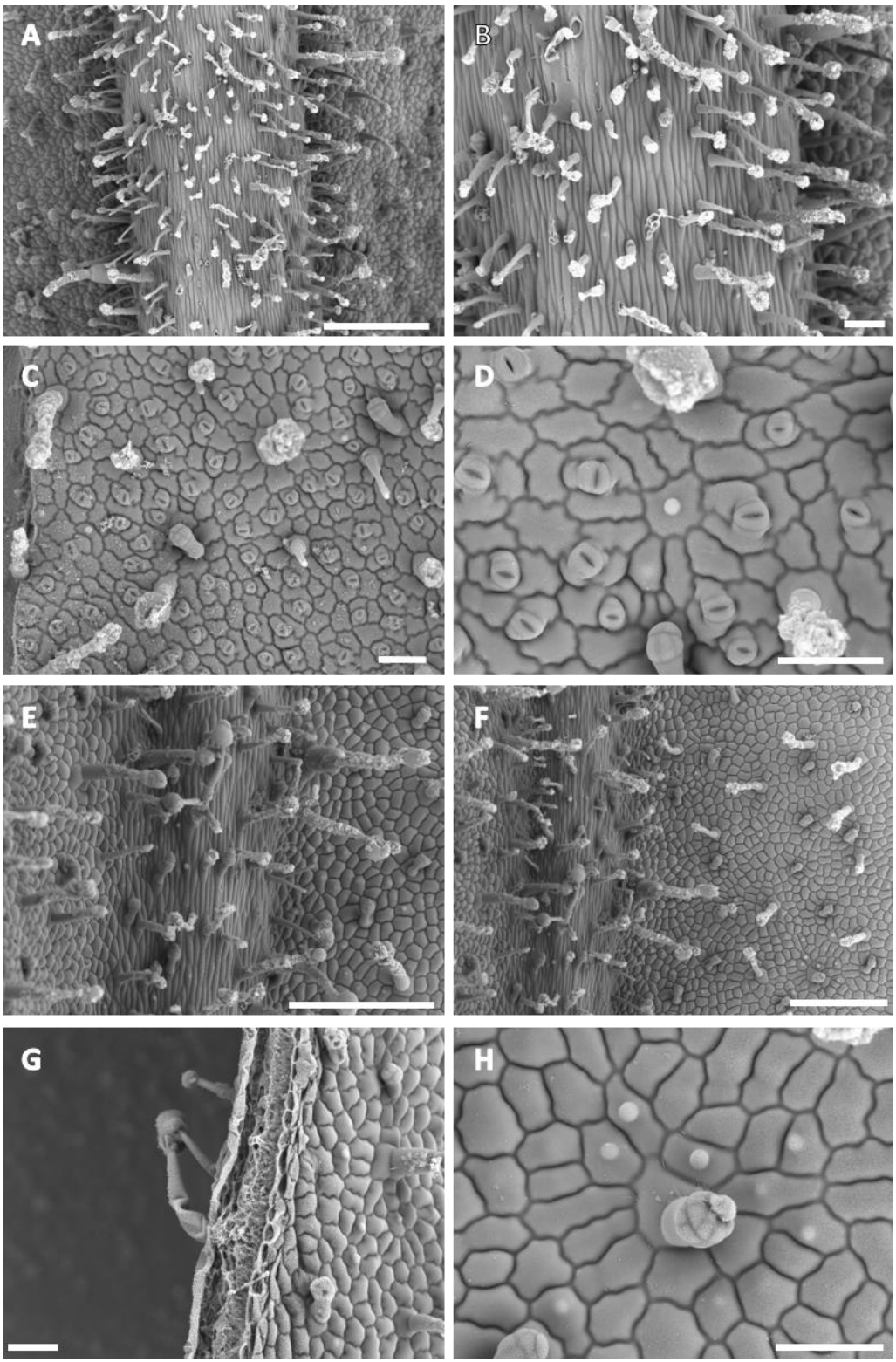

Plate XXIX. Epidermal features of *N. tabacum* lines expressing *NfMYB17-1* (line 11).
Cryo-SEM microphotographs of epidermal features on leaf of *N. tabacum* 35S:*NfMYB17-1*, Line 11. A-D. Abaxial leaf; D-H. Adaxial leaf. Scale bars: A, E-F =500µm, B-D, G-H=100µm

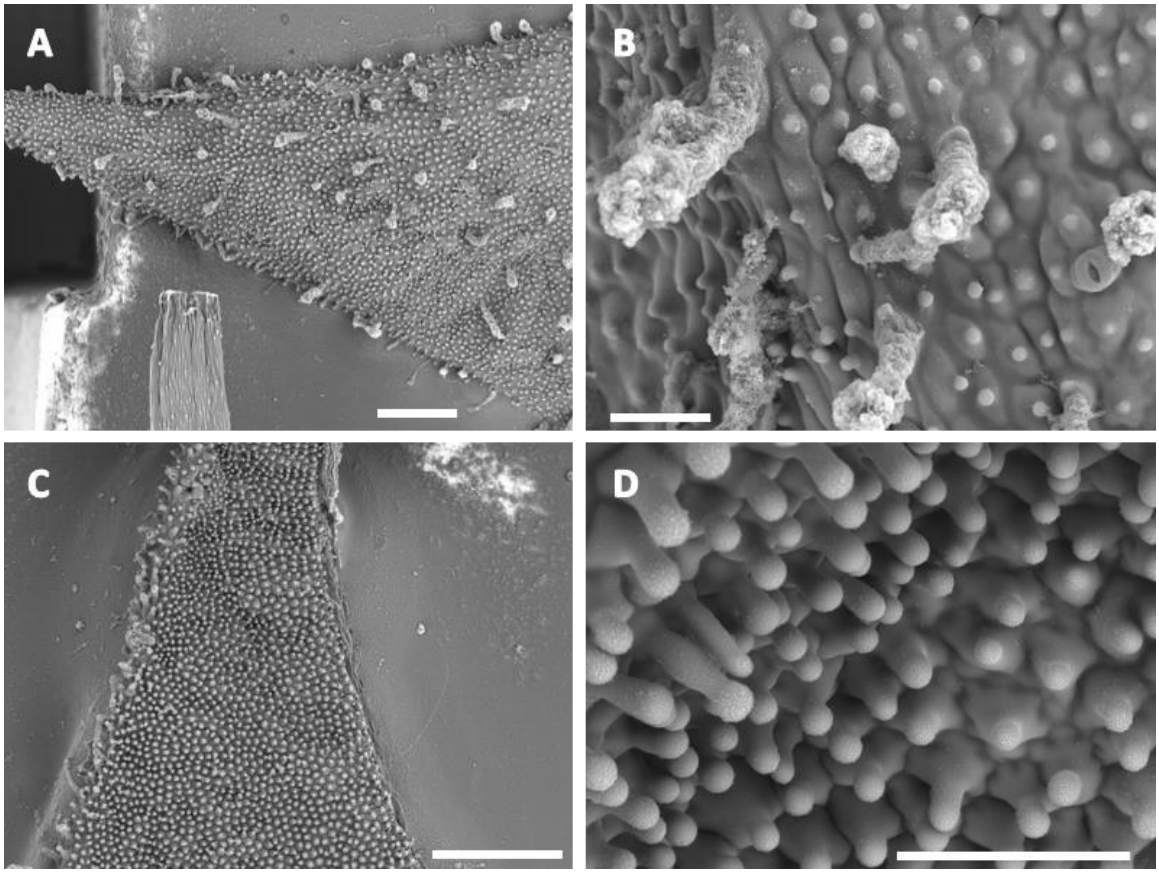

Plate XXX. Epidermal features of *N. tabacum* lines expressing *NfMYB17-1* (line 11).
Cryo-SEM microphotographs of epidermal features on petal of *N. tabacum* 35S:*NfMYB17-1*, Line 11. A-B. Abaxial petal; C-D. Adaxial petal. Scale bars: A, C = 500µm; B, D = 100µm.

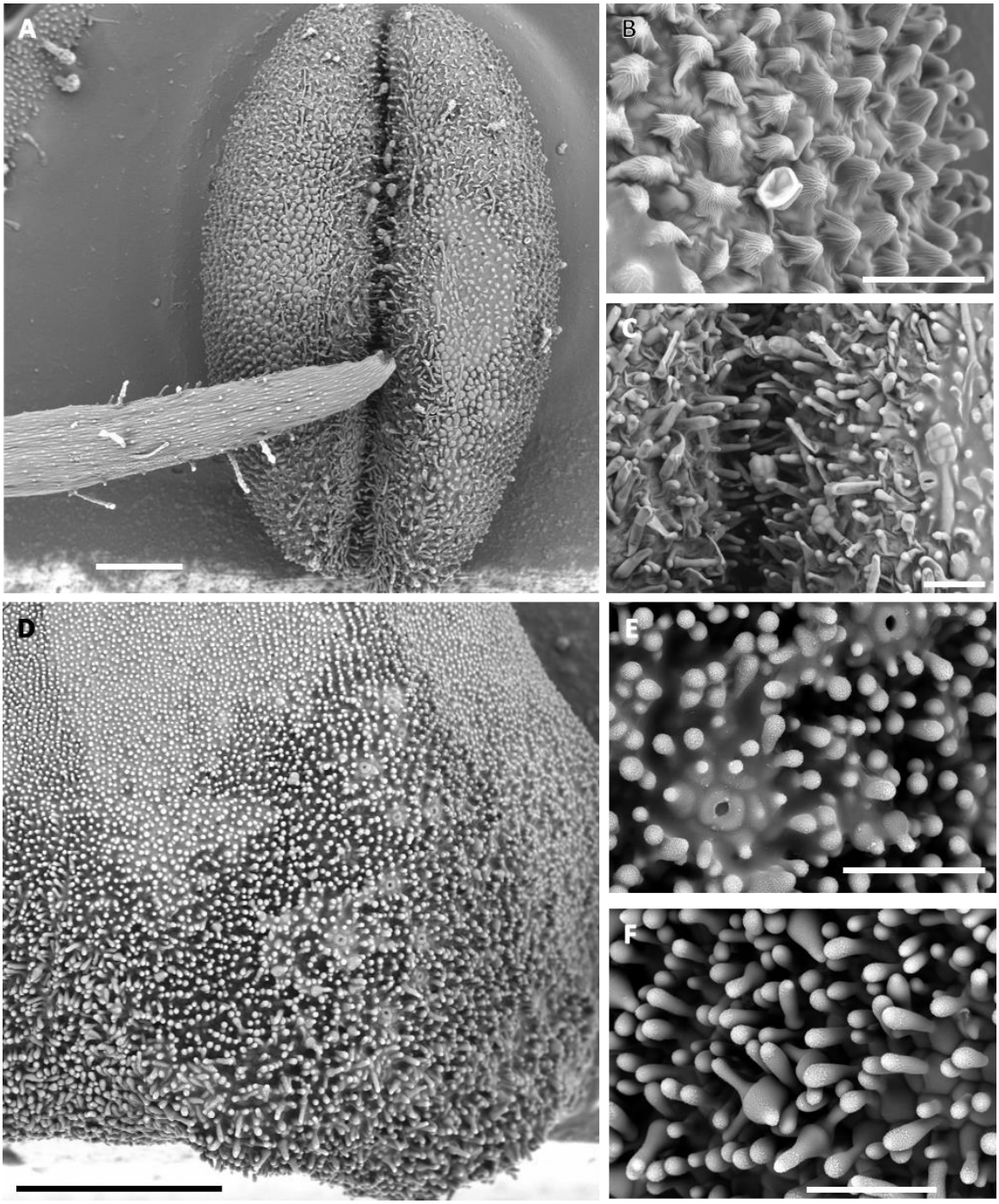

Plate XXXI. Epidermal features of *N. tabacum* lines expressing *NfMYB17-1* (line 11).
Cryo-SEM microphotographs of epidermal features on anther and carpel of *N. tabacum* 35S:*NfMYB17-1*, Line 11. A-C. Anther; D-F. Carpel. Scale bars: A, D = 500µm; B, D, E = 100µm.

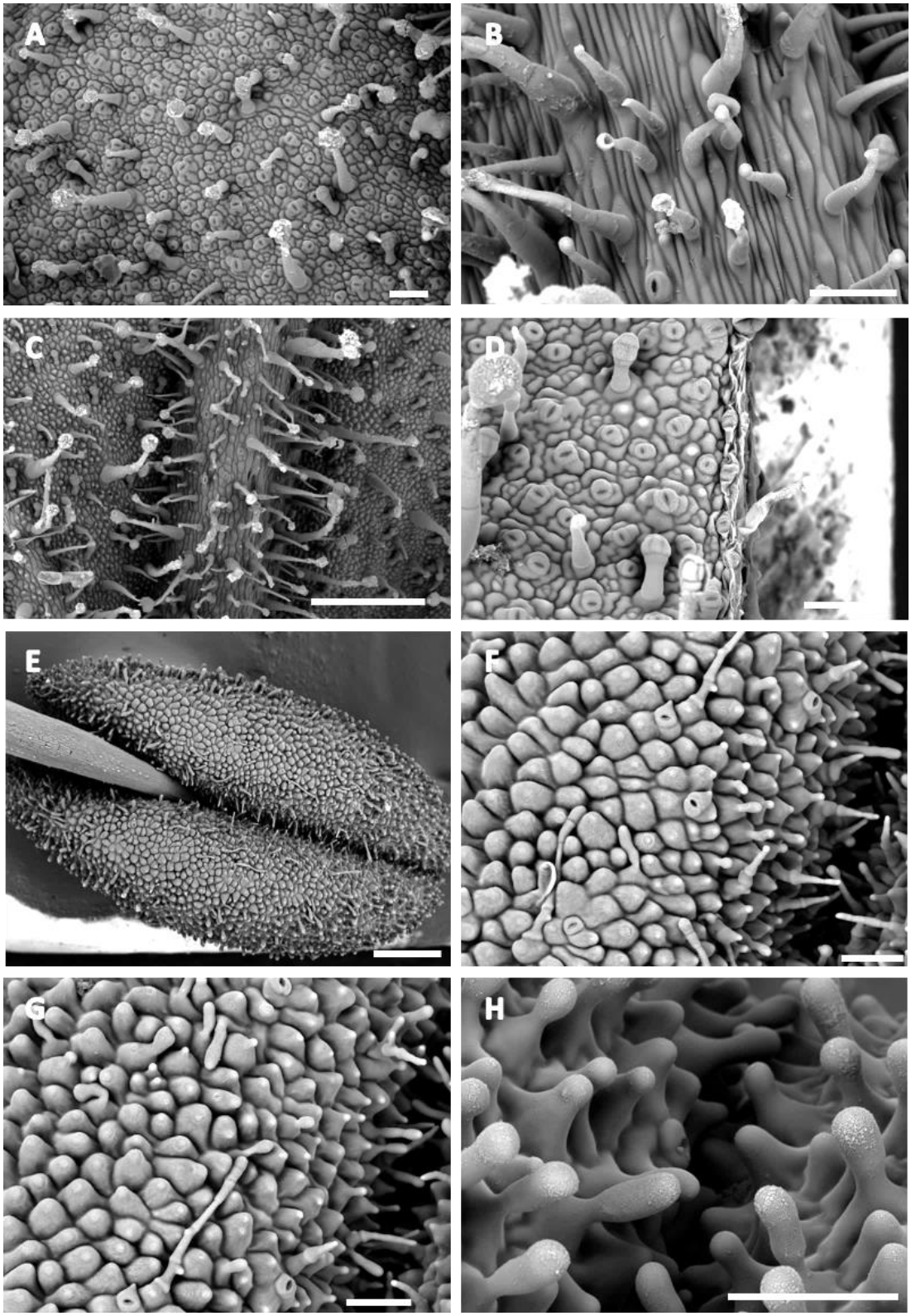

Plate XXXII. Epidermal features of *N. tabacum* lines expressing *NfMYB17-1* (line 12).
Cryo-SEM microphotographs of epidermal features on leaf and anther of *N. tabacum* 35S:*NfMYB17-1*, Line 12. A-B. Abaxial leaf; C-D. Adaxial leaf; E-G. Anther. Scale bars: A, E-F =500µm, B-D, G-H=100µm

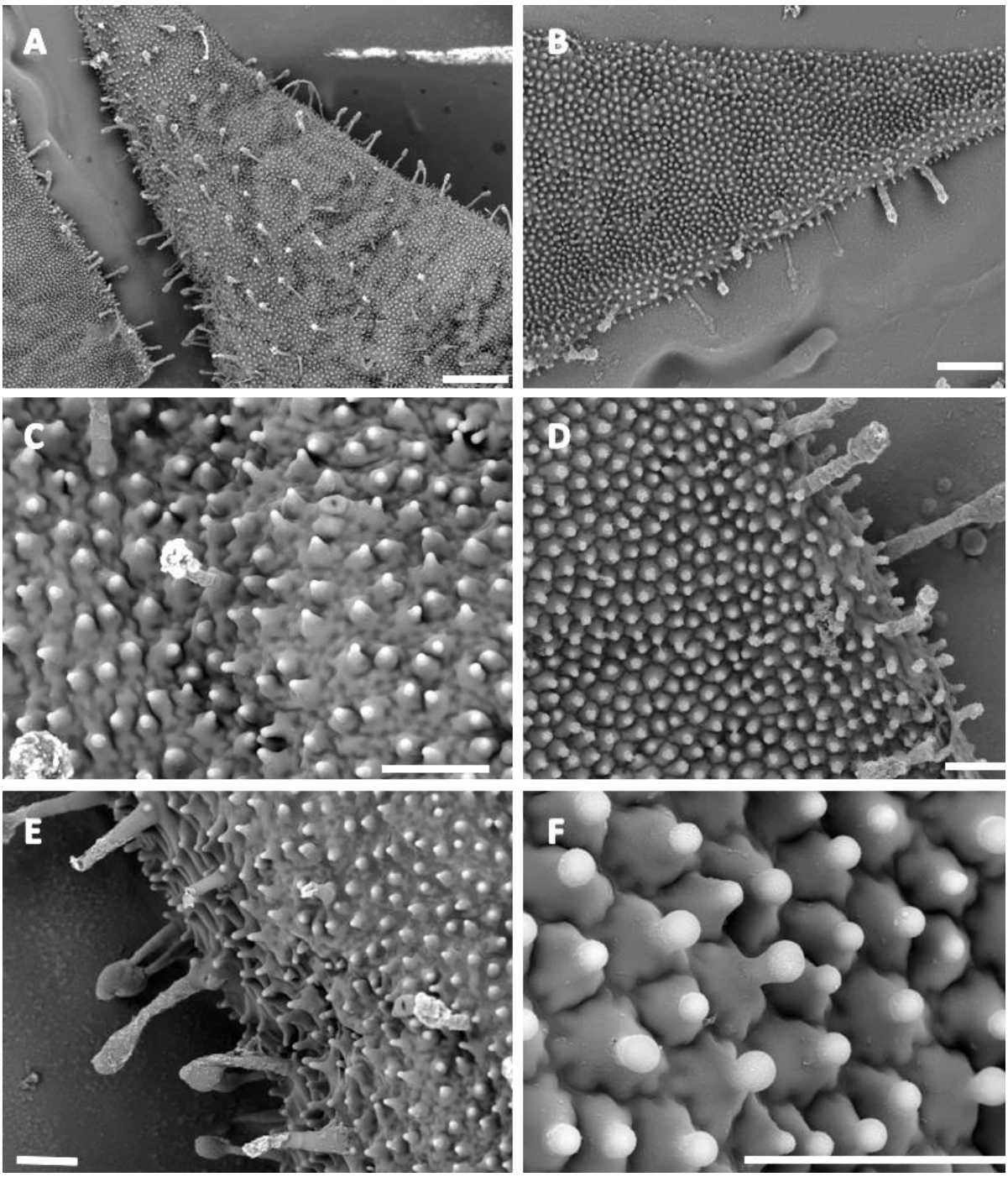

Plate XXXIII. Epidermal features of *N. tabacum* lines expressing *NfMYB17-1* (line 12).
Cryo-SEM microphotographs of epidermal features on petal of *N. tabacum* 35S:*NfMYB17-1*, Line 12. A, C, E. Abaxial petal; B, D, F. Adaxial petal. Scale bars: A-B = 500µm; C-E = 100µm.

Appendix 11. Descriptive statistics for bumblebee behaviour foraging speed experiments

Appendix 11A. General statistical comparisons for foraging speed experiments.

Comparisons between sets of data including all the observations from all the treatments. A. Comparisons between the flight times between "Flower 1-2" and "Flower 2-3". B. Comparisons between times of flight between "Conical" and "Non-conical" flowers. Upper panels: Boxplots. Center panels: Descriptive statistics of the data. Bottom panels: Welch two sample t-tests for comparison between means.

A

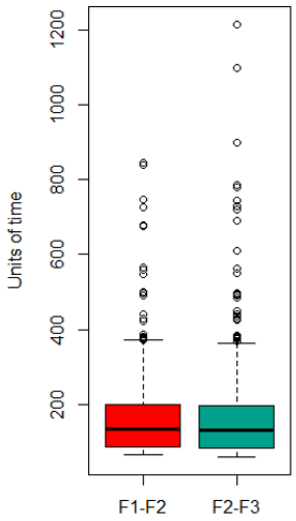

Descriptive statistics	F1-F2	F2-F3
n	354	355
Min	65	60
Extreme of lower whisker	65.0	60.0
Lower hinge	85.0	83.0
Median	133.0	130.5
Mean	173.70	172.37
Upper hinge	200.0	196.0
Extreme of upper whisker	371.0	363.0
Max	844.0	1215.0
Standard deviation	124.60	151.15
Standard error	6.63	8.20

```
Welch Two Sample t-test

t = 0.15781
df = 658.88
p-value = 0.8747
95% confidence interval:
-19.01526  22.33885
sample estimates:
mean of x mean of y
 173.6941  172.0323
```

B

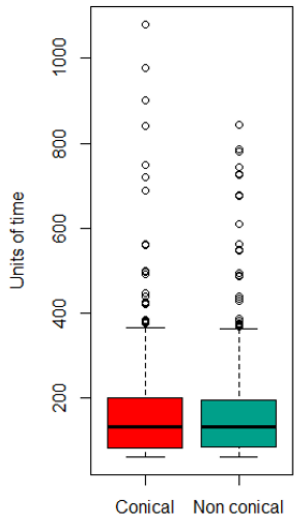

Descriptive Statistics	Conical	Non-conical
n	349	344
Min	62.0	63.0
Extreme of lower whisker	62.0	63.0
Lower hinge	83.0	85.0
Median	132.0	132.5
Mean	171.47	173.90
Upper hinge	200.0	197.0
Extreme of upper whisker	367.0	363.0
Max	1080	844
Standard deviation	137.61	133.81
Standard error	7.37	7.21

```
Welch Two Sample t-test

t = -0.2358
df = 690.87
p-value = 0.8137
95% confidence interval:
 -22.67533  17.81283
sample estimates:
mean of x mean of y
 171.4699  173.9012
```

Appendix 11B. Statistic comparisons between different treatments of the foraging speed experiment.
Comparisons discriminate sets of data of the four different treatments: White-conical (WC, dark purple), white-non-conical (WNC, light purple), red-conical (RC, dark red) and red-non-conical (RNC, light red). A. Boxplots of the data distribution of the different treatments. B. Descriptive statistics of the data including parameters of the boxplot. C. One-way analysis of variance model-ANOVA comparing means of the four treatments. D. Tukey multiple comparison of means test.

A

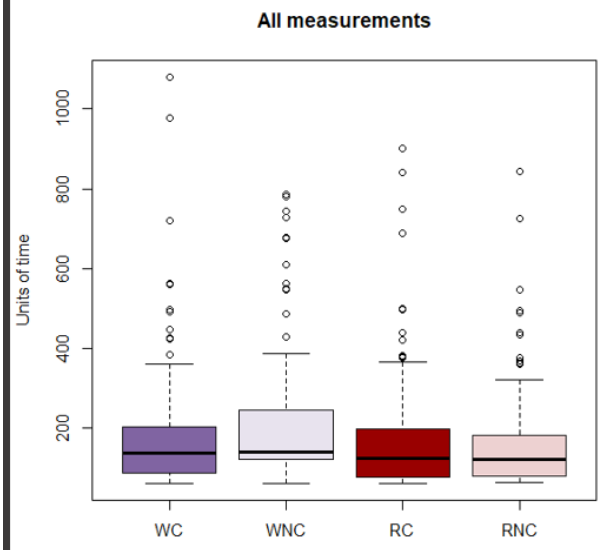

B

Descriptive statistics	WC	WNC	RC	RNC
n	161	151	188	193
Min	62.0	63.0	62.0	64.0
Extreme of lower whisker	62.0	63.0	62.0	64.0
Lower hinge	88.0	122.5	79.0	80
Median	139.0	142.0	125.0	123.0
Mean	185.0	203.7	150.6	159.9
Upper hinge	204.0	244.5	197.5	182.0
Extreme of upper whisker	361.0	388.0	367.0	322.0
Max	1080	785	900	844
Standard deviation	105.41	127.66	135.02	125.63
Standard error	11.71	14.64	8.98	12.62

C

One-way Analysis of variance model-ANOVA

	Df	Sum Sq	Mean Sq	F value	Pr(>F)
Disc Setup	3	294032	98011	5.429	0.00108**
Residuals	689	12438536	18053		

D

Tukey multiple comparisons of means
95% family-wise confidence level
Fit: anova formula = Flower_ALL ~ Disc_Setup, data = treat)

		diff	lwr	upr	p adj
WNC	WC	18.71276	-20.4868	57.91228	0.608343
RNC	RC	-9.30868	-44.7663	26.14895	0.906149
WNC	RNC	53.06928	15.47542	90.66314	0.001693
WC	RC	25.04784	-12.1079	62.20356	0.305727
WNC	RC	43.7606	5.947941	81.57327	0.015740
WC	RNC	34.35652	-2.57651	71.28954	0.078839

Appendix 12. Phenotype of putative *N. benthamina* transgenic lines expressing *NbMYB17-1*
Cryo-SEM microphotographs of abaxial leaf, adaxial petal and carper on *N. benthamiana* WT (yellow boxes) compared to putative lines expressing *NbMYB17-1* (green boxes)

Abaxial leaf

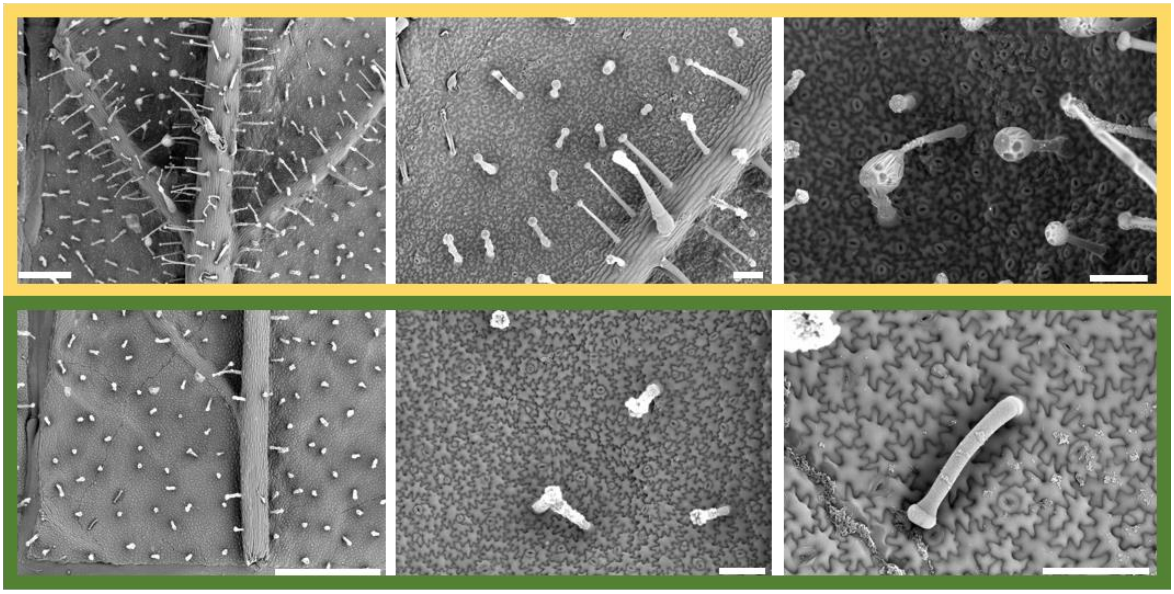

Adaxial petal

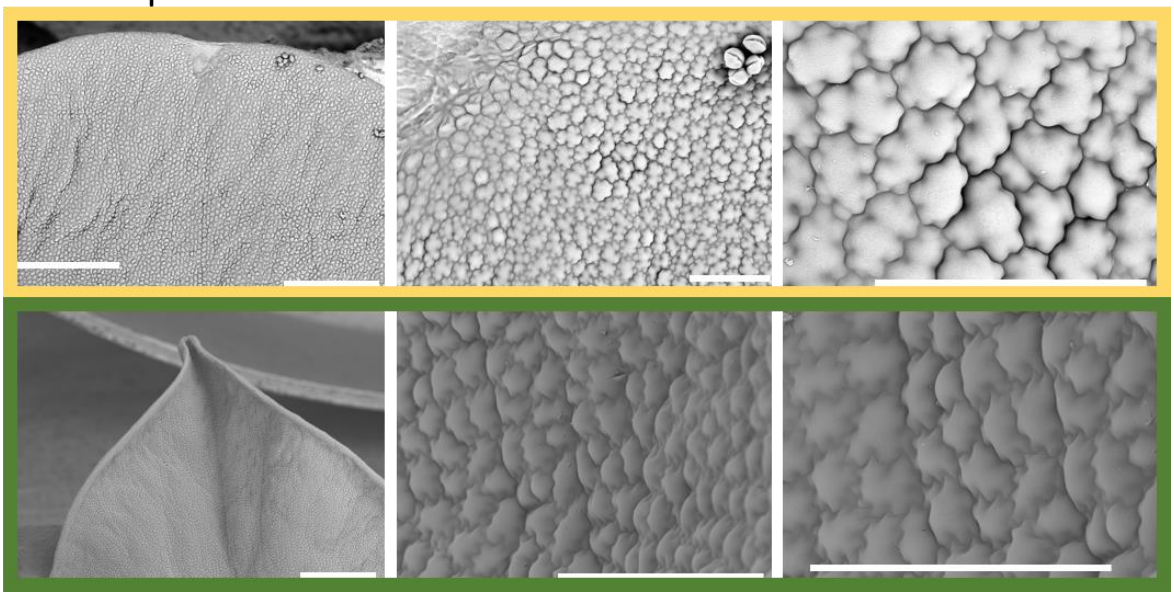

Carpel